GARP

GLOBAL ATMOSPHERIC RESEARCH PROGRAMME

GLOBAL WEATHER EXPERIMENT

GARP PUBLICATIONS SERIES

No. 25

THE GARP ATLANTIC TROPICAL EXPERIMENT (GATE) MONOGRAPH

INTERNATIONAL COUNCIL OF SCIENTIFIC UNIONS

WORLD METEOROLOGICAL ORGANIZATION

GLOBAL ATMOSPHERIC RESEARCH PROGRAMME (GARP)

WMO-ICSU Joint Scientific Committee

THE GARP ATLANTIC TROPICAL EXPERIMENT (GATE) MONOGRAPH

GARP PUBLICATIONS SERIES No. 25

April 1982

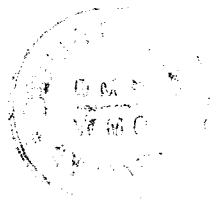

TABLE OF CONTENTS

./...

Page No.

./...

Page No.

* * * * * * * *

F O R E W O R D

The GARP Atlantic Tropical Experiment (GATE), conducted from June to September 1974, was the first experiment organized jointly by WMO and ICSU under the Global Atmospheric Research Programme. This experiment was unprecedented in its scale and in the success of its results. About 70 countries took part, thereby expressing their great interest in the objectives of the programme.

During the field phase of GATE unique data sets were obtained for the Tropical Atlantic area which furthered extensive research in the study of cumulus convection processes and their relation to large-scale weather systems in the Tropics.

Since the time of the experiment a large number of scientific conferences and workshops have been organized in which scientists from various countries have had a good opportunity to discuss common problems relevant to GATE. During the same period about 1000 scientific papers were published thereby showing the magnitude of interest in the problems concerned.

In order to follow up the research and evaluation phase of GATE the Joint Organizing Committee (Mexico City, April 1978), suggested that a monograph be prepared in the GARP Publications Series: "A Synthesis of the GATE Research Programme". Distinguished scientists who were taking an active part in the research and evaluation phase of GATE were invited to write papers on selected topics for the monograph.

The International Conference on Scientific Results of GATE, held in Kiev, USSR in September 1980, was considered as a final stage of the international co-operation in GATE.

The papers presented at the Conference were used as background material for the preparation of the monograph. "Referee-experts" were invited to assist in this work.

Thus, the monograph presents a rather comprehensive overview of the internationally encouraged research activities for the last seven years associated with the GATE programme.

Although the internationally co-ordinated effort comes to an end after the publication of this monograph, it is believed that the available GATE data will continue to encourage scientists all over the world to further study the phenomena of the tropical atmosphere.

I would like to take this opportunity to express my appreciation to all those who contributed to the success of GATE.

John Houghton
Chairman
Joint Organizing Committee

ACKNOWLEDGEMENTS

The editors of the Monograph wish to express their gratitude to all those who have contributed to this volume. First of all special mention should be made of the authors of the individual chapters. (Their names can be found at the beginning of their respective chapter). Secondly, thanks should be given to the formal reviewers of the chapters, the referee-experts who were designated by the Informal Meeting of Invited Authors and Organizers, held in Kiev on 24 September 1980. In alphabetical order they are as follows: A.Arakawa, J.R.Bates, V.A.Bubnov, J.Businger, H.Charnock, B.S.Chuchkalov, S.Cox, M.A.Estoque, H.Grassl, W.M.Gray, V.N.Ivanov, S.A.Mashkovich, T.Matsuno, J.Merle, K.Miyakoda, R.S.Pastushkov, C.J.Readings, J.Sadler, G.Sommeria and M.Yanai.

The scientific planners and organizers of the International Conference on the Scientific Results of GATE (Kiev, 17-23 September 1980), which was a key point in the preparation of the Monograph, also greatly contributed to the final success of the publication. Here we should mention the International Organizing Committee which was chaired by M.A.Petrossiants and whose members consisted of T.N.Krishnamurti, P.R.Rowntree, N.P.Skripnik and J.D.Woods. Concerning the preparation and actual implementation of the Conference thanks are due to the National Organizing Committee which was designated by the USSR State Committee for Hydrometeorology and Control of Natural Environment.

During the preparation of the Monograph many contacts were made with people and bodies responsible for the co-ordination of GATE research at the national level. In particular SCOR should be singled out for their assistance in the development of the GATE scientific programme and in arranging the many workshops and symposia in the analysis phase of GATE.

* * * * * * * *

LIST OF ABBREVIATIONS

ABL	- atmospheric boundary layer
ALPEX	- Alpine Experiment (GARP)
APE	- available potential energy
ASECNA	- Agence pour la Securité de la Navigation Aerienne en Afrique et à Madagascar
ATEX	- Atlantic Tradewind Experiment
BOMEX	- Barbados Oceanographic and Meteorological Experiment
CC	- cloud cluster
CISK	- convective instability of the second kind
CWS	- curl of wind stress
ECMWF	- European Centre for Medium-Range Weather Forecasts
FGGE	- First GARP Global Experiment
FSU	- Florida State University (USA)
GATE	- GARP Atlantic Tropical Experiment
GCM	- general circulation model
GFDL	- Geophysical Fluid Dynamics Laboratory
GTS	- Global Telecommunication System
ISMG	- Interim (and International) Scientific and Management Group (for GATE)
ITCZ	- intertropical convergence zone
MO	- Meteorological Office (UK)
MONEX	- Monsoon Experiment (GARP)
MPF	- mesoscale precipitation feature
NHC	- National Hurricane Center (USA)
NCAR	- National Center for Atmospheric Research (USA)
NMC	- National Meteorological Center (USA)
NOAA	- National Oceanic and Atmospheric Administration (USA)
RFD	- radiation flux divergence
RS	- radio-sound (-sounding)
RSP	- Radiation Sub-programme (in GATE)
SAL	- Saharan aerosol layer
SSDC	- Synoptic-scale Subprogramme Data Centre (in GATE)
TROPEX	- USSR Tropical Experiment, 1972 and 1974
VIHMEX	- The Venezuela International Hydrological and Meteorological Experiment
WAMEX	- West African Monsoon Experiment (GARP)
WWW	- World Weather Watch (WMO)

CHAPTER 1

OPENING LECTURE: MAJOR TASKS OF GATE

by

M.A.Petrossiants*

(Hydrometeorological Research Centre of the USSR,
Moscow, USSR)

1.1 AN EARLIER HISTORY OF GATE

1.1.1 The planning of the GARP Atlantic Tropical Experiment (GATE) has a long history. The necessity of preliminary studies in the tropics prior to the First GARP Global Experiment was recognized by the ICSU/IUGG Committee on Atmospheric Sciences at a very early stage. At its second meeting (Geneva, 22-25 April 1966) it was recommended to carry out "studies in the tropics - including the development of appropriate dynamical models, analyses of the role of convection in energy transformation and detailed observational programmes in low latitudes".

1.1.2 In November 1966 the WMO CAS Working Group on Tropical Meteorology held a meeting in Geneva and proposed "a tropical data-gathering experiment throughout 1968 - as a precursor for the planning of further development of the World Weather Watch and of the Global Atmospheric Research Programme". The report of this working group was considered at the third meeting of the ICSU/IUGG-CAS which decided that the tropical project should be considered as an important GARP sub-programme and the project should be referred to GARP Study Conference for a detailed consideration.

1.1.3 The Study Conference on the Global Atmospheric Research Programme held in Stockholm (28 June - 11 July 1967) gave the first comprehensive analysis of the scientific objectives of GARP and in particularly objectives of the tropical investigations.

During the Study Conference an attempt was made to break down the problems of tropical meteorology into three broad categories as follows:

(A) Planetary scale (the equatorial trough and trade-wind zones, the subtropical highs and subtropical jets, the tropical monsoons, the quasibiennial oscillation in the stratosphere),

(B) Synoptic scale (easterly waves, tropical cyclones, waves and vortices in the upper troposphere and stratosphere),

(C) Moist-convective scale (cumulus clouds and cumulus cloud clusters).

It was strongly emphasized that the outstanding problems of tropical meteorology are associated with interactions of the scales of motion.

The main features of tropical atmosphere subject to investigation have also been pointed out in the Report of the Conference.

After analysing the problems connected with the types of atmospheric motion of the above mentioned scales, the Conference formulated the following recommendation that in fact was the first scientific objective of GATE:

> "The principal problem in tropical meteorology is the mechanism of interaction of the deep cumulus convective systems with the mesoscale circulation patterns in the rain areas and with motions of synoptic scale. This

---

* Present affiliation: The Moscow State University, USSR

mechanism involves the sub-cloud boundary layer in a special way, for it is here that the major moisture supply exists. There are models to be tested, some rather rudimentary, some of fairly precise formulation and we ask for definitive data, on a scale never before attempted in the tropics, but non vastly different from what is routinely available to northern hemisphere middle-latitude meteorologist. What is different is our strong requirement for a small-scale observational network enmeshed in the more normal large-scale framework, and the necessity for a portion of the observational experiment to be conducted in remote, mid-oceanic regions".

1.1.4 The next very important contribution to the planning of GATE was the Report of the JOC Study Group on Tropical Disturbances (Madison, October 21 - November 8, 1968).

The report of the study group subdivides the cloud systems over the tropics into three categories, namely "cloud clusters", "monsoon clusters" and "popcorn cumulonimbi", and points out that "these three categories of cloud systems appear to be the most important contributors to the energy release in the tropics".

It was shown by the study group, that "cloud clusters occur over all the three major oceans, in practically all seasons. With the exception of South America and the monsoon area, these cloud clusters seem to represent the most characteristics pattern over the whole of the tropics. It was therefore concluded that "the first objective of a tropical experiment should be to study intensively their internal structure and their relation with their immediate environment and the general circulation".

The report of the Study Group on Tropical Disturbances was considered by the JOC (Princeton, 27-30 January 1970) at its second session and scientific objectives were approved in general. It was agreed that the first type of tropical experiment might be restricted to studying in detail the cloud clusters and to investigating their relations with the immediate environment. The main objectives would be to clarify the internal structure and the interactions within the clusters "although the relations between the mesoscale and the large scale should also be explored by making use of all available observations in the area". The JOC decided that a progress report on a GARP Tropical Experiment should be submitted to the Executive Committees of WMO and ICSU. In accordance with the decision of JOC the report was prepared under the title "The Planning of the First GARP Tropical Experiment" which took into account as the background material the Report of the Study Conference on GARP and the Report of the First Session of the JOC Study Conference on Tropical Disturbances. The WMO and ICSU Executive Committees considered "The Planning of the First GARP Tropical Experiment" and endorsed the scientific and technical proposals of the JOC as a preliminary definition of the scope of the Experiment and decided that it still requires further elaboration. In response to this JOC decided to convene a meeting of the Study Group on Tropical Disturbances with invitation of experts involved in tropical investigation and to refine the scientific objectives and design of a Tropical Experiment.

1.1.5 The final version of the Report entitled "The Planning of GARP Tropical Experiments" that was approved by JOC Officers in Rome (13-16 January 1970) was submitted by Chairman of the JOC Prof.B.Bolin to the Executive Committees of WMO and ICSU.

In this report there was some revision of classification of motion scales in tropics in comparison with those contained in the report of the Study Conference on the GARP and refinement of goals of Tropical Experiment.

The scales of atmospheric motions in the tropics were stated as follows:

Scale A - the large wave-scale of the order of 2000 to 10000 km,

Scale B - the scale of cloud clusters of the order of 100 to 1000 km,

Scale C - the meso-convective scale of the order of 10 to 100 km,

Scale D - the scale of convective cells of the order of 1 to 10 km.

Main problems in regard to the tropical atmosphere were formulated as follows:

- The small amplitude of the changes in the wind, temperature and water vapour fields in the tropics must be defined by global observing systems on a scale suitable for numerical forecasting modesl;

- It will be necessary to parameterize sub-grid scale processes.

1.1.6 These scientific goals were detailed by a hierarchy of experimental studies in the tropics in the following way:

(1) An experimental study to define the interactions between the large wave-scale and the cloud-cluster scale (Scales A and B).
Objectives:

(a) To determine the necessary and sufficient conditions for the development of a cloud cluster;

(b) To understand the role of large-scale disturbances (2000-10000 km wave length) in the development of a cloud cluster;

(c) To account for the spatial redistribution of heat, moisture and momentum by the cluster during its life cycle in a manner consistent with large-scale numerical prediction models;

(d) To ascertain the effects of this redistribution on the large-scale motion field.

(2) An experimental study to determine the interaction between the scale of the cloud cluster and the meso-convective scale (Scales B and C).
Objectives:

(a) To make intensive case studies of the structure, evolution, dynamics and thermodynamics of selected meso-convective elements in order to

determine how much variability exists between different elements and whether there are fundamentally different types of meso-convective-scale organization with respect to parameterization.

(b) To account for the local redistribution of heat, moisture, momentum an energy due to the individual meso-convective elements within a cluster with reference to the sizes and the spacing of meso-convective elements, the types of meso-convective scale organization (e.g. lines, rings, etc.).

(3) Auxiliary experimental studies on convection over a tropical land mass.
Objectives:

(a) To determine the mechanism for the transfer of heat and moisture from the convective systems to the large scale resulting, for example, in the formation of outflow from anticyclones in the upper atmosphere or in the generation of high level cold troughs.

(4) Auxiliary experimental studies on the planetary boundary layer in the equatorial region
Objectives:

(a) To study the behaviour of the planetary boundary layer in the immediate vicinity of the Equator.

(b) To determine whether convection can be produced by frictional convergence within plus or minus one degree or so of the Equator - that is, on the scale of the meso-convective processes.

(c) To determine to what extent small gradients in sea surface temperatures influence the structure of the planetary boundary layer.

(d) To understand the dynamics of the equatorial dry zone which exists at some longitudes.

1.2 IDENTIFICATION OF GATE

1.2.1 The issue of GARP Publications Series No.4 "The Planning of GARP Tropical Experiments" was the first step in defining the scientific tasks of GATE. The proposals contained in the publication were submitted to the Planning Conference on GARP (Brussels, March 1970). This Conference adopted the scientific ideas and tasks of the Tropical Sub-programme of GARP and approved an experiment dealing with interaction between Scales A and B and/or an experiment dealing with interaction between Scales B and C, including the collective effect of Scale D as it was recommended by JOC.

At the same time it changed the place of the Experiment from Pacific to Atlantic.

The conference pointed out the ways for further planning, designing and implementation of the Experiment. It was recommended to organize the Interim Scientific and Management Group for designing the Experiment and to establish the Tropical Experiment Council and the Tropical Experiment Board for its implementation. These

decisions found their further continuation in the Report of Interim planning group on GARP Tropical Experiment in the Atlantic (London, July 1970) when it agreed with the JOC recommendation that Tropical Experiments should investigate the interactions between all scales - A, B, C and D.

1.2.2 The transfer of the Tropical Experiment from Pacific to Atlantic demanded some additional studies of cloud clusters and tropical disturbances over the new area. In November 1970 the Interim Scientific and Management Group (ISMG) started working in close conjunction with the Joint Planning Staff. A little later JOC Study Group on Tropical Disturbances together with above mentioned bodies and some invited experts produced the Report of their second session (Geneva, 11-16 January 1971) that gave the sound basis to JOC to restate the scientific objectives of the GARP Atlantic Tropical Experiment. It was done in the following way.

The GARP Atlantic Tropical Experiment has been announced in order to provide a basis upon which to develop appropriate schemes for estimating the effects of the smaller tropical weather systems on the larger-scale circulations. It has also aimed to provide data against which the validity of numerical prediction methods can be tested in the tropics.

The tropical atmosphere is noteworthy for the widespread occurrence of cumulus and cumulonimbus cloud and convective storms. The major part of tropical rainfall is produced by such convection, and there is little doubt that convection is a major factor in the vertical transport of heat and water vapour and probably also of momentum . However, convection does not occur at random, and satellite observations of cloud distribution have shown that a major part of the convection occurs in organized 'cloud clusters' with dimensions from 100 to 1000 km.

The GARP Atlantic Tropical Experiment has therefore been designed to provide a description of the internal structure of cloud clusters, to estimate the vertical transport of heat, moisture and momentum in the system and relate them to the larger scale motions of the tropical atmosphere. The experiment was exploratory, inasmuch as no accepted conceptual model for a cloud cluster existed and the experiment aimed to determine its internal organization. However, the observations were designed to measure the bulk effects of the cloud cluster, such as the overall convergence into and divergence from it at various levels, the vorticity changes in the circulation round it, etc.

The observational system must also have been adequate to define the motion of the large scale to which the occurrence and development of the cloud cluster was to be related.

It was anticipated that besides an improvement of our understanding of the physical processes in the tropical atmosphere and the development of adequate numerical models for the simulation of general circulation, the GATE would provide

a solid background for the improvement of weather forecasting in the tropics in general, and forecasting movement and development of tropical storms and associated rainfall in particular.

1.2.3 The next step of formulation of scientific tasks of the Tropical Experiment was the preparation of "The GATE Experiment Design Proposal" by J.P.Kuettner, N.E.Rider, I.G.Sitnikov (ISMG). The Scientific Objectives of the GARP Atlantic Tropical Experiment as formulated by J.S.Sawyer for the JOC were fully accepted. Looking in retrospect there were as follows.

The GARP Atlantic Tropical Experiment has been developed as a major contribution to the Global Atmospheric Research Programme (GARP) which is a joint programme of WMO and ISCU directed towards improving understanding of the general circulation of the atmosphere, its variability and its predictability. The primary aims of GATE are thus to extend our knowledge of those aspects of the meteorology of the equatorial belt which are essential for a proper understanding of the circulation of the Earth's atmosphere as a whole. However, the knowledge and experience derived from GATE will cerainly also provide a basis for a major advance in the understanding of tropical meteorology and for the development of weather forecasting in the equatorial belt.

The atmosphere of the equatorial belt behaves differently from the atmosphere of middle latitudes in many respects, but it forms an integral part of the global circulation. It contains the main heat sources which drive the general circulation of the atmosphere as a whole, and fluctuations in the equatorial belt are undoubtedly linked with variations of the circulation in higher latitudes although the nature of the connexions is as yet obscure.

One of the principal tools in achieving the aims of GARP is the numerical simulation of the behaviour of the atmosphere by the numerical solution of the physical and dynamical equations describing appropriate models of the atmosphere. Such models of the atmosphere have been developed, and their validity in respect of middle latitudes has been extensively tested by comparison with synoptic data. The models are at a less developed stage in regard to the atmosphere within the tropics and comparison with the real atmosphere of these regions has been limited by the lack of synoptic data with adequate resolution and extent.

No mathematical model can represent all the disturbances of the atmosphere and the capacity and speed of even the largest computers set a limit to the number of points which form theintegration grid at which the meteorological variables are evaluated. Disturbances in the atmosphere which are not large enough to extend over several points of the computation grid cannot be properly described by the direct integration of the dynamical equations. Nevertheless such disturbances have important effects in producing transports of heat, momentum and water vapour both vertically and horizontally. These must be taken into account by relating them to larger-scale features of the atmospheric circulation which are adequately represented by the model. Such, so-called, 'parameterization' of the smaller-scale features is particularly important in the tropical belt where much of the atmospheric variability is associated with disturbances less than a few hundred kilometres in extent. Unfortunately, the available knowledge of such disturbances in low latitudes is, as yet, insufficient for such parameterization to be effectively carried out.

The GARP Atlantic Tropical Experiment has aimed to provide a basis upon which to develop appropriate schemes for estimating the effects of the smaller tropical weather systems on the larger-scale circulations. It has also aimed to provide data against which the validity of numerical prediction methods can be tested in the tropics.

The tropical atmosphere is noteworthy for the widespread occurrence of cumulus and cumulonimbus clouds and of convective storms. The major part of tropical rainfall is produced by such convection, and there is little doubt that convection is a major factor in the vertical transport of heat and water vapour - probably of momentum also. However, convection does not occur at random, and satellite observations of cloud distribution have shown that a major part of the convection occurs in organized 'cloud clusters' with dimensions of from 100 to 1,000 km. It has long been recognized that disturbances in the equatorial wind field also exist on a larger scale. In the lower troposphere these disturbances have been studied as 'easterly waves' and in the upper troposphere they have been more recently identified as mixed Rossby-gravity waves. In principle their size is such that numerical models can be used to describe and predict their behaviour, but it is necessary to know the interrelations between them and the cloud clusters. To obtain this knowledge is one of theobjectives of GATE.

Recent experiments on numerical simulation of the behaviour of the tropical atmosphere have used a grid-length of 250 km and, with a grid-length as short as this and a rather elementary parameterization of the convective processes, it has been possible to reproduce precipitation areas with features similar in some respects to those of cloud clusters. With present computers a grid-length of 250 km approached the maximum resolution which was practical for global simulation experiments, but the results held promise that with the improved parameterization which may be achieved following GATE, successful prediction of the wave-like disturbances in the tropical wind field and of the associated cloud clusters may be achieved.

The GARP Atlantic Tropical Experiment has therefore been designed to provide a description of the internal structure of a number of cloud clusters, to estimate the vertical (and horizontal) transport of heat, moisture and momentum associated with these systems and to relate them to the motion of the tropical atmosphere on a larger scale. The experiment has been exploratory in as much as no accepted conceptual model existed for cloud clusters, and the experiment has aimed to describe their internal organization. However, the observational network in GATE was designed to measure the bulk effects of a cloud cluster, such as the overall convergence into and divergence from it at various levels, the changes in the total vorticity of the circulation round it, the total release of latent heat and exchange of heat and water vapour between levels. An important aspect of the experiment was the comparison of the observations with numerical calculations using dynamical models employing a fine grid. It was expected that the combined observational and theoretical approach will reveal significant aspects of the life cycle of cloud clusters with applications both to forecasting and to the understanding of the role of tropical disturbances in the general circulation of the atmosphere.

The GARP Atlantic Tropical Experiment therefore required observing systems on several different space scales. On the largest scale the observational system had to be adequate to define the large-scale disturbances of the wind field to which

the behaviour of the cloud cluster was to be related. This required the determination of the wind and temperature field of the tropopsphere between 10°S and 20°N extending across the Atlantic and covering the African and South American continents in this belt. The observational density needed to be sufficient to resolve features with dimensions of 1,000 km and upwards. Winds obtained from cloud movements as observed from geostationary satellites were an important supplement to more conventional observing networks.

A finer network of observations was required to resolve the internal structure of the cloud clusters and the effects of the clusters on the circulation in their immediate environment, e.g. convergence of wind and other fluxes into and out of the system. Time sequences of observations providing evidence of the changes as the cluster moves through the observing network helped to fill in details. Satellite images of the cloud distribution employing enhancement of the contrasts to delineate active convective areas were important for the interpretation of the surface-based observations. The area for the fine network of the ship-based observations has been selected in the eastern Atlantic where the climatological frequency of cloud clusters is notably high.

A full understanding of the behaviour of the cloud clusters and the transports of heat, water vapour and momentum arising from them could not be achieved without consideration of the fluxes of these quantities produced by individual cumulus cells and even smaller-scale motions. It is not possible to measure these fluxes throughout the whole volume within a cloud cluster, but sample measurements by aircraft of relevant parts of the spectra and co-spectra of turbulence and also detailed measurements of air motion during precipitation using Doppler radar should have been very valuable in indicating the distribution and significance of such transports. Radar observations of precipitation distribution also helped in building up a composite description of the tropical disturbances.

The energy of tropical disturbances is largely derived from the heat input from the sea into the atmospheric boundary layer, most of it as latent heat. The energy released in a particular cloud cluster has not been derived from the sea surface immediately beneath it, but has been collected from a substantially wider area. Nevertheless, the effect of the cloud cluster itself on the evaporation and heat transfer may be of significance and should have been studied. Also it was believed that the effects of frictional convergence in the atmospheric boundary layer played an important part in the control of the growth of organized convective systems (convective instability of the second kind - CISK) and some knowledge of the turbulent stresses in the boundary layer in different parts of the system was desirable.

Thus, although GATE has not been primarily directed towards measurement of boundary-layer exchanges, measurements were required from ships in order to establish variations in the boundary-layer fluxes of heat, water vapour and momentum which occurred in association with cloud clusters - down-draughts produced by the convective systems may have been particularly effective in influencing the air-sea transfer processes.

Knowledge of the radiative flux divergence is of importance in the long-term control of the structure of the tropical atmosphere and may play a role in the

maintenance of conditions in which convective disturbances can develop. It was, therefore, hoped that GATE would include sufficient radiation observations for an assessment of radiative flux divergence and its comparison with theoretical models.

The GATE programme has also provided an opportunity for oceanographic experiments and was particularly appropriate for the study of phenomena which are affected to an important degree by temporal variations in the wind field with periods from a few hours to a few weeks such as examined by the meteorological network.

It is appropriate to recall the implications of GATE in the broader context. The experiment was the first GARP endeavour directed to the investigation of the least known part of the global atmosphere, namely the tropical belt. As such, its impact extended beyond the limits of its inherent scientific interest and its own latitudinal boundaries. It hopefully contributed to the solution of some of the outstanding meteorological problems of our time which, in turn, may result in tangible, economic benefits of major significance. Among the main results of this wider sense we may expect:

i. a definition of the necessary and sufficient conditions for the generation and development of tropical disturbances, including the early stages of tropical cyclones;

ii. improvements in the quality and time range of forecasts for the tropics;

iii. improvements in extended forecasts in extra-tropical latitudes by taking the tropical heat sources properly into account;

iv. progress towards an understanding of the possibilities for modifying tropical weather.

It is difficult to foresee any substitute for GATE in the solution of these problems which are of significance for the whole population of the world.

1.2.4 The GATE Experiment Design Proposal was submitted to JOC VI (Toronto, 20-25 October 1971) and approved by it and subsequently by the second session of the Tropical Experiment Board, Geneva, December 1971. The International Scientific and Management Group has been established. It was the time for the beginning of elaboration of the comprehensive GATE Plan. It was approved that the content of GATE should include the Central Programme and five sub-programmes, dealing namely with the synoptic-scale motions, the convection, the boundary layer, the radiation and the oceanography.

1.3 MAIN SCIENTIFIC OBJECTIVES OF GATE

In accordance with this architecture of the scientific plan of GATE, the major scientific objectives of GATE were stated as follows:

- To provide a means of estimating the effects of smaller tropical weather systems on the large-scale (synoptic-scale) circulations,

- To facilitate the development of numerical modelling and prediction methods.

The special diagram was elaborated as presented in Figure 1.1, taken from the GATE Report No.3 "The Central Programme for the GATE". The diagram shows how these objectives were translated into the necessary components of the Central Programme. For each component identified in Figure 1.1 a brief statement of the scientific considerations was presented and the required data set was identified. The more detailed discussion including analysis methods, experimental design, data management and bibliography was left to the sub-programme documents.

1.4 THE GATE SUB-PROGRAMMES AND THEIR TASKS WITHIN THE CENTRAL PROGRAMME

The primary scientific objectives of the five GATE Sub-programmes were formulated in the following way (see GATE Report No. 3, pp. 25-29):

1.4.1 Synoptic-Scale Sub-programme

The main scientific objectives centre on:

(a) Description of the synoptic-scale disturbances in the tropical troposphere and lower stratosphere from West Africa to the western Atlantic Ocean;

(b) Description of the averaged state of the troposphere over the GATE area particularly in terms of the jet streams, meridional circulations and the Inter-tropical Convergence Zone (ITCZ);

(c) Description of the synoptic-scale environment of cloud clusters passing through the B-scale area in sufficient detail to allow investigation of the interaction between the clusters and the larger-scale motions;

(d) Development of complete and internally consistent data sets for tropical numerical prediction models.

Provide time series, time-space sections, composites and daily synoptic analyses to identify the nature of oscillations in the troposphere and lower stratosphere with periods greater than or equal to 3 days. Include analysis for A-scale vorticity divergence and vertical motion distribution.

Provide averaged values of the horizontal wind velocity V_H, pressure p, temperature T, moisture q, and cloudiness distributions, with the characteristics of jet streams, ITCZ and latitudinal circulations well defined particularly near the B-scale area.

Determine for 20-day periods the available potential energy, momentum and moisture budgets for rhe eastern tropical Atlantic, including internal conversions and boundary fluxes for 5^{o} latitudinal bands.

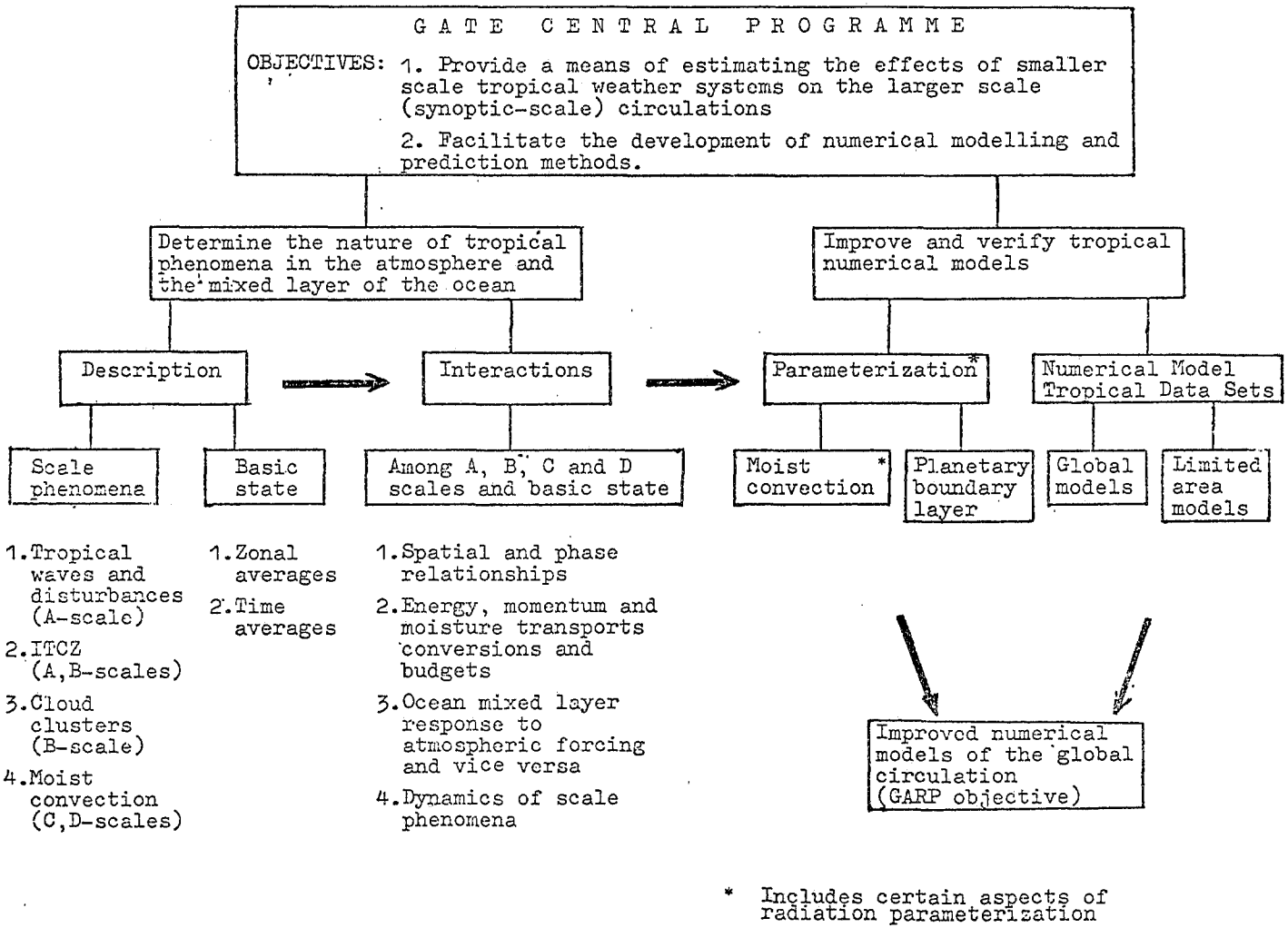

The thick arrows indicate the inter-relationship of the components noting the general order in which scientific work may proceed. The box at the lower right hand corner and the two arrows leading into it indicate the aim of the numerical experimentation programme which will follow after the objectives of the GATE Central Programme are accomplished

Figure 1.1 - The objectives and components of the GATE Central Programme

Provide detailed analyses of the energy cycles and momentum budgets of tropical waves and clarify the nature of interactions between the mean flow and tropical waves on the one hand and between convection and the tropical waves on the other.

Provide internally consistent and complete data sets for numerical models representing synoptic-scale motions and certain aspects of sub-synoptic scale phenomena.

1.4.2 Convection Sub-programme

The main scientific objectives centre on:

(a) The description of the life cycle of cloud clusters and mesoscale convection as well as of the undisturbed state. This will be done by the four-dimensional fields of fundamental parameters (p, T, q, V_H, precipitation, cloudiness) and by derived quantities (for example vertical velocity w, divergence and vorticity fields or radiative heating rates). Description includes studies of selected cases, composites, time series and statistical relationships;

(b) The study of interaction between scales (B $\leftrightarrow$ C and C $\leftrightarrow$ D), with the boundary layer and (to mention it separately because of its special importance) with the large-scale systems such as the ITCZ and tropical waves (B $\leftrightarrow$ A and C $\leftrightarrow$ A). Among the basic approaches to be used for scale interaction analyses are the determination and interpretation of spectra and cross spectra and of the "interaction terms" (covariances). The latter ones can be obtained as residuals from budget computations or directly using the measured deviations from the basic state;

(c) Provision of data sets appropriate for testing and developing models for convective interaction and parameterization schemes.

Primary tasks within the Central Programme:

Provide cloud cluster census by location, frequency and size within the A-scale domain.

Provide studies of selected cases, composites, time series and statistical relationships for B-scale features of cloud clusters, of the ITCZ and in the trade wind regions.

Provide similar studies of C-scale convective systems, either within cloud clusters, the ITCZ or the trade wind region.

Evaluate budgets of mass, energy, momentum and moisture to describe the life cycles for the individual and composited systems listed above and the derive interaction terms (inputs from the Synoptic-Scale, Radiation, Boundary Layer and Oceanographic Sub-programmes are needed here).

Determine the validity of parameterization schemes for moist convection and provide an observational base for development and testing of improved parameterization.

1.4.3 Boundary Layer Sub-programme

Primary tasks within the Central Programme:

Determine the sensible and latent energy and momentum transfers at the lower boundary relevant to the B, C and D-scale phenomena.

Determine the magnitude and distribution (in relation to convective systems of B, C and D-scales) of boundary layer mass and moisture convergence in the subcloud layer.

Investigate the changes of boundary-layer structure at low latitude in the vicinity of the ITCZ and cloud clusters.

Improve parameterization methods of surface and cloud base fluxes of mass, energy and momentum appropriate to low latitude flows with emphasis on the relationship to the ITCZ and cloud clusters.

1.4.4 Radiation Sub-programme

Primary tasks within the Central Programme:

Determine the vertical profiles of net radiative temperature change at the time and space resolution of the B and C-scale in dependence of principal parameters (clouds, aerosol, etc.), thus providing an essential factor required to study the formation of tropical clouds and the interaction of tropical cumulus convection and the larger-scale phenomena.

Determine the net radiation and its components at the ocean surface in the B-scale area, since these parameters are essential for air-sea interaction studies and for objectives of the Boundary Layer and Oceanographic Sub-programmes.

1.4.5 Oceanographic Sub-programme

The main scientific objectives relevant to GATE which are to be investigated:

(a) Response and feedback of the mixed layer of the ocean to atmospheric disturbances over the B-scale area. The oceanic mixed layer interacts directly with the atmospheric boundary layer. Thus this study will essentially focus on the measurement of the temperature and salinity in the upper ocean, and the determination of the energy and momentum fluxes across the ocean's surface from changes in the structure of the oceanic mixed layer.

(b) Coupling between the position of the ITCZ and the changes of currents and other characteristics of the tropical ocean. The ITCZ activity depends (among others) on the distribution of the sea-surface temperature, which

is in turn influenced by advection processes due to oceanic circulation. Thus the study of the structure and dynamics of the ocean currents in the tropics (including the Equatorial Undercurrent) and of their response and feedback to the atmospheric dynamics is essential;

(c) Sea-surface temperature distribution at the A, B and C-scale in order to study its influence on atmospheric circulation and to verify oceanic numerical models. Mapping of the sea-surface temperature at these scales will be done using measurements from satellites, ships and aircraft where possible.

Primary tasks within the Central Programme:

Determine the detailed response and feedback of the mixed ocean layer to B, C and D-scale disturbances in terms of its temperature and salinity structure.

Provide estimation of precipitation patterns in cloud cluster and ITCZ convection from salinity measurements in the mixed layer.

Identify the role of oceanic circulation by studying the sea-surface temperature field and the structure of the oceanic mixed layer. Particular emphasis will be given to the interaction of ITCZ with the structure of the ocean.

Provide maps of surface temperature distribution with A, B and C-scale resolution.

The above stated illustrates the fact that the elaboration of the main scientific objectives of GATE was a very long and difficult process in which many scientists from different countries of the world were involved. The collective efforts of many people through which the main scientific objectives of GATE have been determined served as the basis of the successful implementation of the GATE field phase as well as data collection and processing. The success of GATE has contributed in every way to the successful implementation of the First GARP Global Experiment (see also Chapter 12).

* * * * * * * * *
* * * * * * * *

CHAPTER 2

GATE OBSERVATIONAL STRATEGY: A LOOK IN RETROSPECT

by

Joachim P. Kuettner

(National Center for Atmospheric Research, Boulder, Colorado, U.S.A.)

2.1 INTRODUCTION

The strategy for a large field experiment such as GATE begins with the first day of the Experiment Design. It continues throughout the field operations but it receives its last judgement only in retrospect, that is, in and after the scientific analysis phase. Strategy implies a counter-player, normally a human being, friend or enemy. In scientific research the main counter-player is nature, but technology and economy are second players in the cast.

2.2 OBSERVATIONAL STRATEGY IN THE PLANNING PHASE

The experiment design for GATE was a two-year full-time effort with a large team of outstanding consultants. It addressed the question of how and where best to observe the mechanism and related scale interactions of the tropical heat engine.

The first decision was to use a composite observing system that would have "nested" resolution from the cumulus scale (D scale) over the meso and cloud cluster scales (C and B scales) to the synoptic-planetary scale (A scale) and to place its centre into the Eastern Atlantic. The next decision was to select a geographical longitude far enough from Africa to suppress continental influences but close enough to make it accessible to long-range aircraft from the operations centre in Dakar. The latitude was chosen so as to intercept the Intertropical Convergence Zone (ITCZ) and the cloud clusters developing and travelling in it in an optimum fashion. Based on all data available since 1887, including the sea-surface temperatures, the selected centre point was placed at 22.5°W and 8.5°N. The A, B and C scale ship array was constructed around this point. We can say today that this centre point was in a nearly ideal position and that the tracks of the cloud clusters in the ITCZ during the three phases of GATE (late June to mid-September) were successfully intercepted (Figures 2.1 and 2.2).

It is also interesting to compare the originally-estimated long-term sea-surface temperature field (Figure 2.3) with the one actually measured during GATE (Figure 2.4, after Krishnamurti and Pasch, Chapter 3, this volume; see Düing et al., 1980). One can see that the selected centre point of the array was placed near the 27°C isotherm as intended.

2.2.1 Configuration of the Observing System

A difficult question facing the experiment design was how to configure the B scale (cloud cluster scale) ship array for upper-air soundings. On one hand, it should intercept as many cloud clusters as possible travelling west from the African coast; this would favour a large north-south extension. On the other hand, one wanted to get an insight into the life cycle of the cloud clusters and their heat budget. This would require a good overlap of quantitative radar ranges and favour strong east-west extension.

As it happened, only four of the nine available radar ships had digital 5cm radars suitable for quantitative precipitation measurements. Furthermore, the need for upper-air soundings on the A/B scale suggested a well-spaced distribution of the wind-finding ships. The actually selected double hexagon configuration (Figure 2.5) turned out to be a good compromise satisfying both the grid point and the precipitation requirements. With four strongly overlapping radars (Figure 2.6) unprecedented quantitative information on the convective precipitation systems over the tropical oceans was obtained (see Chapter 9, this volume).

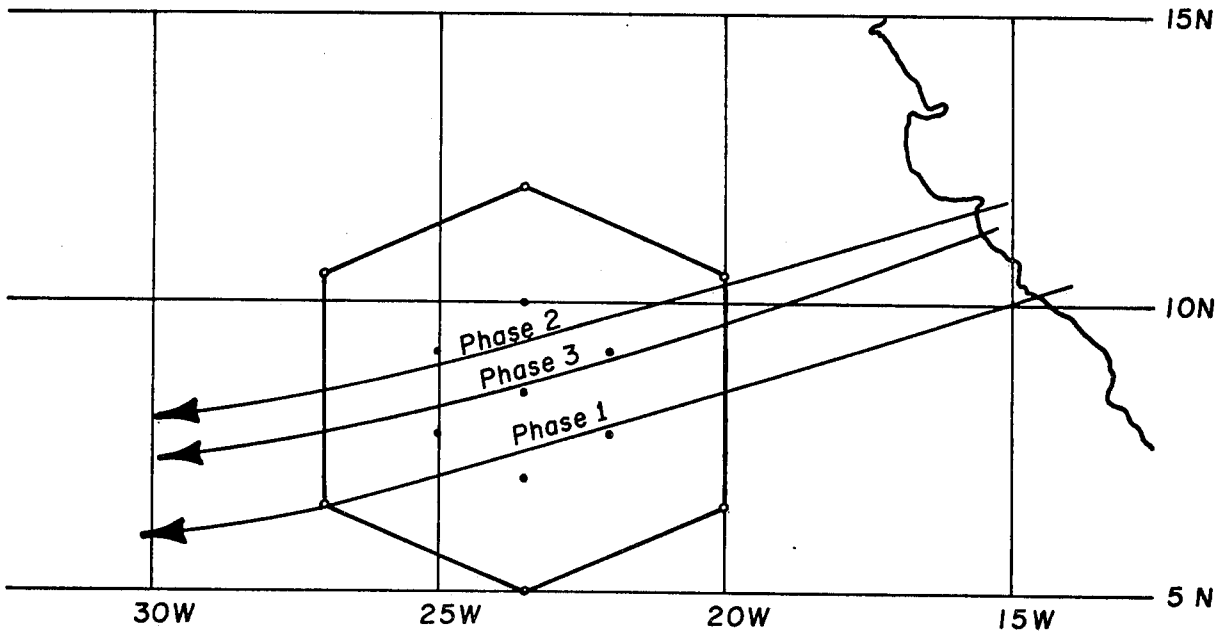

Figure 2.1 - Interception of cloud clusters by the ship array. The arrows show the mean path of the convective systems during each phase as determined from satellite IR pictures.

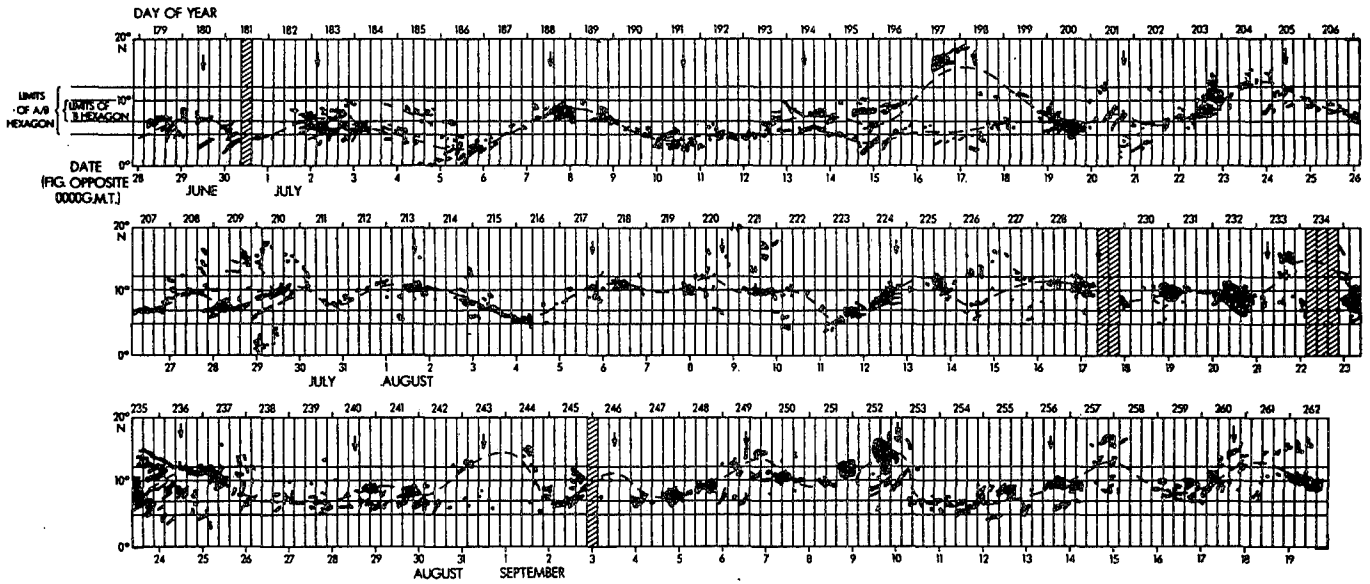

Figure 2.2 - Time section of the upper-level clouds between 0° and 20°N in a 1 1/2 degree longitude band centred on the midpoint of the ship array at 23 1/2°W. The arrows near 15°N indicate the time when the 700 mb troughs of each easterly wave crossed 23.5°W. Latitudes of A/B scale ship array (double hexagon) are also shown.

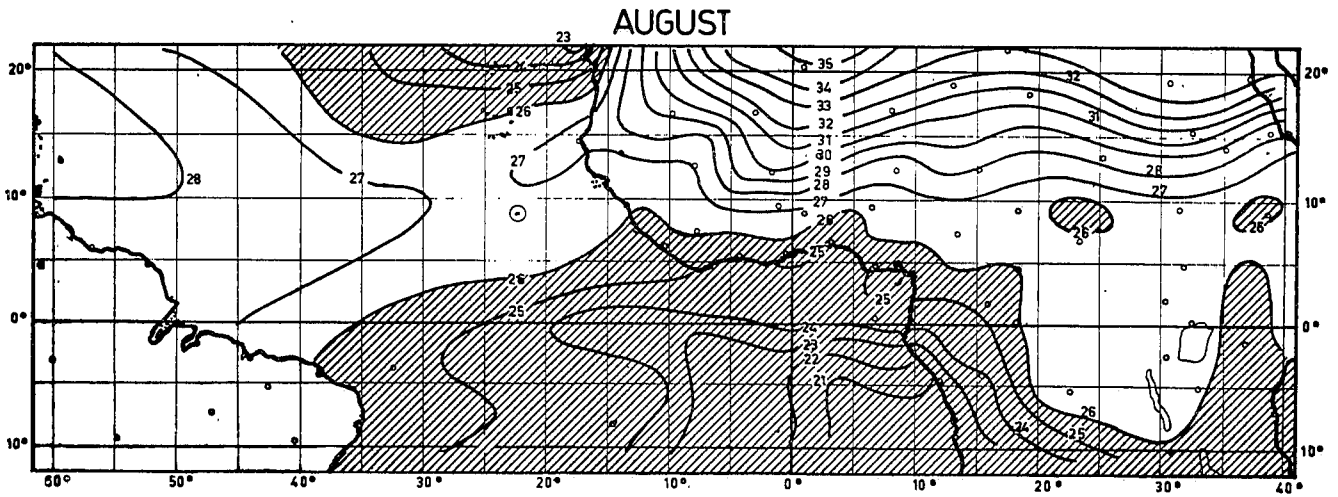

Figure 2.3 - Expected mean surface temperature in ^{o}C in August based on data available since 1887. Circle denotes centre of ship array.

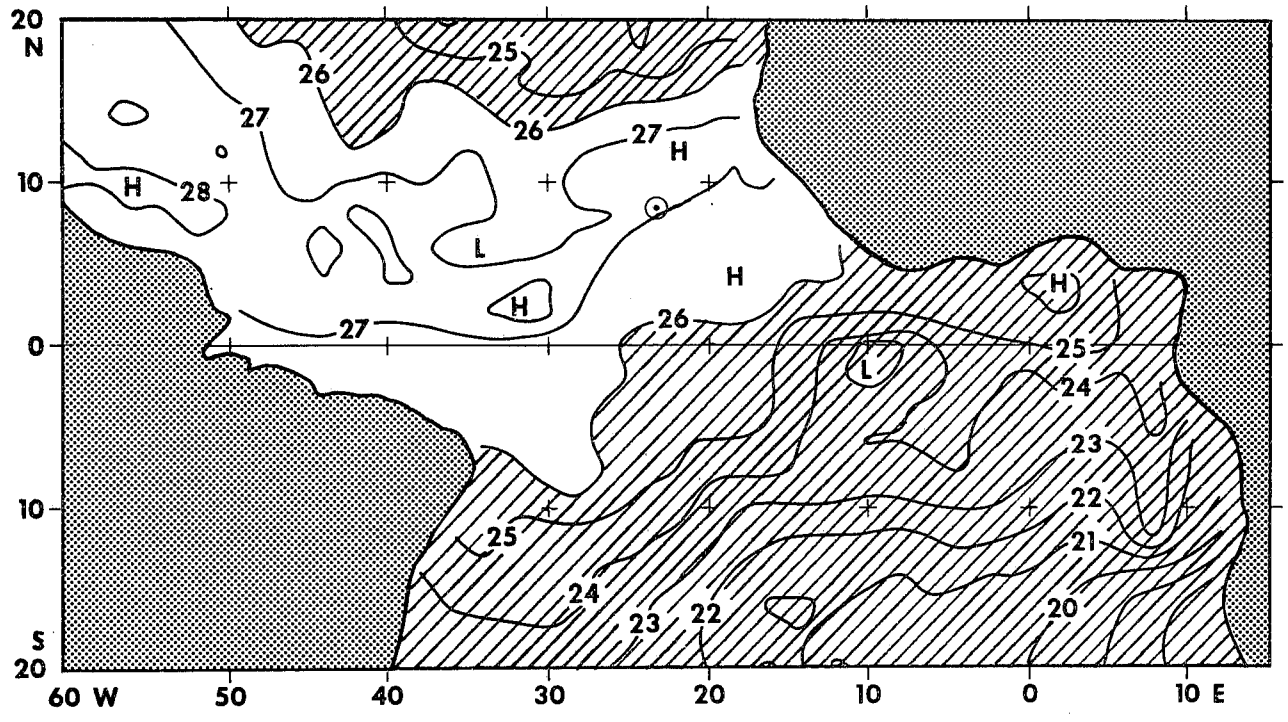

Figure 2.4 - Actual sea-surface temperature in August 1979 during GATE (after Krishnamurti and Pasch, Chapter 3, this volume). Compare to Figure 2.3.

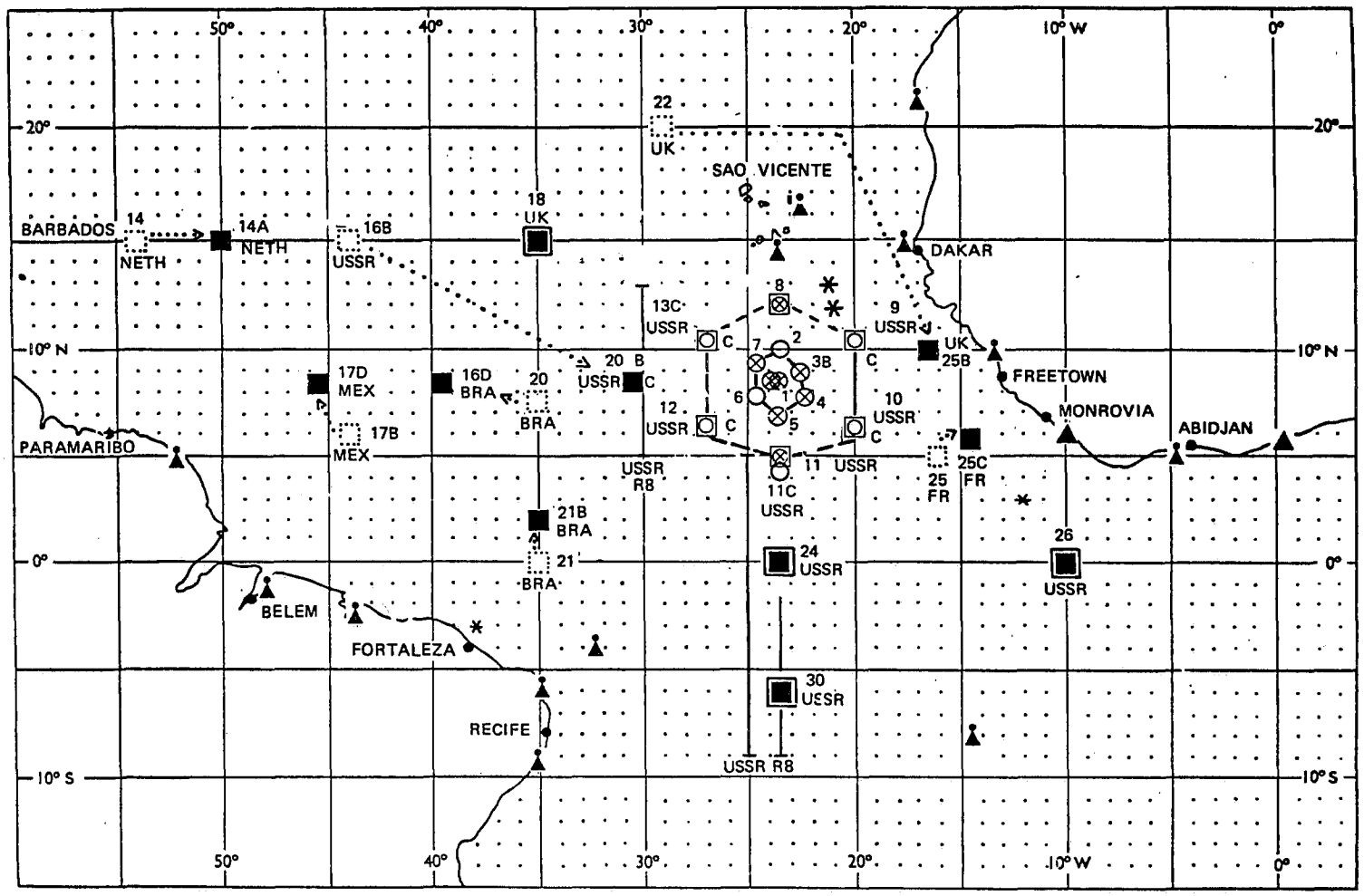

Figure 2.5 - Ship distribution, Phase 3 (30 August-19 September 1974). Numbers are ship positions. Dotted arrows denote adjustments of ship positions from originally planned locations.

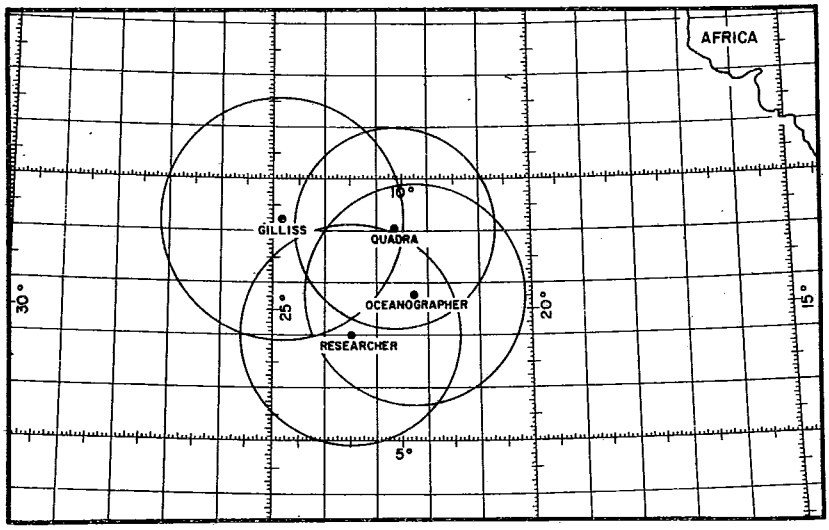

Figure 2.6 - Positions of ships carrying quantitative (digital) radars during Phase 3 of GATE.

2.2.2 Synoptic network and WWW

Another problem of the experiment design was the optimum coverage of the synoptic/planetary scale (A scale) by upper-air stations over land and over the ocean within the GATE area. On land, one obviously had to rely on the World Weather Watch but past records had shown that critical gaps existed in the WWW observing network and the Global Telecommunication System (GTS), especially over Africa. Over water, the competing ship requirements of the various scales presented some problems. In spite of the fact that eventually 39 ships with upper-air capability became available. Numerical studies on optimum ship distribution were conducted during the experiment design phase by the U.S.S.R. and the U.S.A. and an A scale ship array of 12 ships reaching as far north as 20°N was foreseen (Figure 2.7).

Life, however, has a way of disregarding the best laid plans. In spite of a lead time of nearly three years, shortcomings of the WWW-GTS in some parts of Africa persisted. Most serious was the critical gap in the upper-air network along the west coast of Africa. Just upstream of the A/B ship array, there were no data between Dhahran and Abidjan, since Freetown and Monrovia did not operate. (As we will describe later, one way to correct the situation in the field was to redistribute the ships thereby diluting the A scale distribution, see Figure 2.5.)

Furthermore, the geostationary satellite placed over the GATE area was to cover any gaps by cloud vector winds at two or even three levels. This proved to be extraordinarily useful, though not perfect.

Besides the missing WWW stations, it was expected that some of the upper-air stations which operated as planned would have communication difficulties via the GTS. It was planned to at least partly correct this by a simple paper-tape collection. As it happened, this increased the synoptic coverage by about 20%.

2.2.3 Option plan

In order to reduce the critical decision time during the actual operations, most of the conceivable options were anticipated in the planning stage, to the degree possible, and the various alternatives were predetermined.

This was especially important for the aircraft planning. Decisions and options were tried and tested in the planning stage making for a rather smooth operation of the aircraft programme in the field phase.

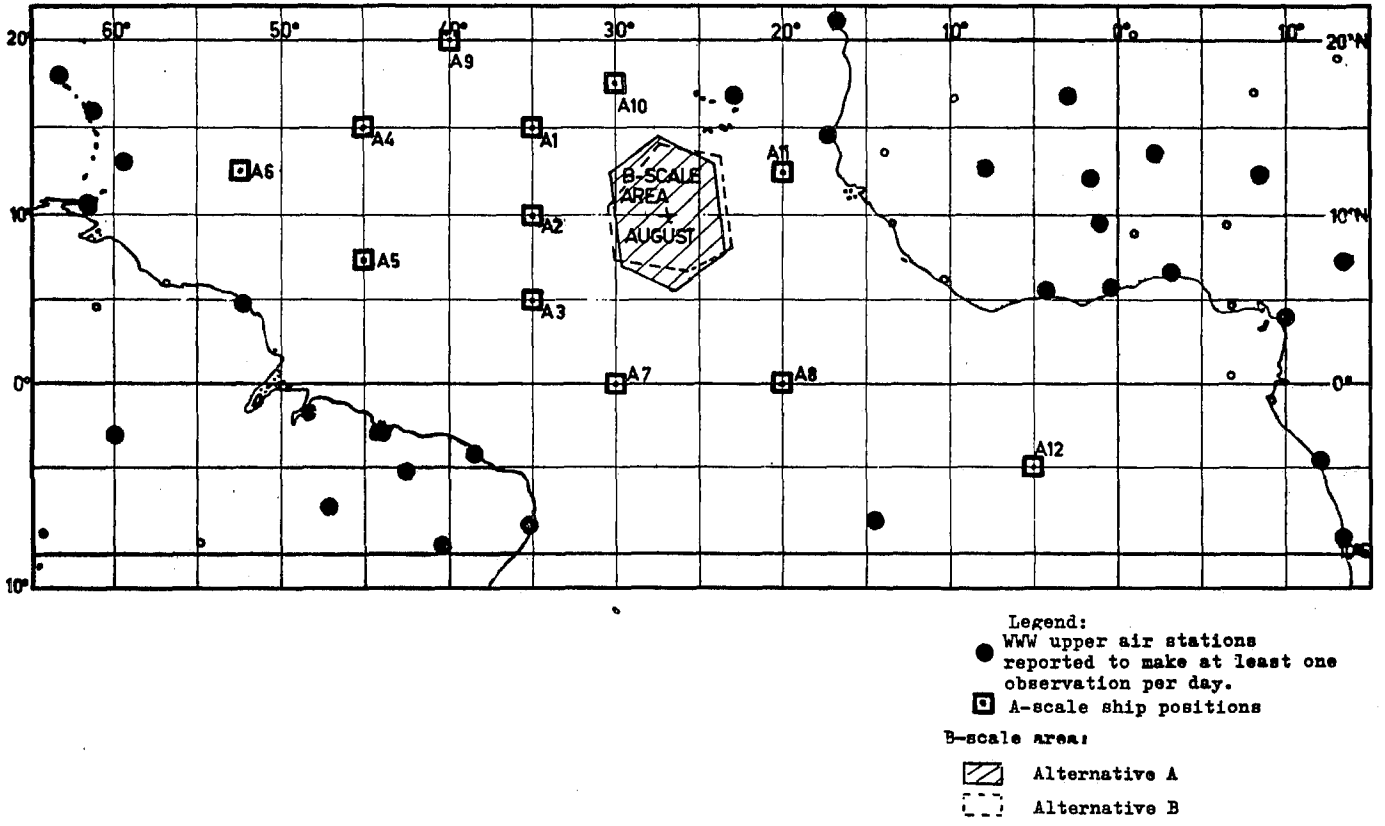

Figure 2.7 - Originally recommended layout of ship array

2.2.4 Subprogrammes and central programme

Due to the complexity of the scientific objectives it was decided to form five subprogrammes which were held together by the "Central Programme". In this way it was possible to attract the top talents of the international scientific community in the fields of boundary layer physics, convection, synoptic-scale dynamics, radiation and oceanography. The Central Programme, in turn, made sure that sight was not lost of the primary objectives, namely the scale interaction and the needs of numerical modelling, such as the parameterization, initialization and verification requirements. The strategy adapted early in the GARP experiments was to combine the numerical objectives with phenomenological and physical research. In this way full scientific use could be made of the enormous resources marshalled by GATE. The vast scientific literature that emerged from this experiment testifies to the stimulation and advance of practically all fields of atmospheric and oceanographic sciences in the tropics by GATE.

2.3 STRATEGY DURING FIELD OPERATIONS

Strategical decisions during the field phase are rendered difficult by two circumstances: the time limitations and the undesirable consequences of any change. Nearly all decisions in the field are urgent. Endless argumentations are entirely useless. The pre-developed option plan was therefore very important - but not all situations and not all consequences could be anticipated. It is good principle to comply, to the extent possible, with the original plans. Attempts to "improve" things during the field phase are dangerous. Usually a chain reaction of technical and logistics difficulties follows such changes. A "better" project often becomes a worse project. Changes should only be made if one of three circumstances arises, namely (in order of priority):

(1) the safety of the participants is endangered

(2) the primary scientific objectives are jeopardized

(3) unexpected natural phenomena demand adjustment (one may call this serendipity).

All three happened during GATE.

2.3.1 Safety considerations

The safety of the aircraft crews demanded certain adjustments with the ship programme due to hazards with the tethered balloons. Also, intercomparison flights between aircraft of different propulsion systems led to some hazardous situations rendered worse by language difficulties. Cases of sickness among ship personnel made it necessary to move ships from their assigned positions. Aircraft were grounded when fuel contamination was suspected. Safety always took priority over science.

2.3.2 Maintaining the scientific objectives

The second problem, a possible jeopardy of the primary scientific objectives, also had to be faced. Two events led to this situation. It was technically and cost-wise impossible to equip all 39 ships with stabilized wind-finding radar; only the U.S.S.R. ships had fully-tested and reliable radar wind equipment. The rest of the ships carried the so-called navigation aid wind-finding system ("Navaid"). This system was newly developed and not sufficiently tested. When it became doubtful that the "navaid" data were reliable, the question arose whether or not the problem of scale interaction between the A and B scale could be solved. There was a possibility that one of the prime objectives of GATE was in jeopardy.

The common human approach to priority problems is to "rob Peter to pay Paul". This was done in GATE too. Peter was the A scale ship array. It was a difficult decision and it was complicated by the second circumstance mentioned earlier, a critical gap in the WWW along the African coast, upstream of the A/B scale area. Therefore, after the first phase of GATE a double adjustment was necessary: some of the U.S.S.R. ships had to be pulled closer to the A/B scale hexagon and other ships farther north had to be moved close to the African coast to cover the upstream conditions (Figure 2.5).

The resulting dilution of the A-scale network in the northern and western Atlantic was considered carefully. It was accepted as the lesser of two evils since a more perfect synoptic observing grid for numerical models would probably be available at some future time, but the chance to repeat the multi-scale central ship array for scale interaction studies was practically nil. Also, the operational forecasts for GATE demanded this decision.

As expected, the shortcomings were felt later, for example in difficulties to track and determine the identity of westward-travelling easterly waves from Africa to the Caribbean Sea (see Burpee and Reed, Chapter 4, this volume). These waves can best be tracked near 15°N at the 700 mb level. The missing ship soundings at this latitude and in the western Atlantic could not be fully replaced by satellite cloud vector winds because these usually refer to levels lower or higher than 700 mb.

All in all, the synoptic subprogramme seems to have suffered under the given situation more than the other subprogrammes.

2.3.3 Unexpected behaviour of nature

The aircraft programme, with its many types of flight tracks, had been designed primarily to explore the nature and life-cycle of the cloud clusters, a phenomenon that appeared rather obscure prior to GATE. Once its nature became more familiar during the GATE field phase the programme had to be swiftly adjusted. The main factor in this adjustment was the unpredictability of the location and the almost explosive growth of the cloud clusters in their initial phase. Mephisto said to Goethe's Faust: "Grey, my dear friend, is all theory". Our well-laid plans of how to disect the cloud clusters were not adequate. The idea to make consecutive flight sorties to follow their development and life-cycle had to be given up. The elusive nature of the phenomenon required decision-making almost on the spot and the practical considerations of crew rest and equipment readiness limited our flexibility. As a consequence, another strategy had to be developed.

The role of the "airborne mission scientist" on the command aircraft was strengthened as compared to the ground mission scientist and the precise flight tracks were determined during the flight itself, often with the help of real-time ship radar and satellite data. This required great skill and excellent communications. Night flights and the so-called "butterfly" pattern (Figure 2.8) had to be given up after a few attempts. This pattern, while very useful in the exploration of quasi-stable vortices (for example, during MONEX) cannot follow the fast changes of the cloud cluster core. The "box pattern" turned out to give better data, also for energy budget calculations. There is little doubt now that this strategy change contributed greatly to the better understanding we now have of the mechanism of tropical convection and the subsystems making up the cloud cluster (see Betts and Houze, Chapter 9, this volume).

On the other hand, the plan to vertically "stack" the research aircraft was not as effective as we had hoped - partly because of failure or inconsistencies of the various on-board systems - partly because of performance problems, especially under icing and turbulence conditions. Data from more levels would have been desirable in many cases.

By combining the high-resolution aircraft data with the multi-scale ship data, it has been possible to establish the interconnection between the larger scale divergence fields, often determined by easterly waves, and the mass fluxes in the cloud cluster system themselves.

2.4 STRATEGY IN RETROSPECT

We said in the beginning that the "best judgement" is only possible in retrospect, that is, when the plans can be compared with the actual accomplishments. For the observational strategy this is easier done than for the scientific strategy. An example of the first type is the aircraft programme.

In Table 2.1 the apportionment of the available flights (322 sorties) to the various subprogrammes is shown: first, as it was originally planned; second, as the specific GATE Aircraft Plan visualized it; third, as it was actually flown. To come that close to the planned percentages required three things: careful strategy in the field, co-operation of nature and - luck.

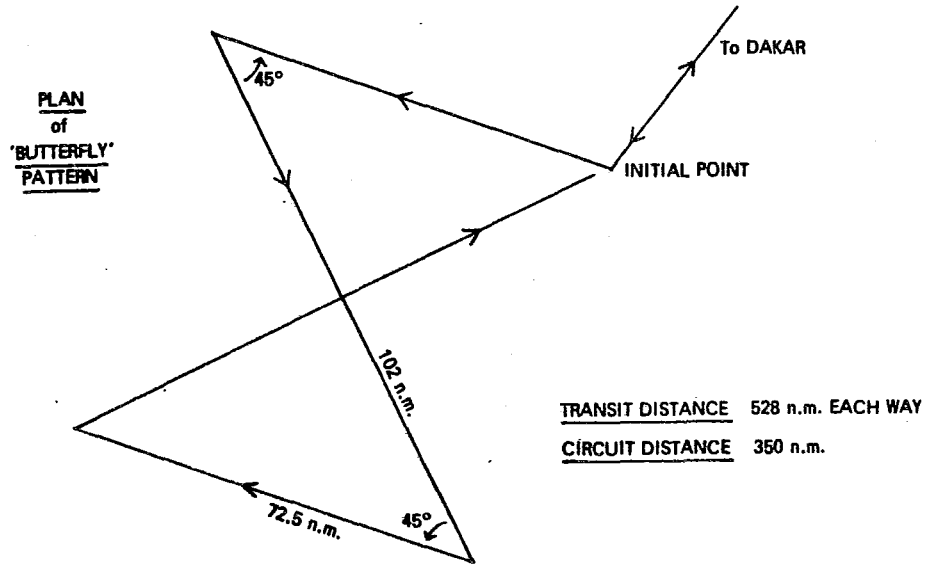

Figure 2.8 - The "butterfly" flight pattern for the exploration of cloud clusters was given up because of unexpected behaviour of nature.

Table 2.1: Apportionment of total flight missions planned for various scientific tasks as compared to actually flown missions

Type of mission	General Goal %	GATE Aircraft Plan %	Actually flown %
Basic GATE Missions plus convection flights	60	62	57
Special Boundary Layer missions	20	18	18
Special Radiation missions	15	18	21
Special Oceanographic missions	5	2	4

In regard to the scientific strategy the results available today indicate that it was successful in producing the needed data sets.

The B scale observations provided much improved information on the vertical distribution of heating, moisture and precipitation in the tropical belt enabling first tests of different parameterization schemes for tropical convection. We do not yet know if certain details of these schemes such as entrainment, mass flux, evaporation can be verified. Progress is already being made in mesoscale parameterization of convective systems but the verification and operational use of advanced cumulus parameterization schemes in large-scale prediction models is still outstanding.

The first systematic use of satellite data in a major field project provided excellent coverage by cloud vector winds, useful, for example, in the determination of the large-scale mean state (see Krishnamurti and Pasch, Chapter 3, this volume). In addition, it resulted in the first "Satellite-Derived Precipitation Atlas for GATE" (1980), including satellite-ship radar comparisons.

2.5 SOME LESSONS LEARNED

GATE's unique operational and scientific experience was useful to the planning of later large-scale field projects such as MONEX and ALPEX. It also provided several strategic lessons, of which only three shall be mentioned here:

(1) Advances in technology do not in themselves justify the introduction of new observing systems.

(2) The experiment design must be "frozen" sufficiently ahead of the experiment and should be altered only for exceptional reasons.

(3) Research should be started as early as possible and should not wait for "perfect" data. In other words, a comprehensive early "Quick-Look Data Set" is of overriding importance.

Finally, we should all remember that the human factor is more important than technology in international field research of such magnitude and complexity. If human relations between the scientists of many nations are as good as they were in GATE, success is almost assured. Without such relationship the best technology will be useless.

REFERENCES AND OTHER RELEVANT PUBLICATIONS

Düing, W., F. Ostapoff and J. Merle, 1980: "Physical Oceanography of the Tropical Atlantic during GATE" (Atlas), University of Miami.

Kuettner, J. P. and D. E. Parker, 1976: "GATE: Report on the Field Phase". Bull. Am. Meteorol. Soc. 57, 11-27.

"Satellite-Derived Precipitation Atlas for GATE", 1980: U.S. Dept. of Commerce, NOAA.

CHAPTER 3

LARGE-SCALE MEAN STATE

by

T. N. Krishnamurti and R. J. Pasch
(Department of Meteorology, Florida State University,
Tallahassee, Florida 32306, U.S.A.)

3.1 INTRODUCTION

The region of the GATE A-scale was monitored by some thirty research ships which provided four times daily upper-air soundings. In addition some ten research aircraft provided high resolution atmospheric measurements over the GATE A/B-scale during its three phases. About 1,500 marine surface observations were available during each 24-hour period over the 100 days of GATE. For the first time very high resolution cloud winds became available from a geosynchronous satellite SMS-1 over the Atlantic Ocean. This covered nearly 90 days of the 100-day experiment. GATE provided a unique experience in the collection of commercial aircraft data sets for the upper troposphere. Wide-bodied jets with multiple inertial navigation systems provided very high resolution winds. Some half a million wind reports were collected during the 100 days of GATE. A special effort by the Synoptic-Scale Subprogramme Data Centre at Bracknell provided a means to collect delayed data for the World Weather Watch. A polar orbiting satellite provided very high resolution measurements of the sea-surface temperature for the entire period of GATE. This collection surpassed all previous inventories of data sets over land areas, islands and oceans.

In many ways what was happening in the GATE data collection effort during the summer of 1974 was a precursor for the then forthcoming First GARP Global Experiment (FGGE). Many of the successful efforts of GATE were directly extended into FGGE.

These so-called GATE A-scale data sets were collected and archived at the World Data Centres (WDCs) for the domain which covered the region 20°S to 34°N and 100°W to 50°E.

Table 3.1 identifies a number of basic variables and derived fields that were analysed with these data sets for different periods extending from individual phases to the entire 100-day period. Tapes of the daily analysed fields have been made available to many scientists internationally. Relevant to this work are the time averaged fields. For this purpose a detailed tape of the 18 fields identified in Table 3.1 was prepared and is being sent to the World Data Centres. The large volume of data provided a unique opportunity for defining the mean state over West Africa and the tropical Atlantic Ocean. Waves, depressions and hurricanes occur in this complex basic state, which we shall show varies considerably in space and time from West Africa to the Caribbean and from 30°N to 20°S.

This review is divided into various sections that describe the mean motion field, the mean precipitation fields, the field of cloud cover, the sea-surface temperatures, the oceanic wind stress and the wind stress curl distributions and heat balance of the upper ocean. We believe that the selected topics are extremely relevant for our understanding of the mean state during the three phases of GATE which span from the middle of June through the last part of September 1974. A number of other fields, identified in Table 3.1 are not covered in this text. It is hoped that research workers desiring to study these areas would have access to the final mean state tape and would be able to carry out their research.

3.2 MEAN SURFACE WINDS

The low-cloud motion vectors describe the motion field near the cloud base level which is roughly at the height of 1 km above the sea level. Since a significant turning of wind with height occurs in the lowest km these winds cannot be used directly to describe the surface wind. However, the fact remains that this is a very powerful data base and deserves to be exploited somehow for the surface analysis. The data sources include:

(i) Marine ship data base;

(ii) Research ship data base;

(iii) World Weather Watch surface data base;

(iv) Low-cloud motion vectors from geostationary satellites.

During a 24-hour period the amount of data from these categories were of the order of 1,400, 180, 2,150 and 1,500 observations, respectively. The flow field was constructed on a daily basis for 100 days of GATE over 00Z ± 5.9 hours and 12Z ± 5.9 hours.

Table 3.1. Contents of GATE Mean State Tape

Field	Domain	Resolution	Phases	Period
1. Sea-surface temperature	GATE A-Scale oceans	1/2° lat./long.	I,II & III + 100 days	6/16-9/23
2. Surface winds	20°S-34°N 100°W-14°E	2° lat./long.	"	"
3. 850 mb winds	20°S-35°N 105°W-60°E	2.5° lat./long.	"	"
4. 700 mb winds	15°S-25°N 50°W-10°E	1° lat./long.	III	8/30-9/16
5. 300, 250, 200 mb winds	25°S-45°N around the globe	2.5° lat./long.	I,II & III + 100 days	6/16-9/23
6. Vertical motions 250, 300 mb	"	"	"	"
7. Temperatures 225, 275 mb	"	"	"	"
8. Geopotential height 300, 250, 200 mb	"	"	"	"
9. Surface wind stress	20°S-34°N 100°W-14°E	2° lat./long.	"	"
10. Surface wind stress curl	"	"	"	"
11. Surface air temperature	"	"	"	"
12. Surface relative humidity	"	"	"	"
13. Sensible heat flux over GATE oceans	"	"	"	"
14. Latent heat flux over GATE oceans	"	"	"	"
15. Net heat gain over GATE oceans	Over GATE ship array	"	I,II & III	During phases only
16. Mean temperature soundings	"	All ships	"	"
17. Mean humidity soundings	"	"	"	"
18. Mean profiles of radiative fluxes	"	"	"	"

The screening of the marine data base required computation of departure of winds from the standard deviation of a local region. About 1/6 of the marine data base was eventually used in the final analysis. The surface wind data from the GATE research ships were of very high quality and almost all of these data are used.

The collection of the surface data from the World Weather Watch was carried out, very efficiently, by the Synoptic-Scale Subprogramme Data Centre at Bracknell. Nearly 80% of the total data set was available for the surface analysis.

The geostationary satellite, SMS-1, provided a very unique data base over the Atlantic Ocean and was handled by Krishnamurti and Krishnamurti (1979) in the following manner for each map time of GATE:

(i) A first guess analysis of the motion field was performed at the surface level utilizing the data sets from the World Weather Watch and those from the GATE and the marine data base.

(ii) An independent analysis of the motion field was made with all available cloud winds. A knowledge of the level of best fit is not required for the proposed analysis method.

(iii) The A-scale domain was subdivided into nine subdomains. Within each domain the mean vector difference from (i) and (ii) above was estimated. This includes a mean turning angle as well as a mean speed difference at the two levels.

(iv) All of the individual cloud winds were next brought down to the surface level, prorating their speed by the wind difference between the two levels and turning each cloud wind by the appropriate mean turning angle of each domain.

(v) The surface level data set is now enhanced by the addition of these 'modified' cloud wind vectors. This level is now re-analysed. Steps (iii), (iv) and (v) are repeated several times to obtain a convergence of the surface analysis within an acceptable vector difference tolerance among successive scans.

This analysis showed that the turning of wind with height in the first km shows veering north of 10°N and backing south of 10°S. There is considerable variability in the vicinity of the intertropical convergence zone where the winds are very light.

Figure 3.1a, b and c shows the final analysis of the mean state of the surface. The salient features in the surface flows are the trade wind systems of the northern and southern hemisphere over the Atlantic and southern trades of the eastern Pacific Ocean. The col point around 25°W and 5°N is a very well known feature of the eastern Atlantic Ocean. It separates the West African monsoonal flows from the northerlies along the Morocco-Mauritania coasts. The major circulation centre over North Africa lies close to 20°N, well north of the rainfall belt over West Africa which is usually found near 7°N. This circulation centre describes a heat low. The flows described here are an average for the two analysis periods (00 and 12Z) and for the duration of each phase. The surface flows show a marked northward penetration over the region of the West African monsoon, a feature that is not so pronounced at the 850 mb level (see Figure 3.2a, b and c).

The intertropical convergence zone (defined here by the location of the asymptote of confluence) lies around 5°N over the Atlantic Ocean during Phase I and near 10°N during Phase II and somewhat north of 10°N during Phase III. Throughout the period of GATE, the intertropical convergence zone stays somewhat north of the axis of the warmest sea-surface temperature shown in Figure 3.4a, b and c. The maximum speeds of the trade wind system are close to 15 kts during the first two phases; the increase to roughly 20 kts during Phase III of GATE. A characteristic feature of the surface flows is the persistent pulses of strong northerly flows along the northwest African coast where speeds around 35 kts were frequently noted. This flow evidently is a response to the strong thermal differential along 20°N from relative cold waters with temperatures around 20°C and over land where surface temperatures during daytime frequently exceed 50°C.

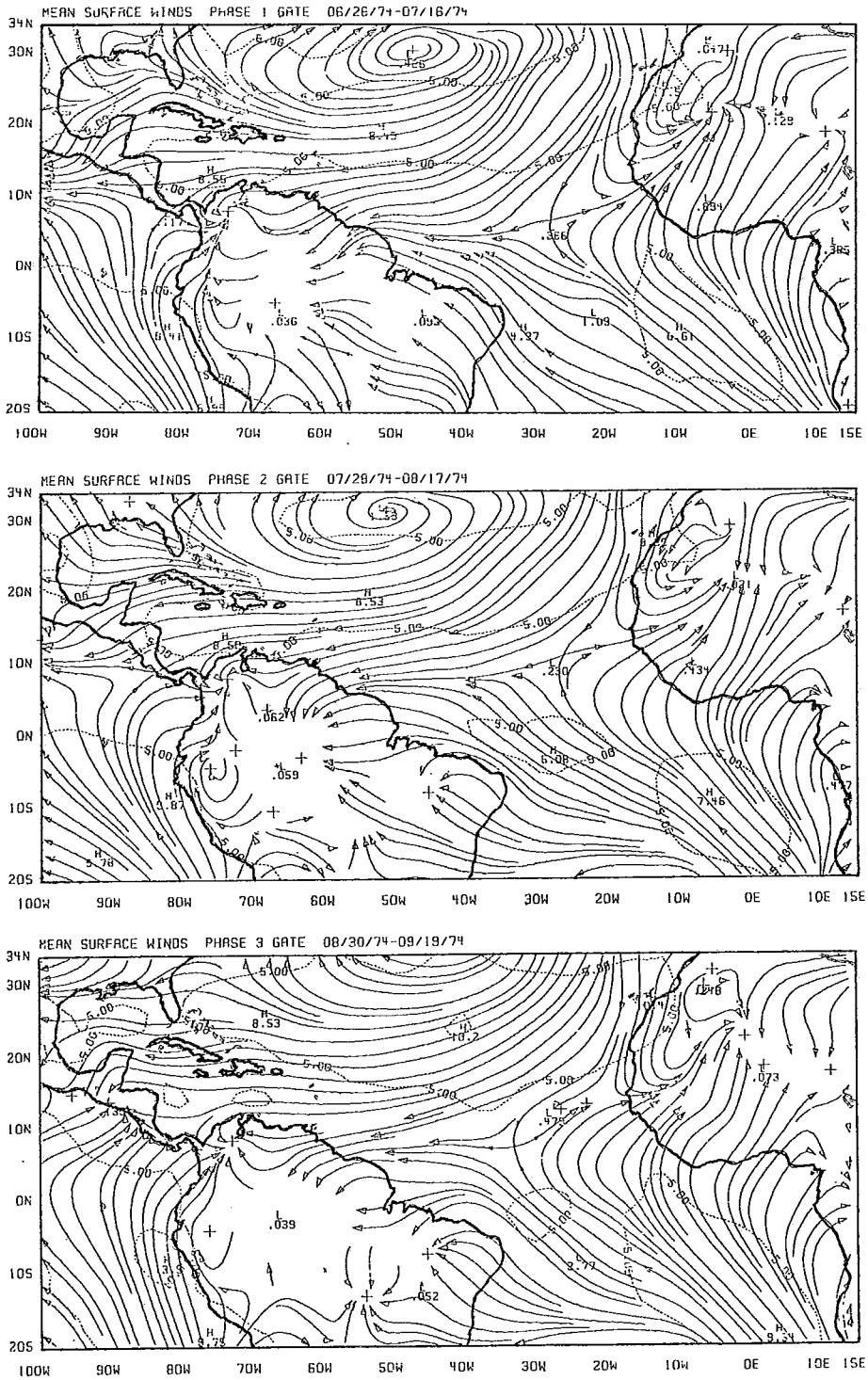

a

b

c

Figure 3.1 - Mean surface streamlines and isotachs (m s^{-1}) for (a) Phase I, (b) Phase II and (c) Phase III of GATE.

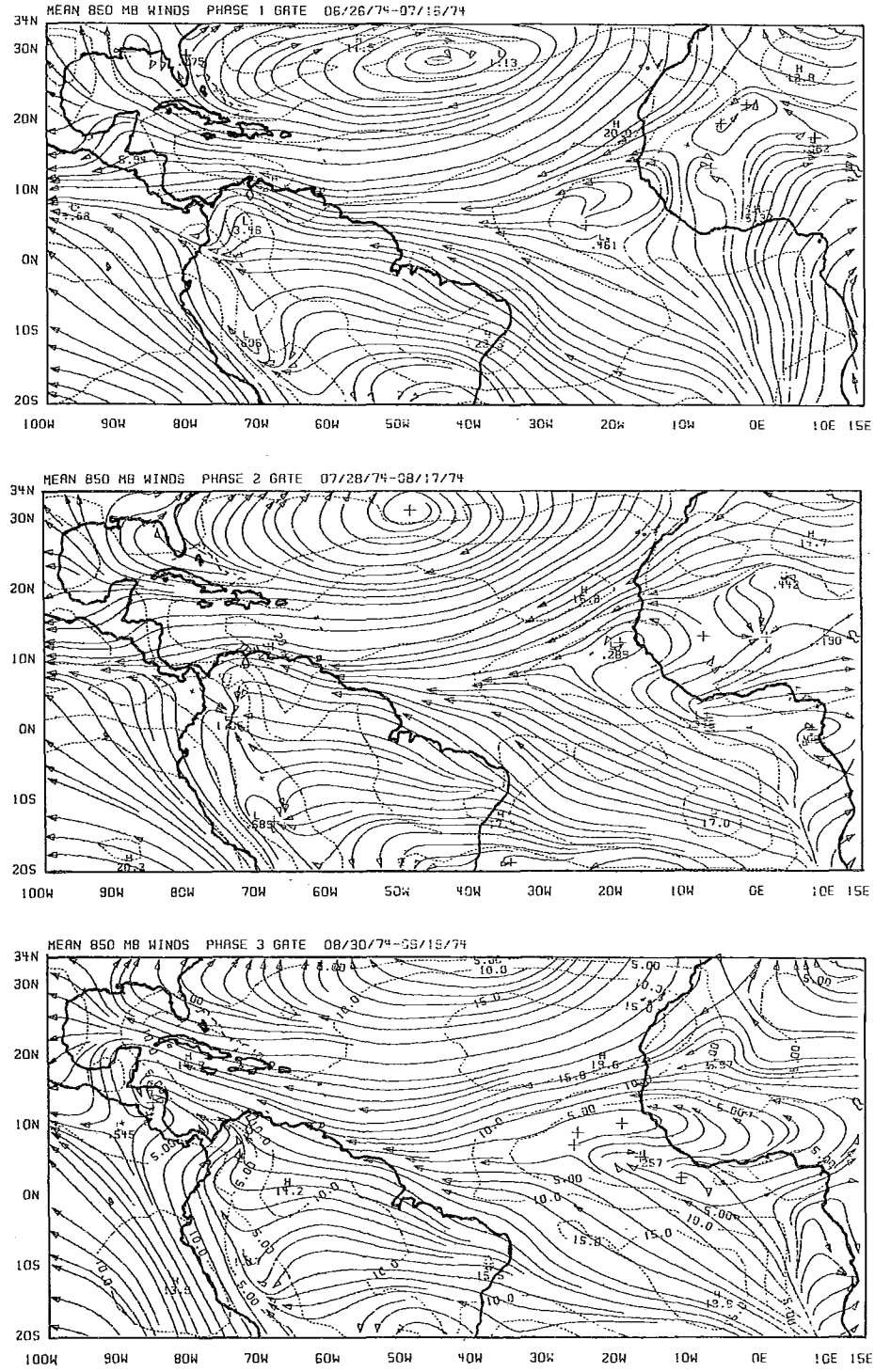

a

b

c

Figure 3.2 - Mean 850 mb streamlines and isotachs (knots) for (a) Phase I, (b) Phase II and (c) Phase III of GATE.

The subtropical high over the northern Atlantic Ocean exhibits a slow northward migration during the three phases. The southern trades exhibit more of a southerly component and the northern trades exhibit more of a northerly component at the surface level in comparison with the flows at 850 mb level. This (as stated earlier) is to be expected since the northern trades veer with height while the southern trades back with height.

The flows over the western Gulf of Mexico exhibit a diffluence during all the three phases. Overall, we believe that a definitive structure for the surface mean state has been obtained with some half a million surface wind observations during the 100 days of GATE. This is a very useful data set for the measurement of the mean wind stresses, the wind stress curl and many other dynamical fields. We do not believe that this data set has been fully exploited as of this stage.

3.3 THE MEAN STATE AT 850 MB

Figure 3.2a, b and c illustrates the three respective phase mean charts of the motion field. The tropical Atlantic is for the first time mapped with a large volume of diverse data sets. The analysis here is based on the data from the following platforms:

(i) Low cloud motion vectors from geostationary satellites. Roughly 1500 vectors per 24-hour period were available from the geostationary satellite. The level of best fit for the assignment of low cloud winds varies between 900 and 800 mb. The choice of 850 mb was suggested by Hubert (1975) although we believe now that the level of best fit is closer to the cloud base level, which is around 900 mb.

(ii) Low resolution flight level data from GATE research aircraft at the 1.5 km level.

(iii) 850 mb winds from the GATE research ships. These ships and their locations are identified partly in Chapter 2 of this Monograph (see also ICSU/WMO GATE Report No. 15, 1975).

(iv) The radiosonde network data at 850 mb over the domain.

(v) Some 400 pilot balloon data were available per day over the entire domain. Winds at the 1.5 km level were used in the present analysis.

The analysis procedure is a successive correction method originally proposed by Bergthorsson and Döös (1955) and Cressman (1959). It was modified by Tripoli and Krishnamurti (1975) and includes a manual correction cycle which provides a better spatial continuity between the data rich regions and the data void regions; the latter uses as a first guess a climatology which is somewhat modified by this process.

Salient features of the 850 mb mean state

The trade wind systems of the Southern Atlantic, Southern Pacific and the Northern Atlantic are the three main wind systems at this level. The intensity of the trade wind systems varies between 15 and 20 knots. Both the southern as well as the northern trades over the Atlantic are somewhat stronger during Phase III in comparison to the other two phases.

The easterly flow over North Africa is most organized during Phase III around 12°N. Here the easterly winds increase with height to about 4.5 km level. The monsoonal flows over West Africa have a southerly component over the ocean (the eastern Atlantic Ocean) during Phase I. In the subsequent phases the trades over the ocean acquire more of a southeasterly component and the monsoonal flow enters West Africa as a westerly current. The intertropical convergence zone at the 850 mb level appears as a trough region over the eastern Atlantic Ocean near 10°N.

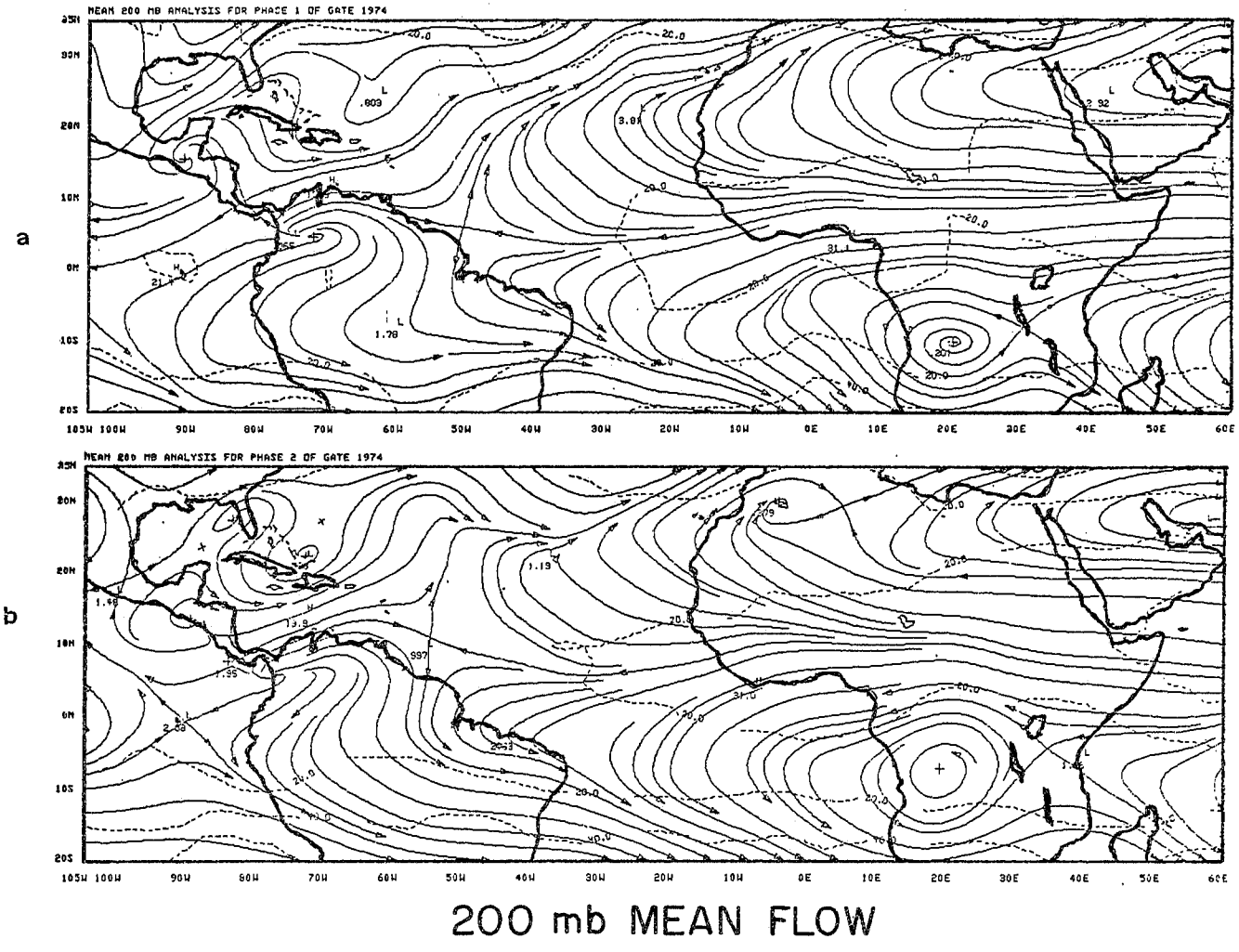

Figure 3.3 - Mean 200 mb streamlines and isotachs (knots) for (a) Phase I, (b) Phase II of GATE.

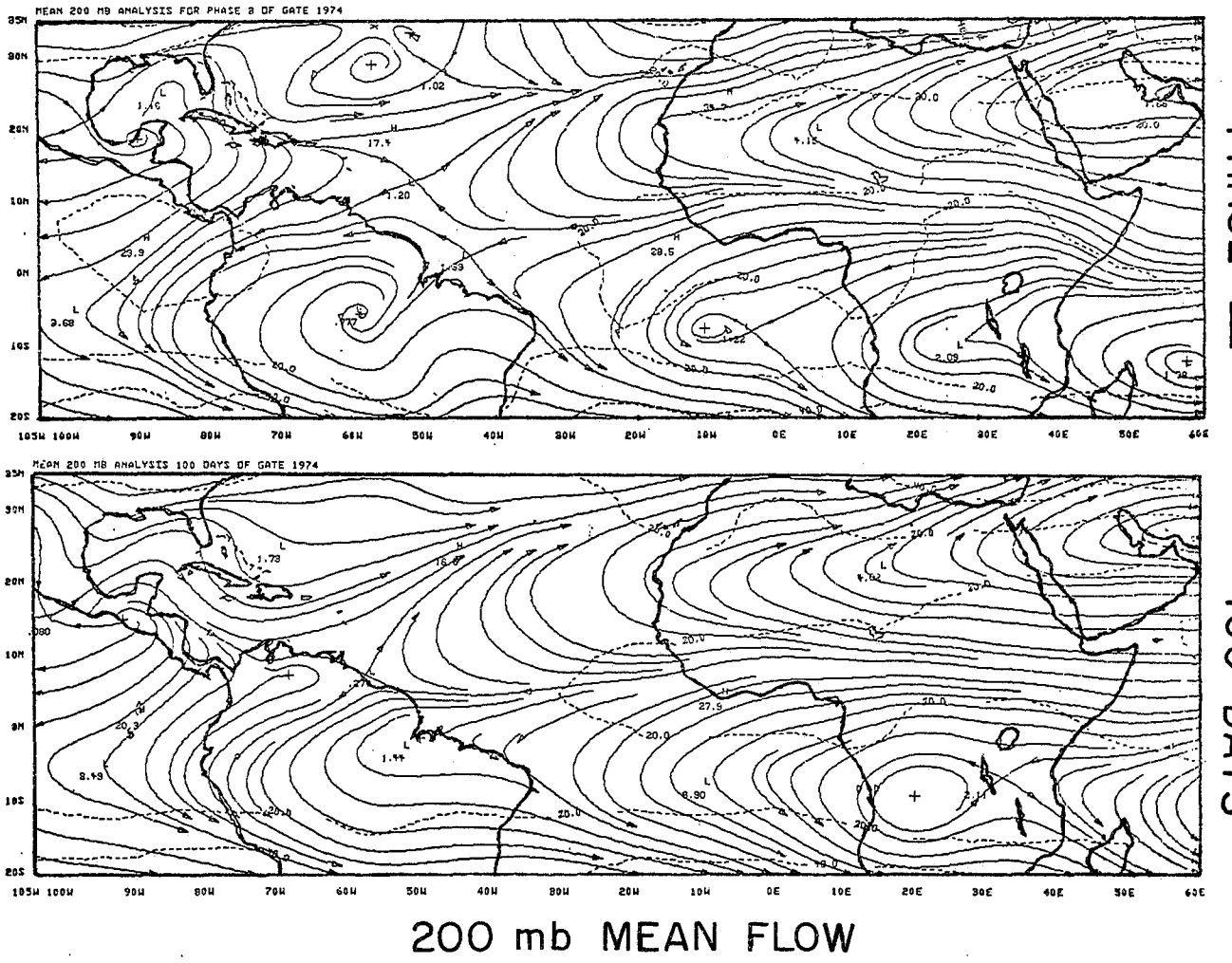

Figure 3.3 - As Figure 3.3(a) and (b) but for (c) Phase III, (d) the 100 days of GATE.

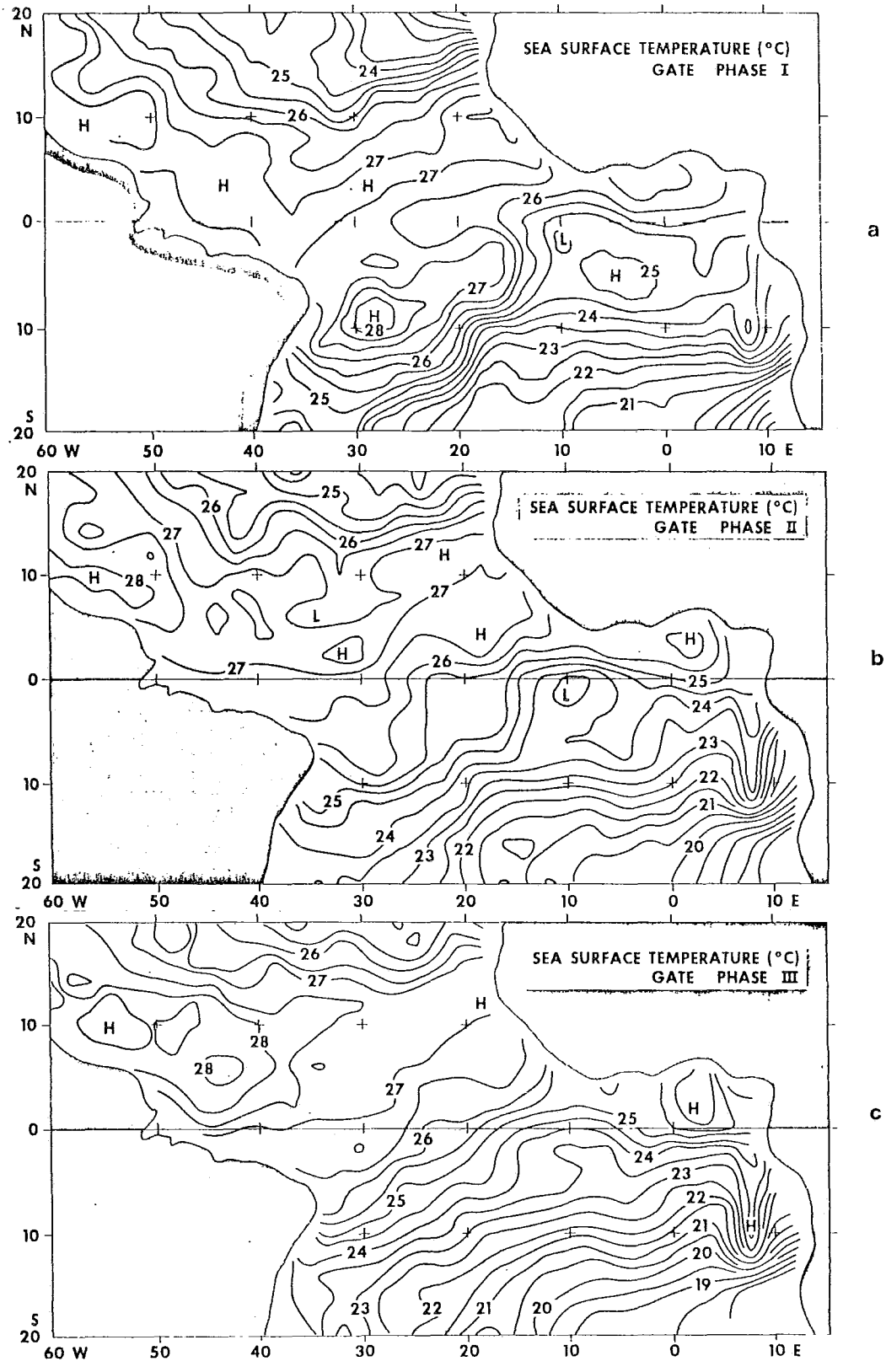

Figure 3.4 - Mean sea-surface temperature (°C) for (a) Phase I, (b) Phase II and (c) Phase III of GATE.

The dry belt over Northeastern Brazil is characterized by a diffluence of the southeast trades. One branch of this flow continues to the northwest while the other branch has more of an easterly component over South America. An interesting finding is a low-level jet around 10°S on the Brazilian coast which is most intense during early summer, i.e., Phase I. This feature reduces in intensity from around 24 knots to around 15 knots during the three phases.

Another interesting velocity maximum appears north of Venezuela (12°N, 68°W). This feature is most pronounced during the first two phases. This feature extends as a low-level velocity maximum into the Caribbean Sea and is an important feature for the development of storm systems over the Caribbean which could draw some of the energy from the horizontal shear flow of this current during July, August and September. The cyclonic shear side of this current occupies most of the Caribbean, especially in September.

African waves generally propagate westward from West Africa to the Caribbean, and are most active between 10° and 15°N. Calculations of the meridional gradient of absolute vorticity along several meridians show that the zonal velocity profile over West Africa and across the GATE B-scale region satisfies the necessary condition for the existence of barotropic instability. This is however not the case in the Western Atlantic Ocean west of 50°W. Thus, it appears that barotropic processes may be of primary importance over the eastern part of the GATE A-scale and only of secondary importance over the western part where the role of convection can be more important. Warm core disturbances such as hurricane Carmen and Fifi formed over the western Atlantic Ocean during GATE.

The most important and fundamental question is that of the maintenance of the mean state. For example, one might want to know how are the large-scale flow fields such as those shown in Figures 3.2a, b and c maintained. Unfortunately, this basic question was not addressed by any of the investigators at the stage of this review. This question requires an examination of the relative intensities of interaction among:

(i) the mean state and the mean state; and

(ii) the mean state and the transients.

Both such interactions can, in principle, contribute to the maintenance of the mean state. Here one could address the maintenance of any of the following parameters:

(i) Mean momentum;

(ii) Mean non-divergent part of the wind;

(iii) Mean kinetic energy;

(iv) Mean vorticity.

All parameters would be functions of horizontal co-ordinates, and even pressure. Although this is not fundamental to the objectives of GATE, we have always assumed that the trade wind systems are well understood on classical grounds. However, this is the first time that such complete and definitive descriptions of the mean state have become available, and it seems that these basic questions on the general circulation of the tropical atmosphere require re-examination and possible reconfirmation.

In a series of atlases, Sadler and Oda (1978, 1979, 1980) have presented the synoptic scale circulations during the three phases of GATE. The atlases describe the daily surface (850 mb over land) and 250 mb flow fields at 1200Z. The analysis covers the GATE A-scale.

3.4 THE MEAN STATE IN THE UPPER TROPOSPHERE

Here we shall confine our attention to 200 mb. For other levels, see Table 3.1. The tropical upper troposphere over the GATE A-scale includes the following features, shown in Figure 3.3a, b, c and d:

(i) Mid-Atlantic trough;

(ii) Tropical easterly jet;

(iii) North African ridge;

(iv) Cross-equatorial flows;

(v) Belt of westerlies about 20° latitude away from the equator.

Here an important contribution of GATE were the special data sets for the analysis of the motion field over the upper troposphere. Florida State University provided a major archive of the commercial aircraft data for GATE. In all over half a million wind reports were collected for GATE. This data base was further enhanced by the high cloud motion vectors from the geostationary satellite SMS-I. Finally, the final validated GATE data tapes provided by the Synoptic-Scale Subprogramme Data Centre at Bracknell provided a nearly complete set of radiosonde/rawinsonde observations. Three atlases of the GATE upper tropospheric motion field were prepared by Krishnamurti et al. (1978), Pasch et al. (1978) and Depradine et al. (1978). The atlases provide details on the daily analysis procedure, and an inventory of the data types. The mean states presented here are extracted from these atlases.

The monsoonal easterlies have a strength of around 60 kts at 200 mb. The easterlies penetrate gradually westwards reaching to about 40°W during Phase I, to about 50°W during Phase II and to about 75°W during Phase III. The Mid-Atlantic trough has a tilt from southwest to northeast and extends from 10°N-80°W to roughly 30°N-60°W in its mean position during the 100 days of GATE. If this trough extends to very low latitudes (i.e. south of 10°N), then upper westerlies prevail over the Caribbean and hurricanes usually do not develop over the Caribbean Sea. The trough did extend into the Caribbean Sea during Phases I and II and no hurricanes were noted during this period. The trough moved north of 15°N (Figure 3.3c) during Phase III and two hurricanes, Carmen and Fifi, developed in this region during late August and the middle of September.

A feature of the monsoonal easterly jet relevant to the GATE A/B-scale dynamics is the diffluence of the flow pattern over the eastern Atlantic Ocean. This feature was most pronounced during Phase III of GATE (Figure 3.3c). The northern branch of the diffluent flow curves anticyclonically northwards while the southern branch often describes a near-equatorial counterclockwise eddy motion. This feature was most pronounced during Phase III of GATE and several near-equatorial eddies formed whose signature can in fact be seen as a close circulation in the Phase III mean circulation.

Calculation of the meridional gradient of absolute vorticity can be made along selected longitudes to inquire whether or not the mean zonal profile satisfies the necessary condition for the existence of barotropic instability. The upper easterly jet over West Africa satisfies this condition. We believe that the diffluence and formation of eddies to the north and south of the jet axis is largely governed by barotropic dynamics. Since this region of upper diffluence lies over the ITCZ of the Eastern Atlantic, upper divergence above the ITCZ cloud clusters could account for the generation of the anticyclonically curved flows north of the upper jet axis. The relative importance of the horizontal shear and the cloud cluster dynamics need to be assessed.

A striking feature of the entire A-scale domain in the 100 day mean circulation is the dominant cross-equatorial flow (Figure 3.3d). Nearly at all longitudes of the A-scale domain the flow is directed from the summer to the winter hemisphere. During different years the active longitudes of cross-equatorial flows seem to shift somewhat. Krishnamurti and Kanamitsu (1980) noted that the data set for 1972 showed very weak cross-equatorial flows over the Atlantic Ocean when most of the strong meridional motions were confined to the Indian Ocean. During 1967 the meridional motions were strong over the eastern Atlantic Ocean (Krishnamurti, 1971). The pattern of cross-equatorial flows during 1974 over the Atlantic Ocean was quite similar to that during 1967. Krishnamurti (1971) noted a very pronounced tilt of the long waves of the tropical upper troposphere during northern summer. To a large extent this is contributed by the geometry of the African and Tibetan anticyclones and the mid-oceanic upper troughs over the Atlantic and Pacific Oceans.

During GATE this pronounced tilt was equally evident in Figure 3.3d. The anti-cyclonic circulation axis extends from the Venezuelan coast (5°N) to the Tibetan High (30°N). This feature on Figure 3.3d contributed to a transfer of westerly momentum away from the tropical easterlies. With reference to global energetics this feature contributes to an energy exchange from the long waves to the zonal easterlies (Krishnamurti, 1978, and Depradine, 1978).

In summary, the 100 day mean flows during GATE in the tropical upper troposphere are characterized by very pronounced tilt north of the equator and pronounced cross-equatorial and northerly flows between the equator and 10°S.

3.5 MEAN SEA-SURFACE TEMPERATURE

An axis of warmest sea-surface temperature migrates slowly northward as we go from Phase I to Phase III of GATE. During the early part of Phase I (June 20th) the sun has reached the Tropic of Cancer and started on its southward march while the axis of warmest sea-surface temperatures continues on the move northwards during middle August and early September as well. The axis of the warmest winter is very close to the equator during Phase I; it lies near 5°N during Phase II and near 10°N during Phase III. A number of important questions naturally arise as to what are the interrelationships among the mean thermal state of the ocean, the radiative fluxes in the atmosphere, heat balance of the ocean surface, the distribution of cloud cover, the location of the intertropical convergence zones and the fields of fluxes of latent and sensible heat at the ocean surface. One should also add the fields of surface wind stress and its curl, since they are relevant to the upwelling and sinking of surface water and their effects on the distribution of sea-surface temperature. An understanding of tropical convection is a central objective of GATE; it seems that in some distant way the answer to the questions raised here are also central to the same GATE objectives. These are among the many questions that have not been adequately addressed by the GATE scientists as of this stage. What is however accomplished is the presentation of this climatology. This is reviewed here with some remarks on plausible answers to the question of interrelationships among the variables listed above.

Figure 3.4a, b and c illustrates the mean sea-surface temperatures T_w for GATE during the individual phases. These were obtained from analyses of the daily fields. The observational platforms include some 30 GATE research ships, some 350 merchant ships, polar orbiting satellites and low resolution data sets from GATE research aircraft. The analysis procedure was based on the assumption that satellite derived sea-surface temperatures have larger absolute errors ($\sim 3^\circ C$) but smaller relative errors ($\sim 0.5^\circ C$). Thus, it is possible to exploit for instance the field of the Laplacian of the sea-surface temperature obtained from the satellites (a field that depends on relative accuracy and not on absolute temperature). The field of $\nabla^2 T_w$ is relaxed back to obtain T_w. In this process we use:

(i) Normal gradient boundary conditions across the irregular coast line.

(ii) A very fine mesh of the order of 50 km to define the field of $\nabla^2 T_w$.

(iii) The reliable research ship data of sea-surface temperatures are located to the nearest grid point. This can produce a mislocation which does not exceed 25 km.

(iv) A screening of merchant ship sea-surface temperature data is performed to remove any data for which the absolute value of the deviation from the mean for a 2.5° square exceeds 3 standard deviations. The remaining data are relocated to the nearest grid point of the 50 km square. This again has a maximum mislocation error less than 25 km. Some 300 ship observations per day are used in the GATE analysis.

(v) During the relaxation process the ship values are frozen and do not change at their assigned locations.

The final product satisfies the Laplacian of the satellite derived sea-surface temperatures where there are no other observations; it also satisfies the research and reliable merchant ship observations wherever they are available. A limitation of this method is that it does not provide any correction of the satellite derived product for clouds or excessive humidity. Recent studies show that the early NOAA-2 and NOAA-3 satellites did encounter some contamination in cloudy areas. To a large extent the use of some 300 ship observations per day alleviates this problem especially over the eastern Atlantic Ocean. The method proposed here is a very powerful scheme for incorporating observations from a mix of diverse observing systems.

Over the GATE A-scale the mean sea-surface temperatures vary from around 18°C to 30°C. In the far western part of the Atlantic GATE A-scale the sea-surface temperatures are quite warm throughout the three phases. The western Gulf of Mexico shows very warm temperatures approaching nearly 30°C in the mean. The eastern Atlantic Ocean shows a gradual warming north of 10°N. An axis of cold water extends from the Mediterranean to the central Atlantic Ocean. Several tropical wave disturbances exhibited a clear tendency of weakening during their passage across this region. Among these was a tropical depression, which eventually became hurricane Carmen. This storm showed considerable disorganization as it passed between 30°N to 45°W during the last week of August 1974. This disturbance regained its organized structure as it passed over warmer sea-surface temperatures over the western Atlantic Ocean.

The West African monsoons are thought of as being driven by a field of differential heating that extends from colder waters of the southeastern Atlantic Ocean and the warm continent over West Africa. The GATE observations provide a very definitive analysis of the sea-surface temperatures of the colder waters for studies of this problem.

No marked interphase variation in the sea-surface temperatures was noted over the region of the southeast trades of the eastern Pacific Ocean. The region just north of 10°N is important for our understanding of eastern Pacific tropical storms; here the sea-surface temperatures exceed 27°C during all the phases. The number of such storms in a hurricane season is known to exceed 20. The role of warm sea-surface temperature is evidently quite important here.

Our analysis does not have adequate resolution to depict the coastal cold upwelling regions since the smallest resolvable scale ($2\Delta X$) is of the order of 100 km, although there is some indication of cold tongues of water along the coast of eastern oceans. For further details see Krishnamurti et al. (1976).

Griffith et al. (1980) have provided an intercomparison of the analysed sea-surface temperatures with the GATE rainfall rates. Their study includes an independent assessment of the quality of the A-scale sea-surface temperatures presented here.

3.6 THE MEAN CLOUD COVER

Murakami (1979) carried out an extensive analysis of the digital infrared data sets from the geostationary satellite SMS-1. His analysis covered the period 27 June to 20 September 1974. This includes all three phases of GATE. The raw data have a resolution of 4 n mi by 4 n mi. These data were averaged over 60 n mi^2 and subdivided into 16 counts of IR brightness (0-15). On this scale 0 corresponds to about +50°C in blackbody temperature, while 15 corresponds to very cold temperatures, i.e., -100°C. One count roughly measures an interval of 8°C.

Figure 3.5a, b and c shows the phase mean distribution of IR brightness during the three phases of GATE. In these charts a well-defined axis of maximum cloud cover extends across the Atlantic Ocean; the largest values are found over West Africa. The implied cloud top temperature is around -36°C which corresponds to a cloud top of around 12.5 km. The cloud cover falls off sharply away from this axis in the trade wind belts of the two hemispheres. This axis has a very distinct planetary scale orientation, being near 5°N over the western Atlantic and around 7°N over West Africa. The slow monotonic increase of latitude from west to east appears to describe a quarter wave (about 45° longitude) of a planetary scale wave. This is strongly suggestive of the organization of cloud cover on zonal wavenumbers 1 and 2.

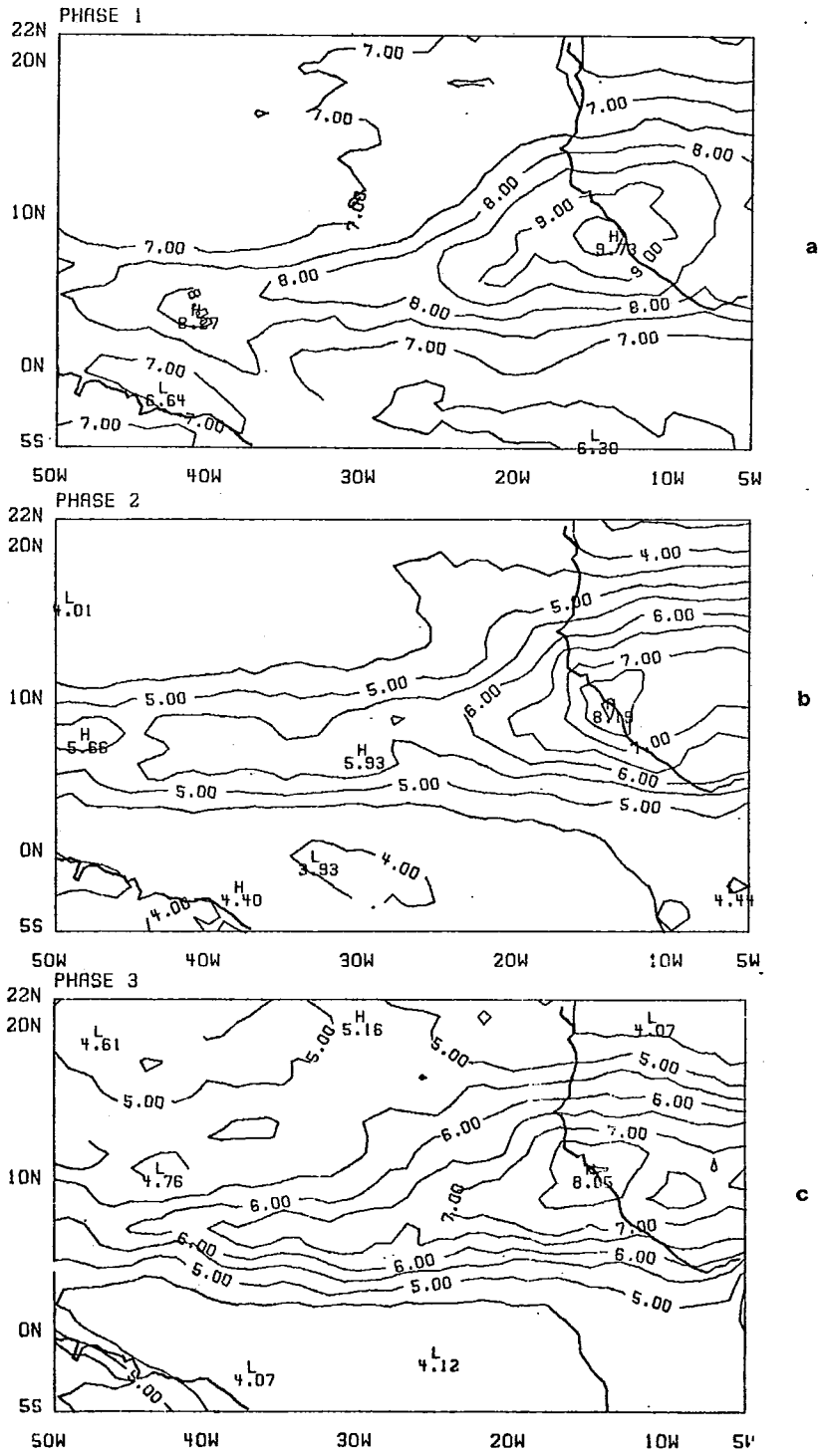

Figure 3.5 - Mean IR brightness count for (a) Phase I, (b) Phase II and (c) Phase III of GATE.

Krishnamurti (1978) has examined the tropical energetics and noted that the generation of eddy kinetic energy occurs primarily on the planetary scale in spite of the fact that there are many cloud clusters with ascending and descending motion on much smaller scale. The conclusion was then drawn that there was in fact an organization of the cloud clusters on the planetary scale which transfers this energy directly to the planetary scale. The orientation of the cloud cover during GATE shown in Figure 3.5a, b and c clearly shows the planetary scale organization. The central objective of GATE seeks answers to the control of convection by the larger scale motion field and vice versa. Here one always felt that the mutual interaction of the cumulus (10 km) scale - the meso (100 km) scale and the synoptic (1,000 km) scale was the central problem. With most of the zonal variance of the cloud cover being on the long planetary scales, the scope of the scale interaction covers a much larger spectrum of scales than was conceived in the earlier planning of the GATE central objectives.

The aforementioned GATE data sets were also stratified by Murakami (1979) into four diurnal categories. Figure 3.6a, b, c and d illustrates the composite anomalies of the cloud cover at 00, 06, 12 and 1800 GMT. The local time is indicated below each panel. The main results of the diurnal change are that both afternoon as well as early morning maxima occur over the tropical Atlantic Ocean. An afternoon maximum occurs roughly along 10^{o}N; it extends from West Africa to the middle Atlantic Ocean. An early morning maximum occurs to the south of it along roughly 5^{o}N. The general rule seems to be that where the 24 hour average cloudiness is largest the afternoon maximum is dominant and the early morning maximum tends to occur in the equatorward side of the 24 hour maximum cloud cover. Murakami attributed this feature to a daily meridional shift of the diurnal oscillation. This problem may be related to a radiative-convective interaction which deserves further exploration.

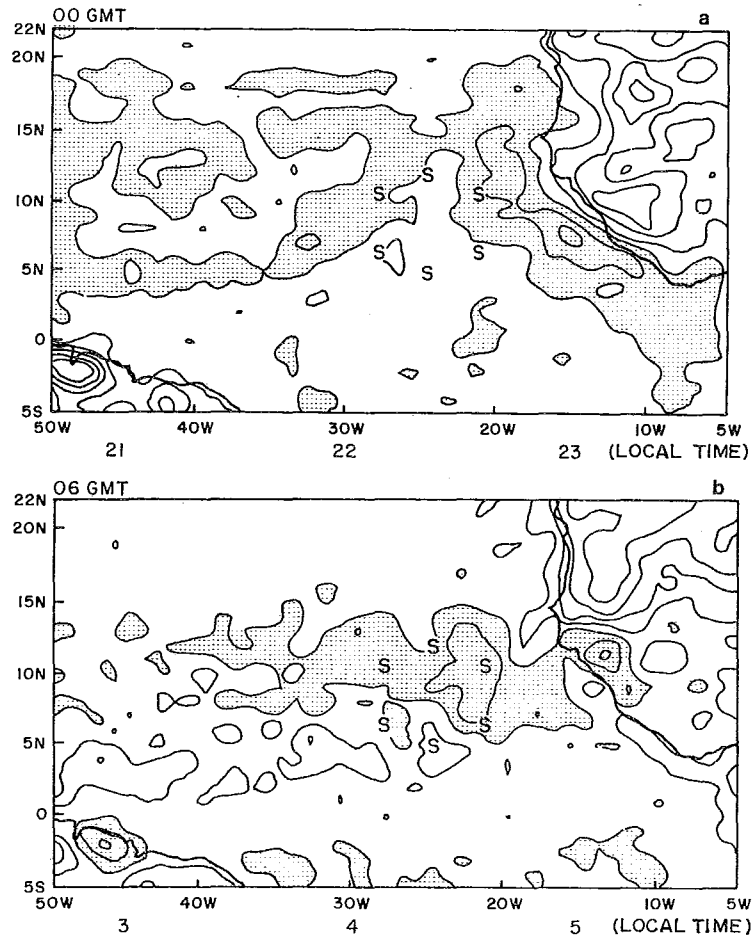

Figure 3.6 - Field of composite diurnal anomalies of IR brightness counts (a) 0000 GMT, (b) 0600 GMT (see Murakami, 1979 for details). Contour interval is 0.2 units. Negative anomalies are shaded. Local time is shown on the abscissa.

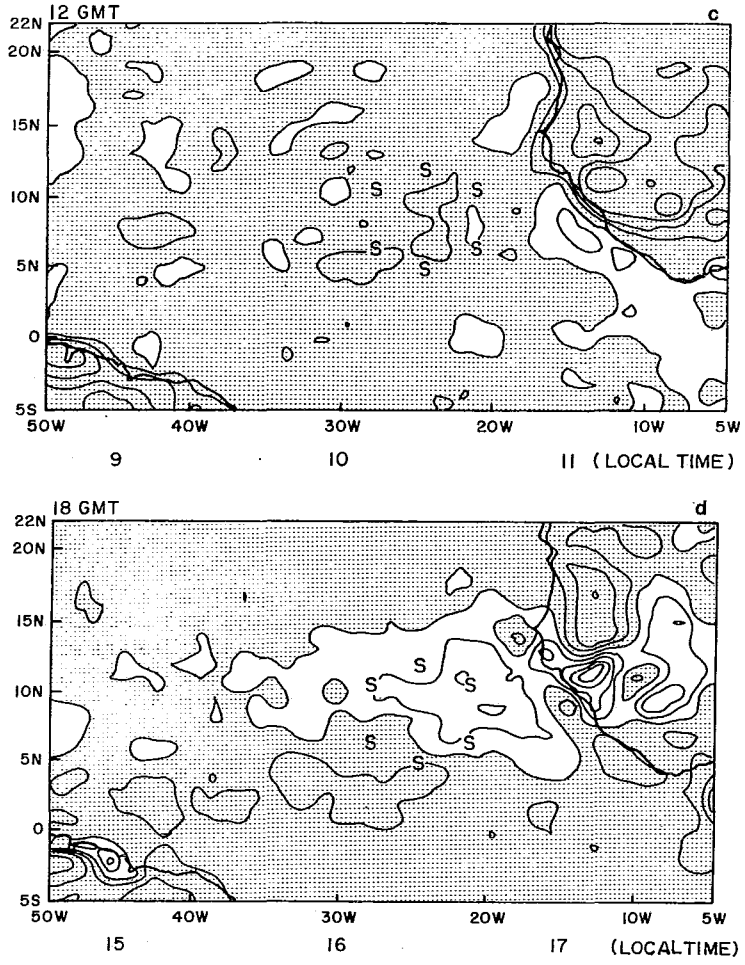

Figure 3.6 - As Figure 3.6 (a) and (b) but (c) 1200 GMT, (d) 1800 GMT.

3.7 THE MEAN RAINFALL RATES

Aside from raingauge measurements, shipboard radar as well as satellite infrared digital data sets provided indirect means for the determination of GATE rainfall rates (Griffith et al., 1980). This mix of observing systems was exploited to provide a three way intercalibration among raingauge, radar and satellite measurements, the intercalibration procedure consisting of the application of an empirical relationship between rainfall rate and cloud size, cloud top temperature, and cloud life cycle. The procedure for the determination of satellite cloud parameters is discussed in some detail by Griffith et al. (1980). This method unfortunately has large errors - the satellite estimates of rainfall rates differ from those obtained from radar by as much as 40 to 60%. The radar estimates were provided by Hudlow and Patterson (1979) and are highly reliable measures. At present the only available products on the entire GATE A-scale is the satellite derived product and we shall review the phase mean rainfall distributions from this source. Figure 3.7a, b and c from Griffith et al. (1980) illustrates the rainfall totals in mm for each of the phases of GATE. Over the region of maximum IR brightness over West Africa rainfall totals are around 400 mm during each phase. The ITCZ over the eastern Atlantic experienced a rainfall total of around 200 mm during each phase. Rainfall amounts were higher during Phase III.

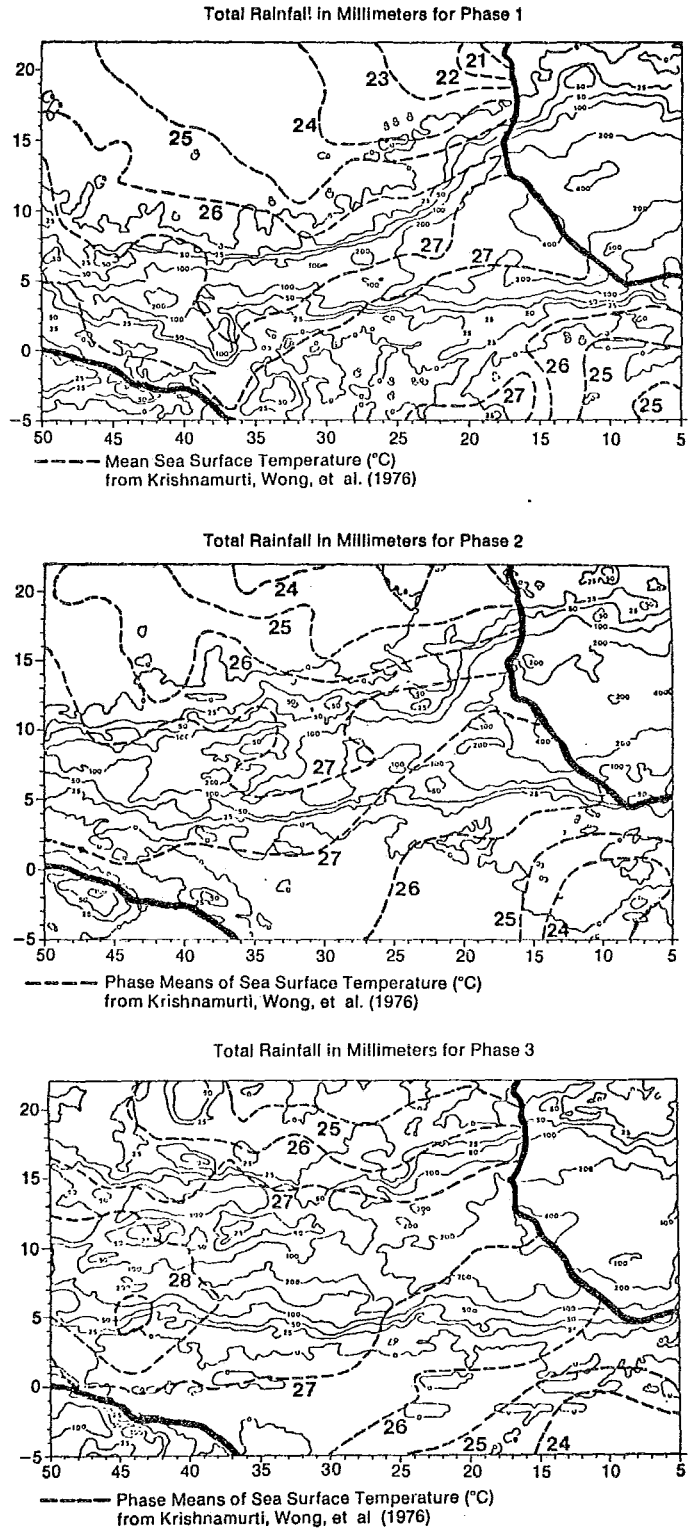

Figure 3.7 - Total rainfall (mm) for (a) Phase I, (b) Phase II, and (c) Phase III of GATE.

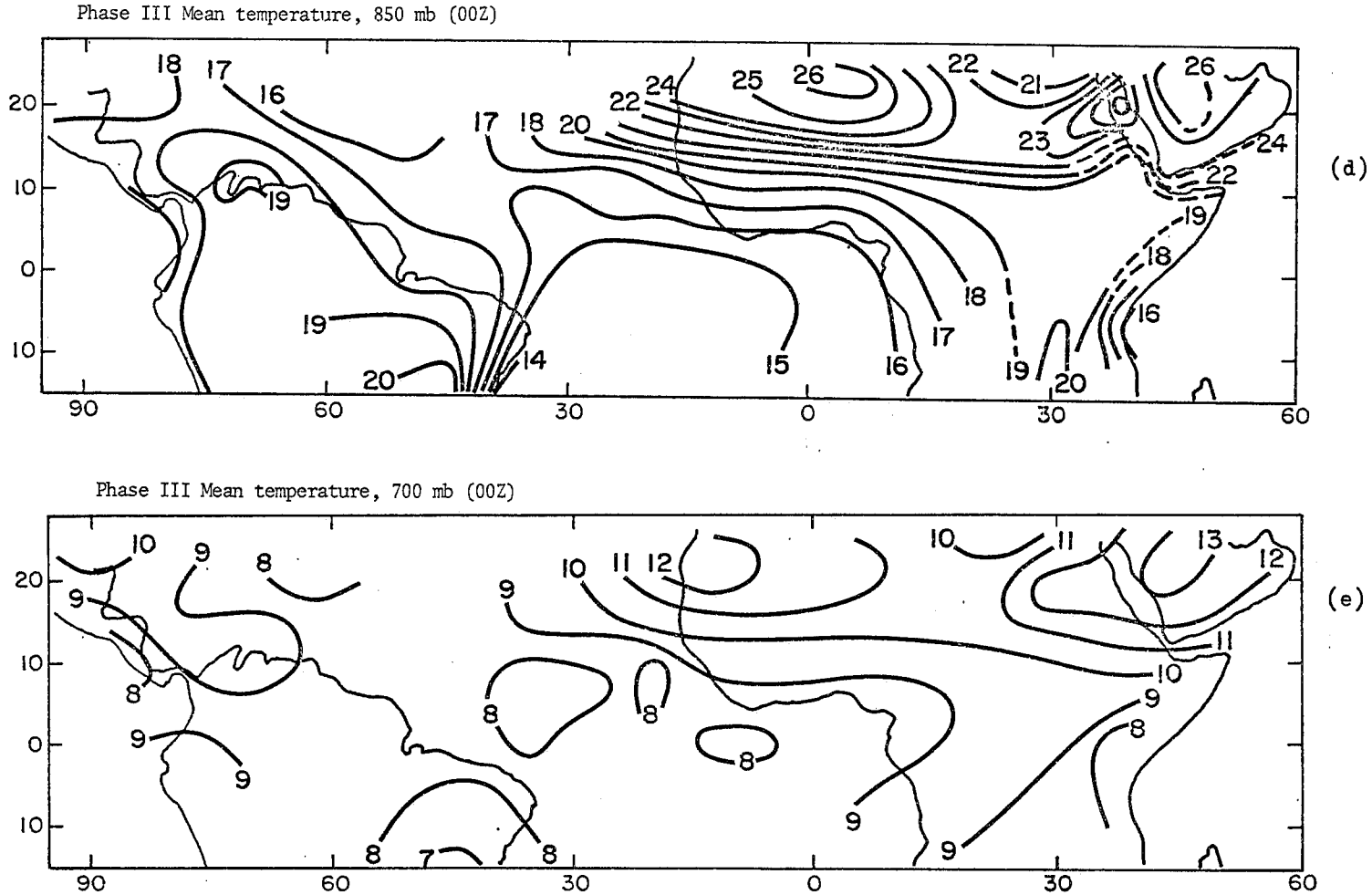

Figure 3.7 (contd.) - GATE Phase III mean temperatures (°C) for 0000 GMT (Reynolds, 1977). (d) 850 mb, (e) 700 mb.

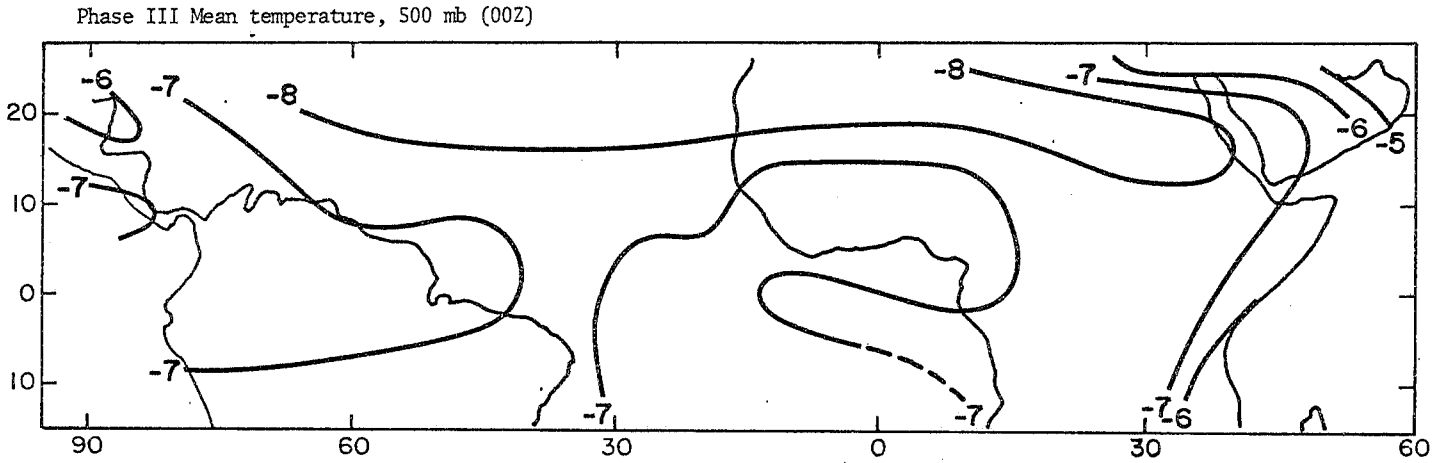

(f)

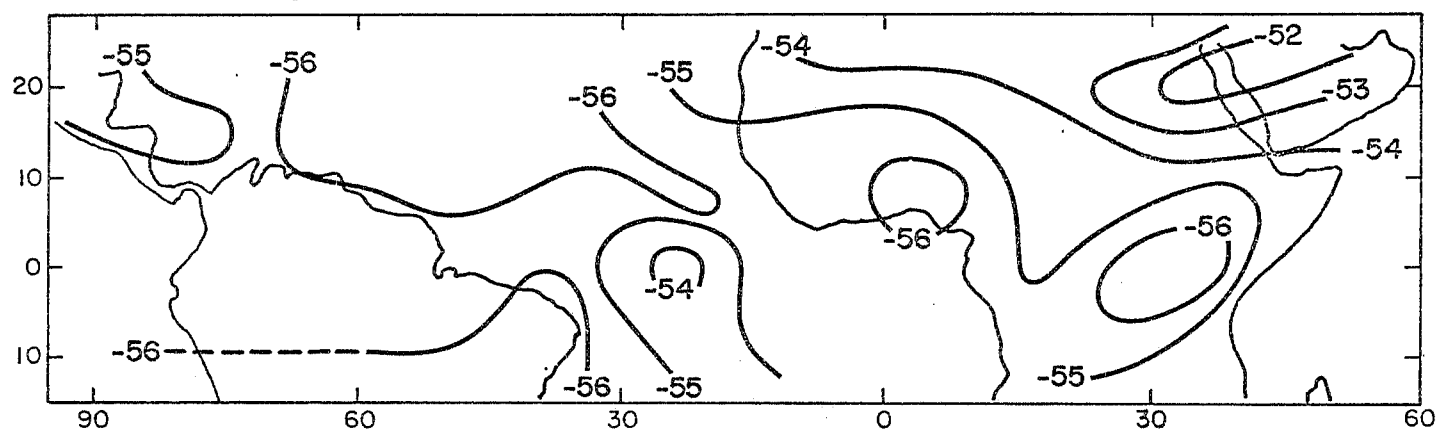

(g)

Figure 3.7 (contd.) - As Figure 3.7 (d) and (e) but for (f) 500 mb, (g) 200 mb.

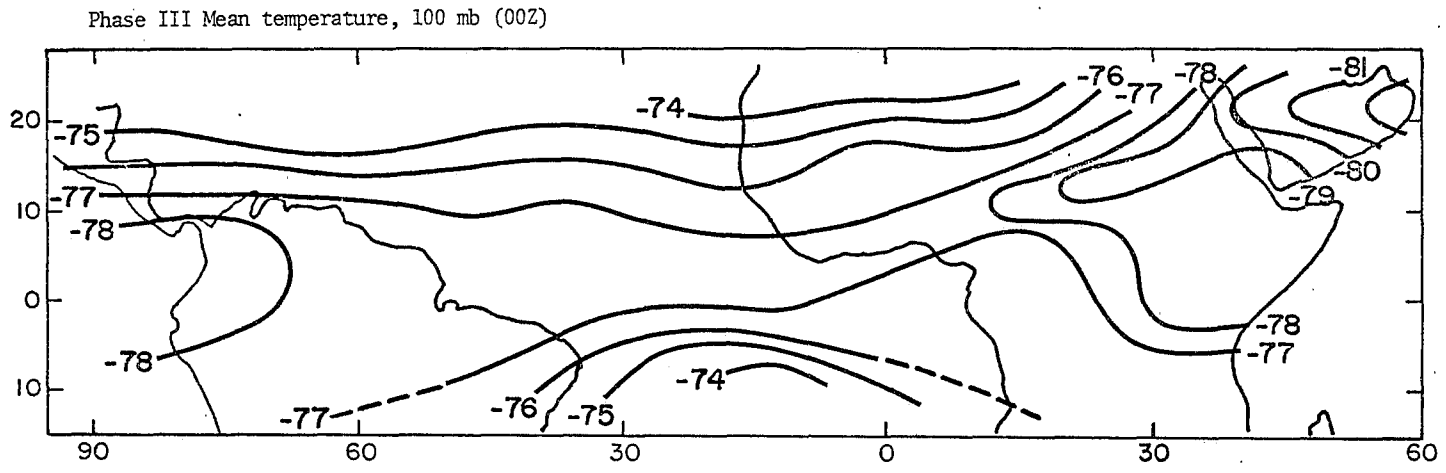

(h)

Figure 3.7 (contd.) - As Figure 3.7 (d) and (e) but for 100 mb.

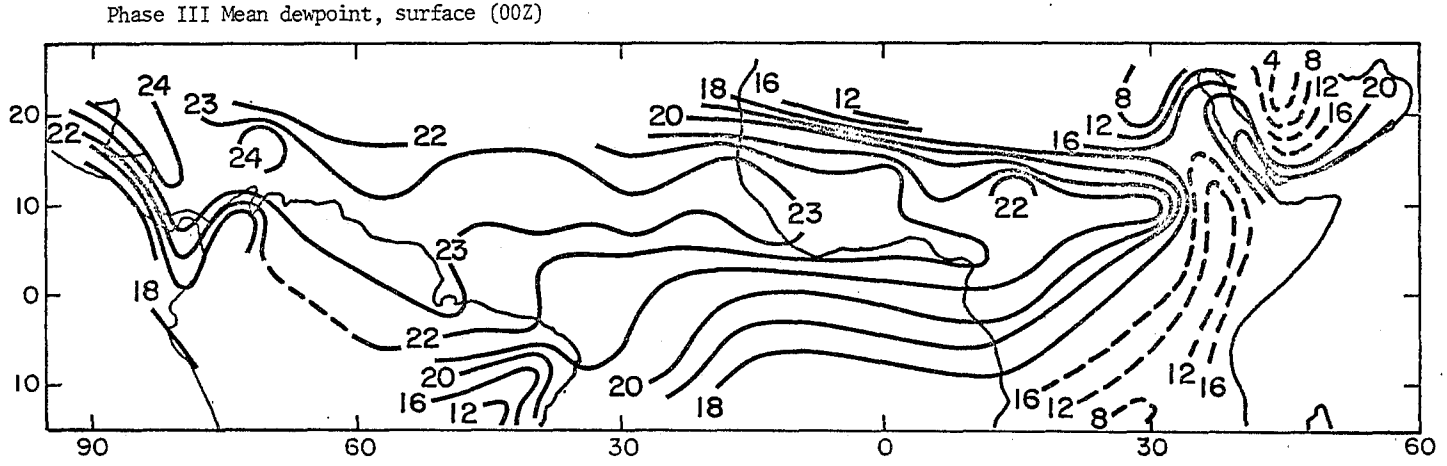

(i)

Figure 3.7 (contd.) - (i) GATE Phase III mean dew point (°C) for 0000 GMT (Reynolds, 1977), surface.

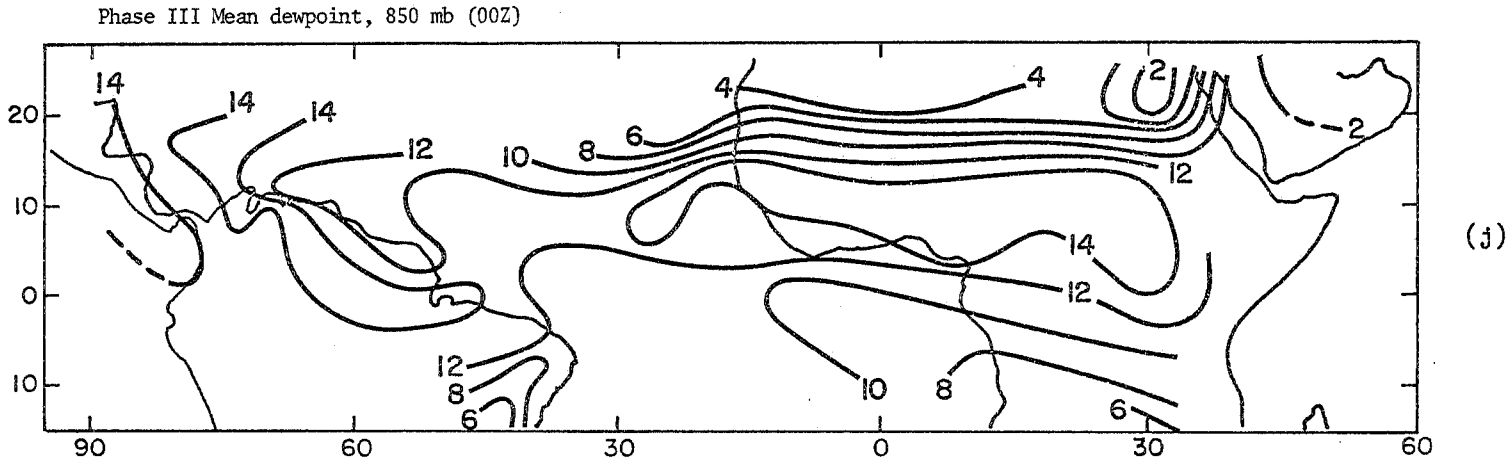

(j)

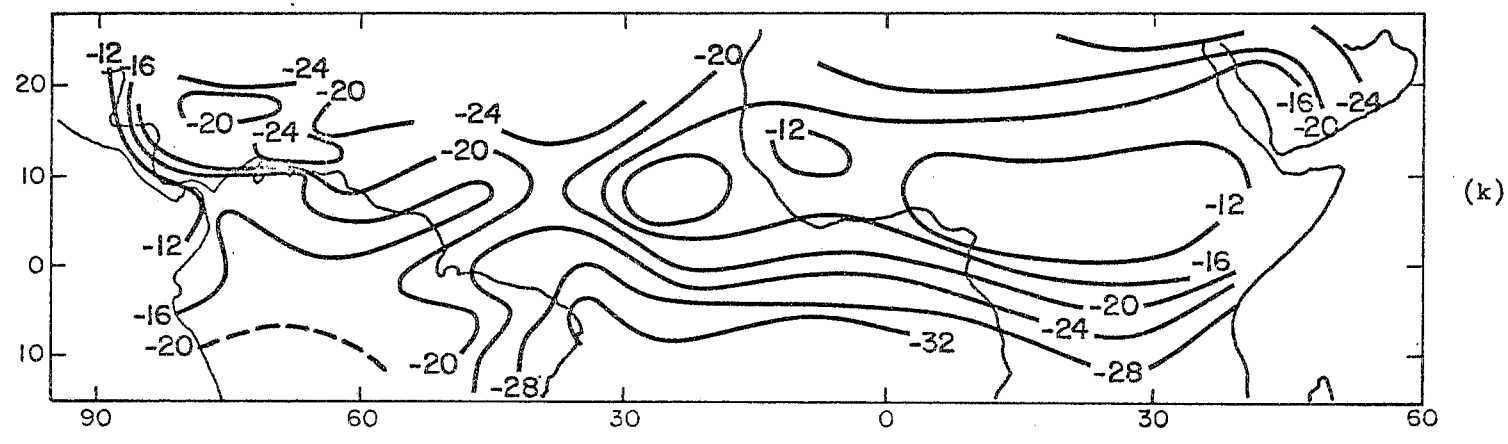

(k)

Figure 3.7 (contd.) - As Figure 3.7 (i) but for (j) 850 mb, (k) 500 mb.

The last phase was characterized by a steady stream of westward propagating African waves. The frequency of these disturbances was roughly one every 4 to 6 days (Thompson et al., 1979). The wave passage was accompanied by rain which usually occurred just prior to and during the trough passage. Some of the precipitation was associated with squall systems which are known to augment the wave precipitation. Clearly what was surprising was that substantial rainfall amounts (~200 mm) also occurred during Phase I when the intensity of African waves was much weaker. A closer look at the rainfall amounts on a smaller scale (the A/B scale array) shows that there were some major differences over local regions between the first and the third phase (Griffith et al., 1980).

The dashed isopleths in Figure 3.7a, b and c show the phase mean sea surface temperatures (Krishnamurti et al., 1976). In general we note that most of the significant phase mean rainfall occurred over oceanic regions warmer than 26.5°C. Thus, it is of considerable interest to examine the radiative heat balance of the ocean surface. Although our analysis reveals a single axis of mean surface streamline convergence along the axis of the warmest sea-surface temperature, Chuchkalov (private communication) points to the need for a double line of low-level convergence lying in close proximity. The northern one of these is associated with the northern trades and the southern with the southern trades. Chuchkalov points as evidence for their presence to the behaviour of diurnal cycle of the cloud cover we have alluded to. He, furthermore, notes that the diurnal variation of precipitation data, composited from Soviet ship observations, also confirms the need to identify a double convergence zone.

3.8 PHASE MEAN TEMPERATURE, HUMIDITY, PRESSURE AND GEOPOTENTIAL FIELDS

Only a few examples will be presented here. Figures 3.7d, e, f, g and h taken from Reynolds (1977) illustrate the temperature field during Phase III at the 850, 700, 500, 200 and 100 mb. The 850 mb field illustrates the well marked baroclinic zone south of the desert regions over Africa. A marked thermal differential between the oceans to the west and the land mass of North Africa is an important feature at this level.

A baroclinic zone is again evident over North Africa at 500 mb. This is related to the westerly regime of the upper troposphere over the Mediterranean. The 850 mb baroclinic zone in fact tilts equatorward and disappears below 600 mb and does not appear to have any continuity with the field at 500 mb. Temperatures at 200 mb are cold over the Atlantic Ocean. They are relatively warm over the eastern end of the A-scale region. A marked east-west thermal differential is evident even at 200 mb. The 850 mb baroclinic zone and that at 500 mb may be continuous in reality; the lack of it may be related to sparsity of data.

The humidity fields (the dew point temperatures) at surface, 850 and 500 mb (Reynolds, 1977) are illustrated in Figure 3.7i, j and k. The most striking feature is the sharp humidity gradient over North Africa that, in fact, extends over the Atlantic Ocean. Here the dry desert air with a dew point of 2°C is separated from the humid West African monsoon air with a dew point of 14°C. The humidity field at the 500 mb exhibits somewhat weaker meridional contrasts; the moist and dry regions are nearly vertically stacked between 850 and 500 mb. These maps are relatively easy to construct since the final validated mean data sets are available on tapes.

A significant three part GATE atlas (Chuchkalov, 1977) presents daily (beginning from 1 July) charts of weather and geopotential from the sea level up to 100 mb level for both 00 and 12Z for, practically, the entire A-scale area. This atlas also includes mean maps for several years over the region of the GATE A-scale and is a very useful reference. We recommend the source to those who are interested in tropical geopotential height distribution.

3.9 TIME AVERAGES OF THE WIND STRESS AND THE CURL OF THE WIND STRESS

During GATE, the buoy observations from the ship 'METEOR' were used to estimate momentum fluxes by the eddy correlation method (Dittmer et al., 1978). From a comparison of their results with those obtained using the Bulk Aerodynamic Method, Businger and Seguin (1977) recommended that the drag coefficient C_D for undisturbed as well as disturbed conditions lies in the range $1.4 \pm 0.4 \times 10^{-3}$. We feel that for large-scale flows (i.e., on the GATE A-scale) this is certainly an

appropriate choice. However, noting the fact that there were several hurricanes during the 100 days within the GATE A-scale domain, we feel that a variation of drag coefficient with wind speed is appropriate for the mapping of the stress charts. Angular momentum budget studies in tropical disturbances clearly show that the drag coefficient does vary with the radial distance from the centre of the hurricane as well as with respect to the wind speed in a hurricane (Miller, 1962; Ooyama, 1969). During GATE on the A-scale, our tabulation on the 2° latitude/2° longitude mesh size does not resolve the fine structure of the high speed region (the inner rain area) of a hurricane. However, we note occasional wind speeds as large at 45 knots during such events. Thus, following Roll (1965) and Miller (1962), we estimate the stresses for wind speeds ≤ 10 mps by using the formula

$$\tau_{\substack{x \\ y}} = C_D \rho_v^u \sqrt{u^2 + v^2}; \qquad C_D = 1.4 \times 10^{-3}.$$

Wind speeds >10 mps are estimated by using

$$C_D = 0.7 + 0.07|V| \times 10^{-3}.$$

This is consistent with the value of 1.4×10^{-3}, for a wind speed of 10 mps suggested by Businger and Seguin (1977). It also gives reliable estimates at high wind speeds. The choice of a constant drag coefficient for speeds less than 10 mps is also suggested by the results from 'BOMEX' observations.

Holopainen (1967), Hantel (1970) and Düing (1968) have examined the distribution of the curl of the wind stress (CWS) over wide areas from long-term time-dependent motion fields. Hantel and Düing examined the Indian Ocean region in considerable detail and noted large zonal gradients of the wind stress curl in the southwesterly monsoonal current. Hantel's charts clearly bring out a relationship between the wind stress curl and the observed regions of cold upwelling in the western Arabian Sea. They also noted that the surface winds in the Indian Ocean were quite large, and as a consequence, stresses of the order of 1 dyne/cm^2 and curl of wind stress of the order of 2.5×10^{-8} dynes/cm^3 were noted in their calculation. Hantel used a drag coefficient of 1.2×10^{-3} which is closer to the value we have used in the present study for the GATE A-scale region.

We examined the GATE phase mean and 100 day mean distribution of the wind stress curl defined by the relation

$$C_{WS} = \frac{\partial \tau_y}{\partial x} - \frac{\partial \tau_x}{\partial y} .$$

The fields were computed by straightforward centred differences over a distance of ΔX and ΔY on the order of 200 km.

The resolution of the data (two maps per day) limits the scope of this study. It should be noted that the smallest resolvable wave in the present context is $\sim$400 km in space and two days in time. Furthermore, since only oceanic and near coastal data are used for the analysis of the wind stress curl over the oceanic domain of the GATE A-scale, the near coastal analyses within a few hundred km are not too reliable. This limits the usefulness of the presented data sets for studies of coastal problems.

The field of the total stress for the three phases is illustrated in Figure 3.8a, b and c. The total stress is larger in the northeast trades in comparison to the southeast trades. The maximum value exceeds 2 dynes/cm^2. The mean value of the total stress for the 100 days over the GATE A/B-scale is around 0.3 dynes/cm^2. This is slightly smaller than the magnitudes of 0.4 dynes/cm^2 reported by Jacobs (1978). The regions along the Peruvian coast, along the western Gulf of Mexico, around 10°N and 100°W and around 20°S and 5°E are other regions with large stresses. It is of interest to compare the magnitudes of the stresses estimated here with the earlier estimates given by Hellerman (1967).

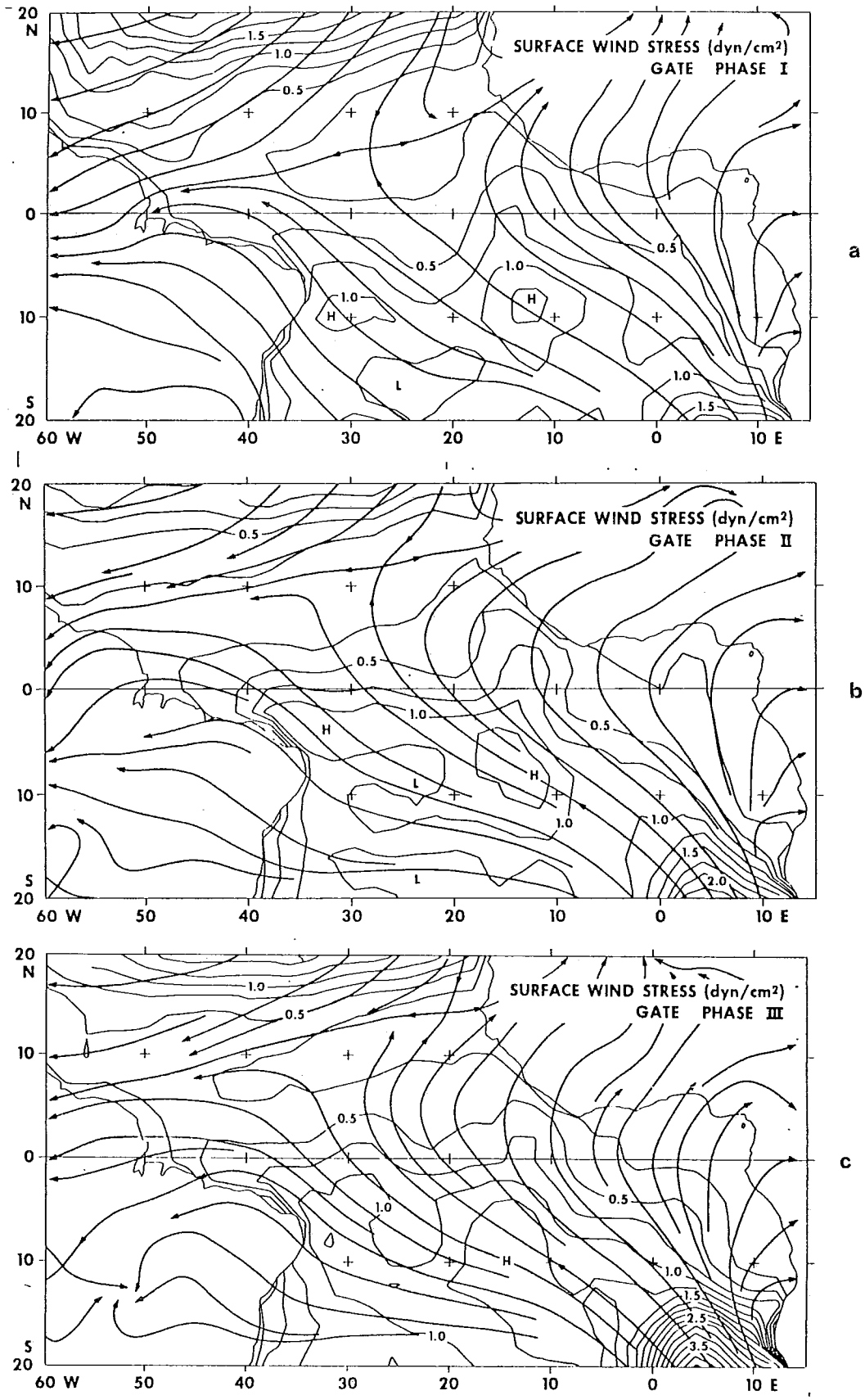

Figure 3.8 - Mean fields of total surface wind stress ($dyn \cdot cm^{-2}$) for (a) Phase I, (b) Phase II and (c) Phase III of GATE.

Hellerman's (1967) well known seasonal mean tabulations of wind stresses (τ_x and τ_y) were based on U.S. Navy Hydrographic Offices' Marine Climatic Atlas of the World. This atlas was based on roughly eight years of marine surface data. We do not show here Hellerman's mean field of the wind stresses τ_x and τ_y for the summer months (June, July and August). Although there is a general agreement between our analyses, during GATE (mean stresses for the period 16 June through 23 September), there are some major differences as well:

In the northern trade wind belt our analysis shows a belt of easterly zonal stress around roughly 20°N. The corresponding latitude of strongest zonal easterly stress in Hellerman's study is located closer to the equator (17.5°N to 7.5°N). The trade belt of strongest winds during GATE seems to be located somewhat farther north. The strongest magnitudes of the stress in Hellerman's tabulations are around 1 to 1.4 dynes/cm^2 while those shown in the present study are around 1.6 dynes/cm^2. The major difference is due to differences in the intensity of the trades. For steady trade wind speeds on the order of 10 mps, we have used a drag coefficient of 1.4×10^{-3} based on recent GATE summaries presented by Businger and Seguin (1977). Hellerman used a value of 2.6×10^{-3} for the same wind speeds. It should also be noted that we have used daily values of the wind in estimating our mean stresses, while those of Hellerman's study are based on long-term mean motion field and wind roses that contain some information on the frequency distribution of daily stresses.

In the region of the northeast trades, the meridional stress is largest around 17.5°N to 7.5°N in the tabulations of Hellerman, while our study shows that the strongest trades are, in fact, found farther north and closer to 20°N. This is primarily due to the differences in the mean motion fields of our study versus those found in the U.S. Hydrographic Marine Climatic Data Summary. The southern trades exhibit winds greater than 10 mps over a wide region of the southeastern Atlantic Ocean. The use of a drag coefficient of 2.6×10^{-3} in Hellerman's tabulation again leads to rather large magnitudes of the meridional stresses. In this region the magnitude of largest meridional stress in Hellerman's study is on the order of 0.5 dynes/cm^2, while in our study it is somewhat larger in spite of our use of much smaller drag coefficients due to stronger winds and transients. Details of stresses within the Gulf of Mexico and in the eastern Pacific Ocean are not described by the climatological data set of Hellerman.

We shall next examine the mean fields of wind stress curl for phases of GATE (Figure 3.9a, b and c). The trade wind belts contain an east-west oriented zero line separating regions of negative and positive wind stress curl. In the northern trades this separation line is located around 20°N, and for the southern trades this line is located along 10°S. In general, a positive and an adjacent negative centre is found over most regions of strong wind stress curl. The positive centre is to the left of the strong wind stress vector while the negative centre is to its right. Such couplets are clearly evident in the western Gulf of Mexico, the Caribbean Sea, the eastern Pacific Ocean, the northeast trades (20°N) and the southeast trades over the eastern Atlantic Ocean. The Guinea coast is a region of some interest here. The only region with a positive wind stress curl along this coast is located near 3°E where a meandering of the zero line may be noted. Over most of the remaining regions along this coast, the wind stress curl does not show positive values north of the equator. This situation is quite different from that along the Peruvian coast. The winds along the Peruvian coast contain a stronger southerly coastal flow, while in the Atlantic Ocean stronger southwesterlies are found and the flows parallel to the African coast are not as large.

3.10 THE SURFACE HEAT BALANCE OF THE GATE OCEANS

During Phase I of GATE the axis of maximum sea-surface temperature is oriented from southwest to northeast across the Atlantic Ocean. It lies close to the equator near South America and near 10°N near the West African coast. This axis of warm sea-surface temperature migrates northwards during the second and third phases of GATE.

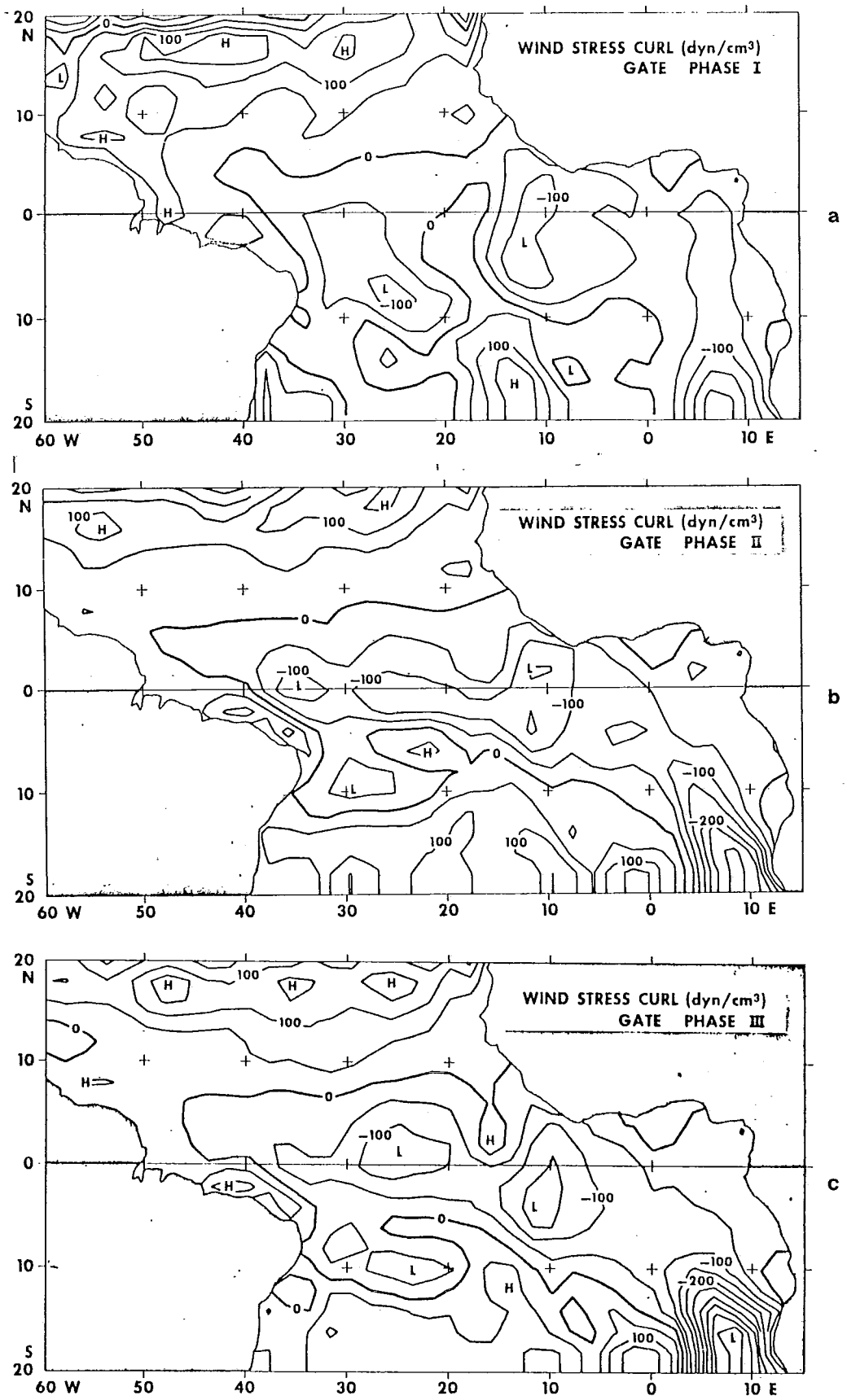

Figure 3.9 - Mean field of the curl of the surface wind stress ($dyn \cdot cm^{-3}$) for (a) Phase I, (b) Phase II, and (c) Phase III of GATE.

The ITCZ, identified by the surface asymptote of confluence on the phase mean surface streamline charts, is located very close to the axis of the warmest phase mean sea-surface temperatures. The surface flows contain an interesting flow separation point (a col point) which may be seen around 25°W and 5°N in Figure 3.1a, b and c. Rainfall maxima tend to occur just north of the ITCZ where the northeast trades acquire a strong easterly component over western Atlantic and south of the ITCZ where the southeast trades acquire a strong westerly component over the eastern Atlantic Ocean.

The GATE A-scale, A/B-scale and the B-scale ship data sets were processed on a 12-hourly basis to evaluate the surface heat balance for the entire three phases of GATE. All calculations are done for 00 and 12 GMT.

In the following all units are in watts/m^2. Separate calculations for 00 and 1200 GMT were averaged to provide 24-hour averages of the oceanic heat balance. In all we include surface and upper-air data from some 30 GATE ships during each phase in this analysis. The exact periods of the three phases are described elsewhere in GATE catalogues.

The following components of oceanic heat balance are considered here:

(i) Downward flux of short-wave radiation (Fs $\downarrow$). The results shown in Tables 3.2, 3.3 and 3.4 (for Phases 1, 2 and 3 respectively) were obtained from the detailed vertical soundings of temperature, humidity and estimates of cloud cover. The calculations follow the method proposed by Joseph (1966), Katayama (1972) and Chang (1979). Here we take into account the scattered as well as the absorbed parts of solar radiation; furthermore, reflection as well as absorption by clouds, water vapour and the ocean surface for a prescribed albedo are included in this analysis.

(ii) Upward flux of short-wave radiation (Fs $\uparrow$). Using the oceanic albedo estimates of Kondratyev (1972) for northern summer the magnitudes of Fs $\uparrow$ are derived from Fs $\downarrow$ (see Tables 3.2, 3.3 and 3.4).

(iii) Downward flux of long-wave radiation (Fl $\downarrow$). The estimates are obtained by the so-called emissivity method following Danard (1969). Here we evaluate the black body fluxes along a vertical sounding of temperature and humidity. The absorption and emission of the black body fluxes include the effects of water vapour, clouds and the ocean surface (see Tables 3.2, 3.3 and 3.4).

(iv) Upward flux of long-wave radiation (Fl $\uparrow$). These are derived from the estimates of sea-surface temperatures for GATE (Krishnamurti et al., 1976; see Tables 3.2, 3.3 and 3.4).

(v) Sensible heat flux from the ocean to the atmosphere (Sen $\uparrow$). The estimates, based on Bulk Aerodynamic methods, are described elsewhere in the atlas (Krishnamurti and Krishnamurti, 1980; see Tables 3.2, 3.3 and 3.4 for estimates at the GATE-ship locations).

(vi) Latent heat flux from the ocean to the atmosphere (Lat $\uparrow$). These were also estimated following the Bulk Aerodynamic methods (see Tables 3.2, 3.3 and 3.4).

(vii) Oceanic heat balance: The net downward heat fluxes obtained from (i) through (vi) above are given in Tables 3.2, 3.3 and 3.4, as well as in Figure 3.10a, b and c, for the three phases of GATE. Here the net flux is defined by the relation:

$$\text{Net}\downarrow = \text{Fs}\downarrow - \text{Fs}\uparrow + \text{Fl}\downarrow - \text{Fl}\uparrow - \text{Sen}\uparrow - \text{Lat}\uparrow.$$

The fields of Net $\downarrow$ exhibit a large positive centre on the GATE A-scale and are enclosed by a region of negative values all around it. A very distinct meridional motion of the region of positive (i.e., net downward flux region) from the first to the third phase of GATE is evident here. The maximum value (located around 10°N, 25°W) of the downward flux is largest during Phase I ($\approx$ 75 watts/m^2), decreases to around 55 watts/m^2 around 12°N, 25°W during Phase II, decreases further to around 30 watts/m^2 during Phase III and is located near 14°N, 25°W. The zero line separating

the downward flux (to the north) from the upward flux moves from the equator to roughly 7°N between the three phases of GATE. This meridional motion of the net oceanic heat flux is consistent with the meridional motion of GATE cloud cover (Murakami, 1979), and the motion of the warm sea-surface temperature belt during GATE (Krishnamurti et al., 1976).

The region of net heat gain by the ocean lies between 5° and 15°N during Phase I and gradually weakens in the subsequent phases as the sun moves towards the equator from the Tropic of Cancer. The axis of warmest sea-surface temperature seems to move towards the region of the net heat gain with a lag of about two months. The other features such as cloud cover, rainfall and the flow field (the ITCZ) also move slowly northwards.

The estimates of the net heat gain rely on observations of sea-surface temperatures, surface and upper-air observations of temperature, humidity and cloud cover. An error analysis of the problem suggests that the final estimates presented here may be in error by as much as 50% if the errors in sea-surface temperature, and air temperature are of the order of 1°C and the humidity error is of the order of 20%. Thus we believe that the different authors using the same data sets but using different analysis methods may differ by as much as 50% in their estimates. The error could be reduced considerably if the calculations are made only on the B-scale domain. However, our intention has been to cover the A-scale and as such is not entirely free of analysis errors. Koprov (1980), Zaitseva et al. (1980) have examined the problems of energy budgets of the equatorial atmosphere and radiation models relevant to the topic of this section. Koprov in particular demonstrates the much stronger fluxes of heat by the ocean currents than is implied by our review.

3.11 MEAN SOUNDING ON THE GATE A-SCALE

In Tables 3.2, 3.3 and 3.4 we present a list of GATE ships that operated during the three phases. Roughly four daily soundings were available during the phases. A mean GATE sounding (Figure 3.11) was prepared from the ship data utilizing the final validated GATE data sets. This sounding describes the mean state during the period 26 June to 20 September 1974. Figure 3.11 also includes a tabulation of the pressure, temperature, dew point and the potential temperature. The mean sounding is heavily weighted by the A/B-scale ship array. As such it describes a sounding in the vicinity of the ITCZ over the tropical Atlantic Ocean. The sounding is very moist in the lowest km. Over most of the troposphere the dew point depression is less than 10°C.

3.12 CONCLUDING REMARKS

GATE has provided a valuable climatology for various meteorological parameters over the tropical Atlantic and West Africa during the northern summer season. High quality data sets from research ships, research aircraft, geostationary satellites, a near complete World Weather Watch and a special collection of data from commercial aircraft were provided for a 10-day period. In this chapter we have presented a summary of the mean state, based on these observations.

The most interesting aspects of the mean state are the inter-phase evolutions of sea-surface temperatures, the sea-level motion field, the field of cloud cover, rainfall totals and the net heat gain by the oceans. The response of the maximum sea-surface temperature to the net heat gain by the ocean is slow (a lag of about eight weeks is evident). While the sun starts to move equatorward after its zenith position over the Tropic of Cancer the field of net heat gain begins to weaken somewhat in the 10° to 20°N latitude belt over the eastern Atlantic Ocean. However, due to the slow response of the ocean the warm axis continues in its mean northernmost position until the third phase of GATE. Mean fields of the oceanic wind stress and the wind stress curl are prepared to provide an understanding of the thermal behaviour of the upper ocean. During this northward excursion of the axis of warm sea-surface temperature other features such as the surface streamlines, the rainfall belt and the axis of maximum cloud cover exhibit a very slow northward motion. Rainfall maximum over the eastern Atlantic tends to occur where the southeast trades acquire a westerly component around 10°N near West Africa. The axis of maximum rainfall is somewhat farther north over the western Atlantic ocean where the northeast trades become due easterlies just north of the ITCZ.

Table 3.2. Oceanic heat budget

Phase I: 26 June-16 July 1974. (Watts.m^{-2})

SHIP	LAT	LONG	Fs↓	Fs↑	Fl↓	Fl↑	Sen↑	Lat↑	Net↑
1 *Korolov*	12.0	23.4	174.2	11.1	397.3	451.7	1.9	40.5	66.3
2 *Poryv*	10.4	20.0	145.5	9.3	417.5	464.9	4.2	42.1	42.5
3 *Krenkel*	6.5	19.9	111.0	7.1	425.1	460.7	5.7	58.4	4.3
4 *Zubov*	5.0	22.9	123.7	7.9	420.1	461.6	1.8	55.9	16.6
5 *Okean*	6.4	26.9	121.5	7.7	423.2	459.9	2.1	49.3	25.7
6 *Priboy*	10.3	26.9	175.9	11.2	399.5	456.9	0.1	31.1	76.1
7 *Oceanographer*	8.5	23.5	118.9	7.6	423.4	458.4	2.3	39.2	34.8
8 *Vize*	10.1	23.5	142.2	9.1	417.8	458.3	2.0	36.6	54.0
9 *Quadra*	9.3	22.1	152.9	9.7	422.3	458.9	3.8	45.0	57.7
10 *Meteor*	7.8	22.1	116.7	7.5	423.0	458.9	4.6	49.8	19.0
11 *Researcher*	7.1	23.5	132.3	8.5	414.1	459.6	2.3	52.5	23.5
12 *Dallas*	7.7	24.8	131.0	8.3	415.1	458.7	1.3	33.5	44.3
13 *Gillis*	9.3	24.8	119.7	7.7	426.0	457.2	3.5	41.0	36.2
14 *Lomonsov*	−5.6	23.5	232.7	14.9	349.7	462.3	19.9	171.1	−85.8
15 *Saldanha*	0.0	35.0	145.0	9.3	386.5	460.9	−1.3	100.6	−37.9
16 *Sirius*	7.5	35.0	168.8	10.7	398.9	457.7	1.4	45.1	52.7
17 *Endurer*	20.0	29.0	256.7	16.4	279.5	437.7	7.8	125.3	−51.0
18 *Charterer*	8.0	16.0	91.4	5.9	432.3	459.2	5.2	62.3	−8.9
19 *Passat*	0.0	10.0	251.4	16.0	355.6	442.8	1.1	86.8	60.3
20 *Kurchatov*	0.0	23.5	180.5	11.5	380.7	451.1	6.5	86.2	5.8
21 *Charcot*	15.0	35.0	204.1	13.0	326.5	443.8	1.2	75.1	−2.5
22 *Volna*	12.5	44.0	206.3	13.1	336.5	455.5	1.3	103.5	−30.7
23 *Onversaagd*	15.0	54.0	159.3	10.1	340.4	459.2	−1.7	131.4	−99.4

Table 3.3. Oceanic heat budget

Phase II: 28 July-7 August 1974. (Watts.m^{-2})

SHIP	LAT	LONG	Fs↓	Fs↑	Fl↓	Fl↑	Sen↑	Lat↑	Net↑
1 *Korolov*	12.0	23.4	151.3	9.7	416.3	462.9	1.8	41.5	51.7
2 *Poryv*	10.4	20.0	153.7	9.8	415.1	459.6	4.3	61.5	33.6
3 *Krenkel*	6.5	19.9	140.7	9.0	421.9	459.3	4.6	86.5	3.1
4 *Zubov*	5.0	22.9	130.7	8.3	418.9	457.5	4.3	91.2	−11.7
5 *Okean*	6.4	26.9	127.6	8.1	417.9	461.0	1.9	85.5	−11.1
6 *Priboy*	10.3	26.9	178.3	11.4	393.9	461.1	1.3	42.7	55.7
7 *Vize*	8.5	23.5	126.2	8.1	419.1	461.1	2.0	70.6	3.4
8 *Vanguard*	10.1	23.5	139.3	8.9	416.9	462.9	1.5	52.1	30.7
9 *Quadra*	9.3	22.1	134.9	8.6	422.8	460.3	4.5	48.0	36.3
10 *Meteor*	7.8	22.1	122.5	7.6	416.1	459.1	2.5	69.1	0.3
11 *Researcher*	7.1	23.5	115.9	7.4	425.1	460.1	2.7	91.1	−20.5
12 *Dallas*	7.7	24.8	166.7	10.7	401.3	459.9	0.4	69.6	27.4
13 *Gillis*	9.3	24.8	109.6	7.0	424.8	461.9	3.4	42.0	20.0
14 *Lomonosov*	−5.6	23.5	162.0	10.3	368.7	449.7	4.6	155.2	−89.1
15 *Passat*	0.0	10.0	240.2	15.3	359.9	435.7	−5.6	57.0	97.7
16 *Kurchatov*	0.0	23.5	188.9	12.1	382.2	448.3	14.7	132.2	−36.2
17 *Anton Dohrn*	0.0	29.0	112.5	7.2	390.1	457.0	1.1	124.5	−87.2
18 *Volna*	8.5	33.0	139.7	8.9	415.5	462.1	0.9	41.1	42.2
19 *La Perle*	6.0	14.5	137.1	8.7	419.4	457.4	4.6	109.0	−23.2
20 *Charterer*	15.0	33.0	135.3	8.7	368.6	450.9	4.5	54.7	−14.9
21 *Endurer*	10.0	16.5	122.9	7.9	423.7	459.5	3.6	77.9	−2.3
22 *Onversaagd*	15.0	50.0	114.1	7.3	415.5	458.4	2.8	84.8	−23.7
23 *Sirius*	7.5	40.0	113.5	7.3	421.4	464.2	1.4	44.1	17.9
24 *Saldanha*	2.0	38.0	135.9	8.7	372.7	461.3	−3.3	90.5	−48.6
25 *Matamoros*	6.5	48.5	131.5	8.4	362.3	463.9	−2.6	56.2	−32.1

Table 3.4. Oceanic heat budget

Phase III: 30 August-19 September 1974. (Watts.m^{-2})

SHIP	LAT	LONG	Fs↓	Fs↑	Fl↓	Fl↑	Sen↑	Lat↑	Net↑
1 *Korolov*	12.0	23.4	127.5	8.1	427.2	462.5	2.6	48.7	32.3
2 *Poryv*	10.4	20.0	148.5	9.5	421.5	460.1	5.9	63.7	30.8
3 *Krenkel*	6.5	19.9	128.4	8.2	425.3	459.6	3.4	76.6	5.9
4 *Zubov*	5.0	22.9	110.3	7.1	421.1	458.8	5.3	111.0	−48.7
5 *Okean*	6.4	26.9	115.5	7.3	422.1	462.2	5.1	97.7	−34.7
6 *Priboy*	10.3	26.9	145.4	9.3	407.1	461.7	4.2	53.8	23.5
7 *Vize*	8.5	23.5	114.1	7.3	427.5	461.1	3.4	63.7	6.1
8 *Vanguard*	10.1	23.5	115.9	7.4	425.5	464.0	4.4	56.5	9.1
9 *Quadra*	9.3	22.1	126.1	8.1	428.1	461.0	5.0	53.0	27.1
10 *Oceanographer*	7.8	22.1	126.5	8.1	422.5	460.3	5.1	66.3	9.2
11 *Researcher*	7.1	23.5	113.1	7.2	419.7	461.9	2.5	90.6	−29.4
12 *Bidassor*	7.7	24.8	122.9	7.9	425.6	461.5	4.2	68.8	6.1
13 *Gillis*	9.3	24.8	114.5	7.3	425.3	461.5	5.0	58.0	8.0
14 *Lomonosov*	−5.6	23.5	159.5	10.2	349.3	447.7	−10.3	118.4	−57.2
15 *Passat*	0.0	10.0	223.9	14.3	384.4	439.7	−4.1	83.4	75.0
16 *Kurchatov*	0.0	23.5	191.9	12.3	405.3	450.9	6.6	132.4	−5.0
17 *Charterer*	15.0	35.0	113.5	7.3	409.8	455.1	6.4	60.1	−5.6
18 *Capricorne*	6.0	14.5	141.1	9.0	418.5	458.5	4.8	83.6	3.7
19 *Endurer*	10.0	16.5	135.4	8.7	413.0	458.9	3.7	63.8	13.3
20 *Onversaagd*	15.0	50.0	107.3	6.9	402.1	460.5	7.5	112.0	−77.5

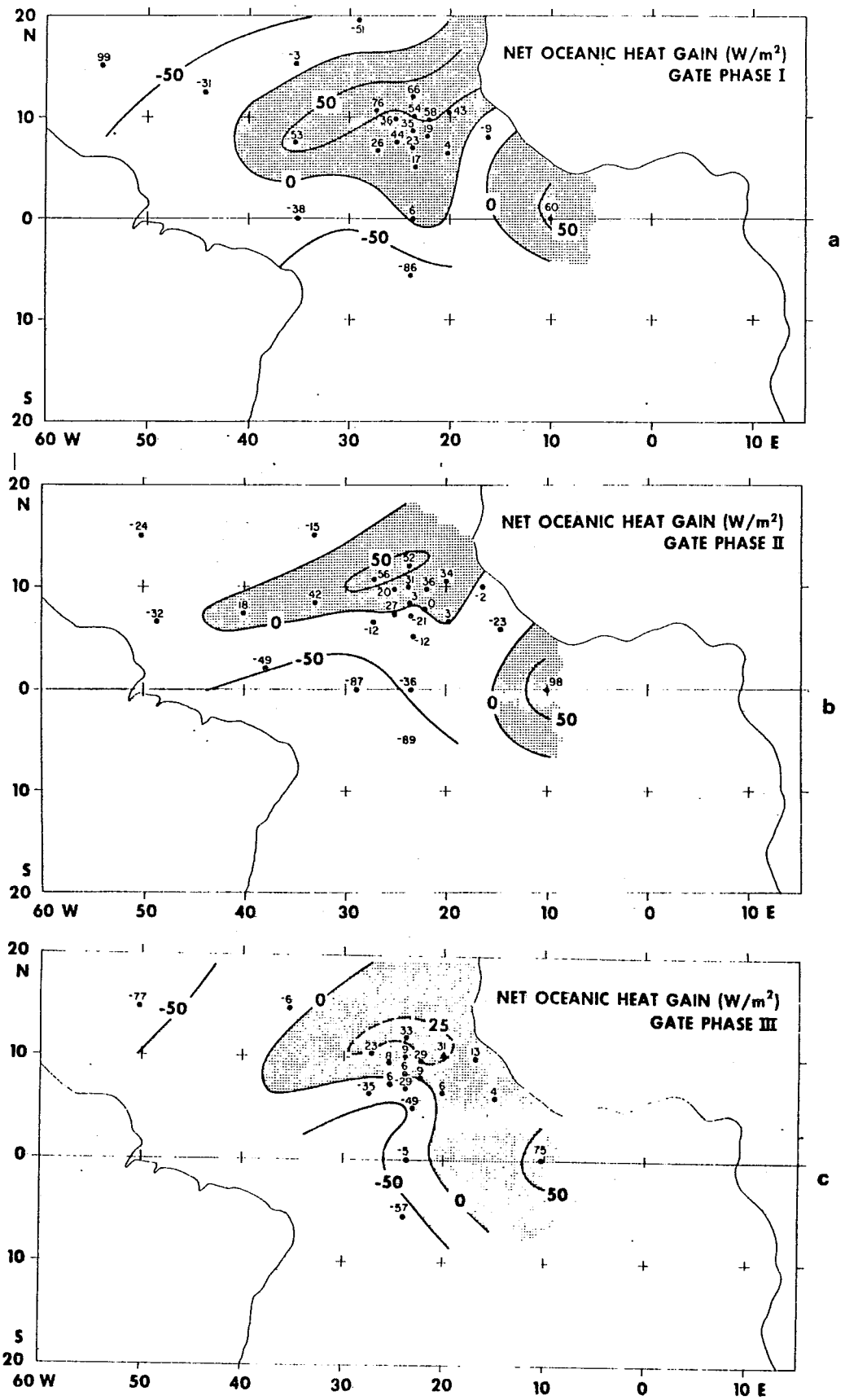

Figure 3.10 - Mean net oceanic heat gain ($W \cdot m^{-2}$) for (a) Phase I, (b) Phase II and (c) Phase III of GATE.

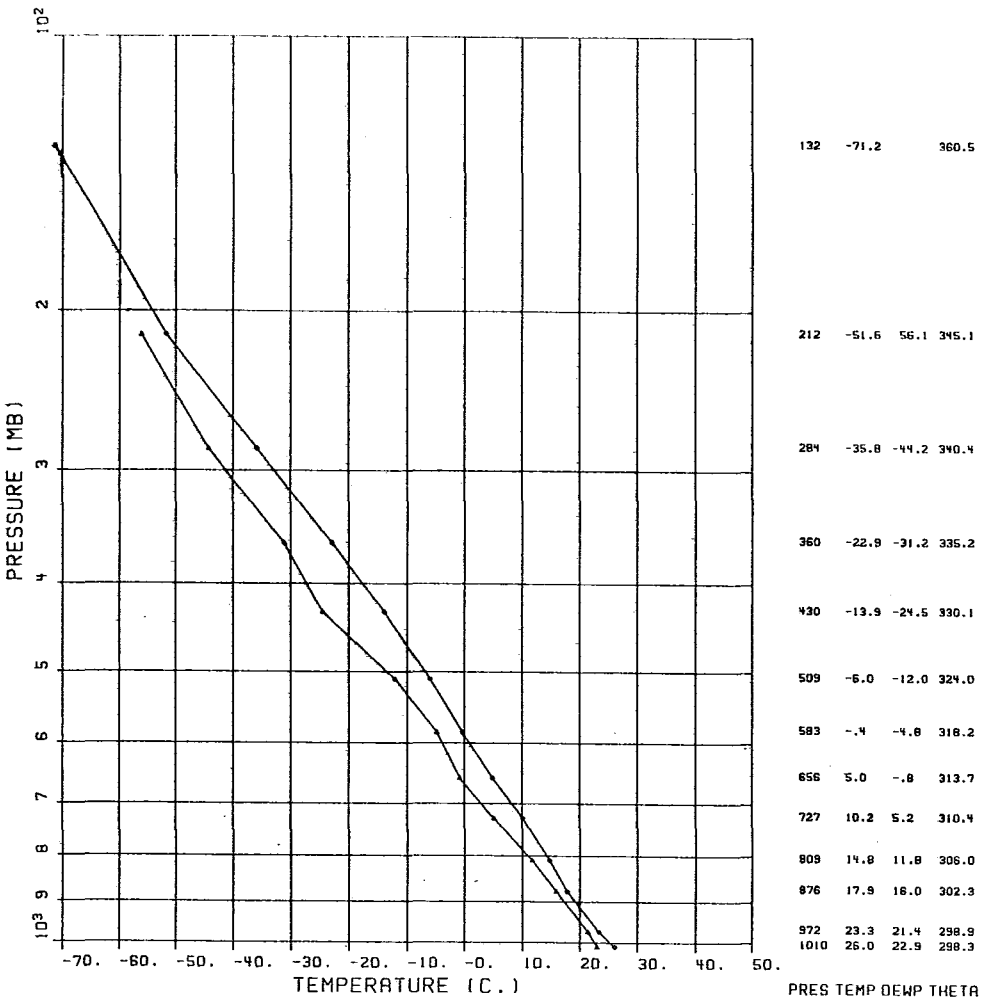

Figure 3.11 - Mean sounding of temperature and dew point (^{o}C) for the period 26 June to 20 September 1974 for the GATE ships listed in Tables 3.2, 3.3 and 3.4. Potential temperature (^{o}K) is tabulated on the right margin.

The tropical upper troposphere over the Atlantic Ocean was, for the first time, mapped with the largest valume of data sets from a variety of platforms. The mix of observing systems included the satellites, commercial aircraft and the World Weather Watch. The tropical easterly jet that has its origin in the Asian monsoons, culminates as a weak diffluent flow over the Atlantic Ocean. This region was very well described by GATE; the diffluent geometry was clearly evident over the eastern Atlantic Ocean in the phase mean flow fields. What was not quite clear was the extent to which the upper diffluence was related to the developing cloud clusters on the A/B-scale of GATE or whether it was a dynamic consequence of the instability of the jet over West Africa. Some of these broader-scale problems have not been adequately addressed at this stage.

The maintenance of the mean state evidently is related to the interaction of (i) mean state with the mean state; and (ii) mean state with the perturbations. Since time averaged motions carry a large proportion of the total variance of the motion field in low latitudes, its maintenance deserves a careful formulation and evaluation.

ACKNOWLEDGEMENTS

Our research work on GATE was supported by the National Science Foundation (NSF) Grant No. ATM78-19363. We wish to convey our appreciation to the former members of the U.S. GATE Project Office who encouraged and made it such a successful experiment. Computations were carried out at the Florida State University and National Center for Atmospheric Research (NCAR) computer facilities. NCAR is sponsored by the National Science Foundation.

REFERENCES

Bergthorsson, P. and B. Döös, 1955: Numerical weather map analysis. Tellus, 7, 329-340.

Businger, J. and W. Seguin, 1977: Sea air flows of latent heat and sensible heat and momentum. Proceedings of the GATE Workshop, published by the National Center for Atmospheric Research, Boulder, Colorado, U.S.A., pp. 441-453.

Chang, C. B., 1979: On the influence of solar radiation and diurnal variation of surface temperature on African disturbances. Tech. Rept. No. 79-3, Florida State University, Tallahassee, Florida, 1-157 pp.

Chuchkalov, B. S. (Editor), 1977: Weather maps of the Atlantic Tropical Experiment (GATE). Volumes I, II, III. Published by the Hydrometoeorlogical Research Centre of the U.S.S.R., Moscow.

Cressman, G. P., 1959: An operational objective analysis system. Mon. Wea. Rev., 87, 367-374.

Danard, M., 1969: A simplified method of including radiative cooling in numerical weather prediction models. Mon. Wea. Rev., 97, 77-85.

Depradine, C. A., 1978: Energetics of long waves in the tropics during the summer of 1974. Ph. D. Dissertation, Department of Meteorology, Florida State University, Tallahassee, Florida.

_____, R. Pasch and T. N. Krishnamurti, 1978: An atlas of the motion field over the GATE area Phase III, 300 mb. Report No. 78-4, Department of Meteorology, Florida State University, Tallahassee, Florida.

Dittmer, K., M. Gruenewald and L. Hasse, 1978: Turbulent flows in the surface layer from profile measurements during GATE. "Meteor" Forschungsergebnisse, Riehe B.

Düing, W., 1968: The monsoon regime of the currents in the Indian Ocean. Tech. Report, Department of Oceanography, University of Hawaii, Honolulu, 1-81 pp.

Griffith, C., W. L. Woodley, J. S. Griffin and S. C. Strowatt, 1980: Satellite-derived precipitation atlas for GATE. NOAA Technical Report, published by U.S. Department of Commerce, 1-20 pp.

Hantel, M., 1970: Monthly charts of the surface stress curl over the Indian Ocean. Mon. Wea. Rev., 95, 607-626.

Hellerman, S., 1967: An updated estimate of the wind stress on the world ocean. Mon. Wea. Rev., 95, 765-773.

Holopainen, G. O., 1967: A determination of wind driven ocean circulation from the vorticity budget of the atmosphere. PAGEOPH, 67, 156-165.

Hubert, L. F., 1975: Evaluation of wind data derived from SMS-1 of characteristics of satellite wind data. Paper presented at the 9th Technical Conference on Hurricanes and Tropical Meteorology, 1-8 May 1975.

Hudlow, M. D. and V. L. Patterson, 1979: GATE rainfall Atlas. NOAA Special Report, Center for Environmental Assessment Services, NOAA, Washington D.C., 155 pp.

Joseph, J. M., 1966: Calculations of radiative heating in numerical general circulation models. Department of Meteorology, University of California at Los Angeles, California. Technical Report No. 1, 1-60 pp.

Katayama, A., 1972: A simplified scheme for computing radiative transfer in the troposphere. Technical Report No. 6, Department of Meteorology, University of California at Los Angeles, 1-77 pp.

Kondratyev, K. Ya, 1972: Radiative processes in the atmosphere. World Meteorological Organization Publication, Geneva, Switzerland, 1-21 pp.

Koprov, B. M., 1980: Energy budget of equatorial atmosphere and meridional heat transfer. Preprint IFA AN SSSR and CAO, Moscow, U.S.S.R.

Krishnamurti, T. N., 1971: Observational study of tropical upper tropospheric motion field during northern hemisphere summer. J. Appl. Meteor., 10, 1066-1096.

_____, 1978: Large-scale features of the tropical atmosphere. "Meteorology over the tropical oceans". Published by Roy. Meteor. Society, James Glaisher House, Grenville Place, Bracknell, Berkshire, RG12 18X.

_____, V. Wong, H. L. Pan, G. Van Dam and D. McClellan, 1976: Sea-surface temperatures for GATE. Report No. 76-3, Department of Meteorology, Florida State University, Tallahassee, Florida, 1-268 pp.

_____, R. Pasch and C. Depradine, 1978: An atlas of the motion field over the GATE area, Part I, Report No. 78-1, Department of Meteorology, Florida State University, Tallahassee, Florida.

_____ and R. Krishnamurti, 1979: Surface meteorology on the GATE A-scale. Deep Sea Research (December 1979 issue).

_____ and M. Kanamitsu, 1980: Planetary scale monsoons during drought and normal rainfall months. Proc. on Monsoon Dynamics, published by Cambridge University Press.

Miller, B. I., 1962: On the energy and momentum balance of Hurricane Helene, 1958. National Hurricane Research Project Report No. 53. U.S. Weather Bureau, 1-19 pp.

Murakami, M., 1979: Large-scale aspects of deep convective activity over the GATE area. Mon. Wea. Rev., 107, 994-1013.

Odyama, K., 1969: Numerical simulation of the life cycle of tropical cyclones. J. Atmos. Sci., 26, 3-40.

Pasch, R. J., T. N. Krishnamurti and C. Depradine, 1978: An atlas of the motion field over the GATE area Part II, 250 mb. Report No. 78-3, Department of Meteorology, Florida State University, Tallahassee, Florida.

Reynolds, R., 1977: Large-scale (A-scale) mean features of the GATE atmosphere during Phase III. Publication Number 'Met 020 Tech. Note No. 105', Meteorological Office, London Road, Bracknell, England.

Roll, H. V., 1965: Physics of the marine atmosphere. Academic Press, New York, 1-426 pp. (Ref: Page 160.)

Sadler, J. and L. K. Oda, 1978, 1979 and 1980: The synoptic (A) scale circulations during Phases I, II and III of GATE. Technical Reports Nos: 78-02, 79-14 and 80-01. Published by the Department of Meteorology, University of Hawaii, Honolulu, Hawaii.

Thompson, R. M., Jr., S. W. Payne, E. E. Recker and R. I. Reed, 1979: Structure and properties of synoptic scale wave disturbances in the intertropical convergence zone of the eastern Atlantic. J. Atmos. Sci., 36, 53-72.

Tripoli, G. J. and T. N. Krishnamurti, 1975: Low-level flows over the GATE area during 1972. Mon. Wea. Rev., 103, 197-216.

Zaitseva, N. A., G. N. Kostyanoy and E. M. Feigelson, 1980: Radiation models of the tropical Atlantic atmosphere. Preprint IFA AN SSSR and CAO, Moscow, 1980.

CHAPTER 4

SYNOPTIC-SCALE MOTIONS

by

Robert W. Burpee
National Hurricane Research Laboratory
Coral Gables, Florida 33146, U.S.A.

and

Richard J. Reed
Dept. of Atmospheric Sciences, University of Washington
Seattle, Washington 98195, U.S.A.

4.1 INTRODUCTION

The GARP Atlantic Tropical Experiment (GATE) was designed to measure phenomena ranging in size from small convective elements to large planetary-scale circulations. A major objective of the experiment was to study the interactions of different scales of motion with particular emphasis on the interaction between convective and synoptic scales. In order to achieve the required definition of the synoptic-scale systems, special observational networks were established and the collection of data from pre-existing sources was enhanced. At the conclusion of the experiment a data set of unprecedented quality existed for investigating large-scale tropical motions. An expanded number of surface and upper air observations were available in readily accessible form for large parts of Africa and South America. Observations from the A-scale ship network, commercial aircraft and the SMS-1 satellite yielded unique data coverage for the Atlantic Ocean. Most importantly, the surface, upper air and radar observations taken in the A/B and B-scale ship networks of the eastern Atlantic provided the basis for intensive study of synoptic systems within a limited region.

The purpose of the present chapter is to review the knowledge that has been gained from analysis of the synoptic data. Principal emphasis is placed on the African or easterly waves which proved to be the dominant, transient synoptic-scale feature in the area of main interest. Topics treated to a lesser extent are the tropical storms and hurricanes that developed in the western part of the GATE region, the upper level vortices that formed in the tropical upper tropospheric trough of the Atlantic, and the ITCZ disturbances, or small synoptic systems of non-wave origin, that were occasionally observed in the vicinity of the Intertropical Convergence Zone (ITCZ).

In treating the foregoing topics, occasional mention is made of the ITCZ. However, in view of the contributions appearing elsewhere in this volume (Chapters 3.8 and 9), a self-contained discussion of the subject is not attempted here. Entirely omitted from discussion are the mixed Rossby-gravity waves and Kelvin waves that are known to be important features of the circulation of the tropical stratosphere. These have received such little attention in GATE analysis that it has seemed appropriate to relegate the discussion of them to the chapter on theoretical studies of tropical waves (Chapter 5). Also discussion of theoretical or modeling results has been kept to a minimum in order to avoid needless duplication of material treated in Chapters 5 and 6.

4.2 AFRICAN OR EASTERLY WAVES

The existence of westward propagating, synoptic-scale disturbances that traverse the region from western Africa to the Caribbean during the period from late May until mid October has been noted for many years. First identified by Piersig (1936), these wavelike disturbances are frequently referred to as African or easterly waves. They are observed to have a typical east-west length scale of 2500 km, a period of about 3.5 days, and a

speed toward the west of 7-8 m s^{-1}. While the majority of the 45-50 waves that cross the African coast each summer weaken as they traverse the ocean, 4 or 5 strengthen and become tropical cyclones in the central and western ocean region, particularly during August and September (e.g., Simpson et al., 1968). Forecasters at the National Hurricane Center (NHC) frequently track these systems as far west as the eastern Pacific, where satellite images are often the only source of information (e.g., Frank and Clark, 1978). On the basis of this operational tracking, the forecasters estimate that about 60% of the tropical cyclones that form in the eastern Pacific are linked to wave disturbances that were first observed over Africa. As a result of the important role that the wave disturbances have in modulating rainfall and initiating tropical cyclones, these African waves have been the subject of many observational and numerical studies in recent years.

4.2.1 The Large-Scale Mean State in the Region Traversed by the Waves

Since research in the early 1970's had already indicated that the waves probably originate and strengthen as a result of the instability of the easterly zonal current over Africa, it is appropriate to discuss some of the basic features of the mean state in western Africa and the eastern Atlantic before the structure of the waves is discussed further. Studies completed before GATE in tropical northern Africa had provided considerable information about the monthly mean patterns and some knowledge of the basic characteristics of the easterly waves and squall lines that occur in this region. In the eastern Atlantic, however, relatively little was known about the vertical structure of the atmosphere since surface ship and commercial aircraft observations were only sufficient to define the monthly mean flow at the surface and in the upper troposphere near 250 mb. On the basis of historical ship observations, Hann (1915) had been able to identify several of the typical characteristics of the surface wind field over the tropical Atlantic. Many years later, the major features of the mean state in the latitudinal band where the wave disturbances are typically observed were described by Aspliden et al., (1965), Burpee (1972), and Sadler (1975).

The major differences in the mean state between tropical western Africa and the eastern North Atlantic occur near the surface. Over the Atlantic, the mean surface wind and pressure patterns were discussed by Aspliden et al. Their 50-year mean streamline and isotach analysis for September shows a col in the wind field near 10°N, 27°W with a zone of confluence extending approximately east-west through the center of the col (Fig. 4.1). These features move poleward from a location near 5°N in February to the position near 10°N during August and then progress equatorward toward 5°N during the fall and early winter. Surface streamline analyses of GATE data suggest that the col and confluence line are observed not only on the long-term monthly means but also in the average for Phase III (Reynolds, 1977) and on many individual map times as well (e.g., Sadler and Oda, 1978, 1979, 1980). In general, the surface confluence line in the A/B ship array marked the boundary between surface southwesterlies to the south and northwesterlies to the north.

During the summer over Africa, the warmest daily average surface temperatures occur near 25°N in the Sahara (Fig. 4.2). South of this region, the surface air becomes cooler and more humid as the southwesterly flow progressively deepens toward the southern coast of the African bulge at about 5°N. Monthly mean maps show that there is a 10°C difference in daily average surface temperature in the latitude band from 10-20°N. In response to this low level temperature gradient, an easterly jet is observed near 15°N with maximum zonal winds on the order of 10-15 m s^{-1} at 600-700 mb. The horizontal and vertical shears of the zonal flow in the vicinity of this jet are quite large when compared to those observed in the middle and lower troposphere at other tropical longitudes (Burpee, 1972).

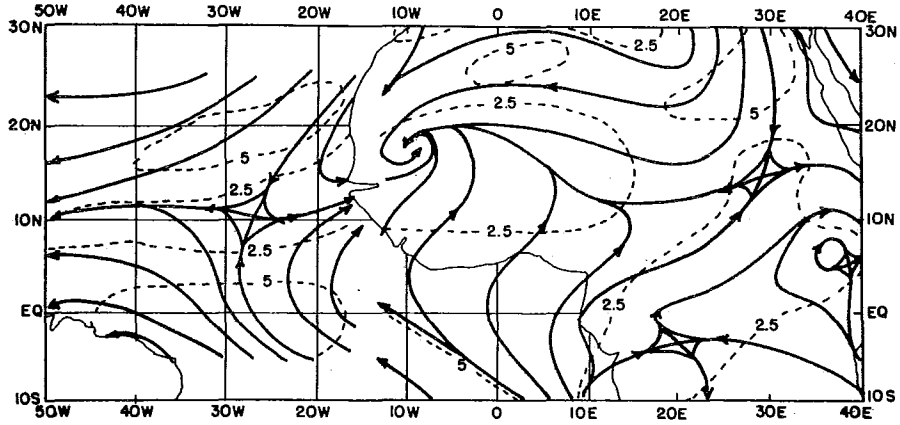

Fig. 4.1 Long-term mean streamline and isotach patterns for September near the surface in the GATE area. The figure has been adapted from the surface analyses of Aspliden et al. (1966a) in the region west of 15°W and from the gradient-wind analyses of Atkinson and Sadler (1970) in the area to the east of 13°W.

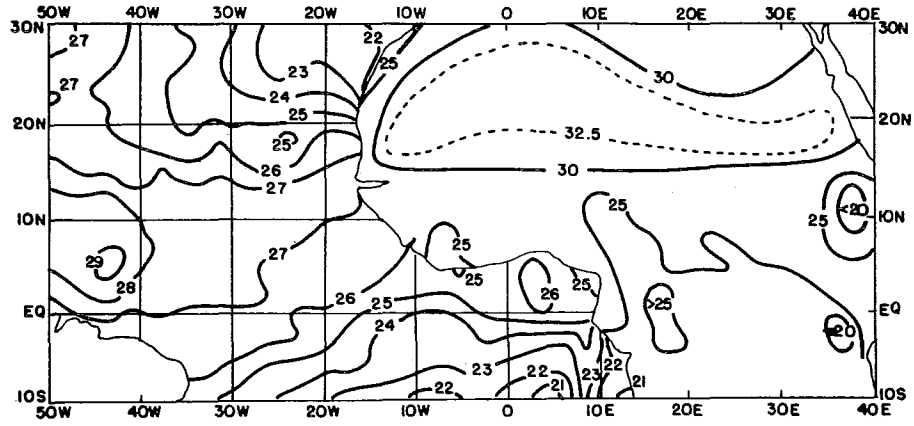

Fig. 4.2 Daily averaged air temperatures at the surface for Africa during September (1951-1960) from Burpee (1971) and mean sea-surface temperatures during Phase III of GATE from Krishnamurti et al. (1976). Note that the land temperatures have been analyzed at intervals of 5°C and the sea-surface temperatures every 1°C.

While the surface temperature maximum occurs near 25°N in western Africa during the summer months, the sea-surface temperature maximum in the eastern Atlantic (Krishnamurti et al., 1976) slopes west southwestward from the coast of Africa near 10-15°N, and through the northern part of the A/B ship array. Thus, north of 10-15°N, the north-south gradient of sea-surface temperature in the eastern Atlantic is in the opposite direction to the gradient of air temperature observed at the surface over Africa (Fig. 4.2).

It had been anticipated before GATE that the horizontal and vertical shears of the midtropospheric easterly jet would be weaker in the eastern Atlantic than in western Africa. Burpee and Dugdale (1975) pointed out, however, that the mean zonal flow during GATE was rather similar in both

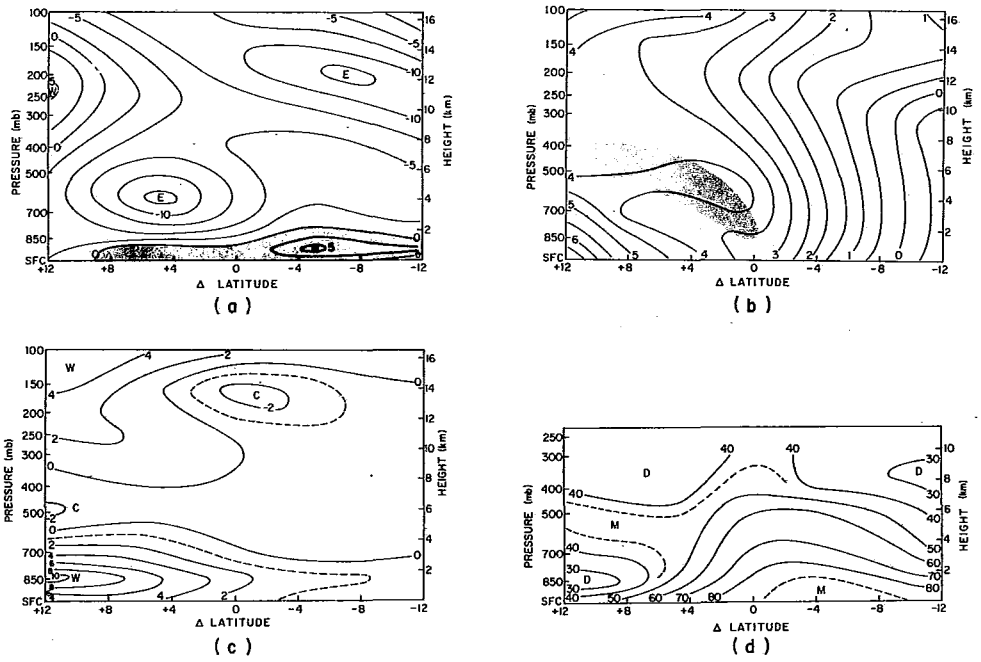

Fig. 4.3 Zonal mean fields (space and time) for period 23 August to 19 September, 1974. "Zero" latitude corresponds to average latitude of disturbance path, 11°N overland and 12°N over ocean. (a) Zonal wind (m s^{-1}); (b) absolute vorticity (10^{-5} s^{-1}); (c) temperature deviations (°C) from values at Δ latitude = -12; (d) relative humidity (percent).

regions except for the layer nearest the surface that is affected by the southwesterly monsoon flow over Africa. Figure 4.3 shows zonal mean fields of zonal wind, absolute vorticity, temperature deviations, and relative humidity that were computed by Reed et al. (1977) for Phase III and the preceding interphase period in the region from 10°E - 31°W. The low-level temperature gradient, the midtropospheric easterly jet, and the moisture distribution are similar to those described in earlier studies. The cross section of absolute vorticity indicates that the necessary condition for barotropic instability of the mean zonal flow was satisfied, as Burpee (1971) had also found for each month from June to September on the basis of observations averaged from 1957-1964.

Detailed knowledge of the atmospheric structure in the region of the A/B ship array was not available before the field experiment. Sadler (1975) summarized previous studies of the mean flow, presented analyses of a few radiosonde observations taken by a research ship in 1963, and related these to satellite information. Chen (1980) determined the average atmospheric structure during each phase of GATE for a 2.5° longitude band centered on 23.5°W in the ship array. His results for zonal and meridional wind, vertical velocity, and temperature deviation for each phase are shown in Figs. 4.4, 4.5, and 4.6. The cross sections of zonal wind indicate that the ship array was on the cyclonic shear side of the midtropospheric easterly jet as would be expected from the results presented earlier in Fig. 4.3 from Reed et al. (1977) for the longitudinal area from 10°E - 31°W. This jet accounts for much larger values of positive relative vorticity in the middle troposphere of the eastern Atlantic than are observed in either the western Atlantic or Pacific. The meridional wind cross sections reveal the presence

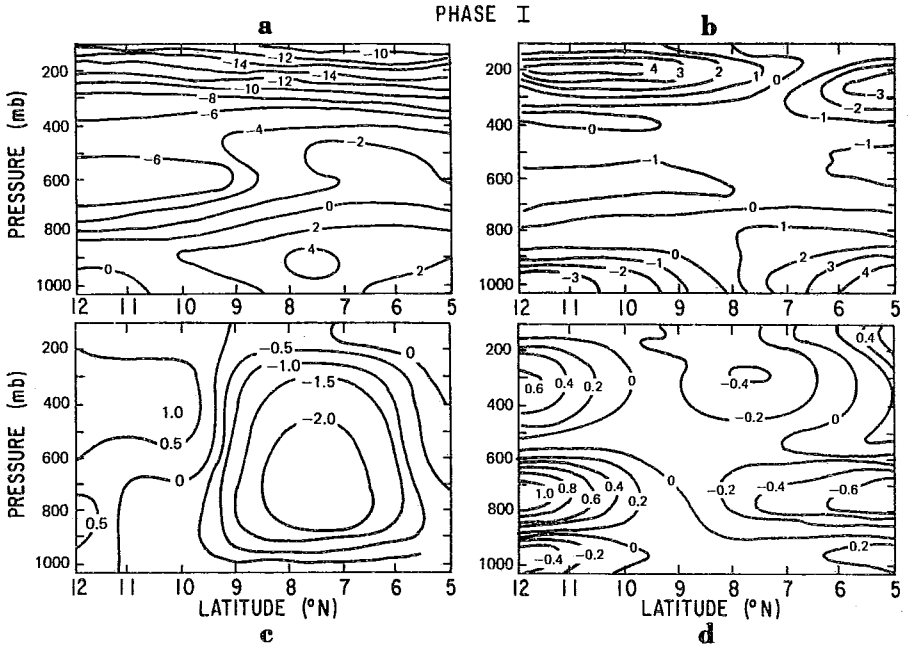

Fig. 4.4 Meridional cross sections of objectively analyzed parameters, averaged for Phase I in the longitude band from 22.25 - 24.75°W. The cross sections represent zonal (a) and meridional (b) wind in m s^{-1}, vertical velocity (c) in μ b s^{-1}, and temperature (d) in °C computed as deviations from the average at each pressure level.

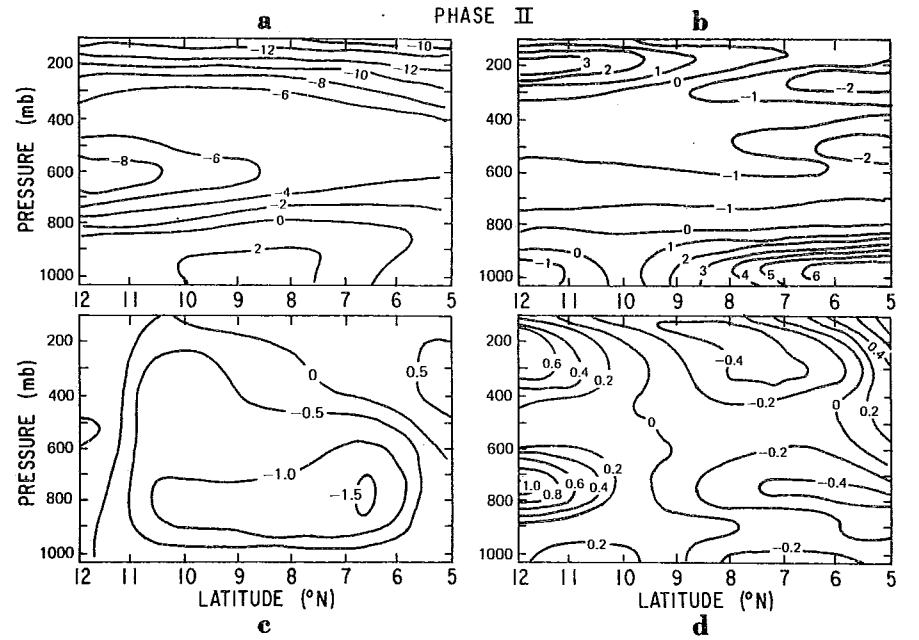

Fig. 4.5 Meridional cross sections during Phase II. See Fig. 4.4 for further description.

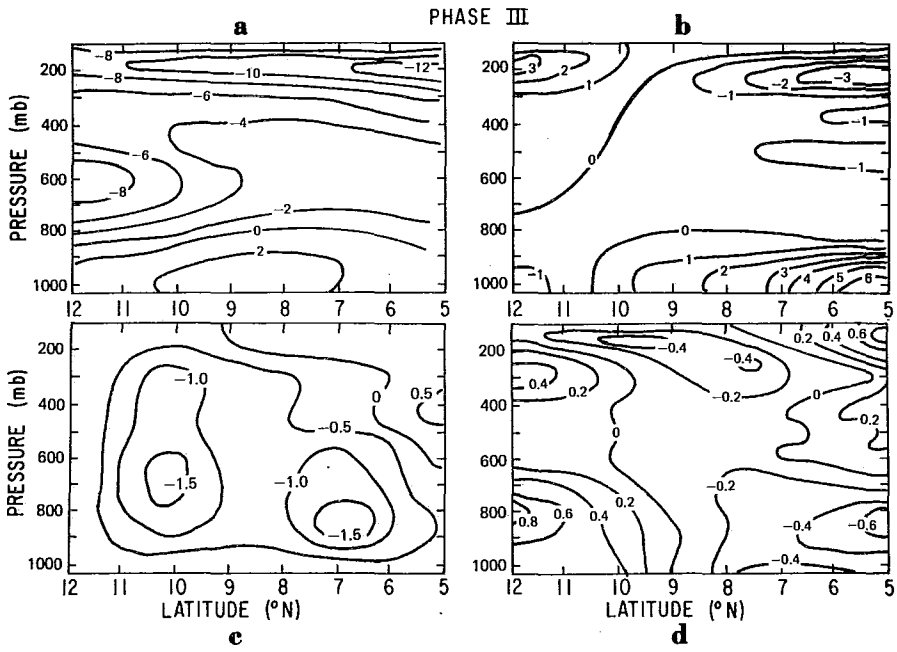

Fig. 4.6 Meridional cross sections during Phase III. See Fig. 4.4 for further description.

of the low-level confluence zone that was located near 8.5°N in Phase I and 10.5°N in Phases II and III with a corresponding region of diffluence near 250 mb. The divergence patterns (not shown) indicate regions of low-level convergence and upper-level divergence as well as weaker regions of convergence and divergence in the middle troposphere. The vertical motion diagrams show that there was a single maximum of ascent near 7°N and 700 mb during Phases I and II, but during Phase III there were two separate low-level maxima: one at 7°N and the second 10°N. In the lower and middle troposphere, ascent occurred at all latitudes within the region of analysis except north of 11°N during Phases I and II. The temperature cross sections, determined by Chen as deviations from the north-south mean at each pressure level, indicate that, when averaged for an entire phase and on the scales that can be resolved by the ship winds, the most rapidly ascending air is cool relative to its surroundings in the latitude band from 5-12°N.

Comparisons of GATE temperature and humidity soundings with those in the western oceans indicate that the A/B ship array is a more stable region, largely as a result of lower specific humidities that can likely be attributed to cooler sea-surface temperatures in the eastern Atlantic (e.g., Thompson et al., 1979). The more stable environment in the GATE region helps to account for the observations of relatively low tops of the deep convective clouds and the frequent occurrence of multiple cloud decks during GATE.

The geostationary satellite, SMS-1, was launched shortly before the beginning of the field experiment and located approximately above 45°W in the central Atlantic, several thousand km to the east of the position occupied by the earlier geostationary satellites. For the first time, this satellite provided infrared images at 30-minute intervals throughout the daytime and nighttime hours. Analyses of the infrared images in the area bounded by 5°S,

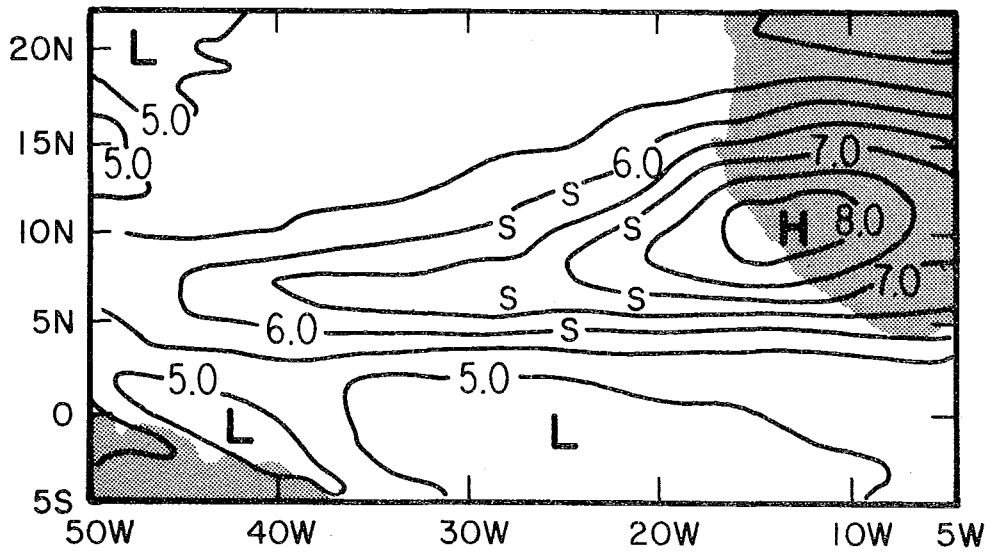

Fig. 4.7 Horizontal distribution of the mean IR values. S's denote the scheduled positions of GATE A/B ships.

50°W, 22°N, and 5°W and averaged for all days of GATE by Murakami (1979) reveal an east-west oriented zone of convectively generated high clouds that was located near 10°N (Fig. 4.7). This figure shows that convectively generated high clouds occurred most frequently near the southwest coast of West Africa and that the total amount and latitudinal extent of high cloudiness decreased considerably from east to west across the Atlantic. Woodley et al. (1980) used the same satellite data to estimate convective rainfall. Their computations show that almost all of the oceanic rainfall occurred in the region bounded by the 26°C isotherm of sea-surface temperature and that there was a large decrease of rainfall to the west of the African coast. Comparisons of the rainfall estimates along four longitudes during each phase suggest that precipitation covered a wider latitudinal area during Phase III than the two earlier phases (Fig. 4.8).

In the region between the surface col and the coast of Africa, pre-GATE satellite studies indicated that the major cloudiness occurs in the westerly flow on the south side of the surface confluence line (Sadler, 1975). Estoque and Douglas (1978) composited GATE observations of cloudiness and rainfall relative to the surface confluence line during those situations when the satellite-observed clouds were oriented in long east-west lines. They found that the maxima of cloudiness and gage measured precipitation were about 100 km to the south of the confluence line. Between 5 and 20°N over Africa, where the surface flow is dominated by the southwest monsoon during the summer months, the area of maximum rainfall is near 10°N, about 1000 km to the south of the northern limit of the monsoon flow.

This brief review of the mean state in western Africa and the ITCZ region of the eastern Atlantic indicates that this part of the GATE area has several unique features that are not observed elsewhere in the tropics. Among the more important features are the sizable temperature gradient at the surface over tropical northern Africa, the large horizontal and vertical shears of the mean zonal wind connected with the midtropospheric jet, the barotropic instability of the mean flow, and the greater stability of the lapse rate in the lower troposphere of the eastern Atlantic in comparison

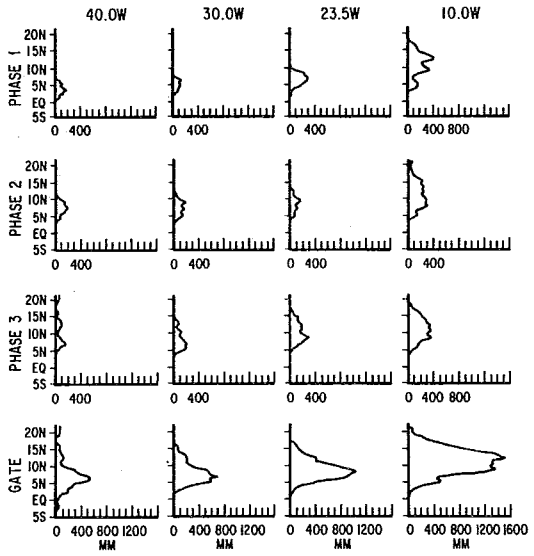

Fig. 4.8 Longitudinal slices of satellite rainfall between 5°S and 22°N over four locations for each phase and all GATE.

with western ocean regions. Some of these features, as will be shown in later sections, have an effect on the structure of the African wave disturbances as well as the distribution, intensity, and amount of deep convection associated with these disturbances.

4.2.2 Structure and Properties of the Wave Disturbances

4.2.2.1 Review of Pre-GATE Knowledge

Piersig (1936), in his study of surface weather maps from 1881-1911, noticed that the disturbances regularly influence the surface wind field in the tradewind belt near the coast of West Africa. Since the cyclones occurred during the season of greatest frequency of hurricanes in the western Atlantic, he speculated that those hurricanes that had been tracked back to the Cape Verde Islands may have been initiated by the disturbances and, therefore, that the precursors of such hurricanes may actually have originated over Africa. Hubert (1939) recognized that the disturbances passed observing stations from the region near the Greenwich meridian to the West African coast at regular intervals of 3 or 4 days. He noted that the extrapolated track of one cyclone, that he followed with surface observations from 5°W to the African coast, could have been at the same location in the central Atlantic as the 1938 New England hurricane at the time that the hurricane was initially observed. On the basis of this extrapolation, he speculated that the storm had developed from a disturbance that originated over Africa.

While studying surface pressure maps in the Caribbean, Dunn (1940) noticed westward propagating isallobaric centers that appeared at intervals of 3 or 4 days. He hypothesized that these wavelike disturbances were the same as those described previously near the coast of West Africa by Piersig. The vertical structure of the waves in the Caribbean was investigated by Riehl (1945), who noted that the maximum pressure and wind amplitude occurred around 700 mb, that the trough regions were relatively cool in the lower troposphere, and that the moist layer was deeper to the

east of the trough. Later, Riehl (1954) summarized the typical structure of the disturbances in the Caribbean. He showed that the waves normally had a wavelength of 15-20° of longitude and a westward propagation speed of 6-7 m s^{-1} and that disturbed weather was most frequently observed on the east side of the trough.

At nearly the same time, Schove (1946) commented on the vertical structure of the waves over Africa and suggested that the wave troughs sloped eastward from the surface to 750-700 mb where the maximum amplitude occurred and then tilted westward with decreasing pressure. He stated that he initially observed many of the troughs as far east as the region around Khartoum and then was able to follow them as they travelled toward western Africa. Since the waves could be tracked across Africa during most of the rainy season, several investigators attempted to determine whether there were preferred regions of the waves for enhanced cloudiness and rainfall and for the development of the squall lines that were described by Hamilton and Archbold (1945) and Eldridge (1957). Gilchrist and Matthews (1960), in a study of rainfall at Nigerian stations, noted that thunderstorms and heavy rainfall were more likely during or just after the passage of the lower tropospheric trough than to the rear of a ridge. Regula (1936), Schove (1946), Gilchrist and Matthews (1961), and Okulaja (1970) concluded that squall lines sometimes occurred in the general vicinity of the wave troughs; however, they did not agree on the preferred location of the squall lines relative to the troughs. For example, Regula noted squalls to the east of the surface pressure trough along the west coast of Africa while Gilchrist and Matthews found that the squall lines in the Nigeria region were usually to the west of the synoptic-scale trough. Schove, on the other hand, stated that the stronger squalls were normally located near the midtropospheric wave troughs.

With the launch of the first weather satellites, it became possible to view the cloud patterns over the tropical Atlantic and thus to follow the wave disturbances routinely from Africa to the western Caribbean. Using satellite pictures and surface ship reports, Erickson (1963) showed that Hurricane Debbie of 1961 quite likely reached hurricane force only 1000 km west of Africa. He demonstrated unambiguously, with analyses of conventional land and ship observations, that the disturbance that developed into Debbie could be tracked eastward to at least 10°E. Later, Arnold (1966) showed that Hurricane Ana of 1961 also developed from a wave disturbance that originated over Africa. On the basis of time series analyses of upper air winds, he tracked several wave disturbances from 15°E to the coast of West Africa. West of that point, he used satellite photographs and infrared information to follow these disturbances across the Atlantic. Most of the waves that originated over Africa during his study reached the Caribbean and no additional wave disturbances developed over the ocean. Arnold speculated that changes in the satellite observed convective structure over the ocean might have been caused by a decrease in the amplitude of the waves between the eastern and central Atlantic and then an increase in wave strength near the Caribbean.

Frank (1969) noted that the waves had characteristic "inverted-V" cloud patterns on visible satellite images and that these cloud patterns could be used to track the waves across the Atlantic. The inverted-V was most frequently observed in the eastern and central Atlantic during the months of June, July, and August. In corroboration of Arnold's deductions from satellite analyses, Frank presented time series of upper air winds that showed that the African waves were much stronger near the west coast of Africa than in the eastern Caribbean.

NHC has compiled annual statistics of the disturbances and their role in generating Atlantic tropical cyclones since the summer of 1967 (e.g., Simpson et al., 1968). In their review of these annual summaries for six pre-GATE years from 1968-1973, Frank and Hebert (1974) indicate that, although the total number of Atlantic tropical cyclones varied considerably from year to year, the total number of easterly waves leaving Africa during each year remained essentially unchanged. For these years, therefore, there was no simple relationship between the number of waves and the occurrence of Atlantic tropical cyclogenesis. It was suggested by Carlson (1971), however, that anomalously cold sea-surface temperatures in the area, 10-20°N and 30-40°W, during August 1965 and August 1968 may explain the fact that fewer African disturbances became Atlantic tropical cyclones during those two summers than in the summers of 1966, 1967, and 1969 when sea-surface temperatures in that area were warmer.

More recently, the focus of research on the African waves has been aimed at understanding the structure, origin, and energetics of the waves. Carlson (1969a) was the first to examine these subjects with his analyses of the conventional surface and upper air observations from Africa for a two-week period in August and September 1967 when there were six strong wave disturbances, three of which ultimately became Atlantic hurricanes. Later, Carlson (1969b) investigated the structure of 33 wave disturbances that travelled across central and western tropical Africa in a 3 1/2 month period that began in July 1968. While average patterns of rainfall relative to the waves had not been clearly specified before GATE, Carlson (1969b) and Burpee (1974) determined that the maximum cloud cover and precipitation occurred near the 700-mb wave trough at 10-15°N and east of the trough farther to the north. This pattern was corroborated by Dhonneur et al. (1973), who studied two relatively strong waves that became tropical distubances just offshore from the coast of Senegal. In both cases the rain and cloud maxima were slightly to the east of the trough in the surface pressure field. In his surface analyses, Carlson (1969b) found that there were two separate cyclonic centers with many of the disturbances. The northernmost center was typically near 20°N and appeared to be thermally induced while the second center was located about 10-12°N in the area of the convective cloud maximum. The disturbances reached their maximum amplitude at longitudes of 10-20°W and the majority weakened as they propagated westward from that region toward the Caribbean.

The large spacing between observing stations over tropical Africa and the Atlantic limited investigations of the vertical structure of the wave disturbances to analyses of time series at a few locations. Burpee (1972) used spectral analysis to show that the wave features sloped eastward from the surface to about 700 mb, approximately the level of the strongest midtropospheric winds, and then sloped toward the west in agreement with the earlier statements by Schove (1946). Composites of upper air observations from Dakar indicated that the maximum temperature variations occurred near 850 mb, with warmest temperatures in the northerly flow to the west of the wave trough. The highest relative humidities, however, were observed to the east of the trough where the winds associated with the wave disturbances were typically from the south (Burpee, 1974). Thus, these findings indicate that temperature and moisture advections in the lower troposphere are nearly out of phase.

For the most part, detailed information on the structure of the waves in the oceanic region was not available before GATE; however, Carlson and Prospero (1972) used upper air observations from western Africa, the Cape Verde Islands, and the eastern Caribbean along with special data from the

Barbados Oceanographic and Meteorological Experiment to examine the atmospheric structure in the middle troposphere. In the region from 850-600 mb, they observed a layer of hot, dry dust-laden air that had a nearly dry adiabatic lapse rate. They showed that this air originated over Africa and referred to it as the Saharan Air Layer. This layer of air was typically most pronounced in the ridge region between the troughs of successive African waves, where the stable base of the Saharan Air Layer acted to suppress deep convection in the tradewinds of the tropical North Atlantic.

One hypothesis for the initiation of the waves was offered by Carlson (1969b), who found that about half of the waves that he tracked during the summer of 1968 originated somewhere to the east of his data network (18°E) and that about 20% were initially observed near the Cameroon Moutains (10-12°E). On the basis of this information, he suggested that the generating mechanism for the waves might be related to convective processes over the elevated terrain of Cameroon and other mountain ranges to the east of 18°E in the Sudan and Ethiopia. Frank (1970), on the other hand, implied that the waves might form as a result of the mechanical effect of the easterly flow of air over the mountains of Ethiopia, although from a dynamical viewpoint, an easterly flow of air over a mountain barrier should be damped on the lee side and consequently not produce wave oscillations (e.g., Holton, 1979, p. 91). These suggestions were based on speculation, however, rather than on direct observations in the region where the waves formed. While Schove (1946) and Okulaja (1970) stated that the waves could be tracked eastward from western Africa to a region around 30°E, they did not systematically document a source region for the waves.

To specify the source region more precisely, Burpee (1972) computed spectral analyses of the meridional wind component at several stations with observations from the summers of 1960-1964. The results of these calculations suggest that the wave disturbances typically originate between Ft. Lamy (15°E) and Khartoum (32°E) since the meridional wind spectra in the middle troposphere at both Khartoum and Aden (45°E) did not show significant peaks at the periods corresponding to the wave disturbances. Later, Dean and LaSeur (1974) tracked 18 synoptic-scale waves during August 1958 and claimed that they could initially identify the waves near Sudan. Evidence that a few waves may occasionally develop as far east as Aden was provided by Aspliden (1974) in time cross sections from September 1954.

With the source region specified, Burpee (1971) noted that the mean zonal flow in the middle troposphere is barotropically unstable above the surface baroclinic zone to the south of the Sahara during the same months and in the same latitude band that the disturbances are observed. Subsequently, Burpee (1972) showed that the midtropospheric easterly current over Africa also satisfies the Charney-Stern (1962) criterion for the instability of an internal jet. His calculations based on the Charney-Stern theory suggest that both the horizontal and vertical shears of the mean flow are unstable and, therefore, that the wave disturbances grow as the result of the combined barotropic and baroclinic instability of the midtropospheric easterly flow.

4.2.2.2 General Wave Description during GATE

The synoptic-scale wave disturbances were tracked across central and western Africa and the eastern Atlantic by Burpee and Dugdale (1975), Reed et al. (1977), and Sadler and Oda (1978, 1979, 1980) while McBride and Gray (1978), Thompson et al. (1979), and Chen (1980) followed the wave features across the A/B ship array. The waves appeared to propagate westward with little or no interruption throughout the experiment. The average

period, wavelength, and speed of westward propagation were 3.5 days, 2500 km, and 7-8 m s^{-1}, respectively: values that are consistent with those found in earlier years. Reed et al. (1977) indicated than the wavelength and period were slightly longer over the African continent than in the eastern Atlantic during Phase III, but the wave speed was about the same in both regions. The waves appeared to strengthen most rapidly over Africa in the longitude band between 10°E and the Greenwich meridian (Albignat and Reed, 1980), to affect a greater vertical depth of the atmosphere as they cross Africa, and to modulate the cloudiness and precipitation increasingly as the experiment progressed from Phase I to Phase III (Burpee and Dugdale, 1975; Viltard and de Felice, 1979).

4.2.2.3 Horizontal and Vertical Structure of the Waves in Western Africa and the Eastern Atlantic

Several studies that investigated the structure of the waves concentrated on Phase III when the easterly wave disturbances were particularly well developed and in the longitude band from 10°E - 31°W where observations were most numerous. During Phase III and the preceding interphase period, Reed et al. (1977) tracked the vorticity centers of eight wave disturbances across this region. They determined the average structure by compositing the observations relative to the 700-mb vorticity center at the mean latitude of the disturbance paths, called the reference latitude, which was about 11°N over the continent and 12°N over the ocean. Each wave was divided into eight east-west categories on the basis of the location of wave features at the reference latitude, in a manner similar to that used earlier by Reed and Recker (1971), and all available observations were averaged in 4° latitude bands for each category. At the reference latitude, they defined category 4 as the 700-mb trough, category 8 as the 700-mb ridge and categories 2 and 6 as the maximum northerly and southerly wind components, respectively. The intermediate regions of the waves were designated by categories 1, 3, 5, and 7. Since the average wavelength of these eight waves was about 2500 km, each wave category corresponds to an east-west distance of about 300 km or 3 degrees of longitude. In general, Reed et al. found that the differences in wave structure between the land and ocean regions were relatively minor so they presented results that were averaged for the entire region from 10°E - 31°W. The composited streamline fields with the mean flow removed are shown for the surface, 850, 700, and 200 mb in Fig. 4.9. The perturbation wind fields in the middle and lower troposphere depict a cyclonic and anticyclonic center near the reference latitude with the circulation centers at 850 and 700 mb almost vertically above the surface centers; but, north of the reference latitude near 15-20°N, the perturbation slopes toward the east between the surface and 700 mb as described in earlier studies. On the equatorward side of these centers, the trough and ridge axes of the composite wave slope from southwest to northeast. There is some suggestion of a second surface vorticity center about 1000 km north of the main center of cyclonic circulation that is approximately in the location of the thermal low that was first pointed out by Carlson (1969b). At 200 mb, the low-level circulation centers are replaced by a region of strong diffluence to the west of the 700-mb trough and strong confluence to the west of the 700-mb ridge.

Vertical cross sections of the composite wave structure are shown in Figs. 4.10 and 4.11 at the reference latitude. The meridional wind (Fig. 4.10a) has a maximum amplitude of about 5 m s^{-1} near 700 mb, a slightly larger value than that found by Burpee (1975b) in an analysis of the waves for the entire GATE period. At the reference latitude, the wave features are nearly vertical below 700 mb, but tilt toward the west above this level.

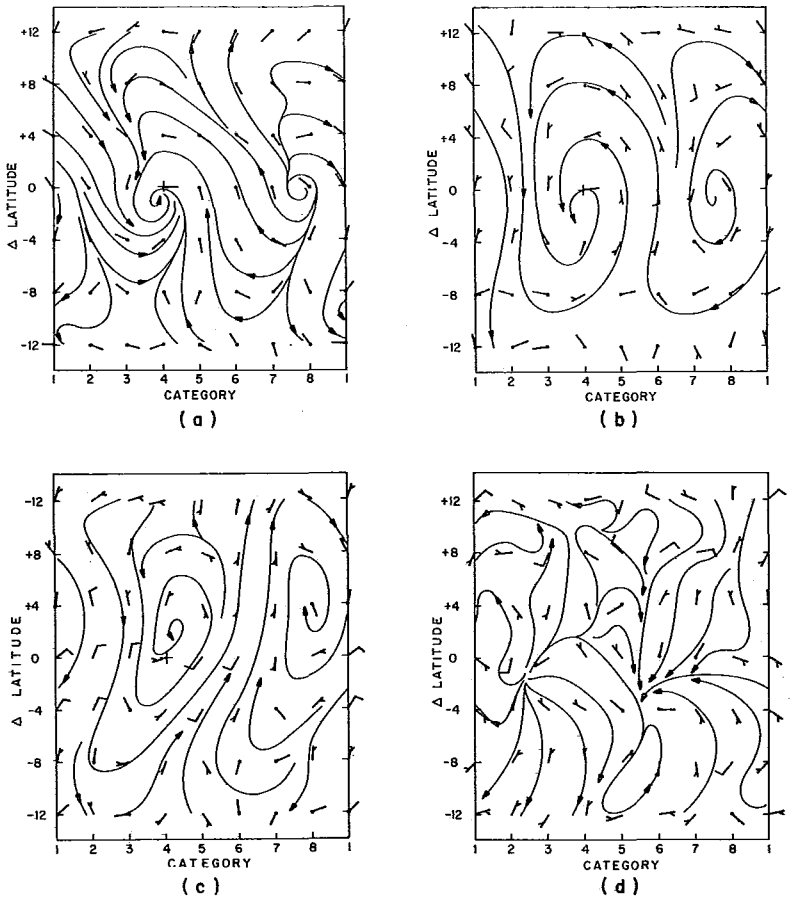

Fig. 4.9 Streamlines for perturbed wind field. (a) Surface, (b) 850 mb, (c) 700 mb. See Fig. 4.3 for further description.

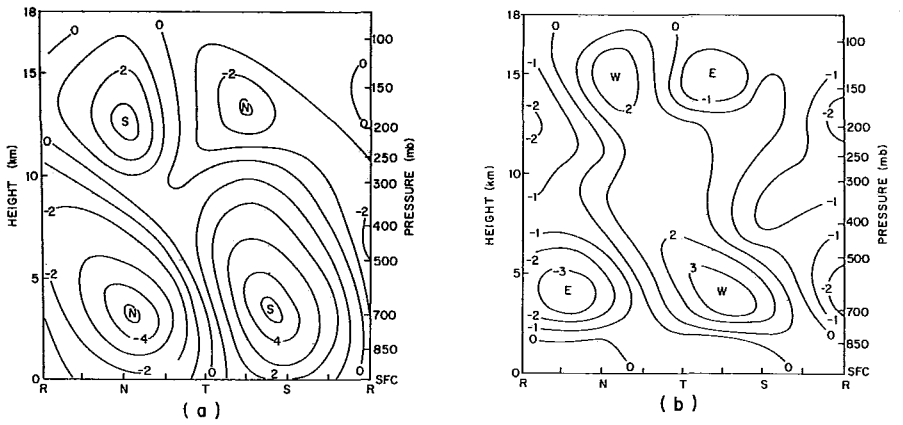

Fig. 4.10 Vertical cross sections along reference latitude. R,N,T,S refer to ridge, north wind, trough, south wind sectors of the wave. (a) Meridional wind deviation (m s^{-1}); (b) zonal wind deviation (m s^{-1}). (Fig. 4.10 continued , next page.)

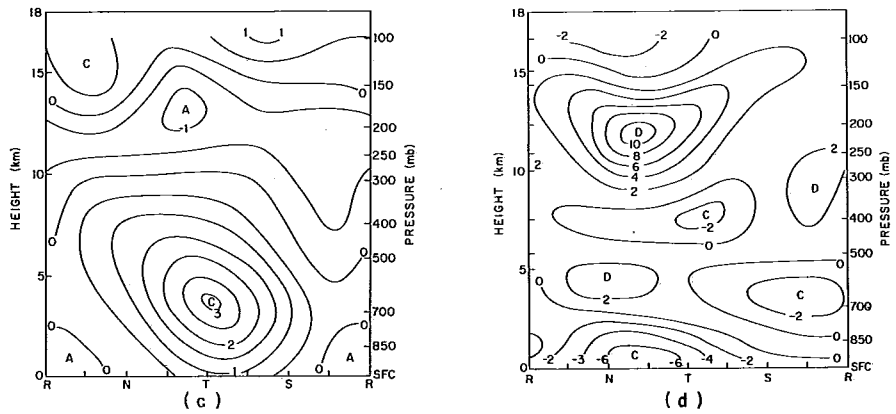

Fig. 4.10 (contd.) (c) vorticity (10^{-5} s^{-1}); (d) divergence (10^{-6} s^{-1}).

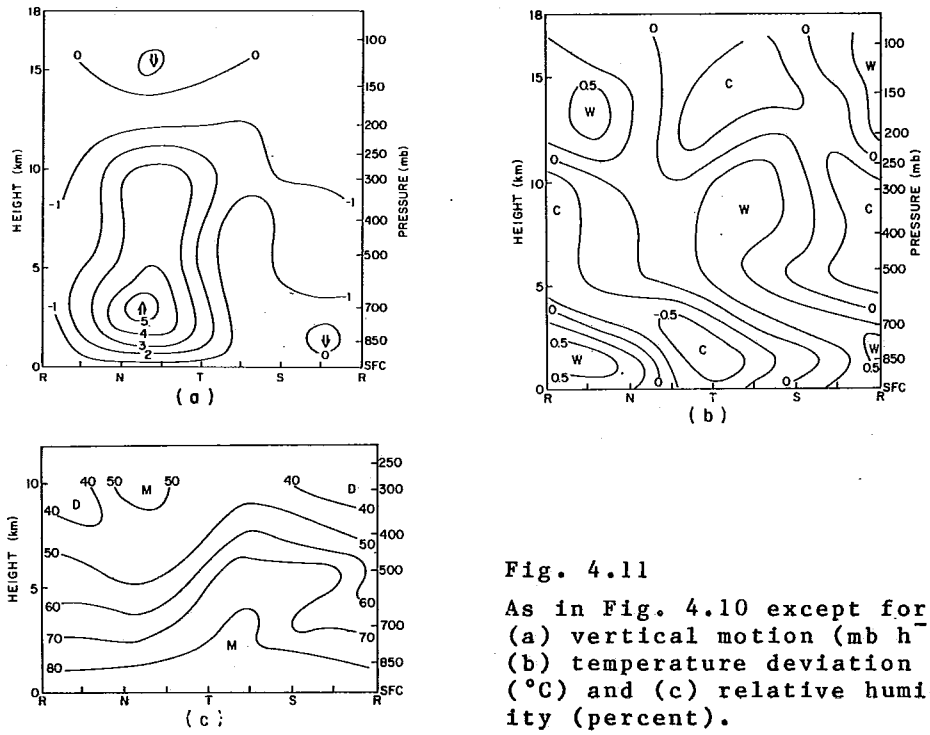

Fig. 4.11

As in Fig. 4.10 except for (a) vertical motion (mb h^{-1}), (b) temperature deviation (°C) and (c) relative humidity (percent).

Near 200 mb, there is a secondary maximum amplitude of 2 m s^{-1} that is nearly out of phase with the wave features at 700 mb. The zonal wind (Fig. 4.10b) is also modulated by the waves; however, at pressure levels between the surface and 350 mb, the amplitude of these fluctuations is less than those of the meridional wind. In general, westerly winds are positively correlated with southerly winds near the reference latitude. The relative vorticity cross section shows a cyclonic maximum near 650 mb at the wave trough (Fig. 4.10c). Since the reference latitude is located on the cyclonic shear side of the midtropospheric easterly jet, cyclonic vorticity is evident everywhere in the lower and middle troposphere except for the region near the ridge. At pressure levels from 300-150 mb, the reference latitude is north of the upper level easterly jet, and consequently, negative relative vorticity is shown in all wave categories.

In the cross section of divergence (Fig. 4.10d), there is a strong convergence near the surface between the northerly wind maximum and the trough. The largest values of divergence occur vertically above this region of the wave in the upper troposphere. In the middle troposphere there are two additional centers of convergence and divergence. This pattern of divergence is considerably more complicated than that observed in the western Pacific (e.g., Reed and Recker, 1971) and may be unique to the region near the midtropospheric easterly jet in western African and the eastern Atlantic. The largest value of upward motion is about 5 mb h^{-1} and is located to the west of the trough near 700 mb (Fig. 4.11a). The temperature anomalies (Fig. 4.11b) show a cold core below 700 mb in the trough that is overlain by a warm anomaly in the middle troposphere. A second area of cold anomalies occurs near 150 mb. The vertical cross section of moisture at the reference latitude (Fig. 4.11c) shows that from the surface to 400 mb the highest relative humidities are located in the same region as the southerly winds and the lowest humidities are observed where there are northerlies. Near 300 mb the pattern is reversed so that the largest values of humidity are above the region that is relatively dry at lower levels.

4.2.2.4 Detailed Wave Structure in the A/B Ship Array

The structure of the waves has been investigated in the ship array during Phase III by Nitta (1978) and Thompson *et al.* (1979), for part of Phase II by Rodenhuis *et al.* (1980), and for all three phases by Chen (1980) and McBride and Gray (1978). These studies have used composite analyses that are defined by the 700-mb meridional wind at the center of the ship array (8.5°N) rather than the reference latitude (about 12°N in the eastern Atlantic), but otherwise follow the method of Reed *et al.* (1977). Three slightly different techniques for determining the wave chronology at the center of the ship array have been used. Nitta (1978), Thompson *et al.* (1979) and Rodenhuis *et al.* (1980) computed quantities at the center of the array on the basis of a least squares regression fit to the surface and upper air ship observations. In the case of Nitta, the regression equation was quadratic in space while Thompson *et al.* and Rodenhuis *et al.* (the analyses of the latter authors are based on the meridional wind computations of Reeves *et al.*, 1979) used regression equations that were quadratic in space and linear in time. Chen (1980), on the other hand, adopted the wave chronology of Thompson *et al.* for Phase III, but determined the wave categories for Phases I and II on the basis of an objective analysis of band-pass filtered, 700-mb meridional winds at each ship. Using a different approach, McBride and Gray (1978) defined the passage of a trough or ridge as the time of the maximum or minimum value of $\partial v/\partial x$ as determined by the 700 mb A/B ship observations at the center of the array.

In general, the vertical cross sections determined by Thompson et al. and Chen at the center of the ship array for Phase III are quite similar to those determined at the reference latitude in the combined land-ocean composite of Reed et al. (1977) and shown previously in Figs 4.10 and 4.11. In particular, the deviations of the meridional and zonal winds from their means at each level and the relative vorticity and the divergence are very much alike, although the amplitude of the zonal wind is larger in the ship array (not shown). The cross section of vertical motion from Thompson et al. (Fig. 4.12a), however, has some slight differences from that presented for the land-ocean composite since ascent occurs at all wave categories in the lower and middle troposphere. The maximum ascent is at low levels (800-700 mb) just to the west of the trough while there is a secondary maximum near 350 mb, close to the level where Reed and Recker (1971) found the primary maximum in the western Pacific. The only region of descent is in the upper troposphere above the low-level ridge.

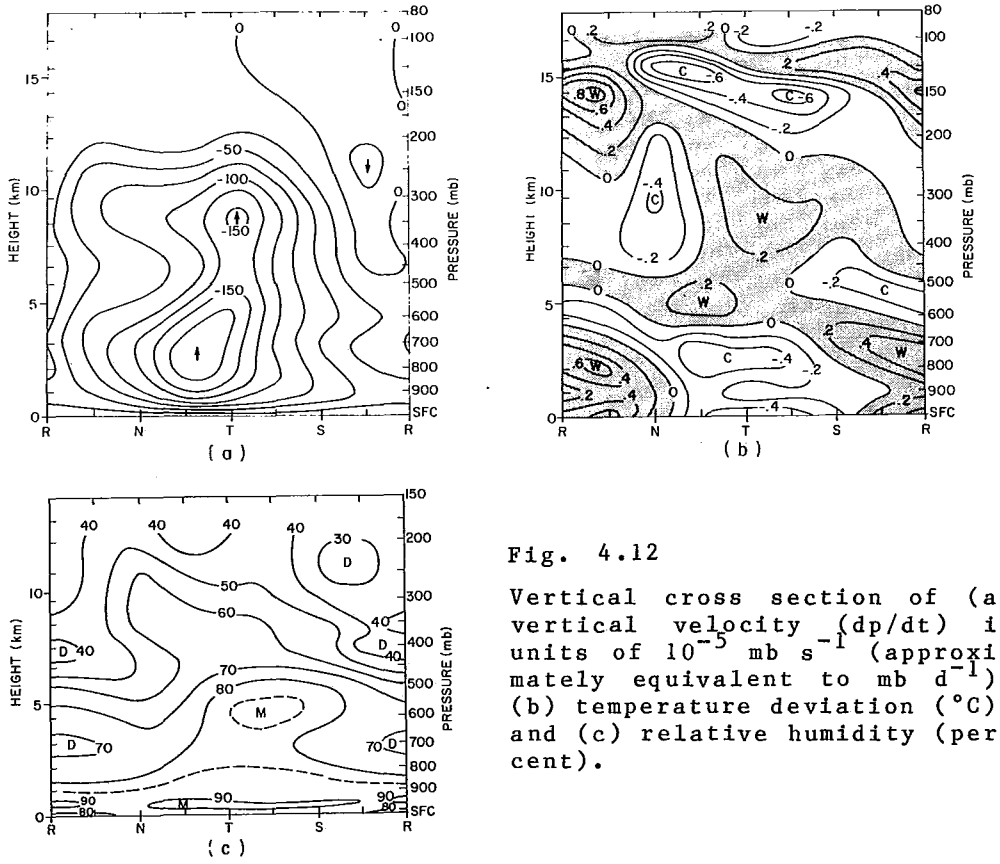

Fig. 4.12

Vertical cross section of (a) vertical velocity (dp/dt) in units of 10^{-5} mb s^{-1} (approximately equivalent to mb d^{-1}), (b) temperature deviation (°C), and (c) relative humidity (percent).

Temperature deviations from the mean at each level (Fig. 4.12b) are very small in the ship array and have a rather complicated pattern that is similar to the land-ocean composite except for an additional warm and cold anomaly near 600-500 mb. Below 700 mb, the cold anomalies occur in the trough and the warm anomalies in the ridge. The low-level cooling in the trough is in the convectively active region of the wave and may be the result of evaporational cooling, a process suggested by Riehl (1954) to explain a similar structure in easterly waves in the Caribbean. The warm anomaly above the trough at 400-300 mb is probably a result of condensation heating by convective clouds.

The relative humidity cross section (Fig. 4.12c) has generally higher values than that shown for the land-ocean composite of Reed et al. (1977), a finding that is consistent with the fact that the ships were located in a convectively active region that typically had ascending motion throughout the troposphere. The highest humidity values are near and to the east of the trough, slightly to the east of the maximum region of ascent. Such a displacement is consistent with relative air motion from west to east at the center of the ship array, an air flow that results from the fact that the wave moves faster than the easterly current at this latitude (Thompson et al., 1979).

Using objectively analyzed data from the ship array, Chen (1980) has compared composites of several variables relative to the waves during Phase III with those of the earlier two phases. He has determined many details of the wave structure; however, only a limited presentation of his results is possible. Figure 4.13 shows the vertical structure of the meridional wind that he determined for each phase. This figure indicates that the 700-mb meridional wind amplitude was 4.5 m s^{-1} in Phase I and 3.5 and 5.2 m s^{-1}, respectively, in the last two phases. At the ocean surface, however, he found that the corresponding meridional winds were 0.5, 2.0, and 2.0 m s^{-1}. Thus, the coupling between the meridional wind at 700 mb and the surface was rather weak during Phase I. The figure also indicates that the meridional wind features in the upper troposphere were nearly out of phase with the lower and middle troposphere during Phases II and III and that, in general, meridional wind oscillations associated with the waves were not as well defined in Phase II as in the other two phases. Most of the other variables presented by Chen also show less organization by the waves in the ship array during Phase II.

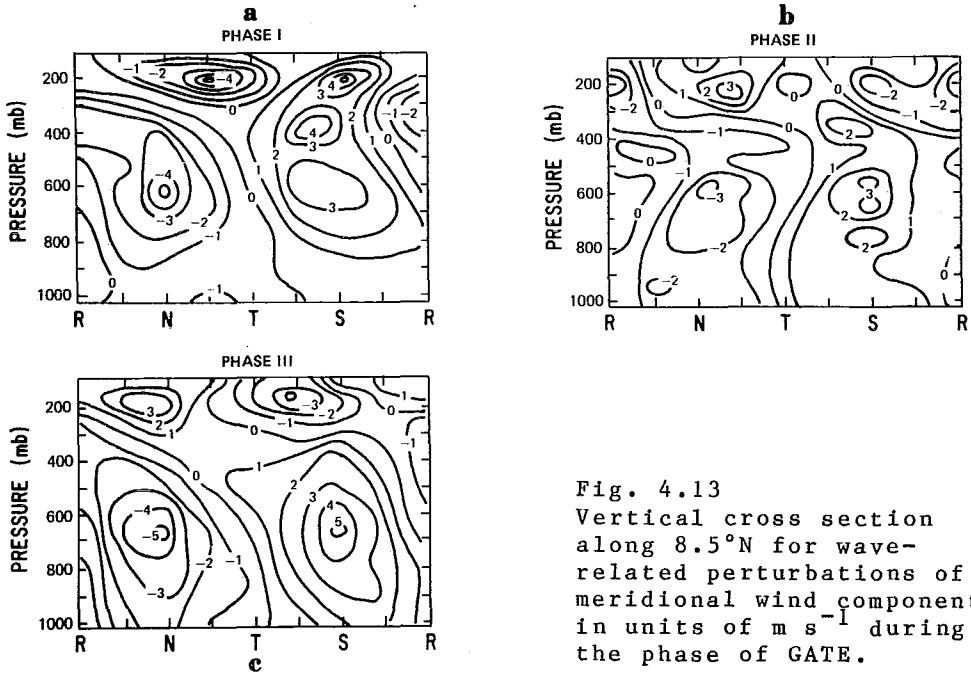

Fig. 4.13
Vertical cross section along 8.5°N for wave-related perturbations of meridional wind component in units of m s^{-1} during the phase of GATE.

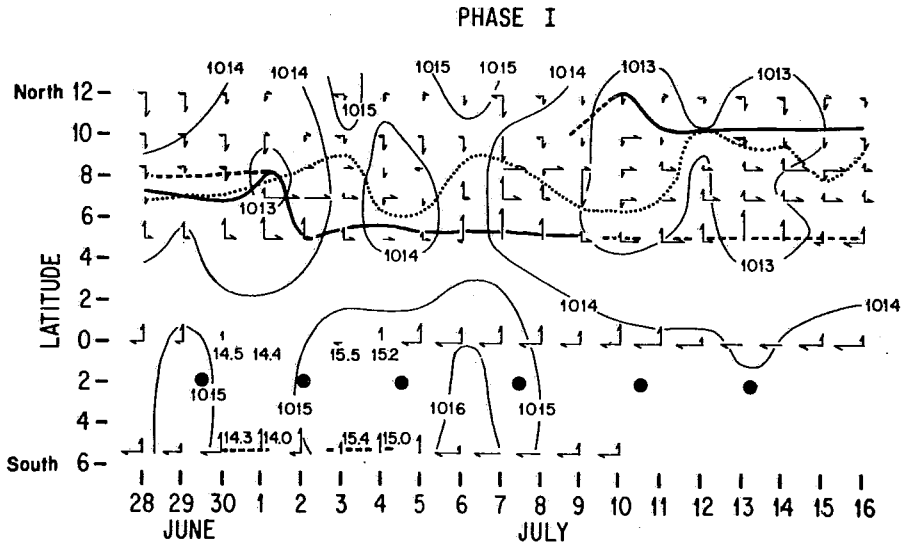

Fig. 4.14 Changes in mean daily surface pressure (thin solid lines) and zonal and meridional wind components along 23.5°W during Phase I. Major features: main equatorial trough line (heavy solid line), secondary trough line (dashed line), and the axis of meridional wind confluence (dotted line). Solid dots show times of passage of easterly wave troughs at 700 mb.

Changes in surface pressure that are related in part to the passage of easterly waves have been analyzed for three phases of GATE by Romanov and Romanova (1980) using hourly observations for ships stationed along 23.5°W. Their time series of surface pressures and wind, a portion of which is reproduced in Fig. 4.14, show that the minimum surface pressure associated with the ITCZ was located near 5-7°N during July, 10-12°N in the first half of August and 8-10°N during the middle of September. In addition to the seasonal north-south displacement of the pressure trough, the time series reveal several minima of surface pressure, called depressions by Romanov and Romanova, that occurred with most of the 700 mb easterly wave troughs tracked by Burpee and Dugdale (1975). The stronger depressions had closed cyclonic wind circulations at the surface that tended to tilt the surface convergence field and the pressure trough from southwest of northeast. In early July, when the centers of the depressions were located closer to the equator than during the rest of the GATE period, the analyses indicate that the depressions produced enhanced areas of disturbed weather near 5°S.

Petrossiants et al. (1975) found evidence of a 4 day periodicity in surface pressures and winds during Phases I and II from spectral analysis of data from USSR ships. They attribute the periodicity to Yanai-Maruyama waves, though African waves would seem to be a more likely explanation.

4.2.3 Relation of Convective Activity and Precipitation to the Waves

4.2.3.1 Introduction

Early in the field phase of GATE it became apparent to the forecasters stationed at the operational center in Dakar that the intensity, amount and latitude of convective activity in the B-scale area were related to the passage of the easterly waves (Burpee, 1975). This finding proved of considerable help in planning aircraft missions, since the waves could be tracked in a more or less regular and predictable fashion from West Africa to

the vicinity of the ship network and beyond. Burpee and Dugdale (1975) in their early summary of the weather systems affecting the GATE area succinctly stated the relationship as follows: "Generally the convection was most intense just before or at the time of trough passage at 700 mb, and the least amount of convection occurred about one day after the trough passed. In addition convective activity occurred farther north in the trough than in the ridge."

An example of cloud and precipitation patterns associated with the passage of a synoptic wave disturbance through the ship array appears in Figs. 4.15 and 4.16, taken from Mower et al. (1979). Fig. 4.15 depicts the cloud pattern as viewed by the SMS-1 satellite in visible imagery. Fig. 4.16 shows the radar echoes with 700-mb streamlines superimposed. The axis of the wave trough at 700 mb is also seen in Fig. 4.16 running from 5°N, 23.5°W to 10°N, 20°W. It is apparent from the cloud pattern in Fig. 4.15 and the precipitation pattern in Fig. 4.16 that the main convective activity does indeed occur near and somewhat in advance of the wave trough. Large areas of suppressed convection are found near 10°W and 30°W. These areas lie within or near the wave ridges. To the east and west of the relatively cloud-free areas are additional large clusters of convective activity marking the positions of the adjacent upstream and downstream wave troughs.

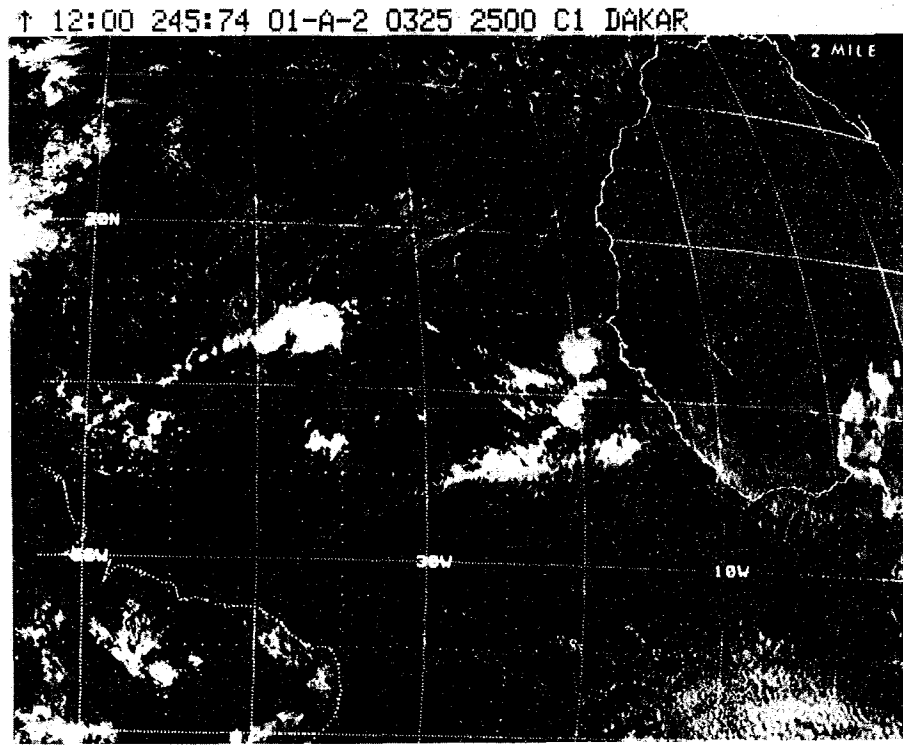

Fig. 4.15 Visible SMS-1 satellite image for 1200Z, 2 September 1974.

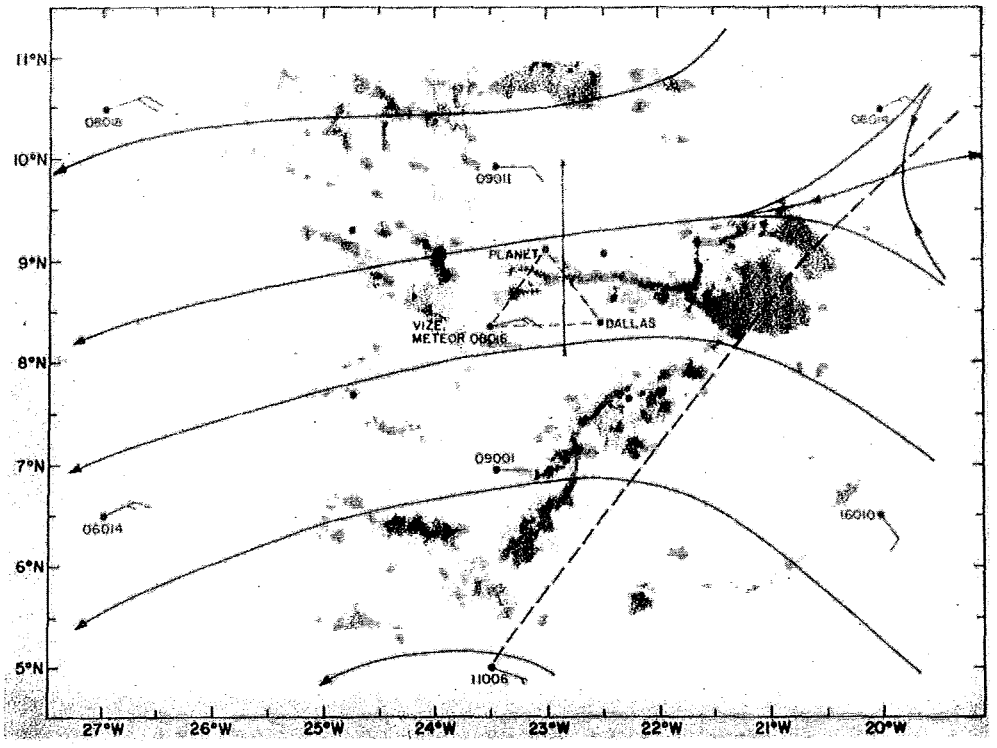

Fig. 4.16 700-mb streamline analysis superimposed on composite radar echoes from the Oceanographer, Gillis and Quadra for 1200Z. The gray shades correspond to rainfall rates of 0.05, 2.0 and 14.0 mm h^{-1}. The vertical line denotes the aircraft tracks during 1130 to 1500Z. The C-scale ship triangle is indicated.

As described by Sadler (1975), the extreme modulation of convection over West Africa and the Atlantic by the synoptic-scale disturbances, illustrated in this example, is characteristic of the August-September period only. During GATE such pronounced patterns were observed mainly during Phase III.

Mower et al. (1979) distinguished two main features in the convective pattern - a broad convective band extending into the wave trough from the ITCZ and long, narrow lines of convection oriented WNW-ESE (seen between 9°N and 11°N and 21°W and 25°W in Fig. 4.15). Other examples of convective patterns in relation to larger scale disturbances appear in Burpee and Dugdale (1975), ISMG (1975), Dean and Smith (1977), Nitta (1977), Zipser and Gautier (1978), Dean (1978), Ogura et al. (1979), Leary (1979) and Cho et al. (1979). A perusal of these examples (and others) reveals that the cloud patterns in the waves are diverse and rapidly changing. It is not possible to construct a model of the cloud and precipitation patterns likely to be seen in a given case, as can be done for middle latitude cyclones. Only in a statistical or composite sense does a well-defined relationship exist. The remainder of this section will be devoted to summarizing the results of the various studies that have documented the relationship. Results obtained for a broad area encompassing West Africa and the eastern Atlantic will be summarized first. Then attention will be focused on the A/B-scale area which is particularly suitable for study because of the more extensive observing facilities that were available there.

4.2.3.2 Results for West Africa and the Eastern Atlantic

Payne and McGarry (1977) examined the relationship of satellite inferred convective activity to easterly waves in the region from the equator to 20°N and 10°E to 30°W. In their study they used SMS-infrared satellite images for Phase III and the preceding interphase period to determine subjectively the percentage of overlapping areas three degrees of latitude and longitude in size that were occupied by bright or white-appearing clouds. It was apparent that the bright clouds were of convective origin. The percentages, determined every 6 hours at intervals of 1° of latitude and longitude, were band pass filtered with respect to time to isolate the 3-4 day wave-related fluctuations, and maps of the filtered values were prepared at 6-hourly intervals. Corresponding 700-mb band-pass filtered winds were also computed and the fields analyzed.

Superposition of the cloud patterns on the wind analyses showed that in general the westward propagating waves were accompanied by regions of positive cloud anomalies in and ahead of the troughs and negative anomalies in and ahead of the ridges. To summarize their results, Payne and McGarry presented histograms of the position of centers of maximum and minimum cloud coverage with respect to the wave categories defined by Reed and Recker (1971) and described in section 4.2.2.3. The histograms are reproduced in Fig. 4.17. The top panel indicates that centers of maximum coverage occur mostly in categories 2-5, a sharp peak in the distribution appearing immediately ahead of the trough (category 4). Centers of minimum coverage (bottom panel) are found predominantly in categories 6-1, being centered in category 7, slightly in advance of the ridge (category 8).

Another depiction of the relationship for the West African and adjacent oceanic regions was obtained by Reed et al. (1977) who composited the raw, unfiltered satellite data of Payne and McGarry (1977) according to the scheme described in section 4.2.2.3. The result is shown in Fig. 4.18a. Again it is seen that the maximum convective activity occurs just in advance of the wave trough. It is also seen that the convection is greatest a degree or two south of the average latitude of the disturbance track, represented in the figure by the zero ordinate. The corresponding geographical latitude is approximately 10°N.

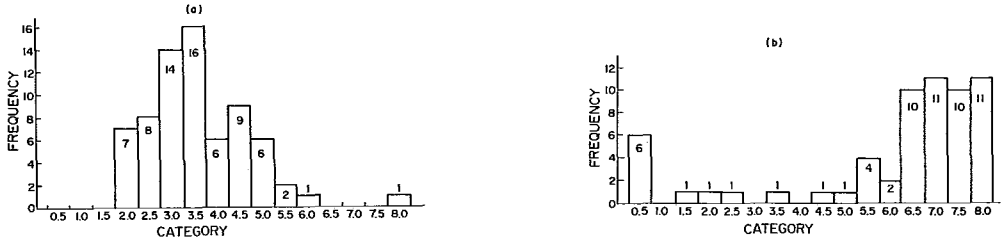

Fig. 4.17 Frequency distribution of maximum values of bandpass filtered category 2 cloud coverage [representing enhanced convective cloud coverage] (a) and minimum values [representing suppressed convective coverage] (b) versus wave phase category for each separate positive and negative region of coverage, respectively, during the 28-day period from 23 August - 19 September 1974.

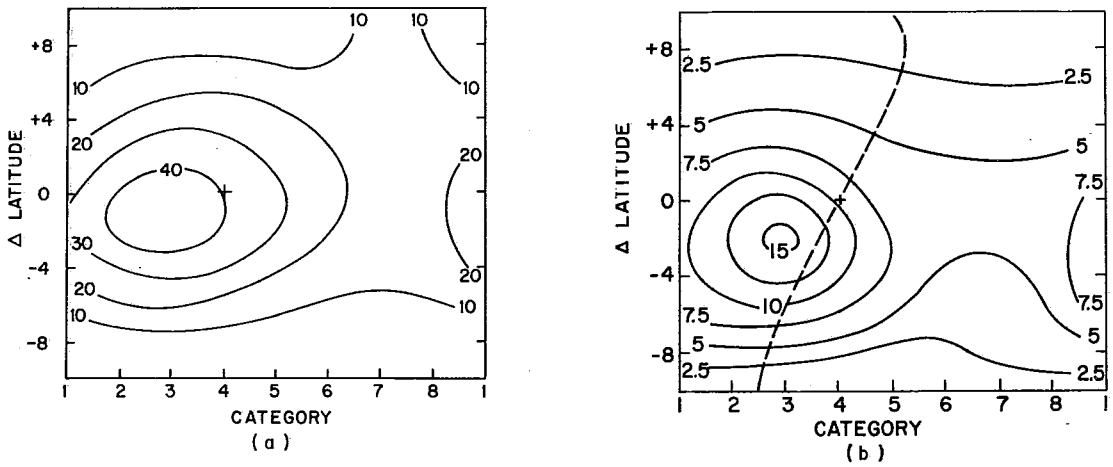

Fig. 4.18 (a) Percentage cover by convective cloud defined as white-appearing cloud in SMS-1 infrared images. (b) Average precipitation rate (mm d^{-1}). Dashed line depicts trough axis at 700 mb.

Shown at the bottom of the figure (Fig. 4.18b) is the average precipitation rate in mm d^{-1} in relation to the composite wave. The location of the trough axis at 700 mb (dashed line) has been added to the figure. The analysis, taken from Reed (1978), is based on 6 h precipitation amounts measured at the GATE A/B and B-scale ships during Phase III (Seguin and Sabol, 1976) and on daily totals for selected stations in Africa. The diagram is a revised version of a similar one appearing in Reed et al. (1977). The correspondence between the precipitation pattern and the convective cloud pattern is obvious.

Much of the precipitation over the African continent occurred in conjunction with the squall lines mentioned in the review of pre-GATE knowledge (section 4.2.1.1). Using SMS-1 satellite images, Aspliden et al. (1976) studied the genesis of the squall lines, including the relatively few that formed over the water, in relation to the wave position. Their results appear in Fig. 4.19. The number of interest here is the second value in each square. This gives the occurrence of squall line formation in the particular square during the three phases of GATE. The first value gives the number of cumulonimbus images on "explosion days", days defined as having an enhanced amount of convection over West Africa. Clearly the region a few hundred kilometers in advance of the wave axis is the preferred position for line formation.

A somewhat similar result was obtained by Payne and McGarry (1977) for 46 squall episodes in Phase III. Fig. 4.20 taken from their paper shows the frequency distribution of the location of the leading edge of squall lines at the beginning and termination of the episodes. Category 2, the region of northerly wind component ahead of the wave trough is the favored genesis region. Decay is most common in Category 1 in conformity with the well known fact that squall lines normally propagate westward at a greater speed than the waves.

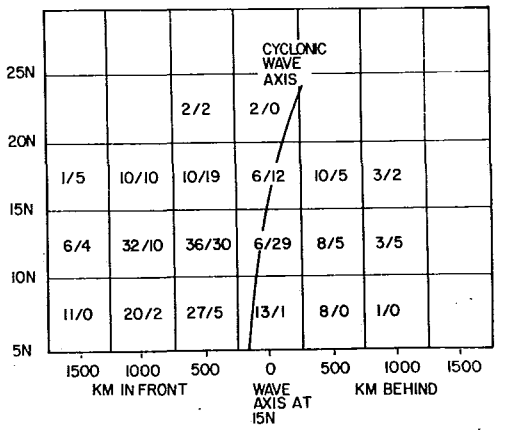

Fig. 4.19
Number of cumulonimbus images on explosion days only (first value) and disturbance lines generated (second value) in each 5° square in relation to the cyclonic axis at 700-mb low-level traveling waves for all three phases.

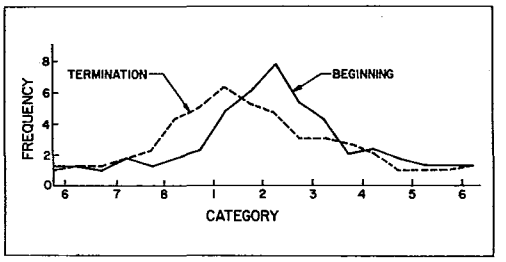

Fig. 4.20
Frequency distribution of the location of the leading edge of squall clusters versus wave phase category for 46 squall episodes at the beginning (solid line) and termination (dashed line) of each squall episode.

Payne and McGarry (1977) also investigated the behavior of non-squall cloud clusters with respect to the easterly waves observed during Phase III. A particularly striking result was obtained for the larger (maximum area 20° square), long-lived (lifetimes 24 hrs) clusters. Put simply, these clusters occurred most commonly in the region ahead of the trough axis and as a rule moved westward more slowly than the waves so that their preferred region of genesis was ahead of the axis and their preferred region of decay behind it (Fig. 4.21 a,b).

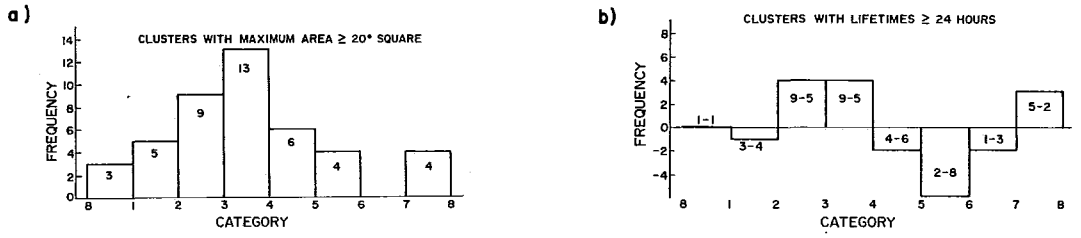

Fig. 4.21 Frequency distribution of (a) the mean location of the center of each cloud cluster versus wave phase category for all clusters with maximum area $\geq (20°)^2$ and (b) the excess (positive ordinate values) or depict (negative ordinate values) of cluster genesis over cluster decay by wave phase category for clusters with lifetimes $\geq$ 24 h.

4.2.3.3 Results for the A/B Scale Area

The day-by-day relation in the B-scale network of radar-derived precipitation (Hudlow and Patterson, 1979) to the wave induced variations in meridional wind component v and vertical velocity (= dp/dt) at 700 mb during Phase III is shown in Fig. 4.22 taken from Thompson et al. (1979). Wave troughs and ridges are denoted by T and R, respectively; N and S refer to regions of strongest northerly and southerly wind components. It is apparent from the figure that the heavy rain events generally occurred at or

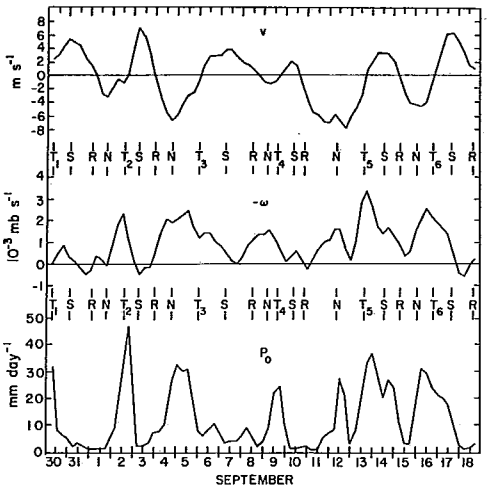

Fig. 4.22
Variations at the center of the B-scale network of the meridional wind component v and vertical velocity $-\omega$ at 700 mb and precipitation rate P_0 during Phase III.

Table 4.1 Lag correlation coefficients between 700-mb vertical p-velocity (ω) and percent convective cloud cover (C) and between vertical velocity and precipitation minus evaporation ($P_0 - E_0$) over the B-scale network during Phase III of GATE. Positive value of lag signifies number of hours that (ω) lags the other quantities.

	Lag (hours)						
	-18	-12	-6	0	6	12	18
C	-.21	-.51	-.71	-.58	-.31	-.08	-.02
P_0-E_0	-.05	-.25	-.56	-.68	-.47	-.18	-.07

before the time of the 700-mb trough passage and that they were well correlated with upward motion (negative ω) at 700 mb.

Precise values of the correlation, for different time lags, are given in Table 4.1 based on Thompson (1977). The surface evaporation has been subtracted from the precipitation but this has little effect on the results since the evaporation, as will be shown later, is relatively insensitive to the wave passage. From the table it is estimated that the precipitation lags the maximum upward motion by an hour or two on the average. Also shown in the table is the lag correlation of the vertical motion with convective cloud cover over the B-scale array. The cloud cover was determined from Payne and McGarry's (1977) data. The lag in this case is a few hours longer, indicating that the heaviest rainfall occurred somewhat prior to the time of maximum extent of bright or cold clouds. This finding is not surprising, since the cirrus canopies continue to expand and yield light precipitation after the most vigorous convection has ceased (Leary and Houze, 1979).

McGarry and Reed (1978), in studying the diurnal variation of rainfall over the GATE area, noted a strong preference for the wave-related precipitation in the vicinity of the A/B-scale area to occur in the late morning and afternoon hours (1200-1800 GMT). This preference can be seen from close scrutiny of Fig. 4.22. Why the diurnal variation should exert a

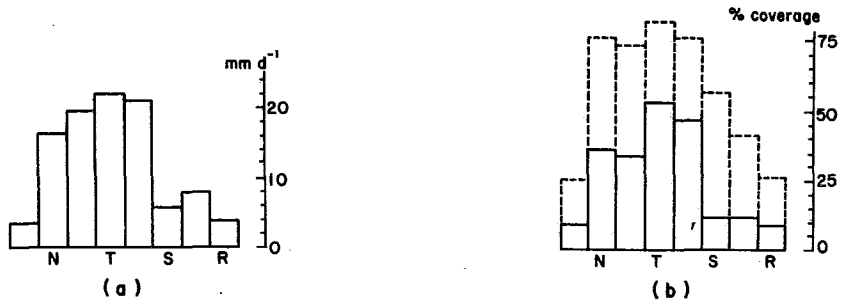

Fig. 4.23 Precipitation rate (a) and bright cloud amount (b) for B-scale area as function of wave position. Solid curve in (b) refers to bright or convective cloud only and dashed curve to sum of middle and high cloud amounts, as determined from SMS-1 IR photographs.

control on the wave-related precipitation over the ocean is a subject of continuing investigation.

When the time series of precipitation and convective cloud coverage for the B-scale area are composited according to wave category at the center of the area, the results shown in Fig. 4.23 are obtained (Thompson et al., 1979). This figure reveals again the tendency for the convective activity to be located in and ahead of the wave trough. The precipitation amount diminishes from about 20 mm d^{-1} to 4 mm d^{-1} in proceeding from trough to ridge, the decrease occurring suddenly with the onset of the strongest southerly winds. Conversely, the strong northerlies signal a sudden rise in the rainfall.

Johnson (1980) has utilized the satellite results depicted by the dashed curve in Fig. 4.23, in conjunction with ground-based cloud observations by Holle et al. (1979), to estimate the percentage of clouds with bases at low (< 2 km), middle (2-6 km) and high (> 6 km) levels as a function of wave category. His results appear in Table 4.2. It is seen that middle and high cloud have their greatest extent in the vicinity of the trough, while low clouds are most extensive in the region ahead of it.

Table 4.2 Percent coverage of clouds based at different levels.

Cloud type	WAVE CATEGORY							
	1	2	3	4	5	6	7	8
High	25	67	65	71	67	24	20	17
Middle	30	67	65	71	67	52	34	40
Low	18	64	50	44	32	36	28	22

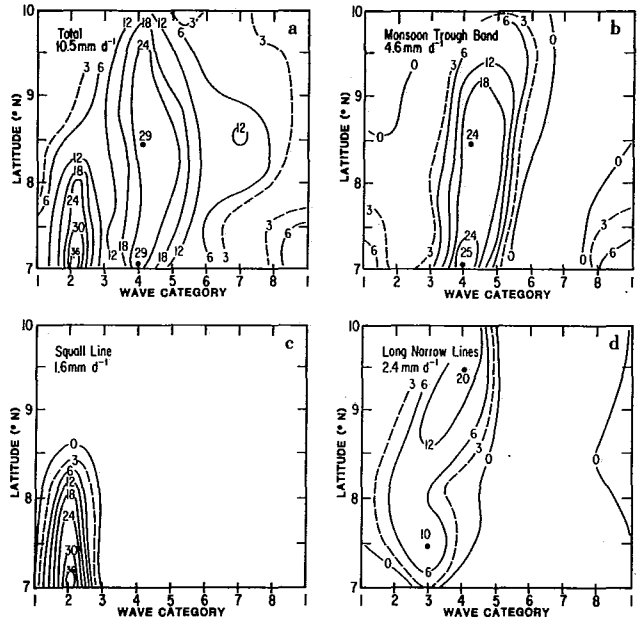

Fig. 4.24
Composites of radar precipitation analyses (mm d^{-1}) relative to wave categories for Phase III (a) total, (b) monsoon trough bands, (c) squall lines and (d) long narrow lines.

Marks (1981) (Fig. 4.24), with use of the radar rainfall data for a one-half degree longitudinal strip centered on 23°W, has obtained a finer depiction of the relation of precipitation to the waves during Phase III in which latitudinal variations are taken into account and the precipitation is partitioned according to the feature producing it. The features delineated are squall lines, monsoon trough bands and long, narrow lines. Examples of the latter two features were given earlier in Fig. 4.15. The total amount (Fig. 4.24a) shows a N-S extended maximum in the vicinity of the trough line (Category 4). The contribution of the monsoon trough bands is largest at the south end of the maximum. The long, narrow lines make their largest contribution at the north end and tend to produce greatest amounts somewhat ahead of the trough. The precipitation from squall lines was confined to the southern half of the B-scale network and was even further ahead of the wave trough. The position is close to that found by Payne and McGarry (1977) for the genesis region of the lines.

The results presented thus far have been for Phase III when, as remarked earlier, the wave disturbances were largest in amplitude, most regular in behavior, and always associated with a distinct pattern of convective activity. It remains to examine the relationship between the convection and the waves during the first two phases. Reeves et al. (1979) have investigated the relationships between convective precipitation and various aspects of the large-scale motions for all three phases in the B-scale area. Their results for the vertical motion at 700 mb, in the form of a time series based on data for overlapping 12 h periods centered every 6 h, are shown in Fig. 4.25. Except during parts of Phase II, a good relationship is obtained between the precipitation rate and vertical motion. However, they do not show a wave chronology. Hence, it is not possible from their diagram to know whether there is a one-to-one correspondence between the features they show and the easterly waves (except during Phase III when the features shown by them are identical to those in Fig. 4.22).

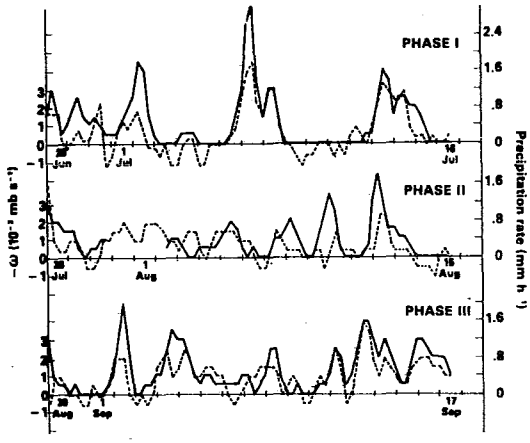

Fig. 4.25
Time series of 700 mb vertical velocity (dashed) and precipitation rate.

Chen's (1980) study, cited earlier, provides additional information on the earlier phases. According to Chen's wave chronology, well marked waves passed through the array on July 8, 11 and 15. From the results of Reeves et al. (Fig. 4.25) it appears that, at least in the B-scale area, only two of the waves were marked by enhanced convective activity in and ahead of the trough.

Despite discrepancies in individual cases, Chen was able to show a well defined statistical relationship between the waves and the precipitation rate during all three phases. His results appear in Fig. 4.26. The relationship during Phase III resembles that of Marks (1981) except for the minor minimum in the trough at 8°N. In Phase I the precipitation is small at and north of 10°N. Otherwise the relationship is similar to that for Phase III. Phase II displays a somewhat different pattern, as also pointed out by Rodenhuis et al. (1980). During this phase the pattern was displaced eastward by one-eighth wave length such that largest precipitation amounts occurred near the trough axis in the southern part of the network and east of the trough axis in the central and northern parts.

Chen (1980) explained the observed relationship in terms of two causative factors, the easterly waves and the confluence line associated with the ITCZ. He did not consider squall lines as a separate factor, as did Marks. During Phases I and II the precipitation remained near or south of the confluence line, the latter moving only slightly in response to wave passages. In Phase III the confluence line underwent larger north-south excursions and a substantial amount of rain fell to the north of it in the vicinity of the wave trough.

Murakami (1979) employed a different compositing scheme to determine the relationship between convective activity and the waves in the A/B-scale area for the three phases of GATE combined. Infrared brightness data from the SMS-1 satellite were used to define the wave categories and the vertical and meridional motions were composited with respect to the categories so defined. The vertical motions were found to correlate well with the deep convection, as in other studies, but the strongest upward motion and convective activity were associated with the region of maximum southerly winds at the surface rather than with the region in and ahead of the trough. It is hard to explain this latter result which, except for the above-mentioned anomalous pattern during Phase II, is unlike that obtained by any other GATE investigator.

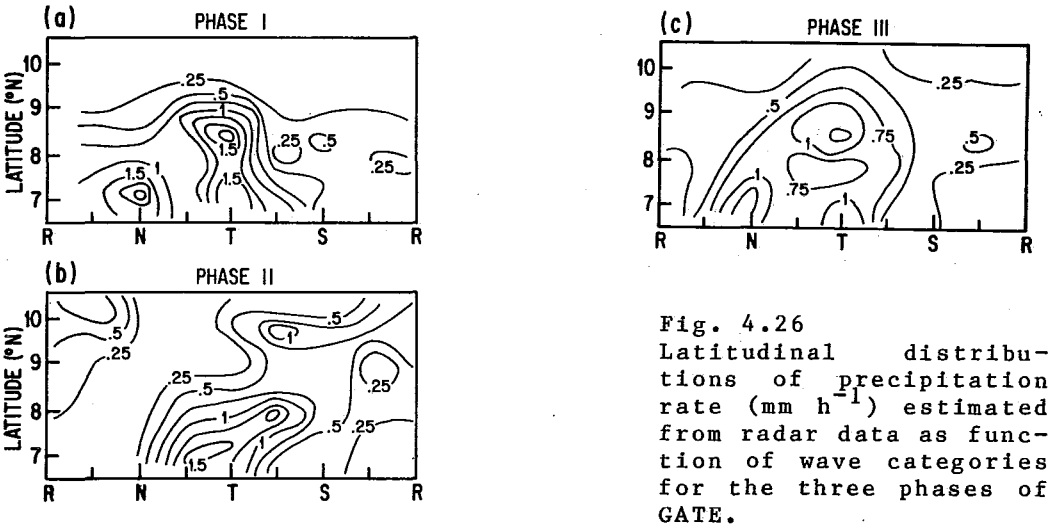

Fig. 4.26 Latitudinal distributions of precipitation rate (mm h^{-1}) estimated from radar data as function of wave categories for the three phases of GATE.

4.2.3.4 Cause of the Relationship

The foregoing results strongly support the view that the observed modulation of the convective activity by the waves is attributable to the associated variations in the large-scale fields of divergence and vertical motion. All studies in which large-scale vertical motions have been computed show them to be highly correlated with indicators of deep convection, for example, precipitation or satellite infrared brightness.

Table 4.3 Properties of undilute air parcels displaced upward from 1000 mb. LCL, lifting condensation level; LFC, level of free convection; LZB, level of zero buoyancy; NEG, energy needed to lift to LFC; POS, energy released above LFC.

WAVE CATEGORY	LCL (mb)	LFC (mb)	LZB (mb)	NEG (10^1 J kg^{-1})	POS (10^4 J kg^{-1})	NET (10^4 J kg^{-1})
1	951	937	182	-0.136	0.111	0.111
2	960	937	177	-0.356	0.119	0.119
3	964	937	197	-0.576	0.082	0.081
4 (trough)	964	922	202	-0.783	0.066	0.065
5	963	937	192	-0.372	0.070	0.070
6	960	932	187	-0.604	0.087	0.086
7	955	932	182	-0.391	0.098	0.097
8 (ridge)	956	947	182	-0.253	0.107	0.107
Mean	959	935	188	-0.434	0.092	0.092

That the variations in convective activity cannot be explained thermodynamically is made clear from the work of Thompson et al. (1979). Table 4.3, taken from their study, shows the energy needed to displace an undilute air parcel from 1000 mb to the lifting condensation level (LCL) and thence to the level of free convection (LFC) in various parts of their composite wave. Also shown is the energy released above the LFC and the net energy released. It is apparent that the LCL is lower and the LFC is higher in the trough, or convectively active region of the wave, than in the ridge and that more energy is required to lift parcels until they can freely rise in the trough than in the ridge. Also the net energy released is much smaller in the trough. Thus a nearly out-of-phase relationship exists between the convective activity and the thermodynamic instability, as seen on the large scale.

4.2.4 Vertical Transports and Budgets in Relation to the Waves

In this section we review the work that has been done in relating the vertical transports of heat, moisture and mass by subgrid-scale motions to the synoptic-scale wave disturbances and in determining the budgets of heat, moisture, vorticity and momentum in different parts of the waves. We consider first the turbulent fluxes at the ocean surface and the surface energy balance. Next the turbulent and convective fluxes in the atmospheric mixed layer and above are examined. Heat, moisture and static energy budgets for the atmospheric column between the surface and 100 mb derived from the flux measurements are then treated. Finally, results of studies of the vorticity and momentum budgets in the waves are summarized briefly.

4.2.4.1 Surface Energy Balance

Following Thompson et al. (1979), we write this in the form

$$R_o = S_o + LE_o + G, \qquad (4.1)$$

where R_o is the net radiation received at the surface, S_o the surface flux of sensible heat, LE_o the surface flux of latent heat ($L \equiv$ latent heat of condensation, $E_o \equiv$ evaporation rate) and G is the surface heat flow into the ocean. Thompson et al. (1979) measured, for Phase III only, the terms in the energy balance as a function of wave category, obtaining G as a residual. The radiation measurements were based on observations taken aboard four B-scale ships. Sensible and latent heat fluxes were determined by the bulk aerodynamic method with use of observations from the same ships. A revised version of their tabulated results is presented in Table 4.4.

From the table it is evident that, of the terms measured, the net radiation undergoes the largest variation with wave passage. Its magnitude is greatest in the vicinity of the ridge and least in and ahead of the trough. This feature undoubtedly can be attributed to the effect of cloud cover in modulating the amount of solar radiation reaching the surface. The latent heat flux also undergoes a variation, being less in and behind the ridge than in and behind the trough. This behavior can be traced to the lesser wind speeds in the former area than in the latter. The sensible heat flux is small but undergoes relatively large changes such that the flux is greater in the convectively active region of the wave than in the convectively suppressed region. The net effect of the foregoing variations is to extract heat from the ocean and in and ahead of the wave trough and to supply heat near the ridge. The net heat supply to the ocean is small.

Table 4.4 Surface energy budget for B-scale area, Phase III. Units: W m^{-2}. R_0 net radiation at the surface; LE_0, surface latent heat flux; S_0, surface sensible heat flux; G, heat flow into the ocean.

Wave Category	R_0 =	LE_0	$+S_0$	+G
1	174	79	6	89
2 (Northerly)	95	97	11	-13
3	55	108	15	-68
4 (Trough)	104	114	19	-29
5	121	121	18	-18
6 (Southerly)	123	122	13	-12
7	192	119	8	65
8 (Ridge)	170	95	7	68
MEAN	129	107	12	10

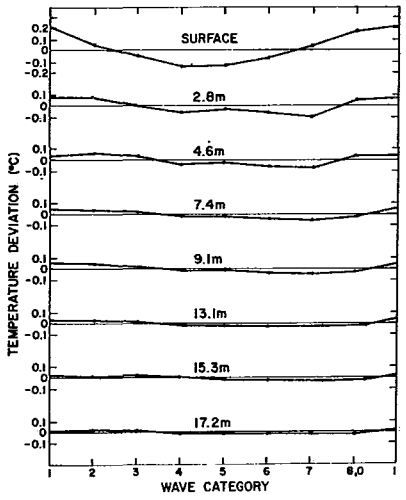

Fig. 4.27 Variation of temperature with wave category and depth.

Reed and Lewis (1979), with use of data from the buoy E3, located in the C-scale network at approximately 8°N, 23°W, have documented a variation of temperature in the upper layer of the ocean that is consistent with the variation of the surface heat flow G shown in Table 4.4. Fig. 4.27 from their paper shows that the sea-surface temperature is about 0.4°C cooler in the synoptic wave trough than in the ridge. The cooler temperatures extend to a depth of nearly 20 m, and the sub-surface cooling lags somewhat behind that at the surface.

4.2.4.2 Turbulent and Convective Heat and Moisture Fluxes

Following the treatment of Nitta (1972) and Yanai et al. (1973), as presented in Thompson et al. (1979), the sensible heat and moisture budgets per unit mass of air may be written

$$\frac{\partial \bar{s}}{\partial t} = -\nabla \cdot (\bar{\underset{\sim}{v}}\, \bar{s}) - \frac{\partial}{\partial p}(\bar{\omega}\, \bar{s}) - \frac{\partial}{\partial p}(\overline{\omega' s'}) + L(\bar{c} - \bar{e}) + Q_R, \quad (4.2)$$

$$\frac{\partial \bar{q}}{\partial t} = -\nabla \cdot (\bar{\underset{\sim}{v}}\, \bar{q}) - \frac{\partial}{\partial p}(\bar{\omega}\, \bar{q}) - \frac{\partial}{\partial p}(\overline{\omega' q'}) - (\bar{c} - \bar{e}) \quad (4.3)$$

Symbols are defined as follows:

s	dry static energy ($= c_p T + gz$)
c_p	specific heat at constant pressure
T	temperature
g	acceleration of gravity
z	geopotential height
q	specific humidity
$\underset{\sim}{v}$	wind velocity (u ≡zonal component, v ≡meridional component)
ω	vertical velocity ($= dp/dt$)
p	pressure
t	time
c	rate of condensation per unit mass of air
e	rate of evaporation of liquid or solid water per unit mass of air
Q_R	radiational heating rate averaged over area
$(\bar{\ })$	area average of the quantity
$(\ )'$	deviation from the area average.

Integration of Eqs. (4.2) and (4.3), the latter multiplied by the latent heat L, from a pressure level p to the surface p_o, yields the following expressions for the sensible heat flux F_s and latent heat flux F_q at the level p

$$F_s = -g^{-1}\,\overline{\omega' s'} = g^{-1}\int_p^{p_o} [Q_1 - L(\bar{c} - \bar{e}) - Q_R]\,dp + S_o \quad (4.4)$$

$$F_q = -g^{-1} L\overline{\omega' q'} = -g^{-1}\int_p^{p_o} [Q_2 - L(\bar{c} - \bar{e})]dp + LE_o \qquad (4.5)$$

where Q_1 and Q_2, the apparent sensible heat source and apparent latent heat sink, respectively, for the large-scale motion, are defined by

$$Q_1 \equiv \frac{\partial \bar{s}}{\partial t} + \nabla \cdot (\bar{\underset{\sim}{v}}\ \bar{s}) + \frac{\partial}{\partial p}(\bar{\omega}\ \bar{s}), \qquad (4.6)$$

$$Q_2 \equiv -L \quad \frac{\partial \bar{q}}{\partial t} + \nabla \cdot (\bar{\underset{\sim}{v}}\ \bar{q}) + \frac{\partial}{\partial p}(\bar{\omega}\ \bar{q}) \quad . \qquad (4.7)$$

Summing (4.4) and (4.5) yields the flux F_h of moist static energy defined as $h = s + Lq$. Thus

$$F_h = g^{-1}\int_p^{p_o} (Q_1 - Q_2 - Q_R)dp + S_o + LE_o. \qquad (4.8)$$

Budgets for the entire atmospheric column are obtained by integrating Eqs. (4.2) and (4.3) from the surface to some high level at which the vertical fluxes become negligibly small. It is convenient to express the budgets in the symbolic form

$$A_s = -D_s + S_o + LP_o + Q_R \qquad (4.9)$$

$$A_q = -D_q - (P_o - E_o), \qquad (4.10)$$

$$A_h = -D_h + S_o + LE_o + Q_R. \qquad (4.11)$$

Here the A's denote accumulation or storage rates of the respective quantities in the column and the -D's denote net horizontal convergences of the quantities into the column. P_o is the precipitation rate at the surface. Instantaneous precipitation of net condensed moisture is assumed.

Payne (1978) used Eqs. 4.4, 4.5 and 4.8 to determine fluxes of sensible heat (dry static energy), latent heat and moist static energy in the mixed layer during the passage through the B-scale area of the synoptic scale wave labeled T_6 in Fig. 4.23. Surface fluxes were computed by the bulk aerodynamic method. Values of Q_1, Q_2 and Q_R were taken from the measurements of Thompson et al. (1979). Evaporation (and condensation) were assumed to be negligible within the layer.

Profiles of the eddy fluxes for three different regions of the wave are shown in Fig. 4.28: the ridge region (7, 8, 1), the region in and ahead of the trough (2, 3, 4) and the region behind the trough (5, 6). The profiles of the moist static energy flux are extended into the overlying cloud layer. Profiles of dry static energy and latent heat fluxes are represented by solid lines to the top of the mixed layer and by dashed lines in the cloud layer. The dashed lines indicate the uncertainty of the estimates above cloud base where the condensation and evaporation terms in Eqs. 4.4 and 4.5 have been neglected. The indicated mixed layer depths are means for the regions based on large numbers of soundings from the B-scale ships.

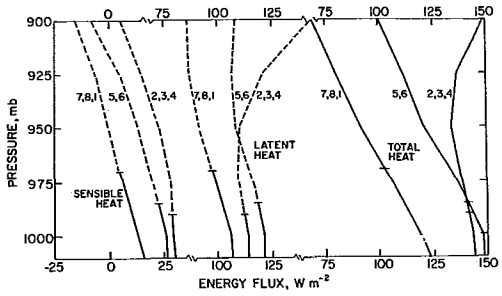

Fig. 4.28

Eddy flux profiles of sensible heat (dry static energy), latent heat and total heat (moist static energy) averaged for wave categories 7, 8, 1; 5, 6; and 2, 3, 4. Sensible and latent heat profiles are dashed above the mixed layer where the measurements neglect possible effects of net condensation in clouds.

In the ridge region the sensible heat flux decreases relatively rapidly with height and approaches zero near the top of the layer. The negative flux just above is a well known effect of the mixing of potentially warmer air downward in the more stable transition layer. The mixed layer is relatively deep in this part of the wave. In the trough region the sensible heat flux remains positive and approximately constant up to cloud base. The depth of the mixed layer is much less than in the ridge. The latent heat flux diminishes upward in all regions, though least rapidly in the disturbed region where the upward transport of moisture into the clouds is largest. The moist static energy flux also diminishes with height in the mixed layer. However, in categories 2, 3 and 4 it reaches a minimum near 950 mb and increases sharply above. The upward increase signifies a divergence or loss of moist static energy due to convective motions. The energy needed to balance this loss is supplied by the large-scale convergence of air of high moist static energy into this portion of the wave.

Thompson et al. (1979) integrated Eq. 4.8 to a height of 200 mb to obtain the moist static energy flux (or flux of total heat, as they termed it) throughout most of the troposphere. Their result appears in Fig. 4.29(a). It is seen that the flux increase in categories 2-4 noted by Payne continues to a height of 800 mb, above which a decrease occurs everywhere. The vertical resolution is too coarse to show the above mentioned minimum near 950 mb. The flux convergence, or cumulus heating as it is sometimes called, is depicted in Fig. 4.29(b). A divergence of 5 x 10^{-2} W kg^{-1}, corresponding in thermal units to a cooling of roughly 5°C d^{-1}, occurs at low-levels in, and in advance of, the trough. A more extensive region of convergence or heating of similar magnitude occurs aloft, centered near the 500 mb level.

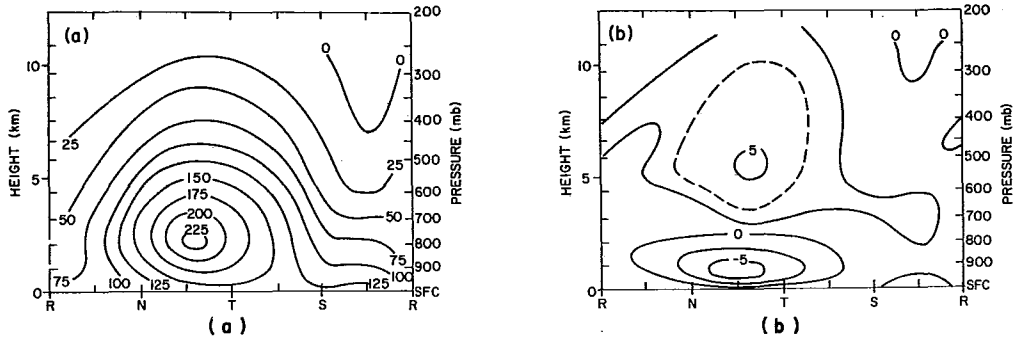

Fig. 4.29 (a) Vertical eddy flux of total heat (W m^{-2}) and (b) its convergence or cumulus heating (10^{-2} W kg^{-1} or approximately equivalent to °C day^{-1}) as functions of wave position.

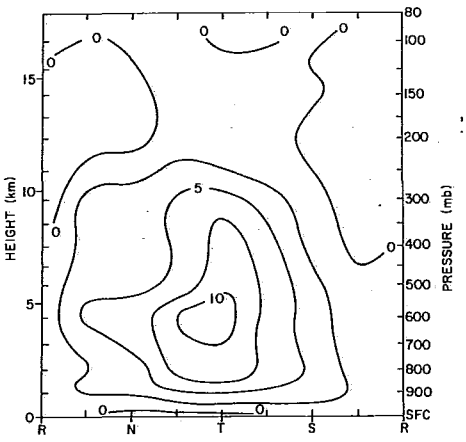

Fig. 4.30
The apparent sensible heat source Q_1 as function of wave position. Units: 10^{-2} W kg^{-1} (approximately equivalent to °C day^{-1}).

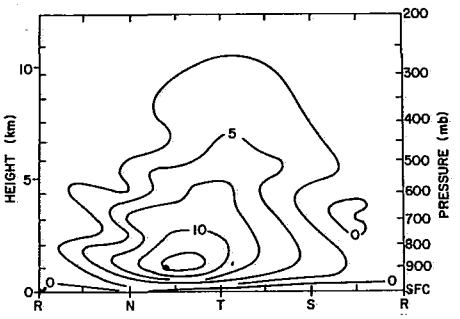

Fig. 4.31
The apparent latent heat sink Q_2 as function of wave position. Units: 10^{-2} W kg^{-1}.

The measured values of Q_1, the apparent sensible heat source, and Q_2, the apparent latent heat sink, upon which the results shown in Fig. 4.29 are based, are displayed in Figs. 4.30 and 4.31. Largest values of Q_1 are found in the trough region at the 600 mb level. Q_2 is largest at 850 mb in the region just ahead of the trough.

Methods have been developed in recent years for deducing cloud mass fluxes from the large-scale heat and moisture budgets and cumulus ensemble models (Yanai et al., 1973; Ogura and Cho, 1973; Nitta, 1975; Johnson, 1976; and Cho, 1977). Johnson's model, Cho's model and a later model of Nitta (1977) include both convective updrafts and downdrafts in the computation of mass fluxes. A recent model of Johnson (1980) also takes into account the effect of mesoscale downdrafts.

Figs. 4.32 and 4.33 show results of Nitta's (1978) computations carried out for the A/B scale area at 6 h intervals during Phase III and composited according to wave position. The first figure gives the cloud base mass flux as a function of the detrainment level, the second the cloud downdraft mass flux. From Fig. 4.32, it is seen that two main detrainment levels are present, a low-level one connected with shallow cumulus and a high-level one associated with deep cumulonimbus. The shallow clouds are most active in the vicinity of the ridge and tend to become less active in the trough region where the deep cloud activity is most pronounced. It is of interest to note, however, that the variation of shallow cloud activity, as expressed by mass detrainment, does not parallel the low cloud coverage as given in Table 4.2. This apparent discrepancy may result from the fact that low clouds, as defined in the table, are not necessarily shallow. Strong downdrafts, extending through a considerable depth, occur in conjunction with the deep clouds (Figs. 4.33). Outside the trough region, downdrafts are weaker and confined to a shallow layer near the surface.

Johnson (1978), with use of a different method for modeling downdrafts, diagnosed cloud base flux and downdraft mass flux for the waves observed during Phase III. His computations, based on the wave composite of Reed et al. (1977), give results that resemble in part those of Nitta. However, they do not show such a strong tendency for the shallow cloud activity to be contentrated in the ridge region. Evidently this difference

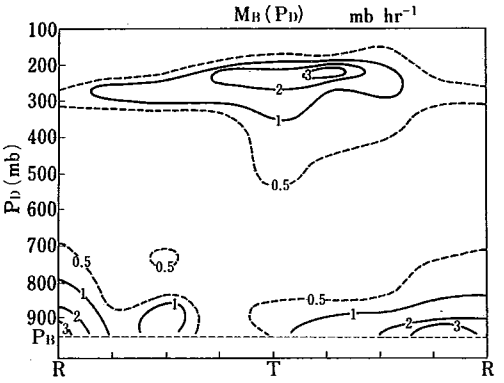

Fig. 4.32
The cloud base mass flux as a function of the detrainment level.

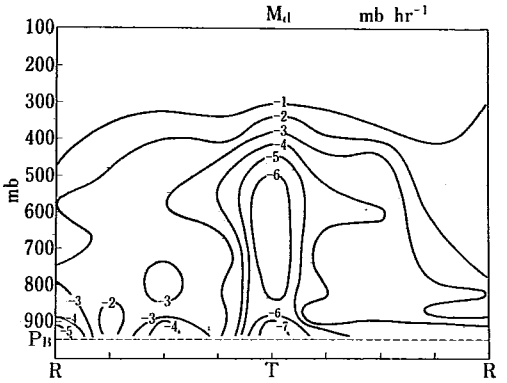

Fig. 4.33
The cloud downdraft mass flux.

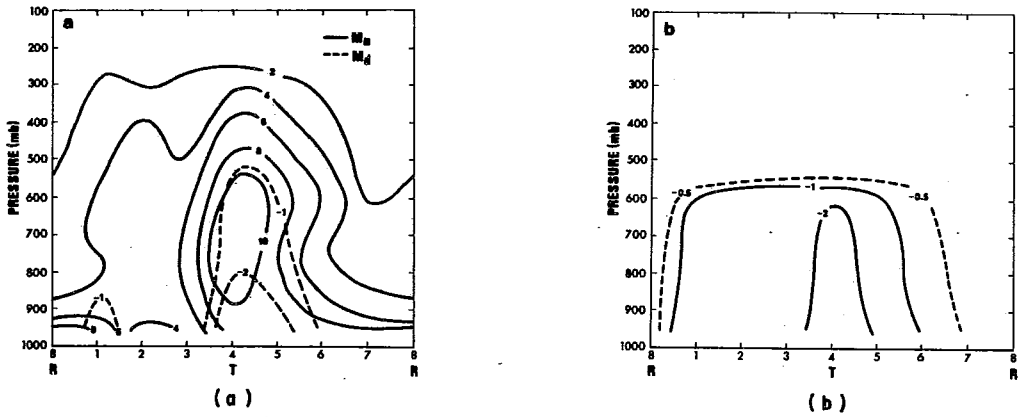

Fig. 4.34 Updraft and downdraft mass fluxes M_u and M_d for composite wave and (b) mesoscale downdraft mass flux M_{md}. Units: mb h^{-1}.

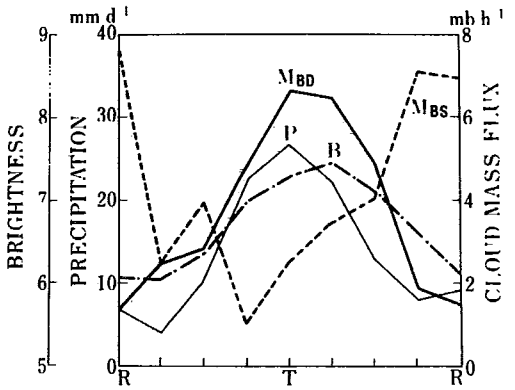

Fig. 4.35 The IR brightness B, observed precipitation rate P, cloud mass flux M_{BD} due to deep clouds and cloud mass flux M_{BS} due to shallow clouds for the composite wave. T and R denote wave trough and ridge respectively.

results from the use of data regions outside the A/B-scale network, since Johnson's (1980) later calculations, which apply to the B-scale area only, yield a picture of detrainment rates from cumulus updrafts that is consistent with Nitta's findings. The inclusion of mesoscale downdrafts in Johnson's analysis, however, does reduce the magnitude of the convective-scale downdrafts well below the values computed by Nitta, as can be seen from Fig. 4.34a. The contribution of the mesoscale downdrafts to the downward mass flux appears in Fig. 4.34b.

Nitta (1979) later compared his computed cloud mass fluxes with cloud and precipitation observations. His results are summarized in Fig. 4.35 which shows, as a function of wave position, the cloud base mass flux due to deep clouds (tops above 400 mb), the cloud base mass flux due to shallow clouds (tops below 700 mb), average IR brightness over the A/B-scale area and average precipitation rate over the B-scale area. The deep mass flux M_{BD} parallels closely the precipitation rate P. The peak IR brightness B lags somewhat behind, an indication of the spreading of the cirrus shield beyond the time when the activity of the deep convection is at a maximum. The shallow cloud activity, as expressed by M_{BS}, is out of phase with the deep activity. Johnson (1980) has computed similar variations for the deep and shallow cloud mass fluxes in the B-scale area.

4.2.4.3 Heat, Moisture and Moist Static Energy Budgets

These appear in Tables 4.5-4.7, taken from Reed (1980). The tables are revised versions of those in Thompson et al. (1979) that make use of Cox and Griffith's (1979) estimates of the radiative cooling. The budgets apply to the layer from the surface to 100 mb and to the period from 30 August to 18 September. The notation of Eqs. 4.9-4.11 is employed.

Table 4.5 Sensible heat budget for B-scale area, Phase III. Units: W m^{-2}. A_S, storage rate; L, latent heat of condensation; $-D_S$, convergence; S_0, surface sensible heat flux.

Wave Category	A_S =	$-D_S$	$+LP_0$	$+S_0$	$+Q_R$	+Residual
1	28	-148	101	6	- 95	164
2 (Northerly)	-62	-307	431	11	-139	- 58
3	27	-439	532	15	-116	35
4 (Trough)	-26	-573	670	19	-114	- 28
5	2	-366	582	18	-126	-106
6 (Southerly)	25	-179	211	13	-122	102
7	12	- 49	196	8	-118	- 25
8 (Ridge)	- 6	- 1	141	7	-143	- 10
MEAN	0	-258	358	12	-122	10

Table 4.6 Moisture budget for B-scale area, Phase III. Units: mm d^{-1}. A_q, storage rate; P_0, precipitation rate; $-D_q$, moisture convergence; E_0, surface evaporation rate.

Wave Category	$A_q = -D_q$	$-P_0$	$+E_0$	+Residual
1	2.4	7.2	- 3.5	2.8	-4.1
2 (Northerly)	1.0	13.3	-15.0	3.4	-0.7
3	2.3	21.0	-18.5	3.8	-4.0
4 (Trough)	3.6	22.6	-23.4	4.1	0.3
5	-1.0	12.0	-20.3	4.3	3.0
6 (Southerly)	-3.5	3.5	- 7.3	4.3	-4.0
7	-2.1	0.9	- 6.8	4.2	-0.4
8 (Ridge)	-2.7	0.1	- 4.9	3.7	-1.6
MEAN	0.0	10.1	-12.5	3.8	-1.4

Table 4.7 Total heat budget for B-scale area, Phase III. Units: W m^{-2}. A_h, storage rate; $-D_h$, convergence.

Wave Category	$A_h = -D_h$	$+S_0$	$+LE_0$	$+Q_R$	+Residual
1	97	59	6	79	- 95	48
2 (Northerly)	-32	76	11	97	-139	-77
3	93	164	15	108	-116	-78
4 (Trough)	77	77	19	114	-114	-19
5	-27	- 22	18	121	-126	-18
6 (Southerly)	-77	- 78	13	122	-122	-12
7	-48	- 22	8	119	-118	-35
8 (Ridge)	-83	0	7	95	-143	-42
MEAN	0	32	12	107	-122	-29

All terms in the sensible heat budget (Table 4.5) show some modulation by the waves, but the principal effects are on the latent heat release by precipitation LP_0 and the compensating heat divergence D_s (essentially the adiabatic cooling). In thermal units, the condensation heating and adiabatic cooling range from about 6°C d^{-1} in the trough region to 1°C d^{-1} in the ridge region.

Again in the moisture budget (Table 4.6) it is the precipitation and divergence terms that dominate. Wave related variations are large - of the order of 20 mm d^{-1} between trough and ridge. The table supports the view expressed earlier that the large-scale forcing is responsible for the relationship of the precipitation to the waves. Local supply of moisture from the surface is considerably less than the import of moisture from the surrounding atmosphere, and the supply, or evaporation rate, varies little

with wave passage. A moderate variation in storage rate is seen, the atmosphere moistening with approach of the trough and drying as it retreats.

The wave modulation of moist static energy (Table 4.7) is relatively small and somewhat erratic. Generally, the largest import and storage are found in advance of the trough and the largest energy supply from the ocean is in, or just to the rear of, the trough.

4.2.4.4 Vorticity and Momentum Budgets

Vorticity budgets have been used increasingly as a means of diagnosing the effects of cumulus convection on the large-scale circulation. The procedure is to expand the vorticity equation into terms that can be measured from the large-scale variables and terms involving sudgrid-scale processes that cannot be measured. In the absence of sud-grid scale processes, the large-scale terms must balance and hence their sum must be zero. In general, however, measurements yield a non-zero sum or residual which, if errors of measurement are sufficiently small, can be regarded as evidence of small-scale effects. In convectively active regions, the residuals, except near the surface, are assumed to arise from processes connected with cumulus transports.

Employing data for the composite Pacific wave disturbance of Reed and Recker (1971), Reed and Johnson (1974) found large residuals in the region of the wave trough. A negative residual or large-scale vorticity sink appeared in the lower troposphere and a positive residual or large-scale source in the upper troposphere. They attributed this behavior to the effect of deep convection in removing vorticity rich air from the near surface layer and depositing it aloft in the cirrus outflow region. Results of related Pacific studies by Williams and Gray (1973) and Hodur and Fein (1977) support Reed and Johnson's observational findings.

Two studies have been conducted using GATE data to investigate vorticity budgets in the synoptic-scale wave disturbances. Shapiro (1978) determined residuals at three different latitudes based on the composite wave of Reed *et al*. (1977). His result for 11°N is shown in Fig. 4.36. The pattern is more complex than in the Pacific wave and does not lend itself to easy interpretation. An examination of individual terms in the vorticity equation reveals that the divergence term is the dominant one in determining the pattern. Thus the greater complexity is consistent with the finding of a more complex divergence pattern in the GATE disturbances than in the Pacific systems.

The second study, by Stevens (1979), is based on data for the A/B scale area only. The data were composited according to wave category and then fitted to quadratic surfaces. The residuals obtained (Fig. 4.37) bear some similarity to those of Shapiro but are even more complex. In view of the complexity, a question must be raised concerning the degree to which the results reflect errors of measurement, or, if they are real, the degree to which they represent only the effects of the convective processes. A possible source of error in both Shapiro's and Stevens's studies, as noted by Chu *et al*. (1981), is the evaluation of the mean vorticity advection from the composite wind and vorticity fields rather than from the mean of the vorticity advections for individual synoptic hours. However, attesting to the reality of the pattern in the vicinity of the wave trough are the results of a recent study by Shapiro and Stevens (1980) in which they were able to reproduce the residuals by a method of cumulus parameterization.

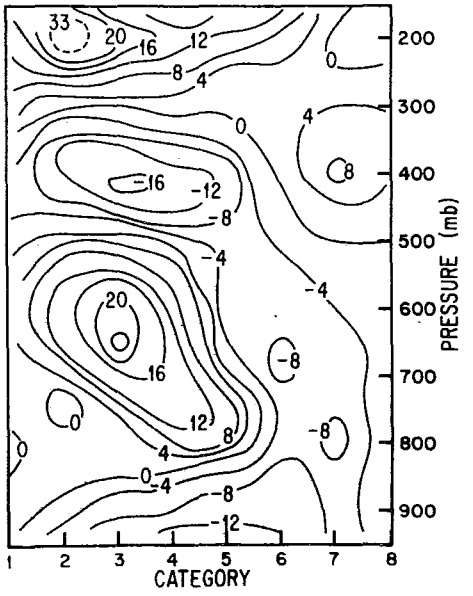

Fig. 4.36
Apparent vorticity source Z at 11°N (10^{-11} s^{-2}) from Shapiro.

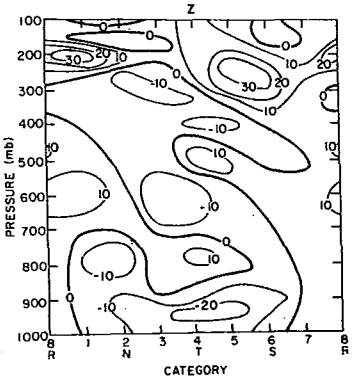

Fig. 4.37
Apparent vorticity source Z(10^{-11} s^{-2}) in the A/B scale area from Stevens.

Reeves et al. (1979) also determined vorticity residuals in the A/B-scale area. Although they did not stratify the data according to wave position, they did separate it into convectively disturbed and suppressed categories. As a consequence, the residuals should resemble those of Stevens for the trough and ridge regions, respectively. Comparison of their results (not shown) with Fig. 4.37 reveals a fair degree of resemblance.

The determination of large-scale sources and sinks of momentum, or residuals in the momentum budget, presents a severe problem in view of the difficulty of measuring pressure gradients with sufficient accuracy at tropical latitudes. To surmount this difficulty, Stevens (1979) derived equations for the perturbed motion that eliminate systematic biases in the pressure measurements. The residuals he obtained for the perturbed zonal and meridional momentum equations appear in Fig. 4.38. A sink for zonal momentum occurs more or less at all heights in the wave trough and a source in the ridge. For the meridional momentum, the reverse is the case.

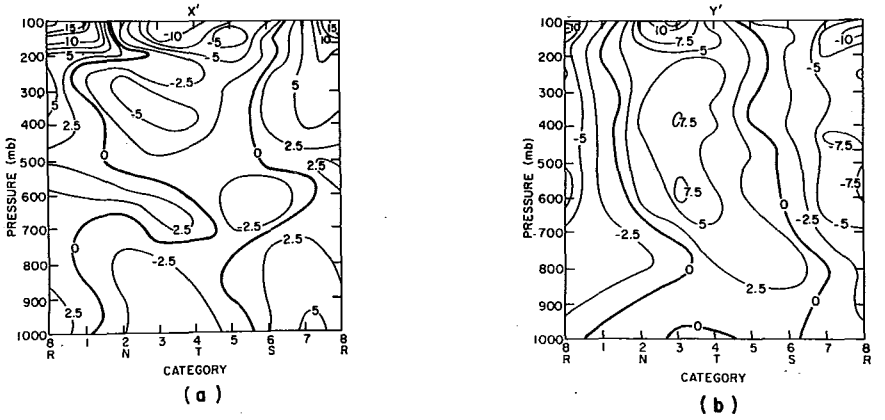

Fig. 4.38 Perturbation zonal and meridional momentum budgets. Units: 10^{-5} m.s $^{-2}$.

These results, if correct, are difficult to reconcile with the idea of cumulus friction (Stevens et al., 1977), at least as applied to a single or predominant cloud population, since the observed residuals are generally of the same sign in the vertical, while a vertical exchange of momentum by cumulus should produce opposite signs in the lower and upper parts of the convective layer. The results also are not consistent with dissipation by a Rayleigh type friction. Either cumulus friction operates in a more complex manner than assumed in simple theories, possibly because of the effect of multiple cloud populations, or errors of measurement are obscuring the true picture.

4.2.5 Wave Energetics and Origins

In this section we review the observational and diagnostic studies that have been carried out with use of GATE data for the purpose of determining the processes responsible for the growth and maintenance of the wave disturbances and the geographical region of their formation. Pre-GATE findings on these subjects are reviewed in section 4.2.1. Theoretical aspects of wave formation are treated elsewhere in this volume (See Chapter 5).

4.2.5.1 Wave Energetics

Following Lorenz (1955), the equations expressing the growth of eddy or wave energy may be written in the symbolic form

$$\frac{\partial K_E}{\partial t} = C_E + C_K + BK_E + B\Phi_E - D_E \qquad (4.12)$$

$$\frac{\partial A_E}{\partial t} = C_A - C_E + BA_E + G_E \qquad (4.13)$$

where K_E is the eddy kinetic energy, A_E the eddy available potential energy, C_E the conversion of eddy available potential energy to eddy kinetic energy, C_K the conversion of zonal kinetic energy to eddy kinetic energy and C_A the conversion of zonal available potential energy to eddy available potential energy. The remaining terms measure boundary fluxes of energy (BK_E, B_e and BA_E), the generation of eddy available potential energy by heat sources and sinks (G_E) and frictional dissipation of eddy kinetic energy (D_E).

Norquist et al. (1977) made use of the composite wave fields derived by Reed et al. (1977) to compute the foregoing conversion terms. The data were not adequate for evaluating the remaining terms. Their results are presented in Fig. 4.39 in which the familiar energy flow diagram of Lorenz is utilized. Three diagrams appear: one for a composite wave based on data for both land and ocean areas and separate ones for composite waves based on land data only and ocean data only.

The composite for the combined areas (top panel) indicates that the kinetic energy of the waves was supplied almost equally by the barotropic conversion C_K and the baroclinic conversion C_E. These conversions were associated with a positive u, v correlation, or northward flux of westerly momentum, south of the mid-tropospheric jet stream and a positve correlation between vertical motion and temperature. The conversion of zonal to eddy available potential energy C_A, was positive, or indicative of a down-gradient heat flow in the baroclinic zone of the jet, and its magnitude was comparable in size to the magnitudes of the other conversions.

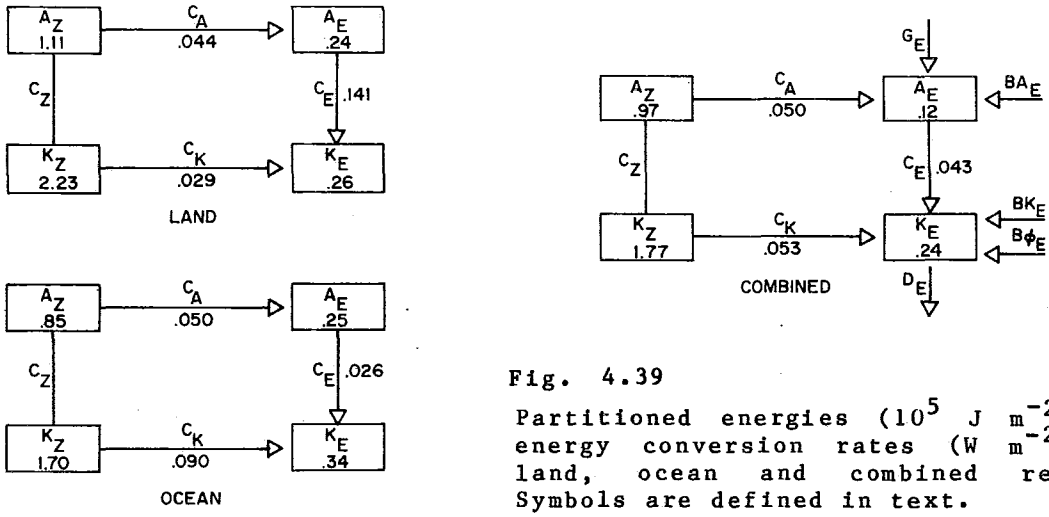

Fig. 4.39

Partitioned energies (10^5 J m^{-2}) and energy conversion rates (W m^{-2}) for land, ocean and combined regions. Symbols are defined in text.

As shown by Nitta (1970) and Wallace (1971), wave disturbances in the tropical Pacific derive their kinetic energy almost entirely from the diabatic generation G_E associated with condensation heating. From the diagram it appears that such a source is not required for the growth of the African waves, barotropic and dry baroclinic processes being sufficient, as first proposed by Burpee (1972). However, this conclusion is altered somewhat when the energy conversions for the separate areas are examined (middle and bottom panels). Over land the baroclinic conversion C_E is relatively large, suggesting from balance considerations that an appreciable generation of eddy available potential energy by condensation heating may take place. On the other hand, over the ocean the barotropic conversion C_K predominates, and it appears, again from balance considerations, that the diabatic generation may be negative. Later measurements by Thompson et al. (1979) confirm this inference and reaffirm the predominate role of the barotropic conversion process in the offshore region.

Further interpretation of the foregoing results will be delayed until the work on the wave origins is reviewed. The maintenance of the kinetic energy of the large-scale disturbances in the eastern Atlantic has also been studied by Kung and Burgdorf (1977) with use of a different formulation of the energy equation.

4.2.5.2 Wave Origins

Albignat and Reed (1980) took advantage of the aforementioned appearance of unusually well developed and easily identified wave disturbances during Phase III to look into the question of their geographical origin and the factors connected with their formation. Attempts to determine the source region by Carlson (1969b), Burpee (1972), Aspliden (1974), Dean and LaSeur (1974), Mass (1978) and other investigators mentioned in section 4.2.1.2, based on pre-GATE data, have yielded a variety of results, some of them seemingly conflicting. In view of the different analysis techniques, time periods and lengths of record employed, the results may not be truly contradictory, but they do indicate the need for obtaining further information on the subject.

Albignat and Reed (1980) based their study on spectrum analysis of 850 mb and 700 mb winds for a large number of African stations during the

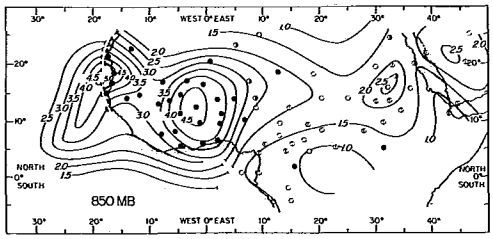

Fig. 4.40
Amplitude of meridional wind oscillation in the frequency band .2-.4 cpd at 850 mb. Units: m s^{-1}. Isopleths over land based on 28 day period of record, over the ocean on 20 day period. Solid circle signifies a pronounced spectral peak in the .2-.4 cpd band, half solid circle a secondary peak, circle with line a weak peak, open circle no detectable peak.

period 23 August - 19 September. A main result of their investigation is shown in Fig. 4.40. The isopleths in this figure represent the amplitude of the meridional wind component at 850 mb in the .2-.4 day frequency band (periods between 2.5 and 5 days). Solid circles indicate stations which exhibited sharp, primary spectral peaks in the .2-.4 cpd band, half-solid circles stations that possesed a secondary peak in that band, lined circles stations with a weak peak that was neither primary nor secondary and open circles stations devoid of a peak.

It is apparent that all stations west of 8°E in the latitude belt between 5°N and 20°N possessed pronounced peaks at the period known from synoptic studies to represent the wave period. East of that longitude peaks were generally weak or absent. Thus it can be concluded that the main growth of the disturbances at this level took place quite rapidly in the region between 10°E and the Greenwich meridian. Cross spectrum analysis yielded a wave length of 2500 km for the oscillations in the .2-.4 cpd band in the region between 10°E and the coast, confirming that they could indeed be identified with the waves analyzed on synoptic maps.

In an attempt to trace the waves further to the east, Albignat and Reed carried out cross spectrum analyses using time series of the meridional component for pairs of stations along a number of approximately east-west lines. However, coherences between the series were generally very small east of 10°E, and no consistent direction of phase propagation could be found. Hence it was concluded that the disturbances were essentially absent east of 10°E. Synoptic analyses of Sadler and Oda (1978) support the view that at 850 mb the disturbances first made their appearance somewhere in the vicinity of 10°E.

The spectrum analysis was repeated at 700 mb with similar results, except that along a line from Fort Lamy (12°N, 15°E) to Djibouti (12°N, 43°E) coherences were moderate in size and the phase propagation was consistently westward. Moreover, the wave length of the coherent oscillations was about 2500 km. It was concluded from these findings that at the higher level, where the waves are generally stronger, evidence could be found of an origin as far east as southern Arabia. However, any waves emanating from this region were very weak. For all practical purposes the wave growth at 700 mb, as at 850 mb, took place near 10°E.

Albignat and Reed (1980) also determined cospectra of the meridional and zonal wind components at both 850 mb and 700 mb for the various stations and, in addition, the phase differences between the meridional wind fluctuations at the two levels. From the cospectra it was concluded that the direction of the momentum flux at 700 mb was such that the mid-tropospheric jet supplied kinetic energy to the waves across nearly the full breadth of Africa. However, this barotropic source of energy was found to be especially large in the offshore region in line with the results of Norquist et al. (1977) and Thompson et al. (1979).

The phase differences allowed the vertical slope of the wave systems to be determined objectively. It was found that poleward of 15°N the waves had the tilt characteristic of dry baroclinic disturbances but that south of that latitude where the waves produced a large modulation of the rainfall, and hence of the latent heat release, no systematic tilt existed. This result is consistent with Carlson's (1969b) finding that the disturbances often possess two centers near the surface, a northerly one believed to be thermally induced and a southerly one of convective origin.

4.2.5.3 Interpretation

From the foregoing studies of the wave origins and energetics and the studies of wave structure and properties reviewed in earlier sections, the following picture of the genesis of the wave disturbances in Phase III can be drawn.

Weak, precursory disturbances of uncertain origin were perhaps present in central and eastern Africa upstream of the region of main development. However, these disturbances were too weak to be identified by synoptic wind analyses and were almost certainly not connected with any discernible organization of the precipitation on the 3-4 day time scale. In the vicinity of 10°E, at the eastern end of the African bulge, a rapid growth of the waves took place, so that effectively the region about northern Nigeria and southern Niger may be regarded as the source region of the disturbances. It is likely that the enhanced instability of the mid-tropospheric jet was the primary factor in initiating or accelerating the wave growth in this region. Figs. 4.41 and 4.42 from Albignat and Reed (1980), which depict the 700 mb wind field and 850 mb to 700 mb wind difference or thermal wind field, make clear that the lateral and vertical shears associated with the jet attained nearly their maximum values in this region of accelerated growth.

Once initiated, the disturbances organized the convection in such a way that condensation heating promoted continued growth over West Africa. This conclusion is supported by the results of both the energy diagnosis and the spectral analysis and is consistent with synoptic results that date back at least to Carlson's (1969b) early description. The disturbances attained their maximum intensity in the vicinity of the coast where it is possible that the reduced surface friction over the water contributed to their further intensification.

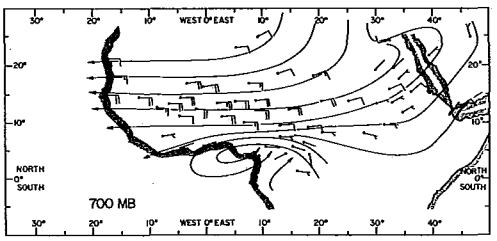

Fig. 4.41
Mean wind fields for the period 23 August - 19 September 1974, 700 mb. Half barb indicates 2.5 m s^{-1}, a full barb 5 m s^{-1}.

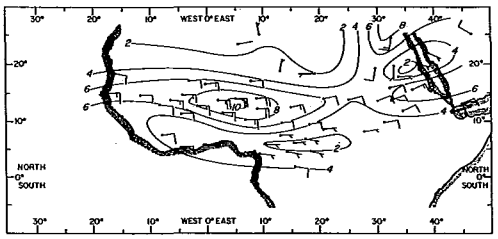

Fig. 4.42
Wind shear between 850 mb and 700 mb for period 23 August - 19 September 1974. Half barb represents 2.5 m s^{-1}, full barb 5 m s^{-1}. Isopleths depict magnitude of the shear.

The disturbances remained relatively strong in and to the east of the A/B ship array but declined rapidly in strength immediately to the west. The general decline over the ocean can be understood in terms of the cessation or diminution of the conditions that gave rise to them: the jet instability produced by the sub-Saharan baroclinic zone that progressively weakens down-stream over the ocean and the convective instability that is greater over the heated continent than over the ocean. Although the general behavior of the disturbances can be understood, the details are harder to explain. Especially puzzling are the energy conversions in the vicinity of the ship array where condensation heating appears to oppose the wave growth and the barotropic conversion attains a much larger magnitude than over Africa. Until such details are explained a completely satisfactory understanding of the wave origins and energetics cannot be said to exist.

4.3 OTHER TOPICS

4.3.1 Synoptic-Scale Disturbances of the ITCZ

4.3.1.1 Historical Perspective

In the years before GATE, when surface ship reports and satellite images were the main sources of information in the lower troposphere of the tropical Atlantic, the identification of different types of synoptic-scale disturbances that affected the cloud patterns in the ITCZ region was extremely difficult. In order to gain a better understanding of the various disturbances affecting the ITCZ, forecasters at NHC began to compile annual summaries of two different types of lower tropospheric tropical disturbances that they observed propagating westward across the Atlantic (e.g., Simpson *et al.*, 1968). One of these disturbances is the African or easterly wave, described earlier in Section 4.2, that frequently can be identified on satellite images by its inverted-V cloud pattern. The second is referred to as an ITCZ disturbance. To be classified as an ITCZ disturbance, a cloud system must have a minimum diameter of 200 km and be tracked along the ITCZ in satellite images for at least 48 hours. In its annual summaries of Atlantic tropical disturbances, NHC typically classifies 80-90% of the Atlantic disturbances as African waves and the remaining 10-20% as ITCZ disturbances. The disturbance summaries for the pre-GATE summers from 1967-1973 indicate that while most African waves and ITCZ disturbances were able to travel across the Atlantic, a few of both types of disturbances decayed and a few others developed over the ocean (Frank and Hebert, 1974). The authors of these summaries cautioned, however, that operational tracking of these systems, particularly the weaker ones, can be extremely difficult and that these summaries may overestimate the number of disturbances that decayed and developed over the Atlantic by failing to maintain continuity of the weak systems over the Atlantic between the rawindsonde stations at Dakar and Barbados (e.g., Frank, 1969).

In an earlier study of the synoptic-scale features of the tropical northern Atlantic, Aspliden *et al.* (1965, 1966a,b) analyzed twice daily surface maps during the summer of 1963 and tracked 32 cyclones that formed between 26 July and 17 October as well as 3 additional cyclones that were already in a mature stage at their first map time on 26 July. After comparing their wind analyses with the corresponding TIROS satellite images, Aspliden *et al.* found that the surface cyclones were generally located either in the center of or along the southern or northern edge of large cloud masses. Although the majority of these cyclones were initially identified near the African coast and then travelled along paths that closely paralleled

the mean location of the surface confluence line in the ITCZ region, Aspliden et al. claimed that these surface cyclones were not easterly waves. LaSeur (1971), on the other hand, speculated that most of the cyclones identified by Aspliden et al. near the African coast were most likely easterly waves; but, he indicated that some of the cyclones that they initially observed in the central Atlantic were probably ITCZ disturbances.

Thus, pre-GATE literature suggested the existence of two types of synoptic-scale disturbances that modulated the cloudiness in the ITCZ: the easterly waves and the ITCZ disturbances. With the observations available before GATE, however, only the most general characteristics of the modulation of the ITCZ cloudiness by the easterly waves had been determined. Frank (1969) indicated that about half of the easterly wave disturbances that had inverted-V patterns also modulated cloudiness in the ITCZ region, while the inverted-V patterns associated with the remaining half of the waves were confined to the tradewind area and did not affect the cloudiness in the ITCZ. To assess how the ITCZ cloud patterns associated with the African waves might change with longitude, Frank (1971) tracked several African waves from Africa to the western Atlantic during June, July, and August of 1970 and 1971. He determined that the total cloudiness and the brightest cloudiness associated with the wave disturbances at the latitude of the ITCZ decreased as the waves travelled westward across the Atlantic. In addition, he showed for all longitudes that the wave-related cloud amount and the brightest cloud amount in the ITCZ were larger from 15 July - 30 August than from 1 June - 14 July (Fig. 4.43). In agreement with Frank's results, Sadler (1975) found that the intensity of African disturbances increased from June to September and that during this time the modulation of the deep convective activity near 10°N and the north-south displacement of this convection by the African disturbances was greatest during September. Relatively little was known, however, about the structure of the ITCZ disturbances, since these disturbances had only been identified in the images from geostationary satellites.

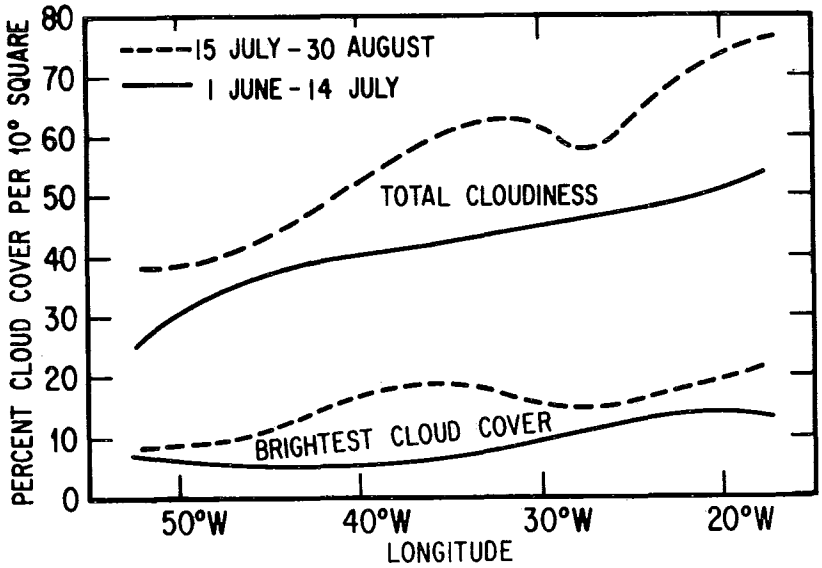

Fig. 4.43 The average longitudinal variation in ITCZ total cloudiness and for the brightest cloud cover for 29 selected African disturbances during 1970 and 1971. The average percentage of a 10° longitude by 10° latitude box centered on the disturbance and 5° North is shown by 5° longitude intervals.

4.3.1.2 Synoptic-Scale Disturbances Affecting the ITCZ Region during GATE

During the 1974 tropical cyclone season, forecasters at NHC used SMS-1 satellite images and radiosonde observations from Dakar and Barbados to track African waves and ITCZ disturbances across the Atlantic (Frank, 1975). In Dakar, however, operational analyses produced by the GATE forecasters utilized the full complement of wind data from the GATE observing network as well as the SMS-1 images. These analyses revealed a regular progression of synoptic-scale African waves, one ITCZ disturbance that ultimately became Tropical Storm Alma, and non-periodic disturbances that had not previously been mentioned in the literature (Burpee and Dugdale, 1975).

The non-periodic disturbances formed near the coast of Africa and reached maximum amplitude near 850 mb. The vortices associated with the disturbances had a typical horizontal scale of about 1000 km, propagated toward the west at 7-10 m s^{-1}, and appeared to decay before reaching 35°W. There was little evidence of these vortices at 700 mb. While enhanced cloudiness was associated with these systems, no preferred pattern of convection was apparent. Seven of the vortices were observed during Phase I, 3 or 4 more in Phase II, but none in Phase III. From the middle of Phase II until the end of Phase III, the flow patterns at 850 and 700 mb in western Africa and the eastern Atlantic were very closely coupled. During that time all of the synoptic-scale troughs and vortices, with the exception of the precursor of Tropical Storm Alma, were the African wave type.

During the entire summer season of 1974, Frank (1975) identified eleven ITCZ disturbances in the Atlantic; however, only three of these occurred during the three phases when the ships in the A/B and B-scale arrays were on station in the eastern Atlantic. The most strongly developed ITCZ disturbance formed along the south coastal area of West Africa, travelled rapidly westward at an average speed of 10 m s^{-1}, and ultimately became Tropical Storm Alma near 10°N and 50°W on 12 August. The two remaining ITCZ disturbances identified by Frank during the active field phases of GATE were observed during September. Examination of the streamline pattern at 700 mb for the first of these disturbances on 12 September (e.g. ISMG, 1975) suggests that this cloud cluster developed near 6°N, 26°W in association with the trough of an easterly wave, while the second September ITCZ disturbance formed on the 17th in the western part of the Atlantic well to the west of the intensive GATE ship array. Thus, there is an indication from this small sample of three, that some of the cloud clusters that are operationally identified as ITCZ disturbances may actually be initiated by the easterly waves.

On the basis of the synoptic-scale research that has been completed with the GATE observations, it is likely that most, or perhaps all, of the synoptic-scale disturbances that modulated the cloudiness in the ITCZ region of the Atlantic were initially observed over the African continent or along the west coast of Africa; however, the physical mechanisms that account for the 850-mb vortices of early summer in the eastern Atlantic and the ITCZ disturbances have yet to be clearly specified. In addition, it seems unlikely that future analyses of the GATE observations will be able to show unambiguously whether the 850-mb vortices and the ITCZ disturbances are different synoptic-scale features or are the same type of disturbance where the former have been identified with wind data and the latter with satellite images.

Detailed descriptions of the kinematic interactions between mesoscale vortices in the African wave troughs and the ITCZ were presented by

Dean and Smith (1977) and Dean (1978), who analyzed maps for six different pressure levels at 6-hour intervals throughout Phase III. On the basis of their analyses, they noticed that many of the African wave troughs contained one or more mesoscale cyclones and that each wave ridge had a single mesoscale anticyclone. In addition to these mesoscale features, the southern part of each wave trough contained a well-defined synoptic-scale cyclonic vortex. Typically, the synoptic-scale cyclonic center in the wave trough moved westward across Africa until it reached the west coast. In the eastern Atlantic, however, this vortex moved toward the northwest and decayed near 15°N, 30°W, while a second cyclonic vortex formed in the wave trough farther to the south and propagated toward the west southwest along the ITCZ.

4.3.2 Hurricanes

During the summer of 1974, seven Atlantic disturbances became tropical storms with four of these storms subsequently reaching hurricane intensity (Hope, 1975). The 1974 storm totals are slightly below the average for the most recent 30 years of ten tropical storms, six of which intensified to hurricane strength. In addition to these statistics, several other factors also suggest that tropical cyclone activity in the Atlantic in the summer of 1974 was less than normal. For example, the date that the first disturbance was classified as a tropical storm was August 12, and the date that the last storm of the season decayed was on October 3. Statistics compiled since 1886 by Neumann et al. (1978) indicate that the tropical cyclone season typically begins in late June and ends in late October; thus, the total time interval between the first and last storm of the 1974 season was less than half as long as the average. Another measure of tropical cyclone seasons is the number of days on which hurricanes were observed. During 1974, there were 19 days with named hurricanes compared to a 20-year average of 29 hurricane days (Lawrence, 1978). Thus, many of the standard measures of tropical cyclone activity indicate that the summer of 1974 was less active than normal in the Atlantic. Analyses of subsequent years have shown that 1974 was part of a seven-year period that lasted from 1971-1977 with fewer storms than normal (Frank and Clark, 1978).

While the 1974 tropical cyclone season was less active than normal, the number of disturbances passing Dakar and the role of African disturbances in initiating tropical storms in the Atlantic was typical of the 10-year average statistics presented by Frank and Clark (1978). Thus the inactivity of the 1974 tropical cyclone season does not seem to be the result of any anomalous behavior of the synoptic-scale disturbances that originated over Africa, but instead, can be attributed to the failure of other generating mechanisms that typically account for tropical storms.

Five tropical cyclones formed within the western part of the GATE A-scale network well to the west of the A/B ship array. Four of these cyclones (Carmen, Elaine, Fifi, and Gertrude) developed from wave disturbances that were originally observed over Africa and all, except Elaine, later became hurricanes. Tropical Storm Alma, the first of the five storms that formed within the GATE region, intensified from a weak ITCZ disturbance that was initially observed near the African Coast, and was not directly associated with any of the synoptic-scale waves. The latitude of the vorticity center of the disturbance was about 300-400 km south of the typical path followed by the vorticity centers of the easterly waves during August and September. On August 10, the center of the disturbance, that later became Alma on the 12th, passed rapidly through the A/B-scale ship array. According to Sadler and Oda (1978), the surface vortices that developed into Hurricane Becky and Tropical Storm Dolly were induced by upper

tropospheric cyclones that were located a little to the north of the GATE A-scale region near 70°W.

While the GATE observing network was not designed to investigate the structure of tropical cyclones in the western Atlantic, the round-the-clock coverage of cloud patterns obtained by the SMS-1 satellite, which was launched a few days before the beginning of GATE, provided researchers with an unprecedented opportunity to view changes of the cloud cover associated with hurricanes. Thompson and Miller (1976) studied the satellite images of Hurricane Carmen and described the evolution of this storm from its weak-disturbance stage over Africa until it made landfall in the Gulf of Mexico some 21 days later. They pointed out that the convective cloud pattern in the ITCZ that was associated with the pre-Carmen disturbance had the shape of a wave. This wave appeared to increase in amplitude, crest, and then break, in a similar manner to a wave on a water surface.

Vincent and Waterman (1979) have described the large-scale atmospheric conditions in the Caribbean region during the 4-day period that Carmen intensified from a tropical depression to a major hurricane. During this time, the Caribbean was characterized by warm sea-surface temperatures, deep moist air, low-level confluence and upper-level diffluence, upward vertical motion, and low values of the vertical shear of the horizontal wind. Climatological studies have shown that all of these conditions are favorable for the formation of tropical cyclones. Edmon and Vincent (1979) computed diabatic heating rates and energy budgets for the large-scale flow surrounding Carmen. They found that large-scale kinetic energy was lost to smaller scales as Carmen intensified, but that large-scale motions gained kinetic energy at the expense of the smaller-scale motions when the hurricane was in its mature stage. The authors speculated that this might imply that kinetic energy was transferred to the storm's circulation as it strengthened and that energy flowed from Carmen to the large-scale surroundings while Carmen was a mature hurricane.

Hawkins (1976) examined conditions in the western part of the GATE A-scale region before and during the passage of Hurricanes Carmen and Fifi. These storms had nearly identical tracks through the Caribbean but were separated in time by slightly more than two weeks. Carmen had a minimum pressure in the western Caribbean of 928 mb while Fifi's lowest pressure in the same region was only 971 mb. Hawkins found little significant difference in the sea-surface temperatures along the tracks of the two storms, and his computations of the high-level mass outflows, based largely on satellite winds, revealed that Hurricane Fifi had a stronger outflow by a factor of two. He concluded that Fifi failed to intensify further because of its proximity to the Honduran landmass rather than as a consequence of any unfavorable environmental conditions.

As the GATE ship Oceanographer headed toward its home port following the field phase of the experiment, Hurricane Gertrude passed a short distance away. This provided an unanticipated opportunity to record digitized radar data of the outer rainbands of the storm from a location about 200 km north of the center of Gertrude, at a time when the hurricane was rapidly decreasing in intensity and convective activity. Analyses of radar, aircraft, satellite, and radiosonde observations by Lewis and Jorgensen (1978) indicated that the storm weakened as it interacted with the strong wind shear and subsidence associated with an upper-level synoptic-scale trough.

4.3.3 Upper Tropospheric Disturbances

Several studies completed before GATE indicated that disturbances in the upper troposphere of the Atlantic and Pacific Oceans occasionally have a pronounced effect in enhancing or diminishing organized deep convection in the tropics. For example, Malkus and Riehl (1964), in their description of the convective structure observed during three research flights across the tropical Pacific, found that they could usually explain the convective organization in terms of the local time rate of change of vorticity in the upper troposphere (250-150 mb). Convection tended to be suppressed (enhanced) as the upper tropospheric vorticity increased (decreased) locally. In the eastern Caribbean, Frank (1969) determined that large cloud clusters were frequently observed when synoptic-scale disturbances in the upper and lower troposphere were favorably aligned. One particular pattern, with the 700-mb trough of an easterly wave located on the southwest side of an upper tropospheric trough, normally produced widespread deep convection. In addition, Sadler (1967) showed that one feature, the tropical upper tropospheric trough, was a factor in initiating some tropical cyclones in the western Pacific.

To assess the possible importance of upper tropospheric features in the development of organized deep convection in the GATE region, upper-level winds have been subjectively and objectively analyzed. Sadler and Oda (1978, 1979, 1980) have completed subjective analyses of the 250 mb wind field for each day during GATE from 26 June - 23 September in the area from 45°N - 30°S and between 105W - 60°E. Their analyses indicate that the upper tropospheric circulation was quite complex with numerous clockwise and counterclockwise eddies appearing on most maps. The major cyclonic activity in the upper troposphere occurred in the general region between the Azores and the northwest Caribbean, near the mean position of the mid-Atlantic trough, where vortices formed in response to eastward propagating troughs in the westerlies. During Phase III, there were ten major vortices that tended to move toward the west-southwest, to achieve maximum intensity near 50 - 60°W, and to weaken when widespread deep convection was initiated. Most of these cyclones decayed before reaching 90°W. Three of the ten upper tropospheric cyclones of Phase III induced surface cyclones, two of which became named tropical storms. During Phases I and II, however, there were only seven and six upper tropospheric cyclones respectively and none of these cyclones was able to induce any circulations in the surface wind field. So far, the other types of eddies that they identified have not been linked to the initiation of disturbances in the lower troposphere or to any role in enhancing the organization of deep convection.

Depradine *et al*. (1978), Krishnamurti *et al*. (1978), and Pasch *et al*. (1978) objectively analyzed the horizontal wind field at 200, 250, and 300 mb on a global domain from 45°N - 25°S for 100 days of GATE beginning with 16 June and ending with 23 September. From these calculations, the Florida State University Group (Krishnamurti, 1978) determined the geopotential field from a dynamical initialization of a one-level primitive equation model, the vertical motion by integrating the continuity equation downward from the 100-mb surface, and the temperature at intermediate levels from the hydrostatic equation. These quantities were then used to describe the time-averaged characteristics and the variability of east-west circulations near the equator. The results presented by Krishnamurti indicate that there were strong divergent circulations in the east-west plane at 200 mb during GATE with three major centers of divergence located near the northern part of the Bay of Bengal, the coast of Nigeria, and northwestern South America. The corresponding centers of convergence were over Somalia and in

the mid-oceanic troughs. In general, the upper tropospheric east-west circulations generated eddy kinetic energy since they were characterized by rising warm air and sinking cold air. Space-time spectral analyses of the average of the east-west flow from $10^{\circ}S$ - $20^{\circ}N$ at 200 mb indicated that the dominant spectral peaks for eastward and westward propagating waves were at periods of 10-20 days and zonal wavenumbers of 4-6. These waves have amplitudes on the order of 1 m s^{-1} and, therefore, are too weak to be observed in the analyses of Sadler and Oda.

The composite structure of the African waves that was presented earlier indicates that the waves have an average amplitude of about 2 m s^{-1} in the upper troposphere. Visual inspection of the analyses completed by Sadler and Oda suggests that, in some cases, the upper tropospheric flow is relatively unperturbed by the waves, while at other times the composite structure can be identified in the 250-mb analyses.

4.4 SUMMARY AND CONCLUSIONS

African or easterly waves were the most prominent transient feature of the synoptic-scale circulation over West Africa and the eastern Atlantic during the three phases of GATE. A considerable body of knowledge concerning the wave disturbances existed prior to the experiment, based on surface and upper air analyses, interpretation of satellite imagery and spectrum analysis of radiosonde data. It was known that the waves generally originate over Africa, that they travel westward at speeds of 6-7 degrees of longitude per day, crossing the coast at intervals of 3-4 days, and that a small fraction of them transform into tropical storms or hurricanes during their passage across the Atlantic. It was also known that the convective activity associated with the waves tended to occur mainly in the vicinity of the troughs, though there were apparent disagreements regarding the precise relationship of convective features and precipitation to the waves. Also prior to GATE a hypothesis for the origin of the waves existed in which the lower tropospheric baroclinic zone, and associated mid-tropospheric jet stream, that form in the sub-Saharan region during the period from May to October, play the central roles. It was shown from observations that the flow in the middle troposphere satisfies the criterion for barotropic instability and that the Charney-Stern criterion for the instability of an internal jet is also satisfied. Many characteristics of the waves were successfully explained by the theory including the time and location of their appearance, their maximum development at middle levels and their tilts in the horizontal and vertical.

Studies based on GATE data have confirmed and refined many of the earlier findings regarding the wave disturbances and in addition have resulted in important extensions of knowledge. The establishment of a dense network of observations in the eastern Atlantic was particularly valuable in the advancement of knowledge, since it allowed accurate measurements of large-scale divergence and vertical motion to be made for the first time. A complex pattern of divergence was found in which the principal features were a region of convergence near the surface in and in advance of the trough and a corresponding region of divergence aloft at 200 mb. Strongest upward motions occurred just ahead (west) of the trough with the primary maximum located near 700 mb and a secondary maximum near 350 mb. Subsidence was exceedingly weak and confined to the region of the ridge.

The relation of other variables to the waves was also documented. Largest fluctuations of winds and vorticity appeared at the level of the mid-tropospheric jet stream (600 mb). Somewhat smaller fluctuations of opposite

sign occurred near 200 mb. The wave coupling in the vertical became stronger during the latter part of the experiment, as evidenced by much larger meridional wind amplitudes near the surface in Phase III than in Phase I. The wave troughs possessed negative temperature anomalies below 600 mb, positive anomalies between 600 mb and 200 mb and negative anomalies again near 150 mb. Highest relative humidities were found behind (east of) the trough and lowest humidities in the region of northerly winds ahead of the trough.

The extensive satellite coverage of the GATE area and the radar coverage of the inner ship network made it possible to define the relationship of convective activity and rainfall to the wave disturbances more precisely than in the past. In conformity with the measured distribution of vertical velocity, convective cloud and the precipitation amounts were greatest near and somewhat in advance of the trough axis and least near and somewhat ahead of the ridge axis. Lag correlations revealed that the heaviest rainfall followed the maximum large-scale ascent by an hour or two and that the maximum extent of convective cloud lagged the ascent by an additional few hours. Squall lines formed most frequently in the northerly wind region ahead of the trough and tended to dissipate as they approached the downstream ridge. Large, long-lived cloud clusters formed most commonly ahead of the trough and moved westward slower that the wave speed, dissipating after being overtaken by the trough axis.

Analysis of soundings from the B-scale ship network revealed that convective instability, as measured by the net energy release, was greatest in the wave ridge and least in the wave trough. Accordingly, variations in forcing by the large-scale motions rather than variations in thermodynamic stratification must be invoked to explain the modulation of convection by the waves.

The unique nature of the GATE data set has also made it possible to compute the wave-related variations in vertical transports of heat, moisture and mass by subgrid-scale motions and the variations in the budgets of heat, moisture, vorticity, momentum and surface energy. Variations in the surface energy budget were caused primarily by the net radiation - principally the short wave component - and secondarily by the latent heat flux. The sensible heat flux from the surface was too small to be of significance. In the region of the wave trough a transfer of heat from ocean to atmosphere was needed to balance the surface energy budget. On the other hand a heat flow into the ocean was required in the ridge region. Observed temperature variations in the upper ocean were in agreement with the implied variations in heat storage. Because of the energy supply by the large-scale horizontal flux convergence, the sensible and latent heat fluxes in the sub-cloud or mixed layer diminished less rapidly with height in the convectively disturbed region of the wave than in the suppressed region. In the convectively active region the total heat or moist static energy flux increased with height above 950 mb, reaching a maximum near 800 mb and decreasing above. The associated flux divergences in the vertical yielded a heating rate by cumulus clouds of about $5°C\ d^{-1}$ at 500 mb and a cooling rate of about the same size at 900 mb. Computations of cloud base mass flux as a function of detrainment level, based on cumulus ensemble models, indicated the presence of two main levels of detrainment, one located near 200 mb in the vicinity of the wave trough associated with deep convection, and the other located close to the surface in the wave ridge associated with shallow convection. Downdraft mass flux was largest in the trough region. Maximum precipitation coincided with maximum cloud mass flux by deep clouds, whereas maximum satellite IR brightness, a measure of the extent of clouds with high tops, lagged somewhat behind.

Wave-related variations in the sensible heat budget were connected mainly with adiabatic cooling and condensation heating. Variations in the moisture budget stemmed mainly from the horizontal moisture convergence and the precipitation. Variations in storage of water vapor were of secondary importance and variations in the supply by surface evaporation were slight. Wave-related changes in moist static energy were relatively small.

Vorticity budgets computed from large-scale variables yield complex patterns of residuals that are presumably caused by cumulus or other subgrid-scale motions. Perturbation momemtum budgets based on large-scale variables yield wave-related residuals that are difficult to explain by simple ideas on cumulus friction.

Studies have been conducted of the energetics and origins of the well developed wave disturbances that occurred during Phase III. The results indicate that both barotropic and baroclinic energy conversions were important for the growth and maintenance of the waves. Over Africa the baroclinic conversion was dominant in the wave growth and depended both on the conversion of zonal available potential energy to eddy available potential energy and on the generation of eddy available potential energy by latent heat release. Over the eastern Atlantic, the conversion of zonal kinetic energy to eddy kinetic energy was the major process in maintaining the waves.

Spectrum analysis of the 850 and 700 mb winds for a large number of African stations revealed that the main wave growth during Phase III took place between 10°E and the Greenwich meridian. At 700 mb it was possible to trace a wave signal as far east as southern Arabia. However, any waves present east of 10°E were too weak to be of practical importance.

During Phases I and II a second type of synoptic-scale disturbance was observed to form irregularly near the African coast. This type of disturbance, which had a horizontal scale of about 1000 km, reached its maximum amplitude near 850 mb and was characterized by enhanced convection that showed no preferred location relative to the center. During Phase III the flow patterns at 850 mb and 700 mb were closely coupled and all disturbances were of the wave type. Prior to GATE it was usual for operational forecasters to distinguish, on the basis of satellite imagery, between ITCZ disturbances and easterly waves in the tropical Atlantic. However, it is not clear whether the second type of disturbance mentioned above can be identified with the ITCZ disturbances inferred from satellite imagery.

Tropical storms and hurricanes constitute another class of synoptic-scale system that occur within the broad region encompassed by GATE. During 1974 seven tropical storms formed in the Atlantic well to the west of the A/B-scale networks and four of these strengthened into hurricanes. Of the seven storms, four developed from wave disturbances that were first observed over Africa. Three of the four later attained hurricane intensity. A fifth tropical storm began as a weak, non-wave type of disturbance near the African coast. Two of the storms were induced by upper tropospheric cyclones located slightly to the north of the A-scale network in the vicinity of 70°W.

The upper-level cyclones were another important class of synoptic-scale disturbance observed during GATE. Such cyclones have long been recognized as a regular feature of the upper level troughs that develop over the Atlantic (and Pacific) in summer. Twenty-three of the cyclones were

detected, seven in Phase I, six in Phase II and ten in Phase III. During the latter phase, three of the cyclones induced circulations in the surface wind field.

Acknowledgments. The contributions of Dr. Burpee and Prof. Reed were supported jointly by the National Science Foundation (grants ATM-8017245 and ATM-8103697, respectively) and the National Oceanic and Atmospheric Administration. Dr. Burpee was a visitor at the Massachusetts Institute of Technology during the planning and initial preparation of the manuscript. The authors appreciate the comments of the formal reviewers, Dr. V. Ivanov and Prof. M. Yanai, and the suggestions made informally by Prof. R. Johnson, Mr. M. Lawrence, Dr. L. Shapiro and Prof. D. Stevens.

REFERENCES

Albignat, J. P. and R. J. Reed, 1980: The origin of African wave disturbances during Phase III of GATE. Mon. Wea. Rev. (accepted for publication).

Arnold, J. E., 1966: Easterly wave activity over Africa and in the Atlantic with a note on the intertropical convergence zone during early July 1961. SMRP Res. Pap. No. 65, Dept. Geophys. Sci., The Univ. of Chicago, 23 pp.

Aspliden, C. I., 1974: The low-level wind field and associated perturbations over tropical Africa during northern summer. Preprint Vol., Intern. Trop. Meteor. Meeting, Nairobi, Kenya, Amer. Meteor. Soc., Boston, Mass., 218-223.

_____, G. A. Dean and H. Landers, 1965: Satellite study, tropical North Atlantic, 1963, Part I, surface wind analyses, July 26-August 31. Final Rept. Grant No. WBG 32, Dept. of Meteor., Florida State University, 110 pp.

_____, _____ and _____, 1966a: Satellite study, tropical North Atlantic, 1963, Part I, surface wind analyses, September 1-September 30. Final Rept. Grant No. WBG 32, Dept. of Meteor., Florida State University, 89 pp.

_____, _____ and _____, 1966b: Satellite study, tropical North Atlantic, 1963, Part I, surface wind analyses, October 1-November 10. Final Rept. Grant No. WBG 32, Dept. of Meteor., Florida State University, 105 pp.

_____, Y. Tourre and J. B. Sabine, 1976: Some climatological aspects of West African disturbance lines during GATE. Mon. Wea. Rev., 104, 1029-1035.

Atkinson, G. D. and J. C. Sadler, 1970: Mean cloudiness and gradient wind charts over the tropics. U.S. Air Weather Service, Tech. Report 215, 2 vols.

Burpee, R. W., 1971: The origin and structure of easterly waves in the lower troposphere of North Africa. Ph.D. Thesis, Mass. Inst. Tech., 100 pp.

_____, 1972: The origins and structure of easterly waves in the lower troposphere of North Africa. J. Atmos. Sci., 29, 77-90.

_____, 1974: Characteristics of North African easterly waves during the summers of 1968 and 1969. J. Atmos. Sci., 31, 1556, 1570.

_____, 1975a: Weather Forecasting for GATE. GATE Report No. 14, Volume I, ICSU/WMO, Geneva, Switzerland, 96-100.

_____, 1975b: Some features of synoptic-scale waves based on compositing analysis of GATE data. Mon. Wea. Rev., 103, 921-925.

_____ and G. Dugdale, 1975: A summary of weather systems affecting western Africa and the eastern Atlantic during GATE. GATE Report No. 16, ICSU/WMO, Geneva, Switzerland, 2.1-2.42.

Carlson, T. N., 1969a: Synoptic histories of three African disturbances that developed into Atlantic hurricanes. Mon. Wea. Rev., 97, 256-276.

_____, 1969b: Some remarks on African disturbances and their progress over the tropical Atlantic. Mon. Wea. Rev., 97, 716-726.

_____, 1971: An apparent relationship between the sea-surface temperature of the tropical Atlantic and the development of African disturbances into tropical storms. Mon. Wea. Rev., 99, 309-310.

_____ and J. M. Prospero, 1972: The large-scale movement of Saharan air outbreaks over the northern equatorial Atlantic. J. Appl. Meteor., 11, 283-297.

Charney, J. G. and M. E. Stern, 1962: On the stability of internal baroclinic jets in a rotating atmosphere. J. Atmos. Sci., 19, 159-172.

Chen, Y.-L., 1980: The relationship between organized convective systems and large-scale fields observed in GATE. Ph.D. Thesis, Lab. for Atmos. Res., University of Illinois, Urbana, Ill., 148 pp.

Cho, H.-R., 1977: Contributions of cumulus cloud life-cycle effects to the large-scale heat and moisture budget equations. J. Atmos. Sci., 34(1), 87-97.

_____, et al., 1979: Atmosphere-Ocean, 17, No. 1.

Chu, J.-H., M. Yanai and C.-H. Sui, 1981: Effects of cumulus convection on the vorticity field in the tropics. Part 1: The large-scale budget (submitted to J. Meteor. Soc., Japan).

Cox, S. K. and K. T. Griffith, 1979: Estimates of radiative divergence during Phase III of the GARP Atlantic Tropical Experiment: Part I. Methodology. J. Atmos. Sci., 36, 576-585.

Dean, G. A., 1978: Atlas of GATE synoptic analyses, Phase III. Dept. of Meteorology, Florida State University, 167 pp.

_____ and N. E. LaSeur, 1974: The mean structure and its synoptic-scale variations of the African troposphere. Preprint Vol., Intern. Trop. Meteor. Meeting, Nairobi, Kenya, Amer. Meteor. Soc., Boston, Mass., 224-228.

_____ and C. Smith, 1977: A study of synoptic and mesoscale interaction over the GATE ship network: 4-5-6 September 1974. NCAR Technical Note - 122+STR, 95 pp.

Depradine, C., R. Pasch and T. N. Krishnamurti, 1978: An atlas of the motion field over the GATE area, Part III, 300 mbs. Rept. No. 78-4, Dept. of Meteor., Florida State Univ., Tallahassee, Florida, 133 pp.

Dhonneur, G., L. Finaud, R. Garnier, L. Gaucher and D. Rossignol, 1973: An analysis of two weather disturbances developing into tropical depressions. ASECNA Applied Research Team Project Report, Dakar, Senegal, 83 pp.

Dunn, G. E., 1940: Cyclogenesis in the tropical Atlantic. Bull. Amer. Meteor. Soc., 21, 215-229.

Edmon, H. J., Jr. and D. G. Vincent, 1979: Large-scale atmospheric conditions during the intensification of Hurricane Carmen (1974) II. Diabatic heating rates and energy budgets. Mon. Wea. Rev., 107, 295-313.

Eldridge, R. H., 1957: A synoptic study of West African disturbance lines. Quart. J. Roy. Meteor. Soc., 83, 303-314.

Erickson, C. O., 1963: An incipient hurricane near the West African coast. Mon. Wea. Rev., 91, 61-68.

Estoque, M. A. and M. Douglas, 1978: Structure of the intertropical convergence zone over the GATE area. Tellus, 30, 55-61.

Frank, N., 1969: The "inverted V" cloud pattern - an easterly wave? Mon. Wea. Rev., 97, 130-140.

_____, 1970: Atlantic tropical systems of 1969. Mon. Wea. Rev., 98, 307-314.

_____, 1971: A note on Atlantic tropical systems and cloud clusters as related to GATE. Experiment Design Proposal, Vol. 2 (Annexes), ISMG/ICSU/WMO, Geneva, Switzerland, Annex VI, 23 pp.

_____ and G. Clark, 1978: Atlantic tropical systems of 1977. Mon. Wea. Rev., 106, 559-565.

_____ and P. J. Hebert, 1974: Atlantic tropical systems of 1973. Mon. Wea. Rev., 102, 290-295.

Gilchrist, A. and L. S. Matthews, 1961: Contour charts for July 1960, in the West African area. Nigerian Meteor. Service Tech. Note No. 19, 12 pp.

Hamilton, R. A. and J. W. Archbold, 1945: Meteorology of Nigeria and adjacent territory. Quart. J. Roy. Meteor. Soc., 71, 231-262.

Hann, J., 1915: Lehrbuch der Meteorologie verlag von Chr. Herm. Jauchritz. Leipzig seite 847.

Hawkins, H. F., 1976: A brief comparison of some of the conditions attending Hurricanes Carmen and Fifi (1974). NOAA Tech. Memo., ERL WMPO-31, Boulder, Colorado, 8 pp.

Hodur, R. M. and J. S. Fein, 1977: A vorticity budget over the Marshall Islands during the spring and summer months. Mon. Wea. Rev., 105, 1521-1526.

Holle, R. L., J. Simpson and S. W. Leavitt, 1979: GATE B-scale cloudiness from whole-sky camaras on four U.S. ships. Mon. Wea. Rev., 107(7), pp. 874-895.

Holton, J. R., 1979: An introduction to dynamic meteorology, 319 pp.

Hope, J. R., 1975: Atlantic hurricane season of 1974: Mon. Wea. Rev., 103, 285-293.

Hubert, H., 1939: Origine Africaine d'un cyclone tropical atlantique. Ann. Physique du Globe de la France d'Outre-Mer, 6, 97-115. Summarized by C. F. Brooks, 1940: Hubert on the African origin of the hurricane of 1938. Trans. Amer. Geophys. Union, 21, 251-253.

Hudlow, M. D. and V. L. Patterson, 1979: GATE Radar Rainfall Atlas, NOAA Special Report, U.S. Dept. of Commerce, Washington, D.C.

ISMG, 1975: Report on the field phase of the GARP Atlantic Tropical Experiment Meteorological Atlas. GATE Report No. 17, ICSU/WMO, Geneva, Switzerland, 179 pp.

Johnson, R. H., 1976: The role of convective-scale precipitation downdrafts in cumulus and synoptic-scale interactions. J. Atmos. Sci., 33, 1890-1910.

_____, 1978: Cumulus transports in a tropical wave composite for Phase III of GATE. J. Atmos. Sci., 35, 484-494.

_____, 1980: Diagnosis of convective and mesoscale motions during Phase III of GATE. J. Atmos. Sci., 37, 733-753.

Krishnamurti, T. N., 1978: Large-scale features of the tropical atmosphere. Meteorology over the tropical oceans. Roy. Meteor. Soc., Bracknell, United Kingdom, 31-56.

_____, R. Pasch and C. Depradine, 1978: An atlas of the motion field over the GATE area: Part I, 200 mbs. Rept. No. 78-1, Dept. of Meteor., Florida State University, Tallahassee, Fla., 133 pp.

_____, V. Wong, H. L. Pan, G. V. Dam and D. McClellan, 1976: Sea-surface temperatures for GATE. Rept. 76-3, Dept. of Meteor., Florida State University, Tallahassee, Fla.

Kung, E. C. and H. A. Burgdorf, 1977: Maintenance of kinetic energy in large-scale tropical disturbances over the eastern Atlantic. Quart. J. Roy. Meteor. Soc., 104, 393-411.

LaSeur, N. E., 1971: A meteorological perspective for GATE. Experiment Design Proposal, Vol. 2 (Annexes), ISMG/ICSU/WMO, Geneva, Switzerland, Annex II, 18 pp.

Lawrence, M. B., 1978: Atlantic hurricane season of 1977. Mon. Wea. Rev., 106, 534-545.

Leary, C. A., 1979: Behaviour of the wind field in the vicinity of a cloud cluster in the Intertropical Convergence Zone. J. Atmos. Sci., 36, 631-639.

_____ and R. A. Houze, Jr., 1979: Melting and evaporation of hydrometeors in precipitation from the anvil clouds of deep tropical convection. J. Atmos. Sci., 36, 669-679.

Lewis, B. M. and D. P. Jorgensen, 1978: Study of the dissipation of Hurricane Gertrude (1974). Mon. Wea. Rev., 106, 1288-1306.

Lorenz, E. N., 1955: Available potential energy and the maintenance of the general circulation. Tellus, 7, 157-167.

Malkus, J. S. and H. Riehl, 1964: Cloud structure and distributions over the tropical Pacific Ocean. Univ. of Calif. Press, Los Angeles, 229 pp.

Marks, F. D., 1981: A tropical mesoscale convection line. Ph.D. Thesis, Dept. of Meteorology, Massachusetts Institute of Technology, Cambridge, Mass., 135 pp.

Mass, C., 1978: A numerical and observational study of African wave disturbances. Ph.D. Thesis, Dept. of Atmospheric Sciences, University of Washington, Seattle, 277 pp.

McBride, J. L. and W. M. Gray, 1978: Mass divergence in tropical weather systems. Atmos. Sci. Paper No. 299, Dept. of Atmos. Sci., Colorado State University, Fort Collins, 109 pp.

McGarry, M. M. and R. J. Reed, 1978: Diurnal variations in convective activity and precipitation during Phases II and III of GATE. Mon. Wea. Rev., 106, 103-113.

Mower, R. N. et al., 1979: A case study of GATE convective activity. Atmosphere-Ocean, 17, No. 1.

Murakami, M., 1979: Large-scale aspects of deep convective activity over the GATE area. Mon. Wea. Rev., 107, 994-1013.

Neumann, C. J., G. W. Cry, E. L. Caso and B. R. Jarvinen, 1978: Tropical cyclones of the North Atlantic Ocean, 1871-1977. National Climatic Center and National Hurricane Centre, NOAA, 170 pp. (NTIS No. 003-017-00425-2).

Nitta, T., 1970: A study of the generation and conversion of eddy available potential energy in the tropics. J. Meteor. Soc., Japan, 48, 524-528.

_____, 1975: Observational determination of cloud mass flux distributions. J. Atmos. Sci., 32, 73-91.

_____, 1977: Response of cumulus updraft and downdraft to GATE A/B-scale motion systems. J. Atmos. Sci., 34, 1163-1186.

_____, 1978: A diagnostic study of interaction of cumulus updrafts and downdrafts with large-scale motions in GATE. J. Meteor. Soc., Japan, 56, 232-242.

_____, 1979: On the comparison of computed cloud mass fluxes with observations over the GATE area. J. Meteor. Soc., Japan, 57, 474-478.

Norquist, D. C., E. E. Recker and R. J. Reed, 1977: The energetics of African wave disturbances as observed during Phase III of GATE. Mon. Wea. Rev., 105, 334-342.

Ogura, Y., Y.-L. Chen, J. Russell and S.-T. Soong, 1979: On the formation of organized convective systems observed over the eastern Atlantic. Mon. Wea. Rev., 107, 426-441.

_____ and H.-R. Cho, 1973: Diagnostic determination of cumulus cloud populations from observed large-scale variables. J. Atmos. Sci., 30, 1276-1286.

Okulaja, F. O., 1970: Synoptic flow perturbations over West Africa. Tellus, 22, 663-680.

Pasch, R. J., T. N. Krishnamurti and C. Depradine, 1978: An atlas of the motion field over the GATE area Part II, 250 mbs. Report No. 78-3 Dept. of Meteor., Florida State University, Tallahassee, Fla. 133 pp.

Payne, S. W., 1978: The large-scale structure and properties of the disturbance of 15 to 18 September 1974, over the GATE B-scale ship array. M.S. Thesis, Dept. of Atmospheric Sciences, University of Washington, Seattle, 112 pp.

Payne, S. W. and M. M. McGarry, 1977: The relationship of satellite inferred convective activity to easterly waves over west Africa and the adjacent ocean during Phase III of GATE. Mon. Wea. Rev., 105, 414-420.

Petrossiants, M. A., V. N. Ivanov, V. V. Galushko and Yu. A. Menshov, 1975: On characteristic time scales of meteorological fields in the tropical Atlantic zone. ICSU/WMO. GATE Report No. 14, Vol. II, pp. 48-63.

Piersig, W., 1936: Schwankungen von Luftdruck und Luftbewegug sowie ein Beitrag zum Wettergeschehen in Passategebiet des ostlichen Nord-atlantischen Ozeans. Arch. Deut. Seewarte, 54, No. 6, Parts II and III have been translated and printed, 1944: The cyclonic disturbances of the subtropical eastern North Atlantic. Bull. Amer. Meteor. Soc., 25, 2-17.

Reed, R. J., 1978: The structure and behaviour of easterly waves over West Africa and the Atlantic. Meteorology over the Tropical Oceans, Roy. Meteor. Soc., Bracknell, United Kingdom, 57-71.

_____, 1980: Energetics and heat and moisture budgets of easterly waves. Proceedings of the Seminar on the Impact of GATE on Large-Scale Numerical Modeling of the Atmosphere and Ocean. Woods Hole, Massachusetts, August 20-29, 1979. National Academy of Sciences, Washington, D.C., 31-38.

_____ and R. H. Johnson, 1974: The vorticity budget of synoptic-scale wave disturbances in the tropical western Pacific. J. Atmo. Sci., 31, 1784-1790.

_____ and R. M. Lewis, 1979: Response of upper ocean temperatures to diurnal and synoptic-scale variations of meteorological parameters in the GATE B-scale area. Deep Sea Research, 25 (Suppl. I): 99-114.

_____, D. C. Norquist and E. E. Recker, 1977: The structure and properties of African wave disturbances as observed during Phase III of GATE. Mon. Wea. Rev., 103, 317-333.

_____ and E. E. Recker, 1971: Structure and properties of synoptic-scale wave disturbances in the equatorial western Pacific. J. Atmos. Sci., 28, 1117-1133.

Reeves, R. W., C. F. Ropelewski and M. D. Hudlow, 1979: Relationship between large-scale motion and convective precipitation during GATE. Mon. Wea. Rev., 107, 1154-1168.

Regula, H., 1936: Druckschwankungen und Tornados an der Westkuste von Africa. Ann. Hydrogs, Maritimen Meteor., 64, 107-111. Translated and printed, 1943: Pressure changes and "tornadoes" (squalls) on the west coast of Africa. Bull. Amer. Meteor. Soc., 24, 311-317.

Reynolds, R., 1977: Large-scale (A-scale) mean features of the GATE atmosphere during Phase III. Meto. O. 20, Tech. Rept. No. II/105, British Met. Office, Bracknell, United Kingdom.

Riehl, H., 1945: Waves in the easterlies and the polar front in the tropics. Misc. Rept. No. 17, Dept. of Meteor., Univ. of Chicago, Chicago, Ill., 79 pp.

_____, 1954: Tropical Meteorology. McGraw-Hill, New York, N.Y., 392 pp.

Romanov, Y. A. and N. A. Romanova, 1980: Atmospheric circulation along the meridian 23.5°W during TROPEX-74. Chapter in Atmospheric Circulation and its Interaction with the Ocean in the Tropical Zone, edited by V. S. Samoilenko, M. Nauka, in Russian.

Sadler, J. C., 1967: The tropical upper tropospheric trough as a secondary source of typhoons and a primary source of tradewind disturbances. Institute of Geophysics, University of Hawaii.

_____, 1975: The monsoon circulation and cloudiness over the GATE area. Mon. Wea. Rev., 103, 369-387.

Sadler, J. C. and L. K. Oda, 1978: The synoptic (A) scale circulations during the third phase of GATE, 20 August-23 September 1974. Dept. of Meteor., University of Hawaii, Honolulu, 41 pp.

_____ and _____, 1979: The synoptic (A) scale circulations during the second phase of GATE, 17 July - 19 August, 1974. Dept. of Meteor., University of Hawaii, Honolulu, 36 pp.

_____ and _____, 1980: GATE Analyses. I. The Synoptic (A) Scale Circulations during Phase I, 26 June - 16 July 1974. II. Means for Phases I, II and III. Dept. of Meteor., University of Hawaii, Honolulu, 32 pp.

Schove, D. J., 1946: A further contribution to the meteorology of Nigeria. Quart. J. Roy. Meteor. Soc., 72, 105-110.

Seguin, W. R. and P. Sabol, 1976: GATE Convection Subprogram Data Center: Shipboard Precipitation Data. NOAA Tech. Rept. EDS 18 (NTIS Ref. No. PB-263 820/3GI).

Shapiro, L. J., 1978: The vorticity budget of a composite African tropical wave disturbance. Mon. Wea. Rev., 106, 806, 817.

_____ and D. E. Stevens, 1980: Parameterization of Convective Effects on the Momentum and Vorticity Budgets of Synoptic-Scale Atlantic Tropical Waves. Mon. Wea. Rev., 108, pp. 1816-1826.

Simpson, R. H., N. Frank, D. Shideler and H. M. Johnson, 1968: Atlantic tropical disturbances, 1967. Mon. Wea. Rev., 96, 251-259.

Stevens, D. E., 1979: Vorticity, momentum and divergence budgets of synoptic-scale wave disturbances in the tropical eastern Atlantic. Mon. Wea. Rev., 107, 535-550.

_____, R. S. Lindzen and L. J. Shapiro, 1977: A new model of tropical waves incorporating momentum mixing by cumulus convection. Dyn. Atmos. Oceans, 1, 365-425.

Thompson, O. E. and J. Miller, 1976: Hurricane Carmen: August-September 1974 - Development of a wave in the ITCZ. Mon. Wea. Rev., 104, 1194-1199.

Thompson, R. M., Jr., 1977: Preliminary heat and moisture budgets over the B-scale ship array during Phase III of GATE. M.S. Thesis, Dept. of Atmospheric Sciences, University of Washington, Seattle, 103 pp.

_____, S. W. Payne, E. E. Recker and R. J. Reed, 1979: Structure and properties of synoptic scale wave disturbances in the intertropical convergence zone in the eastern Atlantic. J. Atmos. Sci., 36, 53-72.

Viltard, A. and P. de Félice, 1979: Statistical analysis of wind velocity in an easterly wave over West Africa. Mon. Wea. Rev., 107, 1320-1327.

Vincent, D. G. and R. G. Waterman, 1979: Large-scale atmospheric conditions during the intensification of Hurricane Carmen (1974) I. Temperature, moisture and kinematics. Mon. Wea. Rev., 107, 283-294.

Wallace, J. M., 1971: Spectral studies of tropospheric wave disturbances in the tropical western Pacific. Rev. Geophys. Space Phys., 9, 557-612.

Williams, K. T., 1970: A statistical analysis of satellite observed trade wind cloud clusters in the western North Pacific. Atmos. Sci. Paper No. 161, Colorado State University, Fort Collins, 80 pp.

Williams, K. T. and W. M. Gray, 1973: Statistical analysis of satellite-observed trade wind cloud. Tellus, 25(4), 313-336.

Woodley, W. L., C. G. Griffith, J. S. Griffin and S. C. Stromatt, 1980: The inference of GATE convective rainfall from SMS-1 imagery. J. Appl. Meteor., 19, 388-408.

Yanai, M., S. Esbensen and J.-H. Chu, 1973: Determination of bulk properties of tropical cloud clusters from large-scale heat and moisture budgets. J. Atmos. Sci., 30, 611-627.

Zipser, E. J. and C. Gautier, 1978: Mesoscale events within a GATE tropical depression. Mon. Wea. Rev., 106, 789-805.

CHAPTER 5

THEORETICAL STUDIES OF TROPICAL WAVES

by

E. M. Dobryshman

(Institute of Atmospheric Physics,
Academy of Sciences of the U.S.S.R., Moscow, U.S.S.R.)

5.1 INTRODUCTION

The structure and contents of this Chapter are in a sense outside of the general plan of the book due to various reasons. The monograph summarizes the results gathered during GATE; no special theoretical investigations on waves in GATE area have been made either during GATE or in the pre-GATE years. Therefore, strictly speaking, it is impossible to sum up the results. At the same time the theory of atmospheric waves was developed and is continuously being developed rather intensively. The great part of the results have been reflected in numerous papers and books and are well known in the meteorological community (U.S. GATE Central Program Workshop; Proceedings of the International Scientific Conference on Energetics of the Tropical Atmosphere (Tashkent, 14-21 September, 1977); several issues of GATE reports; TROPEX-72; TROPEX-74; Journals: Journal of Atmospheric Sciences, Tellus, Quarterly Journal of the Royal Meteorological Society, Journal of the Japan Meteorological Society; La météorologie; Meteorology and Hydrology; Izvestiya AN SSSR - (both are available in Russian and English). The great part of the wave theory is created by linear models. To enumerate the main available results, sometimes contradicting each other, more space is required than the chapter's limit permits.

On the other hand, the development of nonlinear wave theories in various fields of modern physics and the result of the investigation of small-scale (C, D scale) disturbances which occured during GATE stimulated the search of both kinds of solutions and broadened the possibility of interpretation of these very solutions. The author's firm belief is that the nonlinear processes in many cases are much more interesting than the linear ones. The results of nonlinear effects especially for small scale waves are known not so well as the results of the linear models. That is why the chapter treats only some of the findings, with more detailed mathematical presentation given to not too wellknown results which are described in the first four sections (5.1-5.5). These are:

(a) Small-scale waves in the narrow equatorial belt.

(b) The waves in the 5°-15° latitudinal belt, where the variation with coordinate of coefficients even in the linear models strongly affects the wave parameters.

(c) Two effects inherent only to nonlinear models, namely, the resonant interaction of wave triplet and solitary waves of a soliton type. No doubt, the indication to the existence of these nonlinear effects may be found by a careful analysis of the GATE data.

Out of numerous findings on tropical wave theory Section 5.6 emphasizes the following:

- barotropic and baroclinic instability in the generation of waves;
- wave-CISK mechanism.

When arranging the material the author had in mind two somewhat conflicting goals: first, to make the results simple for understanding and illustrative and, second, to describe sophisticated complete physical models which use rather complex instruments of investigation. This task was made most difficult in Section 5.6, for the relevant papers are numerous and the author could name hundreds of those; so the List of References contains only the titles of papers which are being discussed or out of which formulae or figures are being used. Bibliography for Section 5.5 can be found in a number of reviews such as GARP Publication Series N 20 (1978); Yanai, 1975 , as well as in numerous GATE reports and in two already published "GATE Bibliographies". And finally, Section 5.6 briefly treats a basic technique for revealing periodic processes, the illustrations being mainly based on GATE data.

5.2 THE SCALE OF MOTIONS AND DETERMINATION OF THE EQUATORIAL BELT WIDTH

The spectrum of the atmospheric waves is quite large ranging from ultrasonic oscillations to the climatic changes. No theoretical description of the whole spectrum is possible. Moreover it is not reasonable. To study a definite portion of the spectrum certain simplifications are used which would emphasize the features of the spectrum portion under study cutting out (or at least diminishing as much as possible) the rest. Three types of atmospheric waves are important in meteorological processes. They are: inertia, gravity and Rossby waves. These three components of the wave spectrum cannot be isolated on the spectrum diagram or be distinguished physically.

To theoretically study the above mentioned three types of waves it is necessary to retain the terms responsible for the inertial, gravitational and hyroscopic effects, the latter being due to the Coriolis acceleration and is described by the Coriolis parameter and by their variations with latitude. Usually, a well-known β -plane approximation is used. The nearer to the equator, the greater the Rossby parameter $\beta = 2\omega\cos\varphi/r_0$ becomes. Thus, appearance of Rossby waves as well as the β - effect itself would manifest in the low latitudes. But there are two difficulties in analysing and interpreting the theoretical results. Being a physical phenomenon the Rossby waves cannot be very short either in the x -direction or in the y -direction (they should be at least several hundred kilometers). When β is close to the equatorial value

$$\beta_e = 2\omega/r_0$$

we have to consider very short waves along the longitude; it is not allowed to "climb over" the equator.

The second difficulty is due to the fact that the main component $2\omega\sin\varphi$ becomes zero just at the equator. Thus, it is necessary to take into account the term $2\omega\cos\varphi\cdot w$ which is usually omitted when dynamic equations are analysed. A rough value of the equatorial belt width, that is the belt where the term $2\omega\cos\varphi\cdot w$ plays a significant role (or it would be more appropriate to say: where the geostrophical approximation is inapplicable) may be found from a dynamic equation corresponding to the axis x (along the equator eastward). For simplicity let us consider the zonal model $(\partial/\partial x \equiv 0)$

$$\frac{\partial u}{\partial t} + v\frac{\partial u}{\partial y} + w\frac{\partial u}{\partial z} - 2\omega\frac{y}{r_0}v + 2\omega w = 0 \Rightarrow$$

$$\Rightarrow \frac{d}{dt}\left(u - \frac{\omega y^2}{r_0} + 2\omega z\right) = 0 \; ; \; \frac{d}{dt} \equiv \frac{\partial}{\partial t} + v\frac{\partial}{\partial y} + w\frac{\partial}{\partial z}$$

This formula reflects the theorem of angular momentum conservation. Comparing two Coriolis terms $\omega y^2/r_0$ and $2\omega z$ we get an estimation of the equatorial belt width

$$L = \sqrt{2 r_0 h} \quad *)$$

Introducing into this formula h = 17 km, i.e. the thickness of the equatorial troposphere, we get L = 460 km. Thus, the equatorial belt is about 900-1000 km. Within this belt there should exist a certain dynamic regime. The width of the equatorial belt is rather small in terms of large-scale disturbances. Hence two consequences: 1. Within this belt we cannot speak of large-scale disturbances. 2. If any wave disturbances ever occur in this belt, they must be small-scale ones. Since theoretically a disturbance is usually described by a wave, or their sum, we conclude that within this belt waves are smaller as compared to synoptic-scale waves.

A careful and detailed analysis of a complete system of the hydrodynamic equations shows that it is appropriate to divide the tropical atmosphere from the point of view of dynamics of the processes into three parts**: 1. The equatorial belt, 4-5° of latitude on both sides of the equator (by the way tropical cyclones or hurricanes never happen in this belt). 2. The transitional zone from 4°-5° latitudes up to 15°-latitude. It is here that the ITCZ is located and a great number of typhoons and tropical cyclones generate here. In this very zone it is possible to use geostrophical approximation only for u-zonal wind component but not for v. Just here β-effect combined with other effects is stronger than in other latitudes. 3. The tropical zone up to 30°-latitude in which u and v may be replaced by geostrophic wind (it is clear that here a large-scale motion is meant, not a small-scale one). Certainly there are no rigid boundaries between the mentioned zones. Moreover, for different models the positions of the boundaries are different. However the introduction of such zones simplifies theoretical investigations of wave disturbances in the tropical atmosphere.

To analyse the large-scale disturbances in the tropics in a first guess we may neglect the small-scale processes in the narrow equatorial belt; then we should study the equatorial belt independently, but one should be quite careful interpreting theoretical investigations of large-scale disturbances and applying the results in the vicinity of the equator, especially in the equatorial belt.

5.3 LARGE-SCALE DISTURBANCES. ROSSBY WAVES, KELVIN WAVES, MIXED ROSSBY-GRAVITY WAVES

Let us consider the small amplitude deviations from quiet conditions which are met by the static equation. Putting the Cartesian coordinates just at the equator we may use the linear system of hydrodynamic equations in the form:

*By chance this formula is the same as the formula of "length of visibility" on the Earth. This is a rather unexpected result from the nature of Coriolis acceleration.

**For detail see Dobryshman (1980-a).

$$\left.\begin{aligned} &\frac{\partial u}{\partial t} - \beta y v = -\frac{\partial H}{\partial x} \qquad && \frac{\partial v}{\partial t} + \beta y u = -\frac{\partial H}{\partial y} \\ &\frac{\partial u}{\partial x} + \frac{\partial v}{\partial y} + \frac{\partial w}{\partial z} - \delta w = 0 \\ &\frac{\partial H}{\partial z} = \delta R T \qquad && \frac{\partial \bar{T}}{\partial t} + \Gamma w = \varepsilon \end{aligned}\right\} \qquad (5.1)$$

Here H - geopotential, δ - parameter of compressibility of the atmosphere ($\sim 1/\rho \cdot d\rho/dz$ where ρ is density), $\Gamma = \gamma_a - \gamma$ is the parameter of vertical stability; z coordinate is

$$z = -\frac{1}{\delta} \ln \frac{\mathcal{P}}{\mathcal{P}_0}$$ where $\mathcal{P}$ is pressure; R is gas constant.

Let us assume that thermal forcing may be presented in the form:

$$\varepsilon = \varepsilon_1(y)\,\varepsilon_2(z)\, e^{z\delta/2}\, e^{i(mx-\sigma t)} \qquad (5.2)$$

Using the operators $L = \frac{\partial}{\partial z} - \frac{\delta}{2}$; $\bar{L} = \frac{\partial}{\partial z} + \frac{\delta}{2}$

we shall seek the unknown functions in the form

$$\left.\begin{aligned} u &= u_1(y)\, L\, w(z) \\ v &= v_1(y)\, L\, w(z) \\ H &= \varepsilon_1(y)\, L\, w(z) \\ T &= \varepsilon_1(y)\, L\, \bar{L}\, w(z) \\ w &= \varepsilon_1(y)\, w(z) \end{aligned}\right\} \times e^{i(mx-\sigma t)} \qquad (5.3)$$

After conventional procedure of division of variables we come to the following system of equations:

$$\left.\begin{aligned} &i\sigma u_1 + \beta y v_1 - i m \varepsilon_1 = 0 \\ &\beta y u_1 - i\sigma v_1 + \frac{d\varepsilon_1}{dy} = 0 \\ &i m u_1 + \frac{dv_1}{dy} - \alpha \varepsilon_1 = 0 \end{aligned}\right\} \qquad (5.4)$$

$$\frac{d^2 w}{dz^2} + \left(\frac{\Gamma \delta R}{\sigma g h} - \frac{\delta^2}{4}\right) w - \frac{\alpha}{g h}\, \varepsilon_2 = 0 \qquad (5.5)$$

Here h is division constant. It means the "depth" of the atmospheric column. α is the parameter which may be taken in the form

$$\alpha = -\frac{i\sigma}{gh} \qquad (5.6)$$

w must satisfy the two conditions

$$z = 0 : \quad w = 0 \; ; \; z = z_T : \frac{dw}{dz} = i\sqrt{\frac{\Gamma \delta R}{\sigma g h} - \frac{\delta^2}{4}}\, w \qquad (5.7)$$

where Z_T is the level above which $\varepsilon_2(z) \equiv 0$ ($Z_T \approx 20$ km)

One difficulty of a purely mathematical nature arises when one is trying to solve an eigenvalue problem of such kind. This difficulty is due to the fact that Coriolis terms in (5.1) and therefore in (5.4) are not precise. (Later we shall discuss this in greater detail). From system (5.4) it is possible to find the equation for any unknown function u_1, v_1 or ε_1. But it is more suitable to deal with v_1 because we don't need to differentiate with respect to y the nominator. Taking into account (5.6) the equation for v becomes as follows:

$$\frac{d^2 v_1}{d\zeta^2} - \left[\zeta^2 + \frac{\sqrt{gh}}{\beta}\left(m^2 + \frac{\beta m}{\sigma}\right) - \frac{\sigma^2}{\beta\sqrt{gh}}\right] v_1 = 0 \qquad (5.8)$$

where ζ is the dimensionless coordinate

$$y = \sqrt[4]{\frac{gh}{\beta^2}}\,\zeta \qquad (5.9)$$

The equation (5.8) has a limited (when $y \to \pm\infty$) solution if and only if

$$\frac{1}{\beta}\left[\frac{\sigma^2}{\sqrt{gh}} - \left(m^2 + \frac{\beta m}{\sigma}\right)\sqrt{gh}\right] = 2n+1 \qquad (n = 0, 1, 2, \ldots)$$

Hence only discrete values of $\sqrt{gh} = \sqrt{gh_n}$ are suitable

$$\sqrt{gh_n} = -\frac{\beta(2n+1)}{2m\left(m+\frac{\beta}{\sigma}\right)}\left[1 \mp \sqrt{1 + \frac{4\sigma^2 m\left(m+\frac{\beta}{\sigma}\right)}{\beta^2 (2n+1)^2}}\right] \qquad (5.10)$$

Under such conditions the $v_1 = v_{1,n}(y)$ may be expressed by Hermite polinomial H_n, namely

$$v_1 = v_{1,n}(y) = C_n H_n\left(\frac{\beta y}{\sqrt{gh_n}}\right) \exp\left[-\frac{\beta y^2}{2\sqrt{gh_n}}\right] \qquad (5.11)$$

(C_n is constant).

It follows from (5.10) that when $n \to \infty$ one sequence of eigenvalues tends to zero and the second - to the value of $-\beta(2n+1)/m(m+\beta/\sigma)$. In the first case we have a pattern similar to the shallow waves. The corresponding waves are named gravity waves. In the second case, when n is not large, the $\sqrt{gh_n}$ are close to the $-\beta/m^2$ which corresponds to classical Rossby formula. By this fact the waves (n is not large) are called mixed Rossby-gravity waves.

When v_1 is known, there is no problem to find out u_1 and ε_1 directly from system (5.4). It is significant that the spectrum of eigenvalue for the v_1 begins with $n = 0$, but for u_1 and ε_1 - with $n = -1$; $n = -1$ corresponds to the Kelvin waves.

$$v_{1,-1} = 0 \quad ; \qquad u_{1,-1} = \mathcal{D}_{-1} \exp\left[-\frac{\beta y^2}{2\sqrt{g h_{-1}}}\right]$$

$$\varepsilon_{1,-1} = E_{-1} \exp\left[-\frac{\beta y^2}{2\sqrt{g h_{-1}}}\right]$$

$\mathcal{D}_{-1}$ and E_{-1} are constant.

As to W_1, the equation (5.5) must be one of oscillation type. Hence only those n are suitable, for which

$$\lambda_n^2 = \frac{\Gamma \delta R}{g h_n} - \frac{\delta^2}{4} > 0$$

This relation limits the scale of the second sequence of eigenvalue, namely, Rossby type waves. Analysis shows that only $n = -1$, 0, 1 and 2 are applicable. Therefore the greatest part of energy is concentrated in several first modes.

$\varepsilon_2(z)$, the heat source distribution, is a given function. Usually ε_2 is taken in the form

$$\varepsilon_2(z) = \varepsilon_0 e^{bz} \sin \frac{\pi}{z_1} z \qquad *)$$

Parameters b and z_1 have to be chosen under the condition that $\max \varepsilon_2(z)$ lies under or over the tropopause. It is easy to satisfy the conditions (5.7) by this approximation of $\varepsilon_2(z)$.

The system (5.1) is linearized with respect to the state of rest. There is no problem in introducing the mean zonal flow with constant velocity U = const. The only change appears to be that σ should be replaced by $\sigma - Um$. When $U = U(y,z)$, not an analytical but a numerical solution can be found.

Fig. 5.1 gives an idea of the main properties of Kelvin and Rossby-gravity waves: thin line is geopotential; arrows indicate the wind. This picture is taken from Itoh (1977) and presents the results of numerical simulation at altitudes 8 and 16 km when the zonal flow is featured by a weak shear. It should be pointed out that the wind for the Rossby-gravity waves is closer to the geostrophic value than to that for the Kelvin waves.

Here is a short description of analysis of a linear system of equations applicable to the latitude belt 5°-15°.

In these latitudes the belt is influenced both by w from the equator and by v as a result of adjustment processes under a strong impact of β-effect. Bearing in mind these peculiarities, the system of linear equations may take the form:

*In several recent articles the authors use a more complex form for $\varepsilon_2(z)$ which changes quantitatively the results of computations. But the main feature remains without significant changes.

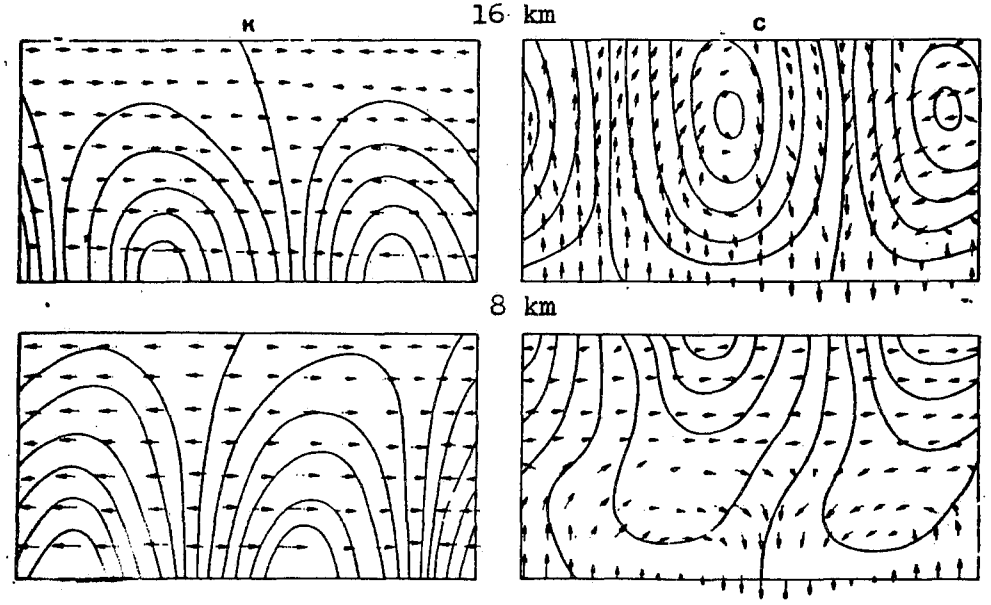

Fig. 5.1 Kelvin waves (K) and mixed Rossby-gravity waves (C) at different levels

$$\left.\begin{aligned}
&\frac{\partial u}{\partial t} - 2\omega \sin\varphi \cdot v + 2\omega \cdot \cos\varphi \cdot w = 0 \\
&\frac{\partial v}{\partial t} + 2\omega \sin\varphi \cdot u + \frac{1}{r_0}\frac{\partial H}{\partial \varphi} = 0 \\
&\frac{\partial w}{\partial t} - 2\omega \cos\varphi \cdot u + \frac{\partial H}{\partial z} = 0 \\
&\gamma \frac{\partial H}{\partial t} + \frac{1}{r_0}\frac{\partial v}{\partial \varphi} + \frac{\partial w}{\partial z} + \delta w = 0
\end{aligned}\right\} \qquad (5.12)$$

Here $\gamma = 1/c^2$ where c is the sound velocity; γ plays the role of a small parameter.

Excluding v and w we obtain the relation between u and H

$$\frac{\partial^2 u}{\partial t^2} + 4\omega^2 u = 2\omega\left[\cos\varphi \cdot \frac{\partial H}{\partial z} - \sin\varphi \cdot \frac{1}{r_0}\frac{\partial H}{\partial \varphi}\right] \qquad (5.13)$$

Excluding u and H we obtain the relation between w and v

$$\gamma\left(\frac{\partial^2 v}{\partial t^2} + 4\omega^2 \sin^2\varphi \cdot v\right) - \frac{1}{r_0^2}\frac{\partial^2 v}{\partial \varphi^2} = \frac{1}{r_0}\frac{\partial^2 w}{\partial \varphi \partial z} + \gamma 2\omega^2 \sin 2\varphi \cdot w + \frac{\delta}{r_0}\frac{\partial w}{\partial \varphi} \qquad (5.14)$$

or

$$\gamma\left(\frac{\partial^2 w}{\partial t^2} + 4\omega^2 \cos^2\varphi \cdot w\right) - \frac{\partial^2 w}{\partial z^2} - \delta\frac{\partial w}{\partial z} = \gamma 2\omega^2 \sin 2\varphi \cdot v + \frac{1}{r_0}\frac{\partial^2 v}{\partial \varphi \partial z} \qquad (5.14')$$

The term $\gamma \frac{\partial H}{\partial t}$ in (5.12) describes fast waves with a small amplitude. The presence of γ in (5.14) or (5.14') shows the influence of these fast waves on v and w. Probably this fact can be interpreted as a stronger influence of high frequency components on v and w than on u and H. Such influence may lead to an increase of variance (σ_0^2), which is proportional to the total energy of random oscillations. An investigation of power spectrum computed from the data collected during the field phase of GATE on 9 ships, showed that $\sigma_0^2(v)$ is greater than $\sigma_0^2(u)$ by about 10-15%, although $|u| > |v|$. (See TROPEX-72 and TROPEX-74).

Under the assumption that the geopotential field varies weaker as compared with the wind field ($\frac{1}{r_0}\frac{\partial H}{\partial \varphi} = \frac{\partial H}{\partial z} = 0$) it may be proved that system (5.12) has a semidiurnal period as an eigenvalue frequency. Indeed applying to (5.12) Laplace transformation according to t-variable, one gets the system:

$$\begin{aligned}
&p\bar{u} - 2\omega \sin\varphi \cdot \bar{v} + 2\omega \cos\varphi \cdot \bar{w} = p u^0(\varphi, z) \\
&2\omega \sin\varphi \cdot \bar{u} + p\bar{v} = p v^0(\varphi, z) \\
&-2\omega \cos\varphi \cdot \bar{u} + p\bar{w} = p w^0(\varphi, z) \\
&\frac{1}{r_0}\frac{\partial \bar{v}}{\partial \varphi} + \frac{\partial \bar{w}}{\partial z} + \gamma p\bar{H} = p H^0(\varphi, z)
\end{aligned}$$

Here a bar denotes the same function, but in the domain of transformation; index " 0 " denotes the initial value of the corresponding function.

The determinant of this system is

$$\mathcal{D}et\ A = \eta p^2 (p^2 + 4\omega^2) \qquad (5.15)$$

Note that $\mathcal{D}et\,A$ does not depend either on φ or z (!). This is due to a peculiarity of the Coriolis acceleration: $\cos^2\varphi + \sin^2\varphi \equiv 1$ When any kind of "simplification" is used, it is necessary to bear in mind this feature. Otherwise the result might be wrong*. Zero of the determinant corresponds to the eigenvalue frequencies. $p=0$ is double root and related to the stationary solution. The roots $p_{3,4} = \pm i2\omega$ correspond to the semidiurnal period. It is well known that the semidiurnal oscillation in the lower latitudes occurs practically in all meteorological parameters in lower troposphere (see Figs. 5.2 , 5.18 and 5.19).

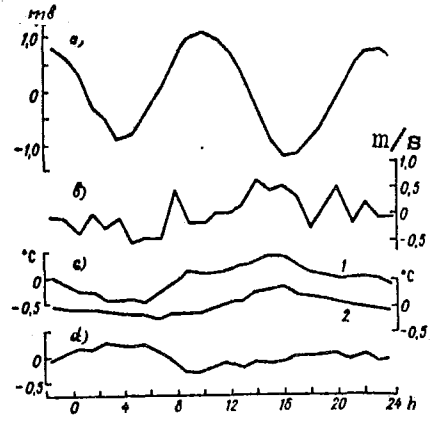

Fig. 5.2 The examples of the diurnal variations of meteorological parameters: a - pressure; b - $\sqrt{u^2+v^2}$; c - temperature of air - 1; surface water temperature - 2; d - air-sea surface temperature difference.

Assuming that wind field, namely w , has semidiurnal oscillation, it is easy to show that temperature has the same oscillation but with a phase lag of $\pi/2$, i.e. 3 hours. Really, taking the equation for T in the simplest form

$$\frac{\partial T}{\partial t} - (\gamma_a - \gamma) w = 0$$

and substituting $T,\ w \sim e^{i2\omega t}$ we find the mentioned result. Such phase lag has been documented with the help of GATE data.

---

*If $\sin\varphi$ and $\cos\varphi$ are replaced by y/r_0 and 1 respectively, then $\sin^2\varphi + \cos^2\varphi = 1 + y^2/r_0^2$ and the corresponding coefficients are functions of y instead of being constant. In some cases analytical solutions will differ greatly (in the eigenvalue problem, for instance). In numerous papers the results differ mainly due to the different ways of Coriolis parameter approximation.

5.4 SMALL-SCALE WAVES IN THE NARROW EQUATORIAL BELT

In the equatorial belt the pressure gradient is at least one order smaller than in the middle latitudes, and its component along the equator is 5-7 times smaller than along the meridian. This fact permits us to use as rough approximation zonal models ($\partial/\partial x \equiv 0$). Another peculiarity of the equatorial atmosphere is its temperature distribution with respect to z. The temperature distribution is stable and very close to being linear. It means that pressure gradient can be approximated by linear function on z. Thus, the original dynamic equations can be taken in the form:

$$\left.\begin{aligned}
&\frac{\partial u}{\partial t} + v\frac{\partial u}{\partial y} + w\frac{\partial u}{\partial z} + \left(\frac{uw}{r_0}\right) - \left(\frac{uv}{r_0^2}y\right) = \\
&\quad = 2\omega\frac{y}{r_0}v - 2\omega w + \nu\frac{\partial^2 u}{\partial z^2} \\
&\frac{\partial v}{\partial t} + v\frac{\partial v}{\partial y} + w\frac{\partial v}{\partial y} + \left(\frac{vw}{r_0}\right) + \left(\frac{u^2}{r_0^2}y\right) = \\
&\quad = A(y)\left[1 + b(y)z\right] - 2\omega\frac{y}{r_0}u + \nu\frac{\partial^2 u}{\partial z^2} \\
&\frac{\partial v}{\partial y} + \frac{\partial w}{\partial z} + \left(\frac{y}{r_0^2}v\right) = \delta w
\end{aligned}\right\} \qquad (5.16)$$

(ν is the coefficient of eddy viscosity).

An analysis of this system shows, that the terms in brackets (they reflect the result of noninertiality of spherical coordinate system) are small. It is just that they have an order or h^2/L^2 where h is thickness of the atmosphere, i.e. $\approx$ 17 km, but L is half the width of the equatorial belt, i.e. $\approx$ 400 km. The Reynolds number is of an order of $2^{-7/3} A_0^{5/3} r_0^{1/3} \omega^{-7/3} \nu^{-1}$. Here A_0 is the mean value of pressure gradient. Taking $A_0 = 10^{-5} ms^{-2}$ which fits the GATE data and $\nu = 10^2 m^2 s^{-1}$ we find $1/Re \sim O(10^{-2})$. Due to a considerable role of w in the equatorial belt, we should take the equation of motion corresponding to the axis z in the form:

$$\frac{\partial w}{\partial t} + v\frac{\partial w}{\partial y} + w\frac{\partial w}{\partial z} = -\left(\frac{RT}{\varphi}\frac{\partial \varphi}{\partial z} - g\right) + 2\omega u \qquad (5.17)$$

The terms in brackets are at least three orders greater than any other term. To avoid the "neighbourhood" of terms with quite a different magnitude order, let us build a "vorticity" equation for component $\Omega_x = \frac{\partial w}{\partial y} - \frac{\partial v}{\partial z}$. For simplicity (it is not crucially important) let us use the continuity equation in the form:

$$\frac{\partial v}{\partial y} + \frac{\partial w}{\partial z} = 0 \qquad (5.18)$$

Having introduced streamfunction ψ and having made some necessary substitutions, we shall have the equation for

$$\Omega_x = \frac{\partial^2 \psi}{\partial y^2} + \frac{\partial^2 \psi}{\partial z^2} \equiv \Delta \Psi$$

in the form:

$$\frac{\partial \Delta \Psi}{\partial t} + (\Psi, \Delta \Psi) = 2\omega \left(\frac{\partial u}{\partial y} + \frac{y}{r_0} \frac{\partial u}{\partial z} \right) - \lambda \frac{\partial \rho}{\partial y} + \alpha \frac{\partial T}{\partial y} \qquad (5.19)$$

$$\alpha = g/\tilde{T} \approx 3 \cdot 10^{-2}\ m \cdot s^{-2} (^\circ C)^{-1}\ ;\ \lambda = \alpha \gamma / g \tilde{\rho} \approx 4 \cdot 10^{-3}\ m^2 \cdot g^{-1}$$

(The terms $\lambda \frac{\partial \rho}{\partial y}$ and $\alpha \frac{\partial T}{\partial y}$ - describe the main part of baroclinicity).

The equation corresponding to the axis x - the theorem of angular momentum maintenance, $U = u - \omega y^2/r_0 + 2\omega z$, will take the form

$$\frac{\partial U}{\partial t} + (\Psi, U) = 0 \qquad (5.20)$$

Under the assumption that angular momentum U = const, the underlined expression in (5.19) becomes zero and equation (5.19) can be rewritten in the form

$$\frac{\partial \Delta \Psi}{\partial t} + (\Psi, \Delta \Psi) = \alpha \frac{\partial T}{\partial y} - \lambda \frac{\partial \rho}{\partial y} \qquad (5.19')$$

It is easy to show that $\left| \lambda \frac{\partial \rho}{\partial y} \right| \ll \left| \alpha \frac{\partial T}{\partial y} \right|$ and in many cases the term $\lambda \frac{\partial \rho}{\partial y}$ can be omitted. Thus, equation (5.19) takes the simplest form:

$$\frac{\partial \Delta \Psi}{\partial t} + (\Psi, \Delta \Psi) = \alpha \frac{\partial T}{\partial y} \qquad (5.19'')$$

We will use all three forms of vorticity equation (5.19) - (5.19").

Finally thermodynamic equation may be transformed into the form

$$\frac{\partial T}{\partial t} + (\Psi, T) = -\Gamma \frac{\partial \Psi}{\partial y} + \varepsilon(t, y, z) \qquad (5.21)$$

(5.19), (5.20) and (5.21) are basic equations for simple zonal models of motion in the equatorial belt. It should be stressed that system (5.19)-(5.21) is not applicable to large-scale processes, but only to small ones in the narrow equatorial belt. The characteristic time t_0 is inversely proportional to Brunt—Väisälä frequency $t_0 = (\alpha \Gamma)^{-1/2} \approx$ ≈ 3-5 minutes.

The system of equations has a common group of invariant transformations. From the viewpoint of invariant group theory the heat source ε is the"free element"of the group. Strictly speaking, we have to classify the solution according to the form of the free element. The group methods are rather unwieldly, and we shall give only one example which can be easily interpreted. Assuming that ε has the form

$$\varepsilon = \kappa\left[\varepsilon_0 + \varepsilon'(\tau, \eta, \zeta)\right]$$

it is easy to make sure that the transformation

$$\left.\begin{aligned} &\tau = t \;;\quad \eta = \frac{y}{\kappa} - c_1 t \;;\quad \zeta = \frac{z}{\kappa} - c_2 t \\ &\Psi = \kappa^2\left[c_2\eta - c_1\zeta + \Psi_1(\tau,\eta,\zeta)\right] \;;\quad T = \kappa\left[\mu\varepsilon_0\tau + T_1(\tau,\eta,\zeta)\right] \\ &U = U_1(\tau,\eta,\zeta) \;;\quad \mathcal{P} = \kappa\,\mathcal{P}_1(\tau,\eta,\zeta) \end{aligned}\right\} \quad (5.22)$$

with $$c_2 = \frac{\varepsilon_0(1-\mu)}{\Gamma} \;;\quad (\kappa, \varepsilon_0, \mu, c_1, c_2 - \text{Const}) \qquad (5.22')$$

leaves the system (5.19'), (5.20) and (5.21) without changing. This group of transformation includes the subgroups of "stretching" and "transfers", the former being described by parameter κ and the latter by c_1 and c_2 - the mean meridional and vertical flows respectively. It should be pointed out that time (t) and angular momentum (U) remain unchanged. All other physical parameters: $v = -\partial\Psi/\partial z$; $w = \partial\Psi/\partial y$; $T, \mathcal{P}$ are proportional to the heat forcing $\kappa\varepsilon$.

From (5.22) and (5.22') it is clear that constant heat forcing (ε_0) induces partly the changing of temperature with time ($\varepsilon_0\mu\tau$) and partly the ascent and descent of the air mass ($\varepsilon_0(1-\mu)/\Gamma$). Certainly, the group theory can not give an answer to the question: which part of ε_0 influences the temperature field and what part goes to the dynamics. The answer depends upon the concrete formulation of the problem. Expression (5.22') is also easily interpreted: the mean vertical motion is proportional to the constant heat source but inversely proportional to the stability of the atmosphere.

It is obvious that in the adiabatic case ($\varepsilon \equiv 0$) $v, w, \mathcal{P}$ would be proportional to the thermal forcing but t and U remain the same.

This group of invariant transformations makes it possible to find several kinds of solutions in the form of a wave placed in the main flow (main flow in the y, z plane).

5.4.1 Waves in the layers with stable and indifferent stratification

In the adiabatic case the system (5.19'), (5.20), (5.21) has two subgroups of wave solutions, corresponding to $\Gamma > 0$ and $\Gamma = 0$. Assuming that a temperature disturbance may be presented in the form

$$T = \delta_1 y + \delta_2 y^2 + T_1 e^{i(my + nz - \sigma t)}$$

and seeking the solution for $\Psi, U, \mathcal{P}$ in the form

$$S = S_0 + Qz + s_1 y + s_2 y^2 + S_1 e^{i(my + nz - \sigma t)}$$

(parameters δ_1, δ_2, m, n are given), a system of algebraic equations may be found for unknown parameters including phase velocity σ. The following notations are used:

$$\mathcal{P} = \mathcal{P}_0 - p_1 y + p_2 y^2 + \mathcal{P}_1 e^{i(\ )}$$

$$u = u_0 - \varkappa z + u_1 y + u_2 y^2 + U_1 e^{i(\ )}$$

$$\Psi = \Psi_0 - V z + W y + \Psi_1 e^{i(\ )}$$

$$i(\ ) \equiv i(my + nz - \sigma t)$$

V and W are main flow velocity components. To make the description as short as possible and in order to facilitate a comparison of various kinds of waves, the result is presented in the form of a table (see Table 5.1). Besides the one-component wave solution, the system (5.19')-(5.21) can be also solved as a sum of waves, namely:

$$\Psi = \Psi_0 - V z + \sum_{k=1}^{\infty} \Psi_k e^{i(m_k y + n_k z - \sigma_k t)}$$

but wave numbers m_k, n_k must satisfy the conditions mentioned in the last line of the last column of Table 5.1.

Two facts should be pointed out.

1. In all the cases $\varkappa$ is calculated from the 2ω-value. This is due to the integral of motion - the theorem of angular momentum (5.20). Parameter u_1 (the horizontal gradient of u) in symmetric models is equal to zero but in nonsymmetric models, it depends upon $\alpha \delta_1$. For stationary waves there exists a relation:

$$\frac{W}{V} = \frac{\delta_1}{\Gamma} = \frac{\varkappa - 2\omega}{u_1}$$

The curvature of zonal wind (u_2) is calculated from $\frac{1}{2} 2\omega / r_0$ half of the equatorial Rossby parameter.

2. The wave amplitude in each case is proportional to $\sqrt{\frac{\alpha}{m^2+n^2}} T_1$ and inversely proportional to the parameter responsible for the stability (horizontal and vertical as well) of the atmosphere. This fact permits us to plot in one and the same graph the curves showing relations between $\Psi_1 \sqrt{\alpha (m^2+n^2)}$ and parameter ξ, determining the corresponding wave solution. Parameter ξ should be taken from the line marked by asterisk* (see Fig. 5.3).

In case when a horizontal gradient of mean temperature (δ_1) is noticeable, an "abrupt relation" for wave number m, n exists. The wave cannot be very long in y-direction. The estimation shows that

$$\frac{m}{n} < 300$$

Table 5.1

THE PARAMETERS FOR VARIOUS WAVE SOLUTIONS

Function	Parameter	The kind of solution					
		Stationary solutions; $\sigma = 0$		$\Gamma = 0$	$U = \text{Const.}$	$\mathcal{P}_1 = 0$	Sum of waves.
		I Type	II Type				
T	δ_1	Given	0	0	0	0	0
	δ_2	Given	Given	Given	0	Given When $\delta_2 = -\delta$ δ_{cr} Exists	0
	T_1	Given	Given	Given	Given	Given	Given
$\mathcal{P}$	$-p_1$	Given	0	0	0	Given	0
	p_2	0	0	0	0	Given	0
	$\mathcal{P}_1$	0	0	0	0	Given, but $\frac{\mathcal{P}_1}{T_1} \geq \frac{\alpha}{\lambda_1} - \frac{m}{n}\Gamma$	0
u	$2\omega(\varkappa - 2\omega)$	$\Gamma\alpha$	$\frac{\alpha\Gamma 2\tau_0\delta_2}{\Gamma + 2\tau_0\delta_2}$	0	0	$2\tau_0\lambda p_1$	0
	$-2\omega u_1$	$\delta_1\alpha$	0	0	0	$\alpha\delta_1 + \lambda p_1$	0
	$2\omega(u_2 - \frac{\omega}{\tau_0})$	$-\delta_2\alpha$	$-\frac{2\tau_0\delta_2^2}{\Gamma + 2\tau_0\delta_2}$	$-\alpha\delta_2$	0	0	0
	$2\omega\frac{U_1}{T_1}$	α	$-\frac{2\tau_0\delta_2^2}{\Gamma + 2\tau_0\delta_2}$	$-\alpha$	0	0	0
Ψ	$\pm V\sqrt{\frac{m^2+n^2}{\alpha}}$	$\Gamma/\sqrt{2\tau_0\delta_2}$	$\frac{\Gamma}{\sqrt{\Gamma + 2\tau_0\delta_2}}$	0	Given	0	Given
	$\mp W\sqrt{\frac{m^2+n^2}{\alpha}}$	$\delta_1/\sqrt{2\tau_0\delta_2}$	0	Given	0	0	0
	$\pm\beta\sqrt{\frac{m^2+n^2}{\alpha}}$	$\delta_2/\sqrt{2\tau_0\delta_2}$	$\frac{\delta_2}{\sqrt{\Gamma + 2\tau_0\delta_2}}$	0	0	0	0
*	$\mp\frac{\gamma_1}{T_1}\sqrt{\frac{m^2+n^2}{\alpha}}$	$-1/\sqrt{2\tau_0\delta_2}$	$\frac{1}{\sqrt{\Gamma + 2\tau_0\delta_2}}$	$\frac{1}{\sqrt{2\tau_0\delta_2}}$	$\frac{1}{\sqrt{\Gamma}}$	$\sqrt{\left(1 - \frac{\lambda}{\alpha}\frac{\mathcal{P}_1}{T_1}\right)/\left(\Gamma - \frac{n}{m}\beta_1\right)}$	$\frac{\gamma_n}{h\sqrt{\alpha}} = \frac{1}{\sqrt{\Gamma}}\frac{1}{m_n\sqrt{1+q^2}}$
	σ	0	0	$n'W$	$m\left[V \pm \sqrt{\frac{\alpha\Gamma}{m^2+n^2}}\right]$	$\mp\frac{m}{\sqrt{m^2+n^2}}\sqrt{\Gamma - \frac{n}{m}\delta_1 A}$ $\left(A = \alpha - \lambda\frac{\mathcal{P}_1}{T_1}\right)$	$\sigma_n = m_n V \pm \sqrt{\frac{\alpha\Gamma}{1+q^2}}$
	$\frac{n}{m} = \frac{\lambda_2}{\lambda_1}$	$\Gamma : \delta_1$	Arbitrary	Arbitrary	Arbitrary	$\frac{\alpha\delta_1 + \lambda p_1}{2\tau_0\lambda p_1}$	$\frac{n_n}{m_n} = q = \text{Const.}$

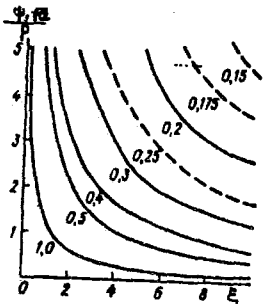

Fig. 5.3 $\Psi_1\sqrt{\alpha}/\rho$ as a function of main parameter ξ.

5.4.2 Response of the atmosphere to the heat sources in stable and unstable layers (quasisolitons)

5.4.2.1 Response in the stable layer ($\Gamma > 0$).

Let the heat source be taken in the form of constant+wave

$$\varepsilon = \varepsilon_0 + i\,\varepsilon_1 e^{i(my+nz-\sigma t)} \tag{5.23}$$

($\varepsilon_0, \varepsilon_1, m, n, \sigma$ are given figures). The solution of the system (5.19'') (5.20), (5.21) takes the form:

$$\left.\begin{aligned} V &= u_0 = const \\ \Psi &= \Psi_0 - Vz + \Psi_1 e^{i(my+nz-\sigma t)} \\ T &= T_1 e^{i(my+nz-\sigma t)} \end{aligned}\right\} \tag{5.24}$$

where

$$\left.\begin{aligned} \Psi_1 &= -\frac{\alpha m \varepsilon_1}{\rho^2(\sigma - mV - nW)^2 - \alpha m^2 \Gamma} \\ T_1 &= -\frac{\rho^2(\sigma - mV - nW)\varepsilon_1}{\rho^2(\sigma - mV - nW)^2 - \alpha m^2 \Gamma} \end{aligned}\right\} \quad (\rho^2 = m^2 + n^2) \tag{5.25}$$

$$W = \frac{\varepsilon_0}{\Gamma} \tag{5.26}$$

The formulae (5.25), (5.22') and (5.26) are quite clear. For instance, (5.26) repeates the (5.22') and shows, that for the constant heat source, the nearer is the atmosphere to instability the larger is the vertical velocity. (5.25) shows that a resonance may occur when the phase velocity of forcing wave σ is equal to the expression:

$$\sigma = mV + nW \pm \frac{m}{\rho}\sqrt{\alpha\Gamma} \qquad (5.27)$$

Let us now suppose that heat source has a more general form:

$$\varepsilon = \varepsilon_0 + i\varepsilon_1(t)e^{i(my+nz)} \qquad (5.28)$$

then seeking solutions for Ψ and T in the form:

$$\Psi = \Psi(t)e^{i(my+nz)} \; ; \quad T = \theta(t)e^{i(my+nz)} \qquad (5.29)$$

We find a system of two differential equations

$$\left.\begin{aligned} &\frac{d\Psi}{dt} + i(mV+nW) + i\alpha\frac{m}{\rho^2}\theta = 0 \\ &\frac{d\theta}{dt} + i(mV+nW) + im\Gamma\Psi = i\varepsilon_1(t) \end{aligned}\right\} \qquad (5.30)$$

An analysis of this system shows that at the initial stage ($0 \leq t < 1$) the temperature field changes first ($\theta \sim t^2$), then Ψ ($\Psi \sim t^3$). The asymptotical solution is periodical with a period $\tau = 2\pi/(mV+nW)$. In case when $mV+nW = 0$ θ vanishes at $t \to \infty$ but $\Psi \to \varepsilon_0/m\Gamma$. It should be noted that temperature reaches the asymptotical value first ($\sim 1/t^2$)

Fig. 5.4 shows schematically the solutions for Ψ and θ when ε is given.

For a purely linear problem

$$\frac{\partial \Delta\Psi}{\partial t} = \alpha\frac{\partial T}{\partial y} \; ; \quad \frac{\partial T}{\partial t} = -\Gamma\frac{\partial \Psi}{\partial y}$$

with the initial conditions

$$t = 0 \qquad T = T^0(y,z) \; ; \quad \Psi = \Psi^0(y,z)$$

the solution is in the form of double Fourier integrals, but the influence function does not vanish when t tends to infinity. Thus, the problem is unstable according to Lyapunov criteria. Apparently the nonlinear terms $(\Psi, \Delta\Psi)$; (Ψ, T) make the problem stable.

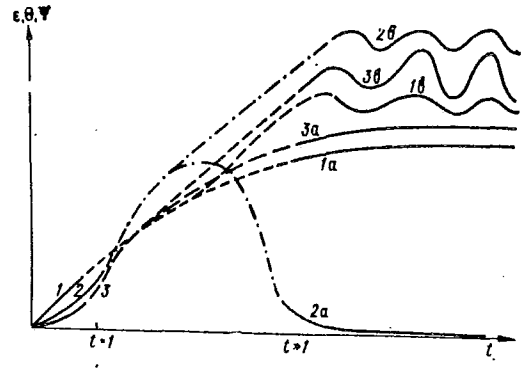

Fig. 5.4 Schematical picture of waves development and asymptotical behaviour for pure stationary solution ($mV+nW=0$) - a and wave solution ($mV+nW\neq 0$) - b. 1 - Heat source - given function. 2 - The response in temperature field. 3 - The response in wind field.

5.4.2.2 Response in the unstable layer ($\Gamma < 0$)

The GATE aerological data showed that there usually exist two layers with moist unstable stratification. The first layer is from the sea surface up to 1.5 km and the second - from 2 up to 10 km. For a qualitative analysis of disturbances in such layers it is sufficient to replace $\Gamma = \gamma_a - \gamma$ by $\Gamma_u = -(\gamma - \gamma_{wa})$ in the equation (6) where γ_{wa} is moist adiabatic lapse rate. A change of the sign before parameter Γ drastically changes the character of the system (5.19) - (5.21) transforming it from the hyperbolic into the elliptic type. There are no solutions of the wave form. Characteristic time $t_0 = (\alpha|\Gamma|)^{-1/2} \approx 300s$ has no relation to any frequency and only indicates the motion scale. In their dimensionless form equations (5.19''); (5.21) become

$$\frac{\partial \Delta\Psi}{\partial t} + (\Psi, \Delta\Psi) = \frac{\partial T}{\partial y}\ ; \quad \frac{\partial T}{\partial t} + (\Psi, T) = \frac{\partial \Psi}{\partial y} + \varepsilon \qquad (5.31)$$

Let us suppose that heat source ε is localized in the narrow band (as a solitary wave). What will be the response in the Ψ and T fields? To study this problem it is convenient to use the set of functions (Proceedings of the Tashkent Conference, 1978).

$$\mathcal{D}_m^n(\zeta) = \frac{d^n}{d\zeta^n}\frac{1}{ch^m\zeta}\ ; (m>0;\ n=0,1,\dots) \quad (5.32) \qquad \text{(quasisoliton)}$$

For several special problems $m=1;2$; $n=-1$

$$\left(\int_{-\infty}^{\zeta}\frac{d\zeta}{ch\zeta} = gd\zeta\ ;\ \int_{-\infty}^{\zeta}\frac{d\zeta}{ch^2\zeta} = th\zeta\right) \text{ is also useful.}$$

It is easy to prove that if

$$\varepsilon(t,y,z) = \varepsilon_0 + \varepsilon_1\,\mathcal{D}_{m+2}^n(\zeta)$$

then Ψ and T are

$$\Psi = \Psi_0 - Vz + Wy - \frac{\varepsilon_1 \lambda^2}{\mu\, m(m+1)} \mathcal{P}_m^{n-1}(\zeta)$$

$$T = -\frac{\varepsilon_1}{m(m+1)} \mathcal{P}_m^{n+1}(\zeta)$$

where

$$\zeta = \mu y + \nu z - \sigma t \quad ; \quad \lambda^2 = \frac{\mu^2}{(\mu^2+\nu^2)(\sigma - \mu V - \nu W)^2}$$

As the main term $\mathcal{P}_{m+2}^{p}(\zeta)$ is $\frac{1}{ch^{m+2}\zeta}$ and $\mathcal{P}_m^p \sim \frac{1}{ch^m \zeta}$ the result is that **if the heat source is narrow in space it generates a relatively** large response in the fields of temperature and wind, "large" both literally and figuratively. This is rather an unexpected kind of instability. Fig. 5.5 shows examples of simplest quasisolitons with zero pedestals:

$$\varepsilon = \frac{1}{ch^4 \zeta} \quad ; \quad T \sim \frac{sh\,\zeta}{ch^3 \zeta} \quad ; \quad v, -w \sim \frac{1}{ch^2 \zeta}$$

It is important to note that quasisolitons for ε, v and w are of the same kind of symmetry whereas ε and T are opposites.

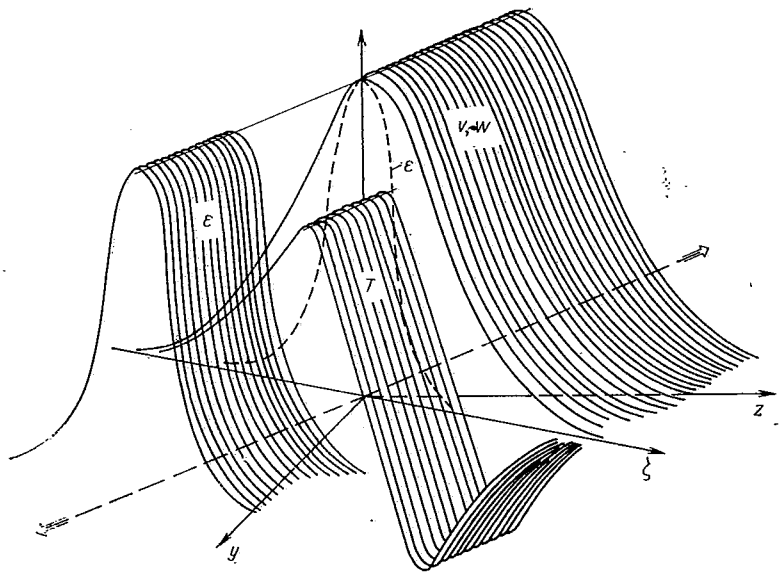

Fig. 5.5 The simplest examples of quasisoliton with zero pedestals. $\varepsilon = sech^4 \zeta$; $v, -w = sech^2 \zeta$; $T = -th\,\zeta \cdot sech^2 \zeta$.

The angle between axes z and crest of the quasisolitons is $tg\,\xi = \nu/\mu$. The quasisolitons move normal to the axis ζ , i.e. to the quasisoliton crest.

5.5 NON-LINEAR EFFECTS

The above solutions: of both wave- and quasisoliton kind are exact solutions for a non-linear system of equations. In this sense they are similar to Rossby wave which is an exact solution of a non-linear vorticity equation. Non-linearity appeared from the fact that in the formulae for amplitude and phase velocity, the components of the mean flow are present. However, all the solutions (the Rossby one included) do not reflect one of important peculiarities of non-linear interaction - energy exchange between the waves. Moreover, the conditions for solitary large-scale waves to exist have not been mentioned here. Herewith these two problems are shortly described.

5.5.1 Wave triplets

The vorticity equation in a barotropic model

$$\frac{\partial \Delta\Psi}{\partial t} + (\Psi, \Delta\Psi) + \beta\frac{\partial\Psi}{\partial x} = 0 \qquad \left(\Delta \equiv \frac{\partial^2}{\partial x^2} + \frac{\partial^2}{\partial y^2}\right) \tag{5.33}$$

is solved in the form

$$\Psi = \Psi_0 - Uy + \Psi_0 e^{-iqy} + \sum_{K=1}^{\infty} \Psi_K e^{-i(m_K x + n_K y - \sigma_K t)} \tag{5.34}$$

where

$$\frac{\sigma_K}{m_K} = U - \frac{\beta}{q^2} \; ; \qquad q^2 = m_K^2 + n_K^2 = const. \tag{5.35}$$

(When the spherical coordinates are used the sum is

$$\Psi = \Psi_0 + A P_n(\cos\vartheta) + \sum_{m=1}^{n} \Psi_m e^{-im\lambda} \mathcal{P}_n^m(\cos\vartheta)$$

where P_n and $\mathcal{P}_n^m$ are the Legendre polynomial and associated Legendre polynomialrespectively). The system (5.19-5.21) has the solution in the form of the sum as well; this solution is presented in the last column of Table 5.1. But these kinds of waves don't interact. The presence of Jacobians indicate the possibility of nonlinear interaction.

Using the hypothesis of "weak interaction" it is possible to find an analytical solution of resonance interaction in wave triplet. The waves' numbers in the wave triplet are not independent.

5.5.1.1 The triplet of Rossby waves. Following the Longuet-Higgins and Hill (1970) let us try to find solution of equation (5.33) in the form:

$$\Psi = \sum_{K=1}^{3} \Psi_K(t)\, e^{-i(m_K x + n_K y - \sigma_K t)} \tag{5.36}$$

where $\Psi_K(t)$ are slowly changing functions of time variable so that $\frac{d\Psi_K}{dt}$ have the higher order of magnitude in comparison with the linear Ψ_K terms.

It is important to note that m_K and n_K may be either positive or negative. Substituting (5.36) for (5.33) we can find three conditions for the linear terms:

$$\left.\begin{aligned} m_1 + m_2 + m_3 &= 0 \\ n_1 + n_2 + n_3 &= 0 \end{aligned}\right\} \qquad (5.37)$$

$$\sigma_1 + \sigma_2 + \sigma_3 = 0 \qquad (5.38)$$

where

$$\sigma_\kappa = \frac{m_\kappa}{\rho_\kappa^2} \qquad (\rho_\kappa^2 = m_\kappa^2 + n_\kappa^2) \qquad (5.39)$$

The conditions (5.37), (5.38) are general to any hydrodynamic triplet nonlinear term of which is caused by Jacobian $(\Psi, \Delta\Psi)$. Relations (5.37) show that three wave vectors form a triangle. Relations (5.38) are "synchronic" condition. For the Rossby waves this condition takes the form:

$$\frac{m_1}{\rho_1^2} + \frac{m_2}{\rho_2^2} + \frac{m_3}{\rho_3^2} = 0 \qquad (5.38')$$

It is significant that in (5.37) none of m_κ can be zero. Otherwise a triplet transforms into a pair of waves for which wave numbers must satisfy the relation $m_1^2 + n_1^2 = m_2^2 + n_2^2 = q^2$ (see (5.35)) and no interaction between the waves exists.

Three relations (5.37) and (5.38') contain 5 unknown components of wave numbers. Therefore there cannot be only one solution of (5.37), (5.38'). We have to nominate at least one vector, say m_3, n_3. In polar coordinates $m_\kappa = \rho_\kappa \cos\varphi_\kappa$; $n_\kappa = \rho_\kappa \sin\varphi_\kappa$ the equations (5.37), (5.38') take the form:

$$\left.\begin{aligned} \rho_1 \cos\varphi_1 + \rho_2 \cos\varphi_2 &= -\rho_3 \cos\varphi_3 \\ \rho_1 \sin\varphi_1 + \rho_2 \sin\varphi_2 &= -\rho_3 \sin\varphi_3 \\ \frac{\cos\varphi_1}{\rho_1} + \frac{\cos\varphi_2}{\rho_2} &= -\frac{\cos\varphi_3}{\rho_3} \end{aligned}\right\} \qquad (5.40)$$

As the given vector (ρ_3, φ_3) can't be zero $(\rho_3 \neq 0)$, we can reduce the number of unknown parameters by introducing the relations

$$\varkappa_1 = \frac{\rho_1}{\rho_3} \quad ; \quad \varkappa_2 = \frac{\rho_2}{\rho_3} \qquad (5.41)$$

The system (5.40) takes the form:

$$\left.\begin{aligned} &\varkappa_1 \cos\varphi_1 + \varkappa_2 \cos\varphi_2 = -\cos\varphi_3 \\ &\varkappa_1 \sin\varphi_1 + \varkappa_2 \sin\varphi_2 = -\sin\varphi_3 \\ &\frac{\cos\varphi_1}{\varkappa_1} + \frac{\cos\varphi_2}{\varkappa_2} = -\cos\varphi_3 \end{aligned}\right\} \qquad (5.42)$$

The system (5.37), (5.38) is symmetrical according to the indices 1, 2, 3. Thus, it is sufficient to study it in one quadrant, say IV: $-\frac{\pi}{2} < \varphi_3 \le 0$.

The first two equations in (5.42) show that

$$2\varkappa_1\varkappa_2 \cos(\varphi_2 - \varphi_1) = 1 - (\varkappa_1^2 + \varkappa_2^2)$$

or $|\varkappa_2 - \varkappa_1| < 1$. This is a consequence of triangle relations. From the first and third equations in (5.42) it follows

$$\frac{\cos\varphi_1}{\cos\varphi_2} = -\frac{\varkappa_1(\varkappa_2^2 - 1)}{\varkappa_2(\varkappa_1^2 - 1)}$$

For given φ_3 there exists a curve of the ends of vector pair, which may interact with φ_3 vector. Such curves are shown in Fig. 5.6 for various values of φ_3. The pair of vectors interacting with given vector φ_3 is located at the ends of any diameter of the corresponding curve. For each given φ_3 the curve has four common points with the circle of unit radius. For these points $\varphi_2 - \varphi_1 = 2\pi/3$. Fig. 5.6 corresponds to $\rho_3 = 1$. For any other ρ_3 $(\rho_3 \neq 0)$ it is sufficient to expand or compress the coordinates in ρ_3 times.

The amplitude functions $\psi_k(t)$ satisfy the system of nonlinear equations

$$\rho_1^2 \frac{d\psi_1}{dt} = \left\{ m_2 n_3 - n_2 m_3 \right\} (\rho_3^2 - \rho_2^2)\, \psi_2 \psi_3$$

and two similar equations with cyclically changed indices. The expressions in the figurative brackets will have the same value for all three equations due to the fact that they present the vector product of two sides of the triangle. Using the notation $\{ \;\; \} = b$ (b may be either positive or negative) we rewrite the equations in the form:

$$\left.\begin{aligned} \rho_1^2 \frac{d\psi_1}{dt} &= b(\rho_3^2 - \rho_2^2)\, \psi_2 \psi_3 \\ \rho_2^2 \frac{d\psi_2}{dt} &= b(\rho_1^2 - \rho_3^2)\, \psi_1 \psi_3 \\ \rho_3^2 \frac{d\psi_3}{dt} &= b(\rho_2^2 - \rho_1^2)\, \psi_1 \psi_2 \end{aligned}\right\} \qquad (5.43)$$

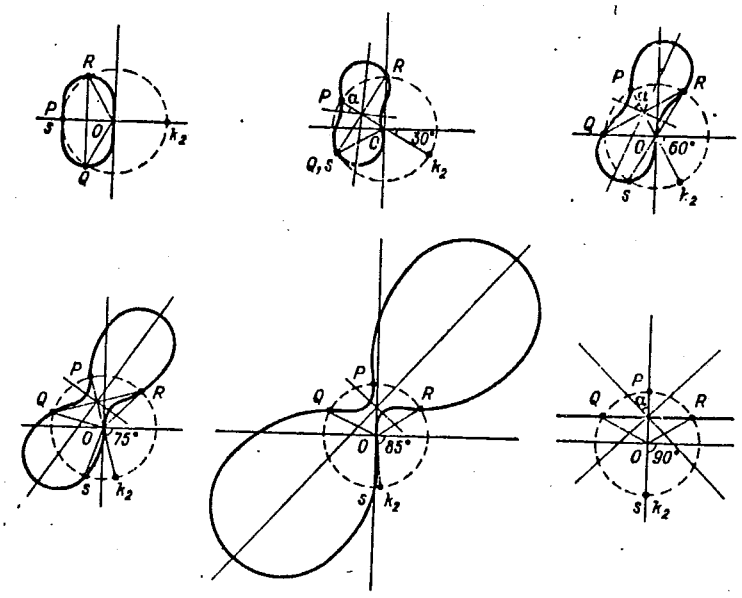

Fig. 5.6 The examples of Rossby waves triplets for various values of given vector ψ_3 . The end of the given vector is indicated by k_2 . The points P, Q, R, S divide the curve in parts where the energy flows either toward the "middle" vector or from it.

There are integrals in system (5.43). For different purposes they may be taken in various forms. For instance, multiplying equation number κ by the

$$\left[B + C\rho_\kappa^2 + D\left(\rho_{\kappa+1}^2 + \rho_{\kappa-1}^2\right)\right]\psi_\kappa \qquad (\rho_4 = \rho_1\ ;\ \rho_0 = \rho_3)$$

where B, C, D are constants and summing up after integration with respect to t , we obtain

$$\sum_{\kappa=1}^{3}\left[B\rho_\kappa^2 + B\rho_\kappa^4 + D\rho_\kappa^2\left(\rho_{\kappa+1}^2 + \rho_{\kappa-1}^2\right)\right]\psi_\kappa^2 = \text{Const} = M \qquad (5.44)$$

If $D=C=0$ we have an energy integral: when $B=D=0$, it is vorticity square integral.

Another integral may be constructed by multiplying the first equation by the $\psi_1/(\rho_3^2-\rho_2^2)$, the second by the $-\psi_2/(\rho_1^2-\rho_3^2)$ and then summing up the results. After integration, we obtain:

$$\frac{\rho_1^2}{\rho_3^2-\rho_2^2}\psi_1^2 - \frac{\rho_2^2}{\rho_1^2-\rho_3^2}\psi_2^2 = \mathcal{N}_1^2 = \text{const} \qquad (5.45)$$

By similar procedure we find

$$\frac{\rho_3^2}{\rho_2^2-\rho_1^2}\psi_3^2 - \frac{\rho_2^2}{\rho_1^2-\rho_3^2} = \mathcal{N}_2^2 = \text{Const} \qquad (5.46)$$

$M, \mathcal{N}_1, \mathcal{N}_2$ can be computed by using the initial values of Ψ_1, Ψ_2, Ψ_3.

Although three integrals of system (5.43) are written, only two of them are linearly independent. It is easy to prove this by computing the range of matrix A, elements of which are the coefficients before Ψ_κ^2 in (5.44), (5.45) and (5.46). The range is equal to two.

Without affecting generality we may count $\rho_1 < \rho_2 < \rho_3$ (if $\rho_1 = \rho_2$, then $\rho_3 = 1 \Rightarrow \rho_1 = \rho_2 = 1$ and no interaction exists). Substituting Ψ_1, from (5.45) and Ψ_3 from (5.46) in the second equation of (5.43) we find the nonlinear equation for Ψ_3 solution of which may be written explicitly by elliptic function. Then from (5.45) and (5.46) Ψ_1 and Ψ_3 may be presented explicitly (an example will be given later). The time of interaction is determined by the double period of elliptic functions. The period in turn depends upon the initial conditions. In special case the period may tend to infinity. In such case the energy exchange processes pass very slowly. According to the conditions $\rho_1 < \rho_2 < \rho_3$ it is easy to show that energy flow may be directed either to the "middle" wave (ρ_2) from "extremal" waves or from the "middle" wave to the both "extremal" waves. It is impossible for any "extremal" wave to pump energy out of the two other waves.

5.5.1.2 Small scale waves in the equatorial atmosphere

In Section 5.3 a number of exact wave solutions for a system of nonlinear equations describing the simple zonal model of small-scale motion were presented. Here are these equations in the dimensionless form:

$$\left.\begin{aligned} \frac{\partial \Delta\Psi}{\partial t} + (\Psi, \Delta\Psi) &= \frac{\partial T}{\partial y} \\ \frac{\partial T}{\partial t} + (\Psi, T) &= -\frac{\partial \Psi}{\partial y} \end{aligned}\right\} \qquad (5.47)$$

Seeking the solution in the form of a wave triplet

$$[\Psi, T] = \sum_{\kappa=1}^{3} [\Psi_\kappa(t), T_\kappa(t)]\, e^{-i(m_\kappa + n_\kappa - \sigma_\kappa t)} \qquad (5.48)$$

Dobryshman (1980-b) found after substituting (5.48) in (5.47) the same equations (5.37) and (5.38). But dispersion equation, instead of (5.39) is $\sigma_\kappa = m_\kappa / \rho_\kappa$. Consequently, the sinchronic condition takes the form

$$\frac{m_1}{\rho_1} + \frac{m_2}{\rho_2} + \frac{m_3}{\rho_3} = 0 \qquad (5.38'')$$

Then the relation between amplitude functions is

$$T_\kappa = \rho_\kappa \Psi_\kappa \qquad (5.49)$$

Repeating the previous procedure, we come to the system (5.42), in which the third equation is replaced by

$$\cos\varphi_1 + \cos\varphi_2 = -\cos\varphi_3 \qquad (5.50)$$

Qualitatively the picture in the m, n plane is similar to the Rossby triplet, but differs quantitatively. Fig. 5.7 shows curves of vector pair ends which may interact with the given vector φ_3. For comparison with Rossby triplet the computations were made for the IV quadrant. When $\varphi_3 \to -\pi/2$ the "vanes" of the curve increase but the "waist" becomes narrower and the curve tends to become a "cross": $n = 1/2$; $m = 0$ as well as for Rossby triplet; the curve centers form circle of radius $r = 0.5$. The longest diameter turns by $\pi/4$ when φ_3 changes from 0 to $-\pi/2$.

The amplitude functions Ψ_k satisfy the same equations (5.43). Introducting new functions:

$$\tilde{\Psi}_k = \frac{\Psi_k}{\rho_k}$$

where

$$\rho_k = \frac{\rho_{k-1}\,\rho_{k+1}}{b\sqrt{|(\rho_k^2 - \rho_{k-1}^2)(\rho_k^2 - \rho_{k+1}^2)}}\;; \qquad (\rho_4 = \rho_1\;;\ \rho_0 = \rho_3)$$

the system (5.43) may be rewritten in the form

$$\frac{d\tilde{\Psi}_1}{dt} = \tilde{\Psi}_2\tilde{\Psi}_3 \;;\quad \frac{d\tilde{\Psi}_2}{dt} = -\tilde{\Psi}_1\tilde{\Psi}_3 \;;\quad \frac{d\tilde{\Psi}_3}{dt} = \tilde{\Psi}_1\tilde{\Psi}_2 \qquad (5.51)$$

Integrals (5.45) and (5.46) take the form

$$\tilde{\Psi}_1^2 + \tilde{\Psi}_2^2 = \tilde{\mathcal{N}}_1^2 \;;\quad \tilde{\Psi}_2^2 + \tilde{\Psi}_3^2 = \tilde{\mathcal{N}}_2^2 \qquad (\tilde{\mathcal{N}}_1 > \tilde{\mathcal{N}}_2) \qquad (5.52)$$

Now, after substituting Ψ_1 and Ψ_3 and integration we find

$$t - t_0 = \int_{\tilde{\Psi}_{2_0}}^{\tilde{\Psi}_2} \frac{d\tilde{\Psi}_2}{\sqrt{(\tilde{\mathcal{N}}_1^2 - \tilde{\Psi}_2^2)(\tilde{\mathcal{N}}_2^2 - \tilde{\Psi}_2^2)}}$$

To make illustration simpler let us assume that $\tilde{\Psi}_2(0) = 0$ and $t_0 = 0$. Then Ψ_k are presented by Jacobian elliptic functions. Namely

$$\tilde{\Psi}_1 = \tilde{\mathcal{N}}_1\,\mathrm{dn}(t|\alpha) \;;\quad \tilde{\Psi}_2 = \tilde{\mathcal{N}}_2\,\mathrm{sn}(t|\alpha) \;;\quad \tilde{\Psi}_3 = \tilde{\mathcal{N}}_2\,\mathrm{cn}(t|\alpha)$$

$$\alpha = \sin^{-1}\tilde{\mathcal{N}}_2/\tilde{\mathcal{N}}_1$$

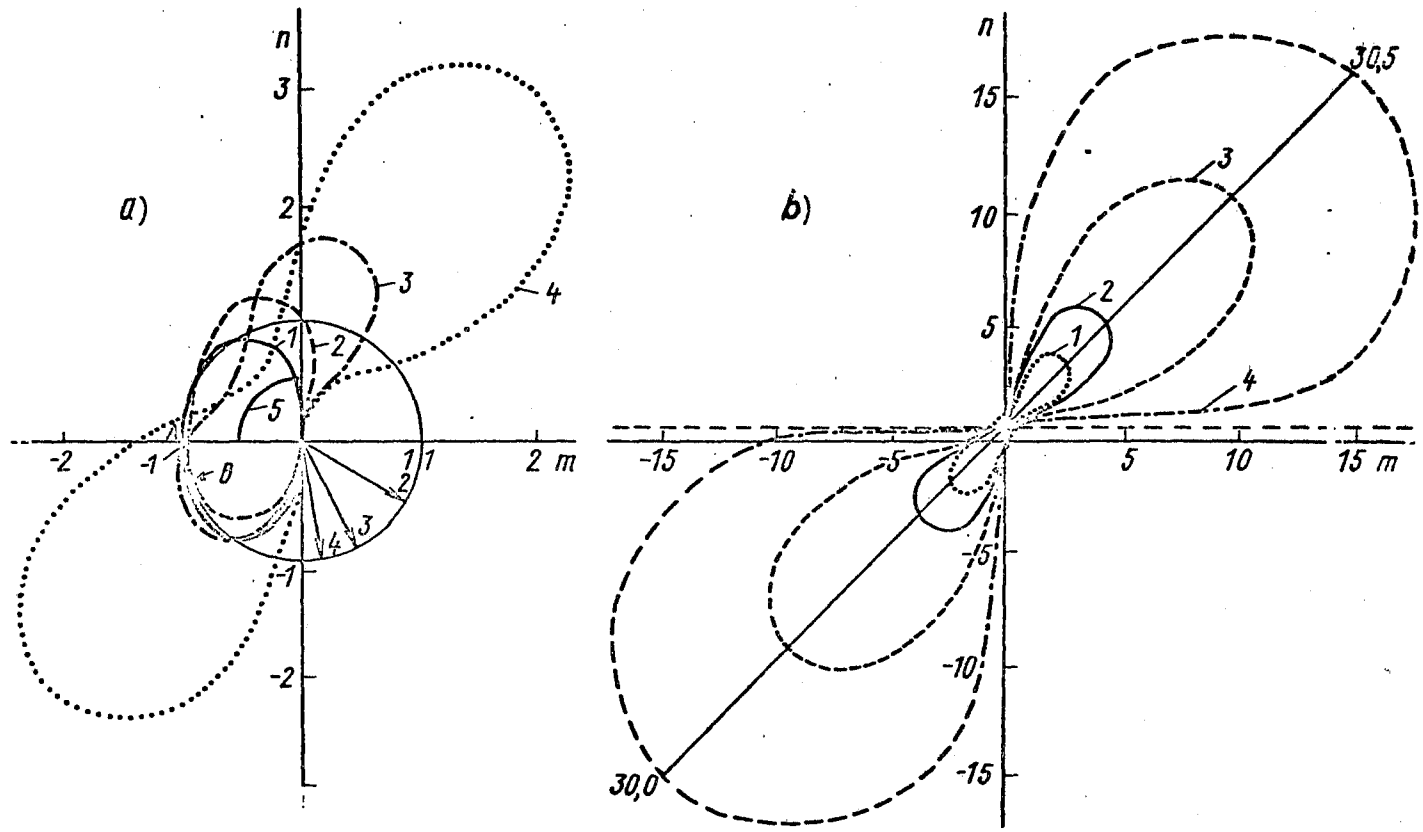

Fig. 5.7 The same as in Fig. 5.6 but for equatorial waves triplet. On the left side the given vector φ_3 is indicated by figs. 1,2,3,4. The figures correspond to the curves. On the right side the curve 1 corresponds to the $\varphi_3 = -80°$, i.e. the curve 4 on the left side; curve 2 - corresponds to $\varphi_3 = -85°$; curve 3 - corresponds to $\varphi_3 = -87.5°$; curve 4 corresponds to $\varphi_3 = -89°$.

Fig. 5.8 shows Ψ_κ as function of t for $\sin\alpha = \tilde{N}_2/\tilde{N}_1 = 0{,}8$

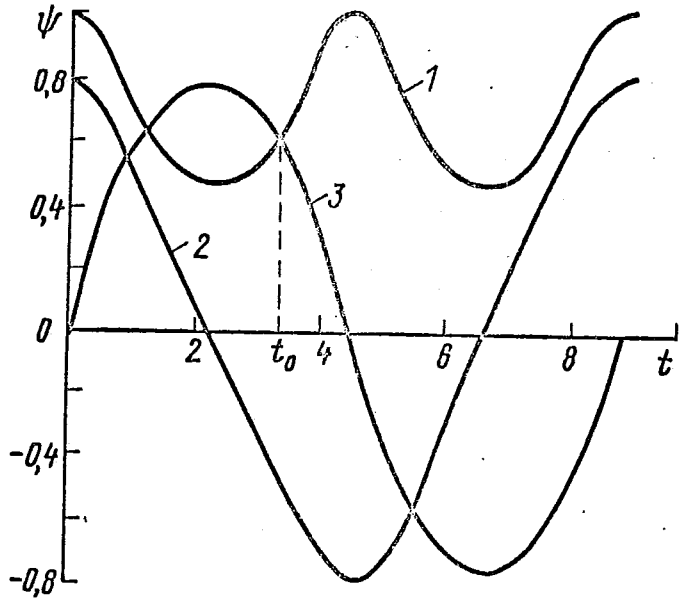

Fig. 5.8 The curves $\Psi_\kappa(t)$ when $\tilde{N}_2/\tilde{N}_1 = 0.8$. The total period is about 9.

The amplitude functions for temperature satisfy the same equations (5.43) with other coefficients. But it is easier to determine them directly from (5.50) because Ψ_κ is already known.

Such "universality" of amplitude functions for both Rossby and small equatorial waves is due to the "weak interaction" approximation (see also Loesch and Deininger, 1979).

5.5.2 Solitary waves (solitons)

Soliton is a stationary solution of a nonlinear equation with partial derivatives, generally in one dimension in space coordinate*. (Usually KDV equation** is used). Therefore to get a solitary Rossby wave it is necessary to use appropriate procedure in a way which transforms a differential operator in vorticity equation into a form having a soliton solution. To date several methods have been worked out. All of them are not simple and require intricate mathematical methods (variational calculations, expansion in formal series, introducing various scaling, etc.). In some methods the physical side of initial equation manipulation is driven aside.

Two examples are shortly described below.

---

* The only more or less known exception is the Kadomtsev-Petriashvily equation. This equation has a solution in form of two-dimensional soliton. But the author does not know of any meteorological applications.

** KDV equation - equation of Korteweg-de Vries.

5.5.2.1 A solitary Rossby wave. The stream function Ψ in the barotropic vorticity equation is being sought in the form of expansion in powers of a small parameter ε. Instead of t and x a new scaling variable is introduced.

$$\xi = \varepsilon x \quad ; \quad \tau = \varepsilon^3 t$$

The variables y and z remain without being scaled. Dependence on z is given in the form of $\cos nz$. Thus solitary wave δ is sought in the form

$$\delta = A(\xi)\, \Phi_n(y)\, \cos nz$$

For n - mode solitary wave Φ_n is determined by the eigenvalue problem. To make this problem correct it is necessary to introduce rigid boundaries at $y = y_1$ and $y = y_2$ and to require that $\Phi_n(y_1) = \Phi_n(y_2) = 0$.

The solution of the problem greatly depends upon the parameter

$$\gamma = \frac{\beta - \frac{d^2U}{dy^2}}{U - c_{on}}$$

where $U = U(y)$ is the mean flow. If $c_{on} = const$ there is no solitary wave. But when $c_{on} = c_{on}(y)$ that is when there is a shear in the mean flow the solitary wave may exist.

After solving the eigenvalue problem the first term of the expansion gives a nonlinear equation (KDV or rather modified KDV equation) for function $A_n(\xi)$

$$\frac{\partial A_n}{\partial \tau} + a_n A_n^2 \frac{\partial A_n}{\partial \xi} + b_n \frac{\partial^3 A_n}{\partial \xi^3} = 0$$

The parameters a_n and b_n are determined by eigenvalue problem and depend upon γ. Fig. 5.9 taken from Redekopp (1977) shows the streamline in the moving coordinate system; the mean flow is

$$U(y) = sn\left(\frac{y}{m}\right)$$

(sn - Jacoby elliptic function). A more sofisticated example is given in (Weidmann and Redekopp, 1980).

5.5.2.2 Solitary wave in the equatorial belt. Introducing the different y and z scales in the system (5.47) and assuming that temperature field is stationary ($\partial T/\partial t \equiv 0$) after expanding the in powers of a small parameter, the following equation for the first term of expansion is obtained

$$\frac{\partial^3 \Psi_1}{\partial t \partial y^2} = F'_{\Psi_1}(\Psi_1) \frac{\partial \Psi_1}{\partial y} \Rightarrow \frac{\partial^2 \Psi_1}{\partial t \partial y} = F(\Psi_1) + A(t)$$

where F is arbitrary function of Ψ_1. Assuming $A \equiv 0$ and $F(\Psi_1) = \sin \Psi_1$ a Sin-Gordon equation is got

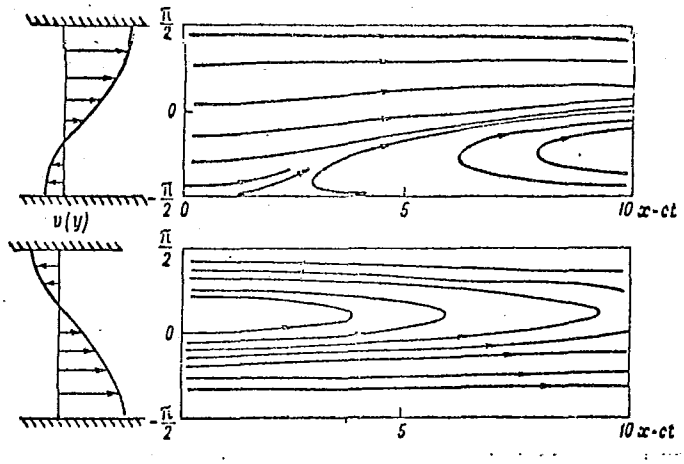

Fig. 5.9 The examples of streamlines in a channel for various zonal current profiles

$$\frac{\partial^2 \Psi_1}{\partial t \partial y} = \sin \Psi_1$$

Between the solutions of this equation there are solitons. Such procedures were suggested by Panchev and Chakalov, 1974.

The most difficult part in such procedures is physical validation of the introduced hypotheses with a view of facilitating mathematical transformations. For instance, it is not clear how observational data can be used either for confirming or disproving the hypothesis $F(\Psi_1) = \sin \Psi_1$. If the solution obtained has a clear-cut physical interpretation based on observational data then the theory is justified a posteriori.

5.6 SOURCES OF LARGE-SCALE WAVE DISTURBANCES IN THE TROPICS

Investigation of wave generation mechanism in physics is one of primary problems arising in the course of the analysis of wave disturbances. Such analysis also helps to better understand wave disturbance energetics. Earlier we described one of mechanisms for energy exchange between wave triplet, the total energy of the triplet is invariant. So in the framework of weak interaction approach none of the triplet waves could become unstable. Wave genesis is of most crucial importance for the tropics, where temporal and spatial variations of meteorological parameters are, on the whole, almost one order less than in middle and high latitudes, while the energy of large-scale wave disturbances is far from weak. Because of the complexity of atmospheric processes it is virtually impossible to single out one and only source of wave generation. Total energy of tropical atmosphere is a sum of energies of various mechanisms which belong to different components of the general circulation mechanism. In order to comprehend energy balance and relations between components, one has to introduce intermediate features and/or mechanisms for the absorption or generation of energy. To make the point clear let us ennumerate the main components of energy cycle in tropical latitudes (inside an air column closed from the flanks. These components are more or less clearly defined after GATE data analyses (see, for example, Report of US GATE Program Workshop)). For the sake of convenience this list can be divided into two parts. The first part will contain mechanisms for the transformation of energy inflow:

1. Total potential energy.
2. Potential energy of zonal flow.
3. Available potential energy of zonal flow.
4. Available potential energy of eddy motion.
5. Kinetic energy of zonal flow.
6. Kinetic energy of eddy motion.

The second part consists of mechanisms which transform, generate and dissipate energy inside the air column. They are:

1. Available potential energy of zonal flow transformed into (a) available potential energy of eddy motion and (b) kinetic energy of zonal flow.
2. Available potential energy of eddy motion transformed into kinetic energy of eddy motion.
3. Kinetic energy of eddy motion transformed from kinetic energy of zonal flow.
4. Production of kinetic energy of eddy motion.
5. Production of available energy of zonal flow.
6. Dissipation of kinetic energy of zonal and eddy motions.

The scales of various components are different. It is obvious that the dissipation of eddy motion is a much more rapid process than the transformation of available zonal flow energy into kinetic energy. The input of energy from each component changes with time. There were periods during GATE when the zonal flow changed but slightly in the course of several days, it was stable. Consequently, only small part of zonal flow energy could be transformed. When zonal flow changed, mechanisms for assimilation and transformation of zonal flow energy were brought into play. In this case we have every right to speak not only of a loss of stability of zonal flow, but of a loss of stability of certain smaller parts of the total circulation mechanism, as well.

Because of different scales, these larger parts of the circulation mechanism in the tropics have to be divided into smaller bits. But there is one inherent difficulty - how to bring all those bits together. For this reason Sitnikov (1977) proposed to make a scale analysis of the dynamics equations in the tropical zone subdividing the latter into several different scale areas.

It is self-evident that dealing with such a complex mechanism one has to know the characteristics of disturbances (waves) as precisely as possible, so as to be able to find their genesis more or less accurately. Prior to GATE, a number of types of large scale tropical waves in the troposphere were assumed to exist. Those waves were, for the most part, discovered by theoreticians who analysed empirical data from several stations only or upper air charts of the 1960s with sparse stations in low latitudes. In one of his lectures Krishnamurti (Dynamics of the Tropical Atmosphere, 1972) gave a "list" of large waves in the troposphere which can be presented as a table (see Table 5.2). After the analysis of GATE data the table became better coordinated and compact (see Table 5.3) (Proceedings of the International Scientific Conference..., 1978).

Table 5.2

Summary of large-scale tropical wave parameters on the basis of data available by 1972

Year of issue	Author	Investigation area and observation period	Name or type of wave	Analysed parameter and investigation method	Wave parameters			
					Direction of motion	Length, km	Phase velocity, $m\ sec^{-1}$	Period, days
(1)	(2)	(3)	(4)	(5)	(6)	(7)	(8)	(9)
1954	Riehl	The Caribbean Sea, summer period	Easterlies	Synoptical analysis	Westwards	1500-2000	8	3-4
1968	Yanai-Maruyama	The Pacific, lower troposphere, April, July 1962	Mixed "Rossby-gravitational"	Time series	Westwards from upper to lower troposphere	$\frac{10000}{5}$	-	4-5
1968	Wallace, Kousky	The same, July-December 1963 and 1964	Kelvin waves (azimuth wave number*)	The same	Eastwards and downwards	$\frac{40000*}{10}$	-	12-20
1969	Carlson	Northern Africa, July-October 1967		Aerological maps of 700 mb. Time series	Westwards	2000	20-35	

*In numerator - along the horizontal
in denominator - along the vertical

Table 5.2 (cont.)

(1)	(2)	(3)	(4)	(5)	(6)	(7)	(8)	(9)
1971	Krishna-murti	Tropical zone, June-August, 1967	(Azimuth wave number 1,7,8)	The same but baric for topography for 200 mb. Harmonic analysis		40000 5800 5000		
1971	Madden and Julian	The Pacific, the whole year	(Azimuth wave mumber*)	(Amplitude of pressure wave about 1 mb)	Westwards	40000		4-5 and 40
1972	Burpee	Northern Africa, July-December, 1957-1964		Aerological maps of 700 mb. Time series	The same	4000	15	3-5

Table 5.3

Wave parameters on the basis of GATE data

Author	Wave parameters		
	Length, km	Phase velocity, m sec^{-1}	Period, days
Reed	2500	8	3.5
Carlson	2500	8	3.2
Mass	2300	8.0	3.3
Burpee	3800	9.8	4.5

The generally accepted concept of wave generation is that of a loss of stability, delivery of instability of a process or processes of a larger scale*. As a rule, we single out four principal mechanisms of delivery of instability: (1) barotropic instability; (2) baroclinic instability; (3) instability caused by heat release during condensation; usually it has a scale of a single cumulus or a small cloud cluster and (4) large-scale convective instability of CISK type. As we are dealing with waves having a scale of 2-3 thousand kilometers, item 3 above is not pertinent here. In item 4 we shall discuss only basic features of wave CISK mechanism.

5.6.1 Barotropic instability

5.6.1.1 General remarks. In an absolutely uniform flow (one-, two-, or three-dimensional) when the behaviour of the flow is independent of its coordinates there are no inherent causes which might bring about any display of instability. Such streams move like solids. Under the impact of external forces gradients of the characteristic appear in the flow, for instance, the temperature, wind velocity fields, etc. Under certain conditions waves might generate in the flow.

Thorough investigations showed, for instance, that solitary Rossby waves (their simplest model was described in Section 5.5) can form only in a flow with a shear. As follows from the general statements of the instability theory (Betchov & Criminale, 1971, and Shakina, 1979) in stratified fluids it is not velocity gradient of the main flow that matters most but the flow curvature characteristic, that is, a second derivative. To be more precise, if $U = U(y)$ is a zonal flow, then the instability criterion under β-plane approximation for barotropic models includes parameter

$$\xi = \frac{d^2U}{dy^2} - \beta \qquad (5.53)$$

*Cases when a large disturbance is formed from the energies of smaller disturbances are but rare. Such processes are sometimes described using a negative viscosity model.

In most cases of linear theory the problem of instability is reduced to the eigenvalue problem. If the imaginary part of the eigenvalue (say $Im\,\sigma$) is not zero then the wave is unstable (the eigenvalue usually has the sense of phase velocity of the wave).

If $U(y)$ profile is sufficiently smooth there can be no purely real eigenvalues outside interval $[U_{min}, U_{max}]$ and, consequently, there is no stability of waves (the waves with $Im\,\sigma = 0$ are sometimes referred to as neutral). Inside the interval in question the analysis is complicated, depending not only on parameter, but also on other characteristics of the flow, for instance, on the sign of difference $c - U(y)$.

5.6.1.2 Analysis of barotropic instability. As stability is largely dependent on characteristics of the main zonal flow, it well be of interest to look at flow profiles along the meridian. Fig. 5.10 shows values of U at 700 mb level obtained from wind observation data and by means of geostrophic formula for various periods of Phase III. Geostrophic wind was calculated for data from Chuchkalov's (1977) Atlas. One seemingly minor detail is worth noting.The real-data profile shown in Fig. 5.10a has no bending point, that is $U''(y) \neq 0$ in none of the points, while the geostrophical curve has a bending point at 18N. Results of investigations of the main flow instability are very sensitive to the procedure used for mathematical transformations and the criteria of stability can vary reflecting subtle properties of the flow. Therefore, the use of real and computed data can yield different results, and it is not always clear which of them is more true. Wind, for one thing, is rather variable and its measurements are more error prone that those of pressure (in compatible units), besides, geostrophical approximation is smoothing the mean flow which, on the whole, will spoil the image of the main flow. Fields $U = U(y,z)$ and $\partial^2 u/\partial y^2 = \phi(y,z)$ in Figures 5.10b and 5.10c taken from Rennick (1976) give some idea of the main zonal flow variability.

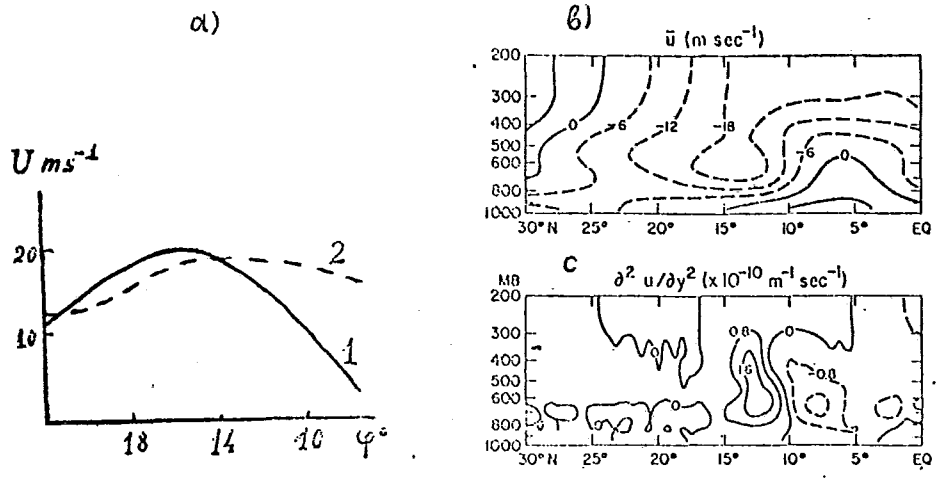

Fig. 5.10 Characteristics of mean zonal flow:
(a) mean zonal profile of wind for 6 days during Phase III of GATE and geostrophical wind computed on the basis of pressure charts (Chuchkalov, 1977)
The profiles of u (b) and $\partial^2 u/\partial y^2$ (c) (from Rennick,1976)

Two types of relatively simple approximations are usually used for the mean flow. If the main flow is a jet it can be readily presented as a function (see Rennick, 1976)

$$U = -U_0 \sin^2(\pi y / 2y_0) \qquad (5.54)$$

which is symmetrical with respect to the jet axis $(y = y_0)$

where 2a is the width of the flow flanked by solid walls, y = 0 and y = 2 y_0; y = 0 usually describes the equator and $y = 2y_0$ - approximately 30N.

Values of the main Coriolis parameter f and Rossby parameter β are calculated on the axis of jet ($y = y_0$).

$$f \approx 0{,}4 \cdot 10^{-5}\, s^{-1} \quad ; \quad \beta \approx 2.2 \cdot 10^{-11}\, m^{-1} s^{-1} .$$

Kuo (1978) used another suitable approximation for a jet

$$U = -U_0 + \frac{U_{10}}{Ch^2(y - y_0)} \qquad (5.54')$$

where U_0 and U_{10} - const and can be of either sign.

If it is necessary to emphasize a wind shear in the main flow, the following formula is applicable (Kuo, 1978)

$$U = -U_0 + U_{10}\, th\,(y - y_0) \qquad (5.55)$$

Calculations based on such models yielded some interesting findings which are supported by data. In model (5.54) the point $y = y_0$ is a critical point within a channel and there is only one neutral wave. The length of such wave is $L_N \approx 2.3\, y_0$. In certain conditions the amplitude of waves whose length is more than L_N increases, while short waves die out. Increment (η_+) or decrement (η_-) depend on U_0 ; the higher U_0, the greater η .

The scales of most unstable waves vary depending on the specific formulation of the problem, but usually their length is around $L \approx 3000$ km; and e-folding time is about 2.5-6 days.

In a flow with a pronounced shear (5.55) there might be two or even more neutral waves. The stability of the flow was found to be dependent on the position of the jet axis. The jet whose axis lies within 6°-10° latitude belt is most unstable.

The above features are in sufficiently good agreement with observations of waves formed in the Eastern Africa and in low latitudes in the Northern Atlantic (Burpee, 1975; Reed et al, 1977; Norquist et al, 1977; Muracami, 1979; Kung and Burgdorf, 1978). However, a scrupulous analysis of wave energetics revealed a substantial difference. In Africa and the Atlantic there is a quasi-stable jet stream over latitudes 5°-30° in the lower troposphere (1.5-3 km), which happens to be a layer of relatively high stability of the atmosphere. The transformation of energy due to barotropic component is rather important here and is more pronounced over sea than over land. It is in these latitudes that the transition from quasi-geostrophic to equatorial regime takes place. It might be that a more uniform ocean surface (from the view point of its smoothness and zonal distribution of temperature and humidity) hinders this transition

to a lesser extent. Hence, mean value of $\partial u/\partial y$ over oceans is higher than over the continent. To approximate the main flow profile over the Atlantic it is better to use formulae of type (5.55) keeping in mind that the westward flow is weaker near the Equator.

As estimations show, up to 70 per cent of total energy of the main flow can be transformed into energy of waves. Baroclinic component is larger over the continent than over the ocean, which might result from the non-uniformity of the underlying surface.

β -effect, as shown by Boyd (1978), on the whole, stabilizes the eastward jet and destabilizes the westward jet with a pronounced shear.

Thus, barotropic instability is the main cause of wave generation or, to put it more precisely, the largest share of the waves energy is caused by barotropic instability.

5.6.2 Baroclinic instability

The conclusion about the dominant role of barotropic instability is only natural, because as far as large-scale processes are concerned, the state of the atmosphere is always close to berotropic. In fact, it is a result of different scales of disturbances along the vertical and horizontal coordinates: the ratio of scales being at least O(0.01). Taking this fact as a basis, one can, as a first guess, analyze the effect of baroclinic instability in the same way as that of barotropic instability. If the main flow smoothly changes with height, flow characteristics may be taken into account for the level under study (U_{min}, U_{max}, dU/dy, d^2U/dy^2). It is only parameters relating to wave amplitude that need adjustment for altitude. Thus, we can take into account the interaction between various layers of the atmosphere. However, such quasi-parametric procedure make it impossible to understand the impact of subtle baroclinic effects. It is also due to the fact that actually the real vertical profile of zonal flow is not very smooth. Shown in Fig. 5.11 are profiles $U(z)$ built on data from "TROPEX-72" and "Meteorology over Tropical Oceans" (1978). As there are several extrema, mathematical and physical analysis of instability is rendered much more difficult. First, to represent such curves analytically, several parameters are needed, which can be understood as the presence of several modes along z -coordinate.

Each mode has to be analysed separately. Second, there might be more than one critical level (that is, the value of z at which the parameter of type (5.53) but with $\partial^2U/\partial z^2$ instead of $\partial^2U/\partial y^2$ becomes zero. No theorem exists to state the existence of only one neutral wave. Third, as we know, vertical stability of the atmosphere is described by the Richardson number, and in tropical atmosphere the value Ri for the main flow changes by more than one order. There are also other difficulties which diminish the possibility of analytical investigations of baroclinic instability effects. Therefore some of recent results have been obtained using computer capabilities. Thus, it has been established that wave velocity depends but little on Ri within the wide range of its variation - from 7 to 100, for both westbound and eastbound waves. Growth rate* in the eastward flow largely depends on Ri, while in the westward flow little. Growth rate maximum depends on the model and ranges from 0.4 to 2.0 in dimensionless units for different models. For each specific model the maximum ranges from 0.2 to 0.3 depending on Ri. With horizontal scale being $L \approx 250$ km, the maximum increment for one of models

*Growth rate is usually characterized by parameters $k\,\mathrm{Im}\,\sigma$, where k - is wave number, $\mathrm{Im}\,\sigma$ - imaginary part of the speed of wave propagation obtained from dispersion equation.

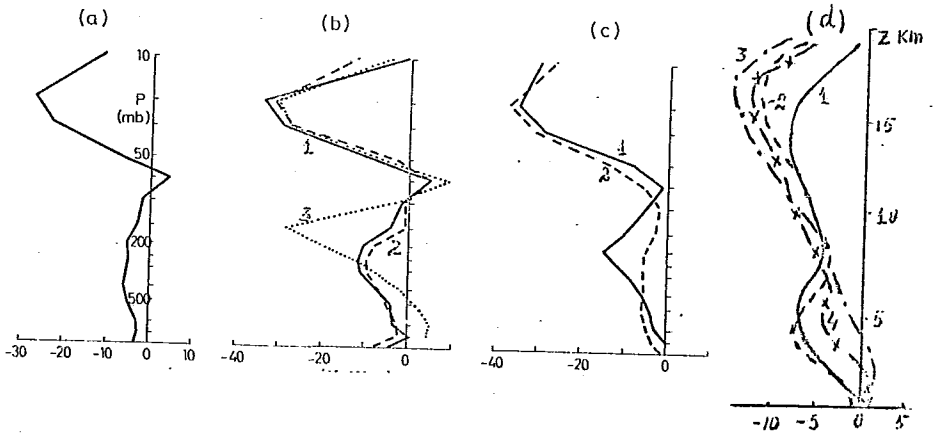

Fig. 5.11 Vertical profile of zonal wind ($m.s^{-1}$):
(a) averaged for the period from July, 1 to September, 30, 1974; observational data were yielded by 18 stations located throughout the equatorial belt from 7°N to 10°S; (b) averaged for same period, but stations were located at 1-0°; 10°W; 2-0°, 23°30'W; 3°-0°30'S, 73°E. (c) Same as for (b) but for: 1°-5°N, 23°30'W; 2°-7°N, 15°E. (d) 1 - averaged on the basis of TROPEX-72 data; 2 - the same, but for TROPEX-74; 3 - research vessel "Professor Zubov" during GATE (5°N); 4 - mean value for all three GATE phases.

based on formula (5.55) lies in 0.4-0.6 interval, which corresponds to $L \approx$ $\approx$ 6 000-3000 km. In other models the maximum of growth rate lies in the interval 1.2-1.4 corresponding to 1000-1500 km. When $Ri < 10$ a westerly is on the whole, more stable than an easterly. If the axis of the shear flow lies below 15° of latitude, the wave number of the most unstable wave becomes larger, just as it happens in a purely barotropic flow.

Fig. 5.12 from Kuo's paper (1978) gives some idea of the difference between barotropic and baroclinic models. In the model the author used two levels thus taking into account only one mode ($Ri = 20$ and flow axis lies at 20° of latitude).

The vertical baroclinity of large-scale motions is described in vorticity equation by a term of the $\alpha\, \partial T/\partial s$ type, where α can be regarded as a parameter and s is a horizontal coordinate. Thus, zones with great horizontal temperature contrasts can also be a cause of baroclinic instability. As was mentioned above, the share of barotropic component over the African continent is less than over the sea. Over the continent a more important role belongs to baroclinic effects which are, on the whole, related to much larger values of $\partial T/\partial y$ over the non-uniform surface. A comparison of the results obtained from analysing the impact of barotropic and baroclinic instability with observational data showed that the components of energy balance are not in good agreement. A hypothesis has been put forward that the loss of stability of the mean flow or even of neutral waves can be caused by energy released in large-scale processes by means of condensation. As warm tropical air is very moist, the latent heat energy is comparable with the energy of wave generation. At a first glance it seemed natural to believe that waves with a period of 3-5 days were formed over the Atlantic due to a release of latent heat energy, because ITCZ with rather a large cloud band is located here. However, a thorough verification of GATE data showed that "The proposal that tropical waves were key elements in the positive feedbacks that determined the ITCZ condition received little support". (Report of the US GATE Central Program Workshop, 1977, p.35).

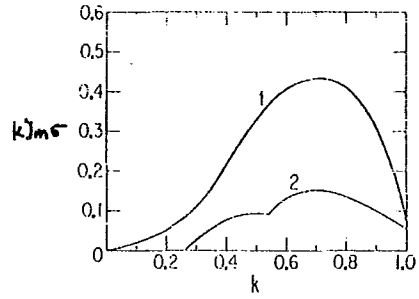

Fig. 5.12 Growth rate of unstable disturbances as a function of wave number for a flow with the centre at 20°N
1 - baroclinic model
2 - quasibarotropic model

Mechanisms responsible for a loss of stability are much more complicated. First, it is practically impossible to single out only one mechanism causing the generation of waves using real data. Second, theoretical investigation of the composite effect of all the three mechanisms is complicated even for modern computer facilities. And third, at present it is difficult even theoretically to formulate the problem of stability or a loss of stability of a large part of general circulation, because the atmosphere and general circulation components are systems with many degrees of freedom. The following, rather simple, example gives some idea about these difficulties. Time-variation analysis of wind velocity horizontal component just at the Equator during the three GATE phases revealed interesting peculiarities which can be interpreted as a break in stable wind picture or as an appearance of instability.

Fig. 5.13 gives an example of time variation for Phase I of GATE based on Zaichikov and Romanov's (1976) data. One can clearly see the intrusion of western winds into east flow in the 2-4-km layer. The duration of such "intrusions" ranged from a few hours (on July 13, 1974 a western wind was observed only at one out of four sounding times) up to six days (July 7-12, 1974). Similar phenomena were also observed in other GATE phases. Most likely, all the three mechanisms are responsible for such loss of stability of the eastern main flow.

The goal set in investigations of stability is not related to global circulation. The waves in low latitudes with a scale of several thousand kilometers should appear in GCMs. Recent, most comprehensive GCMs, for instance, models used at GFDL, ECMWF and Hydrometcentre of the USSR actually include waves of such type. GCMs are very complicated and it is far from easy to find one principal cause for the generation of such waves when analysing results of numerical simulations. In GFDL model, Hayashi and Golder (1978) drew a conclusion that wave generation is caused by release of latent heat, rather than by barotropic or/and baroclinic instability. This conclusion might just as well be prompted by specific features of GFDL model in which dynamic instability is more suppressed by computation procedure than by thermal instability. The latter is already limited by convective adjustment procedure. In the model with fewer layers used in the Hydrometcentre of the USSR (Trosnikov, 1980) dynamic instability is less suppressed, and waves can probably appear even in a "moist" model. It would be of interest to make a series of computations using different GCMs with a view of finding out which mechanism is responsible for the transformation of stability into synoptic-scale waves typical for low latitudes. It might be important not only for revealing some subtle features of a specific GCM, but also for gaining a deeper knowledge of the very mechanism of instability. The fact is, that most findings concerning the stability of atmospheric motions were received in linear approximation, while up-to-date GCMs also take account of non-linear interaction which is responsible for energy exchange between waves of different nature, types and modes.

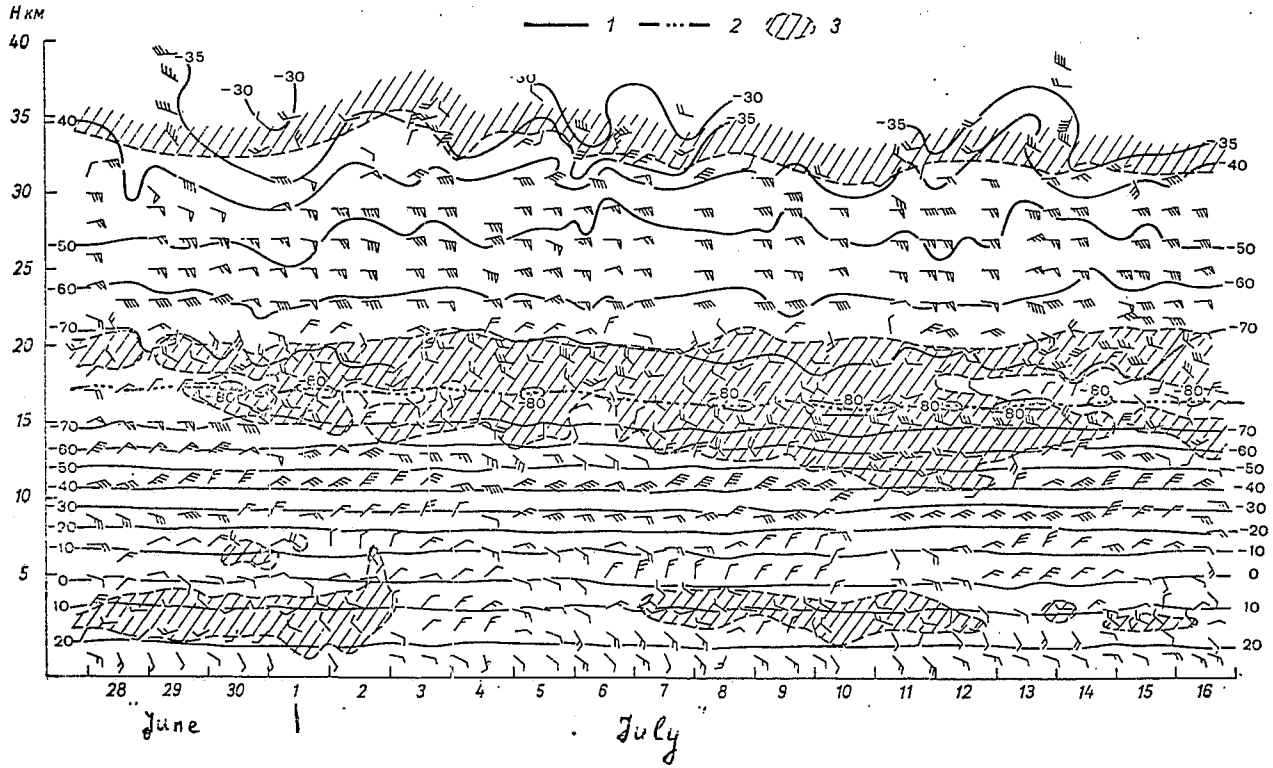

Fig. 5.13 Time-vertical section of the atmosphere at 0°, 23°30'W during Phase I of GATE. 1 - isotherm (0°), 2 - tropopause, 3-westerlies

5.6.3 Wave-CISK mechanism

5.6.3.1 General remarks. CISK hypothesis was put forward by Ooyama (1964), Charney & Eliassen (1964) in an attempt to try to explain the mechanism of instability in processes having a larger scale than a single cumulus. To be more precise, those having a scale of a hurricane or a tropical cyclone. The idea of CISK is rather simple: latent heat of condensation of convective cloud clusters can be expressed (parameterized) through characteristics of large-scale processes inside which cloud clusters are formed. Later on the hypothesis was applied to large-scale disturbances of Rossby-gravitational type and ITCZ. The increasing range of its application brought to light the hypothesis' strong and weak points. For instance , when determining the width of ITCZ-model precipitation zone it turned out that its width is comparable with the size of synoptic disturbance, that is about 3 000 km. This happens because CISK, just as the mechanism of purely conditional instability, brings about too great an increase of instability energy in intensive convection area when condensation is taking place. In order to decrease the width of precipitation zone, Charney (1972) modified CISK hypothesis by developing the so-called movable CISK model. By changing parameters the author obtained a 250-300 km-wide precipitation zone at latitude 10°. A detailed analysis of dynamic equations showed however, that the meridional component of wind speed (v) should be a value about 15 $m \cdot sec^{-1}$ or either v should change by 15 $m \cdot sec^{-1}$ in two days! (two days is a typical time scale of movable CISK). Bates (1973) further makes a distinction between two types of CISK: in one, instabilty largely depends on processes taking place in non-stationary boundary layer, on convergence of moisture and on rotation in subcloud layer, while in the other instability can occur without rotation. So, GATE, among other things, was to verify the CISK hypothesis (but, of course, this goal was not formally included into GATE's programme and terms of reference). It follows from the CISK hypothesis that a line of convergence coincides with a temperature maximum line and, consequently, with cloudiness and precipitation. An ITCZ section constructed from GATE data revealed considerable asymmetry (see Fig. 5.14 based on the Report on US GATE Central Program Workshop, 1977). Temperature maximum is shifted towards the equator with respect to convergence line. This result has considerably narrowed the range of application of the CISK hypothesis. CISK can be applied to processes in which spatial details of 100-km scale are insignificant. Another weak point of CISK is that the less the scale of a disturbance the higher is its growth rate (see Yanai, 1975). But the width of ITCZ is 300-500 km or less, the diameter of a tropical cyclone is about the same, and that of a hurricane is even less (about 100 km), so the CISK hypothesis does not "work" well enough when applied to the above scales for which it was meant.

Though CISK has numerous weak points, at present there is no better alternative and we have to use it at least for qualitative analysis of processes taking place in the tropics.

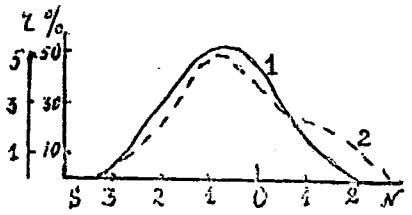

Fig. 5.14 Distribution of precipitation (1) in mm/6 hours and of cloudiness (2) in per cent in ITCZ. Point 0 corresponds to ITCZ axis. Horizontal scale is in hundreds of kilometers

5.6.3.2 The description of the wave CISK mechanism

The energy released during condensation in large-scale convective processes is comparable with other components of energy cycle. But deep cumulus convection in itself can not provide intensive mass convergence in the subcloud layer which is necessary for large cloud clusters to exist. If mass flow balance is not to be destroyed we have to make use of processes with a larger scale than that of cloud clusters.

A model of CISK waves can be presented as the system of linearized equations of hydrothermodynamics

$$\left.\begin{array}{l|l} \dfrac{\partial u}{\partial t} - (f_0 + \beta y)v + \dfrac{1}{\tilde{\rho}}\dfrac{\partial p}{\partial x} = 0 & \dfrac{\partial u}{\partial x} + \dfrac{\partial v}{\partial y} + \dfrac{\partial w}{\partial z} = 0 \\ \dfrac{\partial v}{\partial t} + (f_0 + \beta y)u + \dfrac{1}{\tilde{\rho}}\dfrac{\partial p}{\partial y} = 0 & \dfrac{\partial}{\partial t}\left(\dfrac{\partial p}{\partial z} + \dfrac{1}{H}p\right) + g\S w = Q \end{array}\right\} \quad (5.56)$$

(For details see Lindzen, 1974; Stevens and Lindzen, 1978; Davies, 1979). Here f_0 - the value of main Coriolis parameter for "φ_0" latitude; β - Rossby parameter for "φ_0" latitude; H is about 10 km - scale height of the atmosphere; $\tilde{\rho} = \tilde{\rho}(z)$ - mean density, $q\S$ - parameter characterising vertical statical stability (proportional to Γ parameter from section 5.3; g - gravity acceleration; Q - heat forcing. The remaining symbols have already been explained and for this specific task the unknown functions have a sense of small deviations. Seeking solution of the system in the form of:

$$R(y, z, x, t) = R_1(y) \cdot R_2(z)\, e^{i(kx - \sigma t)} \quad (5.57)$$

where R is any of unknown functions (u, v, w, p) and the prescribed heat forcing is Q; one can, just as it was done in section 5.3 reduce the problem to a third-degree algebraic equation and seek solution by the method of eigenvalues.

The details will depend on specific formulation of the task. The simplest case reflecting several basic features of wave CISK can be obtained from "non-rotational" model ($f_0 = \beta = 0$). In usual "equatorial" approximation

($f_0 = 0$; $\beta = 2.3 \cdot 10^{-11} m^{-1} s^{-1}$) $R_1(y)$ is expressed through the Hermite polynomials (see section 5.3) and equation of dispersion has the form

$$\sigma^3 - \sigma(gh_n)\left\{(2n+1)\sqrt{\beta^2/gh_n} + \kappa^2\right\} - gh_n\beta\kappa = 0 \quad (5.58)$$

where h_n - equivalent depth; $n = -1$ corresponds to the Kelvin waves; $n = 0$ - to Rossby gravitational waves. Dependence on z is found from equations

$$\left.\begin{aligned} &\frac{d^2 w_2}{dz^2} + \lambda_n^2 w_2 = \frac{H^2}{g h_n} q(z) \\ &\lambda_n^2 \approx \left(\frac{gS}{gh_n}\right) H^2 - \frac{1}{4} \end{aligned}\right\} \qquad (5.59)$$

In accordance with the CISK hypothesis, $q(z)$ is not zero only in layer $z_c < z < z_T$, where z_c is cloud base level which coincides with condensation level; z_T - height of clouds. To take account of convergence in a subcloud layer, the value of w_K is assumed proportional to the value of w_K at the upper limit of a mixed intensive layer z_m. So in a general case, we can write

$$q(z) = \left\{ \begin{array}{ll} \alpha w(z_m) \cdot \eta(z) & z_c < z \le z_T \\ 0 & z \notin]z_c, z_T[\end{array} \right\} \qquad (5.60)$$

Parameter α is introduced in order to estimate the degree of feedback.

Details of different models of CISK waves depend on differences in the presentation of heat forcing distribution along the vertical (z).

Fig. 5.15a from Davies (1979) illustrates actual distribution of function $\eta(z)$ and possible analytical approximations. Fig. 5.15b shows distribution with height (w_q) using GATE data (Snitkovsky and Trapeznikova, 1976) (see also Fig. 1 from Chih-Pei Chang, 1976).

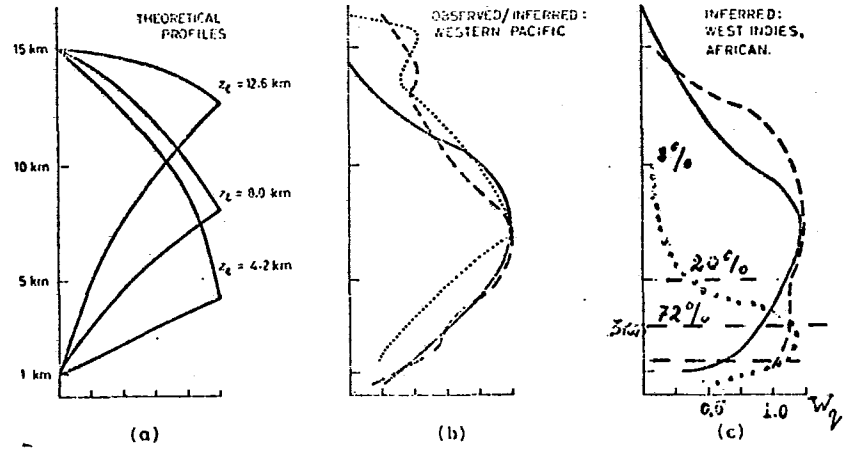

Figure 5.15. Normalized structure of the diabatic heating rate. In (a) a range of theoretical piecewise continuous profiles that correspond to z_1 = 15 km, z_0 = 1 km and with z_4 = 12.6; 8 and 4.2 km, is shown.

In (b) the curves displayed for the western tropical Pacific refer to the long time period structure (dashed curve), cloud cluster environment (solid curve) and one particular sector of the Reed-Recker composite study of easterly waves. Finally in (c) the solid and dashed curves refer respectively to the environment of the cloud clusters in the West Indies and the wave amplitude structure of African wave disturbances over land. Dotted line shows actual distribution of water vapour on the basis of GATE data. Percentage values show vapour content on 0-3 km layer; 3-5 km layer and 5-10 km layer; calculated by Snitkovsky and Trapeznikova (1976).

Analysis of problem (5.59-5.60) with corresponding boundary conditions reveals the following common features for various types of $q(z)$ close to (5.61).

1. As $q(z)$ is proportional to w, eigennumbers of the problem are in fact functions of parameter α. The Fig. 5.16 from Stevens and Lindzen's paper (1978) gives one some idea about the behaviour of eigenvalues depending on parameter α for several first modes. For given α, every unstable solution can be compared with a solution based on induced effect and having a higher value of some complex parameter which determines the ratio of moisture accumulated through divergence to precipitated water.

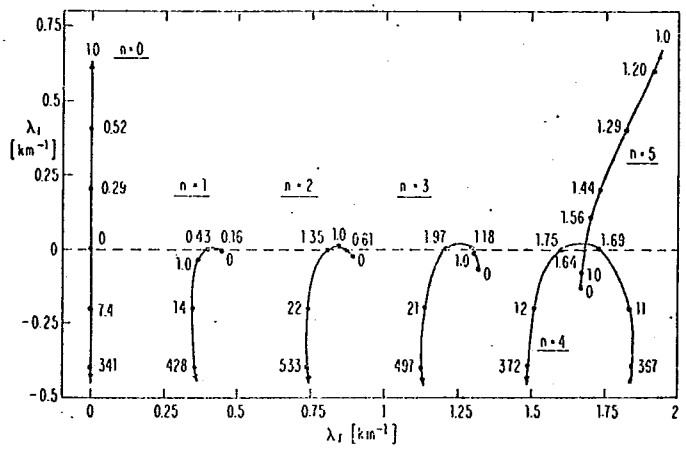

Fig. 5.16 Eigenvalue curves $n = 0-5$. The value of α is denoted at various points on the curves. Unstable/stable solutions are in the upper/lower half-plan

2. If friction is taken into account this will decrease lengths of waves both in horizontal and vertical directions and, naturally, also diminishes time scale.

3. The longer Rossby wave in x direction, the less chance of its becoming neutral. Time scales of long waves are more than 30 days.

4. Phase lag between moisture convergence and heat forcing in case of long waves is rather small, several degrees only.

5. For small scale waves, such as squall lines, with Rossby number exceeding 10 time scale is of the order of several hours.

One of weak points of the above wave CISK mechanism is that the responce of the atmosphere to heat source turns out to be instantaneous. This manifests itself by the same phase of the given heat forcing and unknown functions.

Actually, there is a certain time lapse between divergence (that is, w) and formation of clouds. For instance phase lag between waves of vertical velocity and mean cumulus cloudiness is almost as large as a quarter of a wave (about 80 degrees). That is why Davies in his paper (1979) proposed to write function $w(z_m; x, y, t)$ in the form

$$w(z_m; x, y, t) = \int_{-\infty}^{t} F(t-\tau)\, w(z_m; x, y, t, \tau)\, d\tau$$

where F - is weight function, which becomes zero at the ends of integration interval; $\int F(t-\tau)\,d\tau = 0$ is shown approximately in Fig. (5.17) in dimensionless variables. Function w takes account of the history of events. Computations have shown that thus modified CISK model brings wave parameters closer to real ones. For instance, time scales of most unstable long waves go down to 5-15 days. All modes of the inertia-gravity waves can be stable and the adjustment period is about 12 hours if the wave amplitude of heat source is of reasonable value.

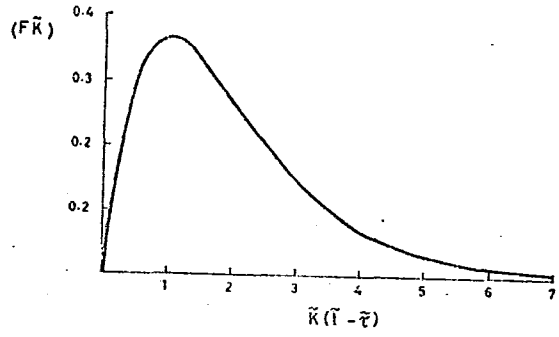

Fig. 5.17 Plot of the non-dimensionalized weight factor against the non-dimensionalized lag time

This new interpretation of CISK model requires special processing of observational data necessary both for verifying the details of the model and for improving the model itself.

Improvements in linear models of tropical waves have been proposed recently by taking into account refined physical effects. For example, Mass (1979) defines more precisely the mechanism of sinoptic-scale wave generation over Africa using a small time step (about 6 minutes). The author analysed the effects of variations of mean wind, latent heat and cumulus momentum mixing in linearized system of primitive equations, which made it possible to obtain values of wave parameters very close to real ones: $L \approx 2500$ km, $c/m \approx 8$ ms^{-1}, $t_0 \approx 3.5$ days. Small-scale processes, such as cumulus momentum friction, boundary-layer and variations in vertical profile of heat forcing, have little effect on the above wave parameters, although they greatly affect vertical wave structure and quantitative characteristics of convective heating parametrization. Undoubtedly, the method in question will also make it possible to take account of non-linear effects which will be very important from the viewpoint of tropical meteorology.

5.7 A METHOD OF SEARCHING THE WAVE FROM THE OBSERVATIONAL DATA

5.7.1 General remarks

As it is know the GATE lasted 100 days; out of them on 58 days (three phases) frequent observations based on special programs have been made. Disturbances which are of more or less periodical character, of T-day period, occured about $n \approx \frac{100}{T}$ times. If T = several days, then n is enough to allow one to speak about an appropriate disturbance and its characteristics. When T~10-30, the results are but slightly reliable. Similar speculations keep valid in reference to space data as well: the GATE area extends along the longitude for about 4 000 km, and along the latitude - 2,500 km. Disturbances the dimension of which exceeds 2-3,000 km should be interpreted with a lot of caution , the more so since the processes in the GATE are strongly influenced by the African continent. The conditions in the Indian ocean and in the Pacific are different.

The disturbances of periodical nature can be divided into two groups. To the first group belong those whose cycle is equal to natural one determined by external factors: by diurnal and yearly earth rotations. Due to some features of dynamics equations in a number of cases semi-diurnal cycle manifests itself like the natural one. To the second group belong waves which propagate with specific phase velocities having nothing to do with the mentioned natural cycles. These phase velocities and hence cycles are determined as eigenvalues of a certain operator describing the dynamics of corresponding atmospheric processes. Such procedure permits to define waves generated by a certain mechanism: Rossby waves, gravitational waves, etc.

Basically two methods are used for searching periodical processes: 1. A direct determination of the oscillation amplitude (and sometimes of the phase) of quite a rigorous apriori of the known cycle - diurnal, annual and semi-diurnal. 2. Veiled cycles are determined by an application of an appropriate procedure based on utilization of statistical characteristics of rather a long observation series. Often these methods are used in their combination: tentatively an approximate period is determined (a quasi-biennial cycle of the zonal wind in the upper troposphere and the lower stratosphere), then on the statistics basis oscillation parameters are found. A most common technique of determining periodicities is plotting a spectral diagram (either directly or as Fourier transformation of a correlation function) - maxima are interpreted as the presence of an oscillation of relevant frequency. Here two facts should be borne in mind: 1. A "throw-out" of Dirac 8-function theoretically corresponds to an oscillation of a known frequency in the spectral function. But on the spectral diagram that is never to be got due to both a limited bank of initial data and due to 2. In atmosphere's nature one never encounters "pure" oscillation with an exact period. These circumstances, namely, limit of data and the absence of an exact physical period lead to "smoothing" of the peak on the spectral diagram. Often it is rather difficult to verify separately the influence of each of the factors, hence a conclusion about the presence of any period is not absolutely fair.

As to the data collected during TROPEX-72, TROPEX-74 and all the GATE period , both methods have been used for determining characteristics of "purely" periodical and quasi-periodical oscillations of meteorological parameters.

5.7.2 Direct determination of characteristics (diurnal and semi-diurnal periods)

On the basis of more frequent observations during the expeditions diagrams of diurnal development of practically all meteorological parameters have been plotted. These parameters can be divided into three groups. To the first one belong those which are directly measured: pressure, temperature, horizontal wind speed and others.
In addition to Fig. 5.2 Fig. 5.18 is given below. To the second group belong those which come from observation data as a result of their processing

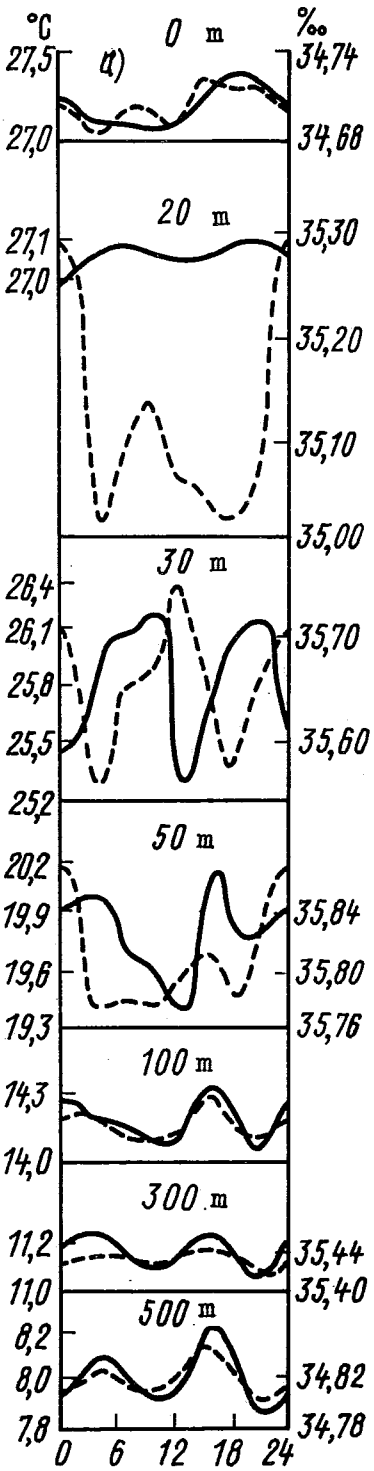

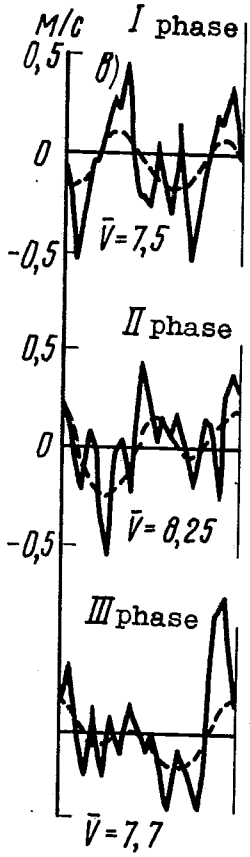

Fig. 5.18 Diurnal variation of the meteorological parameters: a. temperature (solid curve) and salinity (dotted curve) at different depths on the basis of TROPEX-72 and TROPEX-74 data; b. absolute value of horizontal wind velocity at trade-wind zone; dotted line - the representation by two harmonics of Fourier series.

(averaging, revealing separate components, summing up for certain time intervals): zonal and meridional components of wind speed, hourly precipitation sums, etc. (Fig. 5.19). To the third group belong those which are presented in Fig. 5.20. They are parameters computed from dynamics equations. In all the figures time is GMT. To find the local time 2 hours should be substracted.

Analysis of the diurnal variation shows a close interrelation between meteorological parameters and this fact helps to specify methods of measurement and calculation of different values. Moreover it helps to construct theoretical models of circulation mechanisms in low latitudes. The following can serve as an illustration. The diurnal variance of the precipitation in the region of cloud clusters has two maxima: in the morning (7.00-12.00) and the evening (19.00-24.00); apropos the morning maximum is more pronounced than the evening one. On the curve of the diurnal variance (for the second phase of GATE) the maximum of divergence at the sea level falls on 10.00 and 22.00 hours (local time).

5.7.3 Determination of periodical components from spectra power function

Spectra for different parameters began to be constructed immediately after the end of pre-GATE and GATE expeditions. As usual spectra were plotted with $\frac{f S(f)}{\sigma^2}$, $\ln f$- coordinates (f - frequency, S - spectral density related to total variance (σ^2)).

The spectra of pressure P , air temperature T , ocean surface temperature T_{oc}, absolute value of wind velocity (V) are presented in Fig. 5.21

Since one of the main goals of GATE was to investigate ocean-atmosphere interaction, spectra of various hydrophysical parameters measured during GATE were computed. Fig. 5.21 shows examples of the spectra of the current speed of the horizontal components at the 500m depth. A semi-diurnal wave in the velocity field appears very distinctly. It is even more distinct than the diurnal one. In the temperature field these periods are marked very poorly.

The spectra of various values in the atmosphere are presented in Fig. 5.22 a,b (see Petrossiants et al., 1976; Lysenko et al., 1974).

The maximum near 4-5 days is of interest. It is revealed practically in all the spectral curves for all parameters including even those which are not of purely meteorological nature, for example, the geomagnetic index (local feature of the magnetic field disturbances). If waves with a period of 4 days in the fields of wind, pressure, temperature, precipitation are interpreted as a result of the instability of the zonal flow, then what is the meaning of the geomagnetic index here?

The problem here seems to be more complicated, i.e. 4-day variation probably reflects the inner autooscillation regime inherent to the atmosphere (and ocean) of the lower latitudes. If this is the case, then it is necessary to obtain it theoretically from the general equations of the hydrodynamics with "magnetic" interactions applied. But so far it is not clear how to do it. In this respect a further comprehensive processing of the empirical data for longer time periods appears to be quite necessary. It might even happen that the processing will allow us to clarify the general mechanism of the autooscillation regime be mentioned that the maximum near the 30-day oscillation is in good correlation with the 27-day oscillation of the zonal circulation index. The maximum corresponding to 15-16 days is traced over all the heights up to 95 km.

So far the 4-day period appears in each element, so it should be also found in the cross spectra. This diagram is obviously confirmed by Fig. 5.23 which contains examples of the cross spectra curves of various meteorological elements.

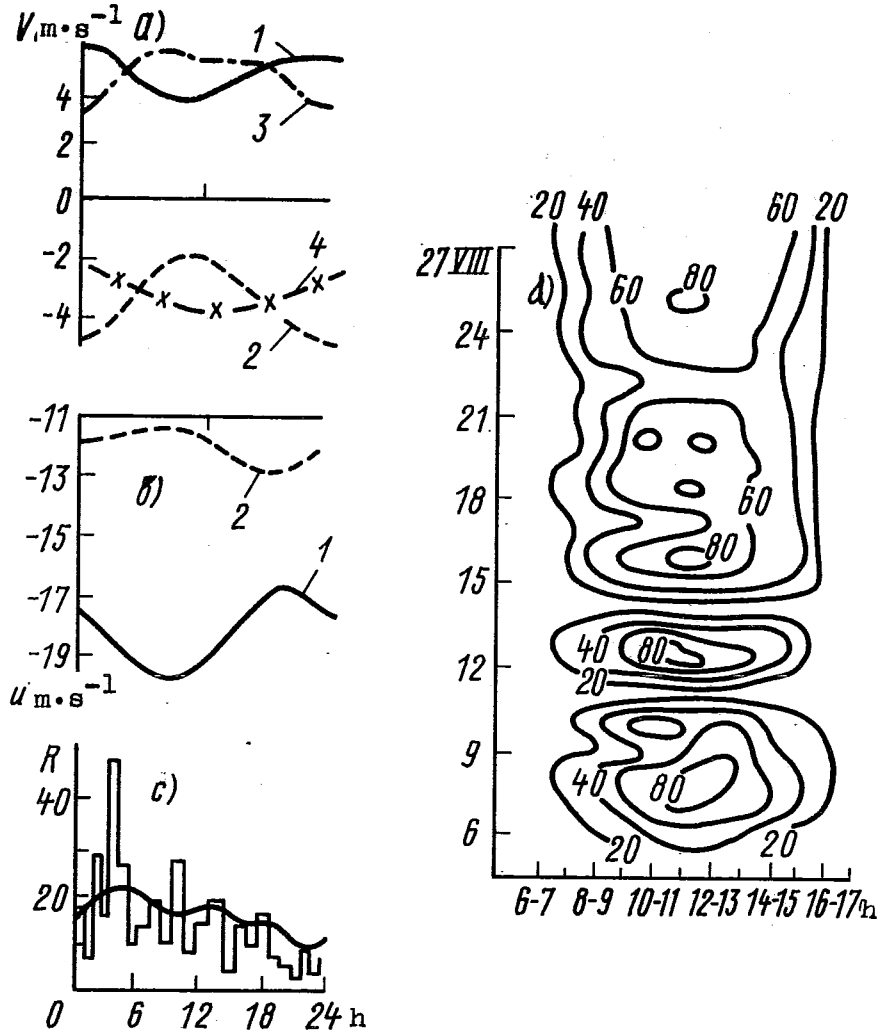

Fig. 5.19 Diurnal variation of the meteorological parameters: a. meridional wind velocity (ms^{-1}): 1-for latitude 12° at 200 mb level, 2-for latitude 5° at 200 mb level, 3-for latitude 12° at sea level, 4-for latitude 5° at sea level; b. zonal wind velocity (ms^{-1}): 1-at the ship located at 6.5°N,20°W; 2-at the ship located at 6.5°N,27°W; c. diurnal variation of precipitation amount in convergence zone (7°30'N, 20°50'W). Hourly sums averaged for the period of July 10-25 and of August 6-21 1974. A smooth curve - the representation by two harmonics; d. hourly sums of total radiation at A-scale area (cal.cm-2) for the period of August 6-27. A distinct wave will be revealed with the 3-5 days period, if one makes a horizontal cross sections. The amplitude of the wave is small in the morning and in the evening and is comparatively large in the afternoon.

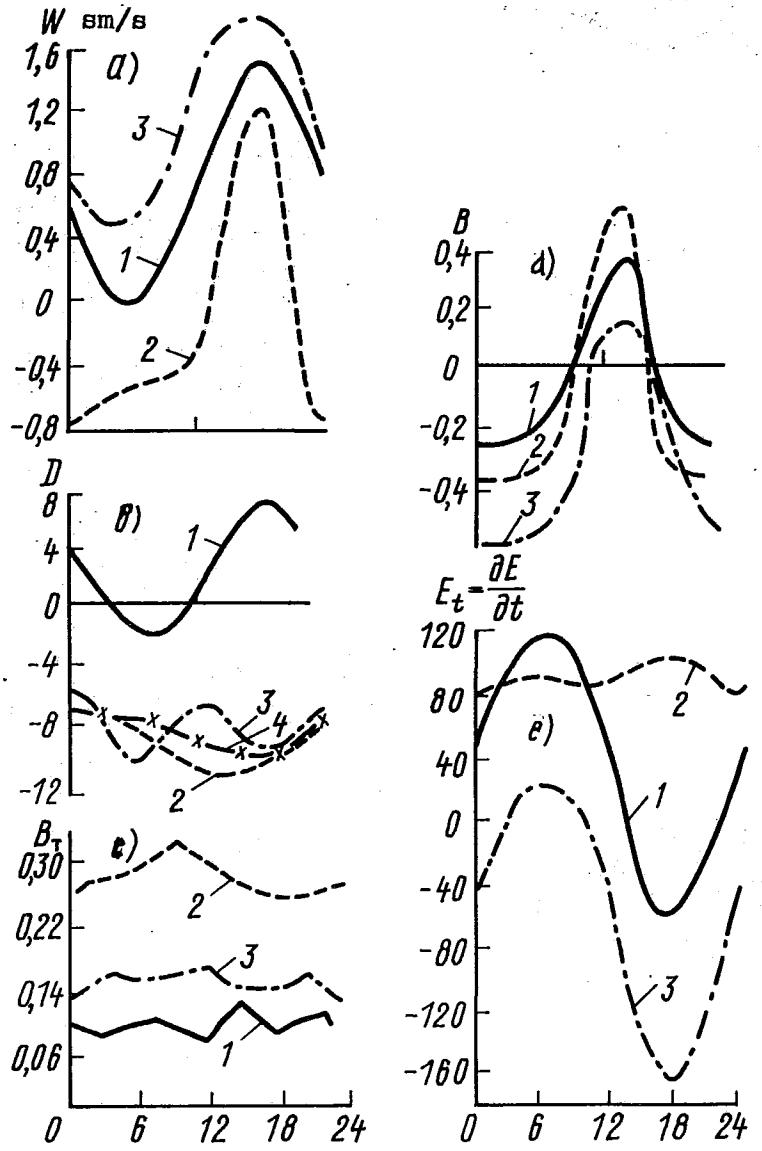

Fig. 5.20 a. Diurnal variation of vertical wind velocity component ($cm \cdot s^{-1}$) at 400 mb level: I - Phase I, 2 - Phase II, 3 - Phase III; b. Diurnal variation of divergence ($10^6 s^{-1}$) I - at 200 mb level, 2-3-4 at sea level for phases I, II, III respectively. c. Diurnal variation of turbulent heat exchange (B_T cal. $cm^{-2} min^{-1}$) at different latitudes: I - 10°N, 2 - 7.5°N, 3 - 5°N. d. Diurnal variation of ocean-atmospheric heat exchange (B cal-$cm^{-2} min^{-1}$) I - Phase I, 2 - Phase II, 3 - Phase III. e. Diurnal variation of energy change due to large-scale motion at A-B scale area for Phase I. I - in the layer 1000-200 mb, 2 - in the layer 1000-700 mb, 3 - in the layer 700-200 mb.

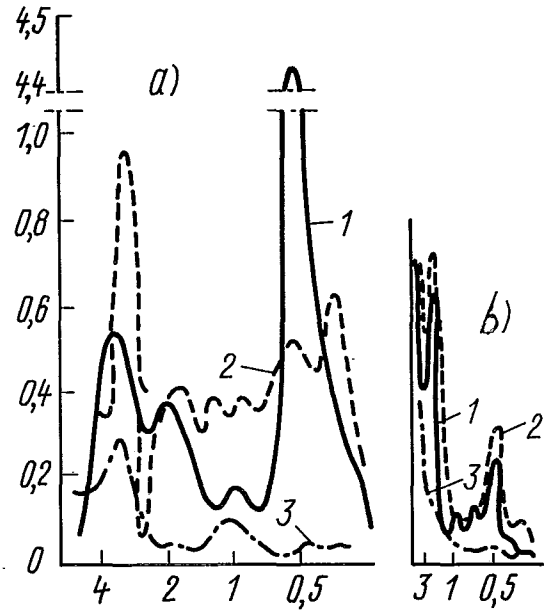

Fig. 5.21 Spectra of the meteorological parameters: (the periods are given by days (24 hours) for all figures dealing with spectra)

a. Spectra of the parameters to be measured: I - surface pressure; the maximum in the range of 12-hours period is shown separately in another scale; 2 - absolute value of wind velocity, averaged over the data; collected by three ships, located at 7.5° latitude; 3 - temperature field.
b. Spectra of zonal - I, meridional - 2 current velocity components and temperature - 3 at 500 mb depth.

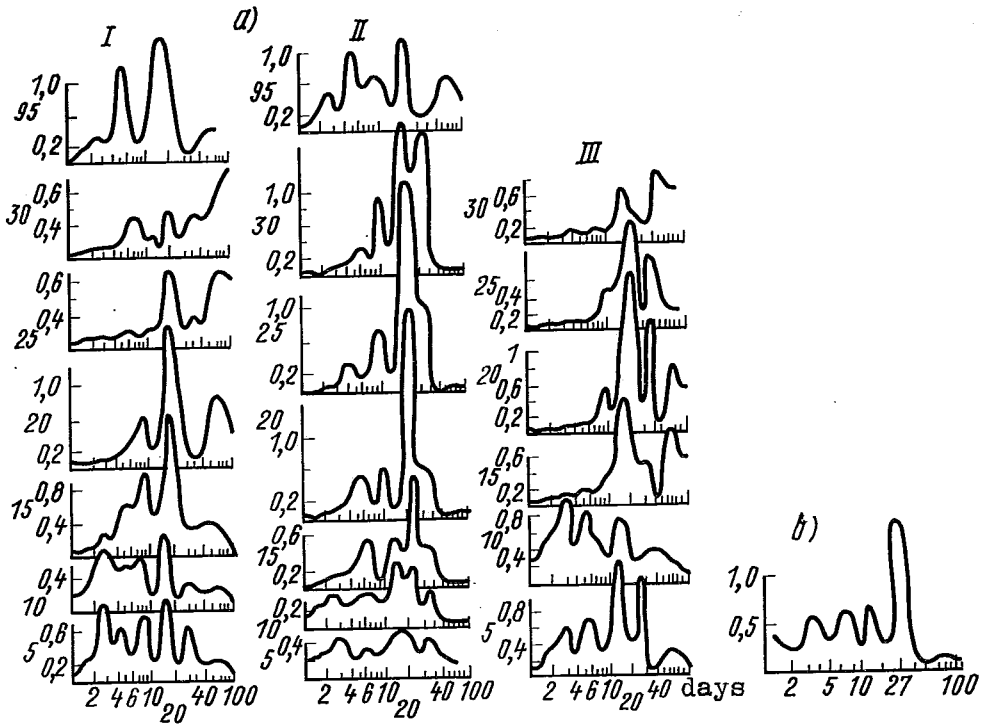

Fig. 5.22 Spectra of zonal - 1, meridional - 2, wind velocity components and temperature - 3 at different levels in the atmosphere; b - spectrum of geomagnetic indice

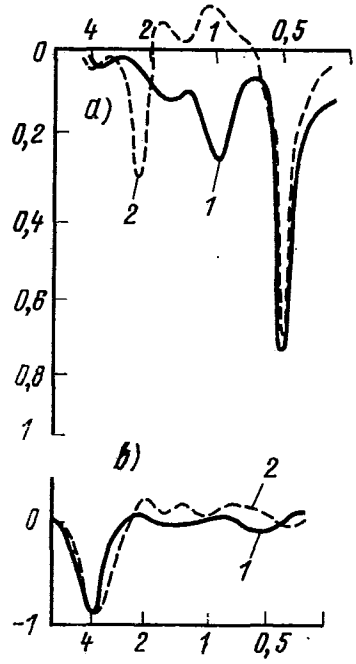

Fig. 5.23 Cross spectra of the meteorological parameters in the near-water surface layer of } on the basis of TROPEX-72 data
a. 1 - precipitation and air temperature
2 - sea surface temperature and air temperature
b. I - meridional and zonal wind velocity components } on the basis of TROPEX-74 data
2 - meridional wind velocity component and air temperature

5.7.4 Approximated definition of characteristics of long-range disturbances

It is practically impossible to detect the variations with a period of 7 to 8 days and longer ones when the length of the series is 100 days. Meanwhile in some cases they occured rather distinctly. We'll give three examples. During GATE, particularly in Phase II (July 28 - August 16) at the layer 6-10 km high the wind changes regularly from south-eastern to north-eastern direction and inversely with a period of 7-8 days. It might be a result of occurrence of inertia-gravity waves with the main period from 3 to 4 days. In Fig. 5.24 (Bubnov et al. (1976)) one can see the variation of daily mean water temperature at different depths. The periodicity of 7 to 8 days is clearly seen at the levels 50-100 m. Fig. 5.24-6 illustrates the time variation of the zonal component at the depth of 75 m. The monthly cycle also occurred.

It is totally necessary to accumulate an extensive series so as to make the best use of spectral analysis methods.

5.7.5 Determination of quasi-biennial phase of zonal wind

A special methodological approach has to be used for investigating the quasi-biennial cycle.

Shown in Fig. 5.25 are mean monthly values of zonal wind speed at various levels obtained by using data from some stations located in lower latitudes. The periodicity is distinctly observed but one harmonic is not enough for its description.

The correlation functions for $U(t)$ - 1 and for noise - 2 are shown in Fig. 5.26. Noise is the difference between $u(t)$ and the sum of oscillations which takes away the greatest part of the variance. The calculation results of the most probable variations for some points are given in Table 5.4. The table contains the following notations: U_0 is the meannvalue of u ; σ_0^2 is the variance of the deviation u' ($m^2 s^{-2}$); $\sigma_1^2(t_m)$ is the variance of the $u - U(t_m)$ which corresponds to the t_m variation period;

$D = \frac{\sigma_1^2}{\sigma_0^2} \cdot 100\%$ is the part of the variance decreasing due to the oscillation with the period t_m; $A(t_m)$ is the amplitude of the oscillation with the period t_m ($m \cdot s^{-1}$).

The table shows that U_0 increases with height, i.e. the eastern wind becomes stronger; at the 9° latitude the energy of the annual variation is in fact equal to the energy of the 28 month cycle oscillation; at the ±18° latitude the quasi-biennial cycle is weakly displayed and only annual cycle is distinctly observed; at the equator the oscillation with the 26-27-28 month periods takes away approximately the same part of energy (the calculations showed that the energy suction "sharply" decreases 2 or 2.5 times as fast for t_m = 25 months and for t_m = 29 months).

The results of presentation of the initial data by several series terms of Fourier expansion are shown by a dotted line in Fig. 5.25. By the way as example we shall give a formula for U at 20 mb surface for Canton Island.

$$u = -7.7 - 13.1 \cos\frac{2\pi}{27}t - 12.2 \sin\frac{2\pi}{27}t - 1.7 \sin\frac{2\pi}{8}t .$$

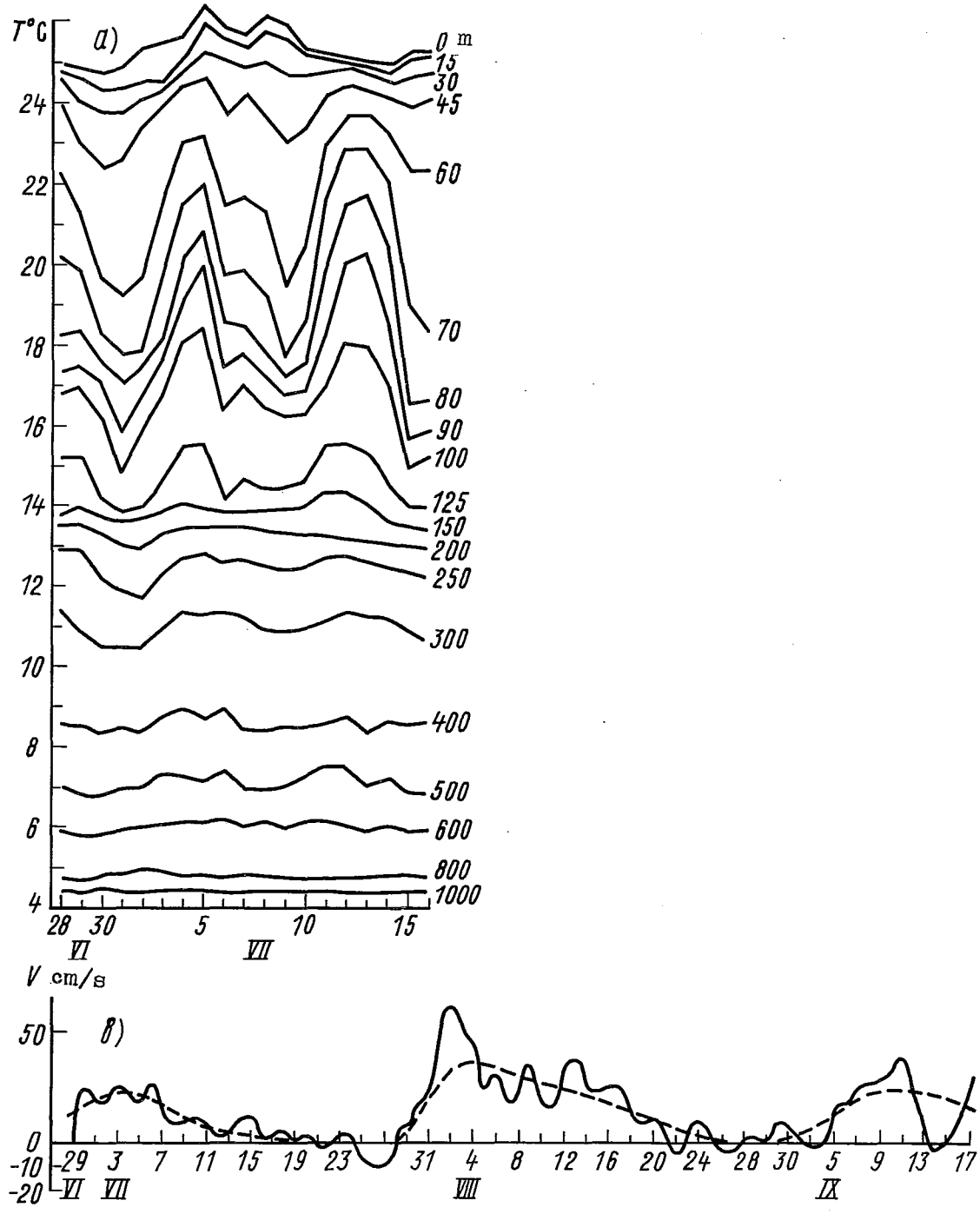

Fig. 5.24 a. Time variation of mean daily water temperature at different depths during Phase-I of GATE. b. Time variation of zonal current velocity component at 75m depth.

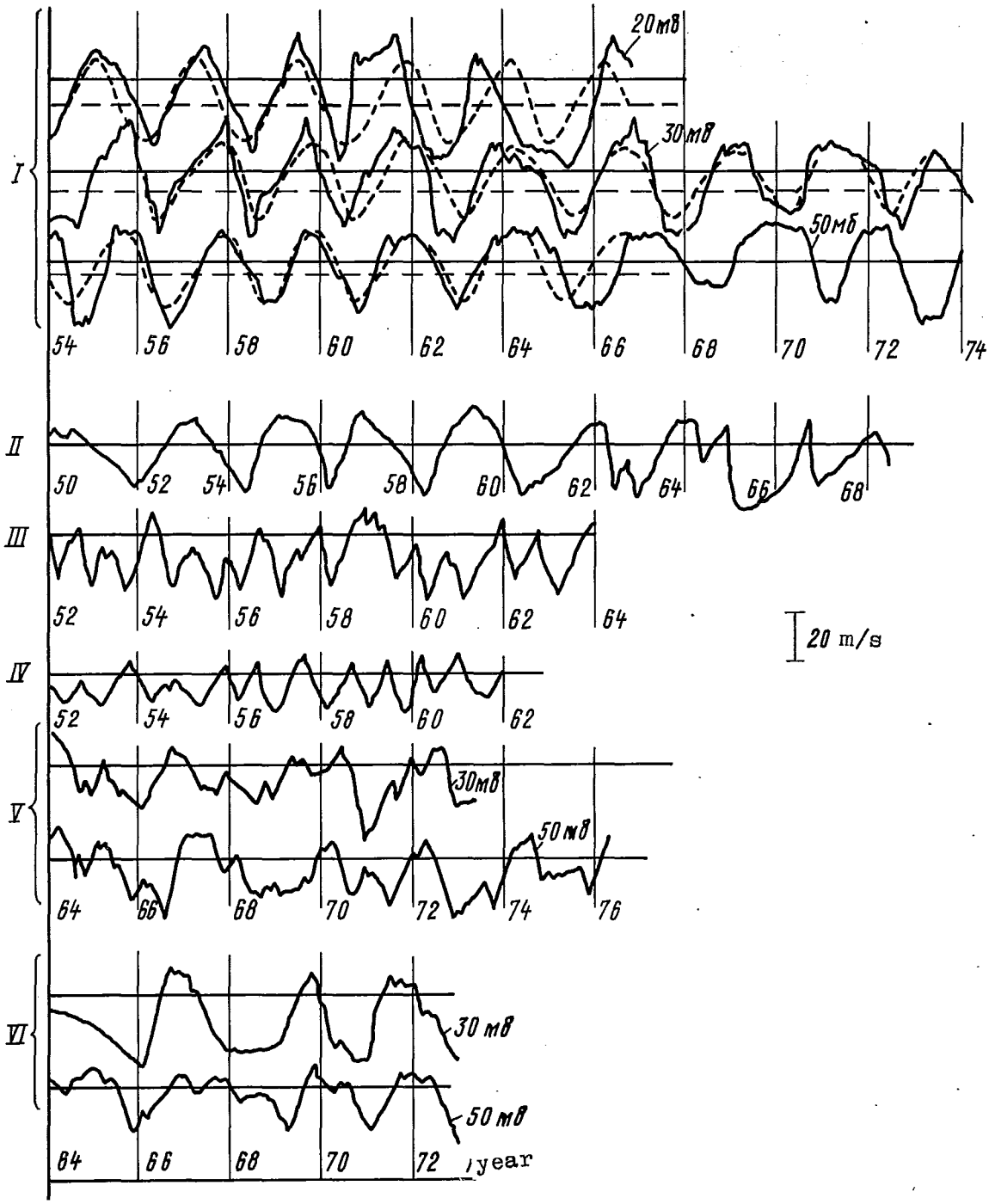

Fig. 5.25 Time variation of zonal wind velocity component (mean monthly values) for the stations located in low latitudes. I. Canton Island (≈3°S) from 1954 till 1967. Gan Island (≈2°S) from 1964 till 1974. II. Howard (≈9°N). III. Kingston (≈18°N). IV. Nandy (≈18°S). V. Trivandrum (≈8°N). VI. Ascension Island (≈8°S).

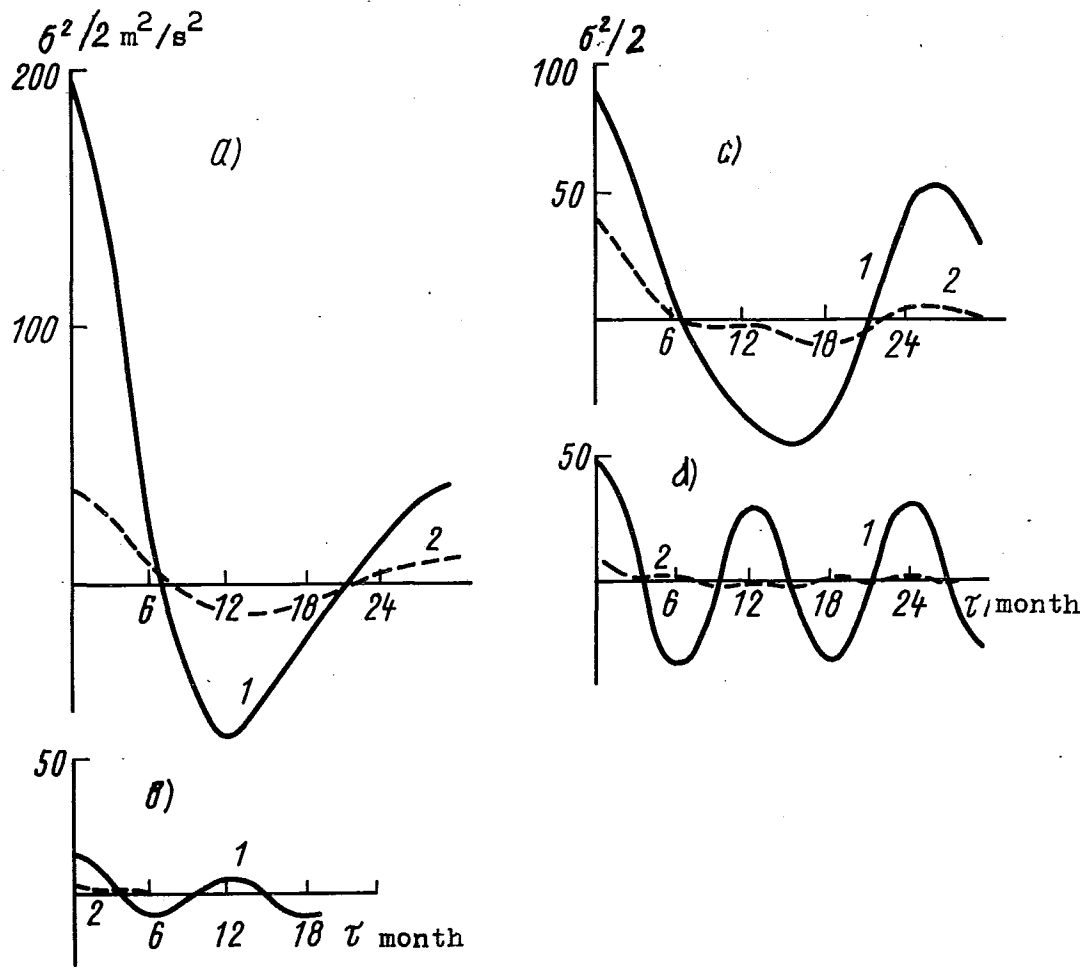

Fig. 5.26. Correlation functions for $u(\tau)$ -1 and "noise"-2. Noise is the difference between u and the sum of the oscillations, which takes away the largest part of the variance: a) Canton, b) Govard, c) Kingston, d) Nandy.

(τ - in months, σ^2 - in $m^2 s^{-2}$).

The correlation functions are "denormalized" by factor $\sigma^2/2$.

Table 5.4

Some characteristics of the quasi-biennial zonal wind oscillation at 50 mb

Parameters	Canton Island (≈3S)	Govard (≈94N)	Kingstown (≈18N)	Nandy (≈18S)
Mean value of u (ms^{-1})	-2	-2	-8	-5
Total variance (m^2s^{-2})	382	184	96	30
The oscillation which takes away the greatest part of variance (months)	27	28	12	12
The amplitude of above oscillation (ms^{-1})	14.9	9.3	8.6	4.8
The portion of variance (%)	58	47	77	78
The second oscillation: period (months)	-	12	28	26
amplitude (ms^{-1})	-	3	2.1	1.8
The portion of variance (%)	-	9	6	11

The fact that the period of 27 months appeared to be the most probable one for all the three surfaces of 50 mb, 30 mb, 20 mb, is also difficult to consider as a random one. Since the quasi-biennial cycle is observed over the entire equatorial zone, it means that this is the result of global-scale circulation mechanism occurrence which can hardly exist independently of other parts of general circulation. That is why it was important to determine and specify the phases of the quasi-biennial cycle during TROPEX-72 and TROPEX-74 expeditions. A comprehensive analysis of the fields in the upper troposphere and lower stratosphere showed that "... in the layer 18.5 to 20.5 km westerly currents of the western phase of the quasi-biennial cycle with a maximum speed of 20 ms^{-1} at 2°S were observed. There were easterly currents of the quasi-biennial cycle with maximum speeds of 40 and 42 ms^{-1} at levels 32 km and 28 km in the regions of 7.5°S and 4.5°N respectively. In the layer 34.5 to 38.0 km westerly currents of a new phase of the quasi-biennial cycle were observed. Those currents were replaced by easterly ones at the layer higher than 38.0 km. In July and August the westerly phase in the lower stratosphere broke and only easterly currents remained in the layer 18 to 34 km. The sinking speeds of the boundaries of westerly and easterly wind of the quasi-biennial cycle were close to normal" (TROPEX-72, p.36). A similar situation took place also in the summer of 1974, when the easterly wind in the upper troposphere and lower stratosphere was sufficiently marked within the latitudes 5° to 12°.

5.8 PLANS FOR FURTHER THEORETICAL AND EXPERIMENTAL INVESTIGATION

The analysis described in the chapter shows that in the tropical atmosphere wave disturbances are quite different not only in scale but in their genesis and features. Despite the seemingly abundant results, the physics of wave disturbances is far from being understood. A number of new problems arose, their list would be too long. So let us name only the most important ones.

The stability problem being the key problem in dynamic meteorology, is emphatically such in tropical meteorology. It is quite important not only to know whether the motion is stable or not (although this fact in itself is important) but it is necessary to know how long the stable state lasts due to various physical factors and it is important to know how and in what form instability destroys the wave of any nature. So far we have no answer to the questions under what conditions a disturbance transforms into a tropical cyclone, although numerical simulations of their life cycles now show quite reasonable results. In section 5.4 we saw examples of wave in y, z plane moving with the mean flow. There are waves in horizontal x, y plane outside the equatorial belt. Probably, there is no linear operator transforming wave (or waves) from y, z plane into x, y plane. It is not absurd to assume that a single disturbance in the 5°-15° belt under strong influence of β-effect begins to twist and under appropriate conditions (what are they?) it rapidly grows into a typhoon.

To what extent are wave disturbances responsible for the processes in the ITCZ? and the ITCZ properties? One of the primary difficulties in analitical studying of wave processes in the tropics is the nonlinearity of hydrodynamic equations. The zonal model for small scale waves in the equatorial belt apparently (section 5.4) is not very good (not to say it is bad). But an inclusion of derivative $\partial/\partial x$ even in the parametrical form sharply limits the usage of conventional analytical methods. There arises a necessity to work out a new mathematical procedure and to combine analytical investigation with numerical modelling. But "physics" should always go first. For this very careful analysis we need all the available data gathered in GATE and in pre-GATE studies and we have to organize special studies in the tropics. Let us examine the simplest example to support the previous thought. It is not so clear how to distinguish wave triplets found for different waves (Rossby waves or those in the equatorial belt) in the GATE data, if these triplets do exist.

What should be the method of processing wind, temperature, pressure, humidity, precipitation, cloudiness data in order to find triplets or to show that they are not there? A similar problem arises with solitary waves. To present a typhoon as a solitary wave it is necessary to learn how to model a nonstationary soliton (or solitons) at least for the two-dimension space coordinate. There is no lack of such examples. It seems reasonable to work out a special scientific programme for studying wave processes in the tropics. In the first rough draft of such a programme the following problems should be included:

1. To determine the stability of a wave motion and to study how and where the energy of the destroyed wave is used.

2. Analytical and numerical modelling of physically sound soliton models in one-and-two-dimension coordinates for various scales of motion.

3. Development of methods of investigation of triplets (or multiplets in general) for waves of different nature.

4. Investigation of the processes transforming the wave motions in the equatorial belt outside the belt and v.v.

5. Investigation of the role of wave processes in equatorial belt in mass, heat and moisture exchange between the northern and southern hemispheres.

6. Studying the developing and asymptotical behaviour of various kinds of waves in relation to the macroscale circulation. (For instance, the generation of orographic waves in low latitudes, quasi-biennial oscillation of zonal wind in the upper troposphere and the lower stratosphere, etc.).

7. Studying wave processes in ITCZ.

8. Development of methods of data analysis (both registered continuiously and time series) for identification of various kind of waves.

9. Working out a detailed plan for observations in the tropics with the processes in the equatorial belt taken into account for the analysis of various waves and for making clearer the relations with the wave processes outside the tropics.

REFERENCES

Bates J.R., 1973. A generalization of the CISK theory. JAS, v. 30, 1509-1519.

Betts A.K., 1976. Modelling subcloud layer structure and interaction with a shallow cumulus layer. JAS, v. 33, No. 12, 2363-2382.

Betchov R. and Criminale W., 1971. The problems of hydrodynamics instability. "Mir" (in Russian).

Boyd J.R., 1978. The effects of latitudinal shear on equatorial waves. P. I; P. II, v. 35, JAS, No. 12.

Bubnov W.A., Kazachkina L.I., Matveeva Z.H., Filippov D.I., 1976. The variability of water temperature at the Equator in the Pacific. TROPEX-74: v. II Hydrometeoizdat (in Russian), 62-70.

Burpee R.W., 1975. Some features of synoptic scale waves based on a compositing analysis of GATE data. MWR v. 103, No. 10, 921-925.

Charney J.G., 1972. Movable CISK. In the book: "Dynamic of the Tropical Atmosphere", Boulder, 1972, p.551-560.

Charney J.G., Eliassen A., 1964. On the growth of the hurricane depression. JAS, v. 21, p. 68-75.

Chih-Pei Chang, 1976. Vertical structure of tropical waves maintained by internally induced cumulus heating. JAS v. 35, No. 5, 729-739.

Chuchkalov (editor), 1977. Weather maps of GATE, v.I,II,III. Obninsk.

Davies H.C., 1979. Phase-lagged wave-CISK. QJ RMS v. 105: 325-353.

Dobryshman E.M. 1980-a. The dynamics of the tropical atmosphere. Hydrometeoizdat (in Russian). 287 p.

Dobryshman E.M., 1980-b. On wave triplets in the equatorial atmosphere. Meteorology and Hydrology, No. 11 (in Russian). 5-15

Dynamic of the tropical atmosphere. Notes from colloquium. Summer 1972. Boulder, Colorado. 587 p.

GARP publication series No. 20, 1978. Numerical modelling of the tropical atmosphere. Chap. 5. ICSU & WMO, Geneva.

Hayashi Y., Golder D.G., 1978. The generation of equatorial transient planetary waves. Control experiments with a GFDL general circulation model. JAS, v. 35, No. 11. 2068-2082.

Itoh M., 1977. The response of equatorial waves to thermal forcing. J.Meteorology Soc. Japan, ser. II, v. 55, No. 3. 222-239.

Kung E.C., Burgdorf M.A., 1978. Maintenance of kinetic energy in large-scale tropical disturbances over the eastern Atlantic. QJRMS, v. 104, p. 393-414.

Kuo H.L., 1978. A two-layer model study of the combined barotropic and baroclinic instability in the tropics. JAS, v. 35, No. 10.1840-1860

Lindzen R.S., 1974. Wave CISK in the tropics. JAS, v. 31, No. 1. 156-179.

Loesch A.Z., Deininger R.C., 1979. Dynamics of closed systems of resonantly interacting equatorial waves. JAS, v. 36, N. 8, 1490-1497.

Longurt-Higgins M.C., Hill A.E., 1970. Resonance interrelation of the planetary waves. In the book "Nonlinear theory of waves propagation". MIR (in Russian). 161-187.

Lysenko I.A., Petrossiants M.A., Portniagin J.I., Svetogorova L.W., 1974. The periodic variations of wind in the lower termosphere, stratosphere and troposphere in winter. Meteorology and Hydrology, No. 10. 16-31.

Mass C., 1979. A linear primitive equation model of African wave disturbances. JAS, v.36, No. 11. 2075-2092.

Meteorology over tropical oceans. 1978. Bracknell, Bershire. 278 p.

Murakami M., 1979. Large-scale aspects of deep convective activity over the GATE area. MWR, v. 107, No. 8. 994-1013.

Norquist D.C., Recker E.E., Reed R.J., 1977. The energetics of African wave disturbances as observed during phase III of GATE. MWR v. 105, No. 3. 334-342.

Ooyama K., 1964. A dynamical model for the study of tropical cyclone development. Geophys. International (Mexico), v.4. 187-198

Panchev S., Chakalov P., 1974. One class of the exact solutions of nonlinear equations of the dynamics of the equatorial atmosphere. Hydrology and Meteorology, No. 5 (in Bulgarian).

Petrossiants M.A., Ivanov V.N., Galushko V.V., Menshov J.A., 1976. Time-space variations of meteorological fields in the tropical zone of the Atlantic. TROPEX-74, v. I. Hydrometeoizdat (in Russian). 249-255.

Proceedings of the International Scientific Conference on the Energetics of the Tropical Atmosphere, 1978 (Tashkent, 14-21 September 1977). ICSU/WMO. Geneva, 442 p.

Redekopp K.G., 1977. On the theory of solitary Rossby waves. J. of Fluid Mechanics, v. 82, p.4. 725-745.

Reed R.J., Norquist D.C., Recker E.E., 1977. The structure and properties of African wavedisturbances as observed during phase III of GATE, MWR, v. 105, No. 3. 317-333.

Rennick M.A., 1976. The generation of African wave. JAS, v.33, No. 10. 1955-1969.

Report of the US GATE Central Program Workshop. Boulder, Colorado, NCAR, 1977, 723 p.

Shakina N.P., 1979. Instability in the atmosphere (review). Meteorology and Hydrology. No. 6,106-112 (in Russian).

Sitnikov I.G., 1977. On the scale analysis of the dynamic equations of the tropical atmosphere. Proceedings of Hydrometcenter of the USSR, issue 197 (in Russian). 3-25.

Snitkovsky A.I., Trapeznikova N.B., 1976. Water content in ITCZ. TROPEX-74, v. I, Hydrometeoizdat. 322-329.

Stevens D.E., Lindzen R.S., 1978. Tropical wave - CISK with a moisture budget and cumulus friction. JAS v. 35, No. 6. 940-961.

"TROPEX-72". 1974. Hydrometeoizdat. 685 p.

"TROPEX-74". 1976. v. I and II. Hydrometeoizdat. 736 p + 217 p.

Trosnikov I.V., 1980. General circulation model of the Hydrometcenter of the USSR. Meteorology and Hydrology No. 11, p. 16-26 (in Russian).

Weidmann P.D. and Redekopp L.G., 1980. Solitary Rossby waves in the presence of vertical shear. JAS, v. 37, No. 10. 2243-2247.

Yanai M., 1975. Tropical meteorology. Reviews of geophysics and space physics. V. 13, No. 3. 685-710; refs. 800-808.

Zaichikov B.P., Romanov Y.A., 1976. The peculiarities of wind, temperature and moisture fields over the Central part of the equatorial Atlantic. TROPEX-74, v. I. Hydrometeoizdat. 338-350.

CHAPTER 6

LARGE-SCALE NUMERICAL MODELLING

by

A. Gilchrist, P. R. Rowntree and D. B. Shaw
(United Kingdom Meteorological Office, Bracknell, United Kingdom)

6.1 INTRODUCTION

Two of the immediate objectives of GATE were relevant to numerical modelling:-

(i) to provide a basis, through improved understanding of the tropical atmosphere, for the development of parametrizations of the effects of smaller-scale tropical weather systems on the larger-scale circulation.

(ii) to provide data suitable for testing numerical models of the tropical atmosphere.

In this chapter we shall discuss the impact of GATE on large-scale numerical modelling. This is not a comprehensive review of numerical modelling of the tropics; such a review was attempted in WMO/ICSU (1978) while Rowntree (1979) has presented a further discussion of the approaches actually used in tropical modelling, and a review of the sensitivity of models to initial data and physical parametrizations. Some overlap with these earlier reviews is of course unavoidable and desirable, but the stress here is on the impact of GATE. The role of GATE in improving the understanding of physical processes is discussed in other sections of this monograph. Only in so far as such improvements have led to new parametrizations which have been incorporated in models, will it be appropriate to discuss them here.

It is possible to identify four distinct aspects of large-scale modelling:-

(i) data collection and quality control;

(ii) the objective analysis of those data;

(iii) prediction of a future atmospheric state;

(iv) simulation of the atmosphere.

We shall have little to say here on the last of these in the context of GATE. GATE can influence numerical simulations in two ways. One is by improving the knowledge of the atmosphere which the models are simulating. Although GATE data have contributed to this knowledge - e.g. by providing better estimates of the mean atmospheric state and variability about that mean over the eastern tropical Atlantic - such data, being for only a single season, must be of limited value, and some time will be needed before the knowledge is properly assimilated and used in assessments of simulations. The other possible contribution will be through the incorporation of new physical parametrizations and other modelling techniques. Such developments are likely to occur first in prediction models using GATE data and will be discussed in that context here.

A considerable part of the effort in any numerical modelling project is devoted to the collection, organisation and quality control of the observed data. Data available for analysis of the GATE atmosphere came from many sources including: surface and radiosonde data from ships and land stations; satellite temperature soundings; upper winds from pilot balloons, radar, rawinsondes or LOCATE systems; aircraft reports; satellite observed cloud motions. In addition to data available on the Global Telecommunications System in real-time, special data collections were organised - e.g. from paper tape records of the

original data from national and regional communications centres, and from ship logbooks and aircraft data collection systems. Detailed accounts of these data collection and quality control efforts can be found elsewhere (e.g. Farmer (1977), Parker (1977) and Pusey (1977) for the final validated data sets of the Synoptic scale subprogramme data centre, Pasch et al (1978) for a brief survey of satellite wind and aircraft data, and Krishnamurti et al (1976) similarly for sea surface temperature data). Substantial sections of the report by the GATE Workshop (1977, pp. 129-197, 599-661) were devoted to assessments of data quality.

Data extraction and quality control techniques used in conjunction with numerical modelling undergo a continuous process of development, and are seldom described fully in publications so that it would be difficult and probably not very useful to isolate the advances due to GATE. The data and some aspects of the quality control used by the groups most involved in GATE modelling have been described by Krishnamurti et al (1979a) (Florida State University (FSU)), Miyakoda et al (1976) (Geophysical Fluid Dynamics Laboratory (GFDL)) and Rowntree and Cattle (1982) (Meteorological Office (MO)).

The subsequent sections of this chapter review the work done using GATE data in objective analyses and numerical modelling. In the final section an attempt is made to summarize the progress made in these areas due to GATE.

6.2 THE IMPACT OF GATE ON OBJECTIVE ANALYSIS TECHNIQUES

The process of objective analysis of the tropical atmosphere has made considerable advances in recent years, stimulated to some extent by GATE. As with numerical modelling generally the development of analysis techniques appropriate to the tropics lagged behind developments applicable to middle and high latitudes.

Increased interest in tropical analysis can be attributed to three different stimuli - firstly the concentration of resources through international programmes such as GATE, also FGGE and its Regional Experiments (MONEX,WAMEX); secondly the increased operational need for tropical analyses by the major meteorological centres, both for their use in tropical forecasting and because of the impact of tropical events on the global circulation in time scales beyond a few days; and thirdly because of the tremendous increase in data availability, principally through the satellite observing systems but also through the more automated reporting of winds from aircraft (the AIDS and ASDAR systems).

It is now clear that the tropics exhibit marked temporal and spatial variability; that the circulations interact with mid latitude weather systems; and that they provide a major source of energy for the global circulation. Effective techniques for objective analysis of the tropics are, therefore, essential.

Basically there are two objective analysis techniques in common use for the spatial interpolation of observational data. The first is the successive correction method, as described by Cressman (1959) and successfully applied to the tropics most notably by Krishnamurti et al (1979a) and Pasch et al (1978) (with similar atlases for 200 and 300 mbs). As applied by Krishnamurti et al, the technique consists of an analysis of surface pressure, surface and upper level winds, and temperature and humidity at successive pressure levels. The analysis is two dimensional, with the necessary vertical consistency being achieved through subjective intervention where necessary or, for the upper level daily analyses at 200 and 300 mb reported by Pasch et al, by using the 250 mb analysis as a first guess. The second analysis technique, which has in recent years become the most commonly used for large scale modelling, is optimum interpolation, originally proposed by Gandin (1963). Many groups now employ this standard technique, though with considerable variations in the actual application of the method. Optimum interpolation takes account of the differing observational accuracies of reporting instruments and so is particularly appropriate for current observing networks, which are made up of several different components. The method can be applied in 1, 2 or 3 space dimensions and may be single or multivariate (in the latter case a wind datum might be used in the analysis of geopotential). Multivariate schemes are most applicable to extra-tropical latitudes; usually a simple analytic form for the geopotential correlation is assumed (e.g. a Gaussian Curve $\mu_{ij} = A \exp(-br^2)$) and other correlations (wind/geopotential, wind/wind) are derived with a geostrophic assumption

(Schlatter, 1975). This assumption is not satisfactory in the tropics and so global optimum interpolation schemes using multivariate analysis incorporate a gradual decoupling of the relationship as the tropics are approached.

In terms of GATE analyses the most notable applications of optimum interpolation have been by GFDL (Miyakoda et al, 1976) and the Meteorological Office (Jones, 1976): each incorporate additional and important aspects of analysis which are briefly summarised here. In the case of the first GATE analyses made at GFDL (Miyakoda et al, 1976) the optimum interpolation technique was only applied in a very limited context for a particular Phase III sequence to a particular subset of the data. The model used for the data assimilation was a global finite difference general circulation model with 9 vertical levels and with a horizontal resolution of approximately 220 km. The vertical coordinate of the model was σ (= P/p_s where p_s is surface pressure), the distribution of levels in the vertical being irregular. The observational data were processed on 13 pressure levels, representing most of the standard pressure levels up to a top level of 4 mb. This use of two distinct vertical coordinate systems required a vertical interpolation between pressure and σ-levels at some appropriate stage in the overall process. The main feature of this first GFDL analysis scheme was the time interpolation/assimilation technique in which data at the model's grid points ('insertion data') were repeatedly inserted over successive time steps as the model progressed from one datum time to the next. The insertion data between these datum times were determined by time interpolation at the model grid point. The insertion data were produced by a spatial interpolation of observational data and it was for this spatial interpolation that optimum interpolation was introduced. The optimum interpolation was applied independently to temperature, wind and surface pressure. The repeated insertion technique was relied upon to produce the necessary balancing of mass and wind. The conclusion from this early work was that the optimum interpolation gave better results than direct insertion of the observational data, but that some difficulties remained, particularly in the tropics.

The first GATE analyses made at the Meteorological Office (Jones 1976, Rowntree and Cattle 1982) also used optimum interpolation. The prediction model used was a limited-area finite difference model with 11 layers and a regular horizontal grid with a 2^o latitude/longitude resolution. As with the GFDL model the vertical coordinate was σ, and the vertical distribution of levels was irregular. The analyses were performed on 11 standard pressure levels ranging from 1000 mb to 70 mb, with an additional analysis level, for geopotential only, at 950 mb. Vertical interpolation between pressure and σ was again required. The analyses of geopotential and wind were made using two-dimensional univariate optimum interpolation, but the means of achieving the necessary balance between the two fields was quite different to the technique used by GFDL. Following the optimum interpolation, a variational adjustment (Sasaki, 1970) is made to both height and wind; it seeks to bring imbalances in the height and wind field towards a state of geostrophic balance. The main areas of doubt in this overall scheme are the forms of the structure functions and background error variances to be used in the optimum interpolation, and the amount of change that should be permitted in the variational adjustment step.

The question now to be asked is whether, in the light of experience gained from GATE, improvements in objective analysis of the tropics have come about. As far as the writers know only three aforementioned groups (FSU, GFDL, MO) have carried out objective analyses using GATE data specifically. Consequently we seek to answer the question by reviewing the most recent documents from the three centres which are available to us.

The successive correction method continues to be employed by FSU, notably in their recent catalogue of analyses relating to MONEX (Krishnamurti et al, 1979b). Four passes of the successive correction technique are applied to produce 2-D analyses of wind, starting from a first guess field which is a FGGE level IIIa NMC analysis. The radius of influence is reduced in each successive scan, starting at approximately four times the mean station separation and ending at approximately the mean station separation. Subjective intervention remains an important feature of the scheme, to provide reasonable continuity in areas where data and first guess fields disagree, as sometimes occurs in the region on the edge of data voids. The general method of analysis is very similar to that employed during GATE; the quality of the analyses is impressive and the MONEX atlas is an authoritative source of tropical analyses.

Turning to the GFDL scheme, the analysis technique has been improved based on the experience of their earlier GATE analyses. Details of the revised method are found in Miyakoda et al (1980), and in the GFDL account of their FGGE analysis system (GFDL Staff, 1980). The revised analysis scheme preserves the features of optimum interpolation to provide insertion values at model grid points, and of repeated insertion of such interpolated data. The principal difference is the introduction of a static analysis every 12 hrs, with the dynamical assimilation restarted from this static analysis. The static analysis is also by optimum interpolation, but uses the 4-D assimilation result as a first guess and a radius of influence of 500 km (the interpolation used in the preparation of insertion data has climatology as a first guess and a radius of influence of 250 km). A further change is the introduction of wind data in the two lowest layers of the model as well, and the use of moisture data at all levels. The introduction of the static analysis based on the 4-D assimilation field as a first guess permits an additional quality control check to be made and provides a better fit to the observational data. The prediction model used for the assimilation has been changed from the GFDL 220 km modified Kurihara grid point model to a spectral transform (R30) model. In addition to the revision of the analysis scheme, the more comprehensive data base of the SSDC final validated data set has been used.

Comparing results of the GFDL reruns with the original analyses, Miyakoda et al (1980) identify appreciable improvements in the representation of easterly waves, and of the East Africa jet, and note that the streamline analyses are smoother. These improvements are due in part to the enhanced data base.

The Meteorological Office analysis scheme as applied originally (Jones, 1976) is described in more detail in Rowntree and Cattle (1982). The scheme has been improved since that time, principally in the use of revised structure functions and in the specification of background error variances (Spalding, 1980). These two improvements have been made based on statistics produced from the original near real time Phase III analyses and forecasts. A third improvement has been achieved through a stronger linkage between wind and height analyses via the variational adjustment. The analysis scheme remains 2-D and univariate. The structure functions are now different for heights and winds and are specified for each of the analysis levels in turn. Originally a single correlation function was universally applied with a radius of influence of 2200 km. The revised structure functions have a more limited radius of influence for winds ($\sim$ 1100 km or less). The revised structure functions for height have a marked dependence on pressure level. In the lower troposphere the function is broad with a wide radius of influence ($\sim$ 4400 km). In the upper troposphere derivation of an adequate structure function for geopotential is difficult because of the high noise level in the observational data. As at lower levels they are broader than that used originally. The functions are expressed as polynomials, deduced by a least squares fit to the correlations found over the area covered by the GATE ships. The variational adjustment has been revised subjectively so that the adjustment factor λ' (see Rowntree and Cattle, 1982) is now an order of magnitude larger; however, south of $\sim 15^{o}$N the effects of the adjustment remain quite small (typically less than 1 m sec^{-1} change in wind, and less than 1 dam in geopotential). These revisions produce improvements in the analysis in that (a) the detection of incorrect data (particularly geopotential height errors) has significantly improved in the quality control check, (b) the analysed geopotential height gradients, particularly in the equatorial zone, are now weaker and more realistic, (c) the ill-conditioning of the covariance matrices in the optimum interpolation no longer occurs. The analyses have also been improved by the use of a better convection scheme in the forecast step. The analyses for Phase III have now been repeated using this revised scheme and the SSDC final validated data set, the analyses being carried out at 12 hour intervals.

It is of interest to compare the analyses produced by GFDL and the Meteorological Office, based as they are on the same delayed-mode data. Figs. 6.1-6.4 show the analyses at 850 mb and 250 mb for 12 GMT 5 September 1974 produced by GFDL and the Meteorological Office. Fig. 6.5 is the 250 mb subjective analysis of Sadler and Oda (1978). In examining this same case, Miyakoda et al (1980) noted very close agreement between the GFDL

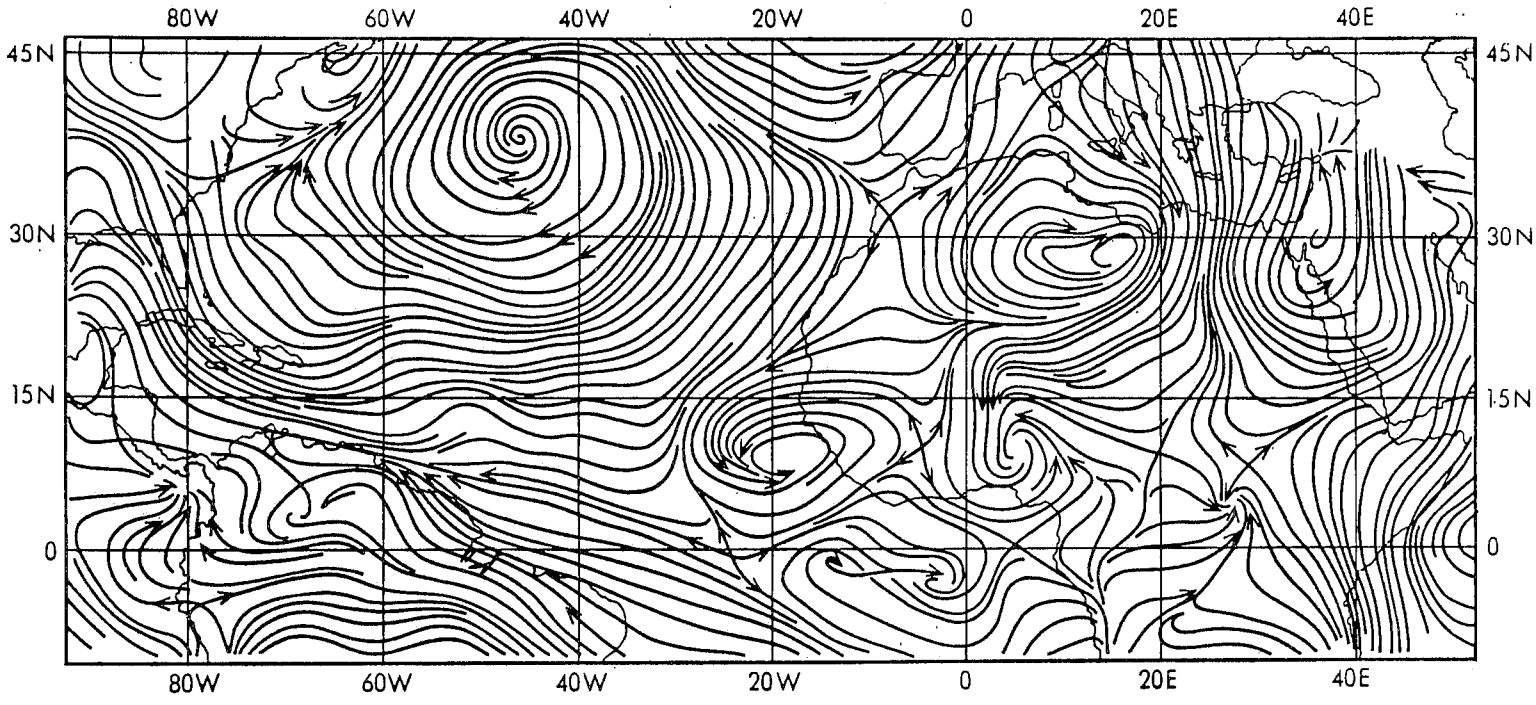

Figure 6.1: Streamline analysis for 850 mb at 12 GMT 5 September 1974 from Miyakoda et al (1980) using GFDL analysis scheme.

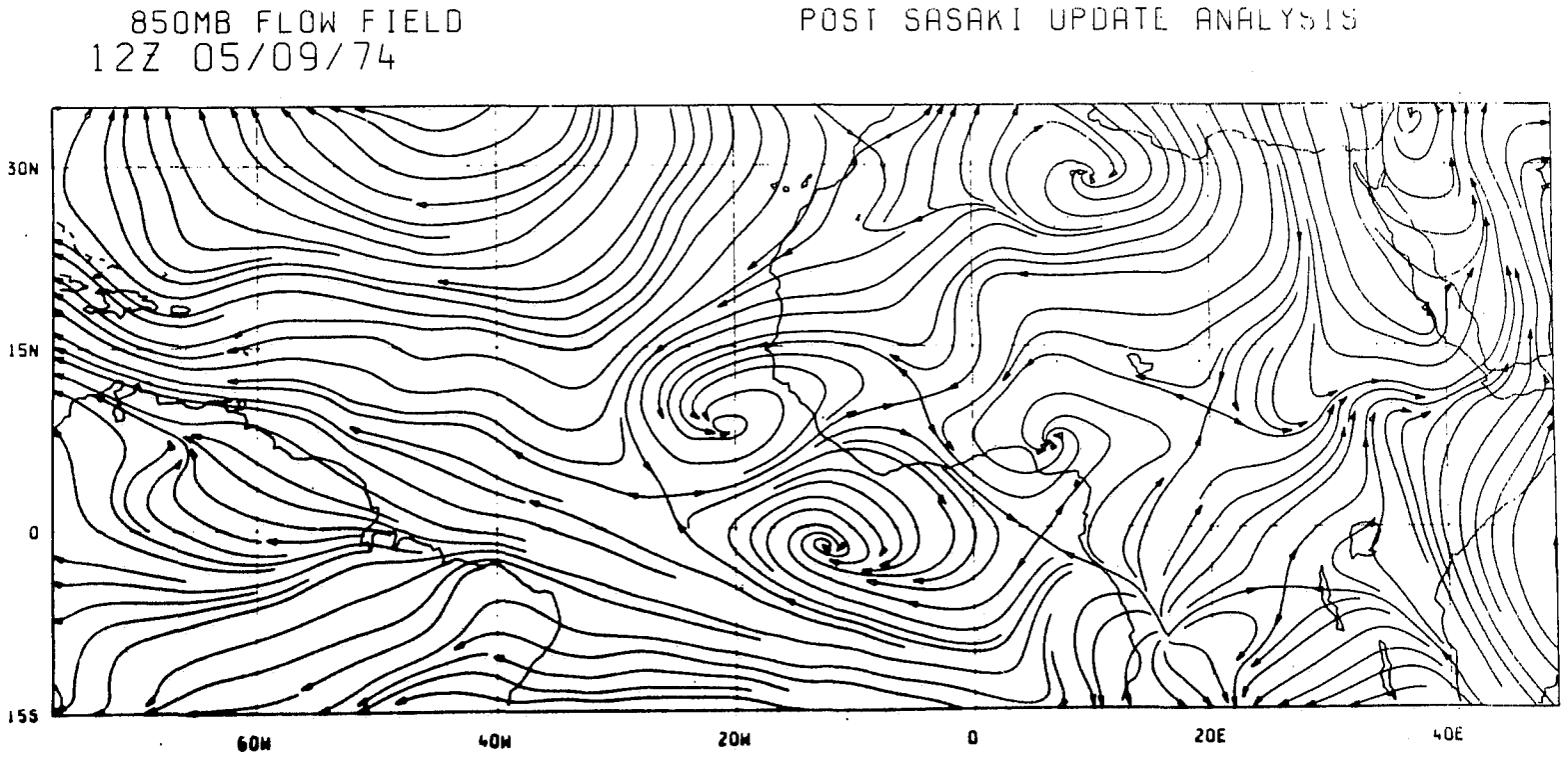

Figure 6.2: As Fig. 6.1 using MO analysis scheme.

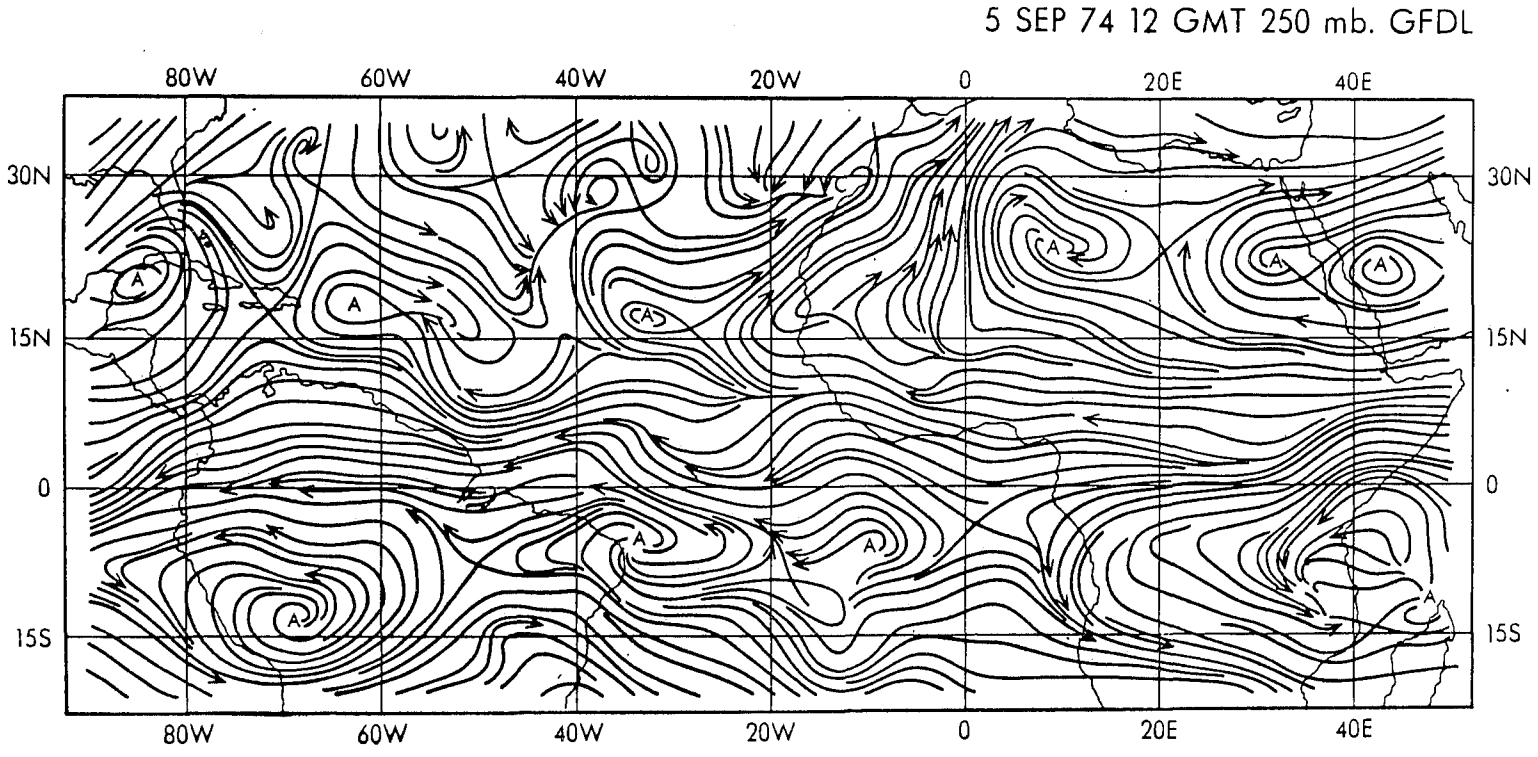

Figure 6.3: As Fig. 6.1 but for 250 mb.

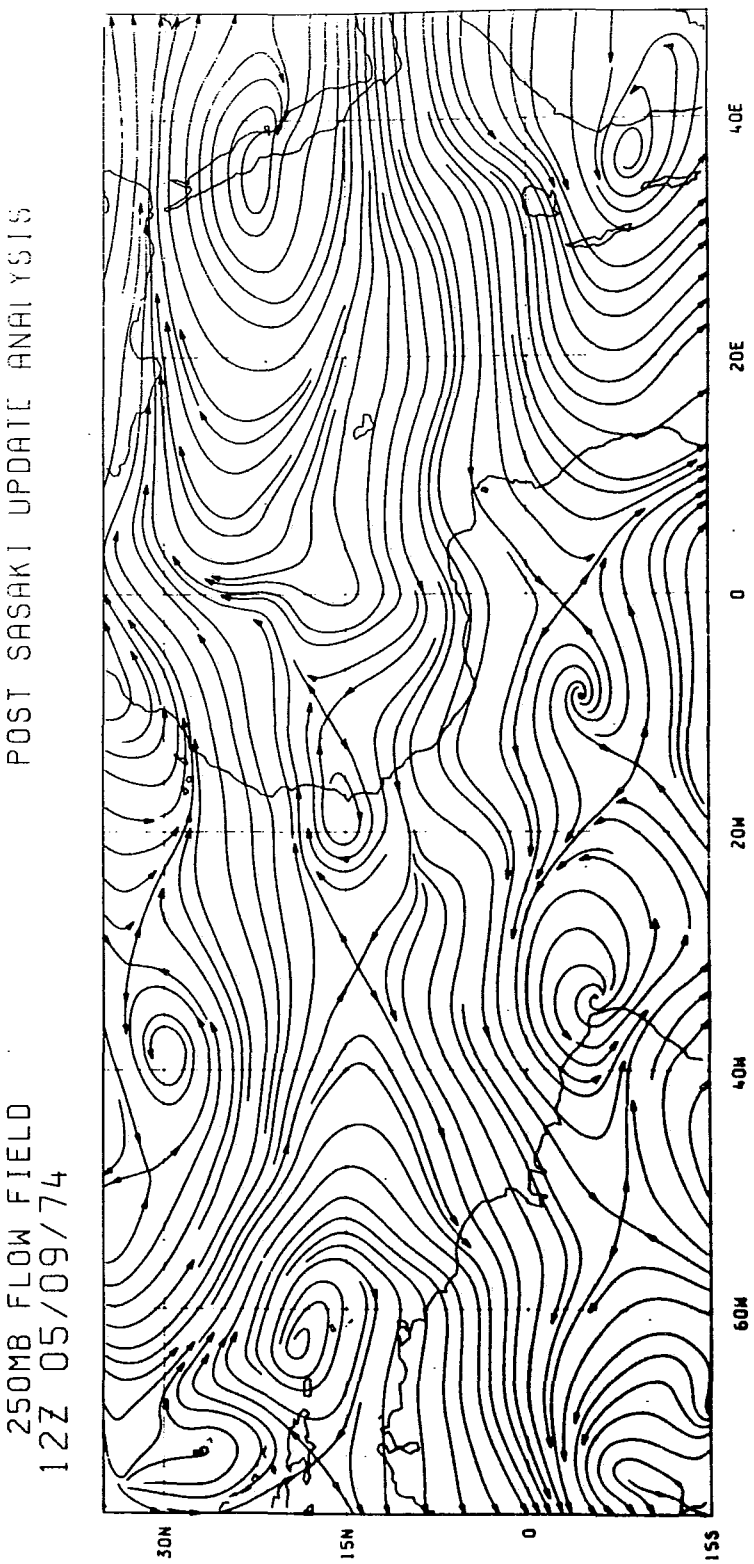

Figure 6.4: As Fig. 6.3 but using MO analysis scheme.

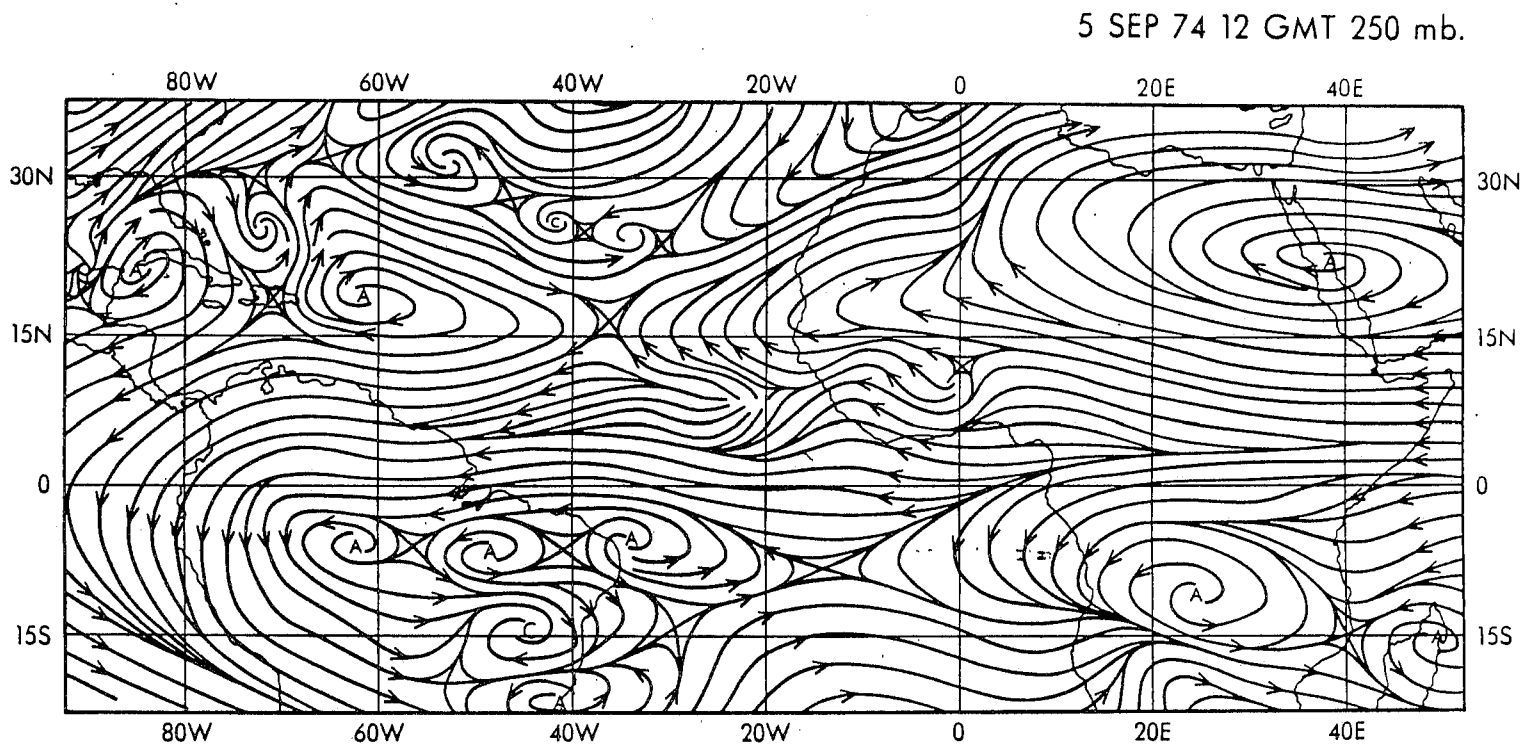

Figure 6.5: As Fig. 6.3 but subjective analysis from Sadler and Oda (1978).

analysis and the subjective analysis at lower tropospheric levels (1000, 850 mb), but greater differences at 250 mb. Comparison of the GFDL 850 mb analysis (Fig. 6.1) with the corresponding MO analysis (Fig. 6.2) also shows a very close agreement. At 250 mb the three analyses shown (Figs. 6.3, 6.4, 6.5) have areas of marked difference particularly, though by no means only, south of the equator. In some regions there is consistency in two, but not three, of the analyses. Pasch et al (1978)'s FSU analyses are for 00 GMT. They are generally in agreement with the consensus of the three analyses shown though nearer to Sadler and Oda's over south Africa. A comprehensive comparison of the analyses is not within the scope of the present paper. Clearly it would be desirable to make a detailed comparison of the different objective analysis schemes looking at such questions as data rejection, data selection, closeness of fit to observational data, biases and rms differences.

The foregoing demonstrates that GATE provided the impetus for improvement of objective analyses in the tropics, although the number of large scale modelling groups carrying out analyses of the data is surprisingly small. Outstanding problems remain. One of the most serious, in the context of optimum interpolation, is the derivation of appropriate structure functions for tropical regions other than the GATE area, and for other times of the year. A second problem is that of data selection; there is considerable variation among different global analysis schemes in the manner in which data are selected in the analysis at a particular point. Comparisons of the different schemes in this context would be beneficial. Analysis of relative humidity in the tropics merits closer attention; it has not been referred to earlier as it is not clear if any improvement in the analysis of this parameter has been achieved through GATE. The revised GFDL analysis scheme now incorporates an analysis of humidity in the final static analysis (Miyakoda et al, 1980); the Meteorological Office analysis incorporated an analysis based on the method proposed by Atkins (1974).

6.3 VERTICAL INTERPOLATION AND INITIALIZATION

Two further steps, vertical interpolation and initialization, may be required before the objectively analysed fields are used as initial data for a prediction. The Meteorological Office analyses of mass and wind fields using GATE data were made on standard pressure levels so that it was necessary to interpolate to the model's σ levels (σ = pressure normalised by surface pressure) and to derive temperatures from the analysed height fields, as described by Rowntree and Cattle (1982). Particular care was needed to ensure that the heights implied by the derived temperatures were sufficiently accurate.

Unless a four dimensional assimilation scheme is used, it is usual to include an initialization step to balance the mass and wind fields. Both Krishnamurti et al (1979a) and Lyne et al (1975, 1976) used a dynamical initialization procedure involving alternating short forward and backward integration steps, the mass and wind fields being allowed to adjust mutually during these integrations. Krishnamurti et al obtained convergence after about 18 hours, with each step being 1 hour in length while Lyne et al found 6 hours, with steps of one ($7\frac{1}{2}$ minute) timestep each, to be sufficient. Krishnamurti et al first removed the vertical integral of the divergence but Lyne et al found that external gravity waves present in the analysed data were removed after only a few hours of initialization. Temperton (1976) obtained similar results for a hemispheric multi-layer model. Both Temperton and Lyne et al noted that omission of the initialization step did rather little damage to the forecasts except to cause some roughness; in particular rainfall was little affected. These differences between the FSU and MO schemes may be partly due to the mutual adjustment of mass and wind fields caused by the Sasaki adjustment step in the MO objective analysis scheme.

6.4 TROPICAL PREDICTIONS USING GATE DATA

The primary aim of GATE according to the GATE Experiment Design Proposal (WMO/

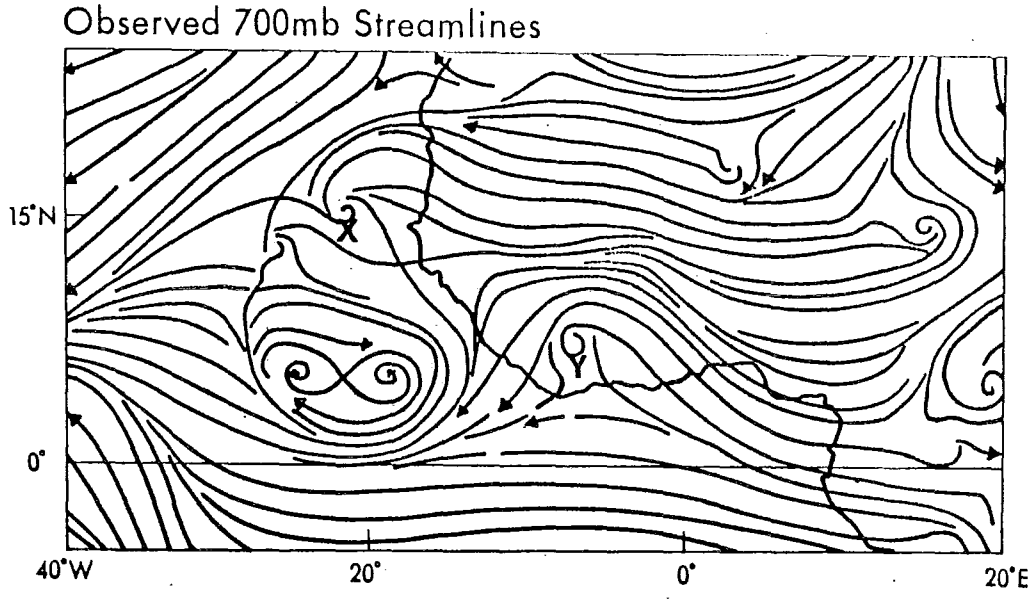

Figure 6.6(a): Analysed 700 mb streamlines for 12 GMT 13 July 1974.

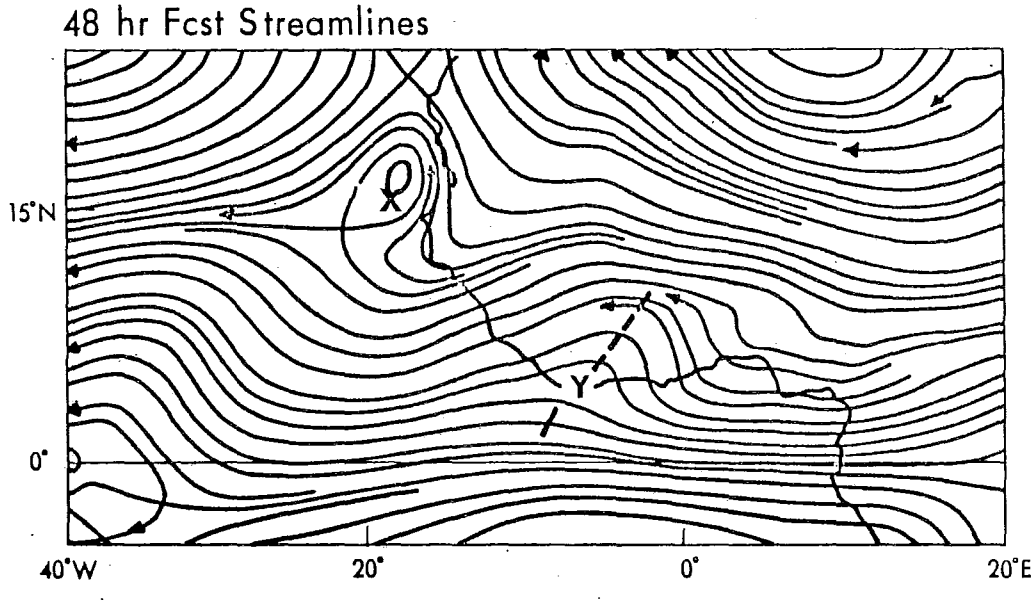

Figure 6.6(b): 48 hour forecast of 700 mb streamlines for 12 GMT 13 July 1974 using the FSU one-level primitive equation model.

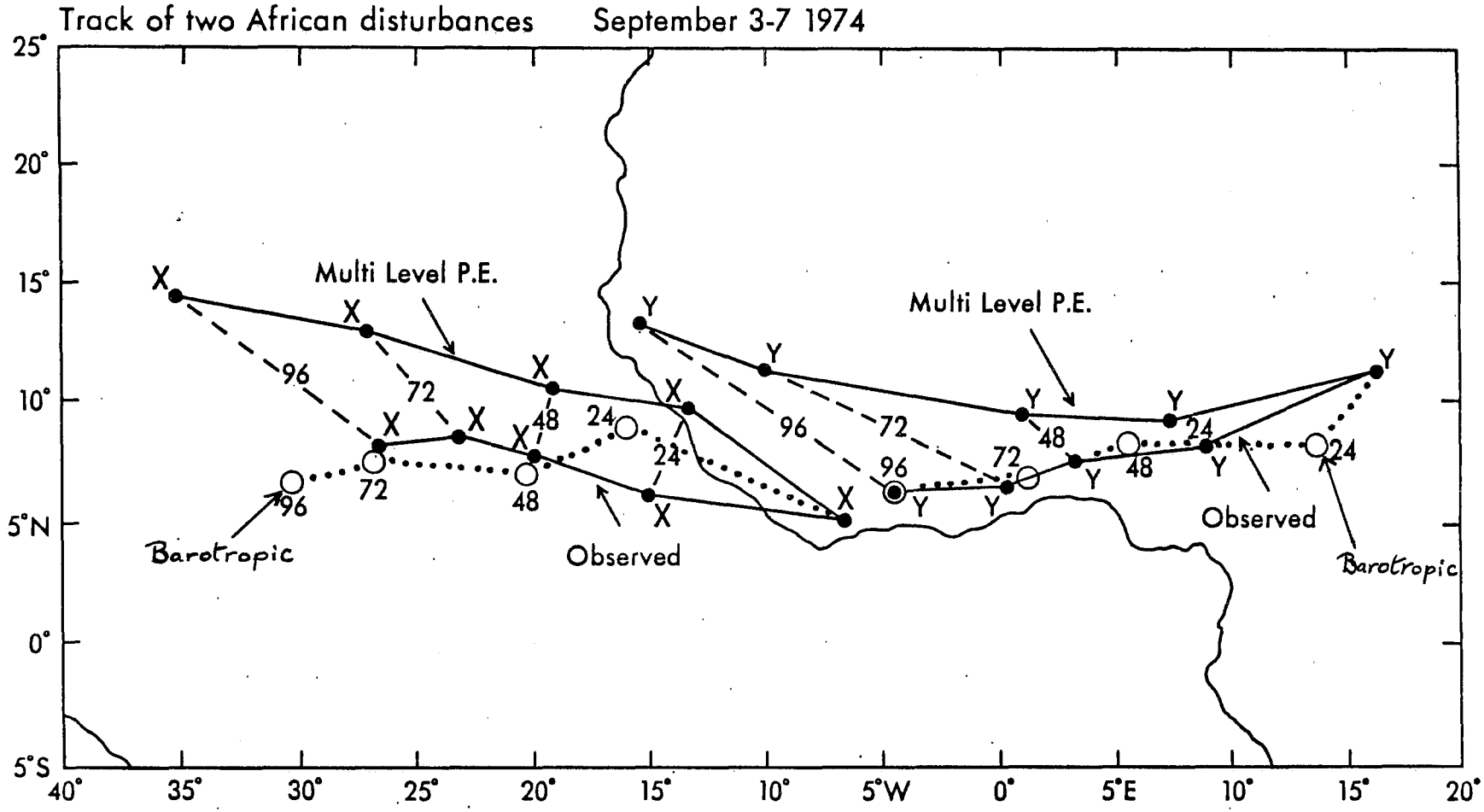

Figure 6.7: Tracks of two African disturbances for 3-7 September 1974, as observed and predicted with the FSU 5-layer (labelled 'multi-level P.E.') and barotropic (dotted track) models (redrawn from Krishnamurti et al. (1978)).

ICSU (1972)) was to extend our knowledge of those aspects of the meteorology of the tropics which are essential for a proper understanding of the earth's atmosphere as a whole. However it was envisaged that GATE would also provide a basis for a major advance in the understanding of tropical meteorology and weather forecasting. Some ways in which developments in tropical modelling capabilities can contribute to these aims of GATE are:

(1) Short-range (1-3 days) prediction:- Requirements for forecasts for aviation, construction etc. are similar to those in higher latitudes (e.g. upper and surface winds, rainfall). Most tropical countries have predominantly agricultural economies which are very dependent on rainfall, so that accurate predictions of rainfall occurrence and amount are of particular value. Detailed prediction of severe storms, (e.g. West African squall lines) which can cause damage through strong winds and floods, will require models of rather high resolution but often such storms are associated with large-scale flow features and precipitation areas whose prediction may be possible with lower resolution models.

(2) Medium-range (1-2 weeks) prediction:- These may allow prediction of, say, the next one or two easterly waves or it may prove possible to predict major changes such as the onset of monsoon flow and associated rains.

(3) Extratropical prediction:- Forecasts of middle latitude and subtropical weather are likely to be sensitive to the predictions in the tropics after the first few days.

Studies prior to GATE (see Chapter 4 of this Monograph) had shown that summer weather over West Africa at 5°-15°N and the Atlantic to the west was controlled to a substantial extent by the easterly or African waves. Thus one of the major aims of forecasts with GATE data was to predict the development and movement of these waves and the associated weather.

Forecasts using GATE data have been made by the Florida State University (FSU) and the Meteorological Office (MO) groups and by Lepas (1980). The FSU model was a development of that used by Krishnamurti et al (1973). It used the primitive equations and had 5 levels spaced regularly in pressure coordinates with a rigid top at 100 mb and a 1° latitude-longitude mesh with data from 5°S-25°N, 40°W-20°E. A semi-Lagrangian advective scheme was used with cyclic boundary conditions at the eastern and western boundaries with an extension of the initial data area to 26°E to allow cyclic continuity. The MO model used during GATE was a limited-area version of a global primitive equation general circulation model and has been described briefly by Lyne et al (1976) and in more detail by Lyne et al (1975) and Rowntree and Cattle (1982). There were 11 layers in σ-coordinates (σ = pressure/surface pressure) with vertical resolution greatest in the boundary layer and the stratosphere. The horizontal grid length was normally 2° of latitude and longitude and the region covered was 16°S-36°N, 78°W-50°E. Boundary values were held constant. Physical processes represented in both models included convection, surface energy and momentum fluxes and radiation. Linear horizontal diffusion was used in the FSU model with larger diffusion coefficients near the boundary while in the MO model a filter was applied four times a day which damped only the shortest waves except near the boundary where all scales were affected. Results for two GATE cases were reported by Krishnamurti et al (1977, 1979a), Encouraging forecasts were obtained with barotropic and one-layer primitive equation models with satisfactory forecasts of the movement of African waves out to 96 hours (e.g. Figs. 6.6, 6.7). Forecasts with the multi-level primitive equation model were less successful. For the case shown in Fig. 6.7 the forecast trough positions from 48 hours onwards were increasingly farther west and north than observed. It seems possible that these errors could be partly due to use of cyclic boundary conditions with boundaries at 40°W and 20°E. In the Caribbean and Indian regions, for which these conditions had been used previously, the boundaries were in longitudes with rather similar mean flow throughout the troposphere. Between 20°E and 40°W the 200 mb easterlies weaken westwards, while near the surface there is generally easterly flow at 40°W but south-

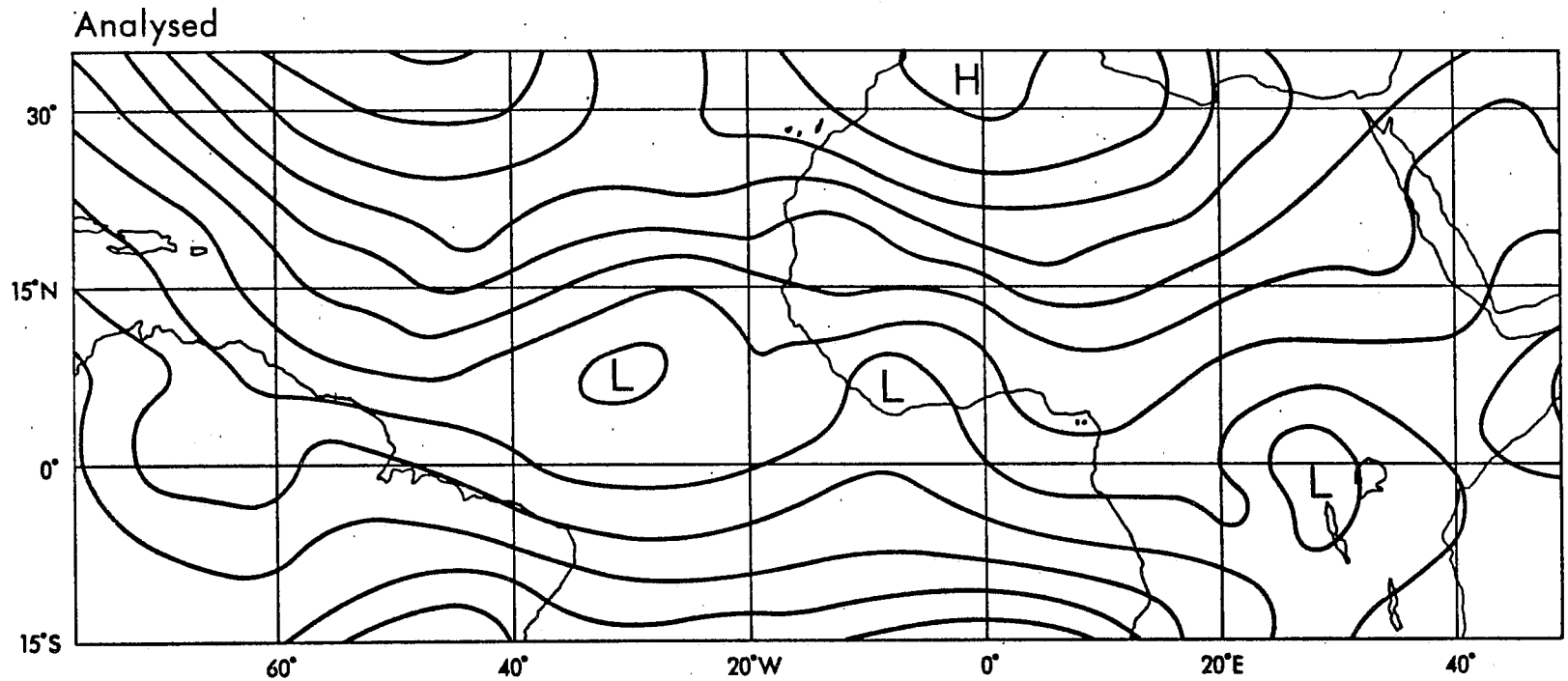

Figure 6.8(a): Analysed stream function at σ = .844 (about 850 mb) for 12 GMT 7 September 1974. (Contour interval 4 $km^2 s^{-1}$).

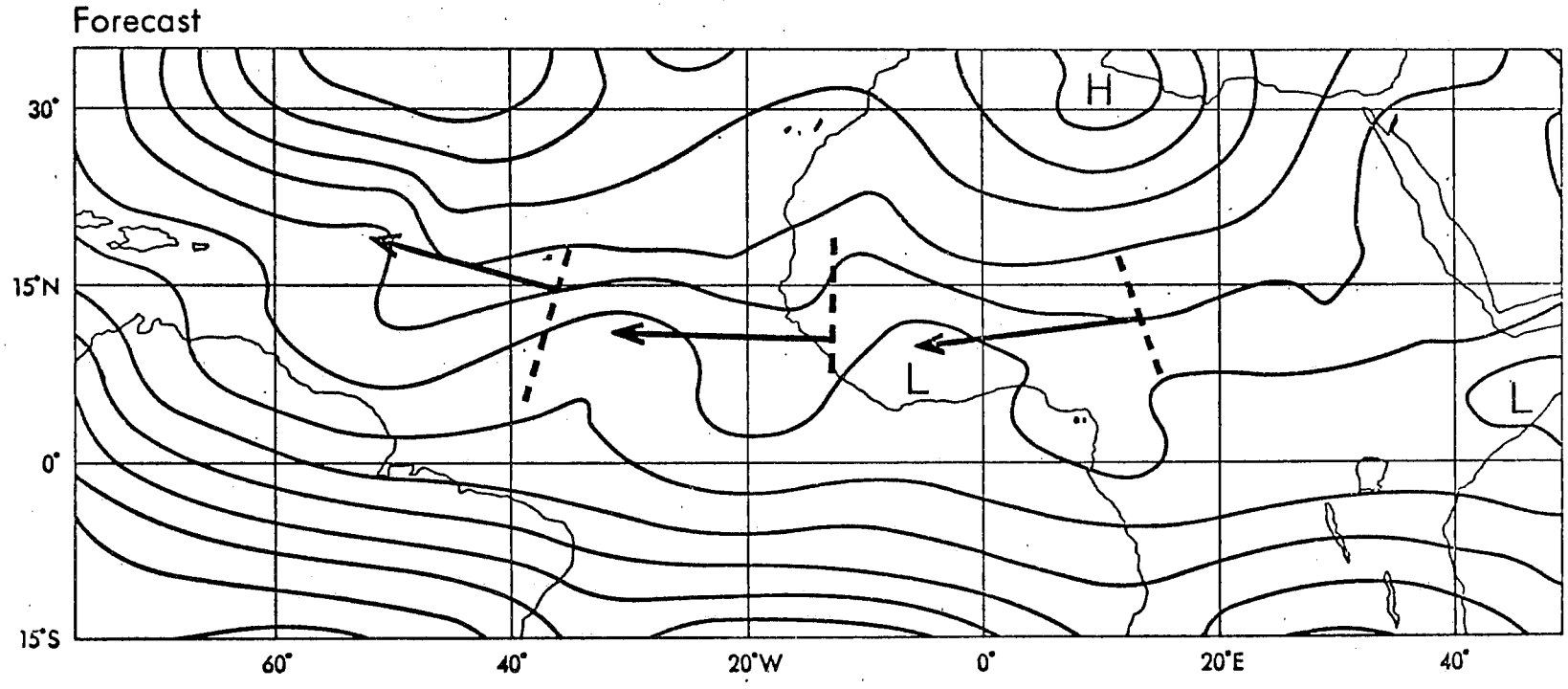

Figure 6.8(b): As Fig. 6.8(a) but for 72 hour forecast with MO tropical model. Arrows show analysed trough movements over the 72 hours.

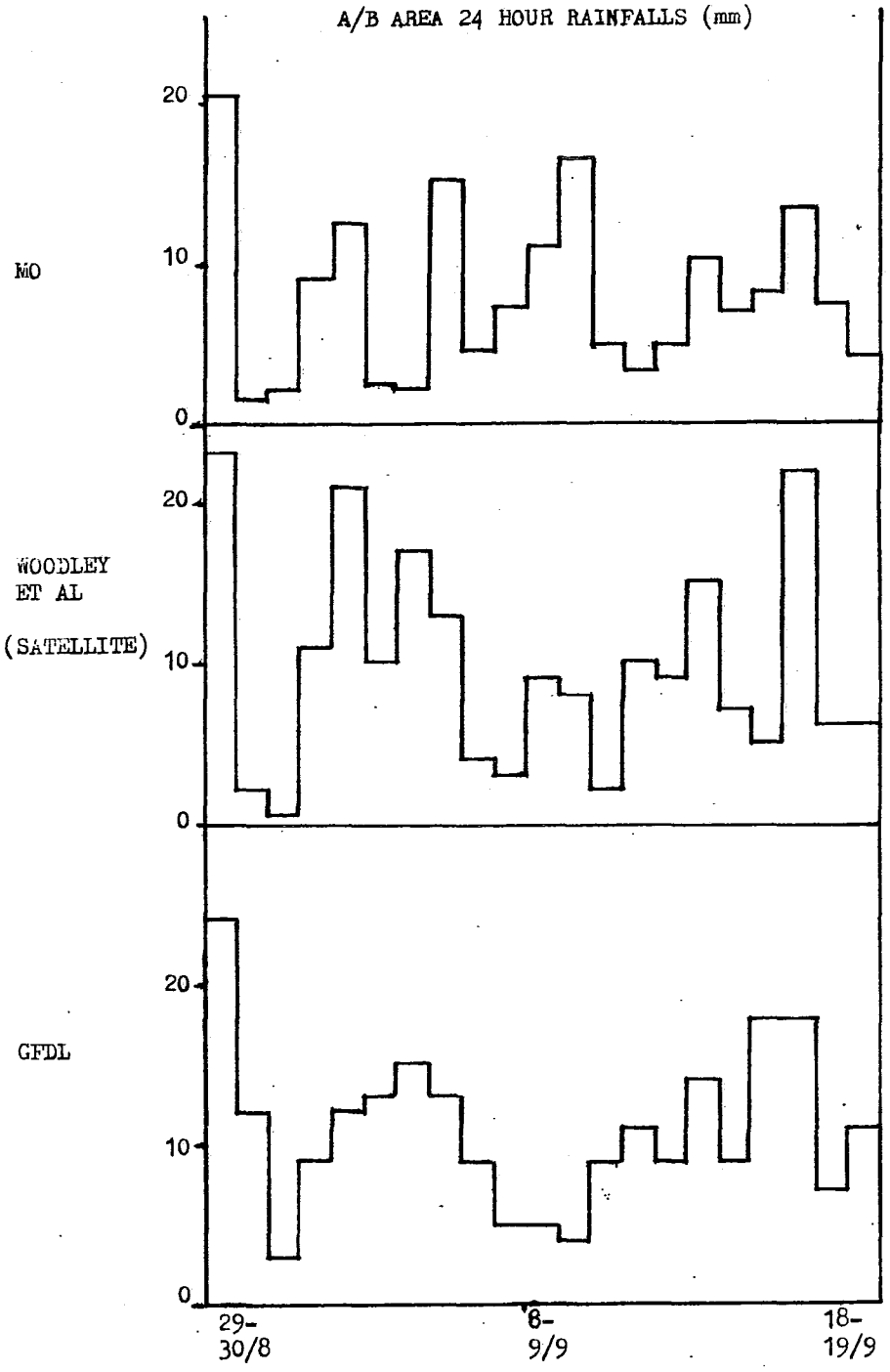

Figure 6.9: Observed (Woodley et al 1980) and modelled rainfalls for 24 hour periods to 12 GMT from 29-30 August to 18-19 September 1974 in GATE ship array.

westerlies along much of the eastern boundary at 20°E. Even with a 600 km linking region it seems possible that distortions of the flow will occur. The fact that good barotropic forecasts were obtained is not inconsistent with this suggestion because at 700 mb the eastern and western boundaries have quite similar easterly flow.

Krishnamurti et al (1979a) constructed diagrams following the wave trough line and showed the variations across the trough to be quite similar to those of Reed et al (1977) based on observed data, with ascent concentrated west of the trough line and maximum relative humidity east of the trough line; however, relative humidity unrealistically increased upwards near the trough. They also documented a westward-propagating transient disturbance which they suggested might be the model's 'gross representation of a squall line'.

In subsequent work Krishnamurti et al (1979c) have reported on barotropic and one-level primitive equation forecasts from GATE Phase 3 data sets. In these experiments the 'cyclic' east and west boundary conditions were replaced by fixed boundary conditions "to prevent the retrogression of domain-scale waves". Forecasts of wave trough movements to 24 and 48 hours are compared with analyses for eight of the cases with each model. The two models have comparable accuracy and overall the predictions shown are in reasonable agreement with observations. For an inner domain, root mean square wind errors over all the primitive equation forecasts are 5.15 ms^{-1} at 24 and 6.20 ms^{-1} at 48 hours, compared to 6.98 and 8.41 ms^{-1} for forecasts using persistence and 6.87 ms^{-1} for a climatological forecast. A method of predicting squall-line positions is also developed, based on observational studies, and the results illustrated in detail. On each of the 8 days on which the squall-line forecast criteria were met, a squall line was observed; the mean errors in forecast position were about 2° longitude at 30 and 39 hours after the initial time. (See Krishnamurti et al (1980) for a less detailed report).

The MO model was run in near real time throughout GATE as part of a data extraction-analysis-forecast cycle described briefly by Lyne et al (1976) and in more detail by Lyne et al (1975), Shaw and Rowntree (1976) and Rowntree and Cattle (1982). The analyses suffered from erroneous data and forecast errors largely attributable to the convection scheme. Most subsequent forecasts, like the rerun Phase III analyses described above, have used a new convection scheme (Lyne and Rowntree, 1976) which gave much improved forecasts compared with those obtained during GATE. Figure 6.8 compares the 72-hour forecast of the stream function for the lower troposphere with the analysed field. The movements of the waves initially located near 15°E and 10°W have been quite well forecast and their intensities are generally realistic. A wave initially west of the GATE B scale array is difficult to locate in the analysis and is probably overdeveloped by the forecast. Quite realistic movements of wave troughs near 15°N were maintained out to 8 days in an extension of this forecast (GATE Workshop 1977, p. 105, Rowntree and Cattle (1982)) although trough shapes were not well forecast after the first 4 days. Some skill was also evident in the forecasts of upper tropospheric flow and rainfall over the first 2 to 3 days (Rowntree, 1979, pp. 223-225).

The precipitation data diagnosed for 6 hour periods from the GFDL four-dimensional assimilations were shown by Miyakoda et al (1980) for the A/B scale area (not defined precisely by them) together with observed estimates by Woodley et al (1980) based on satellite data. Figure 6.9 shows these data accumulated for 24 hour periods ending 12 GMT and also the 24 hour forecasts for 6°-12°N, 20°-26°W for the same periods obtained during the MO reruns of the GATE analysis /forecast cycle. The mean rainfalls for the 21 days of Phase III are 11.0, 9.7 and 8.0 mm/day for GFDL, observed and MO respectively. Root mean square errors are 5 and 5.5 mm/day for GFDL and MO. There are reasonably high correlations between forecast (or diagnosed) and observed time series (0.67 for GFDL, 0.61 for MO, both significant at the 1% level) though some major errors are evident. The MO rerun forecasts from 00 GMT analyses, with no 12 GMT data used, were generally less successful.

Lepas (1980) has run several 48-hour forecasts from the MO's real-time GATE analyses over the period 7th-12th September 1974, using a 15-level σ- coordinate semi-implicit limited-area model with a Mercator grid having an equatorial mesh length of 120 km. With the convective parametrization of Kuo (1974) modelled rainfall near the GATE ship array over five forecasts (between 12 and 36 hours from the initial time) totalled 22 mm compared to an observed figure of 32 mm.

A hemispheric version of a primitive equation model has been tested for Phase III of GATE by Sitnikov and Rubinshtein (1975). Including the GATE-dedicated ships in the analysis scheme associated with the model was shown to reduce the mean relative forecast geopotential errors at up to 48 hours by 2 to 5%. The moist convective adjustment scheme included in the model predicted a reasonable latitudinal distribution of precipitation in the tropics.

In the next section the aspects of the sensitivity of these models to variations in the initial data and in the model formulations will be discussed. These results are drawn from the papers mentioned above and also from recent experiments with the MO model.

6.5 SENSITIVITY OF TROPICAL PREDICTIONS TO INITIAL SURFACE DATA

6.5.1 Introduction

The consequences of varying most features of the initial state have been examined using GATE data. The effects of varying conditions at the earth's surface have not been presented in great detail but sufficient results are available to indicate significant sensitivity to sea surface temperatures, mountain elevations and soil moisture specifications.

6.5.2 Sea Surface Temperatures

Although the FSU group produced daily analyses of sea surface temperature they have not discussed the effects of varying these. Rowntree (1979) reported the effects of a hypothetical change in Atlantic sea surface temperatures on a 5-day forecast with the GATE model. Rainfall increased substantially over warmed water, and decreased over cooled water and an intense cyclonic development was noted over the warmed water. Significant increases in the southward extent of rainfall in the ITCZ were obtained in another experiment in which July climatological sea temperatures were replaced by an analysis of Phase III data which gave generally higher temperatures.

6.5.3 Mountain Elevations

The effect of removing mountains has been discussed by Krishnamurti et al (1979a) for their one-level primitive equation model. Although the overall character of the forecasts with and without mountains was similar at 48 hours, there were some significant differences of detail which the authors attribute mainly to the Guinea and Cameroon mountains. There are no known experiments on mountain effects with multi-level models.

6.5.4 Soil Moisture

As discussed by Rowntree (1979) there have been several experiments with numerical models which have demonstrated their sensitivity to the soil moisture availability. The mechanisms involved, as discussed by Walker and Rowntree (1977), are that the net radiation is compensated in the surface heat balance by upward sensible heat flux with a dry surface but mainly by upward latent heat flux with a moist surface. Thus with a dry surface the air is heated and relative humidity falls while with a moist surface relative humidity tends to increase. The temperature contrast between the hot air over the dry Sahara and the moist air over the African tropical forests arises mainly from this mechanism, and this temperature contrast is largely responsible for the mid-tropospheric

easterlies over West Africa. Development and maintenance of the westward-moving African waves which dominate the weather over West Africa and the east Atlantic in summer are generally supposed to be associated either with this easterly flow through barotropic energy conversion processes or with the temperature contrast through baroclinic processes. Linearised models which prescribe the flow field (e.g. Rennick, 1976, Mass, 1979) have generally indicated barotropic instability processes to be most important. Observational studies (Burpee, 1972, Norquist et al, 1977) have indicated that both barotropic and baroclinic processes play a part while in the numerical experiment by Walker and Rowntree (1977) with an idealised land-sea configuration, baroclinic processes were dominant. This also appears to be the case with the results of Krishnamurti et al (1979a) though these refer both to the oceanic and African domain.

However, as both barotropic and baroclinic processes depend on the soil moisture contrast, as discussed above, it is to be expected that proper representation of soil moisture is crucial for accurate predictions in the GATE area. An example of the effects of misrepresenting the soil moisture was given by Rowntree (1979), substantial weakening of an African wave occurring when the Sahara was represented as wet. A further aspect of the importance of soil moisture is the positive feedback effect discussed and demonstrated by Walker and Rowntree (1977) whereby lack of soil moisture tends to reduce rainfall and so maintain the initial aridity. However, this has not been investigated with GATE data.

6.6 SENSITIVITY TO INITIAL ATMOSPHERIC DATA

6.6.1 Introduction

The sensitivity of tropical models to initial data has been reviewed by Rowntree (1979). It is clear that tropical predictions are sensitive to the rotational part of the initial horizontal flow fields as demonstrated by the success of Krishnamurti et al (1979)'s predictions with a barotropic model. As discussed by Rowntree (1979) the necessity for a good specification of the initial divergent flow is not obvious from experiments to date. There do not appear to have been any relevant experiments with GATE data except for those described by Lyne et al (1975) and Rowntree and Cattle (1982) which showed that removal of external gravity waves by a dynamic initialization step, whilst providing somewhat smoother forecast fields, had little effect on the flow fields after 24 hours or on the first day's rainfall. Significant sensitivity to initial analyses of geopotential and relative humidity has been evident in predictions with GATE data as discussed in the following subsections.

6.6.2 Sensitivity to initial mass fields

During the near-real-time GATE modelling experiment with the MO tropical model, the initial height fields were derived from analyses almost independently of the wind data (Rowntree and Cattle, 1982) and then modified by 6 hours of dynamic initialization allowing mutual adjustment of the wind and mass fields. Some problems with the model were traced to incorrect height fields due mainly to erroneous data. Experiments were therefore made with the analysed height field replaced by a height field derived from the wind field using the reverse balance equation with analysed heights as boundary conditions. This technique was previously used by Krishnamurti et al (1973) but was criticised by Kanamitsu (1975, p. 101) because it gave unrealistic temperatures with unstable lapse rates in some regions; Krishnamurti et al (1976, 1978) used analysed mass fields. The height fields obtained from the GATE winds were generally similar to but smoother than the analysed fields. To obtain satisfactory analyses of the 1000 mb height field over North Africa it was necessary to incorporate a special treatment of the surface friction in the reverse balance equation. The effects on rainfall forecasts during the first 24 hours were considerable, with elimination or reduction of several intense rainfall maxima (Rowntree and Cattle, 1982). However, recent application of this technique with the model area shifted east to the Indian Ocean has been less successful apparently because of the difficulty of defining boundary values

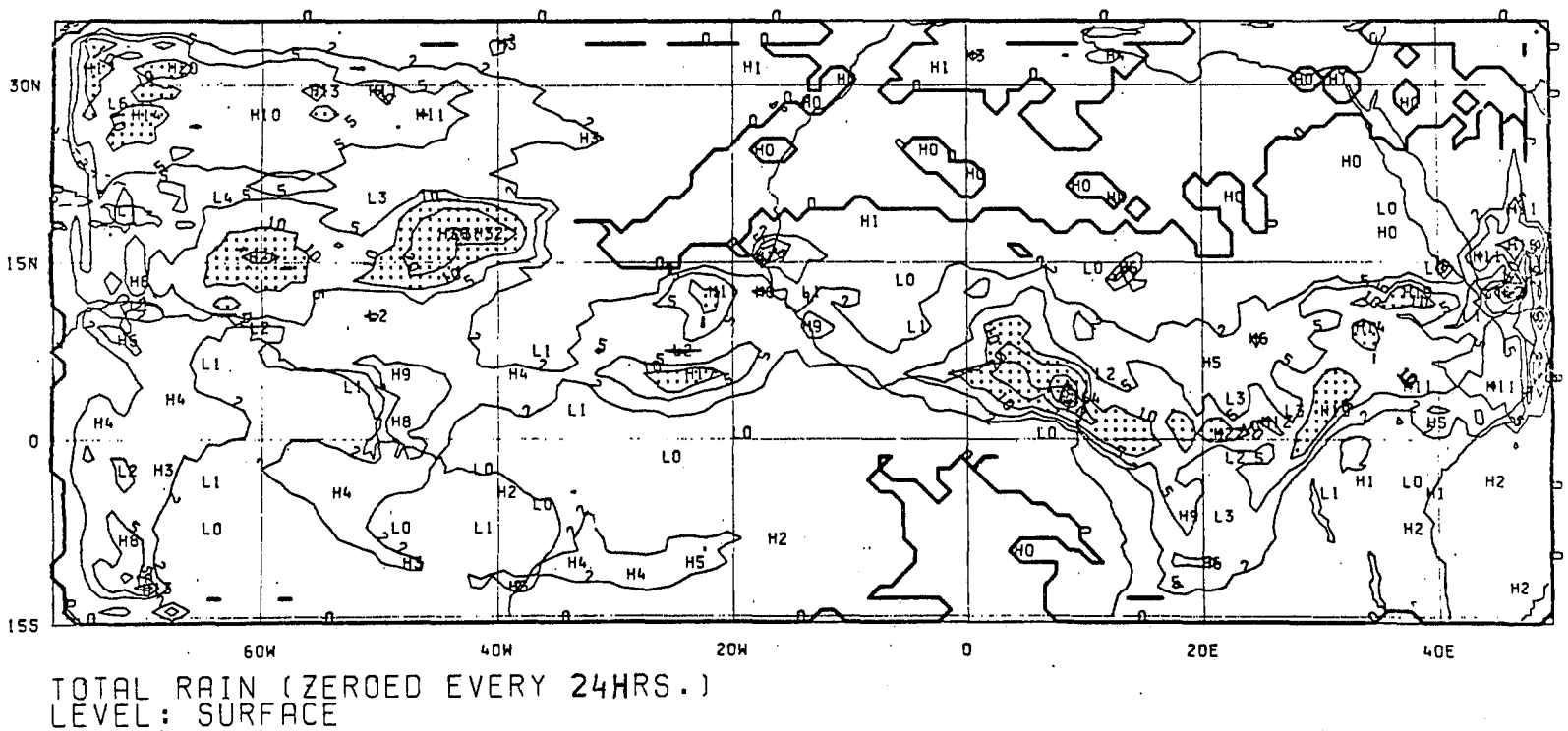

Figure 6.10(a): Precipitation for 24 hours to 12 GMT 6 September 1974 from forecast starting 12 GMT, 4 September 1974. (1^{o} resolution model).

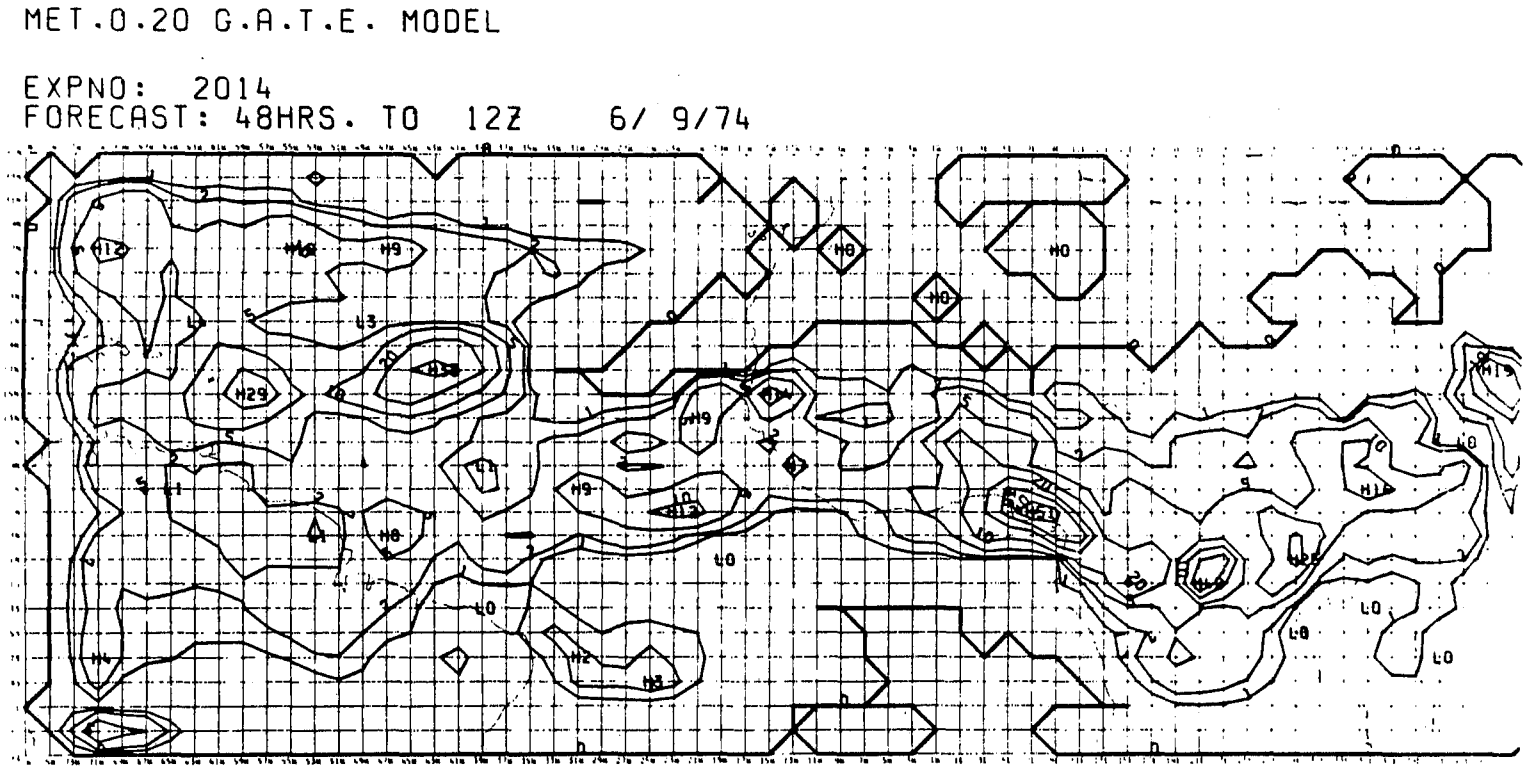

Figure 6.10(b): As Fig. 6.10(a) using a 2^{o} resolution model.

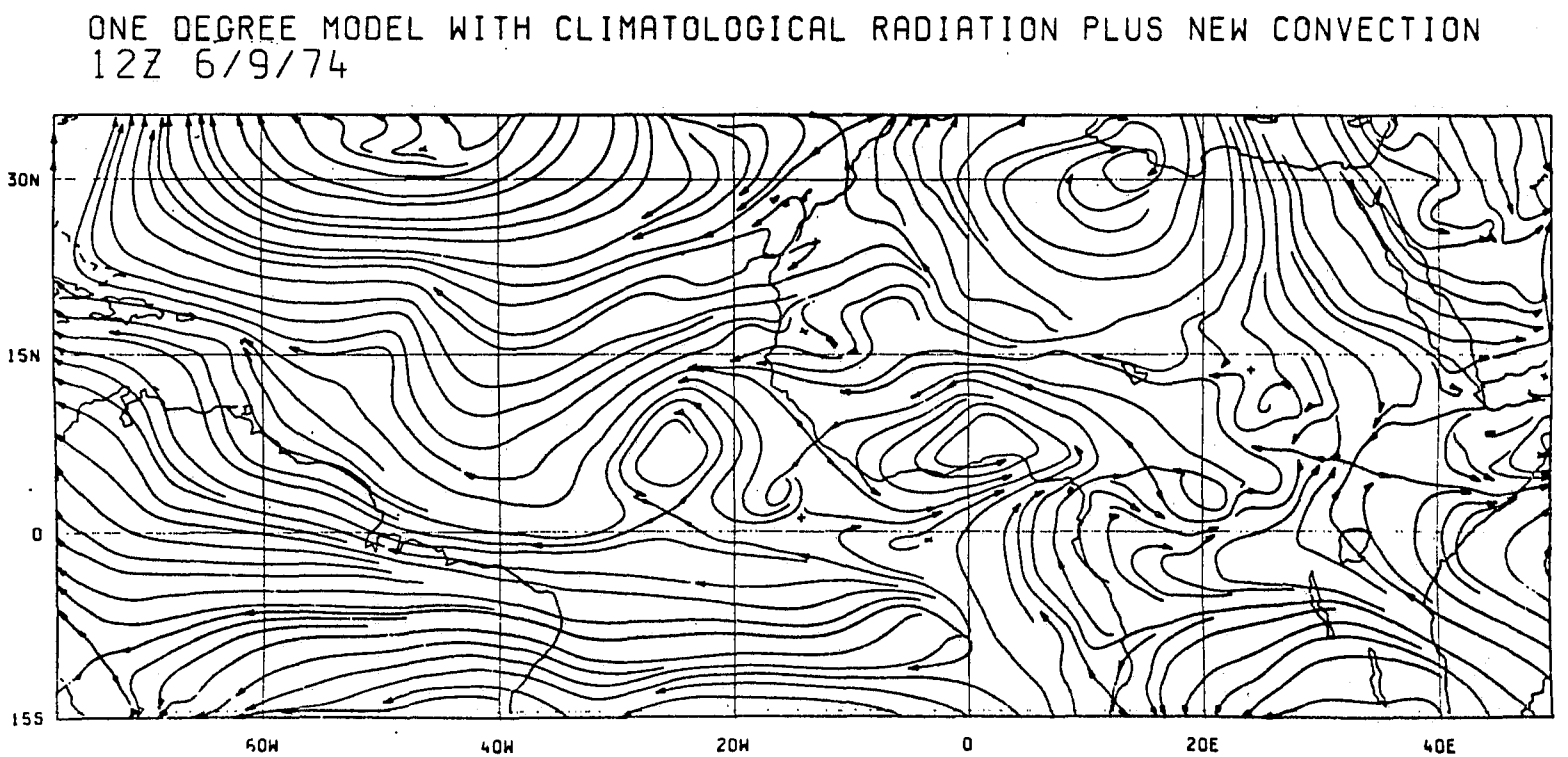

Figure 6.11(a): Streamlines near 850 mb from 48 hour forecast for 12 GMT, 6 September 1974 using 1°resolution model.

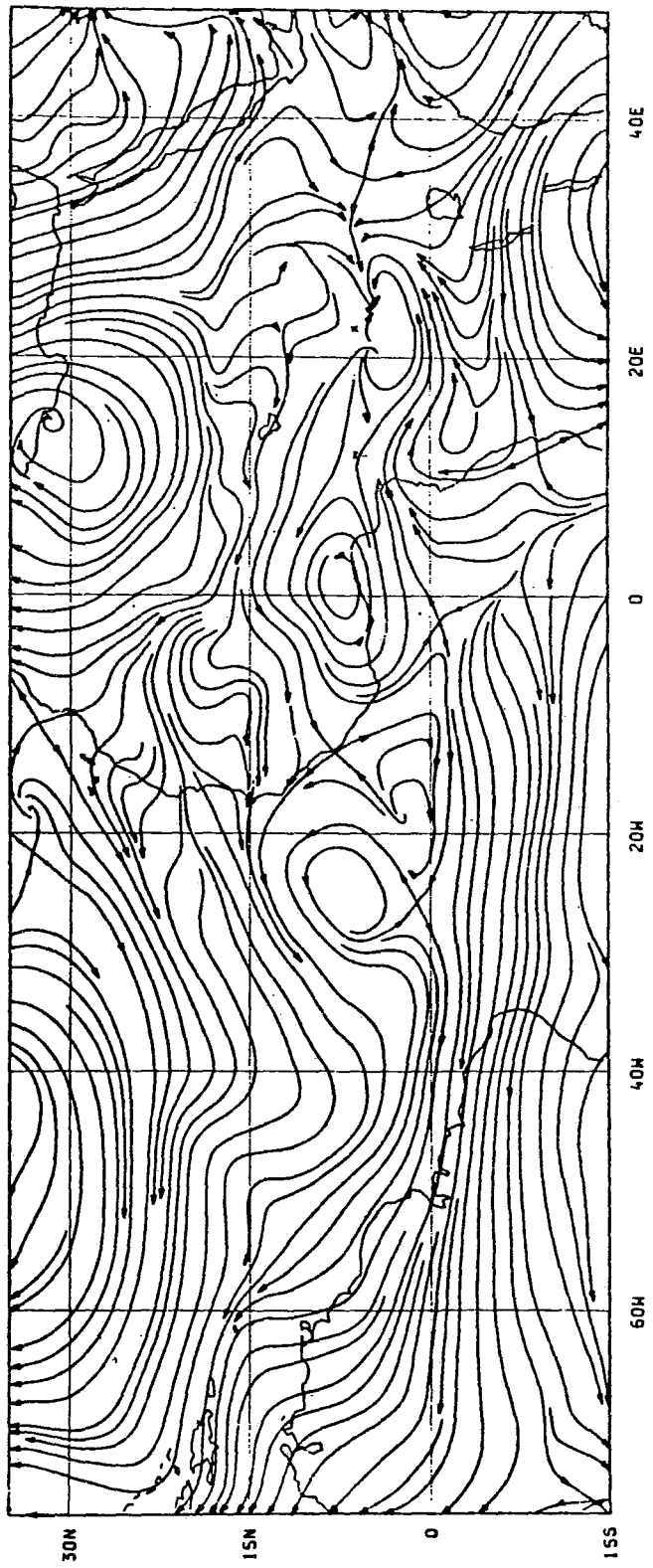

Figure 6.11(b): As Fig. 6.11(a) for 2^{o} resolution model.

of the height field at pressure levels below the Asian mountains. The reruns of the GATE analyses for Phase III discussed earlier have used the analysed height fields in the forecasts from which the background fields for the subsequent analyses were obtained; these have been free of the unrealistic features obtained with the original scheme partly because of better analysis and data quality control procedures and partly because of the improved convection scheme.

6.6.3 Sensitivity to moisture

The replacement of analysed relative humidities by 70% everywhere was shown by Rowntree (1979) to have major effects on flow and rainfall on the first day of a forecast with the MO tropical model. The largest effects occurred over the Sahara where moistening of the air produced a convectively unstable atmosphere, but there were also marked changes in moister areas where the rainfall during the first day was much reduced by the drying of the air. Initial errors in rainfall over land will generate errors in the soil moisture distribution which tend to persist because of the positive feedback mechanism already discussed. For example, it has been found in general circulation experiments that quite different mean rainfall distributions have been obtained over the Sahara for 21 to 50 days from the start of the experiments because of initial differences in atmospheric humidity over North Africa (Cunnington, 1980); with a wet initial atmosphere, mean rainfall at 18^{o}-32^{o}N, 10^{o}W-30^{o}E over Africa averaged about 3 mm/day, compared to much less than 1 mm/day for the dry initial state and for climatology.

6.7 SENSITIVITY TO MODEL FORMULATIONS

6.7.1 Grid Length

Rather inconsistent results have been obtained concerning the grid length required for tropical predictions as discussed by Rowntree (1979). In particular, Krishnamurti et al (1979a) reported that predictions for the GATE area with 11 July 1974 data were poor with a 2^{o} latitude/longitude mesh compared with predictions using a 1^{o} mesh, and suggested that the 2^{o} mesh was not adequate to resolve the African waves. However the 1^{o} mesh multi-level forecast was not wholly satisfactory perhaps because of the cyclic boundary conditions remarked on earlier and the 2^{o} mesh forecast shown by Krishnamurti et al (1977), though certainly too slow in moving one (though not both) of two African waves, did produce more realistic amplitudes than did the 1^{o} model. With the 2^{o} mesh, the east-west boundaries were more remote(110^{o}W and 60^{o}E) so that the cyclic conditions should have had less effect. Experiments with 1^{o} resolution have also been made with the MO model. One, from 4th September 1974, was taken to 48 hours. In Figs. 6.10 and 6.11 it is compared to the corresponding 2^{o} forecast. There are very few differences of any importance to be seen in either the rainfall or the wind fields near 850 mb though the vortices near 25^{o}W and 0^{o} are 1^{o}-2^{o} further south in the high resolution model.

6.7.2 Boundary Layer and Surface Fluxes

Sensitivity experiments on the formulation of surface fluxes have been made by Lepas (1980) but no details are available yet. Rowntree (1979, Fig. 16) noted the sensitivity of the atmospheric temperature structure to the surface wind speeds to which the surface fluxes are roughly proportional. He also discussed the marked sensitivity of rainfall to surface and boundary layer treatment found by Miyakoda and Sirutis (1977).

In the MO forecasts reported by Lyne et al (1975), the boundary layer wind structure was often poorly maintained, especially near the equator where, using a mixing-length formulation for diffusion between the three layers in the bottom 2 km, the model removed the observed shear between weak SSE winds at 850 mb and strong SE winds at 1000 mb, developing within 24 hours an ESE flow with a weak maximum near 950 mb. However, there has, as yet, been little development of boundary layer parametrizations in models on the basis

of GATE data, although, as pointed out in WMO/ICSU (1978), the GATE data set should be very useful in this area.

6.7.3 Convection

A description of convection schemes in use in models appeared in WMO/ICSU (1978) and results of some sensitivity tests were reviewed by Rowntree (1979). The relatively expensive scheme of Arakawa and Schubert (1974) has not been used in predictions with GATE data although it has been found to give good results in semi-prognostic tests as discussed by Betts and Houze in Chapter 9 of this monograph. Krishnamurti et al (1979a) used a scheme based on that of Kuo (1974) but did not show results for rainfall. Lepas (1980) found his model to be sensitive to changes in the convective parametrization. With the Kuo (1965) scheme, the total forecast rainfall for five 24-hour periods was only 5 mm compared with 22 mm with the Kuo (1974) scheme and 32 mm observed.

Rowntree (1979) has discussed the sensitivity of the tropical temperature structure to the convective parametrization, noting that quite realistic temperatures can be generated with some types of convection scheme (e.g. the shallow convection between adjacent layers used in the MO model during GATE). The effects of the change from this scheme to a penetrative convection scheme have been illustrated by Rowntree and Cattle (1982). They used initial data for 12 GMT 10 September 1974 using the original wind analysis with height fields derived from those winds using the reverse balance equation. Although, on the first day, the intense small-scale rainfall maxima evident with forecasts from analysed height fields were absent, by the third day with the shallow convective parametrization several intense rain areas (maximum 137 mm/day) had been generated which were not present with the new convection scheme (maximum rainfall 37 mm/day). Quite different movements and developments were also predicted, the old convection scheme generating rather slow moving intense vortical disturbances. It is evident that there is still much to be done in making prognostic tests of convection schemes with GATE data.

The parametrization of the transfer of momentum by convective processes has often been omitted both in general circulation models and in limited area models of the tropics. The MO tropical model was tested with this included, as discussed by Rowntree (1979). The flow fields were substantially modified by the transfers of momentum directly from low to high levels and more gradually downwards in the compensating environmental subsidence. The effects of convecting momemtum at one grid point and not at the next on the vorticity fields appeared somewhat unrealistic and suggested that the more difficult approach of convecting vorticity might be more satisfactory. The question of whether a simple convective transfer of momentum is appropriate for all types of convection was discussed in WMO/ICSU (1978, Section 4.2.2.3); for organized three-dimensional convection it was suggested that countergradient transports of momentum and horizontal vorticity were more appropriate. (See also Chapter 9 of this volume).

6.7.4 Radiation

Radiation is of crucial importance in tropical models because (a) solar radiation is the main heat source at the surface over land and (b) longwave radiative cooling of the atmosphere destabilises the middle and upper troposphere relative to the boundary layer, the heat and moisture content of which are maintained by the surface fluxes so requiring convective energy transfers (e.g. Yanai et al (1973)). The role of solar heating of the land surface in the maintenance of the African summer monsoon and associated waves has been well demonstrated by Krishnamurti et al (1979a)'s experiments, in which either solar heating was eliminated by choice of a fixed (night-time) zenith angle or all non-adiabatic processes were omitted. In both cases eddy kinetic energy fell to a low level within about 48 hours, more especially in the adiabatic experiment.

The diurnal variation of solar radiation (as distinct from the elimination of all solar radiation) may also have an effect on predictions. This matter is of some interest

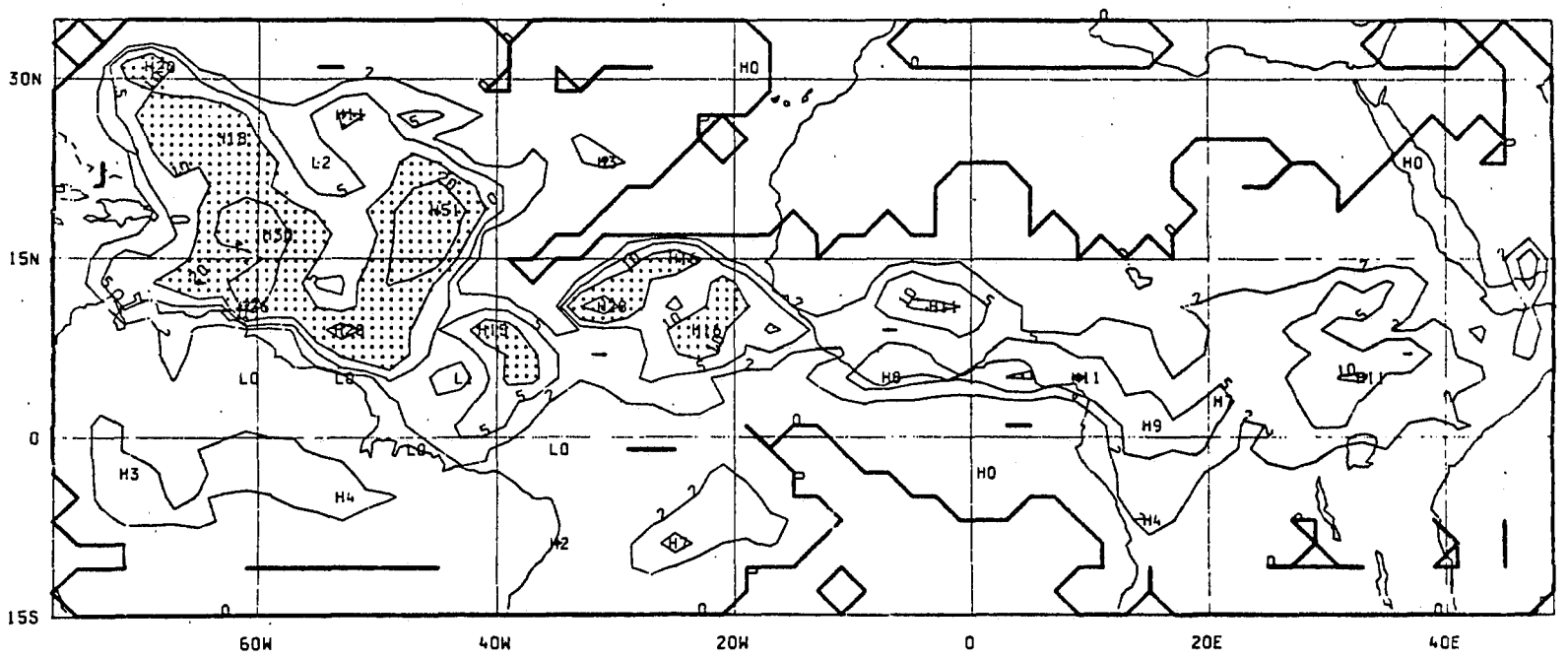

Figure 6.12(a): Forecast of rainfall (mm/day) for 24 hours to 12Z 7/9/74 from initial data for 12Z 4/9/74 with zonal mean clouds and diurnal variation.

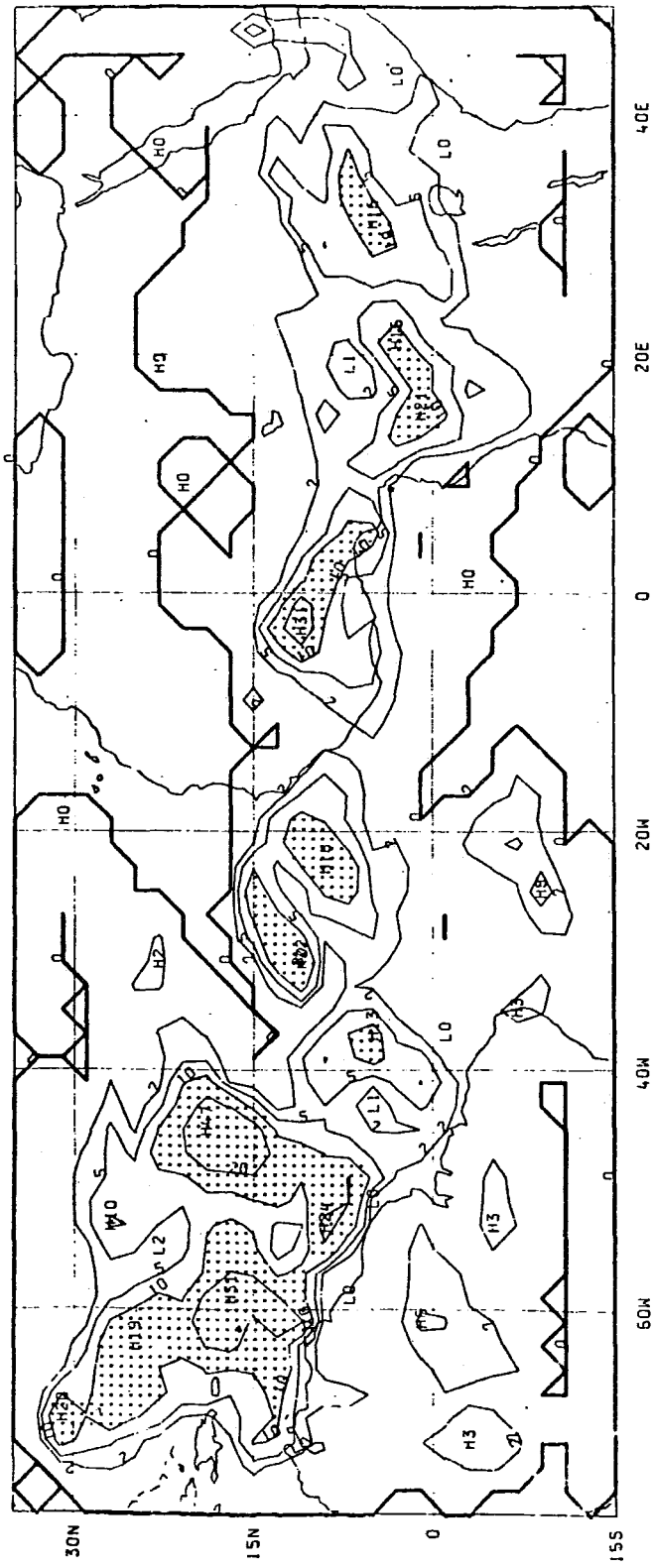

Figure 6.12(b): As Fig. 6.12(a) without diurnal variation.

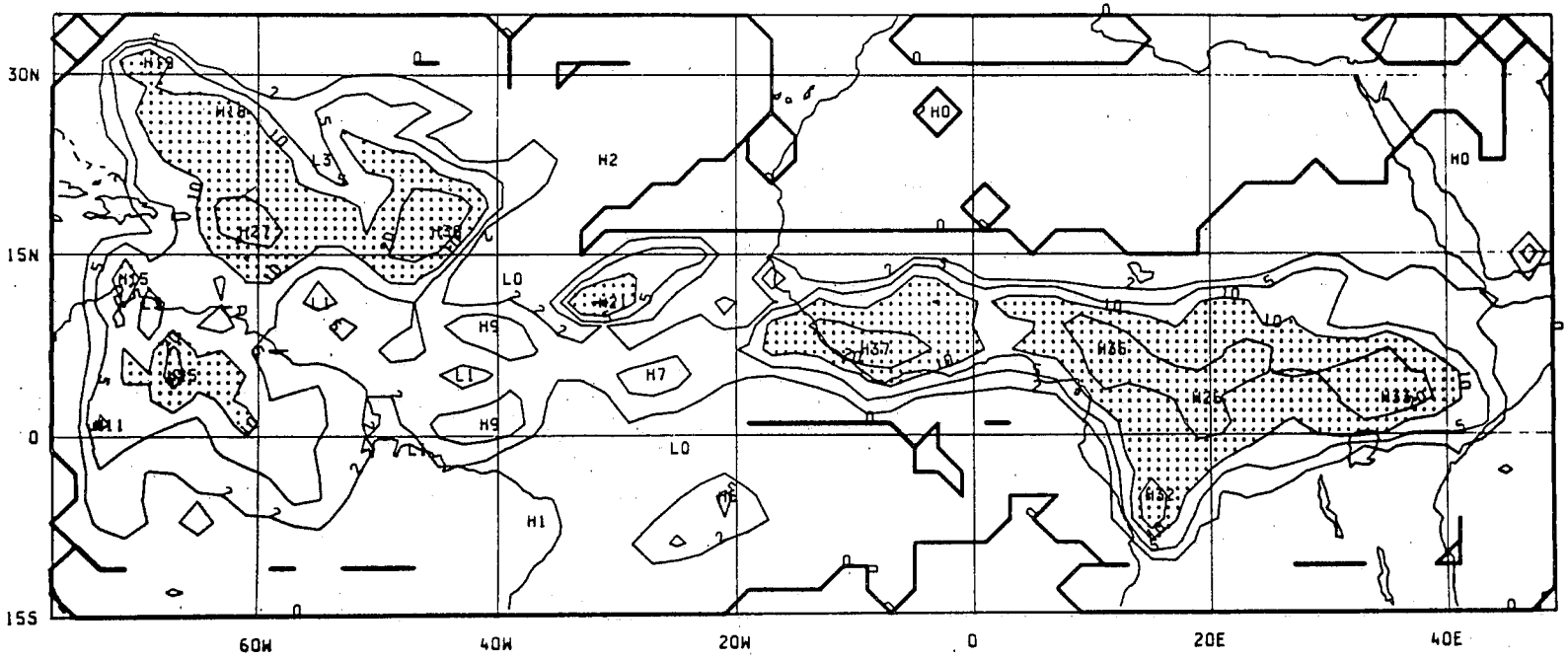

Figure 6.13(a): As Fig. 6.12(a) with interactive radiation and no cloud.

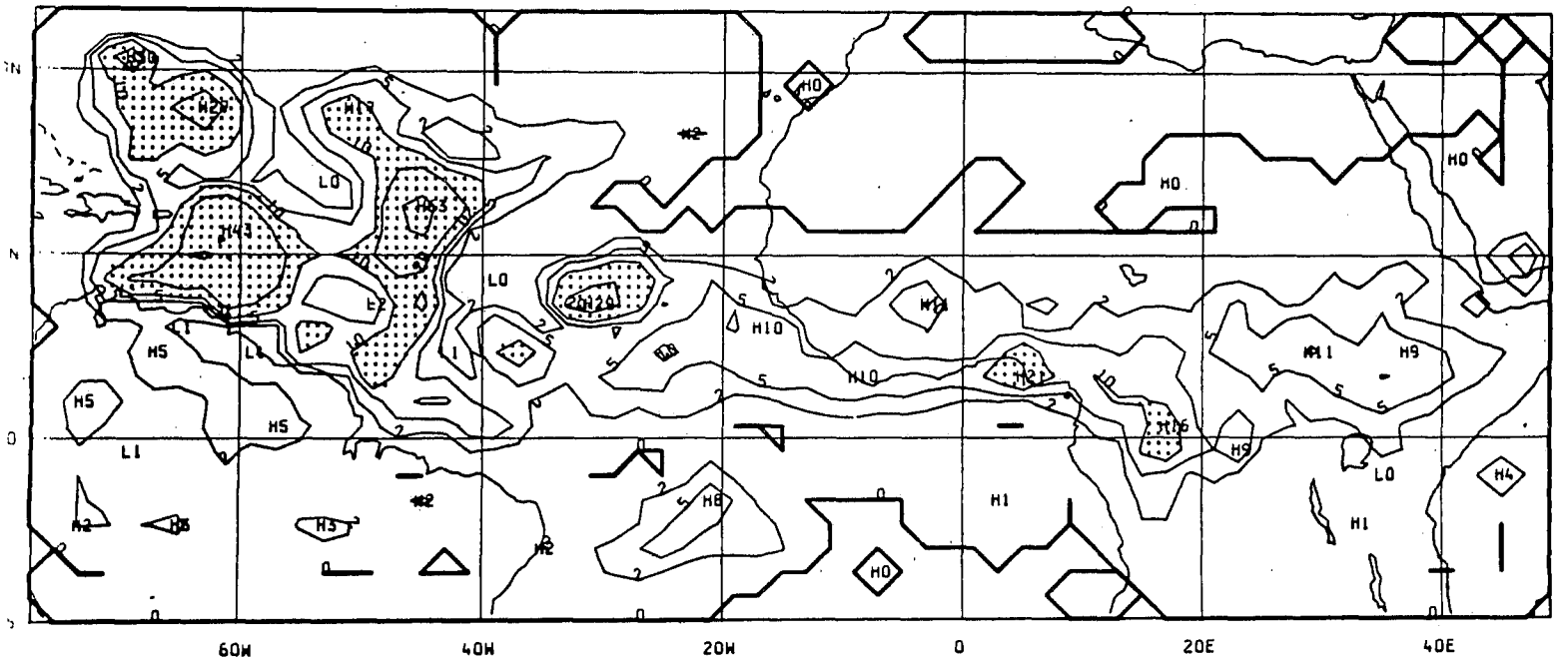

Figure 6.13(b) As Fig. 6.13(a) with interactive clouds.

because some general circulation models have omitted diurnal variations (e.g. Manabe, Hahn and Holloway, 1974). Some experiments to assess these effects have been run using the MO tropical model with zonally averaged fixed cloud (J. Slingo, personal communication). The effects of omitting diurnal variations of solar heating (Fig. 6.12) were still generally small (i.e. rainfall patterns similar and peak values mostly within 10%) after 3 days over the ocean but over land there was a large impact with widespread increases in rainfall including one from 11 to 31 mm on the third day in association with an African wave near 5°W. The explanation for this is not certain. A clear effect of the removal of diurnal variation was to allow moister air to remain in the boundary layer because the daily maximum temperatures were reduced so that this moister air did not become convectively unstable. It may be that this moister boundary layer air allows deeper convection and heavier rainfall in association with developing organised disturbances. The absence of disruption of organised convection by the diurnal variation may also be an important factor. However it should be noted that the model's diurnal cycle of convection was not particularly realistic with a strong afternoon maximum in areas where the observed maximum is in the evening (Burpee, 1977). Similar results were obtained when the interactive cloud scheme of Slingo (1980) was used.

6.7.5 Cloud Feedback

If solar radiative heating of the continental surface and long-wave cooling of the troposphere have a major role in tropical meteorology then it is to be expected that clouds will be important as a modulator of these processes. Thick clouds (e.g. cumulonimbus) can reflect large fractions (70% or more) of the incident solar radiation, transmitting only a small percentage to the underlying surface; if this is a land surface, with its small heat capacity, the energy source for convective activity will be eliminated. Over an ocean surface however, because of its large heat capacity, the surface energy source is not significantly affected on the time scales we are considering so that the absorption of solar radiation by cloud and the long wave radiative effects of cloud on the atmosphere are more important. The long wave effects of cloud depend greatly on the level and thickness of the cloud. Generally the long wave cooling is reduced below cloud while there is an increase in cooling above the cloud. Both these effects are a maximum near the cloud, especially the cooling at the top (Stephens, 1978).

Some effects of cloud on a model of the tropical atmosphere were discussed by Krishnamurti et al (1979a). They found energy conversions to be considerably enhanced when cloud feedback was included; for example, between 72 and 96 hours of their forecast, the generation of eddy available potential energy (APE) was over three times greater while the generation of zonal APE was over fifty times larger (note however that between 24 and 48 hours zonal APE generation was slightly decreased by cloud feedback and only 4% of its later value!). There were corresponding changes in the conversions from eddy and zonal APE to eddy and zonal kinetic energy, and in the magnitudes of the energies themselves. The authors say that the cloud effect is due to cloud top radiative cooling maintaining the convective instability and associated heating.

A series of experiments has been run with the MO model to investigate its response to interactive clouds. Experiments were run with clear skies, with the interactive cloud scheme of Slingo (1980), and with zonally averaged clouds. The initial data were for 12 GMT 4 September 1974; additional experiments from the analyses for 12 GMT, 7 September gave similar results. The forecasts to 3 days showed that the effects of cloud were to damp convective activity and associated rainfall over land and enhance rainfall over the ocean (Fig. 6.13). The changes over land were more striking with rainfalls more than halved over Africa and northern South America. This was attributed to the large reduction in the fraction of solar radiation absorbed by the earth-atmosphere system (mainly at the surface) due to reflection by cloud, the long-wave effects of the clouds being much less. Low-level convergence and upper-level divergence in synoptic scale systems were much reduced and in the 4 September case a West African wave was weakened and displaced southward towards the coast (Slingo, 1978).

Over the ocean the increase in rainfall due to interactive clouds was about 50%. This change is less easy to explain. It is not a large scale response to the decreased ascent and rainfall over the land because an experiment with clouds over the ocean and clear skies over land gave very similar results over the ocean to that with clouds over both land and ocean. An analysis of the radiative cooling rates indicates that the main effect of clouds was a decrease in the cooling through most of the troposphere with radiative warming in some regions. Increased destabilisation was not evident except above 250 mb. It may be that the radiative heating of up to 1 K/day over layers of depth 300 mb in cloudy areas, coupled with similar cooling in clear areas, tended to lower surface pressure in the cloudy regions and so enhance the development of disturbances by increasing low-level convergence and ascent (Slingo, 1978); this mechanism was proposed earlier by Gray and Jacobson (1977) as a possible explanation for the observed diurnal variation in oceanic deep cumulus convection. However it should be noted that some enhancement of rainfall relative to the case with clear skies was also obtained when zonally averaged clouds were used, so removing the cloud feedback effect and indicating that the large scale warming of the oceanic troposphere was partly responsible for the enhanced rainfall. Of course the model's horizontal resolution (220 km) is not really appropriate for modelling the scales observed by Gray and Jacobson.

6.8 SUMMARY AND CONCLUSIONS

Perhaps the most valuable outcome of GATE in the area of large scale numerical modelling will be in the provision of sets of reasonably reliable objective analyses for use in future developments in numerical modelling. It is important that these data sets, using what is certainly the most complete data likely to be available for many years for a tropical oceanic area, should be widely used over the next few years. The GFDL analyses have been rerun using the final GATE data sets for 34 days including Phase III, the MO analyses similarly for the whole of Phase III and FSU analyses have been made for three upper tropospheric levels for the whole of GATE and for 700 mb for Phase III.

Substantial developments of objective analysis techniques have been achieved. The latest operational techniques rely substantially on optimum interpolation and repeated insertion techniques and the experience gained with these in developing GATE analysis methods has already been of considerable value in the analysis of FGGE data.

Experiments with the FSU and MO models using GATE data have clearly demonstrated the feasibility of numerical prediction of tropical flow and rainfall for periods of a few days given adequate data. The limitations to predictability due to lateral boundary conditions in limited area models may be expected to vary with season and with the synoptic situation and will require careful consideration by those wishing to use such models for forecasting in the tropics.

Most of the advances to date in numerical prediction techniques, for which GATE may take credit, can be attributed to the stimulus provided by the observational experiment and consequent data availability. Without that stimulus the MO tropical model would not have existed and the appreciation of aspects of the tropical atmosphere which that model has provided would not have been gained; one may mention in particular the appreciation of the role of soil moisture in modelling the atmosphere over the tropical continents and of cloud over both oceans and continents. The GATE data provided an excellent testbed for a new convection scheme as well as clearly indicating the inadequacies of a simpler scheme. The FSU model already existed prior to GATE but the FSU group have found considerable use for GATE data and have been led to turn their attention more to modelling over the tropical continents. Especial note should be taken of their advances in the application of relatively simple models to the prediction of wave troughs and squall lines, and of their investigations of the interaction between the African atmosphere's mean state and wave developments and of cloud feedbacks. Progress in developing new parametrizations must be expected to be slow because of the time required for the

analysis of new observational data and for the subsequent development of the better understanding needed before new parametrizations can be designed, developed and tested in numerical models. There is promise of such developments in the areas of radiative transfer, particularly the treatment of tropical cirrus clouds, and of convective processes, especially perhaps the representation of downdrafts, the importance of which was particularly evident in GATE. Boundary layer processes are not clearly separable from convective processes over the tropical ocean - a state of affairs not yet fully allowed for in large scale models - and one of the major tasks remaining is to formulate and test improved parametrizations of these vertical transfer processes. The effects of convection on the momentum and vorticity fields also require further investigation. Numerical models could be used more widely in such developments; at present there may not be sufficient involvement of theoreticians and interpreters of observations in large scale modelling.

It should again be stressed that the data sets obtained during GATE are not likely to be equalled in the foreseeable future in terms of spatial and temporal resolution, especially for the B-scale and A/B-scale ship arrays. They should therefore be used as widely as possible, particularly in the development of parametrizations of convective and boundary layer processes and of initialization techniques.

REFERENCES

Arakawa, A. and W. H. Schubert, 1974: Interaction of a cumulus cloud ensemble with the large-scale environment, Part I. J. Atmos. Sci., 31, 674-701.

Atkins, M. J., 1974: The objective analysis of relative humidity. Tellus, 26, 663-671.

Burpee, R. W., 1972: The origin and structure of easterly waves in the lower troposphere of North Africa. J. Atmos. Sci., 29, 77-90.

_____, 1977: The influence of easterly waves on the patterns of precipitation in tropical North Africa. WMO 492, Part II, 41-71.

Cressman, G. P., 1959: An operational objective analysis system. Mon. Weath. Rev., 87, 367-374.

Cunnington, W. M., 1980: The sensitivity of the Saharan region in an 11-layer model as indicated by rainfall amounts. Research Activities in Atmospheric and Oceanic Modelling, ed. I. D. R. Rutherford, W.G.N.E. (GARP), Report No. 21, 82-83.

Farmer, S. F. G., 1977: Documentation of the final validated data set (upper-air soundings) (available from GATE World Data Centres (Washington and Moscow)).

Gandin, L. S., 1963: Objective analysis of meteorological fields. Leningrad, Gidrometeoizdat.

GATE Workshop, 1977: Report of the U.S. GATE Central Program Workshop. Boulder, 25 July-12 August 1977. NCAR, Boulder, Colorado.

GFDL Staff, 1980: FGGE four-dimensional analysis system at GFDL. Part I. Various assimilation processes.

Gray, W. M. and R. W. Jacobson, 1977: Diurnal variation of deep cumulus convection. Mon. Weath. Rev., 105, 1171-1188.

Jones, D. E., 1976: The United Kingdom Meteorological Office objective analysis scheme for GATE. Met. Mag., 105, 249-260.

Kanamitsu, M., 1975: On numerical prediction over a global tropical belt. Report No. 75-1. Dept. of Meteorology, Florida State University, Tallahassee.

Krishnamurti, T. N., M. Kanamitsu, B. Ceselski and M. B. Mathur, 1973: Florida State University's tropical prediction model. Tellus, 25, 525-535.

_____, _____, R. Godbole, Chia-Bo Chang, F. Carr and J. H. Chow, 1976: Study of a monsoon depression (II), Dynamic structure. J. Met. Soc. of Japan, 54, 208-225.

_____, H. L. Pan, C. B. Chang, J. Ploshay, D. Walker and A. W. Oodally, 1977: Numerical weather prediction for GATE. Presented at U.S. GATE Workshop, Boulder, August 1977.

_____, _____, _____, _____, _____ and _____, 1978: Numerical weather prediction for GATE, Report No. 77-7, Dept. of Meteorology, Florida State University, Tallahassee.

Krishnamurti, T.N., H. L. Pan, C. B. Chang, J. Ploshay, D. Walker and A. W. Oodally, 1979a: Numerical weather prediction for GATE. Quart. J. R. Met. Soc., 105, 979-1010.

_____, P. Ardanuy, Y. Ramanathan and R. J. Pasch, 1979b: Quick look 'Summer MONEX Atlas', Part II. The onset phase. Department of Meteorology, Florida State University, Tallahassee, Report No. 79-5.

_____, R. J. Pasch and P. Ardanuy, 1979c: Prediction of African waves and specification of squall lines. Department of Meteorology, Florida State University, Tallahassee, Report No. 79-2.

_____, _____ and _____, 1980: Prediction of African waves and specification of squall lines. Tellus, 32, 215-231.

Kuo, H. L., 1965: On formation and intensification of tropical cyclones through latent heat release by cumulus convection. J. Atmos. Sci., 22, 40-63.

_____, 1974: Further studies of the parameterization of the influence of cumulus convection on large-scale flow. J. Atmos. Sci., 31, 1232-1240.

Lepas, J., 1980: Numerical forecasting experiments with GATE data (Phase 3, September 1974). Abstract for Kiev conference.

Lyne, W. H., P. R. Rowntree, C. Temperton and J. M. Walker, 1975: Numerical modelling during GATE. Met. O. 20 Tech. Note No. II/37. Met. Office, Bracknell.

_____, _____, _____ and _____, 1976: Numerical modelling using GATE data. Met. Mag., 105, 261-271. H.M.S.O.

_____ and _____, 1976: Development of a convective parameterization using GATE data. Met. O. 20 Tech. Note No. II/70. Met. Office, Bracknell.

Manabe, S., D. G. Hahn and J. L. Holloway, Jr., 1974: The seasonal variation of the tropical circulation as simulated by a global model of the atmosphere. J. Atmos. Sci., 31, 43-83.

Mass, C. F., 1979: A linear primitive equation model of African wave disturbances. J. Atmos. Sci., 36, 2075-2092.

Miyakoda, K., L. Umscheid, D. H. Lee, J. Sirutis, R. Lusen and F. Pratte, 1976: The near real time global, four-dimensional analysis experiment during the GATE period, Part I. J. Atmos. Sci., 33, 561-591.

_____, J. Sheldon and J. Sirutis, 1980: Four-dimensional analysis experiment with the GATE data. Part II. (Submitted to J. Atm. Sci. for publication).

_____ and J. Sirutis, 1977: Comparative integrations of global models with various parameterized processes of subgrid-scale vertical transports: Description of the parameterizations. Beiträge zur Physik der Atmosphäre, 50, 445-487.

Norquist, D. C., E. E. Recker and R. J. Reed, 1977: The energetics of African wave disturbances as observed during Phase III of GATE. Mon. Weath. Rev., 105, 334-342.

Parker, D. E., 1977: Documentation of the Final Validated Data Set (surface) (available from GATE Archives: World Data Centres A and B (Washington and Moscow)).

Pasch, R., T. N. Krishnamurti and C. Depradine, 1978: An atlas of the motion field over the GATE area. Part II (250 mbs), Department of Meteorology, Florida State University, Tallahassee, Report No. 78-3.

Pusey, D. M., 1977: Documentation of the FDDS (aircraft reports and satellite winds) (available from GATE Archives: World Data A and B Centres (Washington and Moscow)).

Reed, R. J., D. C. Norquist and E. E. Recker, 1977: The structure and properties of African wave disturbances as observed during Phase III of GATE. Mon. Weath. Rev., 105, 317-333.

Rennick, M. A., 1976: The generation of African waves. J. Atmos. Sci., 33, 1955-1969.

Rowntree, P. R., 1979: Numerical prediction and simulation of the tropical atmosphere, in Proc. Conf. Met. over Tropical Oceans, Ed. D. B. Shaw, Royal Met. Soc., 219-249.

_____ and H. Cattle, 1982: The U.K. Meteorological Office GATE modelling experiment. Scientific Paper No. 40, Meteorological Office.

Sadler, J. C. and L. K. Oda, 1978: The synoptic (A) scale circulations during the third phase of GATE 20 August-23 September 1974.

Sasaki, Y., 1970: Some basic formulations in numerical variational analysis. Mon. Weath. Rev., 98, 875-883.

Schlatter, T., 1975: Some experiments with a multivariate statistical objective analysis scheme. Mon. Weath. Rev.

Shaw, D. B. and P. R. Rowntree, 1976: Met. O. 20 tropical model and experiments using GATE data. Met. O. 20 Tech. Note No. II/80. Met. Office, Bracknell.

Sitnikov, I. G. and K. G. Rubinshtein, 1975: Numerical experiments in the parameterization of convective heat fluxes for modelling of large-scale atmospheric processes. Trudy Gidrometcentra SSSR 160, 26-40 (in Russian).

Slingo, J. M., 1978: The effect of interactive clouds and radiation on convective activity in a numerical model of the tropics. Met. O. 20 Tech. Note No. II/130, Met. Office, Bracknell.

_____, 1980: A cloud parameterization scheme derived from GATE data for use in a numerical model. Quart. J. R. Met. Soc., 106, 747-770.

Spalding, T. R., 1980: Spatial correlations in the tropics and their use in optimum interpolation. Met. O. 20 Tech. Note No. II/144, Met. Office, Bracknell.

Stephens, G. L., 1978: Radiation profiles in extended water clouds. I: Theory. J. Atmos. Sci., 35, 2111-2122.

Temperton, C., 1976: Dynamic initialization for barotropic and multi-level models. Quart. J. R. Met. Soc., 102, 297-311.

Walker, J. and P. R. Rowntree, 1977: The effect of soil moisture on circulation and rainfall in a tropical model. Quart. J. R. Met. Soc., 103, 29-46.

Woodley, W. L., C. G. Griffith, J. S. Griffin and S. C. Stromatt, 1980: Satellite-estimated rainfall in GATE. NOAA Tech. Memo. ERL/NHEML-6, 54 pp.

WMO/ICSU, 1972: Experiment design proposal for the GARP Atlantic Tropical Experiment. GATE Report No. 1.

WMO/ICSU, 1978: Numerical modelling of the tropical atmosphere. GARP Publication Series, No. 20.

Yanai, M., S. Esbensen and Jan-Hwa Chu, 1973: Determination of bulk properties of tropical cloud clusters from large-scale heat and moisture budgets. J. Atmos. Sci., 30, 611-627.

CHAPTER 7

PHYSICS OF THE UPPER TROPICAL OCEAN

by

Gerold Siedler

(Institut für Meereskunde, Kiel University, F.R.G.)

and

George Philander

(Geophysical Fluid Dynamics Laboratory/NOAA,
Princeton University, U.S.A.)

7.1 INTRODUCTION

The oceanographic component of GATE had as its objective a study of the variability of the tropical Atlantic Ocean. With respect to a possible influence of the ocean on the atmosphere in this area, information was required on surface temperature changes, and hence on the vertical heat flux and the primary processes redistributing heat in the upper ocean. Furthermore, the experiment also provided a unique opportunity for studying the response of the ocean to atmospheric forcing on various scales. The investigations aimed at describing the principal kinematic properties, identifying the dominating dynamic processes that are responsible for the energy and momentum flux in the upper layers, and determining what kind of models must be developed to simulate the oceanic variability. Such studies are closely related to succeeding programmes on climate research. The description of kinematic properties, i.e. the temperature-salinity stratification and the current field, was based on observational arrays that on the ocean-wide and intermediate scales had been determined primarily by meteorological requirements resulting from the dominating scales of the cloud cluster regime and the easterly waves in the Intertropical Convergence Zone (ITCZ). The resulting station separations were often large in comparison to dominating spatial scales of the oceanic variability, however, the arrays for the first time provided simultaneous measurements covering most of the tropical Atlantic. The more closely spaced ships on stations along 23°30'W provided particularly useful data for this part of the programme. Two observational arrays were specifically adjusted to the needs of the oceanographic programme. One area was the zone within a few degrees latitude of the equator. This region, which is dynamically distinct because of the small value of the Coriolis parameter, is characterized by intense currents and strong upwelling. During the planning stages of GATE little was known about the oceanic variability in this region. Some oceanographers speculated that variability would have such long time scales that nothing interesting would happen during the relatively short duration of GATE. The results from GATE surprised these pessimists.

The other focus of oceanographic measurements was the C-scale in the ITCZ region north of the equator. There, experiments were particularly aimed at process studies related to atmospheric forcing of the ocean. This included studies on the slowly varying density and current field, on surface and internal waves, and on the turbulent structure of the mixed layer and the thermocline, with particular emphasis on frontal zones.

The following discussion will highlight some major achievements of the GATE oceanographic programme. A selection of results and ideas will be presented which is not claimed to be complete, but is rather aimed at informing those scientists about principal results who were not engaged themselves in the oceanographic programme of GATE. For further details the reader is referred to the special GATE issues of Deep-Sea Research (Siedler and Woods, 1980a; Düing, 1980), to the GATE Atlas (Düing, Ostapoff and Merle, 1980) and the TROPEX-74, Volume II. The review will start with a description of the large-scale fields, whereafter results will be presented on the variability of these fields and the processes responsible for such changes.

7.2 THE MEAN OCEANOGRAPHIC CONDITIONS

The oceanic circulation is maintained primarily by the wind-stress on the ocean surface. Hellerman (1980) describes the seasonal variability of the winds over the tropical Atlantic, and Krishnamurti and Krishnamurti (1980) describe their variability during GATE. The winds are primarily from the south over the Gulf of Guinea (east of 10°W). Trade winds prevail west of 10°W: northeast trades north of the ITCZ; southeast trades south of the ITCZ. Of particular interest to us is the steady intensification, between June and September, of the winds west of about 30°W. This intensification is associated with a northward migration of the ITCZ.

The surface winds drive the following mean currents. Figure 7.1 presents a meridional section across the currents; Figure 7.2 shows the associated temperature field. The eastward North Equatorial Countercurrent, between 3°N and 10°N approximately, is sandwiched between the westward North Equatorial Current to the north and westward South Equatorial Current to the south. The Countercurrent is fed by the Brazilian Coastal Current at its western extreme (Vazquez de la Cerda, 1978), has a transport of approximately 17 x $16^6 m^3 s^{-1}$ across 40°W (Cochrane, 1978), and weakens further to the east. It can be shown that the Countercurrent is nearly in geostrophic balance and that it is associated with the strong latitudinal slope of the isopycnals between 3°N and 10°N; computed geostrophic velocities and directly measured currents have been shown to compare well (Bubnov et al., 1979). In the mixed surface layer there is, however, a significant non-geostrophic component which is presumably associated with the Ekman layer.

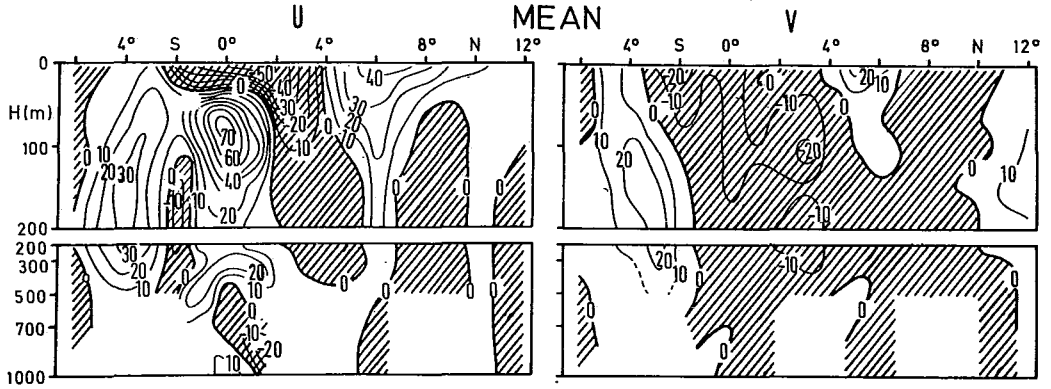

Figure 7.1 - Zonal (u) and meridional (v) velocity components at 23°30'W on the basis of direct measurements averaged over the GATE period. Units are cm s^{-1}, shaded regions indicate westward (u) and southward (v) flows (after Bubnov and Egorikhin, 1980).

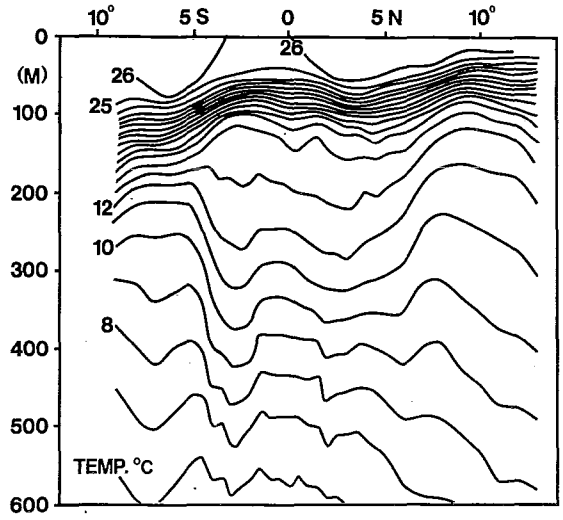

Figure 7.2 - Mean temperature distribution along 23°30'W on the basis of measurements from R/V TRIDENT and R/V SEMEN DEZHNEV (after Philander and Düing, 1980).

An intriguing feature of the hydrographic data shown in Figure 7.2 is the steep sloping of the isotherms near 5°S (at depths between 200m and 600m) and near 6°N (at depths between 200m and 400m). These slopes imply subsurface eastward currents documented by Hisard et al. (1976).

Symmetrically about the equator flows the subsurface, eastward Equatorial Undercurrent (Lomonosov Current) which had an average maximum speed of the order of 75 cm s^{-1}. Transport estimates of the Undercurrent must be interpreted with some caution because of the large variability encountered over short time periods. All estimates fall within the range (12.5 ± 2.5) x $10^6 m^3 s^{-1}$ for transport within the 20 cm s^{-1} isotach, while up to 50% higher values are given for the eastward transport down to 200m depth (Bubnov and Egorikhin, 1977).

Based on five sections, occupied once each, Bruce and Katz (1976) found the transport to increase downstream as far as 16°W, but further eastward, where the zonal pressure force along the equator changes from eastward to westward, the transport rapidly decreased. Associated with the Undercurrent is a core of high salinity water. The salinity maximum is, on the average, about 20m above the core of the zonal velocity. This is probably a consequence of the strong equatorial upwelling. Eastward of 28°W there is a gradual salt flux out of the Undercurrent. This loss of salt is due to upwelling into the divergent surface layers, and downward entrainment into the pycnostad. From the absence of downstream, latitudinal spreading of the salinity fore, Katz et al. (1980) infer a meridional convergence of fluid into the Undercurrent. This meridional circulation is the subject of theories for the Undercurrent and is thought to be important in its momentum balance (Moore and Philander, 1977). During Phase II of GATE two additional maxima of eastward flow were observed below the Undercurrent (Helm, Lass and Sturm, 1980), and an intense westward current was observed below the Undercurrent in Phase III (Bubnov et al., 1979; Bubnov et al., 1980).

The various currents described so far are associated with meridional density gradients. The thermocline also slopes zonally and increases in depth from east to west as shown in Figure 7.3. Sea-surface temperatures are highest where the thermocline depth is greatest (close to the South American coast). The variability of the sea-surface temperature is largest where the thermocline is shallow, near the equator and in the eastern part of the Gulf of Guinea.

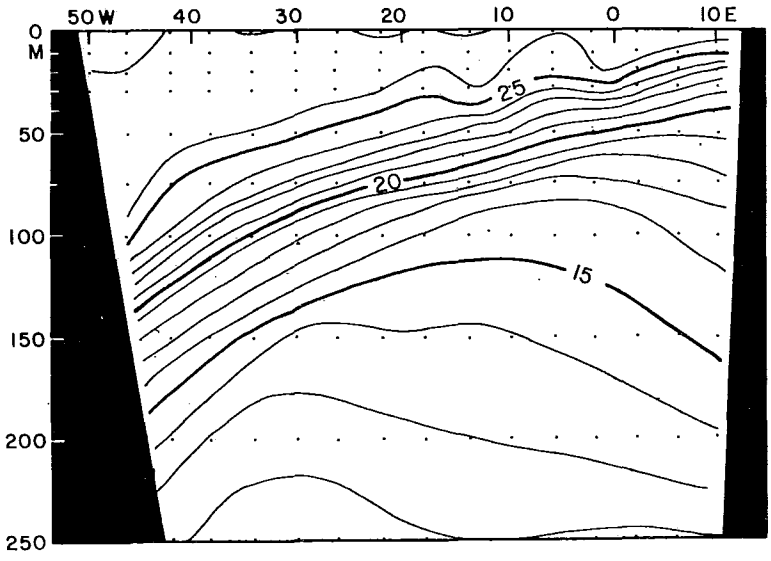

Figure 7.3 - Mean temperature distribution along the equator on the basis of all available Nansen casts (after Merle, 1980).

7.3 MIXING PROCESSES

The dense array of ships north of the equator, centred at $8^{\circ}45'N$, $23^{\circ}00'W$, allowed a study of the variability of upper ocean spatial scales corresponding to the temporal scales (a few minutes up to a few weeks) that were covered by the two-months' duration of the experiment.

Peculiar features of the near-surface temperature and salinity structure are found below the cloud cluster regime of the ITCZ where few high-resolution measurements had been obtained before GATE. Figure 7.4 presents an example of vertical profiles at a fixed position, demonstrating the rapid and strong variations of salinity and temperature in the upper metres. With the fairly steady North Equatorial Countercurrent flowing to the northeast or east with 35 to 40 cm s^{-1}, these variations imply a salinity and temperature patchiness at the surface which must be related to the unique conditions of precipitation and wind stress in the area. When comparing data from different ships in the area, it is found that typical horizontal scales are smaller than the ships' separations of 50 to 100 km. Comparisons with individual atmospheric events during the experiment showed that these near-surface features usually cannot be related to local effects. Water whose properties are changed by vertical heat and water flux at the surface at a certain position is swept away immediately, and mixing is sufficiently effective to redistribute salt and heat on scales of order 10 km or less.

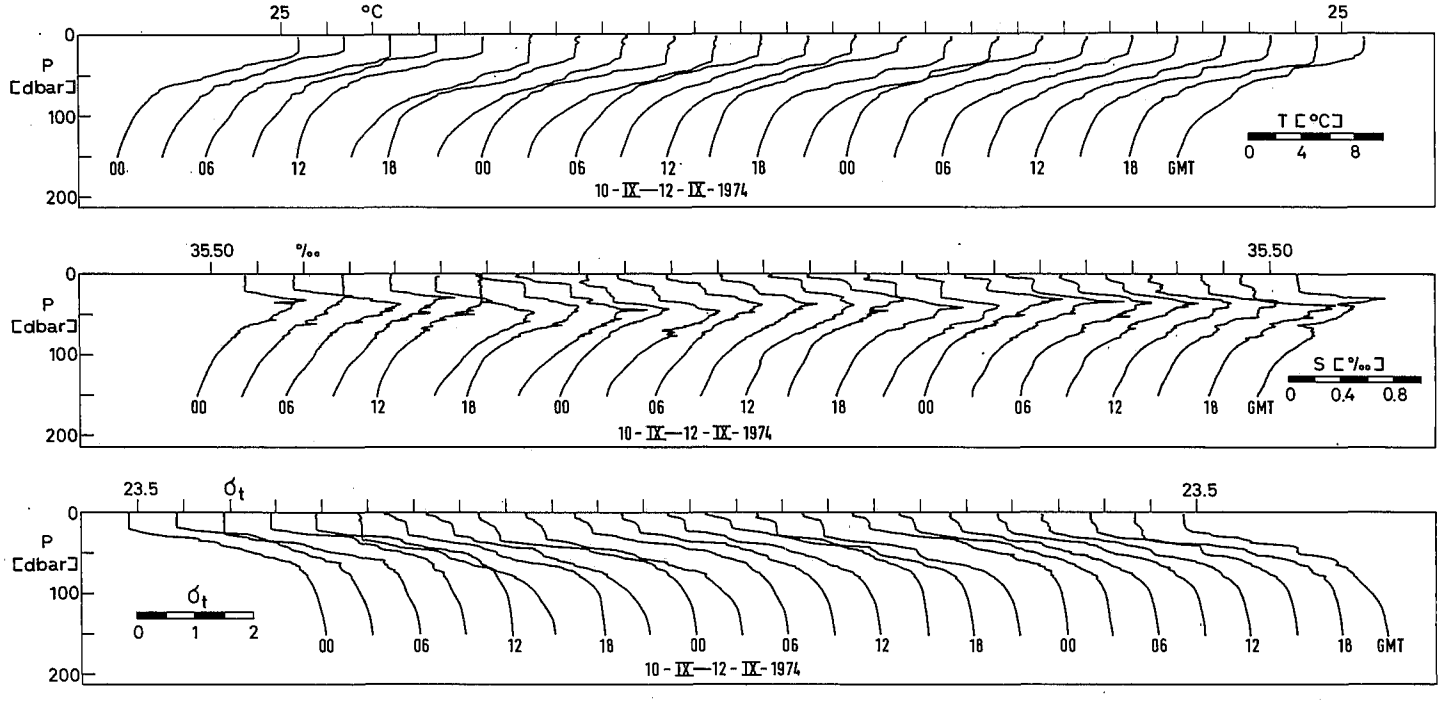

Figure 7.4 - Selected vertical profiles of temperature T, salinity S, and density σ_t in the C-scale array from R/V PLANET on 9°08.4'N, 22°58.8'W (after Peters, 1978).

Progressing down to the steep part of the thermocline, a similarly strong variability is found in the salinity maximum range below the "homogeneous" layer. Vertical salinity gradients of order $0.05^{o}/oo$ per metre at a depth of 30 to 50m, without strong shear in these layers, suggest much reduced vertical mixing, with the high salinity core being maintained by the advection of subtropical waters.

For parameterizing the upper ocean in models, mean vertical diffusion coefficients are required. Elliott and Oakey (1980) used a vertically profiling temperature microstructure measuring instrument for determining the average heat diffusion from the frequency of mixing events that are due to breaking internal waves. For a surface layer 130m thick they arrive at mean vertical eddy diffusion coefficients of 10^{-2} to $10^{-4}m^{2}s^{-1}$. Their estimate of the vertical heat diffusion at the bottom of this layer is 0.5 Watts m^{-2}. Comparing this number with the typical net heat flux of 50 Watts m^{-2} through the surface (e.g. Perkins, 1980) leads to the conclusion that horizontal advection and possibly horizontal diffusion dominate the heat balance of the upper ocean in this area.

A peculiar pattern of turbulence is observed in the region within 2^{o} latitude of the equator (Crawford and Osborn, 1980). A free-fall probe measuring microstructure current shear and temperature gave results such as those presented in Figure 7.5.

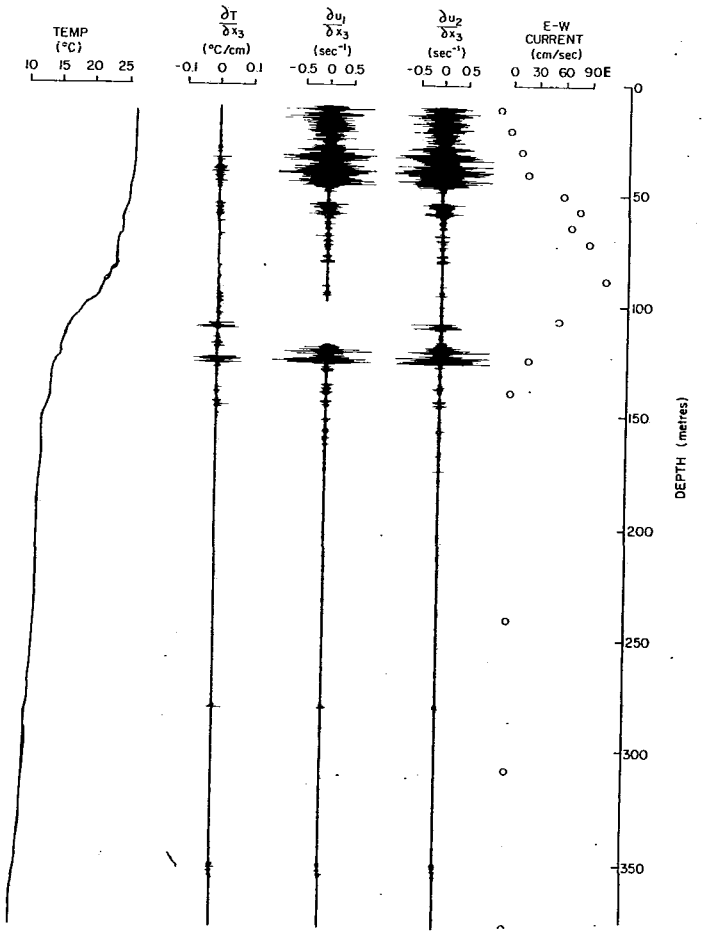

Figure 7.5 - Temperature, vertical microstructure, temperature gradient, east and north component microstructure shear (after Crawford and Osborn, 1980) and east component of current (after Bruce and Katz, 1976) near $32^{o}59'W$, $0^{o}02'N$ in July 1974.

In this plot the data are displayed together with a current profile observed close to this position using an over-the-side current meter (Bruce and Katz, 1976). The current profile on the right indicates the Equatorial Undercurrent core at 40 to 120m depth. The upper layer is well mixed, but has a strong mean shear. Large microstructure shear amplitudes are found in this depth range. In the transition layer between the South Equatorial Current and the Undercurrent there is obviously very active turbulence, and another turbulent region is found near the base of the thermocline. Little or no shear microstructure is found in the Undercurrent core. Richardson Numbers are of order 0.1 in the active depth ranges and of order 1 or higher in the Undercurrent core. It is concluded that strong eddy diffusion and high dissipation rates found are due to turbulence generated by the high large-scale shear existing above the velocity core. Typical eddy viscosity coefficients in this active layer are of order $10^{-3} m^2 s^{-1}$ (Crawford and Osborn, 1980).

Towed undulating conductivity - temperature - depth recorders provided data in the ITCZ region that indicate the existence of well-defined tongues of disturbed water with increased thermoclinicity and possibly a more frequent occurence of billow turbulence due to internal wave breaking (Woods and Minnett, 1979), and frontal structures are observed in the area (Figure 7.6). This result illuminates the difficulties encountered in the determination of spatially averaged turbulent diffusion properties in the tropical ocean, even with the dense observational network that was available in GATE.

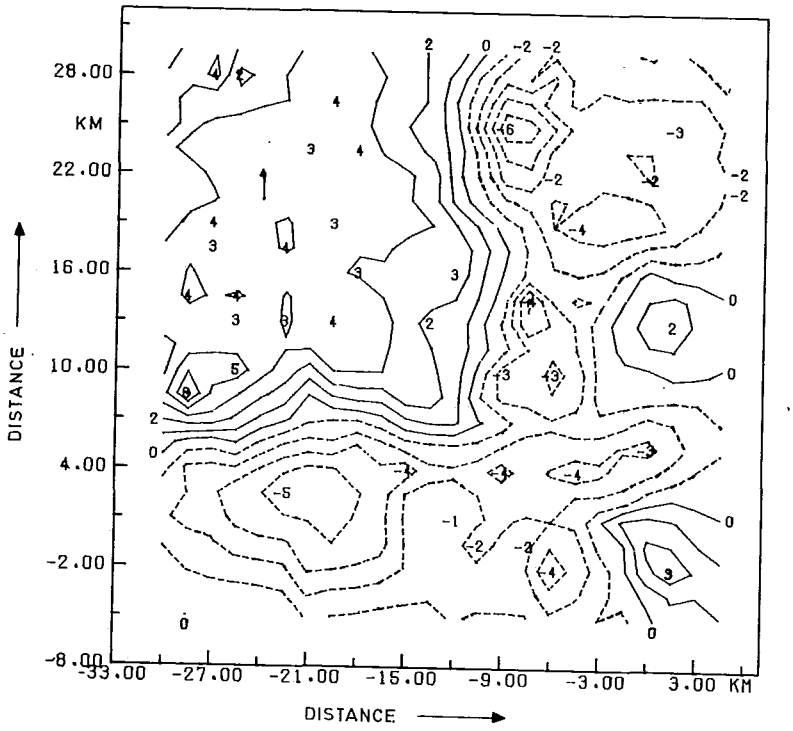

Figure 7.6 - Deviation from mean potential temperature on the density surface σ_t = 23.60 in the GATE C-scale area from undulating bathfish data during Phase III. The distances are measured relative to an origin moving with the mean current at the surface. Units are given in 10^{-2} degrees Kelvin (after Woods et al., 1981).

7.4 HEAT BUDGET OF THE SURFACE LAYER

In the central parts of the subtropical and mid-latitude oceans the heat budget of the surface layer is to a large extent determined by local fluxes across the ocean surface. This is the reason why local one-dimensional mixed layer models, which entirely neglect the dynamical response of the ocean, simulate variations of the surface temperature and the vertical temperature distribution fairly well. It can, however, be argued that the available data do not provide sufficiently stringent tests for these models.

In much of the tropical oceans strong and fairly steady zonal near-surface currents exist, and advective terms in the ocean heat budget can be expected to play a major role. When planning the oceanographic programme of GATE there had been serious doubts whether it would be possible to relate local surface fluxes to heat content variations. Indeed it proved impossible to link deterministically vertical heat flux to surface layer heat content changes. The redistribution is so large that local changes in heat storage are practically unrelated to local fluxes across the ocean surface (Figure 7.7). However, Clarke (1980) was able to show that it is possible to balance the mean vertical heat and fresh-water fluxes in the C-scale area with a horizontal advective flux of heat and fresh water without recourse to large fluxes of these properties across the thermocline. Furthermore spectral properties of heat content fluctuations can be well modelled if local surface heat flux changes due to cloud cover variations, surface mean cloud layer and oceanic mixed layer advection are taken into account (Siedler, 1980).

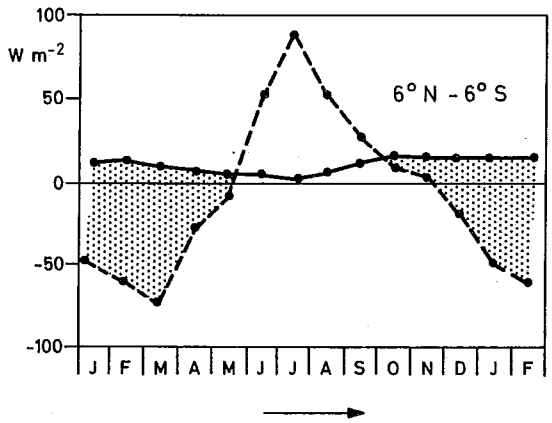

Figure 7.7 - Rate of change of heat content H per month for the region 6°N to 6°S, 30°W to the Brazilian coast (broken line) and oceanic heat gain from the atmosphere for the same region (solid line) (after Merle, 1980).

For future mean heat budget modelling GATE also provided a remarkably good coverage of the area by conventional surface heat flux data. As an example, mean flux distributions for the eastern tropical Atlantic are given in Figure 7.8.

7.5 INERTIA-GRAVITY WAVES

A considerable amount of momentum supplied by the wind stress to the ocean is transferred into surface and internal waves. The C-scale experiment provided an opportunity to observe such processes with simultaneous high frequency surface wind data. The surface wave programme including buoy and aircraft measurements was aimed

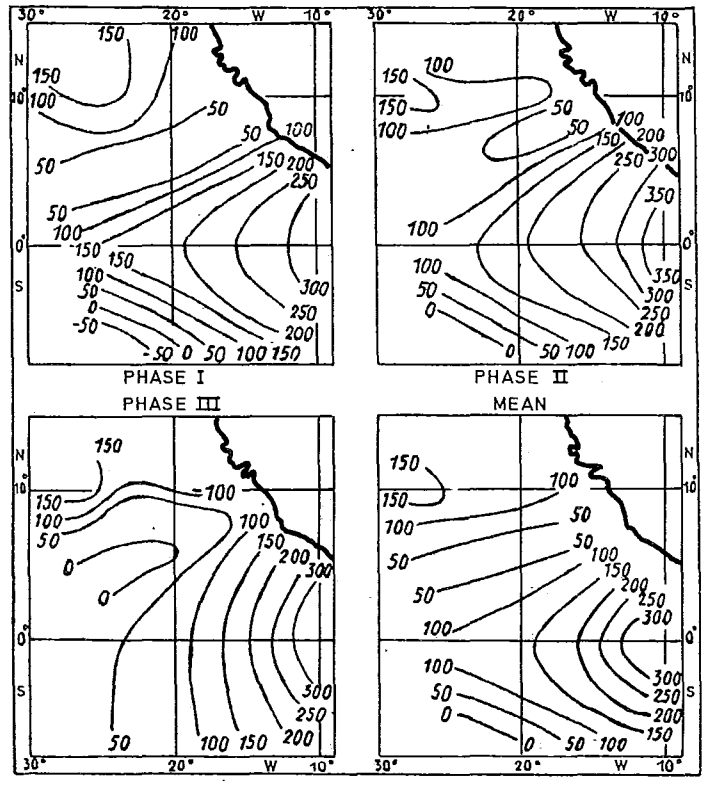

Figure 7.8 - Mean vertical heat flux at the sea surface in cal · $cm^{-2} \cdot day^{-1}$ (after Belevich, 1977).

at testing numerical wave prediction models needed for improved parameterization of air-sea momentum transfer. The data led to estimates of one-dimensional wave spectra and to the mean direction and the spread of wave energy as a function of frequency (Cardone et al., 1981). A complicated superposition was observed of one or often more swell regimes generated by the Northeast and Southeast Trades in addition to the locally generated wave field. Furthermore, early in Phase III swell occurred in the GATE area that had been produced by an intense extra-tropical cyclone crossing the North Atlantic at high latitudes. The locally generated wind waves are evident in the data, but their energy may have been modulated significantly by the low-frequency swell. After elimination of the swell peaks in the spectra, the observed spectral variations usually compare well with the existing spectral ocean wave prediction models.

The GATE C-scale experiment had been planned during a period of rapid theoretical and observational advance in internal wave research. Intensive research on deep-sea inertia-gravity internal waves had been stimulated by the Garrett-Munk (1972) model, but very few data existed then that had been obtained in the near-surface layer on top of the deep ocean.

As expected, a strong near-inertial spectral peak was found in the internal wave band and also usually a peak at semi-diurnal tidal frequency. There exists, however, a third energetic band (Figure 7.9) at medium-depth Brunt-Väisälä frequency in the upper layer (Käse and Siedler, 1980). The observed deviation from a Garrett-Munk type spectrum above the tidal frequency indicates a marked difference in the

behaviour of the internal wave field at high and low frequencies. Below, especially in the inertial range, downward propagating wave groups carry energy from the surface layer to greater depth (Käse and Olbers, 1980). Above, resonant forcing of standing modes with a preponderance of the fundamental mode is possible. In the inertial range a wind-driven simulation model of the mixed layer currents yields an energy input of 3×10^{-3} Watts m^{-2}, and internal waves are generated at a rate of 10^{-3} Watts m^{-2}, with consistent results both from kinematic and dynamic considerations.

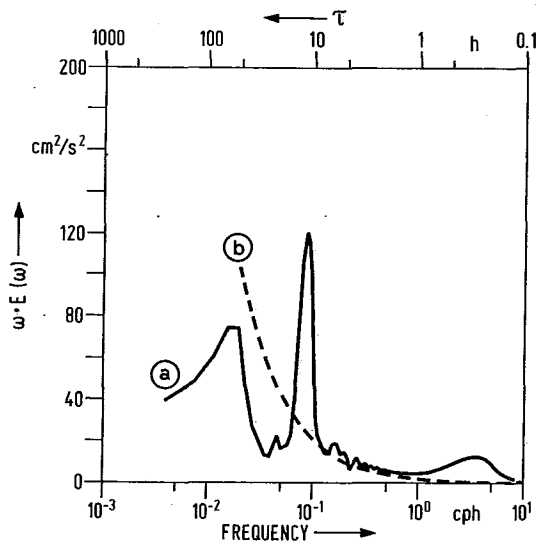

Figure 7.9 - Energy preserving presentation of internal wave energy E observed in the C-scale array (a) and theoretical Garrett-Munk spectrum with energy in frequency band 0.1 to 1 cph equal to that observed (b) (after Käse and Siedler, 1980).

7.6 VARIABILITY NEAR THE EQUATOR

Variability in equatorial regions, as elsewhere in the oceans, occurs over a continuous spectrum of frequencies. The principal difference between equatorial and extra-equatorial spectra is the disappearance of the inertial peak equatorward of 4° latitude approximately. This is evident from Figure 7.10 which shows kinetic energy spectra of ocean currents at a number of locations. Poleward of 4° latitude the inertial peak is prominent because there is a "spectral gap" at lower frequencies. There are no free oceanic waves at sub-inertial frequencies until we are at a radius of deformation from the equator. At that distance equatorially trapped waves are possible at all frequencies. That the shape of the spectrum changes at 4° latitude approximately is therefore consistent with this theoretical result. (The radius of deformation for the first baroclinic mode is about 400 km.) Superimposed on the continuous spectrum of variability are particularly energetic fluctuations at the following periods:

(a) 3 to 5 days: Waves with this period are of special interest because they may be resonant. In the equatorial Pacific Ocean there are, at these periods, pronounced peaks in spectra of sea level fluctuations. Wunsch and Gill (1976) have proposed that these peaks correspond to the gravest equatorially trapped inertia-

gravity waves that have zero zonal group velocity, and that have the vertical structure of the first baroclinic mode. It follows that random forcing will excite these resonant modes. There happen to be energetic atmospheric waves, with the same temporal and spatial scales, in the equatorial Pacific, but Wunsch and Gill (1976) argue that their presence is not essential for the existence of the oceanic waves. Similar atmospheric waves exist in the equatorial Atlantic but here they appear to be entirely responsible for the energetic equatorially trapped inertia-gravity waves with periods between 3 and 5 days. These waves were non-resonant because they had a downward energy flux. The extremely rough ocean floor, due to the mid-Atlantic ridge, prevents the establishment of a standing first baroclinic mode. Curiously, the amplitude of the velocity fluctuations of these non-resonant waves in the Atlantic is substantially larger than the estimated amplitude for the Pacific. (Wunsch and Gill had sea level data only.) Current measurements are necessary in the Pacific to resolve this matter.

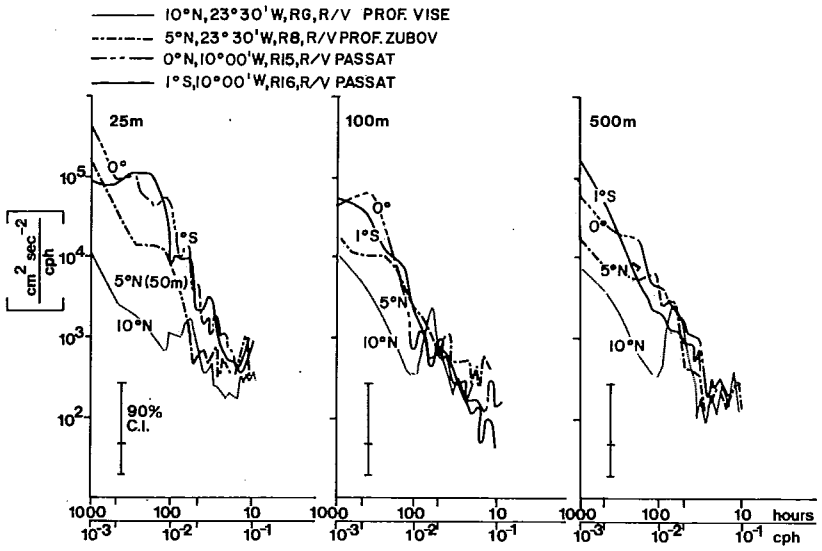

Figure 7.10 - Kinetic energy spectra of ocean currents at a number of locations (after Bubnov, Vasilenko and Krivelevich, 1980).

(b) 16 days: Figure 7.11 shows time latitude plots of the zonal (u) and meridional (v) velocity components as measured along 28°W and 29°W over the three-week period towards the end of July and in early August, 1974. The most striking feature is the meandering of the Equatorial Undercurrent about the equator. Note that the large values of u north of the equator are preceded by northward flow across the equator and large values of u south of the equator by southward flow. A similar pattern is more difficult to discern in the surface layers because the flow there is not symmetrical about the equator. From these figures the period of the oscillations is estimated to be between two and three weeks.

Spectra of 82-day time series of the meridional velocity fluctuations in the surface layers on the equator at 10°W have a strong peak at a period of about 16 days. Time-series measurements, at fixed points, of fields that are symmetrical about the equator, the zonal velocity component u and temperature T at the depth of the core of the undercurrent for example, show twice this frequency as the flow meanders back and forth past the observation point. Vertical phase differences are evident in Figure 7.11: the u fluctuations in the surface layers lead those at the depth of

the core of the Undercurrent by about one week. Time-depth plots of the v-components show an upward phase propagation of about 50 m day^{-1} (Düing et al., 1975). The fluctuations appear to be limited to the upper few hundred metres; there is a vertical decrease of amplitude by a factor of about four between the surface and 200m.

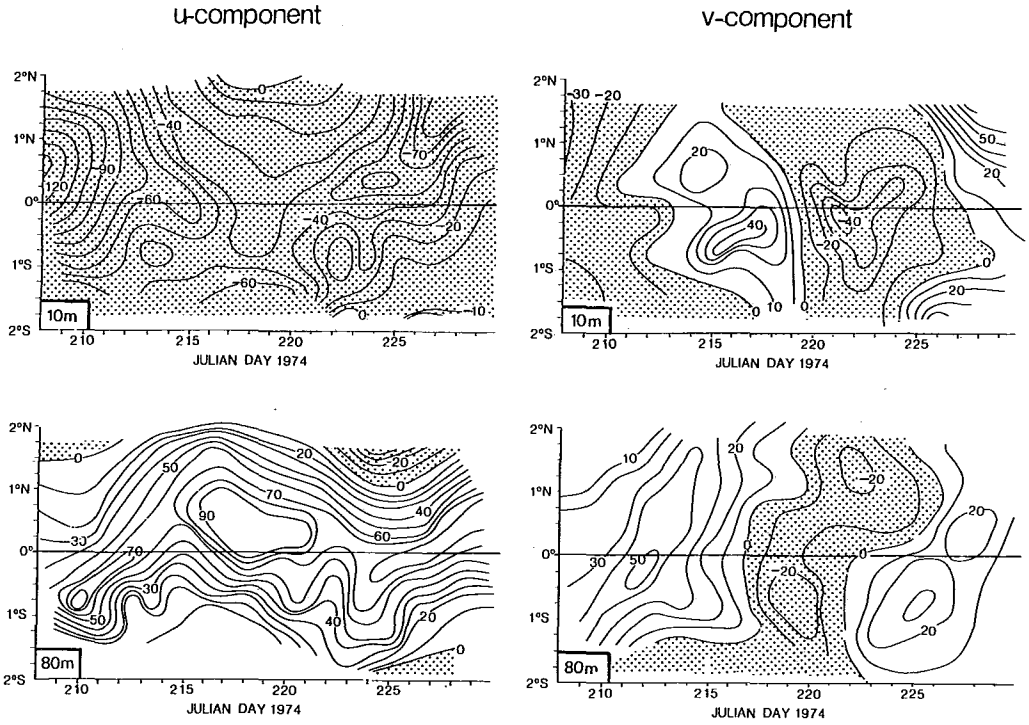

Figure 7.11 - Latitudinal and temporal fluctuations of zonal and meridional velocity components along 28°W (after Düing and Hallock, 1980).

Bubnov et al. (1980) have recently produced daily meridional sections for the three Phases of GATE along 23°30'W, based on current meter moorings, each equipped with ten current meters distributed from the surface to 1000m. Spatially, this data set is of similar density as the current profiling data set obtained by R/V ISELIN along 28°W. On the basis of these data sets Düing and Hallock (1980) estimate the most likely range of values for the east-west wavelength to be from 1750 km to 1980 km. They also show that coherent westward propagation along the equator over the entire distance from 10°W to 29°W is highly probable. Weisberg (1980) came to the same conclusion based on moored current meters at 10°W, 26°W and 28°11'W. The estimates of the scales of these fluctuations are necessarily approximate, since the time-series are insufficiently long and spatial resolution along the equator is inadequate. To make matters worse, there is the energetic bakcground spectrum of higher-frequency fluctuations, and an energetic 30-day oscillation to be discussed below. The time-series measurements of currents on the equator at 28°W and 10°W give more information about the scales, but only at a depth of 200m where the 16-day oscillation was much weaker than in the surface layers. Weisberg (1980) estimates the zonal wavelength of the 16-day wave at a depth of 200m to be approximately 1200 km. This is substantially less than the earlier mentioned value of about 1800 km. The difference between the estimates for the wavelength could be regarded as the range of possible errors.

The cause of these oscillations is yet to be explained. They are apparently not associated with instabilities of the mean currents.

(c) 30 days: The GATE data reveal that, near the equator, there is a westward propagating undulation with a period of about a month and a wavelength of approximately 1000 km. In the surface layers it is most intense in the neighbourhood of 3°N, the boundary between the westward South Equatorial Current and the eastward North Equatorial Countercurrent (Figure 7.1). Fluctuations on a similar time scale at 0°, 10°W are found to be deep-reaching, having a maximum in v and a minimum in u. Only the three months time-series records (current measurements along 10°W, 23.5°W and 28°W; the 100-day sea-surface temperature data set) provide information about this low-frequency wave. Since GATE, however, an array of moorings with current meters below the 500m level has been maintained in the neighbourhood of 0°, 4°W. The dominant signal in these long records is the same 30-day (1-month) wave (Weisberg et al., 1979). Oscillations with practically the same scales have also been observed in the eastern equatorial Pacific so that they appear to be common in the equatorial oceans.

The fluctuations in the surface layers of the ocean can be explained as an instability due to the large latitudinal shear between the South Equatorial Current and North Equatorial Countercurrent (Philander, 1978). This explains the large amplitude near 3°N. The unstable waves in the surface layers will radiate equatorially trapped waves, specifically Rossby-gravity waves, into the deep ocean. The 30-day waves measured at depth do indeed satisfy the dispersion relation of Rossby-gravity waves (Weisberg et al., 1979).

7.7 SEASONAL VARIABILITY

The seasonal cycle in the tropical Atlantic is sufficiently strong to appear as a trend in the GATE data. Studies of this low frequency cycle have motivated investigators to re-examine the historical data set so that a fair amount is now known about the seasonal cycle.

Between June/July and August 1974 the zonal pressure gradient in the upper ocean, along the equator in the western and central Atlantic, nearly doubled. This seems to be part of a seasonal trend from low values in the boreal spring to high values in mid-summer and autumn. This trend is paralleled by the zonal wind-stress over the western equatorial Atlantic (Katz et al., 1977). This result is remarkable because it suggests that on the seasonal time-scale, the response of the equatorial Atlantic is in equilibrium with the forcing function. This rapid adjustment of equatorial oceans to changing winds is, from a theoretical point of view, gratifying. The adjustment of the ocean is effected by planetary waves. In mid-latitudes the Rossby waves travel so slowly that the adjustment-time of that part of the ocean is estimated to be of the order of decades. This is how long it will take the Gulf Stream to respond to a change in the curl of the wind-stress over the North Atlantic for example. The speed of Rossby waves increases with decreasing latitude. There is furthermore a rapid Kelvin wave that is important in the adjustment of equatorial oceans. Theory suggests that the adjustment-time of the equatorial Atlantic Ocean should be of the order of 100 days. The GATE data confirm this result.

From a modelling point of view the changes in the large-scale density gradients have important implications. These changes are associated with an enormous horizontal redistribution of heat in the ocean. In the tropics this redistribution is so large that local changes in heat storage are practically unrelated to local fluxes across the ocean surface (Merle, 1980, see Figure 7.7). This is in contrast to the subtropics and mid-latitudes where local fluxes across the ocean surface can almost entirely be responsible for local changes in heat storage. It follows that whereas local one-dimensional models can often simulate upper ocean variability outside the tropics, such models fail in the tropics: there, simulation of sea-surface temperature variability is possible only with a model of the response of the entire ocean basin to atmospheric forcing.

An example of non-locally forced sea-surface temperature variations occurs in the Gulf of Guinea. Although upwelling in the Gulf is a seasonal phenomenon, the local winds parallel to the shore do not vary seasonally. It has been proposed that wind variations in the western equatorial Atlantic near Brazil change the seasonal modulation of sea-surface temperatures in the Gulf of Guinea. For a further discussion of this topic see Philander and Düing (1980) and Hisard and Merle (1980).

7.8 CONCLUSIONS

It seems appropriate to end this short review by comparing the obtained results with the objectives of the GATE Oceanographic Sub-Programme as described in GATE Report No. 8 (ICSU/WMO, 1974).

One goal had been the determination of surface fluxes from budget measurements in the mixed layer of the ocean. The data led to the conclusion that either long-term mean fluxes or the spectral properties of fluctuations in these fluxes can be related to the mixed layer heat content in the tropical Atlantic. It proved impossible, however, to obtain vertical surface flux variation estimates from local mixed layer heat budget data in a deterministic sense due to the dominating horizontal fluxes in the upper tropical Atlantic.

Another aim had been the determination of the oceanic response to atmospheric forcing on various scales, with projects concerned with the structure and with the currents in the upper ocean. It was recognized in the planning stage for GATE that such response studies would also require a description of the density structure and the kinematics of the tropical Atlantic. It is this group of topics where the most exciting and unexpected results were obtained.

The small-scale structure of the upper ocean being influenced by the peculiar atmospheric conditions and the large-scale slowly varying flow below the ITCZ is much better known now, particularly with respect to dominating scales in time and space. The knowledge about near-surface internal inertia-gravity waves was considerably improved, and vertical diffusion parameters were obtained in the ITCZ region as well as in the equatorial belt including the Equatorial Undercurrent.

One of the observational results that stimulated much theoretical work and further measurements after the GATE field phase was the detection of energetic periodic fluctuations in the equatorial current regime, particularly at about 16 and 30 days periods. It appears that these waves remove kinetic energy from the mean flow that is being driven by the large-scale wind stress field.

Another result, the detected trend in the change of the thermocline slope along the equator, incited studies on the seasonal cycle on the basis of GATE and historical data. It can be concluded that, on the seasonal time scale, the tropical Atlantic is in equilibrium with the varying winds. These changes are associated with an immense redistribution of heat in the ocean.

Although the major part of the GATE oceanographic analysis is finished, it can be anticipated that observational and theoretical results from this experiment will stimulate further studies of the tropical oceans. Last but not least, GATE provided a focus for joint research of meteorologists and oceanographers on a scale not known before, and the experience gained is already beginning to pay off in the World Climate Research Programme.

REFERENCES

Belevich, V. V., 1977: The distribution of heat balance components during the Atlantic Tropical Experiment. Meteorology and Hydrology, 12, pp. 88-94 (in Russian).

Bruce, J. G. and E. J. Katz, 1976: Observations in the Equatorial Atlantic during GATE, June and July 1974 from ATLANTIC II. Technical Report WHOI-76-54, 90 pp.

Bubnov, V. A. and V. D. Egorikhin, 1977: Study of large-scale current structure in the tropical zone of the Atlantic Ocean. Oceanology, 17, pp. 954-961 (in Russian).

_____, _____, Z. N. Matveeva, S. E. Navrotskaya and D. I. Filippov, 1979: Graphical presentation of the U.S.S.R. oceanographic observations in the tropical Atlantic during GATE (June to September 1974). Technical Report TR-79-1 University of Miami, 163 pp.

_____, V. M. Vasilenko and L. M. Krivelevich, 1980: The study of low-frequency variability of currents in the tropical Atlantic. Deep-Sea Research, GATE Suppl. 2 to Vol. 26, pp. 199-216.

_____ and V. D. Egorikhin, 1980: Study of water circulation in the tropical Atlantic. Deep-Sea Research, GATE Suppl. 2 to Vol. 26, pp. 125-136.

Cardone, V., H. Carlson, J. Ewing, K. Hasselmann, S. Lazamoff, D. Ross and W. McLeish, 1981: The surface wave environment in the GATE B/C-scale Phase III. Journal of Physical Oceanography, 11 (in print).

Clarke, R. A., 1980: Changes in the upper ocean within the C-scale array during Phase III. Deep-Sea Research, GATE Suppl. 1 to Vol. 26, pp. 115-127.

Cochrane, J., 1978: The North Equatorial Countercurrent system west of 40°W. Lecture presented at the GATE Symposium on Oceanography and Surface Layer Meteorology, Kiel, F.R.G.

Crawford, W. R. and T. R. Osborn, 1980: Microstructure measurements in the Atlantic Equatorial Undercurrent during GATE. Deep-Sea Research, GATE Suppl. 2 to Vol. 26, pp. 285-308.

Düing, W., P. Hisard, E. Katz, J. Meincke, L. Miller, K. V. Moroshkin, G. Philander, A. A. Rybnikov, K. Voigt and R. Weisberg, 1975: Meanders and long waves in the equatorial Atlantic. Nature, 257, pp. 280-284.

_____ (editor), 1980: Equatorial and A-Scale Oceanography. Deep-Sea Research, GATE Suppl. 2 to Vol. 26, 356 pp.

_____, F. Ostapoff and J. Merle (editors), 1980: Physical oceanography of the tropical Atlantic during GATE. University of Miami, Miami, Florida, 117 pp.

_____ and Z. Hallock, 1980: Equatorial waves in the upper central Atlantic. Deep-Sea Research, GATE Suppl. 2 to Vol. 26, pp. 161-178.

Elliott, J. A. and N. S. Oakey, 1980: Average microstructure levels and vertical diffusion for Phase III, GATE. Deep-Sea Research, GATE Suppl. 1 to Vol. 26, pp. 273-294.

Garrett, C. J. R. and W. Munk, 1972: Space-time scales of internal waves. Geophysical Fluid Dynamics, 2, pp. 225-264.

Hellerman, S., 1980: Charts of the variability of the wind stress over the tropical Atlantic. Deep-Sea Research, GATE Suppl. 2 to Vol. 26, pp. 63-75.

Helm, R., H. U. Lass and M. Sturm, 1980: Some peculiarities of the Atlantic Equatorial Undercurrent core structure and its variation in time and space. Deep-Sea Research, GATE Suppl. 2 to Vol. 26, pp. 249-259.

Hisard, P., J. Citeau and A. Morliére, 1976: The system of equatorial undercurrents, persistence and extension of the southern branch in the Atlantic Ocean. Cahiers ORSTOM Séries Océanographique, Vol. 14, 209-220 (in French).

_____ and J. Merle, 1980: Onset of summer surface cooling in the Gulf of Guinea during GATE. Deep-Sea Research, GATE Suppl. 2 to Vol. 26, pp. 325-341.

ICSU/WMO, 1974: The oceanographic sub-programme for the GARP Atlantic Tropical Experiment. GATE Report No. 8, 135 pp.

Käse, R. H. and D. J. Olbers, 1980: Wind-driven inertial waves observed during Phase III of GATE. Deep-Sea Research, GATE Suppl. 1 to Vol. 26, pp. 191-216.

_____ and G. Siedler, 1980: Internal wave kinematics in the upper tropical Atlantic. Deep-Sea Research, GATE Suppl. 1 to Vol. 26, pp. 161-189.

Katz, E. J., R. Belevich, J. Bruce, V. Bubnov, J. Cochrane, W. Düing, Ph. Hisard, H.-U. Lass, J. Meincke, A. de Mesquita, L. Miller and A. Rybnikov, 1977: Zonal pressure gradient along the equatorial Atlantic. Journal of Marine Research, 35, pp. 293-307.

_____, R. G. Bruce and B. D. Petrie, 1980: Salt and mass flux in the Atlantic Equatorial Undercurrent. Deep-Sea Research, GATE Suppl. 2 to Vol. 26, pp. 137-160.

Krishnamurti, T. N. and R. Krishnamurti, 1980: Surface meteorology over the GATE A-scale. Deep-Sea Research, GATE Suppl. 2 to Vol. 26, pp. 29-61.

Merle, J., 1980: Seasonal heat budget in the equatorial Atlantic Ocean. Journal of Physical Oceanography, 10, pp. 464-469.

Moore, D. W. and S. G. H. Philander, 1977: Modelling of the tropical oceanic circulation. In: The Sea, Vol. 6, Wiley and Sons, New York, pp. 319-361.

Perkins, H., 1980: Low-frequency forcing of the tropical Atlantic Ocean under the ITCZ during GATE. Deep-Sea Research, GATE Suppl. 1 to Vol. 26, pp. 225-236.

Peters, H., 1978: A compilation of CTD- and profiling current meter data from GATE 1974, F.S. "Meteor" and W.F.S. "Planet". Meteor Forschungsergebnisse, A, 20, pp. 49-80.

Philander, S. G. H., 1978: Instabilities of zonal equatorial currents: II. Journal of Geophysical Research, 83, pp. 3679-3682.

Philander, G. and W. Düing, 1980: The oceanic circulation of the tropical Atlantic, and its variability, as observed during GATE. Deep-Sea Research, GATE Suppl. 2 to Vol. 26, pp. 1-27.

Siedler, G., 1980: Heat and momentum transport in the upper ocean. Annalen der Meteorologie (Neue Folge), 15, pp. 114-120 (in German).

_____ and J. D. Woods (editors), 1980: Oceanography and Surface Layer Meteorology in the B/C-scale. Deep-Sea Research, GATE Suppl. 1 to Vol. 26, 294 pp.

TROPEX-74, Proceedings of the Soviet National Expedition on GATE Programme, 17/6-23/9 1974, Hydromet Publ. House (Gidrometeoizdat), Leningrad, 1976, Vol. I - Atmosphere, 736 pp., Vol. II - Ocean, 217 pp. (in Russian).

Vazquez de la Cerda, A. M., 1978: Fluctuation of salinity maximum of the North Brazilian Current and displacement of the high geopotential center. Lecture presented at the GATE Symposium on Oceanography and Surface Layer Meteorology, Kiel, F.R.G.

Weisberg, R. H., 1980: Equatorial waves during GATE and their relation to the mean zonal circulation. Deep-Sea Research, GATE Suppl. 2 to Vol. 26, pp. 179-198.

_____, A. Horigan and C. Colin, 1979: Equatorially trapped Rossby-gravity wave propagation in the Gulf of Guinea. Journal of Marine Research, 37, pp. 67-86.

Woods, J. D. and P. J. Minnett, 1979: Analysis of mesoscale thermoclinicity with an example from the tropical thermocline during GATE. Deep-Sea Research, 26 A, pp. 85-96.

_____, H. Leach and P. Minnett, 1981: The GATE Lagrangian Batfish Experiment: Data Report. Berichte Institut für Meereskunde, No. 89.

Wunsch, C. and A. E. Gill, 1976: Observations of equatorially-trapped waves in the Pacific Sea level variations. Deep-Sea Research, 23, pp. 371-390.

CHAPTER 8

A/B AND B-SCALE MOTION AND BALANCES IN THE ITCZ AREA

by

A. I. Falkovich

(Hydrometeorological Research Centre of the U.S.S.R.,
Moscow, U.S.S.R.)

8.1 INTRODUCTION

ITCZ is a most interesting subject in meteorology, first as for the origin of tropical cyclones that develop most frequently from tropical disturbances moving along the northern boundary of the ITCZ (Gray, 1975), and second, because of the role the ITCZ plays in the energy balance of the tropical zone. In the cumulus cloud ensemble of ITCZ a great amount of latent heat of condensation is released which considerably affects the energy balance of the tropical atmosphere. Besides, the ITCZ area is a unique region to study atmospheric physics. In this area atmospheric processes are expressed most conspicuously and are easier to classify and comprehend on the basis of mean observation values for each class.

Houghton (1977) summarized four theories for the formation of the ITCZ as follows:

(1) A result of either broad general circulation characteristics or the general tropospheric dynamics instead of some boundary layer-convective interaction.

(2) A result of direct ocean-atmosphere interaction.

(3) A product of zonally symmetric CISK (convective instability of the second kind) processes involving the planetary boundary layer (or mixed layer). Charney (1971) was an early proponent of this zonally symmetric thesis.

(4) A product of convective (CISK) and planetary boundary layer (mixed-layer) interactions with tropical wave systems.

The fourth conception is based on the so-called "critical latitudes" hypothesis (Holton et al., 1971; Yamasaki, 1971) according to which the ITCZ expands at the latitudes, where the Coriolis parameter is equal to the frequency of the wave disturbances. The data, obtained during the GATE, may to some extent demonstrate the closeness of these theories to reality.

8.2 CLASSIFICATION OF OBSERVATIONS IN ITCZ

At present the radiosonde data are not sufficiently precise to get by single measurement a reliable quantitative idea of the nature of the atmospheric processes even for a specially organized ship array. Averaging may be used to minimize the effect of measurement errors. The simplest is time averaging when mean values for the phase (month) or for the whole GATE period are used. However, to investigate the structure of the ITCZ and of the tropical disturbances moving along it, it is necessary to consider the cases of deviations from average conditions. For this purpose observations should be classified, particular weather classes over the

studied area identified and then the observations divided according to the class they belong to. All the observations which belong to the same class are averaged, and as a result a reference observation corresponding to the class is obtained.

In Petrossiants et al. (1976a) it is shown that data on cloudiness over the A/B ship array is enough to effectively divide multiple observations into two classes: developed ITCZ when a thick cloud band or a cloud eddy is present and depressed ITCZ when cloudiness is smoothed. In the same paper most informative parameters of such division are investigated using the discriminant analysis method. These parameters are used in Falkovich (1976) for a more detailed division of all observations of Phases I and III on A/B scale area into four classes: Class B (heavy clouds over the area), Class C (virtually clear sky) and two intermediate classes: D and E. Mean values and rms deviations of some atmospheric parameters were computed for each class. Most interesting are two extremes, B and C. The former corresponds to the presence of a strong disturbance over the ship array, the latter to the absence of any disturbance over it. The classification technique was described in greater detail in the book, Falkovich, 1979.

Reed et al. (1975) use a similar composition technique. They analyse the meridional component of the wind at the 700 mb level in the centre of the B ship array and one of 8 wave categories is ascribed to each observation (with three hours interval). The categories follow each other in numerical order, but one category may be repeated from one up to ten times. By averaging observations for each wave category, the authors derive the idea of the movement of the wave disturbance over the studied area. Classes B, D, E, C can also be considered as wave categories following each other. There are also some other averaging techniques. Thus, Frank (1978) when studying the life cycle of deep convective systems, divides observation times with a three-hour interval into seven stages in accordance with the development of a convective system. Augstein and Garstang (1977) describe and analyse several more classification methods. All the suggested methods of classification are eventually associated with the character of cloudiness over the area under study. Therefore, though outwardly different, these methods are nearly identical in their meaning and serve one and the same purpose: averaging of values within a certain class or a wave category helps to appreciably decrease errors due to measurement inaccuracies and to reveal the most typical features of the atmospheric processes.

8.3 ITCZ, ITS LOCATION AND MAIN FEATURES FROM OBSERVATION DATA FOR THE B AND A/B ARRAYS

The GATE data turned out to be very useful for an investigation of ITCZ. It is especially true for the observational material over the GATE B and A/B ship arrays. Indeed the choice of ship arrays has proved to be most successful: during all the three phases of observations, ITCZ cloudiness, the wind convergence line at sea level, maximum precipitation area and maximum sea-surface temperatures as a rule were located within the A/B ship array. Figure 8.1 demonstrates mean atmospheric characteristics obtained by observations during Phases I, II and III from the A/B ship array (Falkovich, 1979). For the Phase I here are also presented isobars at sea level, the axis of the trough and mean rainfall as determined by the ship radars of the B ship array. These data obtained by Seguine et al. are given in Houghton (1977). Figure 8.1 reveals the following main peculiarity: the cloudiness and precipitation are concentrated to the south of the trough and of the wind convergence line at sea level. This is confirmed by Figure 8.2, taken from Estoque and Douglas (1978), where they have processed 25 cases of Phase II observations when cloudiness looked like a band oriented from W to E.

Phase I

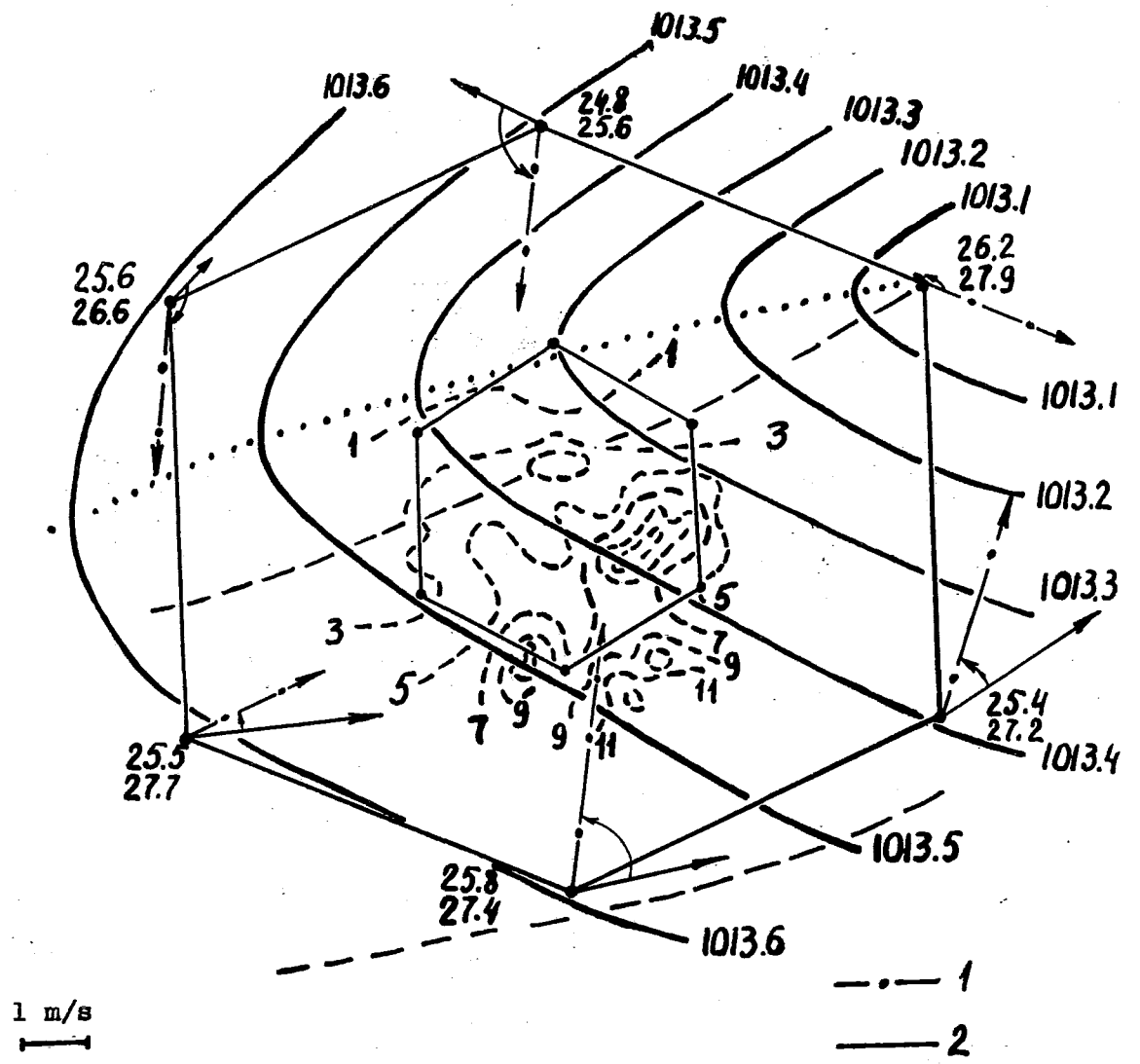

Figure 8.1a - Mean atmospheric characteristics for Phase I from the A/B ship array. At the hexagon vertices velocity wind vectors at sea level (1) and 850 mb (2) are indicated. In figure columns: the top figure - air temperature at sea level; the bottom one - surface ocean temperature. The broken line shows the mean value for the position of the northern and southern boundaries of the ITCZ cloudiness. Also given are isobars at sea level, the axis of a pressure trough (dots) and precipitation rate according to radar data in mm per day (dashes).

Phase II

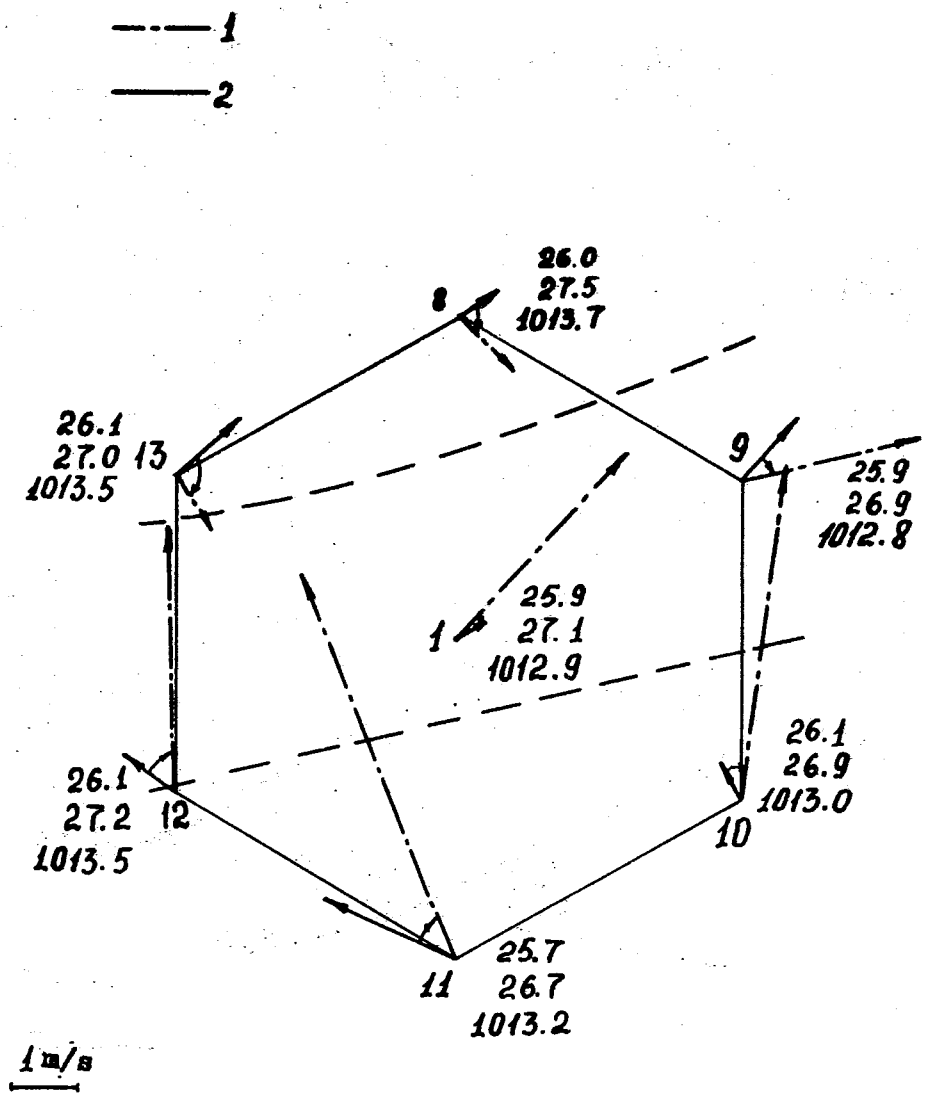

Figure 8.1b - Mean atmospheric characteristics for Phase II from the A/B ship array. At the hexagon vertices numbers of ship locations are indicated as well as velocity wind vectors at sea level (1) and 850 mb (2). In figure columns: the top figure - air temperature at sea level; the middle one - surface ocean temperature, the bottom one - pressure at sea level. The broken line shows the mean value for the position of the northern and southern boundaries of the ITCZ cloudiness.

Phase III

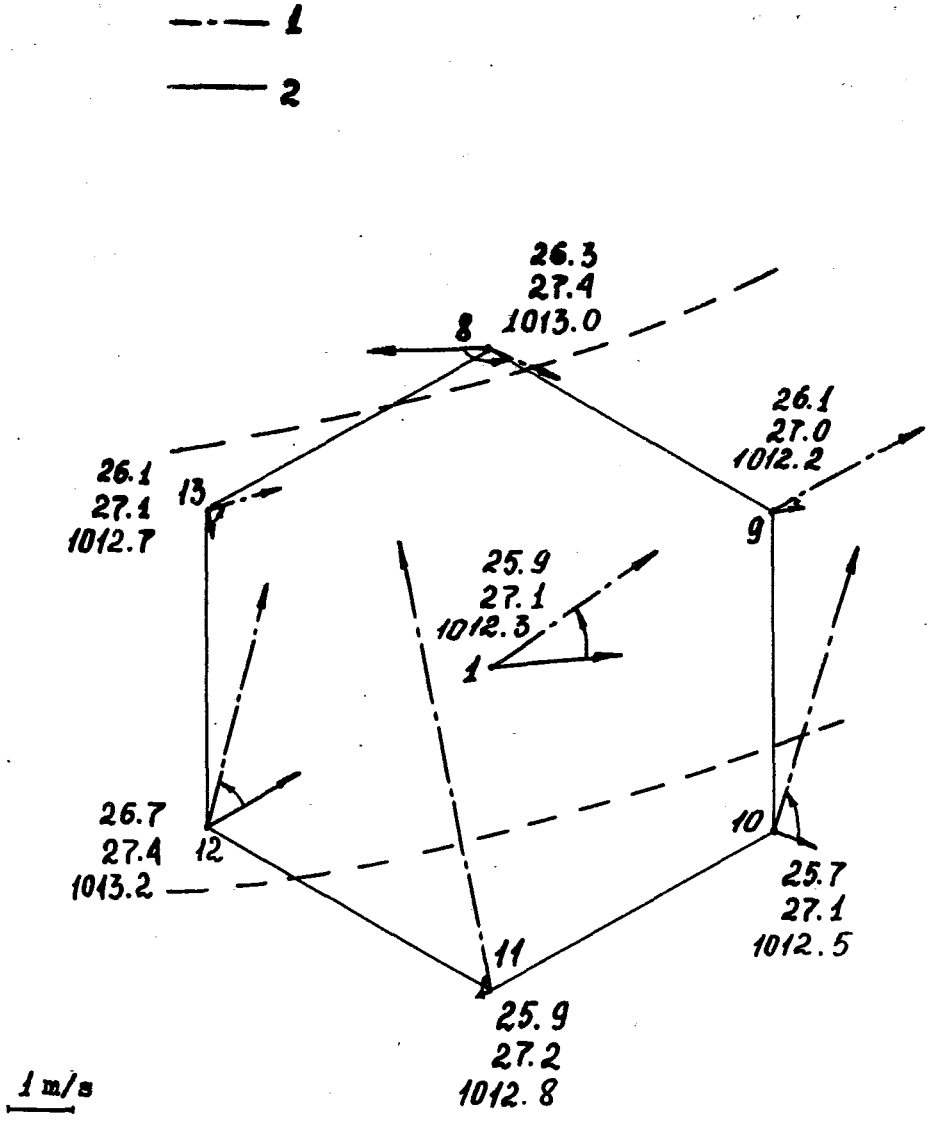

Figure 8.1c - Mean atmospheric characteristics for Phase III from the A/B ship array. At the hexagon vertices numbers of ship locations are indicated as well as velocity wind vectors at sea level (1) and at 850 mb (2). In figure columns: the top figure - air temperature at sea level; the middle one - surface ocean temperature, the bottom one - pressure at sea level. The broken line shows the mean value for the position of the northern and southern boundaries of the ITCZ cloudiness.

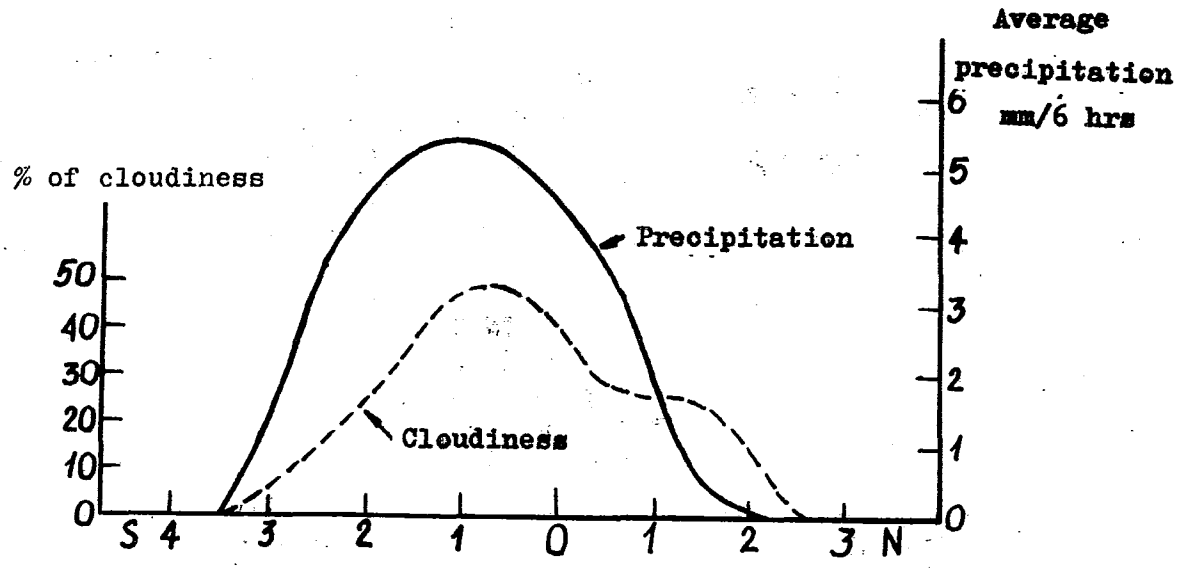

Figure 8.2 - Cloud and precipitation distribution with reference to the wind convergence line at sea level.

The 0-latitude corresponds to the convergence axis of trade winds at sea level. Figure 8.2 shows clearly that the area of maximum rainfall and cloudiness is 1-2° to the south of the surface confluence axis. The same is true for the area of maximum large-scale upward motions. It lies 2° to the south of the convergence line and this is convincingly illustrated by Figure 8.3, that shows a meridional cross-section along 23.5°W obtained by averaging observations for 17 days (during the Phase III from the ship and land stations of the A scale (Falkovich, 1979)). Thus, it is undoubtedly demonstrated that the cloudiness is concentrated to the south of the wind convergence line at sea level, i.e. clouds basically form in the air mass of southern trade winds. This phenomenon so far has not been fully explained. One of the possible explanations is that the air mass of the northern trade wind is drier because it comes partially from Africa and its travel over the colder part of the ocean is short whereas the southern trade wind's travel over the ocean is rather long.

Krivelevich and Romanov (1978) give another explanation of latitudinal shift of the equatorial trough and maximum updraft zone. They show the results of numerical calculations of the equatorial circulations using the stationary atmospheric zonal model with prescribed meridional air pressure. These calculations indicate that when the equatorial trough axis is located at 10-12°N the maximum updraft zone would be shifted 2-3° of latitude closer to the equator. However, when the trough axis is at 2-5° of latitude the maximum updraft zone should be 2-3° of latitude further from the equator then the trough axis.

Bearing in mind that similar calculations lacking advective terms in the equation of motion do not reveal the above effect in the air mass distribution the authors come to the conclusion that the above mentioned effect is closely related to advective terms and hence to the wind flux inertia near the equator.

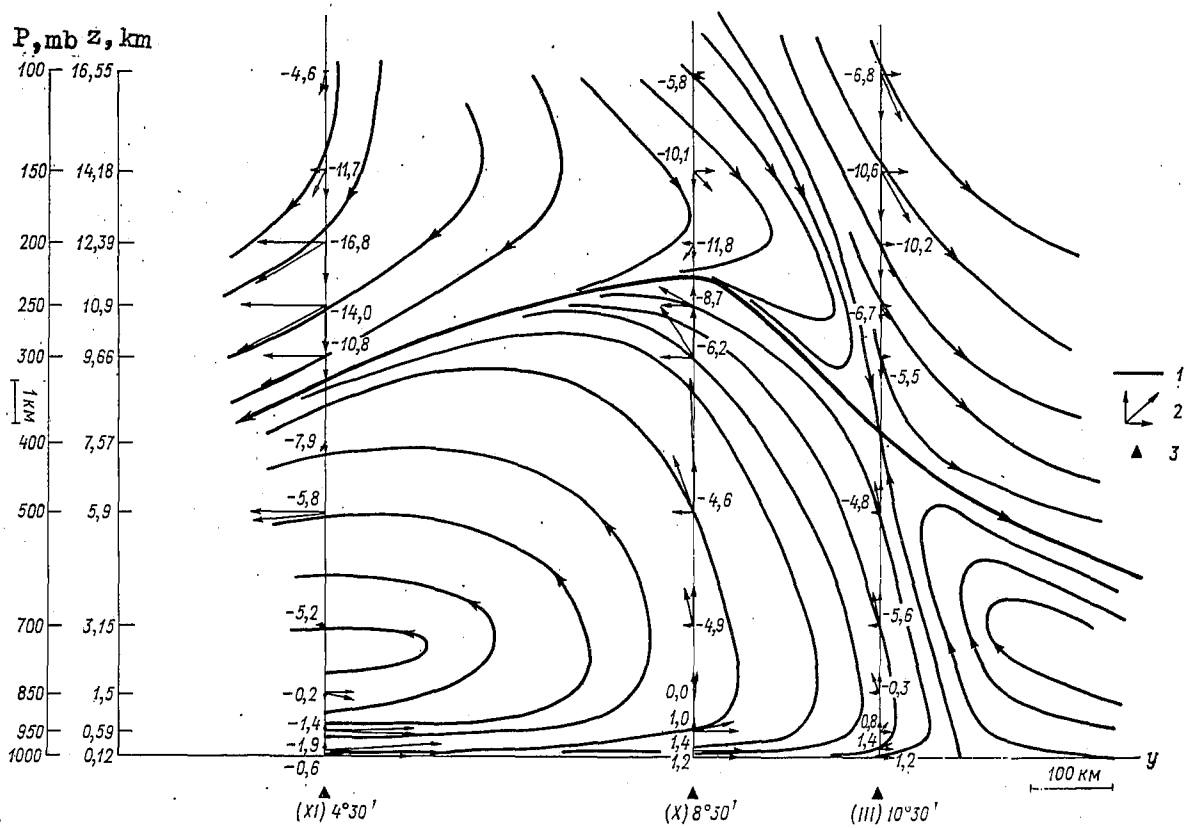

Figure 8.3 - Mean meridional cross-section of the tropical atmosphere along 23.5°W for Phase III. 1) stream lines in the meridional plane; 2) vectors of meridional, vertical and their resulting wind velocity; 3) latitudes, for which computations have been made.

Now let us describe the thermal structure of ITCZ. The presence of the thermal core in the upper troposphere is a typical feature of tropical cyclones. Tropical disturbances which spread along the ITCZ during GATE are noticeably weaker. The analysis of mean values has not revealed any well-expressed thermal core in the upper troposphere of the ITCZ. The cold core in the lower troposphere which has been earlier found in the ITCZ over the Pacific, according to mean data is not practically noticeable either. Estoque and Douglas (1978) used the composition technique to study the air temperature at the meridional cross-section of the ITCZ. In this cross-section one may see a very weak thermal core at 500 mb level, all values for this core being within measurement errors. The investigation of the structure of wave disturbances in the ITCZ (Thompson et al., 1979) over the trough shows a cold core both in the lower and upper troposphere, and a warm one in the middle troposphere. Temperature deviations here are up to several tenths of a degree. Over the trough especially in the middle troposphere moisture maximum can be also found.

In Reed et al. (1975) data are presented of airborne observations on 4 August at the level of 1,100 feet, i.e. in the mixing layer. Here in the ITCZ area one may see a well-marked cold core: temperature in the ITCZ is by 1° lower than at its boundaries. The cold core in the mixing layer evidently is related to the evaporation of precipitation.

The investigation of the mean temperature and moisture values over the A/B ship array (Falkovich, 1979) shows that practically they do not change during their transfer from Class B to Class C, though divergence and vertical velocity change greatly. Thus we should not evaluate the atmospheric conditions by mean stratification values for the A/B scale area whereas dynamic parameters characterize the situation correctly. The cloudy band of the ITCZ spreads along the meridian at $2\text{-}4^{\circ}$ whereas the A/B ship array covers 7°. Even in Class B a considerable part of the ship array is within the zone of trade winds activities. To the north and south of the cloudy band compensating downward motions are frequently observed that can "dry up" the atmosphere appreciably more than it gets moistened in the zone of upward motions (Falkovich, 1979, section 18). That is why the mean moisture for the ship array is not necessarily higher in the presence of thick cloudiness over it than in its absence. This should be kept in mind when parameterizing moist convection in models with 300-400 km grid mesh (the A/B ship array may be considered to be a cell of such a grid). But stratification in these parts of the A/B ship array with clear sky is necessarily different from stratification in the parts where heavy cloudiness dominates. Figure 8.4 taken from Falkovich (1979) presents Phase I averaged static energy profiles of moist and saturated air for the northern ship "ACADEMICIAN KOROLEV" (position 8) located within the zone of northern trade wind activities, and for "ERNEST KRENKEL" ship (position 10), that registered a rainfall maximum during the Phase I. In both cases the atmosphere is conditionally unstable. But convection at position 8 is not possible, because the atmosphere there is convectively stable, and at position 10 according to the data averaged for the entire phase convection can reach the 175 mb level.

Frank (1977) presents very interesting data. He has studied a deviation of temperature and relative humidity from their mean values for the B and A/B ship arrays for different life cycle stages of the convective systems. Stages follow with three-hour intervals. It turned out that as convection is developing, heating is observed in the upper troposphere, cooling in the lower levels and moistening in the middle levels. Heating in the upper troposphere preceeds the development of deep convection. Naturally, the conditions of stability change, that is clearly seen in Figure 8.5 taken from the same paper by Frank where changes are shown of θ_e and θ_e^* for the period from the convection start moment to its peak (for 12-18 hours) for four most interesting convective systems over the B-scale area. Figure 8.5 shows that during the transition from clear sky to deep convection, the convective instability grows rapidly (Falkovich, 1979, section 4). With the development of convection the mixed layer gets thinner and its moisture content lower. On the average for the entire troposphere thickness heating and moisture changes during convection development are close to zero.

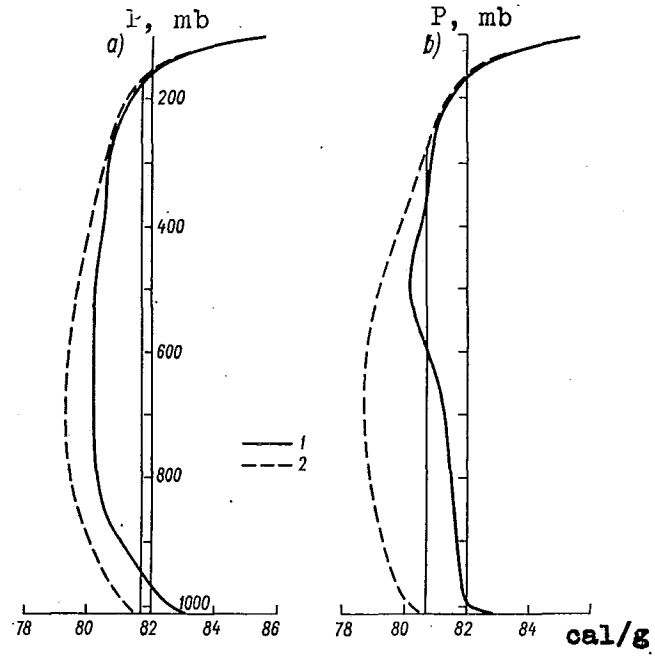

Figure 8.4 - Mean Phase I vertical profiles of $h = c_p T + gz + Lq$ (2) and $h^* = c_p T + gz + Lq^*$ (1) for the ships "ERNEST KRENKEL" (a) and "ACADEMICIAN KOROLEV" (b).

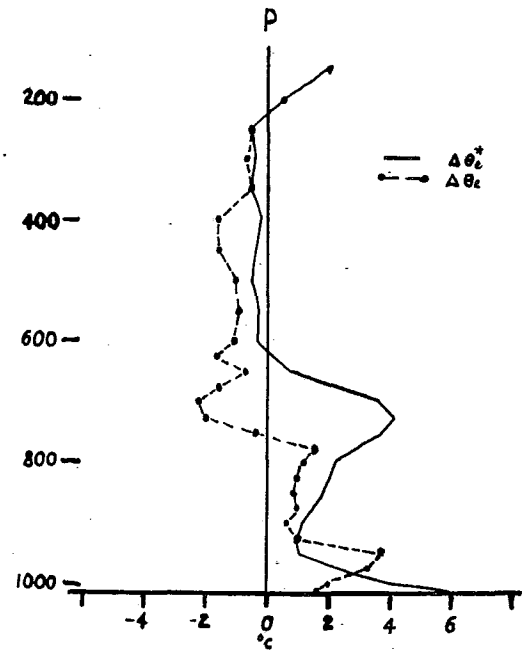

Figure 8.5 - Differences between Θ_e and Θ_e^*, suppressed minus peak activity period.

8.4 EASTERLY WAVES AND DISTURBANCES IN THE ITCZ

At present there is hardly any doubt that the ITCZ in spite of its negligibly small width (2-4° along the meridian) is a link in the general circulation of the atmosphere. The ITCZ is an area of confluence of two most steady circulation systems - trade winds of the Northern and Southern Hemispheres; the ITCZ is clearly seen on averaged weather charts and readily obtained in the general circulation models of the atmosphere. The averaged pattern (for a month, a season) of the ITCZ cloudiness is a continuous band across the Atlantic and Pacific which is nearly parallel to the equator. Murakami (1979) has got interesting results as to a mean cloud pattern for the whole GATE period over the A ship array by processing the satellite brightness measurements in the infrared spectrum. Maximum brightness (the greatest cloud height) is observed in eastern part of the Atlantic near the African coast. Here lines of equal brightness reveal the centre with co-ordinates 10°N, 17.5°W. The brightness "ridge" is located somewhat to the south of the trade wind convergence line and crosses the A/B ship array. Note that even averaging for 100 days has not smoothed this maximum to any great extent. Besides the mean pattern, Murakami has also obtained a meridional-temporal cloud brightness diagram for all three GATE phases. This diagram shows that all the cloud clusters move west and that deep convection much more frequently occurs in the East than in the West Atlantic. The diagram clearly shows that an increase of convection is caused by synoptic-scale disturbances with a period of 3.5-4 days. The same was noticed by Reed et al. (1977) who demonstrated that there is a close correlation between ITCZ precipitation and synoptic-scale disturbances moving from east to west.

In addition to synoptic-scale disturbances Murakami (1979) provided evidence of the presence of diurnal IR variations. The greatest variation turned out to happen near the centre of the maximum convective activity.

According to Murakami maximum convection at the centre occurs at about 1800 hours local time. Over the A/B ship array it is also observed in the evening, not in the morning as in other oceanic areas, for example in the Pacific (Ruprecht and Gray, 1976). That this fact is not accidental is confirmed by studies of diurnal divergence variations at 200 mb, of vertical velocity in the mid-troposphere, of turbulent energy fluxes from the ocean into the atmosphere and of other meteorological phenomena for the A/B ship array (Gray and Jacobson, 1977; Petrossiants and Falkovich, 1977; Falkovich, 1979).

The mechanism of this phenomenon is not yet clear. We can only suppose that this is related to the time difference caused by a disturbance "travelling" from the centre of the maximum convective activity to the area under study. For example, it takes about one day for a disturbance to cover the distance between maximum of diurnal variation at the convective activity centre and the centre of the A/B ship array.

It is interesting to note that as it appears from Murakami (1979) diurnal variation to the north and south of the A/B ship array is quite different from diurnal variations over the array. Thus, to the south-west of the array even an evening brightness minimum was registered. This can be attributed to the fact that at the time of maximum convection development over the A/B ship array there are compensation downward motions around it that suppress convection development. A similar picture is observed over the convective activity centre and its surroundings.

The question is why this centre is located just in this place? In our opinion it is not worth looking for any special reason such as, for example, is suggested by the hypothesis of "critical latitudes" that generate tropical disturbances. To all appearances this may be responsible for all the mechanisms of instability that generate disturbances of synoptic scale in moderate latitudes, and first of all baroclinic and barotropic instability, though Charney (1971) excludes baroclinic

instability. He explains this exception by the fact that horizontal temperature gradients in the tropics are small, besides tropical depressions are most frequently observed over oceanic tropical regions where temperature is distributed most evenly. Indeed, horizontal temperature and pressure gradients decrease the nearer they are to the equator. When observing one and the same disturbance in different latitudes (Falkovich and Yurko, 1976) one easily sees that the pressure gradient needed to sustain the disturbance, decreases as it approaches the equator. Thus an eddy of 500 km radius with a wind velocity of 10 m/s or so in the ITCZ corresponds to pressure gradient of 1 mb per 5^{o}. This is just the gradient observed in nature (Figure 8.1).

In the tropics like in moderate latitudes there are areas where instability manifests itself most conspicuously and where disturbances are borne most frequently. Usually these are frontal areas. So in our case the maximum convective activity centre is located where two air masses (dry from Sahara and moist air mass from Guinea Bay) converge. Here temperature gradients for the tropics are great enough. It is interesting to note that the temperature gradient near the maximum brightness at sea level is directed to the north over land, and to the south over the ocean.

As a result of strong Saharan surface heating along a wide belt east of the maximum convective activity centre between 10^{o} and 20^{o}N, the temperature difference equals about 10^{o}. Though a weak cyclone is located at sea level over Sahara, higher up already at 700 mb level the pressure gradient for this zone is directed to the north. This pressure gradient causes an easterly jet at 15^{o}N near 600-700 mb level. Contrary to the middle latitudes here an easterly jet stream is found, for here it is warmer in the North than in the South. In the southern part of the jet where maximum cyclonic vorticity is observed conditions are created for a barotropic instability. Vertical wind shears near the jet are not weak either and may lead to the formation of baroclinic instability. It is here that easterly waves are generated. Judging from the observations available mean wave length is about 2,500 km with a period of 3-4 days. It is very difficult to trace an easterly wave by pressure field variation: for so close to the equator pressure variations are very small and comparable with measurement errors. Therefore the wave is traced either by cloud field formed in the trough part of the wave, i.e. where the deviation from the mean vorticity is cyclonic (because of this clouds often had inverted-V patterns), or by the meridional wind component. In front of the trough the meridional component is northern, behind it southern in the trough and at the ridge it is nearly zero.

An easterly wave created by barotropic and/or baroclinic instability moves westward reaching maximum amplitude values, i.e. maximum development of disturbances associated with this wave near the maximum convective activity centre.

The cluster motion (though as a rule it develops in the trough side of the wave and is associated with the wave) may differ from the motion of the proper wave. A disturbance over sea travels slower than over land. This is evidently associated with greater temperature gradients developed over land and, consequently, with greater pressure gradient, than over sea. In rainfall the surface and overlying air temperatures over land may drop more than over sea. Maybe this is why squall line clusters are mainly observed over land. As a rule the clusters move westward (southwestward) at speeds of 6-8 m/s. If they form a cloud belt, it is as a rule extended from the west to the east. Squall line clusters usually form a bright cloud belt extended mainly from the north to the south, i.e. perpendicular to the propagation direction. These clusters move at a speed two times higher than the mean flux (higher than wind velocity at any level).

Why it is so is not yet clear, though some GATE data for squall line cluster structure (chapter 4 of the Monograph) inspire some assumptions on this. The front of squall lines is followed by a thickness of cumulo-nimbus tower which is maintained by the warm convective-unstable air moving up ahead of the front. Behind the tower

a downward flux of cold saturated air is formed that on approaching the underlying surface divides into two parts, one of which is oriented towards the front, the other away from it. With the growth and development of the tower, pressure gradient behind the front increases and the front-oriented flux grows too. This flux goes farther under the tower, the front moves on and the upward motions in the back of the tower are weakened since the cold flux has cut it off from the warm air supply, but in front of the tower these motions are strengthened and swallow up new areas unsuppressed so far. When the velocity of the cold flux moving towards the front becomes high enough, the flux may skip under the tower with the frontal division skipping ahead of the tower. As a result the tower is deprived of the supply of the warm air. At the frontal division the formation of a new tower begins. The old one gradually dissipates and adjoins the old exhausted ones in an elongated anvil. Thus we can see that the squall line cloud belt travels faster than the mean flux and its movement sometimes becomes irregular and spasmodic.

The disturbance reaches its maximum development near the convective activity centre (Murakami, 1979) then moves further westward and, generally speaking, it escapes the cyclogenesis area. At the ocean surface the temperature gradient is small and has opposite direction. Indeed by the lower tropospheric easterly jet stream and by the predominating easterly wind in the middle troposphere the properties of the cyclogenesis area are carried a long way westward along the flow. Of course, both jets are weakened while the greater part of the disturbances of African origin are gradually also weakened and then fully decay. Only very few of them are able to reach the western coast of the ocean to acquire new strength there and develop into tropical cyclones.

8.5 THE ITCZ ATMOSPHERIC DYNAMICS

Specific features of the ITCZ atmospheric dynamics are evident in the cross-sections which go along and through ITCZ as they are constructed (Petrossiants et al., 1976b, 1977) for Phases I and III. Calculations have been made for quadrangles formed by ships or by land sounding stations. It was supposed that the circulation along the cross-sections (the meridional cross-section spreads from the equator to 20°N along 23.5°W) is mainly determined by the state of the ITCZ atmospheric process, i.e. in the B and A/B scale areas. This is just what has been confirmed by calculations. The observation data were divided into two classes: a developed ITCZ (heavy clouds over the A/B ship array) and a depressed ITCZ (clouds over the ship array are smoothed out). Mean values of the three wind components have been computed for each class. When the ITCZ is developed the upward motions cover an area from 6° to 13°N and spread from sea level up to 100 mb layer. North of 13°N and south of 5°N there exist zones of downward compensating motions. Of course, each particular sounding gives a considerably narrower area of upward motions for the developed ITCZ. In the depressed ITCZ very weak upward motions are only observed in the lower troposphere, while all the part is occupied by downward motions with an area of marked divergence in the middle troposphere. In both cases just above the ship array at 200 mb level there is an upper-tropospheric eastern jet stream. In the presence of heavy clouds it is more emphasized. This stream generates over the South-East of Asia, spreads over Africa and goes out into the Atlantic. As supposes (M.A. Petrossiants) it is an element of the general atmospheric circulation and is formed in the southern side of high-altitude anticyclones generated in summer over the Tibetan plateau and the Sahara. In both cases near the 600 mb level at 15°N there is a lower-tropospheric eastern jet stream as well. It is less emphasized than the upper-tropospheric jet, but it may be the cause of the zone of barotropic instability near the ITCZ.

Westerly winds with a maximum near the 850 mb surface dominate over the ship array in the developed ITCZ class up to 700 mb. In cases of a depressed ITCZ, speeds of western winds and the layer they occupy decrease considerably, i.e. with strengthening of westerns, processes of convection in the ITCZ also enhance. Let us consider cases of the occurrence of deep disturbance over the ship array (Class B) and of fully depressed ITCZ (Class C).

Shown in Figure 8.6 is the divergence profile on the A/B scale area. First it should be noted that the divergence values are rather great though they are obtained by averaging 20-25 observation times and a ship area with a 3.5° radius.

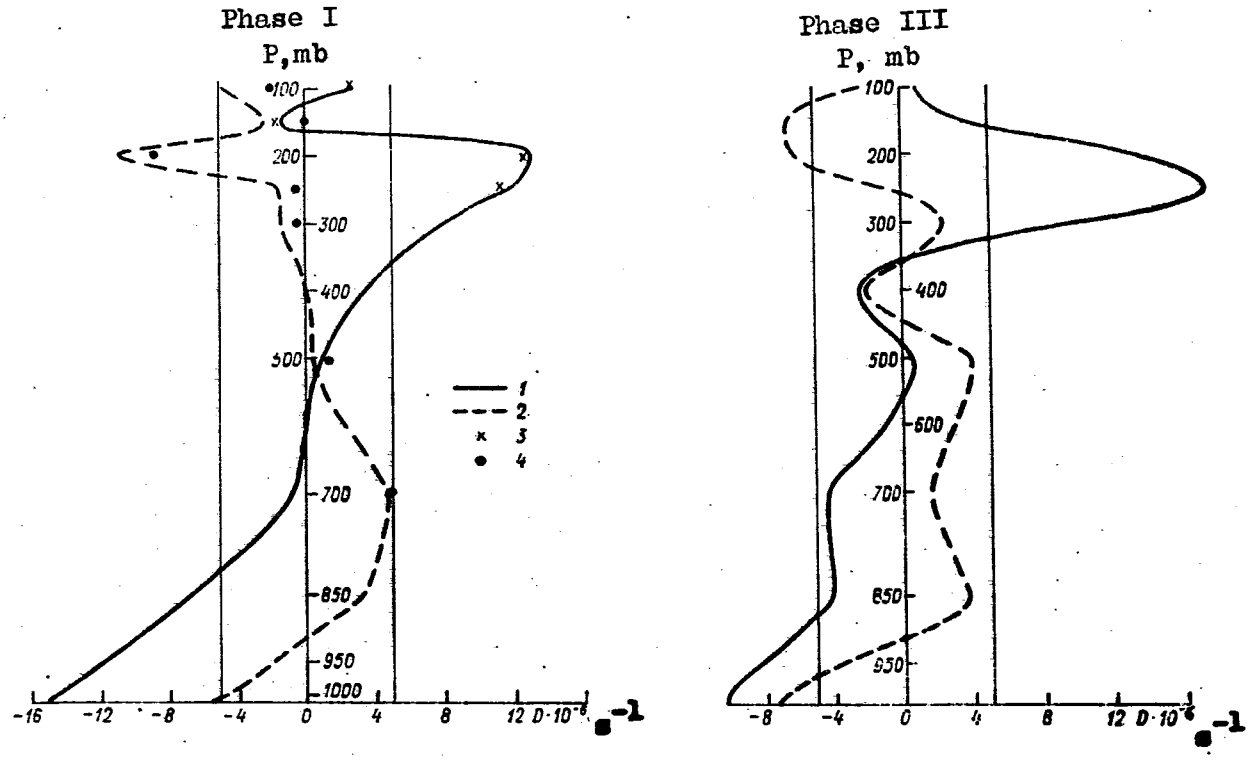

Figure 8.6 - The mean Phase I and III A/B ship array wind divergence profiles. 1) for Class B; 2) for Class C; 3) Class B divergence values without correction; 4) as previous but for Class C.

Wind convergence caused by converging trade winds is dominant in both classes up to a 950 mb level. But the values of convergence in Class B are considerably greater. Under heavy cloudiness (Class B) wind convergence is traced up as far as the 600 mb level. In Class C divergence is observed from 800 to 500 mb, whereas in the rest of the troposphere, convergence is to be seen. Greatest differences in divergence values for both classes are observed at 200 mb level. This is why divergence at this level proved to be the most informative characteristic for dividing all observation times into classes of developed and depressed ITCZ (Petrossiants et al., 1976a).

Likewise, the vertical velocity is different in both classes (Figure 8.7). In Class B upward motions over the A/B scale occupy the whole thickness of the troposphere, with the maximum values of 4-4.5 cm/s in the 400-300 mb layer. In Class C upward motions are observed in the lower troposphere up to 800-700 mb. They are weak and hardly exceed 0.25 cm/s. The rest of the troposphere is occupied by downward motions with their maximum near 250 mb surface. Note that this maximum is not located precisely enough as the calculations have been made for the conditions that $\omega = 0$ on a 100-mb level, for which purpose the divergence values are corrected by the method described in Falkovich, 1979. The correction value is clear from Figure 8.6. Shown in Figure 8.8 are relative vorticity profiles in Classes B and C.

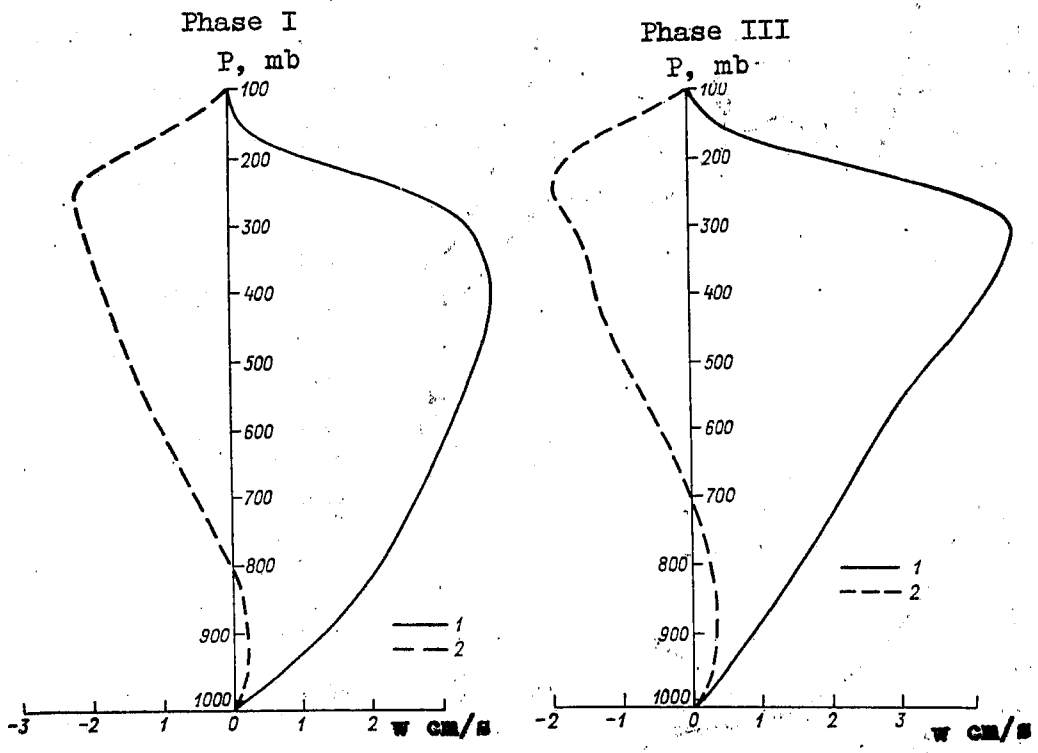

Figure 8.7 - Vertical component of wind velocity for Phases I and III of the A/B ship array observations. 1) for Class B and 2) for Class C.

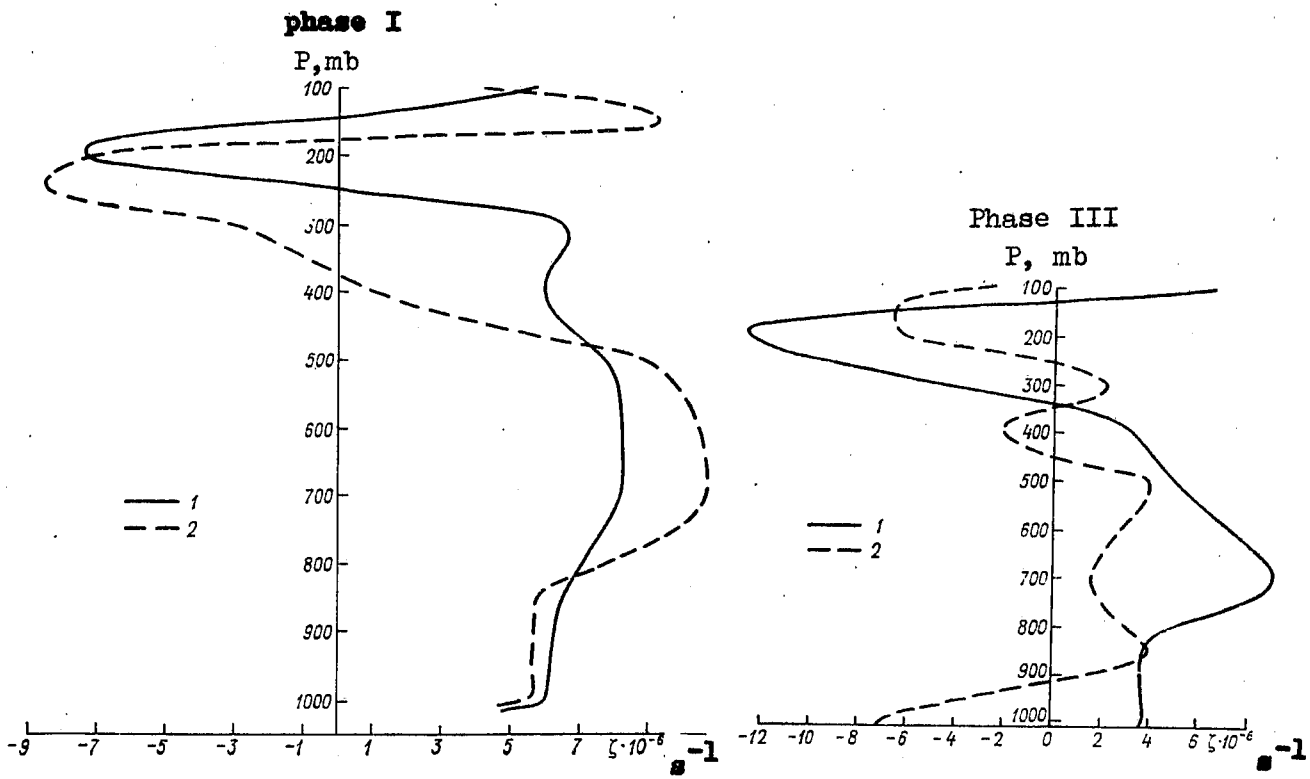

Figure 8.8 - Relative vorticity for Phases I and III of the A/B ship array observations. 1) for Class B and 2) for Class C.

For Phase I they differ but slightly. The difference between them is more noticeable in Phase III, where in the mixed layer in Class C the vorticity is anticyclonic, whereas in Class B it is cyclonic. In the upper troposphere, the layer with an anticyclonic vorticity is considerably thicker, and the maximum values of the vorticity in Class B are two times higher than in Class C. It is probably caused by a different location of ITCZ over the ship array in Phase I and Phase III: in Phase I almost all the northern half of the ship array found itself in the zone of the northern trade winds activity.

In Gray, 1977; Thompson et al., 1979; Falkovich, 1979; Cho et al., 1979, profiles of divergence, vorticity wind velocity are discussed in greater detail. Thus, there the results obtained in the Atlantic are compared with those in the Pacific. A much greater vertical zonal wind shear, with the maximum cyclonic vorticity in the middle troposphere is observed in the Atlantic, which might be explained by the existence of a middle-tropospheric jet stream.

When studying the wind field in the ITCZ area, besides trade winds in the lower troposphere, anti-trade wind streams have been observed (Figure 8.9) at 200-300 mb levels. The ships located north of the wind convergence line at sea level have the northern wind component, south of it they have the southern one. Note the wind veering with altitude in the 300-200 mb layer, i.e. near the upper-tropospheric eastern jet stream. One can assume (Falkovich, 1979) that near the jet stream axis there is a high turbulence zone and that the vertical wind shear is to some extent caused by the force of turbulent friction just like it is in the boundary layer near the underlying surface. In the Ekman boundary layer small-scale turbulent friction brings about vertical wind shear and causes air masses to flow into a low pressure area (a cyclone, a trough). Being close to the Equator, the boundary layer in the ITCZ might be different from the Ekman layer but as shown in Figure 8.1 wind veering with altitude therein also results in air masses flowing into the trough which brings about high absolute values of divergence. Other typical features of a boundary layer are: diurnal variation of meteorological parameters; high vertical gradients of wind, temperature and other atmospheric parameters. In fact, all these features are to be observed in the high-turbulence layer near the axis of the upper-tropospheric jet stream.

Here we come across maximum absolute values of divergence, rather great diurnal variations (Gray and Jacobson, 1977; Petrossiants and Falkovich, 1977; Falkovich, 1979), high vertical wind gradients, vertical wind shear. Besides, the shield of cirrus clouds covering a tropical disturbance frequently lies near a 200 mb surface. The cooling of the upper boundary of cirrus can bring about considerable temperature gradients. With the above-mentioned in mind, this high gradient zone can be referred to as the upper boundary layer of the atmosphere. One can notice that when simulating tropical cyclones the upper boundary layer is implicitly included. It is formed near the upper wall of the model either because of computed viscosity or the growth of the turbulence coefficient.

8.6 HEAT BALANCE AND SEA-SURFACE TEMPERATURE

As mentioned above, the ITCZ is not only characterized by convergence in the lower troposphere, by heavy cloudiness and a pressure trough, but also by a maximum temperature of the sea surface. It is known from observations that an average ITCZ location migrates together with the thermal equator (maximum of sea-surface temperature), therefore the latter is always shifted from the geographic equator towards the ITCZ. From Figure 8.1 one can see that the maximum of water temperature during the GATE is in the A/B ship array. Krishnamurti et al. (1976) has investigated this problem in greater detail. He has computed a mean value of the distribution of the surface water temperature for 100 days of the GATE with a wide zone of the temperature maximum near the ITCZ. The maximum location varies but little from phase to phase though this maximum moves north following the seasonal ITCZ shift (see Figure 8.1) and somewhat increases during the GATE. Analysis has shown that there exist local temperature changes of $1^{\circ}C$ per week.

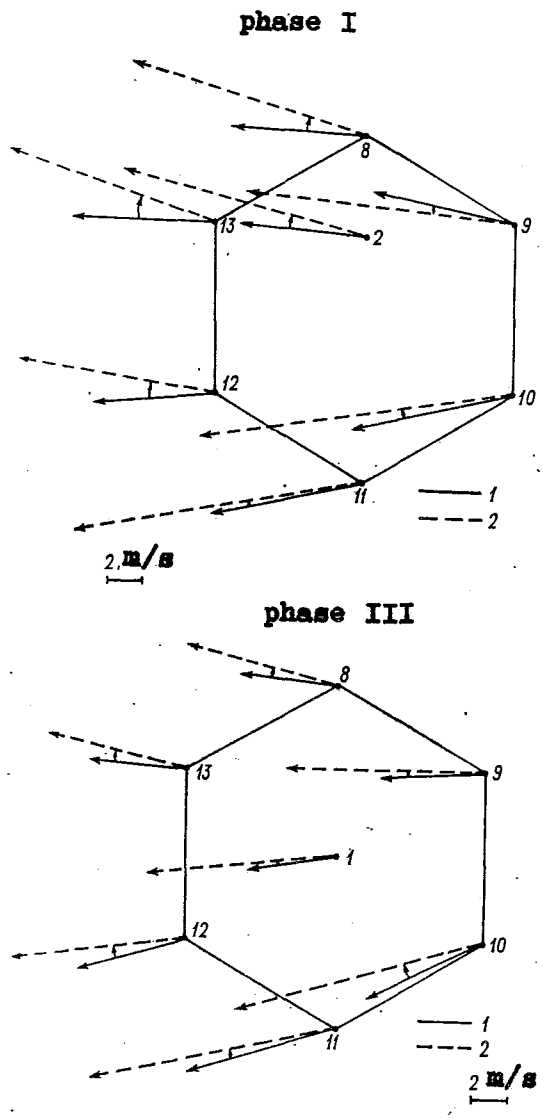

Figure 8.9 - Shear of mean phase wind vector for the A/B ship array for Phases I and III in the layer of 300-200 mb. 1 - 300 mb; 2 - 200 mb.

What explains the location of the thermal equator in the ITCZ latitudes? One can give an exhaustive answer only if one has solved the problem of the circulation of the atmosphere and the ocean. Indeed Pike (1971) showed in a simple numerical model of the ocean-atmosphere interaction that temperature of the sea surface had a very important role in the location of the ITCZ. It follows from his model that the ITCZ is a result of the ocean-atmosphere interaction. Here we shall only consider basic factors altering the sea-surface temperature in the ITCZ area. Let us begin with heat flux from the atmosphere to the sea (T) which is found from the heat balance equation:

$$T = S_a - E_{ef} - H - LE$$

where S_a - short wave absorbed solar radiation, which is usually determined as the difference between total and reflected radiation (taken from actinometric data), LE and H - turbulent fluxes of latent and sensible heat from the sea into the atmosphere, E_{ef} - effective sea radiation. Analysis of the heat balance components showed that its main contributions are absorbed radiation S_a and the flux of latent heat of condensation.

Shown in Figure 8.10 are mean values for each observation Phase T, S_a and LE + H along the meridian 23.5°. These graphs have been made by Belevich (1977) using data from GATE ships which carried out observations on this meridian. From the figure one can see that the maximum heat flux into the ocean occurs at the equator and near 10-12°N, and the minimum flux in the area of 5°N. Here the ocean returns heat back to the atmosphere which is not typical of the tropics at all. This is explained by the maximum turbulent flux of energy from the ocean located here; this maximum is more conspicuous than the minimum of absorbed radiation observed in the zone of maximum cloudiness. The latter travels north following the seasonal ITCZ displacement. Thus, the maximum heat flux into the ocean is not observed where the maximum sea-surface temperature occurs. Moreover, Belevich (1977) shows that in the East Atlantic the maximum heat flux into the ocean is observed where the minimum sea-surface temperature is found (the area covered by the "Passat" vessel, the Equator, 10°W).

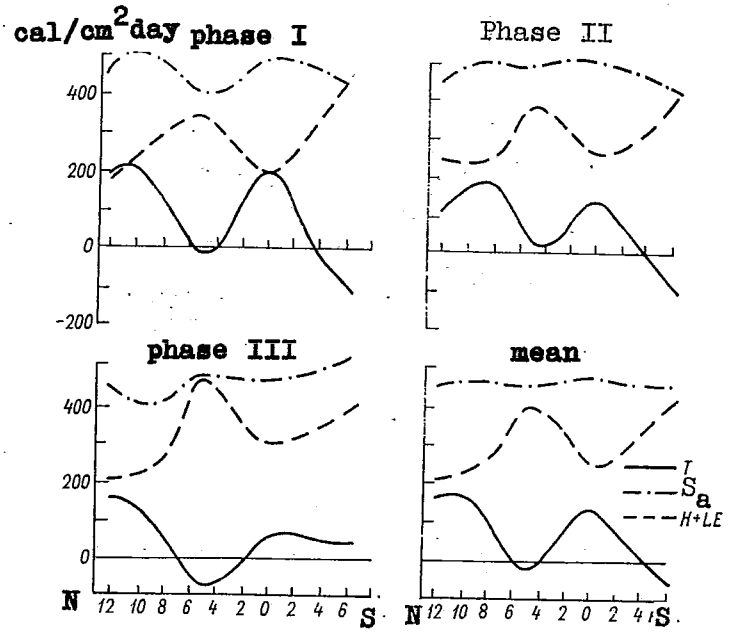

Figure 8.10 - Components of sea-surface heat balance along the meridian 23.5°W from the GATE data.

Shown in Table 8.1 in addition to T and LE + H, are mean phase values of sea-surface radiation balance $R = S_a - E_{ef}$. For clearness the table also contains mean phase values of sea-surface temperatures (t°_w). The sea-surface radiation balance depends on cloudiness and on the aerosol quantity in the atmosphere. In Phase I the A/B scale ships 2, 8 and 13 were located within the zone of the northern trade wind, the clouds over them were thin, rains were very rare. And quite the reverse, the ITCZ cloud band with heavy rains was located over the ship 9-12 most of the time. It is clear from the table that, as it should be expected, greater values R were observed on ships located in the zone of clear sky. The "driest" ship 8 (only 0.6 mm precipitation during the whole phase) was an exception. Low R values here can be explained by the ship staying closer to Africa in the zone where sand is carried out from the Sahara which caused a high content of aerosol over the ocean. The maximum quantity of precipitation was registered on ship 10: here too a minimum R value was noted. Despite the fact that Table 8.1 is the result of averaging hourly observation data for the whole phase (about 20 days), errors in the shown values may be greater than they may seem at first. Of course, of some importance here are not random, but biased, errors, caused by both the systematic inaccuracies of measuring instrumentation and by the computational method used. Thus, errors in the computation of turbulent energy fluxes can reach 10-20% because of an inaccurately determined turbulent exchange coefficient. However, since heat balance values T proved to be rather high, one can expect in the area of ships 2, 8 and 13 a noticeable heating of the ocean, because of heat flux from the atmosphere to the sea.

The sea-surface temperature also depends on heat advection, i.e. on heat transfer by surface sea current. Now we shall not dwell in detail on the role of sea-surface currents. However, note that in the eastern part of the Atlantic between 5 and 10°N in summer there exists so-called inter-trade counter-current and its location practically coincides with the ITCZ position. The counter-current is formed between the northern and southern trade currents but unlike them is directed from the west to the east. Trade currents are drifting. They are caused by trade winds and can be observed all the year round. The trade currents raise sea level near the western Atlantic coasts; it might be the cause of the inter-trade counter-current. As the ocean in the west is warmer, it is natural to suppose that a considerable heat advection is connected with the inter-trade counter-current.

One can add that the northern trade wind becomes north-eastern when it approaches the ITCZ near the A/B array while the southern trade wind, after crossing the Equator, turns to the right and becomes south-western.

In the Ekman layer of the ocean the current integrated over the whole layer in moderate latitudes of the Northern Hemisphere turns 90° to the right of the wind direction, near the Equator it turns less and on the Equator it does not turn at all. Consequently, south of the convergence line the current is eastward, north of it, westward. As the ocean on the ITCZ latitude is warmer in the west, the drifting current south of the trade convergence line can be warmer than north of it.

The easterlies dominating at the equator can cause the upwelling of colder deep water and the cooling of surface water. Indeed, the drifting current generated by the surface friction force, north of the Equator, because of veering in the Ekman layer, must deviate northward and south of it, southward, and this will lead to divergence and upwelling of colder water. This might be one of the reasons why the ITCZ appears very seldom on the Equator. Of course all our speculations are qualitative but they show that in a study of sea-surface temperature distribution it is necessary to take into account all the three factors: heat balance of the sea surface, currents and upwelling.

Table 8.1 - Heat balance components (cal/cm^2·day) and sea-surface temperature ($^\circ$C) for Phases I, II, III, the A/B ship array

Position No. (see Figure 1)	Name of Ship	R	LE + H	T	t_w°
			Phase I		
2	Professor Vise	410	210	200	26.8
8	Academician Korolev	350	180	170	25.6
9	Poryv	330	270	60	27.9
10	Ernest Krenkel	280	280	0	27.2
11	Professor Zubov	320	320	0	27.4
12	Ocean	320	240	80	27.0
13	Pryboi	400	210	190	26.6
The Equator	Academician Kurchatov	370	200	170	-
			Phase II		
1	Professor Vise	400	220	180	27.1
8	Academician Korolev	320	240	80	27.5
9	Poryv	320	200	120	26.9
10	Ernest Krenkel	340	290	50	26.9
11	Professor Zubov	400	340	60	26.7
12	Ocean	360	280	80	27.2
13	Pryboi	360	200	160	27.0
The Equator	Academician Kurchatov	360	240	120	-
			Phase III		
1	Professor Vise	310	240	70	27.1
8	Academician Korolev	345	210	135	27.4
9	Poryv	310	190	120	27.0
10	Ernest Krenkel	325	330	-5	27.1
11	Professor Zubov	390	410	-20	27.2
12	Ocean	330	290	40	27.4
13	Pryboi	390	210	180	27.1
The Equator	Academician Kurchatov	320	270	50	-

8.7 ENERGY BALANCE OF THE AIR COLUMN IN ITCZ

A great number of research works on moisture and energy budgets for B and A/B ship arrays has been done using composite analyses suggested by Reed (Reed et al., 1977) for the study of wave disturbances over the array. These research works are presented in detail in Chapter 4 of the Monograph, so we shall not dwell on them here. Samoilenko et al. (1977) have studied heat and moisture budgets for different TROPEX-72 arrays. The computations of heat and moisture budgets presented further were based on A/B ship array data alone because B ship wind measurements proved to be non-representative.

In Section 8.2 the division of all radiosonde observations at the A/B ship array into four classes was discussed. In each class mean characteristics of the atmosphere can be considered to be reference values of the observations in four cases: thick clouds over the ship array, practically clear sky and two intermediate situations. This division is justified at least by the fact that in spite of averaging for 20-25 observation times the atmospheric parameters proved to be considerably different for each class. Figure 8.11 shows the mean net flux of latent heat of condensation and enthalpy in a unit column of the atmosphere, caused by large-scale motions for different classes of ITCZ. (Calculations were made according to the technique stated in Falkovich (1979).) For clarity the whole troposphere is divided into five layers. The arrows show mean flux for each class of energy (in case of positive sign) to a unit air column between indicated isobaric surfaces. The figures show the variation of energy fluxes in case of transition from clear sky (Class C) to highly developed ITCZ (Class B). In Classes B and D the increase of latent heat of condensation due to large-scale motions is observed throughout the troposphere, while in Classes C and E everywhere above 700 mb level the large-scale motions cause the decrease of latent heat. In lower troposphere the latent heat of condensation flux is observed in all classes. It is interesting to note that in Class B considerable increasing of latent heat takes place not only in the lower troposphere, but in the 500-300 mb layer as well. When comparing the figures it is easily observed that the decrease of the latent heat of condensation is in correspondence with the increase of enthalpy and vice versa.

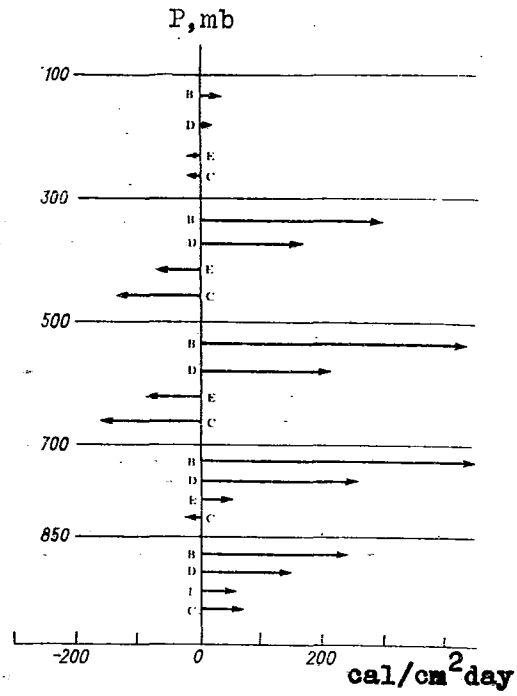

Figure 8.11a - Mean net flux of latent heat of condensation in a single atmosphere column due to large-scale motions for different ITCZ classes during the Phase I observation for the A/B ship array.

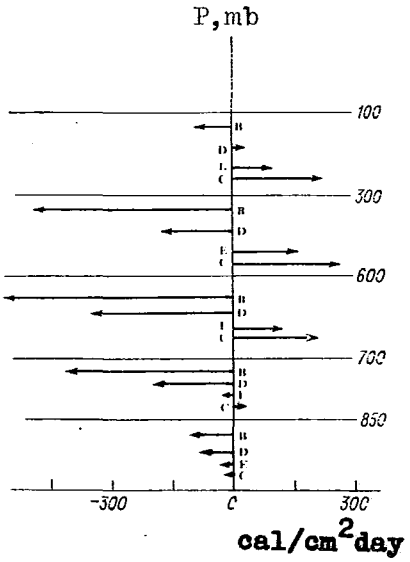

Figure 8.11b - Mean net flux of enthalpy in a single atmosphere column due to large-scale motions for different ITCZ classes during the Phase I observation for the A/B ship array.

Let us consider in more detail the situation in an air column when a disturbance occurs over the ship array (Class B). Tables 8.2 and 8.3 present mean (m) and root-mean-square deviations (σ) for Class B of these kinds of energy due to large-scale motions in Phases I and III, respectively. To facilitate the analysis the lower lines of the table present the turbulent energy fluxes from ocean to atmosphere calculated by the method described in Falkovich (1979).

Tables 8.2 and 8.3 show that large-scale upward motions which in Class B involve the whole thickness of the troposphere tend to increase the amount of latent heat of condensation in the air column and to decrease the enthalpy. Thus, in air column P_s - 200 mb the amount of latent heat of condensation should increase due to large-scale motions by 1453 (1344) cal/cm^2 per day; the enthalpy should decrease by 1686 (1575) cal/cm^2 per day. Here in brackets the values of Phase III are presented, without brackets the values of Phase I.

According to computations based on the data of nocturnal actinometric sounding and estimations of diurnal short-wave warming from the data of hourly actinometric ship observation (Falkovich, 1979) the daily mean radiation cooling of air column P_s - 200 mb at the A/B ship array would be about 100-150 cal/cm^2 per day, Frank (1979) in his calculations uses Cox's and Griffit's data according to which mean value for air column Q_R = 1.16°K/day. For the air column P_s - 200 mb that makes about 230 cal/cm^2 per day. All together on the average for Class B a unit air column P_s - 200 mb loses about 1800 (1630) cal/day of enthalpy due to large-scale motions, radiation and eddy flux from ocean to the atmosphere. At the same time due to all the above factors, except radiation, the same column receives about 1730 (1520) cal/day of latent heat of condensation. It is interesting to note that the decrease of enthalpy is practically equal to the increase of the latent heat of condensation (their difference makes about 100 cal which is within computation accuracy).

Table 8.2 - Mean values (m) and root-mean-square deviations (σ) of fluxes of energy (cal/cm^2 day) in a unit atmospheric column due to large-scale motions for Class B of Phase I, the A/B ship array.

Atmosphere column, mb	Latent heat of condensation Lq		Enthalpy c_pT		Total energy	
	m	σ	m	σ	m	σ
p_s - 1000	2.6	2	0	0.5	2.7	12
1000 - 950	42	20	-19	7	23	15
950 - 850	191	86	-101	37	90	61
850 - 700	469	305	-419	253	50	139
700 - 500	429	240	-596	280	-168	113
500 - 400	183	80	-310	139	-128	82
400 - 300	107	60	-201	118	-94	76
300 - 250	23	16	-38	45	-16	35
250 - 200	6.7	7	-1	29	5	24
200 - 150	0	1.7	14	36	14	35
150 - 100	0	0.2	-14	54	-14	53
p_s - 200	1453	557	-1686	685	-235	218
Turbulent flux from the ocean to the atmosphere	251	80	24	9	275	86

Table 8.3 - Mean values (m) and root-mean-square deviations (σ) of fluxes of energy (cal/cm^2 day) in a unit atmospheric column due to large-scale motions for Class B of Phase III, the A/B ship array.

Atmosphere column, mb	Latent heat of condensation Lq		Enthalpy c_pT		Total energy	
	m	σ	m	σ	m	σ
p_s - 1000	0.9	2	0	0	0.8	2
1000 - 950	30	25	-13	9	17	18
950 - 850	150	104	-70	45	80	65
850 - 700	302	170	-275	126	26	78
700 - 500	521	218	-555	206	-34	79
500 - 400	173	78	-320	117	-148	108
400 - 300	128	54	-286	122	-158	84
300 - 250	29	12	-54	38	-23	30
250 - 200	9	6	-5	24	4	17
200 - 150	0.9	1.1	10	15	11	14
150 - 100	0	0.2	0	58	0.4	58
p_s - 200	1343	475	-1575	501	-235	181
Turbulent flux from the ocean to the atmosphere	247	44	24	7	271	49

In Falkovich (1979) it is shown that almost all latent heat of condensation is converted into enthalpy, vapour condensates and falls out. Frank (1978) also indicates that on the average in the whole thickness of the troposphere, heating and moistening during convection development are near to zero. This is explained by greater size of the A/B ship array and its closeness to the Equator. Even in case of thick clouds over the ship array and great values of mean upward motions there is a region of compensation downward motions over it. In Sections 17-18 from Falkovich (1979) an example of sounding at the A/B scale for 1800 GMT, 7 July 1974, is considered. On that day values of convergence at sea level, divergence at 200 mb surface and vertical velocity at 500 mb surface were the greatest ever observed for Phase I. Between 1800 GMT and 2400 the ship "OKEANOGRAPHER" located in the centre of the ship array registered about 150 mm of rainfall, 90 mm out of it were precipitated between 2030 and 2130. A thick cloud band covered considerable part of the array. The average amount of water vapour over the area was less than average value for the whole phase. This is explained by the fact that in case of very strong upward motions in the cloud band to the north of the band strong compensation downward motions were observed that "dried" the northern part of the ship array. Thus, the northern ships 8 and 13 registered at that hour the lowest for Phase I amount of

water vapour in a column: Ship 8 registered 2.8 g/cm^2 (1.8 g/cm^2 less than the Phase I average value for this ship); Ship 13 registered 3.1 g/cm^2 (1.5 g/cm^2 less than the Phase I average value for this ship). In case of upward motions the deviation from mean values is considerably less.

Tables 8.4 and 8.5 show that in the absence of disturbance over the A/B ship array (Class C) downward large-scale motions tend to decrease the amount of latent heat of air column.

Tables 8.2 - 8.5 also show fluxes of total energy in air column or to be more accurate - the fluxes of $c_pT + Lq + K$. This sum agrees with the total energy only in air column as a whole, but further on for the sake of simplicity we shall call it total energy. It is seen from the tables that the flux of kinetic energy is so small that essentially the tables show nothing but fluxes of the sum of enthalpy and latent heat of condensation. The tables also show that in case of strong upward motions (Class B) in a lower troposphere from the sea level up to 700 mb surface due to large-scale motions and eddy flux from ocean the energy increases while above this layer it decreases. In the absence of moist convection this would lead to warming of the lower atmosphere and to cooling of the upper one, i.e., created convective instability. Moist penetrative convection transporting the energy upwards tends to restore the vertical profile of energy as if compensating the action of large-scale motions.

In order to give the idea of the nature of sea-air interaction, Table 8.6 presents mean and root-mean-square deviations of turbulent momentum flux τ, water vapour E, latent heat of condensation LE, enthalpy H, net energy LE + H from ocean to the atmosphere calculated by the technique described in Section 16 from Falkovich (1979) for four classes of ITCZ and Phase I as a whole. The table also contains sea level pressure p, water temperature t^o_w and the Bowen ratio β for different classes of ITCZ. All the values presented in the table are mean values for the A/B ship array.

Eddy fluxes are considerably stronger in case of thick cloudiness than a clear sky. The developed ITCZ "sucks" additional energy from the ocean. Thus, the eddy flux of energy from ocean to the atmosphere makes 275 cal/cm^2 per day in Class B and only 202 cal/cm^2 per day in Class C.

The results obtained give the idea of interaction between a "cascade" of motions of different scales (it will be considered in Section 8.8 in more detail). Thus, in Class B the organized large-scale motions are responsible for convective instability. They are "exciting" the motions of the next scale, i.e. moist convection. Moist convection transporting energy from the lower half of the troposphere into the upper one, strengthens the motion of the next scale, i.e. eddy transport of energy in the boundary layer of the atmosphere. This is evident from the fact that the turbulent boundary layer in Class B has to transfer from a thin surface layer into the atmosphere significantly more energy than in Class C. Finally, the eddy transport of energy intensifies micro-interaction in a thin surface layer and that causes the increase of net energy flux from ocean to the atmosphere.

8.8 COMPUTATION OF PRECIPITATION AND THE ROLE OF ITCZ IN ENERGY CONVERSIONS IN THE ATMOSPHERE

In the previous section it was shown that for various observation times changes of different kinds of energy in air column averaged over the A/B ship array are small. This is explained by proximity of the ship array to the Equator and its dimensions. This makes it possible to estimate the amount of precipitation over the A/B ship array. Let us consider Table 8.7 which presents the net flux of water vapour amount in a single air column for different classes of ITCZ in Phase I, caused by large-scale (mean over the ship array) motions.

Table 8.4 - Mean values (m) and root-mean-square deviations (σ) of fluxes of energy (cal/cm^2 day) in a unit atmospheric column due to large-scale motions for Class C for the Phase I, the A/B ship array.

Atmosphere column, mb	Latent heat of condensation Lq		Enthalpy c_pT		Total energy	
	m	σ	m	σ	m	σ
p_s - 1000	1	1	0	0.2	1.1	1
1000 - 950	17	18	-7	7	9.6	12
950 - 850	54	71	-24	33	30	40
850 - 700	-22	148	25	140	3	48
700 - 500	-169	169	206	197	37	41
500 - 400	-79	94	137	134	58	61
400 - 300	-51	49	106	96	56	54
300 - 250	-12	12	43	47	32	37
250 - 200	-6	6	37	48	32	44
200 - 150	-1	1.3	9	34	8	33
150 - 100	-0.08	0.1	23	37	23	37
p_s - 200	-265	439	523	546	259	178
Turbulent flux from the ocean to the atmosphere	187	55	15	5	202	58

Table 8.5 - Mean values (m) and root-mean-square deviations (σ) of fluxes of energy (cal/cm^2 day) in a unit atmospheric column due to large-scale motions for Class C for the Phase III, the A/B ship array

Atmosphere column, mb	Latent heat of condensation Lq		Enthalpy c_pT		Total energy	
	m	σ	m	σ	m	σ
p_s - 1000	0.2	2	0	0.3	0.2	2
1000 - 950	20	17	-9	8	10	10
950 - 850	80	86	-36	42	44	46
850 - 700	11	199	-0	173	10	42
700 - 500	-45	168	64	186	20	42
500 - 400	-81	96	111	145	30	52
400 - 300	-30	47	68	100	38	56
300 - 250	-12	14	41	48	29	35
250 - 200	-6	6	26	32	21	28
200 - 150	-1.2	2	27	58	25	56
150 - 100	-0.06	0.2	0	40	-0.1	40
p_s - 200	-62	463	265	514	204	200
Turbulent flux from the ocean to the atmosphere	223	70	21	8	245	76

Table 8.6 - Parameters of the atmosphere/ocean interaction layer for the Phase I, the A/B ship array.

Class	p mb		τ dyn/cm^2		E $g_v/(cm^2 day)$		LE cal/(cm^{2}day)	
	m	σ	m	σ	m	σ	m	σ
B	1013.71	1.17	0.54	0.3	0.43	0.14	251.6	80.2
D	1013.46	0.97	0.40	0.14	0.35	0.08	206.2	47.7
E	1013.66	1.24	0.30	0.11	0.31	0.08	179.6	47.7
C	1013.75	1.34	0.33	0.15	0.32	0.09	186.9	55.1
All Phase I	1013.8	1.2	0.41	0.23	0.36	0.12	208.96	70.8

Class	H cal/(cm^{2}day)		LE + H cal/(cm^{2}day)		t_w °C		Bowen ratio β	
	m	σ	m	σ	m	σ	m	σ
B	23.56	9.03	275.2	86.5	26.81	0.26	0.10	0.02
D	20.83	7.40	227.0	52.0	26.76	0.34	0.10	0.03
E	16.64	5.24	196.3	50.6	27.05	0.21	0.09	0.02
C	15.35	5.01	202.3	57.9	27.01	0.29	0.08	0.02
All Phase I	19.5	7.4	228.5	75.8	26.9	0.3	0.09	0.02

Table 8.7 - Mean values (m) and root-mean-square deviations (σ) of water vapour flux into a unit atmospheric column (g/cm^2 day) due to large-scale motions, and turbulent transfer from ocean into atmosphere for different classes of the ITCZ during the Phase I, the A/B ship array.

Atmosphere layer mb	B		D		E		C		Phase I	
	m	σ	m	σ	m	σ	m	σ	m	σ
p_s - 1000	0.00	0.00	0.00	0.01	0.00	0.01	0.00	0.00	0.00	0.01
1000 - 950	0.07	0.03	0.05	0.04	0.02	0.04	0.03	0.02	0.04	0.04
950 - 850	0.33	0.14	0.20	0.13	0.09	0.13	0.09	0.11	0.19	0.17
850 - 700	0.79	0.50	0.43	0.49	0.09	0.33	-0.02	0.27	0.31	0.51
700 - 500	0.74	0.42	0.36	0.36	-0.15	0.38	-0.28	0.30	0.18	0.56
500 - 400	0.32	0.15	0.12	0.11	-0.07	0.13	-0.14	0.16	0.06	0.24
400 - 300	0.17	0.10	0.06	0.09	-0.04	0.05	-0.09	0.08	0.03	0.14
300 - 250	0.01	0.03	0.01	0.02	-0.01	0.01	-0.02	0.02	0.00	0.03
250 - 200	0.00	0.01	0.00	0.01	-0.01	0.01	-0.08	0.01	0.00	0.01
200 - 150	0.00	0.00	0.00	0.00	0.00	0.00	0.00	0.00	0.00	0.00
150 - 100	0.00	0.00	0.00	-0.08	0.00	0.00	0.00	0.00	0.00	0.00
p_s - 200	2.47	0.98	1.24	1.01	-0.08	0.90	-0.44	0.77	0.81	1.51
Turbulent flux from ocean to atmosphere	0.43	0.14	0.35	0.08	0.31	0.08	0.32	0.09	0.36	0.12

To make analysis complete the lowest line of the table presents eddy flux of water vapour from ocean to atmosphere computed by formulae of the semi-empirical theory. In eddy boundary layer this water vapour is not accumulated but transported upward by turbulent pulsations in a surface layer and by cellular convection up to condensation level. Still higher the main transport is carried out by moist (penetrative) convection. In case of relatively clear sky (Class C) due to eddy flux from ocean, the atmosphere receives 0.32 g/cm^2 of water vapour per day. This is compensated with excess by decreasing water vapour due to large-scale downward motions. In Class B an eddy flux of vapour from ocean to atmosphere results in 0.43 g/cm^2 day; large-scale motions bring 2.47 g/cm^2 day. Consequently, in case of highly developed ITCZ it has to precipitate about 30 mm per day. Based on the data of this table a total precipitation amount for Phase I (73 observations) was computed, taking into account the turbulent vapour flux from ocean to atmosphere. It equalled 210 mm. According to measurement data (Falkovich, 1979) the A/B scale mean precipitation amount for Phase I is between 180 and 220 mm. It should be noted that this is casual coincidence. Precipitation in ITCZ is as concentrated as in cloud clusters. Very heavy precipitation covers the area in the order of 1% of cloud band over the A/B ship array. It is evident that a series of phase averaging (about 80 observations) is too short to have a reliable notion of precipitation amount over such a

sparse grid (7 ships at a ship array with a radius of 3.5°). Thus, in Phases II and III the amount of measured precipitation is proved to be considerably less than the computed amount.

Computed precipitation amount in Phase II accounts for 174 mm, in Phase III, 286 mm. According to observational data the A/B scale mean precipitation amount is about 90-100 mm in Phase II and 120-140 mm in Phase III (Falkovich, 1979). Such a close agreement in Phase I could not be observed if very heavy precipitation on 7 July 1974 (see Section 17 from Falkovich, 1979) has occurred not over the central ship of the ship array, "OKEANOGRAPHER", but at a distance of several scores of kilometers. It should be reminded that for one hour, from 2030 to 2130 GMT, this ship registered 90 mm of precipitation.

As very strong cloud towers cover the area in the order of 1% in cloud clusters, the passage of such a tower over sounding ship is observed very rarely. Therefore, the amount of measured precipitation there could be expected to be usually underestimated. The exception is for the stations located on the islands, atolls and coastal areas of continents. As shown in Section 4 of Falkovich (1979), higher temperature of underlying surface on the islands compared with adjacent regions facilitates the formation of high cumulo-nimbus clouds over them which is very often observed there when the ocean surrounding the isles is comparatively cloudless. Here on the contrary the precipitation data will be considerably higher than mean values over a large area.

Measurements of precipitation in ship conditions on such a sparse network as the A/B ship array is not a very reliable procedure. Frank (1979) compares the results of computations for the A/B ship array obtained by different authors with the estimation received by means of radar methods. However, radar measurements of precipitation were made only by ships of the B scale array and covered the area a little larger than that of the B scale, but smaller than the area of the A/B scale. Table 8.8 presents data from Frank (1979) added to our results (see Table 18 from Falkovich (1979)).

Table 8.8 shows that the results obtained by Frank exceed the results of radar measurements by 42% in Phase I, by 35% in Phase II and by 8% in Phase III. For our computations these values are 6, 7 and 19% respectively.

Frank (1979) received very interesting results on the delay of computed precipitation (i.e. maximum intensity of large-scale motions) in relation to maximum precipitation measured by radar. This delay is about 5-6 hours. Frank explains this fact by variation of liquid water accumulation in the atmosphere.

In spite of the fact that the amount of energy of different kinds of air column of ITCZ in the region of the A/B scale area changes very slightly, this region is of importance for heat exchange of the atmosphere. Table 8.7 shows that in a highly-developed ITCZ (Class B) about 30 mm per day have to precipitate. This value is an average over the A/B ship array. Cloud band of ITCZ is usually considerably narrower, its mean width is about 3°. As soon as a mean eddy flux of water vapour from ocean to atmosphere in a trade wind zone does not exceed 3-4 mm per day a highly-developed ITCZ precipitates water accumulated from the area which is greater than the area of ITCZ by a factor of 10. ITCZ at a width of 3° condensates vapour evaporated from the trade wind band of 30° width. Latent heat of condensation released thereby is transformed into sensible heat and transported to subtropical regions.

Table 8.8 - Precipitation estimation from the water vapour flux into the atmosphere column p_s-100 mb (g/cm^2 day)

Author	Phase I	Phase II	Phase III	Mean for the GATE period
Frank	1.56	1.11	1.35	1.36
Dewart and Gray	-	-	-	1.53
Thompson	-	-	1.33	-
Falkovich	1.17	0.89	1.43	1.16
Radar precipitation	1.10	0.82	1.25	1.06

Figure 8.12 shows horizontal divergence of net energy flux caused by large-scale motions. Arrows of the figure show mean flux of energy $c_pT + gz + Lq + K$ from a single air column between indicated isobaric surfaces (in case of positive sign) for each of four classes of ITCZ. From sea level up to 850 mb surface the energy flux into the air column through side surface is observed in all classes but it varies greatly. In case of thick cloudiness (Classes B and D) the energy inflow is observed up to 700 mb surface and main outflow of energy takes place in the upper half of the troposphere. In Class B a maximum outflow is observed in a 300-100 mb layer. In Classes C and E, the other way round, the energy inflow is observed in the upper troposphere. As for outflow, it prevails in 850-500 mb layer. It should be taken into account that at lower levels great amount of latent heat is supplied to the air column, while at upper levels the outflow consists practically of the sensible heat alone. It follows that the air column in Classes B and D transforms the energy of latent heat into sensible heat and it outflows into subtropical regions.

It is known (Falkovich, 1979) that approximately one half of solar energy obtained by the Earth falls on the tropics - the only region of Earth which receives more solar energy than radiates into the space. The main part of surplus radiation energy is accumulated in the oceans. About one third of energy accumulated in the ocean is carried to middle latitudes by oceanic currents, the remaining two thirds are transported to the atmosphere mainly by evaporation. Almost all the energy comes through ITCZ. The intertropical convergence zone plays the role of a "distributor": when it is well developed (Class B) it transforms all the energy of latent heat accumulated in the tropics into sensible heat which is followed by heavy precipitation and at upper levels of the troposphere it directs sensible heat to the subtropical regions; when ITCZ is depressed (Class C) at the lower half of the troposphere moist air flux goes to the subtropical regions.

It should be noted that such a role is played not only by ITCZ but by any tropical disturbance.

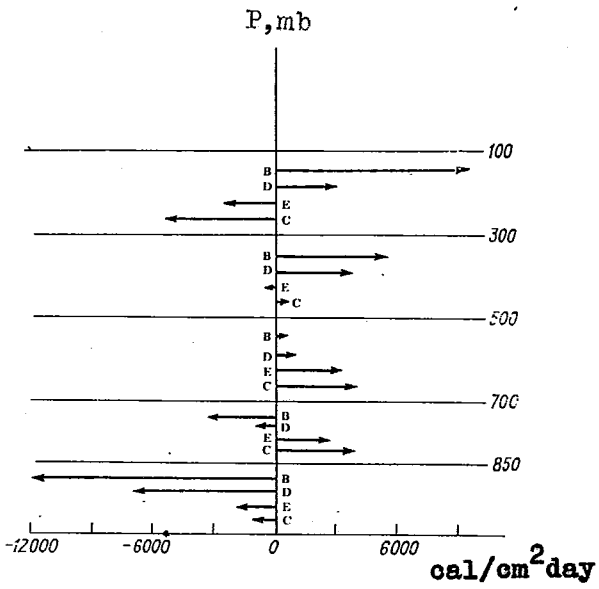

Figure 8.12 - Horizontal divergence of the total energy flux for different ITCZ classes for the Phase I for the A/B ship array.

8.9 INTERACTION OF DIFFERENT-SCALE MOTIONS IN THE TROPICS

The hydrodynamic equations that describe the atmospheric condition are rather nonlinear. Therefore, different-scale motions are not independent of each other. Their interaction leads to energy and impulse transport over the oscillation spectrum. When integrating numerically a weather forecast problem or a general circulation model it is necessary to cut the spectrum parameterizing the influence of cut-off part on the remaining one, introducing one or other additional hypotheses. Therefore, the study of interaction of different-scale motions acquires at present a paramount importance.

Let us consider a tropical disturbance in ITCZ over the A/B scale. At sea surface the disturbance has a cyclonic vorticity. As a result of eddy friction over the underlying surface a boundary layer appears to differ from the Ekman layer due to its proximity to the Equator, but as the processing of observational data shows the boundary layer, like the Ekman one, leads to air mass inflow into the area of low pressure (trough, cyclone). Thus, small-scale eddy friction in the boundary layer of the atmosphere tends as if to fill in the cyclone and throw away extra mass out of the anticyclone, creating great absolute values of large-scale divergence. From this point of view large-scale divergence can be considered as an indicator of the boundary layer of the atmosphere: where it is large (by absolute value) a boundary layer can be found. It was noted earlier that along with a lower boundary layer at 200 mb surface over the A/B ship array an upper boundary layer is observed (more accurately a zone of enhanced turbulence). This can be explained by the fact that in the Atlantic over the ITCZ at these altitudes an upper-tropospheric eastern jet stream is located. We can suppose that the action of the upper boundary layer is opposite to that of the lower one: it tends to deepen still more the disturbance. Relative vorticity in it is anticyclonic and near 200 mb surface it attains its maximum.

So, thanks to lower and upper boundary layers vertical distribution of large-scale divergence is formed and, consequently, distribution of large-scale vertical velocity. The combined influence of boundary layers will not lead to filling in the disturbance. Really, according to experimental data it is possible to compute for each observation time the large-scale (averaged over the ship array) characteristics of the atmosphere as a result of interaction of motion of all scales. Let us see what will occur with tropical disturbance if for some period only the large-scale motions are left. When averaging the vorticity equation over the area it is easy to come to the conclusion that large-scale convergence in the lower troposphere tends to increase the cyclonic vorticity and divergence in upper troposphere strengthens anticyclonic vorticity there. Thus, the large-scale motions tend to intensify disturbance, to increase its vorticity. Besides, large-scale upward motions in the disturbance (Table 8.9) lead to increasing energy in the lower troposphere, P_s-700 mb, and its decreasing in all the remaining part of the troposphere that must lead to the appearance and development of convective instability of the atmosphere (Falkovich, 1979). This convective instability calls forth moist (penetrative) convection that transports the energy upwards and tends to store the vertical profile of energy distribution and to compensate the action of large-scale motions.

What is the nature of feedback? How does penetrative convection affect the large-scale disturbance? It can be assumed that the influence of moist convection on large-scale motions is as follows. First, increasing moist convection can create additional "sucking in", i.e. an increasing of large-scale convergence (divergence) in the boundary layers of the atmosphere. This can occur due to increasing eddy friction coefficient and extending boundary layers of the atmosphere (Falkovich, 1979). Second, moist convection, if it is sufficiently developed, forms a warm core of the disturbance.

Before finishing this chapter let us note that a tropical disturbance (even if it is far from the stage of a tropical cyclone, as is the case over the A/B ship array in the ITCZ area) possesses a great deal of energy. It must "convert" about 1800 cal/cm^2 day latent heat of condensation into enthalpy, i.e. the scheme of moist convection parameterization must "release" this amount of heat to compensate for the activity of large-scale motions and turbulent flux of energy from the ocean into the atmosphere. But difficulty of parameterization is in the fact that it should find small deviations from compensation values responsible for the tendency of disturbance development. Only several per cent of the compensation energy are connected with these deviations, and only a small part of it is spent on generation of kinetic eddy energy. Judging from Reed's calculations (see Chapter 4) less than 0.5 cal/cm^2 day is spent on it.

8.10 SUMMARY

(1) Classification problems of GATE data are discussed. When processing GATE data many authors suggest a number of classification methods for observations. In spite of their outward difference these methods are similar in essence and serve one and the same purpose: averaging based on classes (wave categories) allows to considerably diminish the influence of measurement errors and to pinpoint most typical features of the atmospheric processes.

(2) Data are presented on wind shear, cloudiness, precipitation, water and air temperature in the area of the ship arrays under study. It was shown that cloud cover, maximum precipitation and large-scale upward motions are concentrated south of the ITCZ confluence axis at sea level.

(3) During the convective system development heating in the upper troposphere, cooling in the lower and moistening in the middle troposphere takes place. On the average heating and moistening values for the whole troposphere during the development of a convective system are close to zero.

Table 8.9 - Fluxes of energy $c_pT + K + Lq$ in a unit atmospheric column (cal/cm^2 day) due to large-scale motions and turbulent fluxes from ocean to atmosphere for different ITCZ classes during Phases I and III, the A/B ship array.

Atmosphere layers, mb	Phase I				Phase III			
	B	D	E	C	B	D	E	C
	Changes due to large-scale motions							
p_s-850	115	81	26	41	98	66	78	55
850-700	50	45	17	3	26	16	10	10
700-500	-167	-84	23	37	-34	-52	-4	20
500-300	-222	-83	57	144	-306	-101	1	68
300-200	211	17	34	63	-18	-5	25	51
200-100	0	17	19	31	12	15	6	25
p_s-200	-235	-23	158	259	-235	-75	109	204
	Turbulent flux from the ocean to the atmosphere							
	275	227	196	202	271	259	247	245

(4) Proceedings of satellite data for cloud brightness showed that over land near the African coast at about 10°N, 17°W there exists the centre of maximum convective activity. Convection intensity in this centre oscillates with a period of one and four days.

(5) A diurnal variation over the A/B ship array is discussed. This variation is shown to be in the co-phase with the diurnal variation over the centre of maximum convective activity. Diurnal variations north and south of the A/B ship array and of this centre are, however, quite different.

(6) Dynamic features of the atmosphere over the A/B ship array are studied both in the presence and in the absence of a strong disturbance.

(7) A vertical wind shear is shown to be located in the 300-200 mb layer. It is supposed that near the upper-tropospheric easterly jet stream exists an upper atmospheric boundary layer (a region of enhanced turbulence) which essentially effects the development of the ITCZ disturbances. Great absolute values of large-scale divergence are shown to indicate boundary layer presence.

(8) An equation of heat budget for sea surface along the meridian 23.5°W is analysed. The resulting heat flux into the ocean is shown to be maximum where surface temperature is lower and to become even negative in the ITCZ where a peak in the surface temperature is found. The water temperature maximum in the ITCZ can most likely be attributed to heat transfer by the inter-trade wind counter current.

(9) It was revealed for the A/B ship array that due to its closeness to the Equator and due to its great size, the energy of the whole troposphere column does not practically change in case of transfer from thick cloudy conditions to clear sky.

It means that almost all the latent heat of condensation coming into the atmosphere column due to large-scale motions and due to the eddy flux from the ocean, is converted into the sensible heat.

(10) Agreement of precipitation amount derived from the heat budget and from radar measurements proved to be quite satisfactory.

(11) On the basis of GATE data the interactions of different scales of motion are discussed. Large-scale upward motions are shown to restructure stratification and to cause convective instability of the atmosphere. The latter results in moist penetrative convection tending to restore the initial vertical temperature and moisture distribution. In its turn moist convection when being enhanced may cause an extension and intensification of the boundary layers and the creation of the warm core of the disturbances. Growth of small-scale turbulent friction in the boundary layers leads to the increase of large-scale convergence (divergence) and of large-scale upward motions. An increased warm core of the disturbance is followed by enhancing temperature gradients and, consequently, pressure gradients and intensity of the disturbance.

REFERENCES

Augstein, E. and M. Garstang, 1977: The structure of and transports through the lower atmosphere (surface to 1-2 km). Report of the U.S. GATE Central Program Workshop, NCAR, Boulder, Colorado, p. 455-482.

Belevich, V.V., 1977: Distribution of heat balance equation components during GATE. Meteorologiya i Gidrologiya (Meteorology and Hydrology), No. 12, p. 88-94 (in Russian, abstract in English) (see also English translation in "Soviet Meteorology and Hydrology" Allerton Press Inc., New York).

Charney, J.G., 1971: Tropical cyclogenesis and the formation of the intertropical convergence zone. Mathem. Problems in the Geophysical Sciences, I. Geoph. Fluid Dynamics. Lectures in Appl. Math. Vol. 13, American Math. Soc. Providence, Rhode Island, p. 355-368.

Cho, H.R., L. Cheng and R.M. Bloxam, 1979: The representation of cumulus cloud effects in the large-scale vorticity equation. J. Atmos. Sci., Vol. 36, p. 127-139.

Estoque, M.A. and M. Douglas, 1978: Structure of the intertropical convergence zone over the GATE area. Tellus 30, 55-61.

Falkovich, A.I., 1976: The balance of energy of the intertropical convergence zone. TROPEX-74, Vol. 1, p. 90-116.

_____, 1979: Dynamics and energetics of the ITCZ. Gidrometeoizdat, Leningrad, p. 247 (in Russian, abstract in English).

_____ and T.A. Yurko, 1976: Numerical experiment on propagation of disturbances in the tropical zone. Meteorologiya i Gidrologiya (Meteorology and Hydrology), No. 10, p. 15-22 (in Russian, abstract in English) (see also English translation in "Soviet Meteorology and Hydrology" Allerton Press Inc., New York).

Frank, W.M., 1977: Rawinsonde compositing studies. Report of the U.S. GATE Central Program Workshop, NCAR, Boulder, Colorado, p. 251-260.

_____, 1978: The life cycles of GATE convective systems. J. Atmos. Sci., Vol. 35, p. 1256-1264.

_____, 1979: Individual time period analyses over the GATE ship array. Mon. Wea. Rev., Vol. 107, p. 1600-1616.

Gray, W.M., 1975: Tropical cyclone genesis. Atmos Sci. Pap., No. 234, Colorado State University, 122 p.

_____ and R.W. Jacobson, 1977: Diurnal variation of deep cumulus convection. Mon. Wea. Rev., Vol. 105, p. 1171-1188.

_____, 1977: Cloud-cluster-scale phenomena including undisturbed condition. Mean state and typical conditions. Report of the U.S. GATE Central Program Workshop, NCAR, Boulder, Colorado, p. 199-214.

Holton, J.R., J.M. Wallace and J.A. Young, 1971: On boundary layer dynamics and the ITCZ. J. Atmos. Sci., Vol. 28, No. 2, p. 275-280.

Houghton, D., 1977: Summary for ITCZ. Report of the USA GATE Central Program Workshop, NCAR, Boulder, Colorado, p. 19-37.

Krishnamurti, T.N. et al., 1976: Sea-surface temperatures for GATE. Report No. 76-3, Department of Meteorology, Florida State University, Tallahassee, 268 p.

Krivelevich, L.M. and Yu.A. Romanov, 1978: Numerical study of the atmospheric circulation near the equator for the zonal pressure field with the equatorial trough. Pr. of the Conference on the Energetics of the Tropical Atmosphere (Tashkent, 1977). Geneva, p. 345-352.

Murakami, M., 1979: Large-scale aspects of deep convective activity over the GATE area. Mon. Wea. Rev., Vol. 107, p. 994-1013.

Petrossiants, M.A., A.I. Snitkovsky and A.I. Falkovich, 1976a: The evolution of the intertropical convergence zone. TROPEX-74, Vol. 1, p. 80-89 (in Russian).

_____, S. Slaby, A.E. Snitkovsky and A.I. Falkovich, 1976b: The circulation in the tropical troposphere along the 23°30'W. TROPEX-74, Vol. 1, p. 117-124 (in Russian).

_____, A.E. Snitkovsky and A.I. Falkovich, 1977: On air circulation in the intertropical convergence zone. Meteorologiya i Gidrologiya (Meteorology and Hydrology), No. 5, p. 87-94 (in Russian, abstract in English) (see also English translation in "Soviet Meteorology and Hydrology", Allerton Press Inc., New York).

_____ and A.E. Falkovich, 1977: On diurnal variations in GATE. Meteorologiya i Gidrologiya (Meteorology and Hydrology) No. 7, p. 83-90 (in Russian, abstract in English) (see also English translation in "Soviet Meteorology and Hydrology" Allerton Press Inc., New York).

Pike, A.C., 1971: Intertropical convergence zone studied with an interacting atmosphere and ocean model. Mon. Wea. Rev., Vol. 99, No. 6, p. 469-477.

Reed, R.J., N.E. La Seur and D. Berrill, 1975: Aircraft observations of ITCZ structure on 4 August 1974. In GATE Report No. 14, Vol. 1, ICSU/WMO, Geneva, p. 317-333.

_____, D.C. Norquist and E.E. Recker, 1977: The structure and properties of African wave disturbances as observed during Phase III of GATE. Mon. Wea. Rev., Vol. 105, p. 317-333.

Ruprecht, E. and W.M. Gray, 1976: Analysis of satellite-observed tropical cloud clusters. Tellus, XXVIII, 5, p. 391-413.

Samoilenko V.S., K.V. Voitova and L.G. Luniakova, 1977: The heat balance in the atmosphere of the tropical zone of oceans. Pr. of the Conference on the Energetics of the Tropical Atmosphere (Tashkent, 1977), Geneva 1978, p. 235-241.

Thompson, R.M., S.W. Payne, E. Recker and R.J. Reed, 1979: Structure and properties of synoptic-scale wave disturbances in the meteorological convergence zone of the eastern Atlantic. J. Atmos. Sci., Vol. 36, p. 53-72.

Yamasaki, M., 1971: A further study of wave disturbances in the conditionally unstable model tropics. J. Met. Soc., Japan, Vol. 49, No. 5, p. 391-415.

CHAPTER 9

CLOUDS, CONVECTION AND CONVECTIVE MODELS*

by

Robert A. Houze, Jr.

(Department of Atmospheric Sciences, University of Washington, Seattle, Washington 98195, U.S.A.)

and

Alan K. Betts

(West Pawlet, Vermont 05775, U.S.A.)

9.1 THE UNDERSTANDING OF TROPICAL CONVECTION *CIRCA* 1973

While it had been recognized well before the planning of the Global Atmospheric Research Program's Atlantic Tropical Experiment (GATE) that deep convection over the equatorial oceans is a primary mechanism for transporting heat from the planetary boundary layer to the upper troposphere (Riehl and Malkus, 1958), it was just becoming evident during the planning of the experiment (from accumulating satellite evidence) that this convection was concentrated in "cloud clusters" (Martin and Karst, 1969; Frank, 1970; Martin and Suomi,1972). During GATE planning meetings, a cloud cluster came to be defined as a group of cumulonimbus joined in their mature and dissipating stages by a common **cirrus shield ∿100 to 1000 km in horizontal dimensions** (GARP Publications Series No. 4, 1970). The bright cirriform tops of the clusters were seen to dominate the satellite-observed cloud patterns over the equatorial oceans (Kornfeld et al., 1967). The clusters seen in satellite imagery appeared and disappeared somewhat sporadically (GATE Report No. 1, 1972, p. 28); however, Reed and Recker (1971) showed that cloud cluster frequency over the equatorial Pacific Ocean was modulated by the passage of synoptic-scale waves in the easterlies.

Heat and moisture budgets in the vicinities of tropical cloud clusters were determined from rawinsonde data by several investigators in the early 1970's. Gray (1973) suggested that the budgets that were obtained could be explained only if an average cloud affected its large-scale environment through a combination of dry compensating subsidence, which warmed the environment, and detrainment of hydrometeors, which evaporated and thereby cooled the environment. Yanai et al. (1973), Ogura and Cho (1973), López (1973) and Nitta (1975) used one-dimensional cumulus models to show that this was the case. Betts (1973b) presented similar arguments in his studies of cumulonimbus clouds over Venezuela.

The approaches of Yanai et al. (1973), Ogura and Cho (1973), and Nitta (1975) provided a particularly useful mathematical framework for the study of convection in GATE. Their equations employing simple cumulus models to diagnose convective cloud properties from observed large-scale budgets paralleled those used by Ooyama (1971) and Arakawa and Schubert (1974) in their schemes for the parameterization of convection in numerical models of large-scale atmospheric flow. It was evident, however, that the usefulness of the results of the diagnostic techniques or parameterization schemes depended on the adequacy with which the assumed cloud models actually described the component clouds of clusters.

---

*This chapter is published as an article in Reviews of Geophysics and Space Physics under the title: "Convection in GATE". The article is reprinted here with the permission of the American Geophysical Union.

Questions about this adequacy were already evident in 1973. During the Line Islands Experiment, aircraft and other detailed observations of one cloud cluster showed that its common cloud shield was in the form of a stratiform "anvil" cloud trailing a line of deep cumulonimbus cells (Zipser, 1969). The base of the anvil was at middle levels (4-5 km), and general non-convective precipitation was falling from it. This widespread rain was evaporating as it fell and thereby cooling the air below the anvil cloud. The cooled air was subsiding in a general mesoscale downdraft extending over a region several hundred kilometers in horizontal scale. Similar mesoscale downdrafts were also noted by Riehl (1969) in oceanic cloud clusters and by Betts (1973b) in Venezuelan cumulonimbus.

From these observations, it was apparent that mesoscale as well as cumulus-scale vertical motions could be important circulation features in cloud clusters. Such structure was considerably more complex than the mathematically simpler types of clouds assumed in diagnostic calculations or parameterization schemes.

9.2 THE AIMS OF GATE IN IMPROVING THE UNDERSTANDING OF TROPICAL CONVECTION

Against this background of the general understanding of tropical convection at the time of the planning of GATE, it is not surprising that the experiment was designed "... to provide a description of the internal structure of a number of cloud clusters, to estimate the vertical (and horizontal) transport of heat, moisture and momentum associated with the systems and to relate them to movements of the tropical atmosphere on a larger-scale." (GATE Report No. 1, 1972, p. 7). The descriptions would be made possible by employing a variety of special observing systems. At the same time, the large-scale budgets of mass, heat, momentum and other quantities would be determined from intensive soundings of the atmosphere in the vicinity of the convection. Diagnostic techniques of the type pioneered by Yanai *et al.* (1973), Ogura and Cho (1973) and Nitta (1975) could then be used to deduce cloud properties, and these properties could be compared with those shown directly by the special observing systems. In this way, the physical understanding of tropical convection would be increased and the adequacy of cloud models used in diagnostic studies (and parameterization schemes) would be determined. Moreover, as large-scale atmospheric conditions shown by the soundings were observed to change during the course of the experiment, for example, diurnally or with the passage of easterly waves, associated changes in the observed convective processes could be noted.

9.3 METHODS OF OBSERVING THE CONVECTION IN GATE

In GATE, the standard approach of combining satellite, radar, aircraft, and highly resolved upper-air balloon data was adopted to probe the convective cloud field. These data were supplemented by standard synoptic observations, surface-based cloud photography and a variety of boundary-layer measurements. Each type of data collected contributed in a unique way to an understanding of the cloud fields. The principal types of data are discussed below.

9.3.1 Satellite

During the summer of 1974, the geosynchronous meteorological satellite SMS-1 was positioned to provide detailed imagery over the GATE area. These data, obtained at 15-30 min intervals throughout the experiment, provided a detailed history of the development of cloud patterns over the GATE region. However, since the satellite data portrayed only the tops of the clouds, it was necessary to use other instrumentation to probe their internal structures.

9.3.2 Radar

The internal structures of GATE cloud systems were revealed by a network of weather radars, which showed the precipitation fields of the systems. Eight GATE ships carried radars (Arkell and Hudlow, 1977) of which four were C-band and equipped for digital data acquisition. Characteristics of the digital radar systems, which were arranged spatially to allow overlapping coverage (Fig. 9.1), are described by Hudlow et al. (1980). Three-dimensional fields of radar reflectivity (or precipitation intensity) were recorded simultaneously by all four digital radars at 15 min intervals throughout GATE.

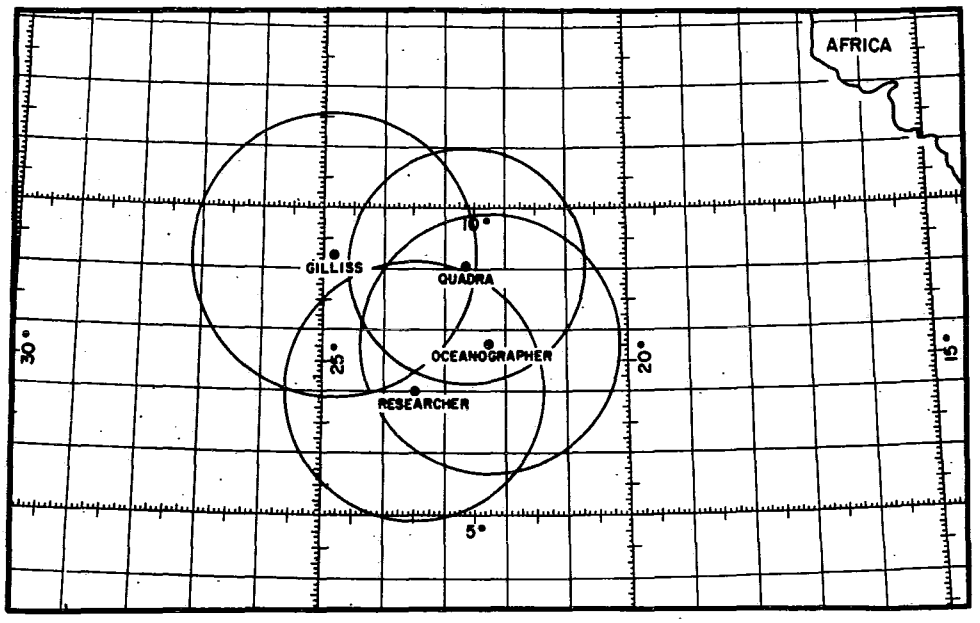

Fig. 9.1 Positions of ships carrying quantitative radars during Phase III of GATE (30 August-10 September 1974). A somewhat different arrangement was used in Phases I and II. From Houze (1977).

9.3.3 Aircraft

Although combined radar and satellite data, with the aid of surface-based cloud photography, gave a fairly complete description of the structure and evolution of the cloud and precipitation fields in GATE, these remote measurements gave no direct information (other than cloud top temperature) on the values of dynamical or thermodynamical variables within or near cloud systems. Measurements of these quantities were obtained by direct aircraft sampling of GATE cloud systems. The aircraft also provided additional cloud photography, turbulent flux measurements, radiation measurements, dropwinsondes, aerosol observations and cloud microphysical data.

Thirteen aircraft were used in GATE to make more than 400 research flights. Many of these flights were made in the vicinity of the shipborne radar network, thus providing detailed measurements near and within the same cloud systems being observed by radar and satellite. Summaries of the various aircraft missions are presented by Kelley (1974) and in GATE Report No. 18 (1975). Listings of the types of measurements and observations recorded during these flights can be found in the GATE Data Catalog (available from World Data Center-A, National Climatic Center, Asheville, North Carolina, U.S.A.).

9.3.4 Upper-air Soundings

Upper-air soundings in GATE were launched at three-hourly intervals from ships arranged within a hexagonal region surrounding the shipborne radar network. With this distribution of sounding sites, it was possible to monitor the structure of the large-scale environment in the vicinity of the cloud systems being observed by satellite, radar, and aircraft.

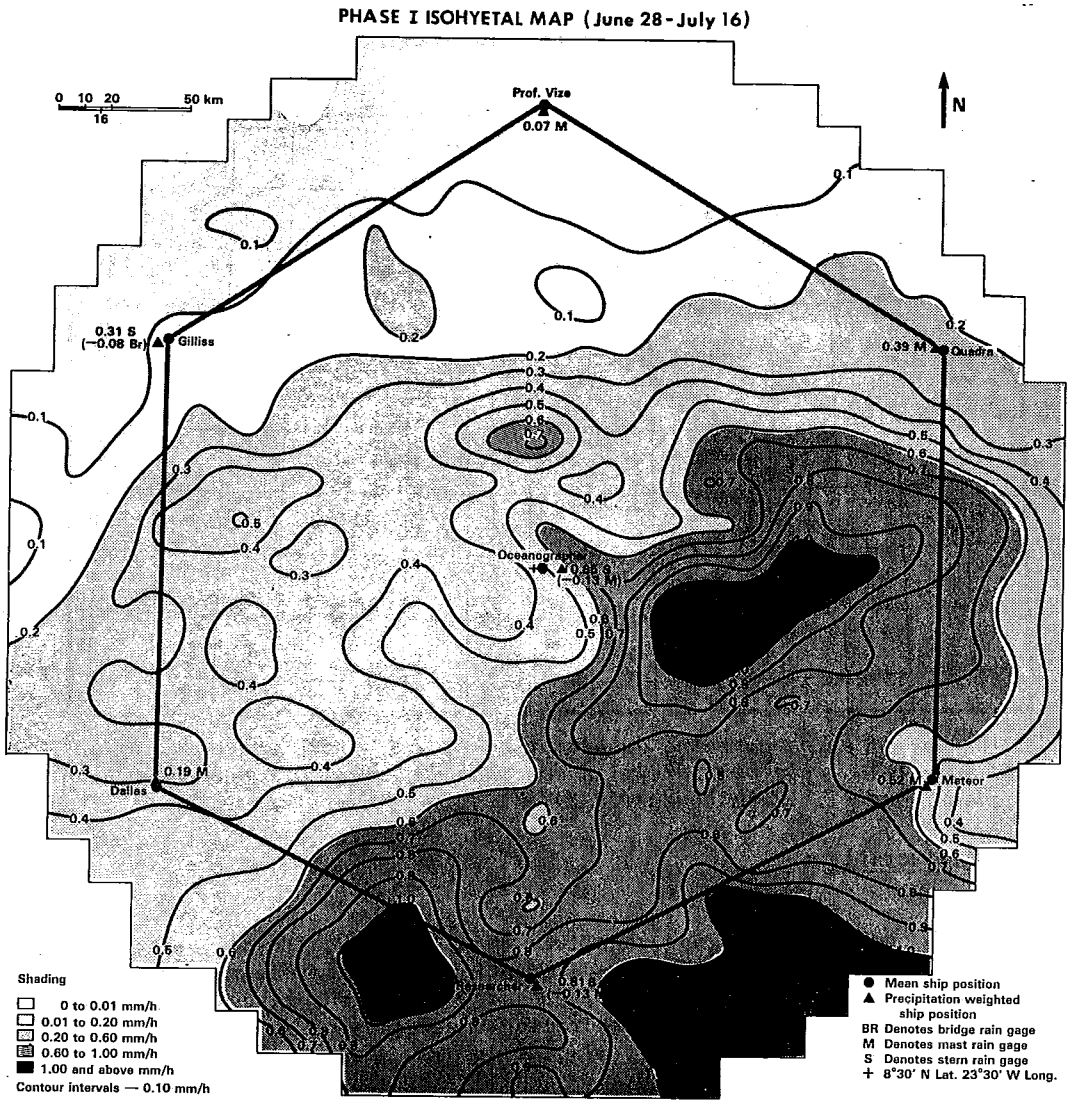

Fig. 9.2 GATE Phase I isohyetal chart derived from ship radar observations. The isopleths give the phase-mean rainfall rates (mm h^{-1}). From Hudlow (1979).

9.4 STATISTICAL SURVEYS OF GATE CONVECTION

The main array of ships in GATE was located so that it would be on or near the axis of the east-west belt of cloudiness and precipitation associated with the Intertropical Convergence Zone (ITCZ) (GATE Report No. 1, 1972). Thus, statistical studies of the various types of data collected within or near the array would reflect the mean properties of the convection in the ITCZ during the experiment. A variety of statistical and quasi-statistical studies have now been performed, and they are summarized below.

9.4.1 The Mean Rainfall Pattern in the ITCZ

The mean rainfall patterns within the GATE ship array were determined from the shipborne weather radars and have been presented by Hudlow (1979) (e.g., Fig. 9.2). These patterns are consistent with shipboard raingauge measurements (Hudlow et al., 1980) and with water vapor budgets derived from the upper air soundings obtained in the ship array (Lord, 1978; Thompson et al., 1979; Reeves et al., 1979). The precipitation pattern over a broader region than the GATE ship array has been estimated from the infrared imagery of the geosynchronous SMS-1 satellite by Woodley et al. (1980) (Fig. 9.3). Over the ship array, the satellite estimates agree reasonably well with the radar measurements and therefore appear to be a useful extension of the GATE precipitation pattern. This pattern confirms that the ship array was, in fact, in the maximum precipitation belt of the ITCZ.

9.4.2 Types of Clouds Occurring in the ITCZ

The types of clouds that formed within the portion of the ITCZ sampled by the GATE ship array have been determined from whole-sky camera photography obtained aboard four U.S. ships (Holle et al., 1979) and one Soviet ship (Bibikova et al., 1977). Simpson (1976), Borovikov et al. (1978), Peskov (1980), and Lebedeva and Zavelskaya (1980) have all commented on the frequent presence of several cloud layers, including cumulus clouds with bases near 500 m and layer clouds with mid-tropospheric bases near 4 km. From the U.S. photographs, Holle et al. (1979) determined that the frequency of low clouds (including deep cumulus and cumulonimbus as well as stratus and stratocumulus) and rainfall duration were maximum just south of 7-8° N. Combined middle and high clouds extended north of this zone in a manner consistent with the classic Hadley cell circulation, with poleward flow of air at upper levels from the equatorial trough.

9.4.3 Contributions of Cloud Clusters to Cloudiness in the ITCZ

Trajectories of cloud clusters over West Africa and the tropical Atlantic during GATE were compiled by Martin (1975) and found to occur in an east-northeast to west-southwest band extending from the African continent to the ship array and then westward across the Atlantic (for example, the cluster trajectories for the first fifteen days of GATE in Fig. 9.4). Thus, Martin (1975) concluded, the GATE ship array "lay squarely in the main cluster track and captured clusters in all stages of growth and dissipation." The cluster tracks, moreover, coincided with the mean precipitation zone shown by radar and satellite (Figs. 9.2 and 9.3), with the region of maximum cloudiness indicated by surface-based photography (Holle et al., 1979) and with global maps of cloud cluster frequency (Semyonov, 1975). Clearly, the mean cloudiness and precipitation associated with the equatorial Hadley cell in the GATE region is largely a composite of individual cloud clusters.

A special type of cloud cluster is the "squall-line" or "squall cluster" (Hamilton and Archbold, 1945; Zipser, 1969). As noted by Martin (1975), squall clusters are evident in satellite imagery by their "explosive growth, oval shape, and very high brightness." Aspliden et al. (1976) identified 176 squall clusters during GATE. The majority formed and decayed over the West African continent (162 and 130, respectively). Over the ocean only 14 formed and 46 decayed. Thus, the cloud clusters sampled by the GATE ship array were predominantly non-squall clusters, while over the continent, cluster statistics, such as the higher cluster speed and longer trajectories seen over land in Fig. 9.4, were strongly influenced by squall clusters.

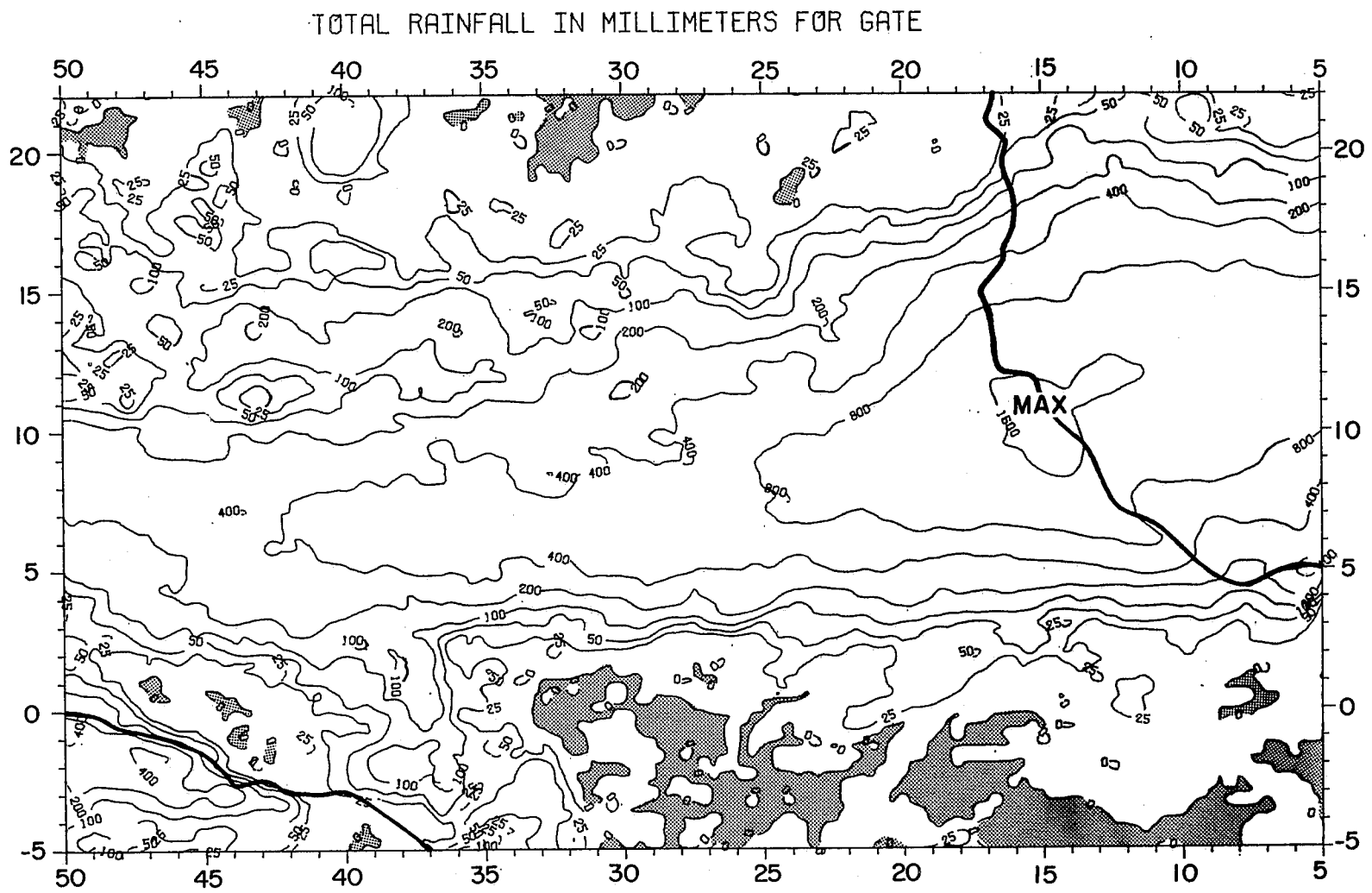

Fig. 9.3 Mapped total rainfall (mm) for all GATE (27 June-20 September 1974, excluding 22 August). Tic marks indicate latitude and longitude. Derived from SMS-1 satellite imagery, from Woodley et al., (1980)

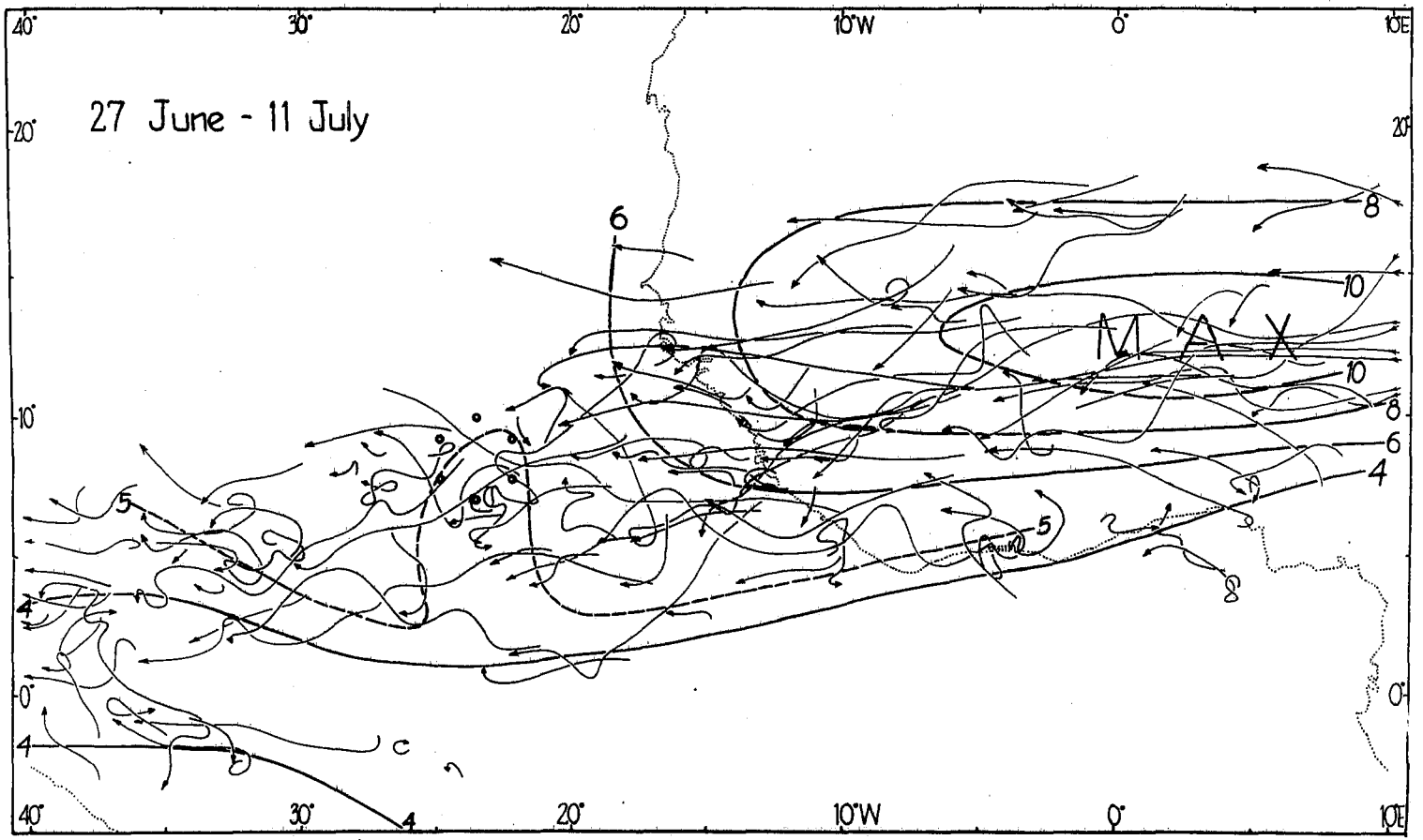

Fig. 9.4 Trajectories of cloud clusters for the first 15 days of GATE. Contours represent averages of cluster speeds over 10° x 10° squares. Circles indicate ship positions. From Martin (1975).

9.4.4 Modulation of Cloud Cluster Frequency by Synoptic-scale Wave Passages

That cloud cluster frequency in the ITCZ can be modulated by the passages of easterly waves was shown by Reed and Recker (1971). Synoptic-scale easterly waves were observed to pass over the GATE ship array at intervals of 3-4 days (Burpee, 1975; Reed et al., 1977). Payne and McGarry (1977) showed that the occurrence of convective cloudiness associated with clusters was enhanced at and ahead of trough axes and suppressed at and ahead of ridge axes (Fig. 9.5). Large non-squall cloud clusters occurred just ahead of the trough and moved at slightly less than the phase speed of the wave. Squall clusters also tended to occur just ahead of the trough but moved at about twice the speed of the wave and tended to die just behind the ridge.

The modulation of GATE cloud cluster occurrence by synoptic-scale waves is also indicated by the correlation of rainfall over the ship array with wave phase (Thompson et al., 1979; Hudlow, 1979; Reeves et al., 1979).

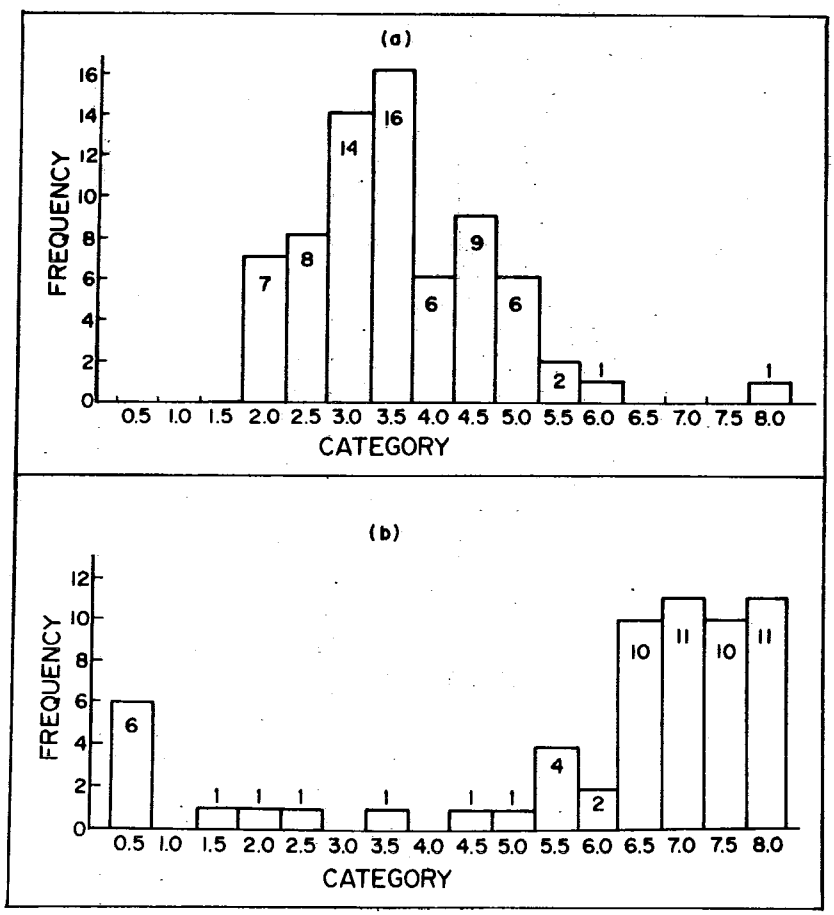

Fig. 9.5 Frequency distribution of maximum values of enhanced convective cloud coverage (a) and minimum values (representing suppressed convective coverage) (b) versus wave phase category for each separate positive and negative region of coverage, respectively, during the 28-day period from 23 August-19 September 1974. Category 4 is the trough and Category 8 is the ridge. From Payne and McGarry (1977).

9.4.5 Diurnal Variation of Cloud Cluster Occurrence

Diurnal variations of convective cloudiness occur in the tropics for various reasons. Over continents destabilization by the daily cycle of insolation can be important. Over and near large islands and peninsulas such as Borneo and Malaya, land-sea breezes control diurnal variations in clouds and precipitation (Ramage, 1971; Houze et al., 1981). Over much of the open equatorial oceans, there is a tendency for an early morning ($\approx$0700 LST) maximum of precipitation, which Gray and Jacobson (1977) and McBride and Gray (1978) attribute to day- night differences in the radiative heating profiles in cloudy and cloud-free regions. They suggest that these differences lead, through adjustments of pressure fields, to a maximum of low-level convergence in the morning in the cloudy areas.

The diurnal variation of deep convective cloudiness inferred from satellite infrared images have been determined for the GATE ship area by Gruber (1976) and for both the ship area and portions of the West African continent by McGarry and Reed (1978), Murakami (1979) and Ball et al. (1980). McGarry and Reed (1978) also analyzed the diurnal cycles in rainfall data and reports of thunder and lightning. McGarry and Reed showed further how the amplitudes and phases of local diurnal cycles vary geographically over both the GATE ship area and the coastal and land areas of western Africa (e.g., Fig. 9.6). Afternoon maxima of convective cloudiness and precipitation occurred over the ship array, while over the northern part of the land area large amplitude cycles occurred with rain amounts greatest shortly before midnight, maximum cloud cover shortly after midnight, and light rain most frequent near dawn.

The diurnal cycles over the northern continental regions are attributed by McGarry and Reed to the tendency noted by Martin (1975) and Aspliden et al. (1976) for intense cloud clusters to form in the afternoon and then take several hours to reach their stage of maximum development. The explanation of the afternoon maximum of cloudiness and precipitation over the GATE ship array is not as obvious. Noting Cox and Griffith's (1979) finding of significant differences in day and night heating profiles in cloudy and cloud-free regions in the GATE area, McBride and Gray (1978) modify their explanation of the 0700 LST cloudiness maximum over other equatorial ocean areas by suggesting that the adjustment of pressure fields resulting from the radiative heating and cooling differences leads to enhanced convergence in the morning but that the tendency for GATE cloud clusters (they say squall lines) to take several hours to reach their maximum stage of development explains the observed early afternoon precipitation maximum.

9.4.6 Sizes and Structures of Precipitation Areas in the ITCZ

In satellite imagery, a cloud cluster typically appears as a rather homogeneous patch of upper-level cloud. However, the precipitation falling from this cloud is seldom, if ever, correspondingly homogeneous. Typically, there are several cumulonimbus features with precipitation areas of a variety of sizes and types interconnected by the same upper cloud shield. Statistical studies of radar echo patterns have determined characteristics of the population of precipitation features that occurred in the GATE ship array.

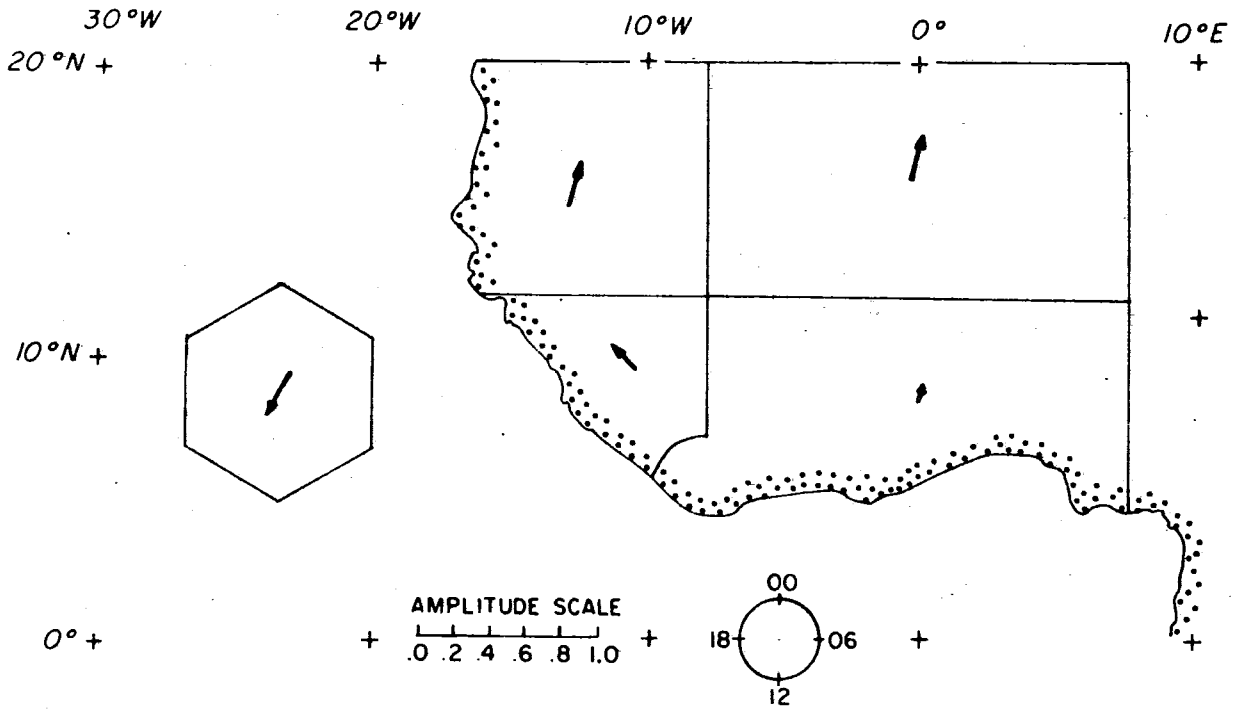

Fig. 9.6 Phase and normalized amplitude of diurnal cycle of convective cloudiness for Phases II and III of GATE based on 6-hourly SMS-1 satellite photographs. Time of the maximum is indicated by direction of arrow according to 24h clock. From McGarry and Reed (1978).

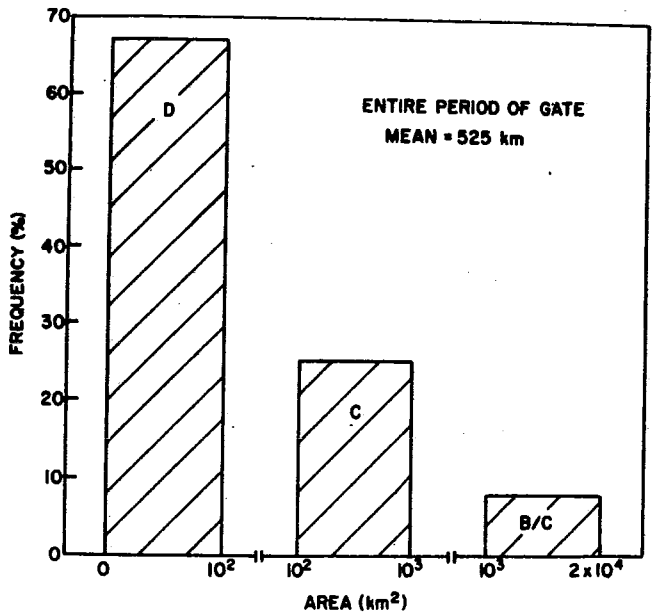

Fig. 9.7 Frequency of occurrence of D, C, and B/C scale radar echoes during GATE. From Houze and Cheng (1977).

9.4.6.1 The Size Spectrum of GATE Radar Echoes

Prior to GATE, convective radar echo patterns over the western tropical Atlantic Ocean had been studied by Iwanchuk (1973) and López (1976), who found that small echoes (<10 km^2 in area) dominated the total number of echoes, while large echoes (>10 km^2 in area) accounted for most of the area covered by precipitation. Convection in GATE (i.e., the eastern Atlantic) has been found to be similar. Using radar observations from the GATE ship Oceanographer, Houze and Cheng (1977) made a comprehensive survey of radar echoes occurring around 1200 GMT on most days of GATE. Some 67% of the echoes in GATE were 1-10 km^2 in area (D scale) and 28% were 10^2 -10^3 km^2 (C scale), while only 8% were >10^3 km^2 (B/C scale) (Fig. 9.7). Yet 79% of the total area covered by echoes was covered by the B/C scale echoes (Fig. 9.8). Hence, the relatively few large precipitation areas present in GATE (and other tropical cloud populations) take on great importance when their areal extent is considered. López (1978), also working with the Oceanographer radar data from GATE, further showed that the largest 10% of the echoes accounted for 90% of the precipitation.

Examined in another way, the size spectrum of radar echoes in the tropics (whether measured in terms of echo areas, heights, durations, or rainfall intensities) is usually found to be basically lognormal (Fig. 9.9) (López, 1976, 1977). In GATE, lognormality of the radar echo population has been found to hold both for long periods of time (Houze and Cheng, 1977; López, 1978) and at individual times during the development and dissipation of a single cloud cluster (Warner and Austin, 1978). GATE shipboard observations indicate that visually observable cloud dimensions also had a lognormal frequency distribution (Kuusk et al., 1978).

Houze and Cheng (1977) found that echo heights and durations were positively correlated with echo areas, and that larger echoes tended to contain multiple cores, with the most intense maxima occurring in the largest echoes (Fig. 9.10). From Fig. 9.10, it can be seen that on average only 10-11 echo cores were observed to exist at any one time in echoes exceeding 10^4 km^2 in area. If the individual cores were typically 10^2 km^2 in area, then only about 10% of the area covered by these large echoes consisted of intense cores. Much of the area covered by these huge echoes consisted instead of relatively uniform rain in which individual echo cores could not be easily identified. It is evident from case studies of cloud clusters (Sec. 9.5) and observations such as those of Borovikov et al. (1975) that this uniform rain was of the type associated with the anvil cloud of the Line Islands cloud cluster studied by Zipser (1969).

9.4.6.2 Types of Radar Echoes in GATE

From the foregoing statistics of echo sizes, four types of GATE radar echoes (precipitation areas) can be identified:

(i) Isolated cells or cores -- these were the smallest in horizontal extent (D scale to smaller C scale), shallowest in vertical extent (≤6 km) and least intense;

(ii) Aggregates of cells or cores -- these were of moderate horizontal extent (larger C scale and smaller B/C scale echoes), containing individual cores reaching 6-9 km in height, and had echo cores reaching moderate intensities;

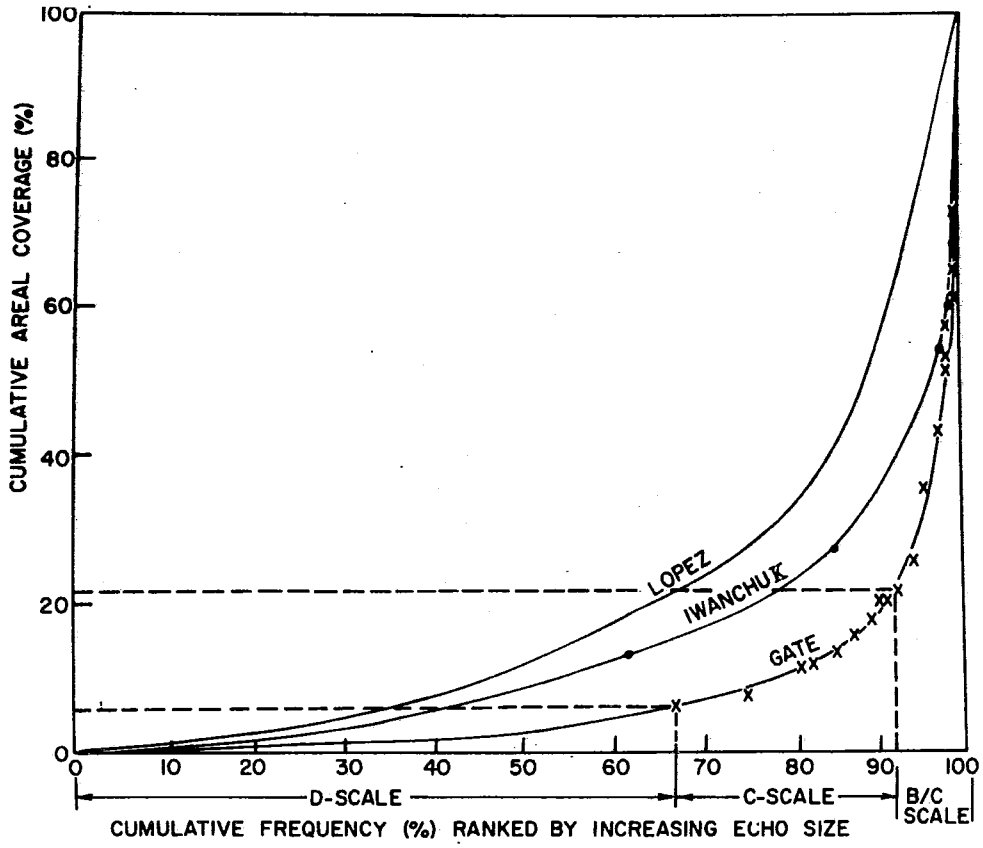

Fig. 9.8 Cumulative frequency distribution of accumulated echo areal coverage. Western tropical Atlantic distributions compiled by Lôpez (1976) and Iwanchuk (1973) are shown for comparison. Dashed lines are referred to in text. From Houze and Cheng (1977).

(iii) Aggregates of cells or cores with associated regions of uniform anvil rain -- these were the largest echoes of GATE (larger B/C scale echoes), containing the deepest (generally >9 km, often overshooting to 16-17 km) and most intense cells;

(iv) Regions of uniform anvil rain containing few if any deep convective cells -- these echoes were the remnants of type (iii) echoes whose convective cells had died but whose anvil rain remained for some time.

These four types of echoes correspond to convection in successively more advanced stages of development. Type (iii) and (iv) echoes occurred only in major cloud clusters (see case studies in Sec. 9.5). Characteristics of the convective cells, which occurred in types (i), (ii) and (iii) echoes, will be discussed in Sec. 9.4.6.3 below, while the structure of the anvil precipitation will be described in Sec. 9.4.6.4.

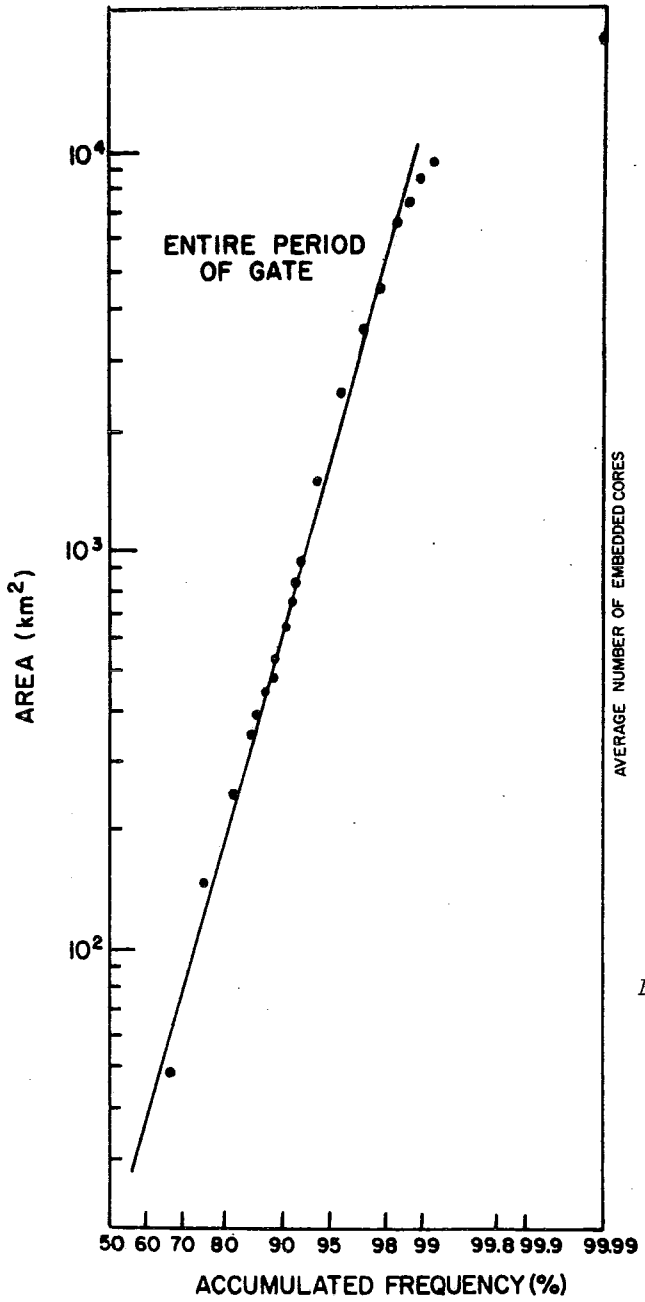

Fig. 9.9 Accumulated frequency distribution of areas covered by GATE radar echoes plotted in log-probability format. The straight line shows the log-normal distribution computed from the mean (1.54) and standard deviation (0.83) of the logarithms of the observed echo areas. From Houze and Cheng (1977).

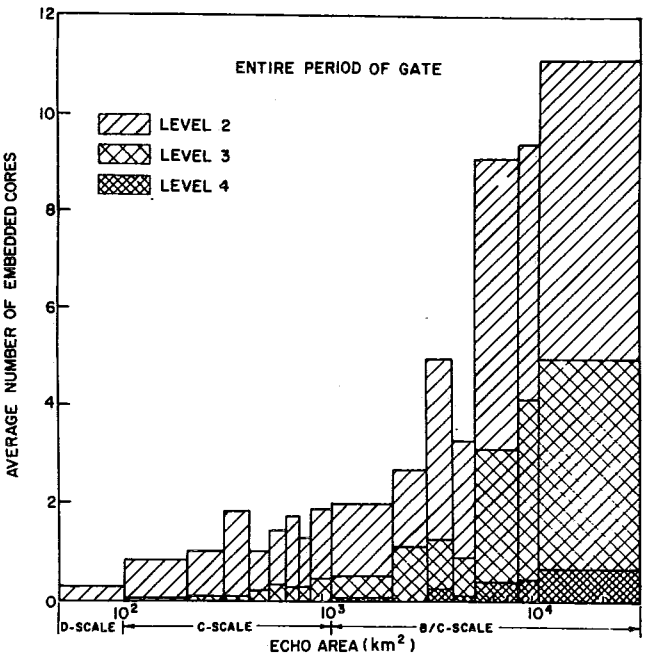

Fig. 9.10 Average number of embedded cores of maximum radar reflectivity located within GATE radar echoes in different size ranges. Shading indicates the fraction of the total number of cores in each size range which exceeded reflectivity threshold levels 2 (31 dBZ), 3 (30 dBZ), and 4 (47 dBZ). From Houze and Cheng (1977).

9.4.6.3 Characteristics of Cells

López (1978) examined a large sample of isolated cells and aggregates of cells [type (i) and (ii) echoes]. The frequency distributions of the maximum areas attained, durations and rainfall intensities of the isolated cells and the cells contained in aggregates were determined. The distributions were found to be lognormal both for the isolated cells and the cells making up aggregates (Fig. 9.11). However, the means of the distributions for the cells in aggregates were greater, that is, the cells making up the aggregates tended to be larger, last longer, and rain more than isolated single-cell echoes. Evidently, as concluded by Lopez, the formation of aggregates affords a measure of protection from entrainment of unsaturated environment air for cells embedded within the aggregates, while such protection is not available to isolated cells.

Direct sensing of the air motions in cells was accomplished by GATE aircraft sampling. LeMone and Zipser (1980) and Zipser and LeMone (1980) have examined aircraft measurements of the updraft and downdraft velocities in cells of type (i)-(iii) echoes on six days of GATE. They divided the data into: "drafts", where the vertical velocity is non-zero continuously for $\geq$ 0.5 km, and "cores", for which the absolute values of the velocity exceeds 1 m s^{-1} for $\geq$ 0.5 km. The distributions of draft and core sizes and intensities were lognormal at all altitudes in each echo- system penetrated (Fig. 9.12). The tendency of convective entities to be lognormally distributed is thus seen to apply not only to gross echo structures from 10^2 to $\approx 5 \times 10^4$ km^2 in area (Fig. 9.9), to echo cells $\sim$10-200 km^2 (Fig. 9.11) and to visible clouds (Kuusk et al., 1978) but also to the individual updrafts and downdrafts $\sim$0.25-50 km^2 in cross-sectional area that were embedded within the cells of the precipitating clouds.

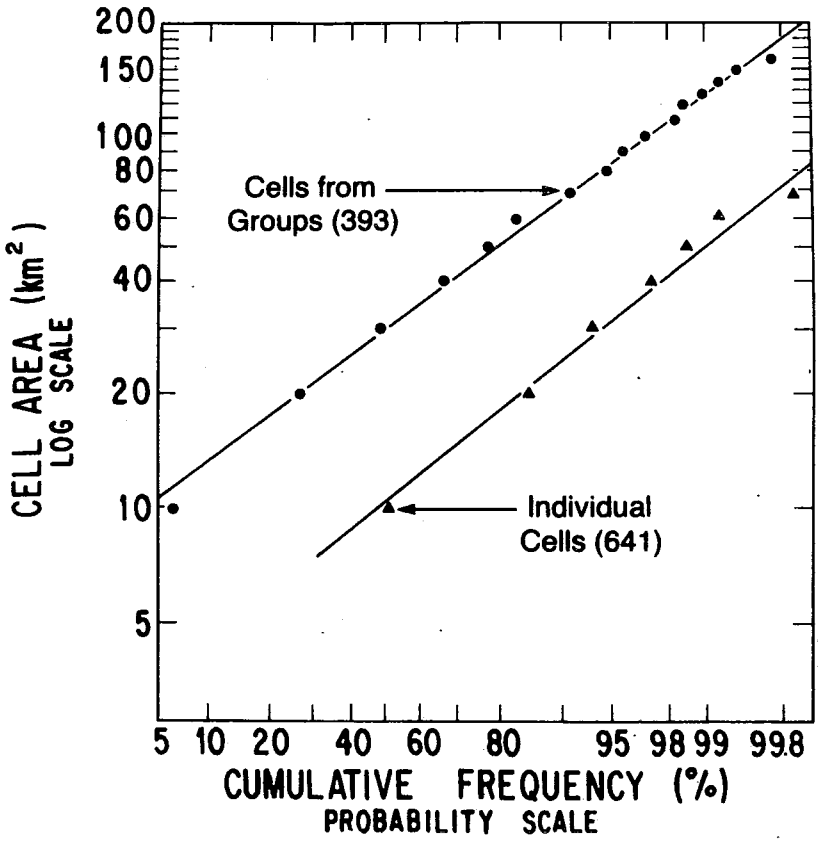

Fig. 9.11 Cumulative frequency distribution of the maximum area attained by radar echo cells that are isolated and members of aggregates. From López (1978).

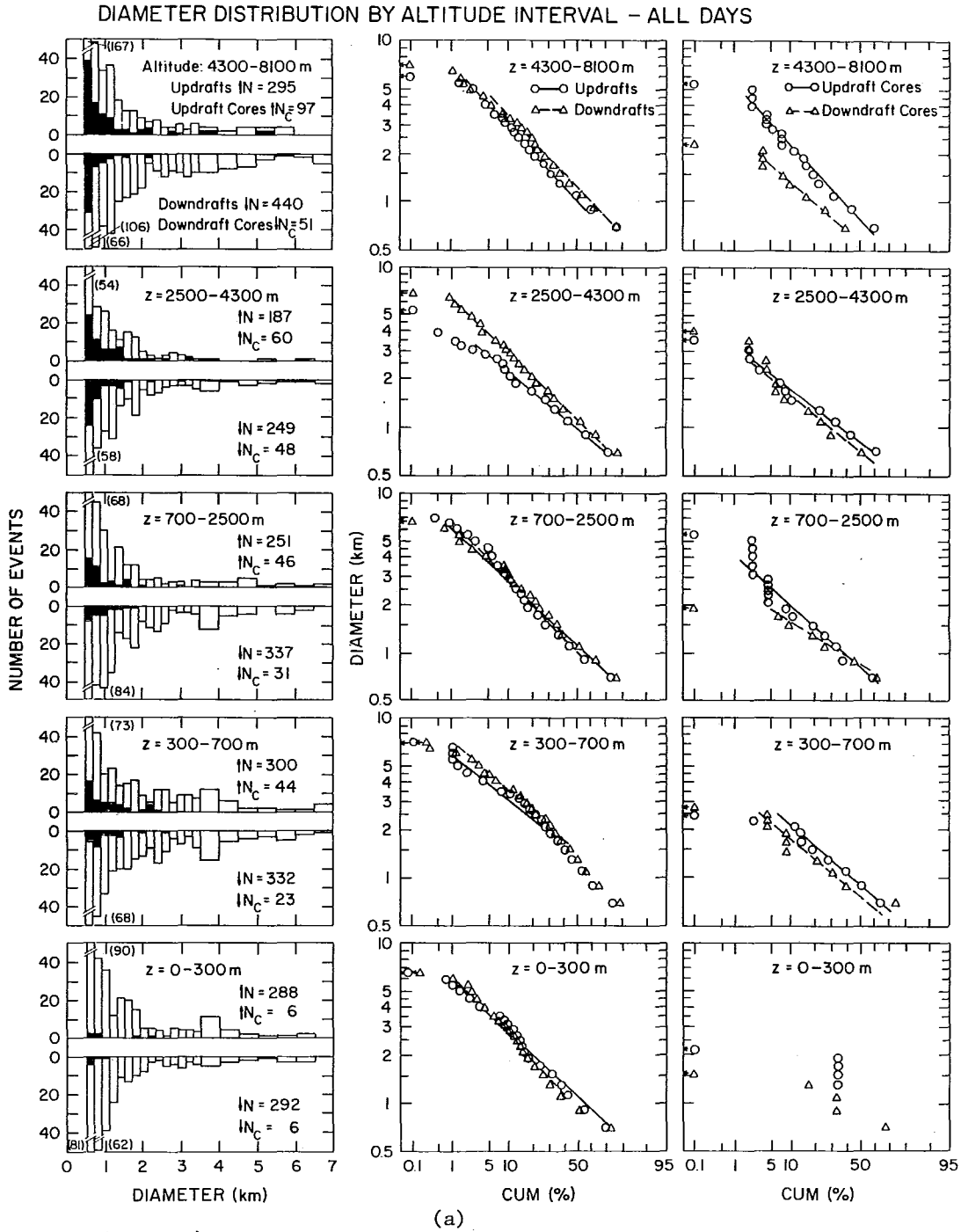

Fig. 9.12 Aircraft measurements in GATE convective cells. Combined draft and core statistics are summarized by altitude group. In bar graphs, total length is total number of drafts and black is total number of cores. Cumulative distributions are in log-probability format. See text for definitions of drafts and cores. From LeMone and Zipser (1980).

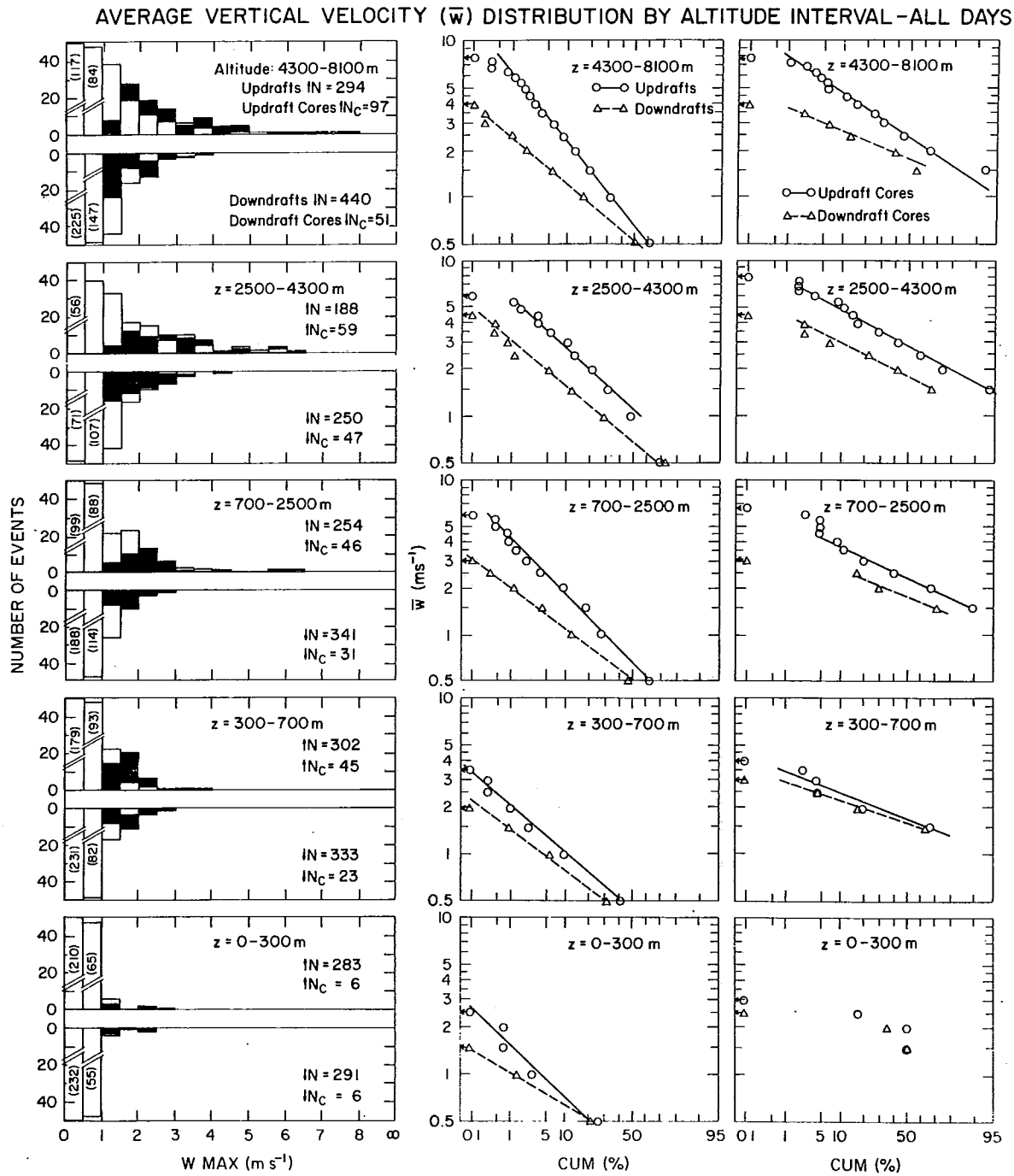

(b)

Fig. 9.12 (cont.)

The majority of the GATE convective cores described by Zipser and LeMone had mean vertical velocities < 3-5 m s^{-1}. (Peak values exceeded the mean values by a factor of 1.6 to 2.0.) In the middle troposphere, only 10% of the updraft cores had mean vertical velocities greater than 5m s^{-1} or diameters in excess of 2 km (Fig. 9.12). Downdraft cores were weaker than updraft cores, except near cloud base, where updraft and downdraft cores were of similar intensity. In general, the GATE cores and drafts were similar in size and intensity to those observed in hurricanes but weaker than those observed in the continental thunderstorms oserved in the U.S. Thunderstorm Project (Byers and Braham, 1949).

9.4.6.4 Anvil Precipitation Structure

The anvil rain in type (iii) and (iv) echoes was a substantial contribution to the total GATE rainfall. Cheng and Houze (1979) estimated its contribution to be 40%. The structure of the anvil rain resembled that of mid-latitude stratiform rain. Leary and Houze (1979b) examined five examples of anvil rain. They found that the radar reflectivity was horizontally stratified with a well defined radar bright band at the melting level (e.g., Fig 9.13). Preliminary analyses of GATE radar measurements had indicated that bright bands were frequently present (Houze, 1975; Shupiatsky et al., 1975, 1976a, b). The presence of the bright band indicates that strong convective cells were absent and ice particles were gently settling downward, melting and falling to the surface as widespread anvil rain.

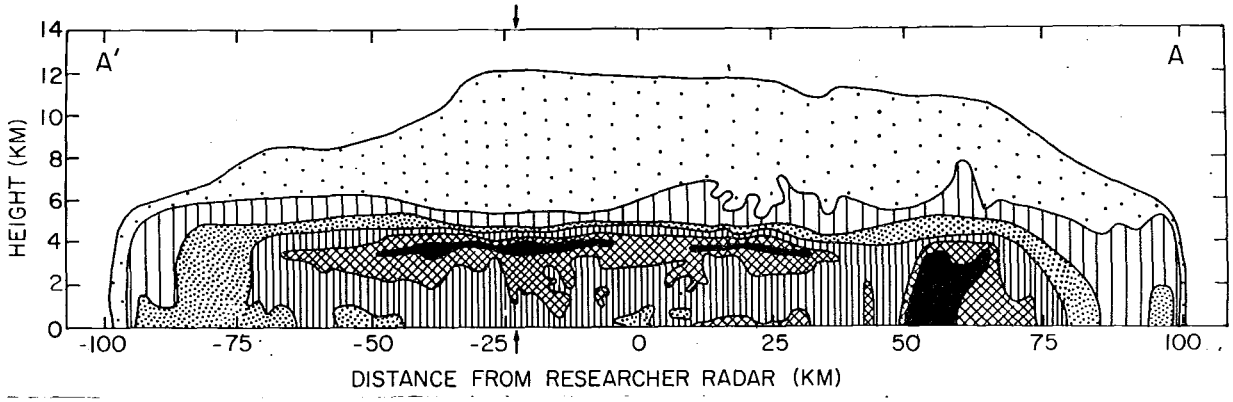

Fig. 9.13 Vertical cross-section showing the uniform precipitation (between -150 and 50 km) in a large GATE radar echo. A radar bright band is in evidence in the melting layer just below 4 km height. Data were obtained with the Researcher radar at 2100 GMT, 4 September 1974. The outside contour is for the minimum detectable echo, inner contours are for 23, 28, 33, 38, and 43 dBZ, and arrows indicate the vertical profile in Fig. 6a. From Leary and Houze (1979b).

The physical processes in an anvil rain region are illustrated schematically in Fig. 9.14. The microphysical structure was deduced indirectly by Leary and Houze (1979b) from observed vertical distributions of radar reflectivity and by determining the types of ice particles that would, upon melting, produce a population of raindrops having a size distribution similar to drop-size distributions observed aboard GATE ships and aircraft (Cunning and Sax, 1977a, b; Austin and Geotis, 1979). It was determined that rimed aggregates and hexagonal graupel were the probable ice particle types just above the melting layer. The existence of riming and graupel is consistent with the observations of Borovikov et al. (1978), who noted aircraft icing and liquid drops co-existing with ice in GATE cirrus clouds. They noted, however, that at altitudes as high as 12-13 km only ice was present. These observations suggest active anvil clouds, in which enough lifting is present to maintain liquid water in the presence of ice. Below the melting level, the primary microphysical process in the anvil region is evaporation of the falling raindrops in dry subsiding air below cloud base.

Air motions within and below the anvil and their relationship to evaporation and melting will be discussed further in the next section of this paper.

9.5 CASE STUDIES OF GATE CONVECTION

In the preceding section, it was seen that the mean cloudiness and precipitation in GATE was accounted for primarily by cloud clusters. To date, twelve GATE cloud clusters have been subjected to various degrees of case-study analysis (Table 9.1). The first six of the case studies listed in Table 9.1 were of squall clusters. The other six were non-squall clusters. In the following subsections, we will first discuss the squall clusters. This will be followed by a discussion of the non-squall clusters and then by a discussion of smaller cumulus and cumulonimbus associated with clusters.

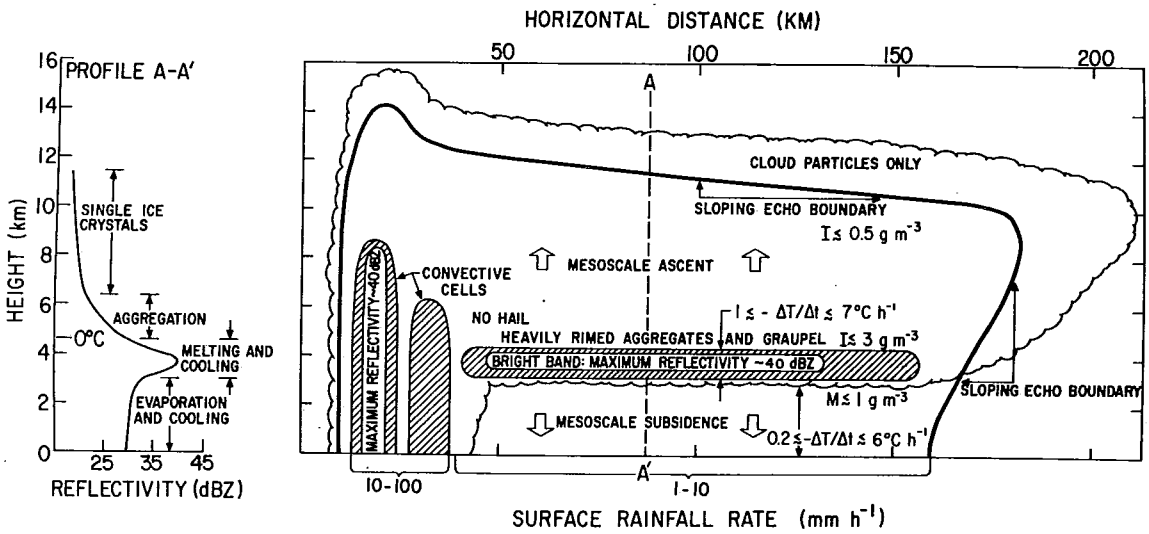

Fig. 9.14 Schematic vertical cross section and vertical profile of radar reflectivity (along dashed line A-A' in the cross section) in horizontally uniform precipitation associated with an anvil cloud. The anvil cloud occurs to the rear of intense convective cells propagating in the direction from right to left in the figure. The dark solid line is the contour of minimum detectable radar echo, lighter solid lines and shading indicate contours of higher reflectivity, and the scalloped line indicates the cloud boundary. From Leary and Houze (1979b).

Table 9.1 Studies of major convective events in GATE.

Investigator	Day of GATE	Type of Convective Event
Reed (1975) Zipser (1977)	28 June	Squall line over the GATE ships
Houze (1975, 1976, 1977) Mansfield (1977) Ogura et al. (1979)	4-5 September	Squall line over the GATE ships
Zipser (1977) Fortune (1980)	4-5 September	Family of squall lines over Africa
Houze (1975) Mansfield (1977) Leary and Houze (1979b)	11 September	Squall line over the GATE ships
Houze (1975) Shupiatsky et al. (1976b) Mandics and Hall (1976) Zipser (1977) Mansfield (1977) Nitta (1977) Gaynor and Mandics (1978) Leary and Houze (1979b)	12 September	Squall line over the GATE ships
Houze (1975) Mansfield (1977)	16 September	Squall line over the GATE ships
Zipser and Gautier (1978)	15 July	Non-squall cloud cluster associated with an oceanic tropical depression northeast of GATE ships
LeMone (1975) Nicholls (1979)	3 August	Weak non-squall cluster in an ITCZ wind pattern over the GATE ships
Shupiatsky et al. (1976b) Ogura et al. (1979)	11-12 August	Non-squall cluster in a well-defined ITCZ cloud pattern over the GATE ships
Betts (1978) Mower et al. (1979) Warner (1980)	2 September	Non-squall cloud cluster over the GATE ships
Leary and Houze (1976, 1979a) Suchman and Martin (1976) Nitta (1977) Ogura et al. (1979) Leary (1979) Nicholls (1979)	5 September	Double non-squall cloud cluster over the GATE ships
Zipser (1980) Zipser et al. (1981)	14 September	Non-squall cloud cluster over the GATE ships
Suchman et al. (1977) Warner and Austin (1978) Warner et al. (1979) Warner et al. (1980) Simpson and van Helvoirt (1980)	18 September	Non-squall cloud cluster and associated small clouds over the GATE ships

9.5.1 Squall Clusters

9.5.1.1 The Formation Process

The statistical studies of Martin (1975) and Aspliden et al. (1976) showed that squall clusters were most frequent over the African continent. In a case study, Fortune (1980) reported on a "family" of five squall lines that developed in series over the African continent. The time-lapse sequence of satellite imagery in this case shows the origin of each squall system and the westward advance of its anvil shield or its leading arc of low cumulus (Fig. 9.15). In high-resolution visible imagery, available for the daylight hours, the arc clouds are seen at the squall front just ahead of the advancing upper-level anvil cloud. The five squall systems were initiated from groups of or individual cumulonimbus identified in Fig. 9.15 as A-C, D-F, G-H, K, and L, respectively. Each of these squall systems produced a distinct anvil whose rapid expansion was tracked and measured. Systems A-C and D-F developed almost simultaneously and eventually merged. The resulting combined squall system appeared to trigger or excite the development of the next system during its late stages, when it approached the developing cells G-H. In a similar way, the squall that developed from G-H subsequently appeared to trigger two new squall lines, one to the south and one to the north, as it spread out and approached the cumulonimbus cells K and L.

The squall-line system studied by Houze (1977) also formed at the advancing arc-shaped edge of a dissipating anvil cloud, in this case, one which had moved from northeast to southwest over the ocean from a position over Africa on the preceding day. Apparently, in addition to being favored ahead of the troughs of synoptic-scale waves or at certain times of the day (cf., Secs. 9.4.3-.5), new squall lines tend to become organized when cumulonimbus cells form along or just ahead of the edges of horizontally expanding pools of dense downdraft air deposited at the earth's surface by older cloud clusters.

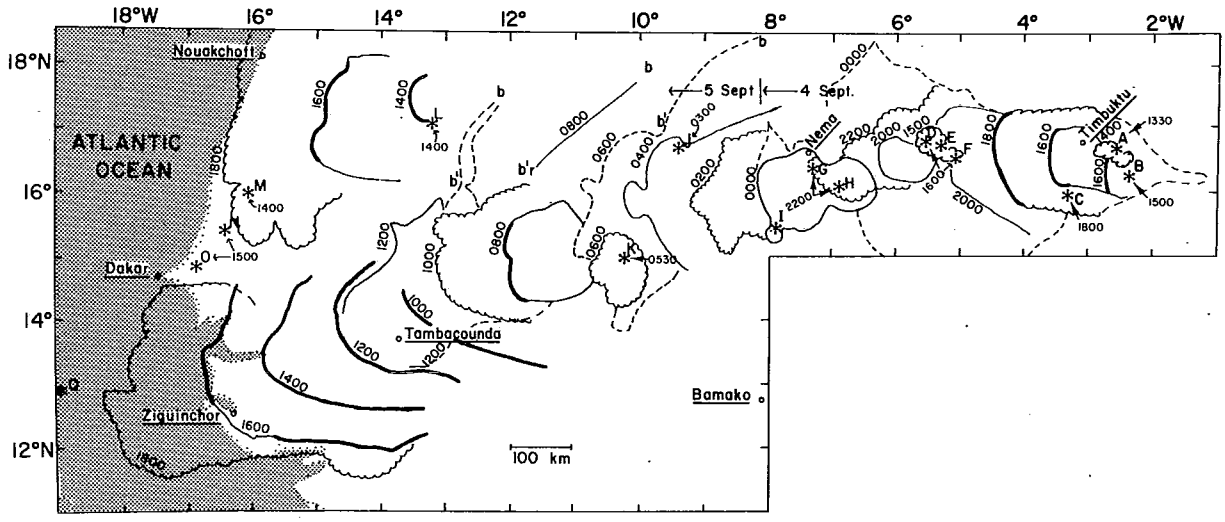

Fig. 9.15 The advance of the squall-line family of 4 and 5 September 1974 from its origins to the Atlantic. Asterisks mark the points of origin of squall line elements A-Q, with the hour of origin indicated. Alternating scalloped and thin lines show the leading edge of the anvil cloud at 2h intervals. Thick solid curves mark the position of the arc front on the visible pictures. Dashed lines outline the anvil every 6h. Line b-b' is a long-lived but dormant arc of middle cloud. From Fortune (1980).

9.5.1.2 Squall-line and Anvil Precipitation

Houze's (1977) case used GATE radar data to document the evolution and internal structure of a cloud cluster, which conformed in general with Zipser's (1969) conceptual model of a squall cluster and with the results of other pre-GATE studies of tropical squall lines (Hamilton and Archbold, 1945; Eldridge, 1957; Tschirhart, 1958; Obasi, 1974; Betts et al., 1976). The system consisted of a "squall line", forming its leading edge, and a trailing "anvil region". The radar data showed that the leading line consisted of discrete line elements (LE's), which formed ahead of the squall line, weakened toward the rear of the line and blended into the trailing anvil region as they dissipated. Each LE progressed through a period of rapid growth, with echo tops typically penetrating the tropopause to maximum heights of 16-17 km, then decreasing to heights of 13-14 km, corresponding to the height of the top of the anvil cloud with which the LE's merged at the end of their durations as active convective entities. This process is indicated schematically in Fig. 9.16.

As the old squall-line elements dissipated, their strong upward air motions apparently ceased and no longer carried precipitation particles upward or suspended them aloft. The fallout of particles from these weakened line elements then took on a stratiform appearance and, as the elements were incorporated into the anvil, they became indistinguishable from the rest of the anvil cloud and precipitation, which was horizontally stratified, with a pronounced melting band. This structure, illustrated schematically in Fig. 9.16 and by actual example in Fig. 9.17, is similar to that shown in Figs. 9.13 and 9.14. The mature squall-line system exemplifies the type (iii) radar echoes that consisted partly of convective cells and partly of stratiform rain (Sec. 9.4.6.2). The anvil precipitation evolved as shown in Fig. 9.18. During the first few hours of the disturbance, little anvil rain fell. As the anvil developed and expanded, the amount of rain falling from it became approximately equal to that coming from the squall line itself.

9.5.1.3 Convective and Mesoscale Vertical Motions

The large portion of the total rain coming from the anvil indicates that mesoscale vertical air motions associated with the anvil cloud as well as convective-scale updrafts and downdrafts associated with the cumulonimbus elements making up the squall line itself were important dynamical components of the squall-line system. Essentially similar conceptual models of the convective-scale and mesoscale vertical motions in GATE squall-line systems have been presented by Zipser (1977, Fig. 9.19), Houze (1977, Fig. 9.16) and Leary and Houze (1979b, Fig. 9.14). These models are consistent with the Venezuelan squall line model of Betts (1976a) and Betts et al. (1976). The updraft and downdraft structures contained in the models are summarized in the following subsections.

9.5.1.4 Convective-scale Updrafts

Convective-scale updrafts occur in the cumulonimbus elements making up the squall line. The rapid growth of the radar echoes traced through their life history to typical maximum heights of 16-17 km by Houze (1977) clearly indicates that buoyant convective updrafts produced these cells. The air feeding the squall-line updrafts comes from the pre-squall boundary layer. The vertical structure of the squall-line convective elements, shown by radar data (Houze, 1977) and in satellite imagery (Fortune, 1980), shows that these updrafts have a distinct tilt.

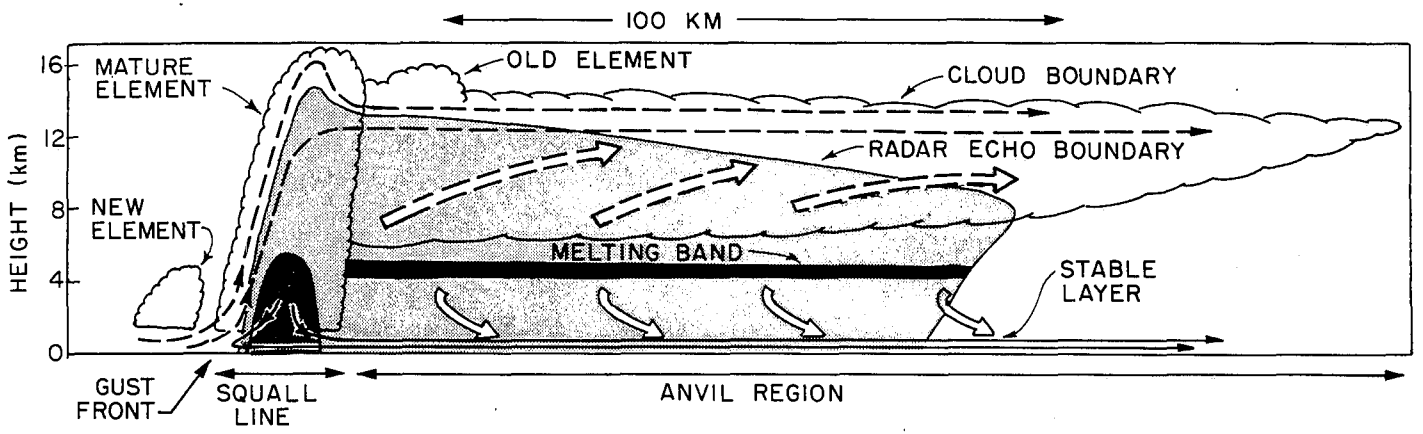

Fig. 9.16 Schematic cross section through squall-line system. Streamlines show flow relative to the squall line. Thin dashed streamlines show updraft circulation, thin solid streamlines show convective-scale downdraft circulation associated with mature squall-line element, and wide arrows show mesoscale downdraft below the base of the anvil cloud. Wide, dashed arrows show mesoscale ascent in the anvil. Dark shading shows strong radar echo in the melting band and in the heavy precipitation zone of the mature squall-line element. Light shading shows weaker radar echoes. Scalloped line indicates visible cloud boundaries. Adapted from Houze (1977).

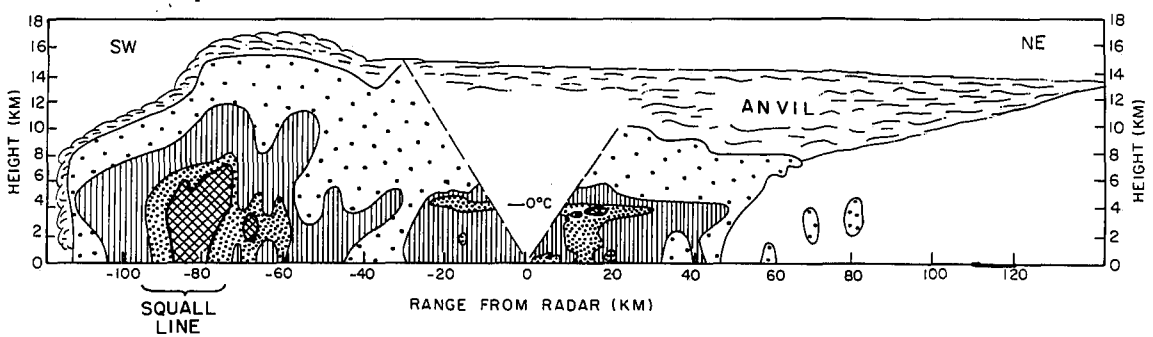

Fig. 9.17 Vertical cross section through entire squall-line system, along azimuths 223° (SW) and 43° (NE) from Oceanographer radar at 1545 GMT 4 September 1974. Inside contours are for 38, 33, 33, 23 dBZ and minimum detectable echo. Outside scalloped contour outlines cloud boundary estimated from infrared satellite imagery. From Houze (1977).

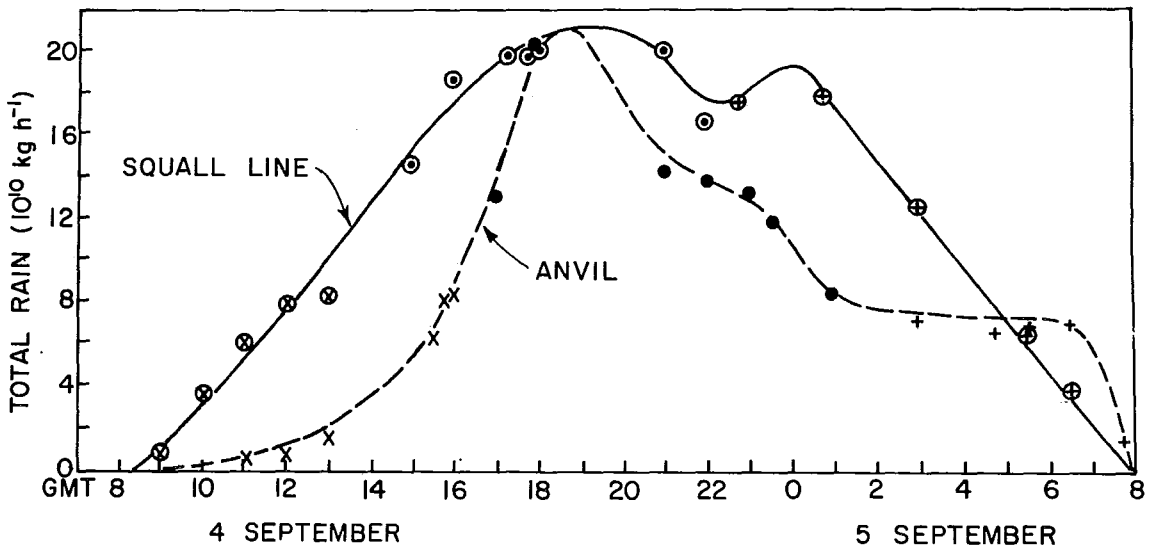

Fig. 9.18 Total rain integrated over areas covered by squall line and anvil portions of a squall-line system. Circled points refer to squall line region. Data points derived from Oceanographer radar echo patterns are indicated by X's. Points derived from composite Oceanographer and Researcher radar echo patterns indicated by dots. Points derived from composite Oceanographer, Researcher, and Gilliss echo patterns are indicated by crosses. From Houze (1977).

9.5.1.5 Convective-scale Downdrafts

Just behind and below the sloping updraft of a squall-line element there is a concentrated downpour of heavy precipitation that contains a convective-scale downdraft. These downdrafts, which are characteristic of cumulonimbus, apparently are negatively buoyant non-hydrostatic features composed of air, whose downward motion is initiated by weight of hydrometeors and sustained by evaporation.

The air feeding the convective-scale downdrafts comes from levels between 900 and 600 mb. At these levels, the mean relative flow is toward the squall line. Consequently, air enters one of these downdrafts after either circumnavigating discrete updraft towers distributed along the squall line or by finding itself behind a new line element that formed just ahead of the current squall line as part of the line's discrete propagation.

When the convective downdraft air reaches the surface, it has a lower moist static energy and is more stable that the pre-squall boundary-layer air (Betts, 1976a; Gaynor and Ropelewski, 1979; Fitzjarrald, 1979; Barnes, 1980). This air spreads out, partly toward the front of the squall-line system and partly toward the rear. The forward-spreading portions of the downdraft outflows of the various cumulonimbus elements along the squall line typically intersect and form a continuous windshift line along the front of the squall system in the manner suggested by Byers and Braham (1949) for mid-latitude squall lines (see their Fig. 113).

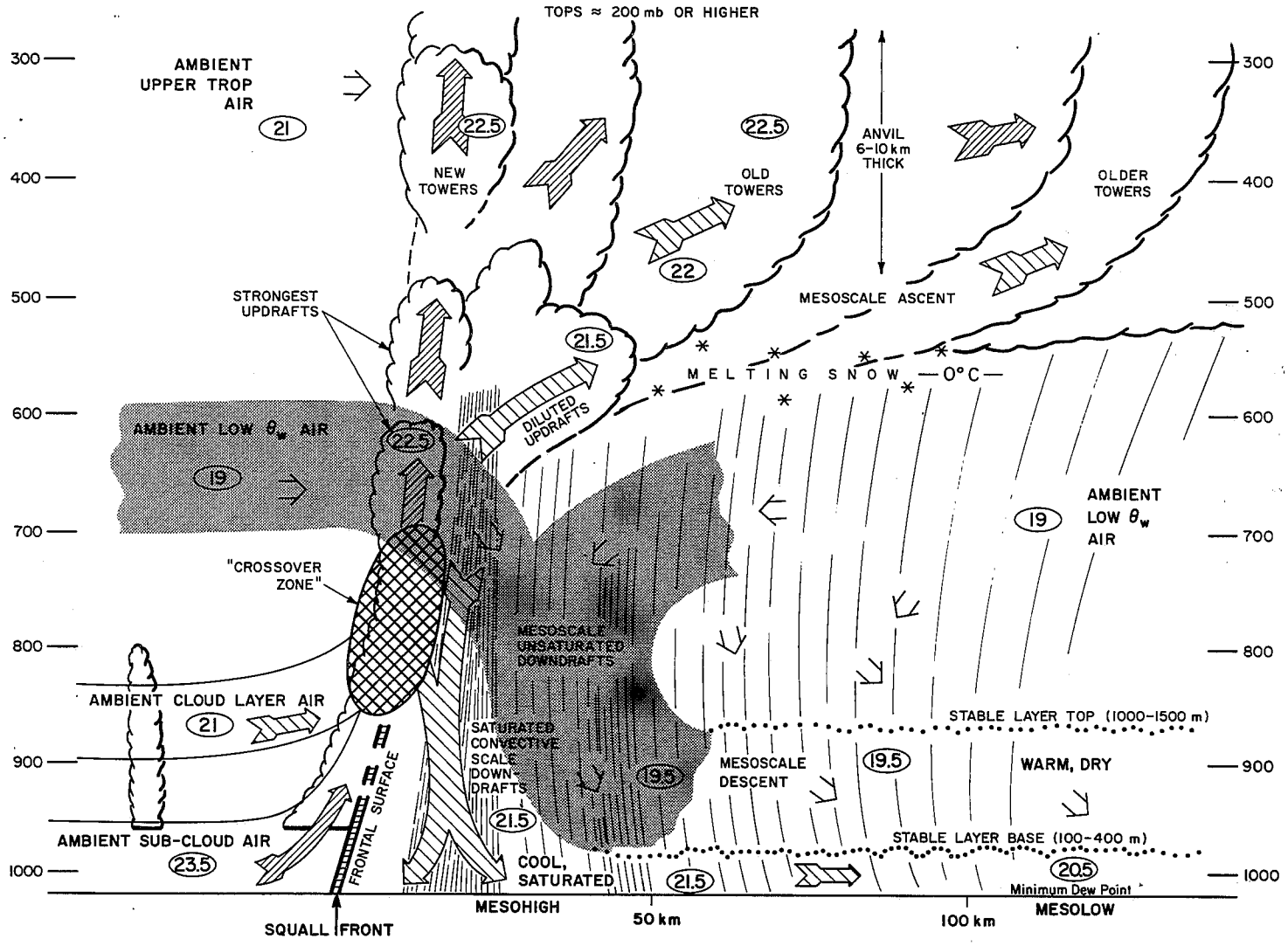

Fig. 9.19 Schematic cross section through a class of squall systems. All flow is relative to the squall line which is moving from right to left. Circled numbers are typical values of θ_w in °C. From Zipser (1977).

The portion of convective-scale downdraft outflow that spreads toward the rear of the squall-line system streams out in a thin layer 50-500 m above the surface. As this layer of cold air moves out over the warm sea surface, enhanced activity of turbulent plumes rising from the surface occurs (Mandics and Hall, 1976; Houze, 1977; Zipser, 1977; Gaynor and Mandics, 1978; Gaynor and Ropelewski, 1979; Fitzjarrald, 1979). The mixing associated with the plumes acts to raise the moist static energy of the convective downdraft air and thereby gradually convert it to air with properties characteristic of the undisturbed (or pre-squall) subcloud layer. This recovery is sufficiently slow that the surface outflow layer, or squall-line "wake", is evident for up to several hundred kilometers behind the squall line (Fig. 9.16 and 19). This surface outflow layer (see next section) is bounded above by a stable layer maintained by widespread subsidence below the anvil cloud. The subsiding air is characterized by low moist static energy, and its entrainment across the stable layer helps slow the recovery of the surface wake to pre-squall conditions.

9.5.1.6 The Mesoscale Downdraft

The subsiding air below the anvil extends over horizontal scales of 100-500 km. By mapping the surface outflow pattern of the 12 September GATE squall- line system, Zipser (1977) estimated the downward velocity at 500 m, near the top of the wake layer, to be 5-25 cm s^{-1} (Fig. 9.20). A downdraft of this horizontal scale and magnitude is a hydrostatic circulation feature, in contrast to the nonhydrostatic convective-scale downdrafts associated with the cumulonimbus rainshowers making up the squall-line. Zipser (1969) proposed that the wide hydrostatic (or mesoscale) downdraft below the anvil of a tropical squall line was thermally-driven by the evaporation of rain falling from the mid-tropospheric base of the anvil. Using a hydrostatic mesoscale numerical model in which both cumulus-scale convection and cloud microphysical processes were parameterized, Brown (1979) demonstrated that this mechanism was feasible for a tropical squall system. His model produced an anvil, below which evaporative cooling led to adjustment of the mid-to-low tropospheric pressure field. The associated ageostrophic wind was convergent near the base of the anvil, divergent at the sea surface and the mesoscale downdraft was located in the intervening layer. The melting of ice particles that produces radar bright bands near the bases of anvils was not included in Brown's model but in real cases this melting reinforces the evaporative cooling in maintaining the mesoscale downdraft (Leary and Houze 1979b).

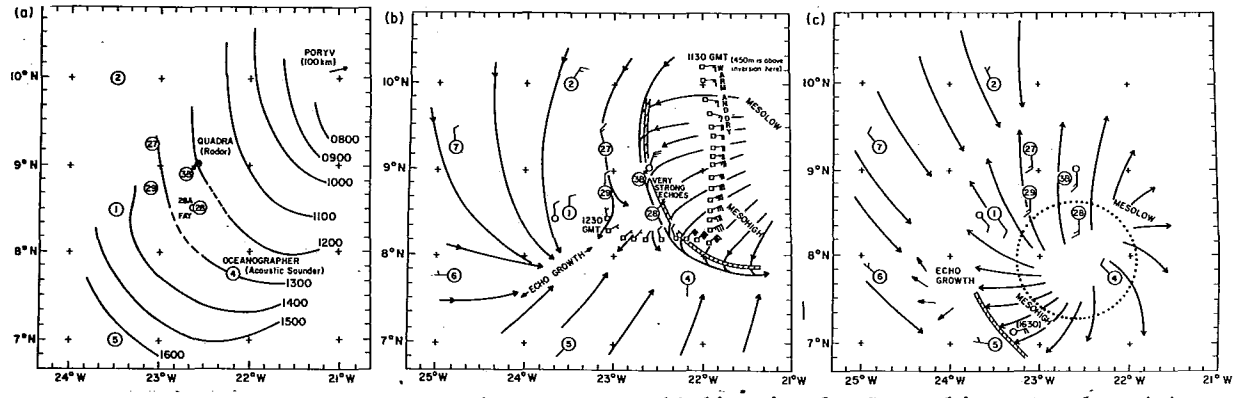

Fig. 9.20 Aspects of the 12 September 1974 squall line in the GATE ship network. (a) Isochrone chart of the leading edge; dotted lines are used to indicate ambiguous squall line location due to interaction with preexisting line of convection. (b) Surface chart, 1200 GMT, with some winds from the NCAR Electra at 450 m included. (c) Surface chart, 1600 GMT, showing 150 km circle over which divergence is estimated at 2 x 10^{-4} s^{-1}. Each full wind barb is 5 m s^{-1}. From Zipser (1977).

The thermodynamic structure of the mesoscale downdraft has been documented by Zipser (1969, 1977). He compiled the seven soundings shown in Fig. 9.21, which were obtained beneath various tropical squall-line anvils. Below the base of the anvil (about the 650 mb level), the soundings show the warming and drying effects of subsidence with a maximum separation between temperature and dew point being reached near 900 mb, at the top of the stable layer bounding the top of the surface wake. The warm dry air just above the wake has about the same value of moist static energy as the air near the base of the anvil. Building on ideas of Betts and Silva Dias (1979), Leary (1980) used a one-dimensional steady-state, hydrostatic model of a downdraft containing a realistic spectrum of evaporating raindrops to show that these soundings below anvils result from a balance between the evaporation of the falling precipitation particles, which acts to increase the relative humidity, and the subsidence, which warms and dries the air.

While the cooling effects of evaporation and melting appear to support and maintain the mesoscale downdraft through hydrostatic adjustment of the pressure field below the anvil, the mechanism that initiates the mesoscale downdraft is not clear. Miller and Betts (1977) suggest on the basis of convective cloud model simulations that the mesoscale downdraft is forced to descend since it overlies a spreading density current of convective-scale downdraft air. In a two-dimensional hydrostatic hurricane model with mesoscale (20 km) horizontal grid spacing, Rosenthal (1980) has shown that, as high moist-static energy air rising from low levels moves upward in the updrafts of squall-type features that form in the pre-hurricane stage, low moist static energy air carried downward in neighboring regions of compensating subsidence is advected into the lower part of the moist updraft. This air forms an unsaturated stable ascending wake which cuts the rising cloud air off from lower levels. The stable ascent in the wake leads to cooling below the cloud and a hydrostatic pressure rise at the surface. A mesoscale downdraft then forms at low levels and builds upward.

9.5.1.7 The Mesoscale Updraft

Within the anvil cloud itself, directly above the mesoscale downdraft, there appears to be a mesoscale updraft. Mesoscale ascent occurs in the anvil cloud in Brown's (1979) numerical model and also in the anvil formed by the successive cutting off of rising cloud elements by the mesoscale updraft wakes in Rosenthal's model. Similar mesoscale updrafts have been produced in mesoscale models simulating mid-latitude convective systems (Krietzberg and Perkey, 1977; Fritsch and Chappell, 1980). The mesoscale ascent in these models is hydrostatic and driven thermally by condensation heating. Observational evidence consistent with (but not proving the existence of) such mesoscale updrafts in GATE squall-line anvils includes: (a) the large amount of rain falling from anvils (Houze, 1977); (b) divergent and anticyclonic 200 mb level outflow centered in anvil cloud regions (Houze, 1977; Fortune, 1980); (c) indications that liquid water existed in anvils (Borovikov et al., 1978; Leary and Houze, 1979b); (d) average upward motion on the resolvable scale of rawinsonde data centered on the anvil clouds of squall-line clusters (Frank, 1978; Betts, 1978; Ogura et al., 1979); and (e) mid-latitude squall line systems that exhibit mesoscale ascent in their anvils (Sanders and Paine, 1975; Sanders and Emanuel, 1977; Ogura and Chen, 1977; and Ogura and Liou, 1980). Work in progress at several institutions indicates that compositing of upper wind observations obtained in the vicinities of squall-line anvils will prove the existence of the mesoscale updraft.

9.5.1.8 The Mesoscale Wind Field Near Squall Clusters

The squall cluster's circulation pattern (Fig. 9.14, 9.16,and 9.19) can have a substantial imprint on the horizontal wind field over an area 1000 km in dimension centered on the cluster. Tourre (1979, 1980) identifies a "squall- line wave"

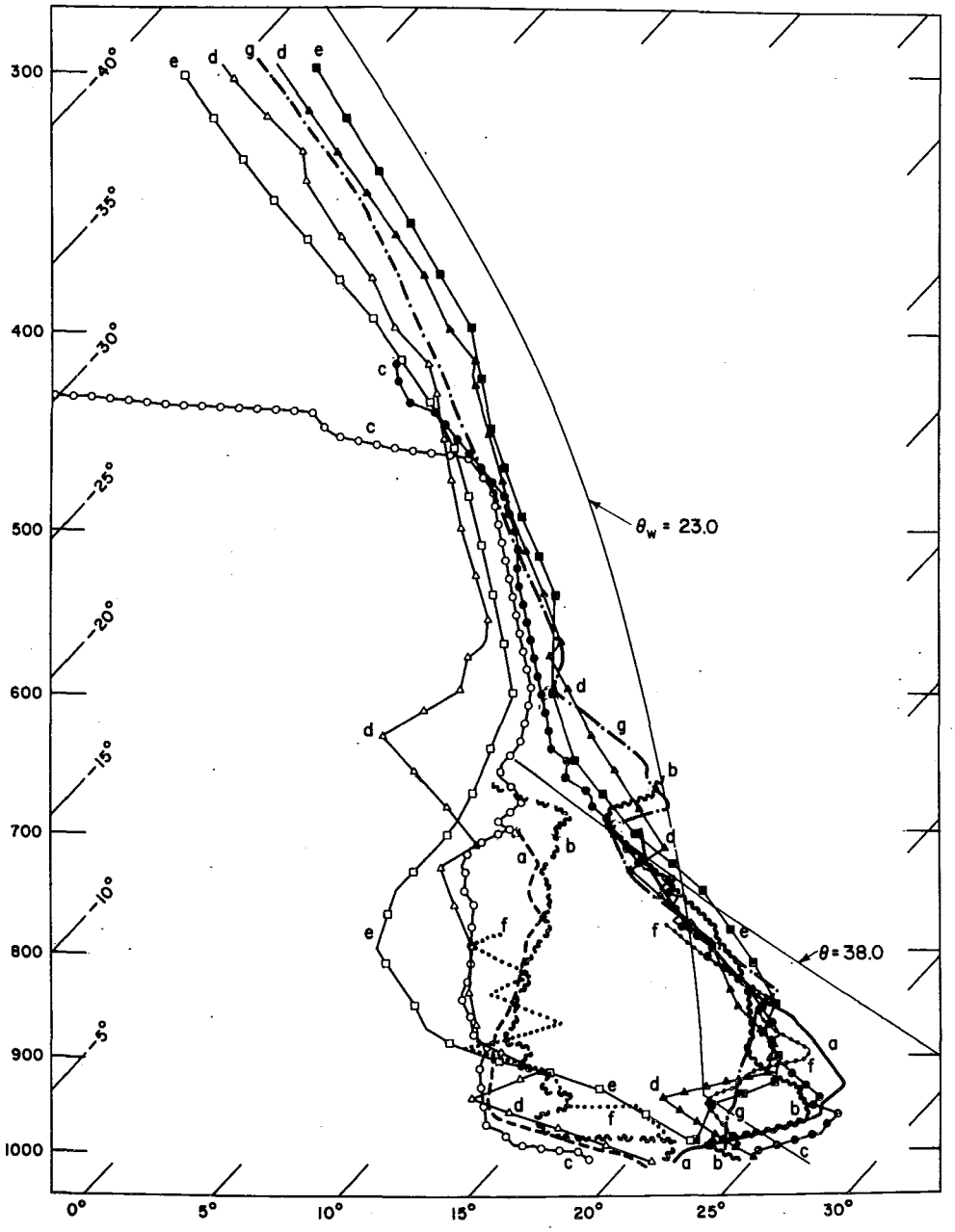

Fig. 9.21 Characteristic soundings in post-squall regions. (a) 5 September 1974 by NCAR Queen Air, mostly in rain; (b) 1630 GMT, 12 September 1974, from the Fay (GATE position 28A, about 200 km behind leading edge and 50 km behind trailing precipitation); (c) 1804 GMT, 12 September 1974, from the Oceanographer (GATE position 4, about 250 km behind leading edge and 100 km behind trailing precipitation); (d) 1130 GMT, 12 September 1974, from the Poryv (GATE position 10, about 350 km behind leading edge and 174 km behind trailing precipitation); (e) 2000 AST, 28 August 1969, Anaco, Venezuela, about 50 km behind trailing precipitation; (f) aircraft sounding from Fig. 9.6; (g) Barbados sounding (no dew point available). from Zipser (1977).

(wavelength about 1200 km), in the vicinity of squall clusters. In other studies, wind patterns are noted in relation to the anvil cloud. At the surface, directly below the anvil, anticyclonic divergent outflow predominates (Fig. 9.20). Near the base of the mature anvil (600-700 mb) a convergent circulation develops; for example, the 4 September oceanic squall (Houze, 1977) and the 5 September African squall (Fortune, 1980) exhibited convergent cyclonic rotation in the 700 mb flow at the base of mature anvils. At upper levels (≈200 mb), divergent outflow was centered on the anvils (Houze, 1977; Fortune, 1980). The pattern of divergence at low levels, convergence in mid-levels and divergence at high levels in the anvil region is apparently associated with the mesoscale downdraft below the base of the anvil and mesoscale ascent in the anvil cloud itself.

9.5.1.9 Squall-line Propagation

Why squall clusters take on a mesoscale organization in which their convective cells line up and move as a group faster than other forms of convection in GATE and indeed often faster than the pre-squall environmental wind at any altitude is a question to which there is not yet a definitive answer. However, several recent theoretical studies provide insight and appear to be consistent with GATE and other tropical observations. Before summarizing these studies, we note that the squall propagation cannot be explained by the density currents formed by the downdrafts of the convective cells within the squall line. These downdrafts are on the scale of the individual cells, while the mechanism that organizes the group of cells into a larger propagating line is necessarily mesoscale. Nor can the line's organization be explained by the mesoscale downdraft that spreads out below the squall's trailing anvil cloud, at least not in the initial stages of the line, since the arc-shaped squall line takes shape well before the development of significant anvil structure (Houze, 1977; Fortune, 1980).

Extending the work of Raymond (1975, 1976), Silva Dias (1979) used a "Wave-CISK" model to show that a small initial convective perturbation in a mean GATE wind environment leads to the development of a propagating gravity wave structure on the scale of a tropical squall line. The wave develops arc- shaped horizontal structure (even though the basic-state wind has no horizontal shear) and exhibits vertical tilt consistent with tilts observed in GATE squall lines (Houze, 1977; Fortune, 1980). The wave is also consistent with the tendency, noted by Houze (1977), of tropical squall lines to move in part by discrete propagation. If the speed of the wave giving rise to the line organization exceeds the speed of individual cells, whose motion is probably controlled by their internal dynamics (e.g., by the density current action of the convective-scale downdrafts), new cells would be expected to be triggered ahead of old ones as the wave continually moves ahead of existing cells.

Another idea relevant to discrete propagation is mesocyclogenesis resulting from compensating downward motion (Fritsch, 1975; Hoxit et al., 1976; Fritsch and Chappell, 1980). This process occurs in Rosenthal's (1980) two- dimensional hurricane model wherein the pre-hurricane squall line propagates in steps. The warming of the air column ahead of an active squall-line element by compensating downward motion leads to lowering of the surface pressure ahead of the line. The convergence into this low is associated with a reversal of the low-level vertical motion and a new squall-line element forms there. It is interesting that compensatory downward motion also is concentrated just ahead of the Silva Dias (1979) gravity wave squall line.

9.5.2 Non-Squall Clusters

As noted in Sec. 9.4.3, the overwhelming majority of cloud clusters over the GATE ship array consisted of non-squall clusters, which traveled more slowly than squall clusters and did not possess the distinctive oval cirrus shield or arc-shaped

leading edge characteristic of squall systems. Despite these differences in motion and appearance, the non-squall and squall clusters in GATE exhibited surprising similarities in other aspects of their structures. In view of these similarities, much of the understanding of squall clusters reviewed above is basic to a universal understanding of convection in the ITCZ. The summary of GATE studies of non-squall clusters presented below is organized around the theme of their structural and dynamical similarities to squall clusters. Their differences from squall clusters will also be discussed.

9.5.2.1 Occurrence of Mesoscale Precipitation Features in Non-Squall Clusters

The GATE non-squall clusters examined in case studies (Table 9.1) all contained mesoscale rain areas. Leary and Houze (1979a) extended the conceptual model of a tropical squall-line system (Figs. 9.14, 9.16 and 9.19) to describe the structure and behavior of these rain areas. They arrived at the more general concept of a mesoscale precipitation feature (MPF), of which the rain area of a squall cluster is an example, but which also applies to the rain areas of non-squall clusters.

9.5.2.2 Typical Life Cycle of a Mesoscale Precipitation Feature

Squall clusters and some non-squall clusters contain just one MPF. Other clusters contain several MPF's interconnected by a common anvil cloud. Intersections and mergers of the MPF's can add complexity to the precipitation pattern of the cluster. However, when the individual MPF's making up the pattern are identified and followed in time, they each exhibit a life cycle similar to that of a squall-line MPF. This characteristic cycle, as postulated by Leary and Houze (1979a), is illustrated schematically in Fig. 9.22.

In its formative stage (Fig. 9.22a), the MPF appears on radar as a group of isolated type (i) (D scale or small C scale) radar echoes, which may be randomly distributed in the horizontal or arranged in a line. Fig. 9.22 follows the evolution of a line. In squall clusters, and in many non-squall clusters, such as those of 15 July and 2, 5, and 14 September (see papers referred to in Table 9.1), the MPF's are linear. The 18 September GATE cloud cluster, however, contained mesoscale features composed of groups of cells which tended to be randomly distributed (Warner et al., 1980), and MPF's in cloud clusters observed at a similar latitude near Borneo during the Asian winter monsoon also evolved from groups rather than lines of cells (Houze et al., 1981).

In the intensifying stage of an MPF, the rain areas of the individual cells grow and merge (Fig. 9.22b). The feature then comprises a single type (ii) (large C scale or small B/C scale) radar echo.

The mature stage of an MPF is reached when a stratiform precipitation area develops from older cells blending together as they begin to dissipate (Fig. 9.22c). In the same way that squall line elements weaken, become stratiform and are incorporated into their associated anvil region (Sec. 9.5.1.2), convective cells of the MPF go through life cycles at the end of which they weaken and become components of a mass of stratiform precipitation falling from the middle-level base of the general anvil cloud of the cluster. For example, the cell at 9°N in Fig. 9.23 was weakening. By 1215 GMT, a melting layer was evident near a height of 4 km, and the cell had taken on the character of light anvil rain. When several neighboring cells reach this stage, they become indistinguishable from each other and together can form an extensive region of stratiform anvil rain with a continuous melting layer. Though in weaker clusters, the size of the stratiform regions that develop in this way may be limited (as on 18 September; see Warner et al., 1980), stratiform areas as great as 200 km in horizontal dimension can occur (Fig. 9.13).

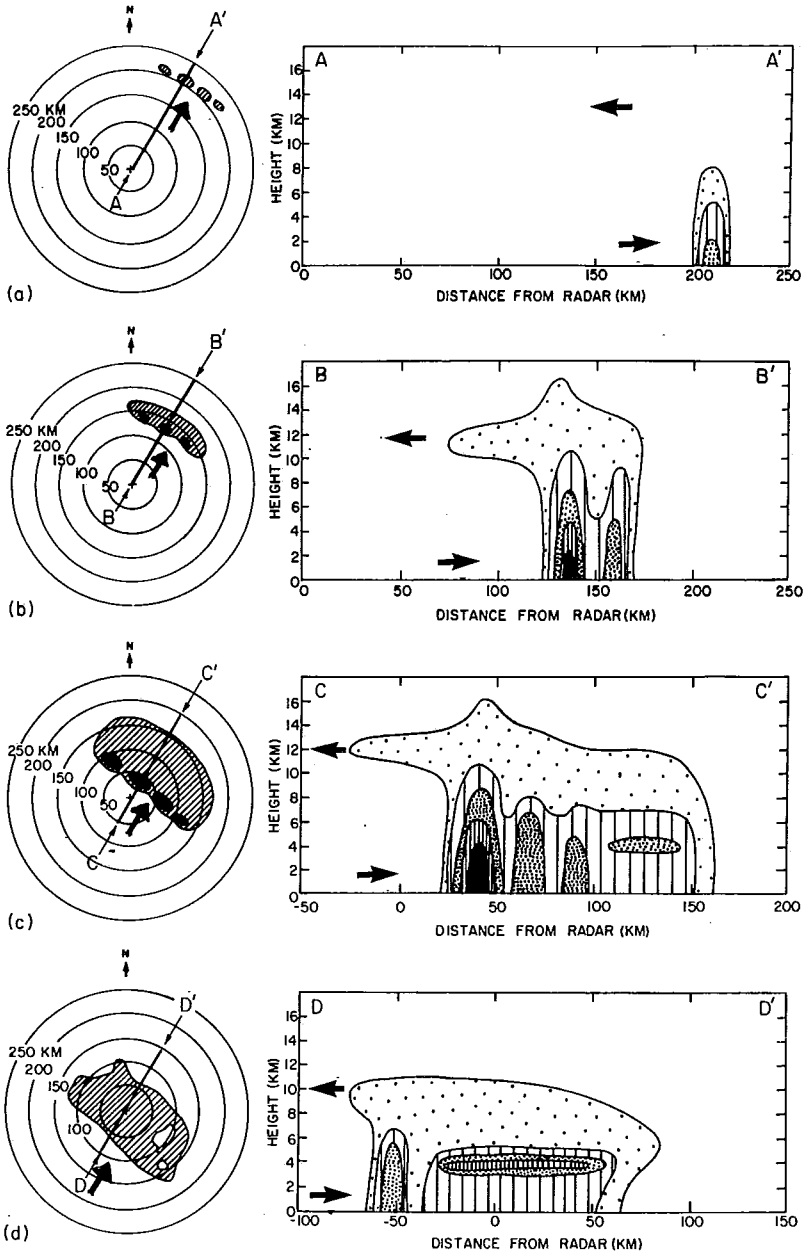

Fig. 9.22 Schematic of the structure of a mesoscale precipitation feature as viewed by radar in horizontal and vertical cross sections during the (a) formative, (b) intensifying, (c) mature and (d) dissipating stages of its life cycle. The outside contour of radar reflectivity is the weakest detectable echo, and the inner contours are for successively higher reflectivity values. Heavy arrows on horizontal cross sections indicate direction of the low-level winds. Arrows on vertical cross sections indicate directions of the low-level and upper-level winds relative to the feature. From Leary and House (1979a).

As long as new convective cells continue to form adjacent to a stratiform region, the mesoscale precipitation feature remains an aggregate of cells with an associated region of stratiform rain, and, as such, composes a type (iii) radar echo.

A common way that a mature mesoscale precipitation feature continues forming new cells is by discrete propagation in a direction opposed to the relative wind at low levels. Byers and Braham (1949, pp. 78-79) found that in mid-latitude thunderstorms the probability of new cell development is: (1) greatest within the zone of overlap of downdraft outflows from neighboring convective cells, and (2) greater in the leading and lateral sectors of cell groups than in the trailing portions of the groups. Applying similar ideas to a line of echoes that evolves into a mesoscale precipitation feature of the type observed in GATE on 5 September, Leary and Houze (1979a) noted that convergence and new cell formation is favored between and upwind of the existing cells. Using a three-dimensional cumulus model, with GATE wind and thermodynamic soundings from the moderately unstable day of 18 September, Simpson and van Helvoirt (1980) showed that an individual deep cumulonimbus cell of the type observed in the cluster observed on that day indeed develops a downdraft outflow at low levels that "acts as an obstacle with stagnation and strong convergence (10^{-3} s^{-1}) at its upwind edge." This convergence would favor the growth of new towers at the edge of the cloud, leading to some propagation upwind. Moreover, "the pressure field and the more favorable vertical stratification could cause new separate cumuli to spring up at horizontal distances of 10 km or more upwind from the old cloud."

In the dissipating stage of the MPF (Fig. 9.22d), the formation of new convective cells diminishes, and as described in Sec. 9.4.6.2, the feature tends to become a type (iv) echo. The feature can persist in this form, i.e., as a large region of mostly stratiform anvil cloud and precipitation, for several hours after the demise of the convective cells (Borovikov et al., 1978; Leary and Houze, 1979a). Mesoscale ascent in the anvil cloud (Fig. 9.14) probably helps to prolong the dissipating mesoscale precipitation feature.

9.5.2.3 Similarity of Air Motions Associated with Squall and Non-Squall Mesoscale Precipitation Features

The mesoscale precipitation features in the non-squall clusters of 15 July, 2 September, 5 September and 14 September all exhibited air motions that resembled those of squall-line systems. Convective-scale drafts were associated with the cells while mesoscale drafts were associated with their stratiform rain areas.

On 15 July, intense convective cells extended northward from the center of a tropical depression along a line of strong confluence and convergence of the low-level wind (Fig. 9.24). Extending some 100 km west of the convective line was a region of lighter stratiform rain falling from an anvil cloud based in the mid troposphere and extending up to the tropopause. Aircraft penetration of the intense cells at the northern end of the convective line revealed a series of closely spaced, exceptionally intense convective-scale updrafts, each 1-5 km wide with peak speeds of 10-15 m s^{-1}. Convective-scale downdrafts ($\lesssim 4$ m s^{-1}) were also encountered in this group of cells. In contrast to these intense convective drafts, the region of uniform anvil rain to the west was characterized at low levels by widespread divergence indicating the presence of mesoscale subsidence below the anvil cloud.

In the stratiform rain area of one of the mature mesoscale precipitation features observed in the 5 September non-squall cloud cluster, aircraft observations, described by Leary and Houze (1979a), showed cool, dry air of low moist static energy at low levels, consistent with the presence of a mesoscale unsaturated downdraft maintained by melting and evaporation of the falling rain (as in Fig. 9.14). In the convective cells at the leading edge of the same mesoscale precipitation feature, a low-level aircraft penetration confirmed the presence of a convective-scale downdraft outflow.

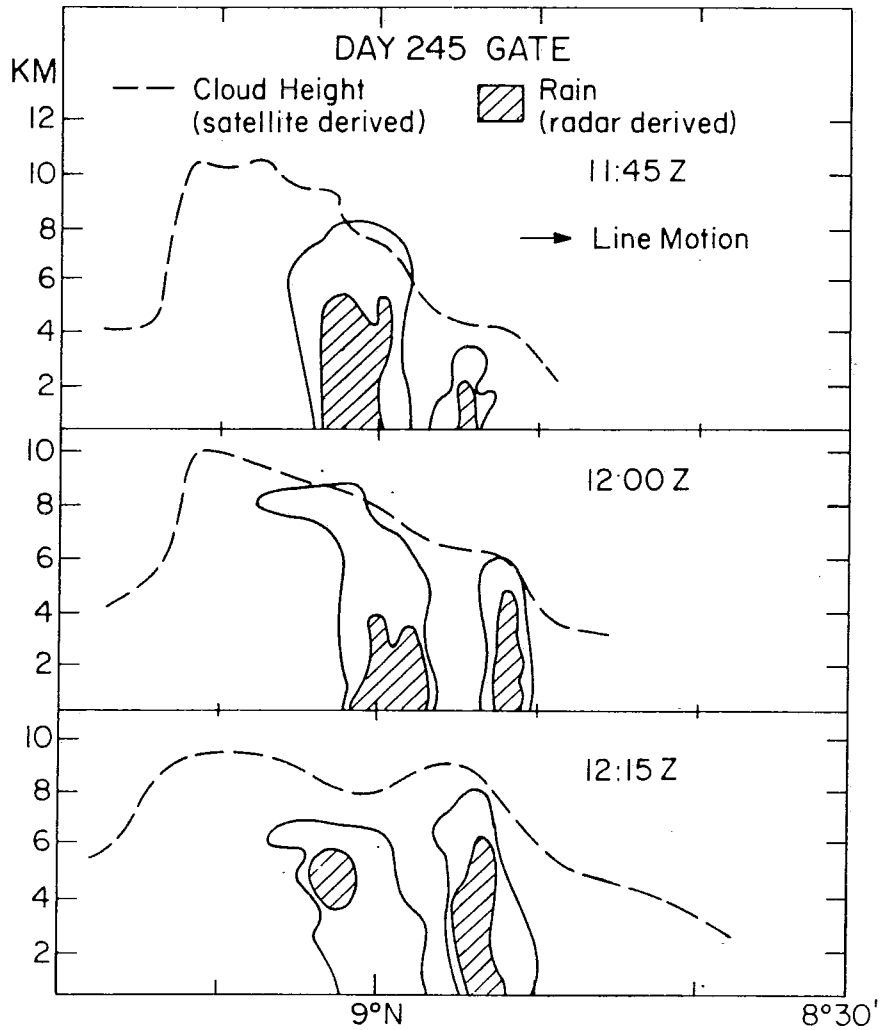

Fig. 9.23 Cross-sections through the convective line along the aircraft flight tracks (north-south on 22° 51'W) on 2 September 1974, showing sequential growth of new cells on the leading edge of a mesoscale precipitation feature. From Mower et al. (1979).

The 2 and 14 September features were propagating similar to the idealized case in Fig. 9.22. Aircraft penetrations revealed convective-scale drafts of up to a few meters per second and gust fronts associated with cells at the leading edges of the systems with broader divergence areas to the rear associated with decaying cells and anvil precipitation. Zipser et al. (1981) constructed a schematic model of the 14 September mesoscale precipitation feature (Fig. 9.25). The similarity of the airflow to that of a squall-line system (Fig. 9.16 and 19) is evident.

9.5.2.4 The Mesoscale Wind Field Near Non-squall Clusters

The similarity of the air motions in non-squall and squall clusters is further seen in analyses of the wind fields in the vicinities of the clusters.

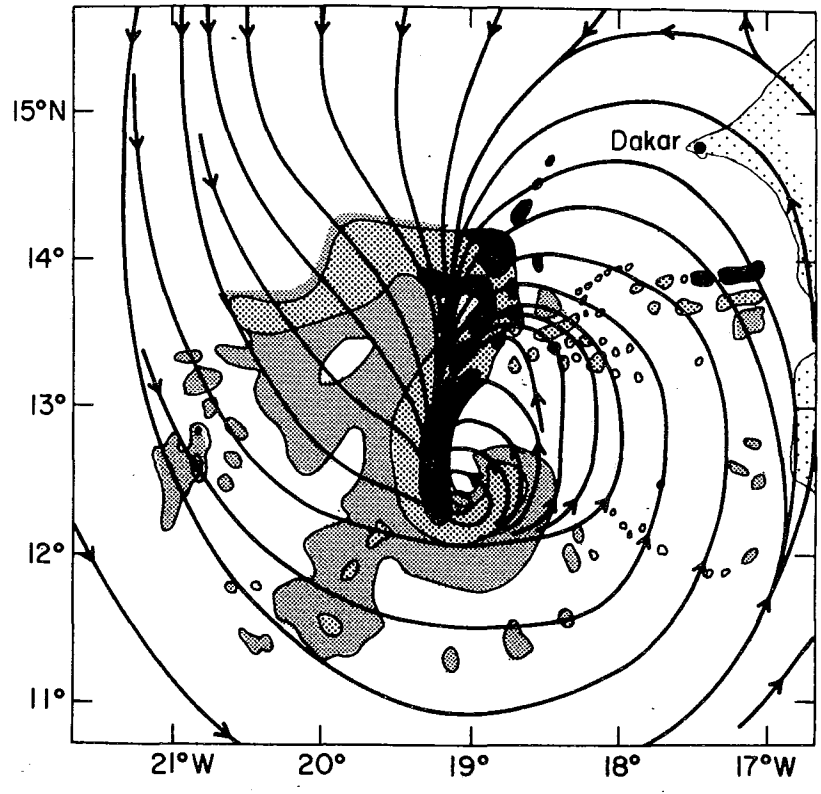

Fig. 9.24 Radar composite, 990 mb streamlines superimposed for 1400 GMT 15 July 1974. Three levels of reflectivity are indicated, determined subjectively. The northwest portion of the echo is not enclosed, as it is believed to extend beyond the limits shown. From Zipser and Gautier (1978).

A prominent characteristic of a squall cluster is the location of its leading line of convective cells within a zone of locally enhanced convergence. Though the MPF's of non-squall clusters do not always exhibit linear shapes and though they may occur in various environmental flows (e.g., tropical depressions, ITCZ patterns, monsoon flows), the convectively active portions of these features can nearly always be associated with a mesoscale convergent perturbation of the low level flow in which they are embedded.

For example, Leary (1979) found that in the early stages of the large 5 September non-squall cluster, when it was dominated by mesoscale precipitation features in their formative, intensifying and early mature stages of development, the confluent asymptote of the ITCZ became intensified about the cluster at low levels. Rather similarly, a cyclonic vortex in the surface flow formed about an intensifying mesoscale precipitation feature on 2 September (Betts, 1978; Mower et al., 1979). The 15 July mesoscale precipitation feature (Fig. 9.24) coincided with a locally intensified line of confluence and convergence (Zipser and Gautier, 1978), and Warner et al. (1980) noted a tendency for the mesoscale precipitation features of 18 September to be aligned parallel to features of the low-level convergence field. A linear mesoscale precipitation feature within the non-squall ITCZ cluster of 12 August studied by Ogura et al. (1979) was shown by objective analysis of GATE wind data to lie within an elongated region of enhanced convergence, which intensified as the precipitation feature and its associated upper level cloud expanded.

Late in the lifetime of the 5 September cloud cluster, when it was dominated by mesoscale precipitation features in their late mature and dissipating stages, the winds at 700 mb formed a closed convergent cyclonic flow centered on the cluster (Leary, 1979), while at 200 mb, a center of divergent anticyclonic outflow developed (Suchman and Martin, 1976; Leary, 1979; Sikdar and Hentz, 1980). Developments in the 700 mb and 200 mb flows similar to those of 5 September also occurred in the vicinity of GATE squall clusters (Houze, 1977; Fortune, 1980) and are apparently associated with the development of mesoscale ascent in deep, extensive precipitating anvil clouds characteristic of the late stages of both squall and non-squall mesoscale precipitation features (Figs. 9.14, 9.16, 9.19, and 9.25). Frank (1978), Betts (1978), Ogura et al. (1979), and Sikdar and Hentz (1980) have shown that large-scale upward motion computed from GATE wind data for occasions when cloud clusters were within the ship array increased and became a maximum in the upper troposphere (i.e., at anvil levels) during the mature stages of the clusters. During the dissipating stages, the upper tropospheric upward motion remained substantial but decreased markedly in the lower troposphere, probably reflecting the mesoscale upraft-downdraft complex, although the computed vertical motion was for a bigger area than that covered by the individual clusters. The vertical motions on the scale of the clusters and anvil rain areas themselves have yet to be determined.

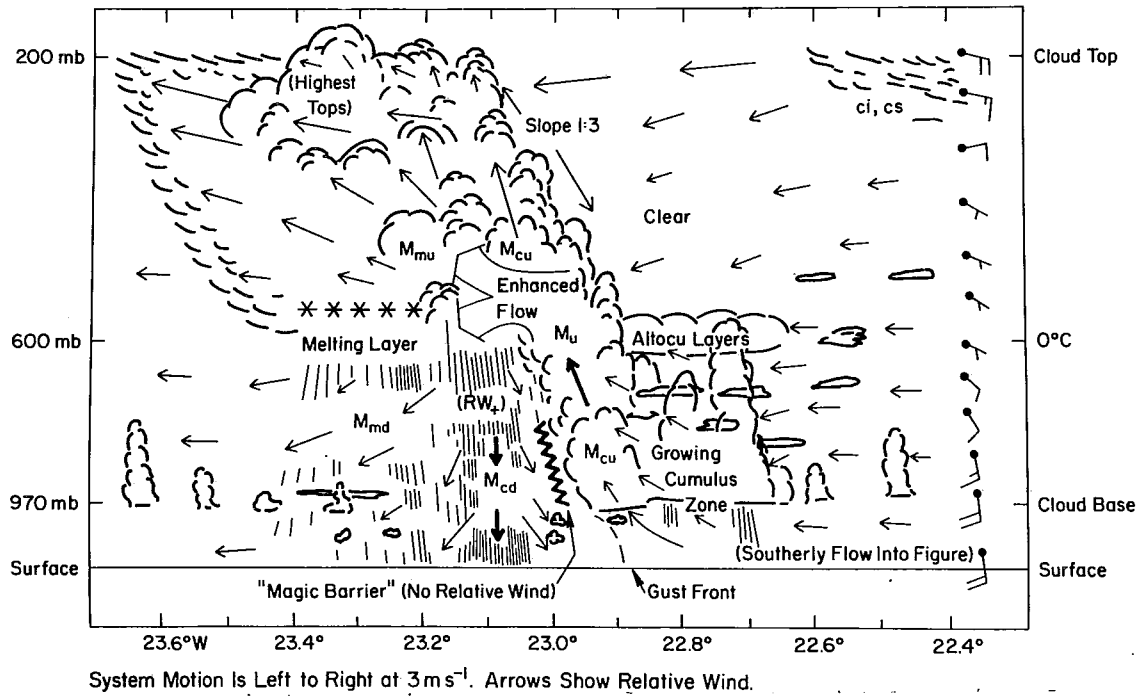

Fig. 9.25 Schematic cross section through September 14 cloud system. From Zipser et al. (1981).

9.5.2.5 Time Series of Mass Flux and Rainfall in a Mesoscale Precipitation Feature

Zipser (1980) hypothesized a time series of mass and precipitation fluxes associated with a typical (squall or non-squall) mesoscale precipitation feature (Fig. 9.26). It was assumed that the MPF originates "by an imposed mesoscale convergence." Then, "...the order or events is as follows: (2) rapid increase in

upward convective mass flux (M_u); (3) rapid rise in rainfall, initially 100 percent convective; (4) rapid rise in mass flux in convective downdrafts ($M_d - M_{md}$); (5) gradual increase in anvil rain; (6) gradual increase in downward mass flux in mesoscale downdrafts." The similarity of this "typical" time series to that observed in the 4-5 September squall cluster (Fig. 9.18) is apparent.

9.5.2.6 Differences Between Squall and Non-squall Mesoscale Precipitation Features

At this stage of GATE research, the similarities of squall and non-squall clusters are more evident than their differences.

The main features that set squall systems apart from non-squall clusters is their rapid motion, which as noted in Sec. 9.5.1.9, may be related to the co-location of the squall systems with well defined northeasterly or easterly jets at 600 to 700 mb (Frank, 1978). For reasons that may be rather complex, involving momentum transformations in downdrafts, or gravity wave dynamics, or both, the convection becomes organized into a line propagating with the 600 to 700 mb flow. Non-squall clusters apparently lack intimate connection with a 600-700 mb jet.

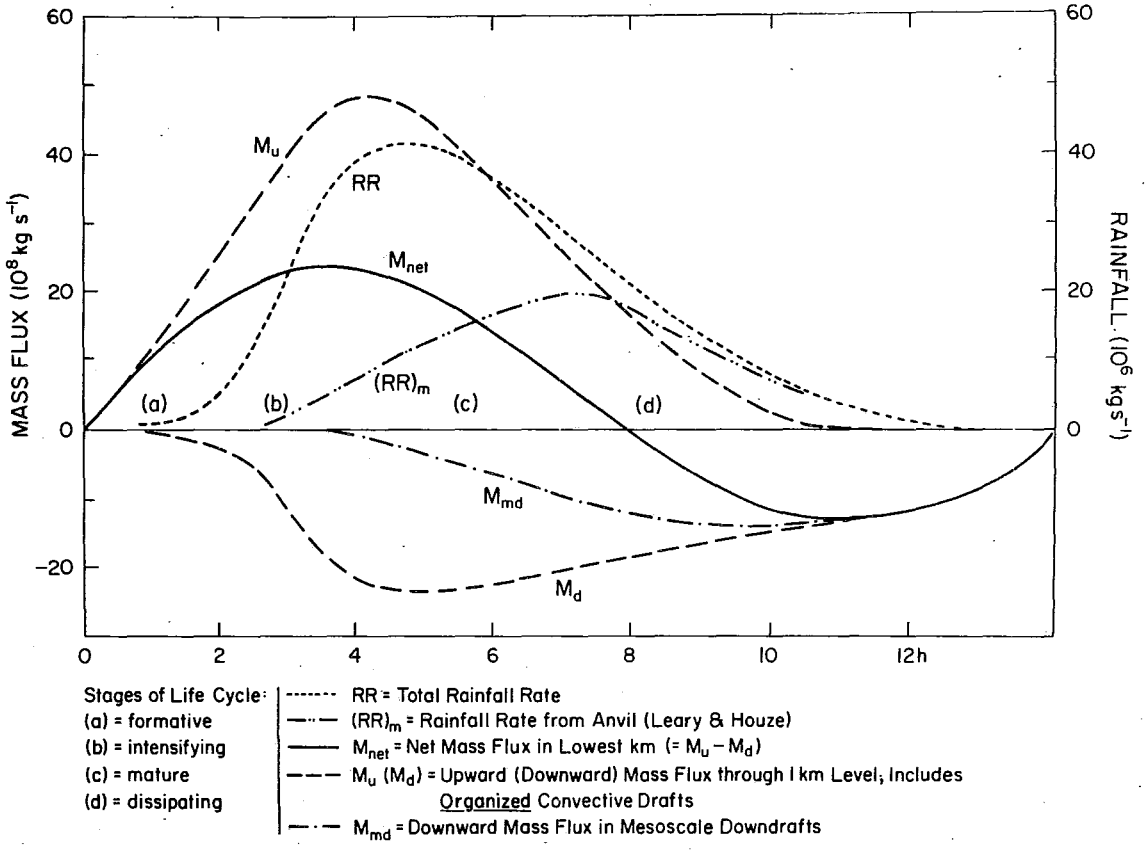

Fig. 9.26 Life cycle of "typical" mesoscale precipitation feature in time series. From Zipser (1980).

Another difference between squall and non-squall MPF's is that their downdrafts (both convective-scale and mesoscale) appear to be less potent than squall downdrafts in lowering the moist static energy of the lower troposphere (e.g., Zipser and Gautier, 1978; Betts, 1978; Mower et al., 1979; Zipser, 1980). The reason for this difference needs further study.

9.5.3 Smaller Convection Associated with Cloud Clusters

9.5.3.1 Occurrence of Smaller Clouds in the Vicinities of Clusters

In discussing squall and non-squall cloud clusters, we have focussed on MPF's, which, in their mature stages, constitute the type (iii) and (iv) (large B/C scale) radar echoes that account for most of the area covered by precipitation in cloud clusters (Sec. 9.4.6.1-2). Though these B/C scale mesoscale precipitation features dominate the precipitation patterns, the lognormality of the size distributions of tropical cloud and rain areas indicates the simultaneous presence of many more smaller precipitating and non-precipitating convective clouds.

9.5.3.2 Cloud Population Associated with a Cloud Cluster

Warner et al. (1979, 1980) have mapped the entire population of clouds associated with the GATE non-squall cloud cluster of 18 September. Photogrammetry applied to airborne cloud photography, quantitative time-lapse satellite imagery and radar data, were analyzed. The mapped clouds (Fig. 9.27) show a gradation, with shallow non-precipitating clouds (< 2.5 km, FIg. 27b) in the southwest of the region studied giving way to deeper precipitating clouds in the northwest (Fig. 9.27a). The largest clouds (> 10 km in height) were components of MPF's located under the cirrus canopy (shown in Fig. 9.27b) of the cloud cluster.

9.5.3.3 Types of Clouds Making Up the Population Associated with the Cluster

Following Warner et al. (1979, 1980) and Simpson and van Helvoirt (1980), we may think of the clouds on 18 September in four categories, to which we assign the following terminology:

(i) Tiny cumulus - less than 1 km in height, non-precipitating

(ii) Small cumulus - 1-3 km in height, occasionally precipitating

(iii) Moderate cumulus - 3-9 km in height, nearly always precipitating

(iv) Penetrative cumulonimbus cells - over 9 km in height, always associated with precipitation, usually embedded in MPF's.

We are concerned here with the first three categories, i.e., with the tiny to moderate convective clouds. Their characteristics are discussed briefly in the following two subsections.

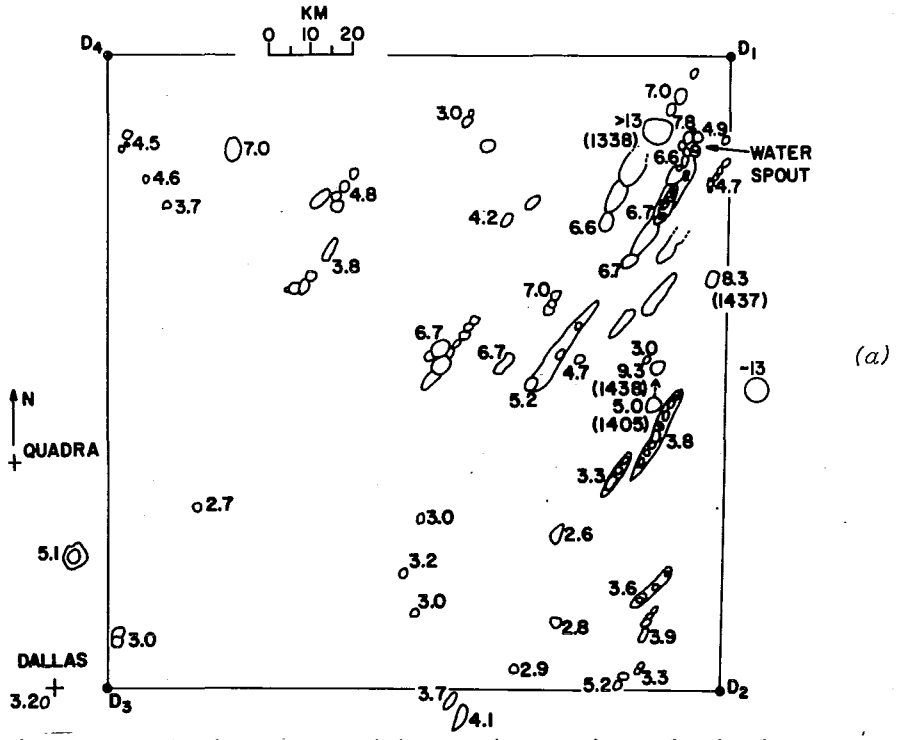

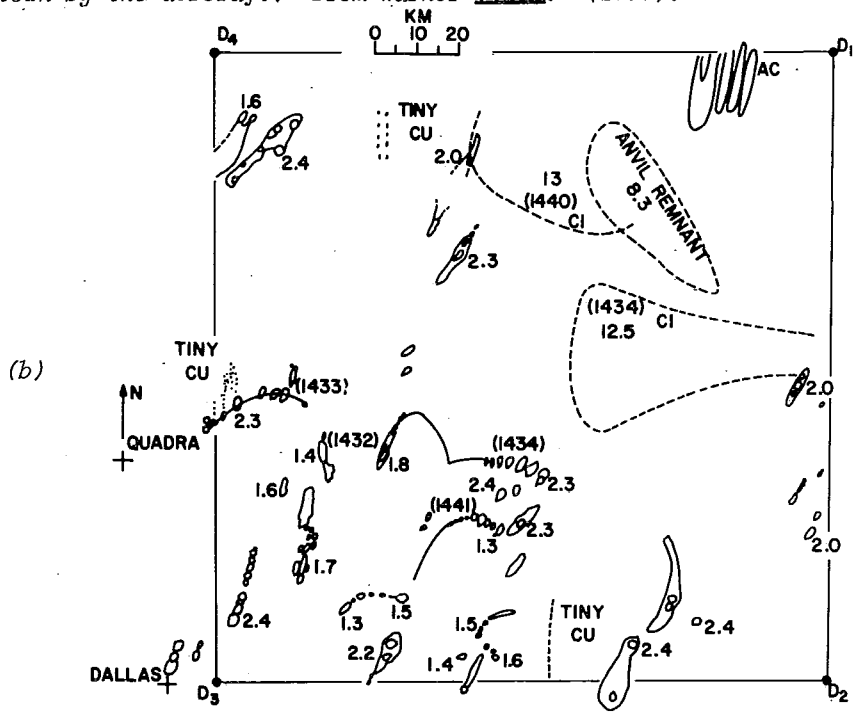

Fig. 9.27 Cloud map from airborne observations obtained from 1300 to 1445 GMT 18 September 1974. (a) (top): Active tops (outlined by contours) in the height interval 2.5 - 13 km. (b) (bottom): Clouds of height <2.5 km, and anvils (dashed). Thin solid lines represent arcs of clouds. Numbers are heights (km) above the sea, and times of measurement. The corners D_1 to D_4 define the box circuit flown by the aircraft. From Warner et al. (1979).

9.5.3.4 Tiny and Small Cumulus

These species differ from the deeper ones in that they do not require strong low-level convergence in order to exist. In fact, they occur over wide areas of the tropical oceans, including regions of widespread subsidence (e.g., the trades), inimical to the development of the deeper clouds. These clouds arise wherever the mixed layer thickens sufficiently that moist turbulent elements can reach the condensation level. The vertical transports effected by the tiny to small cumulus maintain the moist cloud layer and typical inversion capping it against large scale subsidence characteristic of undisturbed regions (Betts, 1978).

Thickening of the mixed layer and occurrence of tiny to small cumulus tends to occur within mesoscale patches where the turbulent flux of moisture at the condensation level exceeds that at the ocean surface (LeMone, 1980). [Nicholls and LeMone (1980) have shown that this behavior is consistent with the parametric boundary layer model of Betts (1976b).] Warner et al. (1979) found that the tiny cumulus on 18 September occurred in mesoscale patches in the forms of rows separated by 1 or 2 km and aligned along the wind shear in the manner of roll vortices (LeMone, 1973; LeMone and Pennell, 1976). The small cumulus on 18 September described by Warner et al. (1979) tended, on the other hand, to occur in mesoscale patches in the forms of arcs and rings (Fig. 9.27). In vertical cross section, the small cumulus of the arcs displayed a rather extreme slope dictated by the ambient wind shear (Fig. 9.28).

9.5.3.5 Moderate Cumulus

The moderate cumulus and penetrative cumulonimbus differ from the shallower tiny and small cumulus in two apparent respects, noted by Simpson and van Helvoirt (1980); viz.,

(i) The deeper clouds apparently require concentrated low-level convergence in order to be maintained, whereas the shallow clouds can exist under large-scale suppressed conditions, and

(ii) The deeper clouds are more effective in modifying the subcloud layer by filling it with downdraft air of low moist static energy, especially when the rainfall rates are substantial (Betts, 1976a; Barnes, 1980).

In Secs. 9.5.1 and 2, the effect of the downdrafts of penetrative cumulonimbus cells associated with the mesoscale precipitation features of squall and non-squall clusters were described. In their three- dimensional cloud-model study using GATE input data from 18 September, Simpson and van Helvoirt (1980) showed that moderate cumulus can also produce strong downdraft modification of the subcloud layer (Fig. 9.29).

9.5.3.6 Downdrafts and Interactions

The arcs of small cumulus described by Warner et al. (1980) appeared near precipitating clouds and were apparently triggered by outflows of dense downdraft air from regions of precipitation. As the arcs progressed through their life cycles, some of the small cumulus making up the arcs grew and became precipitating clouds, which, in turn, developed their own downdrafts that could spawn new arcs of small cumulus. This behavior of the arcs is reminiscent of the generation, on a larger scale, of new squall-line systems in the vicinities of the edges of downdraft outflows of old dissipating cloud clusters (Sec. 9.5.1.1, Fig. 9.15).

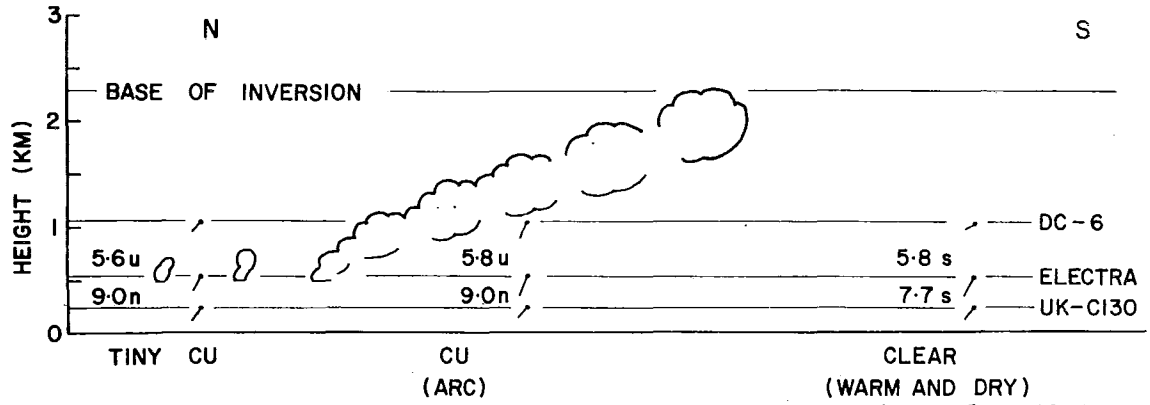

Fig. 9.28 Schematic cross section through a cloud arc of the type observed on 18 September 1974. The clouds were composed of succession of thermals rising in wind shear. Numbers are temperature lapse rates (°C km^{-1}) between the levels of flight indicated, and winds are drawn as short barbs. The letter S means stable, N neutral, and U convectively unstable. The system moved northward (from right to left). Updrafts occurred at the clouds' leading edges, downdrafts behind. The clear air behind the arc was warm, dry and stably stratified, implying subsidence. From Warner et al. (1979).

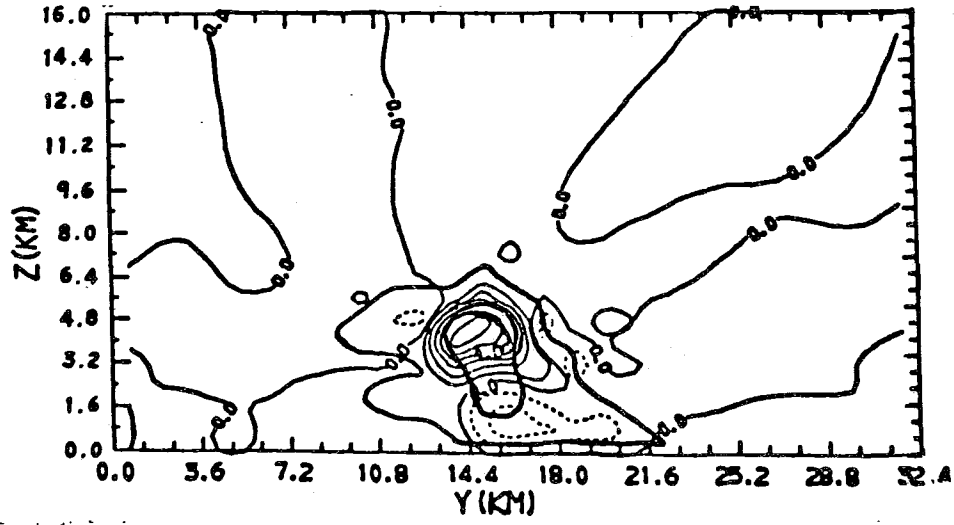

Fig. 9.29 Model simulation of cumulus congestus observed in GATE on 18 September. The Y-axis extends from south to north. Cloud tops at 14 km 20 min. later. Primary isopleths are vertical velocities in m s^{-1}, contour interval 1 m s^{-1}. Updrafts are solid; downdrafts dashed. Heavy inner isopleth 2 g m^{-3}. From Simpson and van Helvoirt (1980).

Examination of the whole spectrum of clouds associated with a cloud cluster in the intertropical convergence zone thus reveals a highly interactive assemblage in which the existence of past clouds affects the location and mesoscale spatial arrangement of future clouds. The primary mode of communication between the past and the future clouds appears to be the outflow of downdraft air from precipitating clouds. Downdraft outflows affect future cloud formation in at least two ways.

Firstly, low-level convergence becomes concentrated at the edges of the outflows and updrafts of new clouds are triggered there. Secondly, the outflow of downdraft air from a precipitating cloud so completely changes the character of the planetary boundary layer (Betts, 1976a; Barnes, 1980) that wherever the outflow spreads the formation of even tiny cumulus is prevented for hours, until the flux of latent and sensible heat from the ocean re-establishes a mixed layer of high moist static energy (Garstang and Betts, 1974; Echternacht and Garrstang, 1976; Houze, 1977; Zipser, 1977; Augstein,, 1978; Gaynor and Mandics, 1978). Once re-established, the mixed layer is ready to serve as updraft air for future clouds.

9.6 INTERACTION BETWEEN CONVECTION AND THE LARGE-SCALE FLOW: DIAGNOSTIC MODEL RESULTS

As noted in Sec. 9.2, a central objective of GATE was to estimate the bulk effects of cloud ensembles on the large-scale flow observationally. It was hoped that these estimates would help our understanding of convective parameterization models (Rodenhuis and Betts, 1974). Prior to the field experiment, most of the emphasis on diagnostic modeling work was directed toward the heat and moisture transports by convection (e.g., Yanai et al., 1973; Ogura and Cho, 1973; Nitta, 1975) using cloud spectral models of the type proposed by Ooyama (1971), Arakawa and Schubert (1974) for cumulus parameterization. Work of this type has continued with GATE data, and there has been a growing awareness of the role of transports of momentum and vorticity by clouds in the dynamics of tropical wave systems and cloud clusters. Considerable progress has been made both observationally and theoretically in understanding these transports. However, the preparation of data sets has been a major task facing researchers undertaking diagnostic modeling studies, and work is still in progress.

9.6.1 Preparation of Data Sets

9.6.1.1 Upper-air Data

Early studies have been compiled using preliminary upper-air data sets (Reed et al., 1977) and the A/B-ship data alone (Nitta, 1977; Falkovich, 1978; Cho et al., 1979b). Many subsequent papers have been based on simple field fits to the A/B and some or all of the B-ship data (Thompson et al., 1979; Reeves et al., 1979; Ogura et al., 1979; Frank, 1979). The disappointing quality of those B-ship winds derived from NAVAID tracking systems (which were not adequately tested before the 1974 field phase) has both delayed production and considerably reduced the quality of wind data sets on the B-scale. A major effort has been in progress for the past seven years to extract wind sets with optimum time and space filtering using spectral objective analysis methods. The Phase III data set has now been completed (Ooyama, 1980). It contains a wealth of information which will be the basis of further B and A/B-scale studies.

9.6.1.2 Radar Data

The data from the four shipborne digital weather radar systems (Fig. 9.1) provide the primary GATE precipitation measurements for use in diagnostic studies involving moisture budgets. Because of the quantitative information they provide on the structure of populations of precipitating clouds, the radar measurements constitute a set of data in addition to budgets derived from upper-air data against which cloud models can be tested and constrained to indicate the properties of ensembles of GATE clouds (Houze et al., 1980).

Preparation of the radar data for quantitative diagnostic purposes has also been a lengthy and complex effort involving radar calibrations, studies of the accuracy of functions relating power measurements to rainfall rates, intercomparisons of radars, comparisons of radar data with shipboard raingauge measurements and studies of raindrop size distributions. As a result of careful planning and testing for several years prior to 1974 and five years of major effort in processing the data after GATE, the desired quantitative radar set has been produced (Hudlow, 1979; Hudlow et al., 1980).

9.6.1.3 Aircraft Data

Quantitative budget studies based on GATE aircraft data have had to await the enormous undertaking of processing the data from over 400 flights by several aircraft, each carrying diverse and unique instrumentation. These data are now in a form which allows such studies to be attempted and initial work is underway (Zipser, personal communication).

9.6.2 Important Budget Study Results

Budget studies have confirmed the close coupling of deep convection and large-scale mean vertical motion ($\overline{w}$). Figure 9.30 (Reeves et al., 1979) shows that for the three phases of GATE deep tropospheric ascent was present only in disturbed deep convective conditions (see also Falkovich, 1979, and Cheng and Houze, 1979). Thompson et al. (1979) and Frank (1979) show the close agreement between observed precipitation and precipitation derived by the budget method, in which the terms involving w dominate (Fig. 9.31). It is thus clear that provided w can be predicted, a reasonable parameterization of rain is possible. The vertical distribution of condensation heating and water vapor modification is more difficult to obtain, since it requires a cloud transport model (Sec. 9.6.3).

The divergence and heating profiles in the GATE area are more complex than shown by earlier studies in the tropical Pacific (Figs. 9.32 and 9.33) (Thompson et al., 1979). The mean GATE divergence structure is the result of averaging various phenomena (ITCZ, wave, diurnal, cloud cluster), which each have divergence structures that are variable in time and space. The resulting complex mean profile shows low-level convergence stronger and shallower in the GATE area than in the Pacific, with mid-tropospheric divergence and convergence below upper level divergent outflow.

Although the vorticity structures in the East Atlantic are also markedly different from those of the Pacific, exact comparisons are difficult since the GATE data set is subject to less averaging in time and space. Low-level mean vorticity values are typically smaller or no larger than low-level divergence (Frank, 1978; Reeves et al., 1979), indicating that the circulation is not frictionally driven as was speculated in the early planning of GATE. Furthermore, convection acts to oppose the tendency for amplification of a low-level vortex driven by convergence in a region of cyclonic vorticity (see Sec. 9.6.3.2).

9.6.3 Diagnostic Studies of Convective Transports

While the preparation of better data sets has been in progress, a considerable number of diagnostic studies of mass, thermodynamic and vorticity transports by GATE convection have been undertaken using preliminary data. This work has been dominated by two themes:

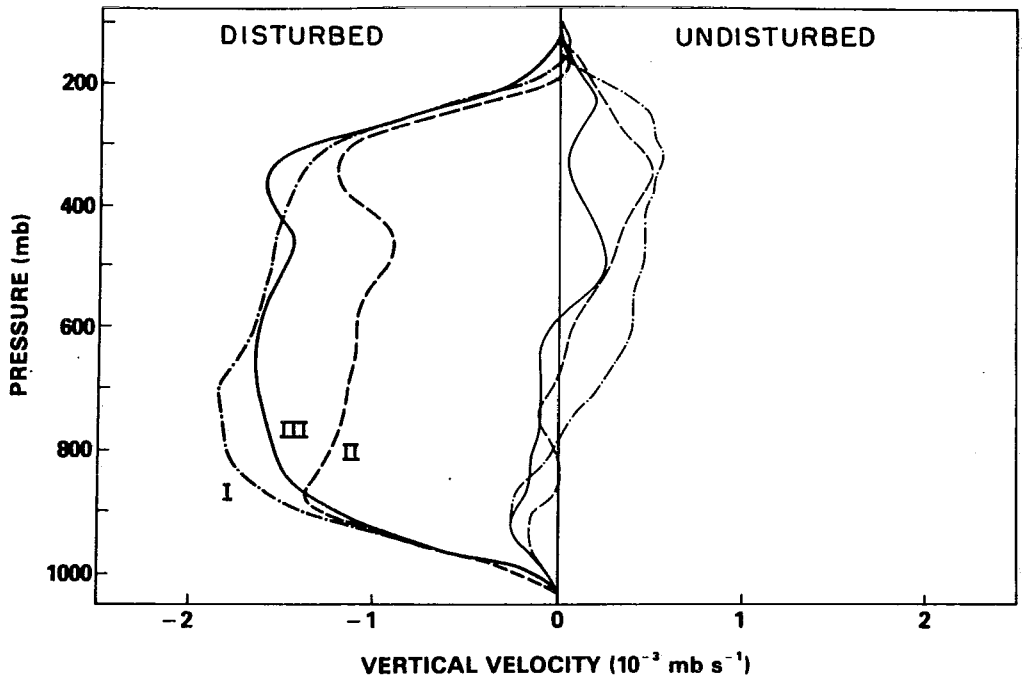

Fig. 9.30 Mean vertical velocity profiles for disturbed (heavy) and suppressed (light) conditions for Phase I (dashed-dotted line), Phase II (dashed) and Phase III (solid). From Reeves et al. (1979).

(i) The development of improved diagnostic models to interpret the data sets and the derived parameters used to characterize a convective field.

(ii) The need to reconcile descriptive studies (Sèc. 9.4-5), which indicate that transports occur on various subsynoptic scales, with the limited information in observed budget data and the highly constrained requirements of a closed parameterization theory. It is here that much work remains to be done.

9.6.3.1 Development of Improved Diagnostic Models for Thermodynamic Transports

The diagnostic studies that have been undertaken with GATE data (see review by Johnson, 1980a) have been carried out in the framework of a large-scale budget equation (for heat, moisture, momentum, or vorticity) in which a residual term represents the vertical convergence of fluxes by vertical motions (presumably associated with clouds) that are unresolved by the available sounding network. A population of model clouds is then constrained to match these residual terms. The model cloud properties required to match the residual are then manipulated to decompose the residual term into physically meaningful components (e.g., detrainment or compensating downward motion effects) and to relate the residual to bulk or spectral profiles of cloud vertical transports of mass, heat, moisture or other quantities. This approach is relevant to parameterization of convection in large-scale numerical models since there the objective is also to represent the residual terms in a proper way. The difficulty with the diagnostic studies is that real clouds are not simple. As shown by descriptive studies, they contain **convective-scale updrafts and downdrafts, they have important entrainment and**

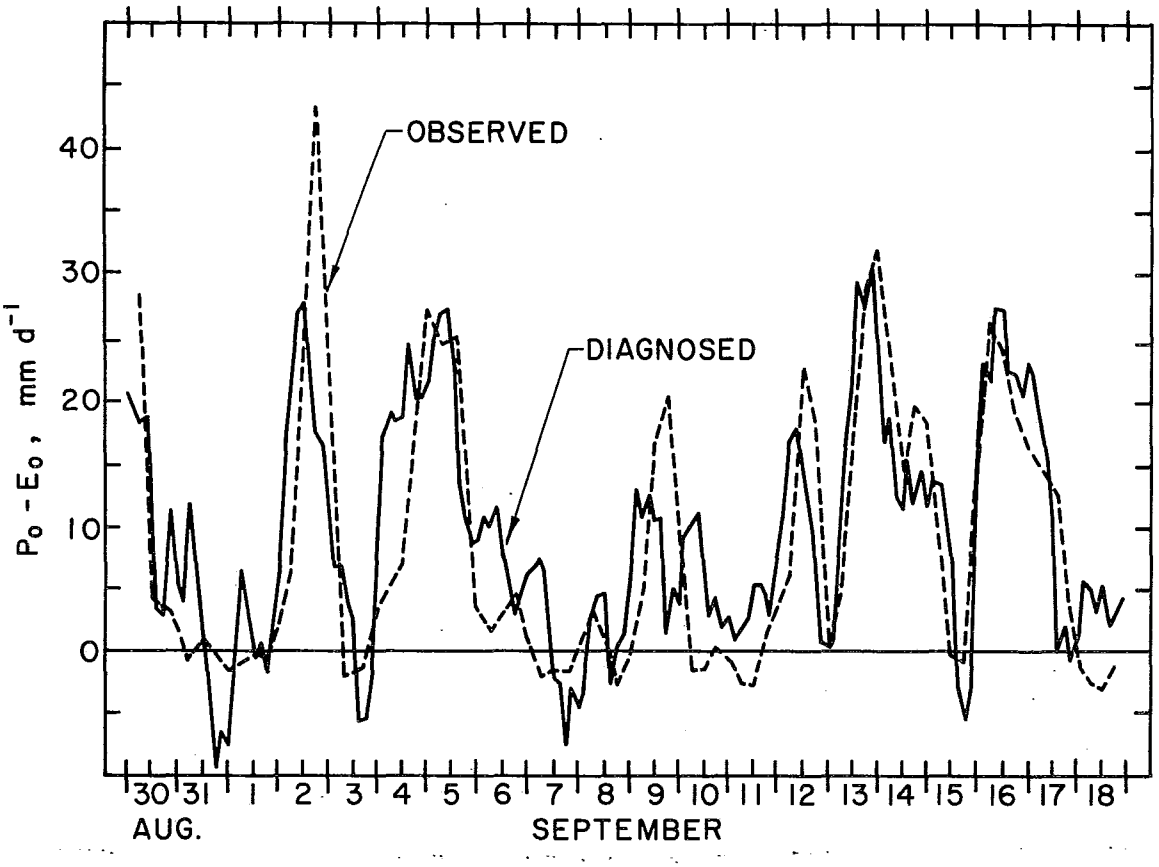

Fig. 9.31 Time series for Phase III of diagnosed (solid) and observed (dashed) precipitation minus evaporation. From Thompson et al. (1979).

detrainment effects, they have mesoscale anvil circulations and they are controlled not only by the resolved synoptic-scale motion field but by mesoscale convergence patterns, downdraft outflows and probably other unresolved features. The diagnostic studies to date have emphasized determining the extent to which these various features of GATE clouds can affect convective transports.

One major area of research has been the extension of the cloud spectral approach (Ooyama, 1971; Arakawa and Schubert, 1974; Ogura and Cho, 1973; Nitta, 1975; Yanai et al., 1976) to include convective downdrafts as well as mesoscale anvil air motions, since GATE descriptive studies have shown their importance (Fig. 9.34, from Houze et al., 1980).

In deriving cloud ensemble fluxes from synoptic data, Johnson (1976, 1978, 1980) has used a spectral convective downdraft, and in the later paper a mesoscale downdraft as well, both related to the updraft mass flux by coefficient of proportionality. An optimum value for the convective downdraft amplitude coefficient is found from matching diagnosed and observed rainfall, since the greater the evaporation associated with increased downdaft mass flux, the smaller the net precipitation. The author suggests that the amplitude of the mesoscale downdraft can be estimated by making plausible assumptions about the environmental mass flux between mesosystems. The main effect of the inclusion of more downdraft processes is to bring the net cloud mass flux closer to $\overline{w}$, particularly at low levels (Fig. 9.35, from Johnson, 1980).

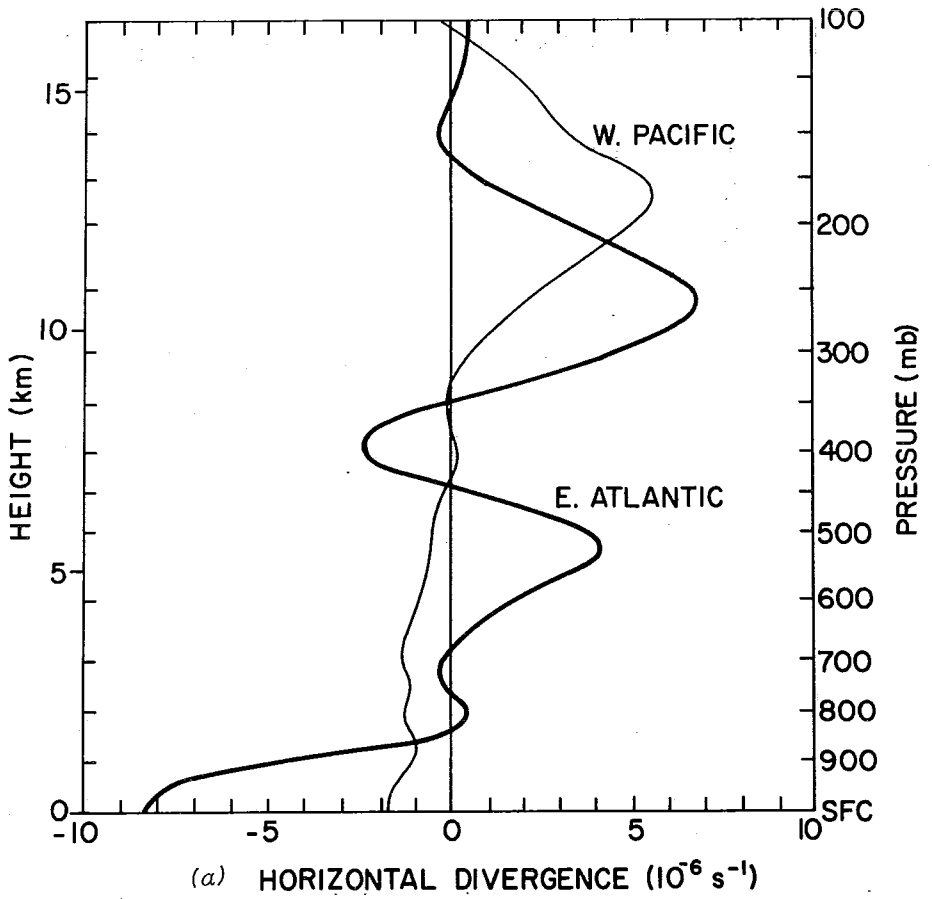

Fig. 9.32 Variation with height of mean horizontal divergence (a) and mean vertical velocity, dp/dt, where p is pressure, (b) for the B-scale area and the West Pacific station triangle. From Thompson et al. (1979).

Houze et al. (1980) extended their earlier work (Houze and Leary, 1976) in comparing diagnosed cloud ensemble fluxes computed from synoptic data by the residual method and from radar echo population data (Austin and Houze, 1973). Ruprecht (1980) has taken a similar approach. Houze et al. (1980) compared GATE Phase III diagnostic results computed by the method of Johnson (1976) with results based on their own radar population studies (Cheng and Houze, 1979). With common model assumptions they found reasonable agreement between the mass fluxes (Fig. 9.36) (and hence the derived heat fluxes) using these synoptic and radar approaches. They concluded both methods were basically sound, although both gave results that depended strongly on model assumptions. Cheng and Houze (1980) then examined the sensitivity of the convective-scale fluxes predicted from radar data to some of these model assumptions and suggested an optimum set based on plausibility arguments. Leary and Houze (1980) showed that the inclusion of mesoscale anvil updrafts and downdrafts consistent with descriptive studies of GATE cloud clusters made major changes to the model-derived profiles of convective mass and heat transports.

The drawback of these increasingly complex spectral convective and mesoscale models is that although these models contain terms for many of the processes now known to exist in nature, they contain several parameters and coefficients, which are not readily determined from the data and must be specified. Betts (1975) pointed out that there are only two independent budget equations. Earlier papers focussed on the moist static energy transport, and the models discussed above (e.g., Johnson, 1980b), still

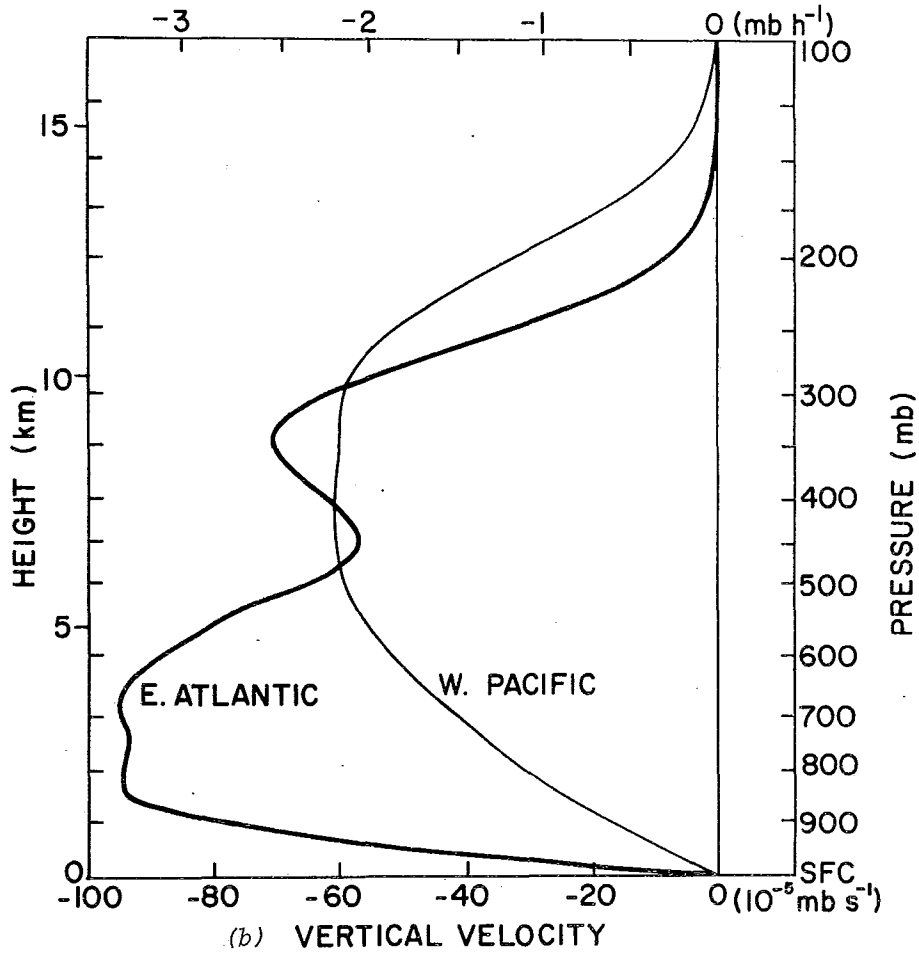

Fig. 9.32 (cont.)

do not use all the information in the second budget equation, despite their excess of variables. Nitta (1977) and Cho (1977), on the other hand, have taken different approaches, both using the information of two budget equations to determine two unique parameters.

Nitta (1977) used the fluxes of moist static energy and the combined flux of static energy and liquid water. This does, however, require a rain parameterization. Cho (1977) and Cho et al. (1979a), extending earlier work of Fraser (1968), Haman (1969), Betts (1973b) and Fraedrich (1973) determined a combined (net) updraft and downdraft convective mass flux from the flux of static energy and liquid water, and then a second parameter from the moisture budget: a vertical profile of a time scale for recycling of air by cumulus cloud life cycles (Fig. 9.37). Almost by design, this method gives a cumulus mass flux very close to the mean $\overline{w}$. The elegance of this theory lies in not attempting to separate updraft and downdraft components. However, the recycling rate is hard to interpret, and it can only be separated from cloud moisture parameters by further assumptions (Cho assumed detrained cloudy air is just saturated), which do not appear to be justified for deep convective ensembles, where the dominant detrainment at upper levels is updraft air and at lower levels unsaturated downdraft air, which the theory in its present form does not separate.

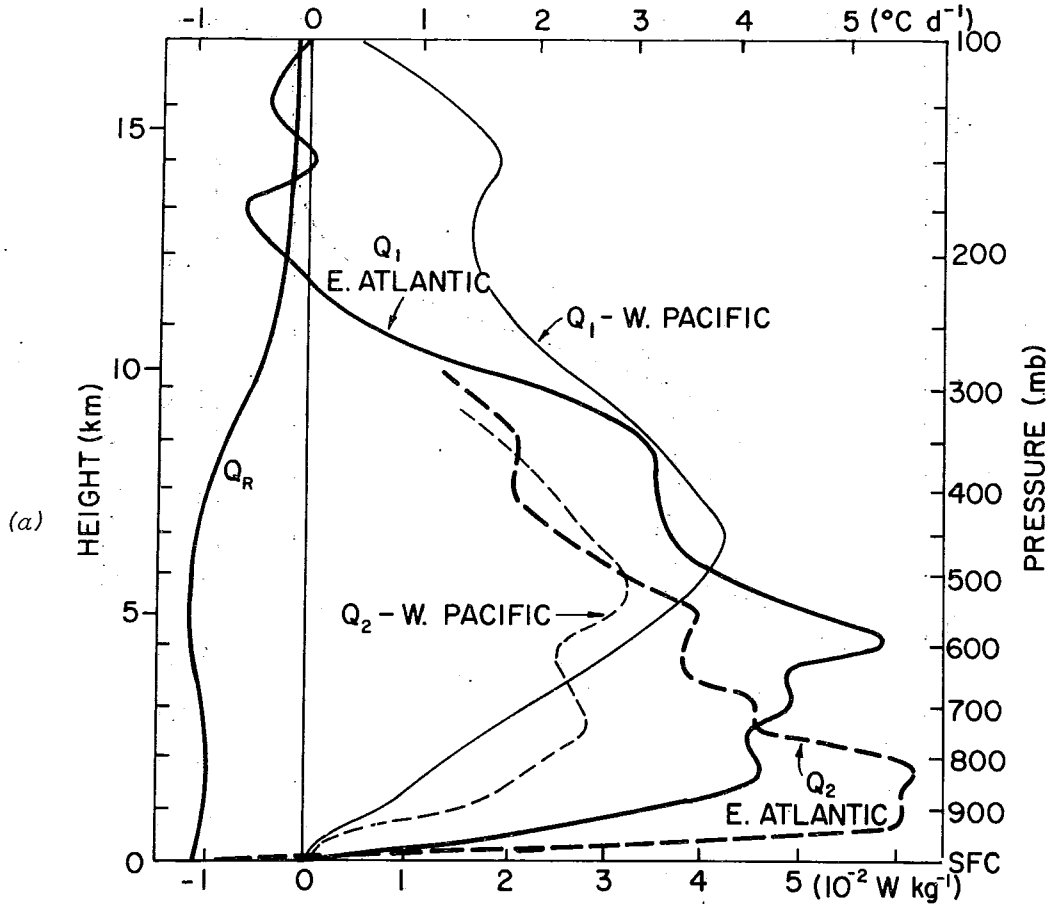

Fig. 9.33 Variation with height of the apparent sensible heat source, Q_1, and apparent latent heat sink Q_2 and the mean radiational heating Q_R (a) and the vertical eddy flux of moist static energy (b) for the B-scale area and the West Pacific triangle. From Thompson et al. (1979).

It does seem, though, that further development of the diagnostic theory for deep convection is possible by combining the ideas of Betts (1975), Nitta (1977) and Cho (1977). Work on this is in progress.

A different aspect of diagnostic models, which has presented some problems, is the transience of cloud systems. On the easterly wave scale, cloud storage terms associated with the changing cloud fields (which synoptic data do not resolve) are relatively small (Johnson, 1980), but for the life cycle of individual cloud clusters, there seem to be significant lags between, for example, synoptic water vapor convergence and precipitation (Betts, 1978; Frank, 1979). Whether this reflects partly unresolved data problems or storage in a changing cloud field is not clear.

Despite their limitations, some of the diagnostic models have been applied to GATE heat and moisture budget data for GATE easterly waves (e.g., Johnson, 1978, 1980b; Nitta, 1978). Nitta's and Johnson's results show that, depending on the moisture stratification, the occurrence of convection and its associated warming and drying of the environment lag the strongest synoptic-scale low-level convergence by as much as half a day, raising questions about the applicability of some CISK ideas. Their results illustrate how the vertical mass flux in deep convection is controlled by wave phase and indicate that during outbreaks of deep convection, the vertical mass flux in shallow convection is suppressed, apparently by downdrafts.

(b)

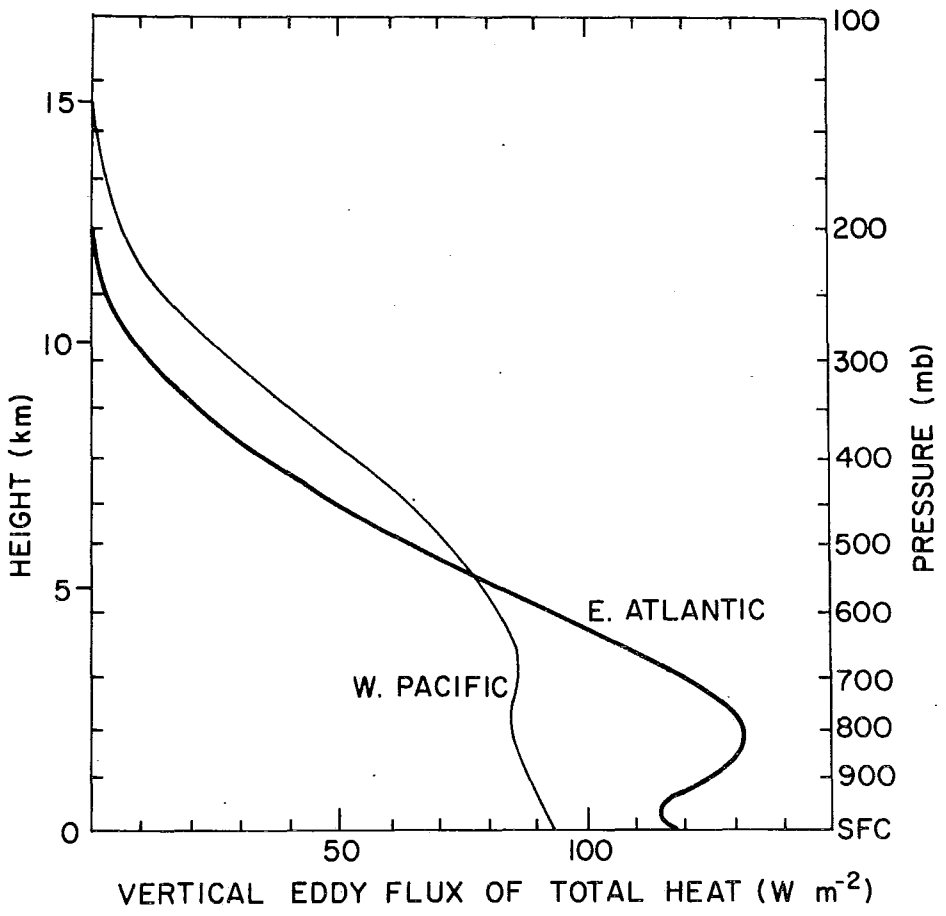

Fig. 9.33 (cont.)

9.6.3.2 Dynamic Transports by Cloud Ensembles

Some progress has been made in understanding the contribution of clouds to the large-scale vorticity budget (Shapiro, 1978; Stevens, 1979; Cho et al., 1979b; Reeves et al., 1979; Cheng et al., 1980; Cho and Cheng, 1980; Shapiro and Stevens, 1980). The observed vorticity source residuals are complex (as are the divergence profiles), but generally show that at low-levels, the convection acts as a sink of vorticity which opposes the amplification that low level convergence in a region of positive vorticity would produce (e.g., Reeves et al. 1979). This is of great dynamic significance, and seems consistent with the observation that very few GATE systems showed signs of low level vorticity amplification. There are some indicators of a similar effect at high levels -- of a convective source opposing anticyclonic amplification -- but different diagnostic studies are not consistent, or show both sources and sinks in the upper troposphere. The higher resolution fields of Ooyama (unpublished) show fascinating upper-level vorticity structure, which clearly needs further study (Fig. 9.38).

Reeves et al. (1979) present phase-average vorticity budget computations and a disturbed-suppressed stratification (Fig. 9.39), which show the increased vorticity sink at low levels during disturbed periods mentioned above. The budgets

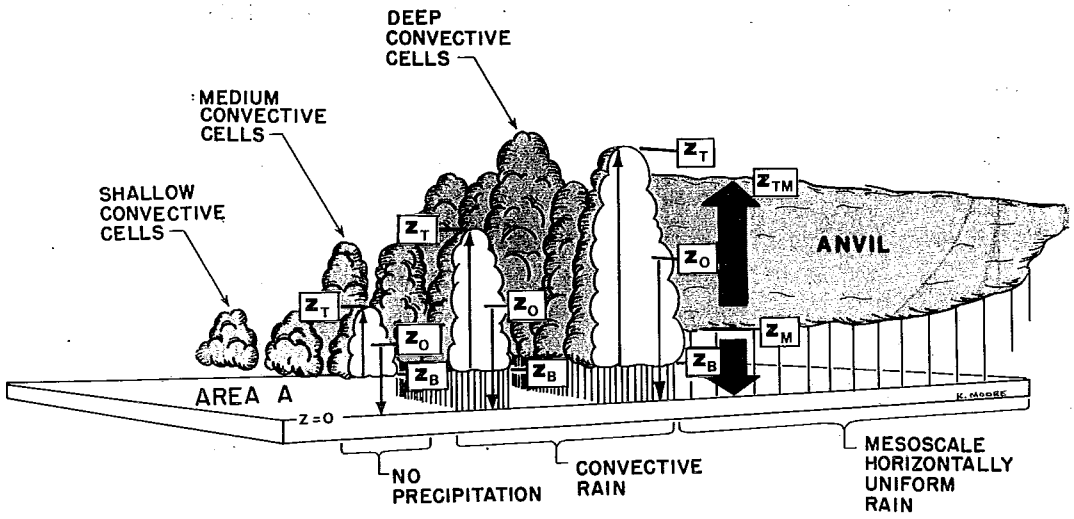

Fig. 9.34 Schematic of a typical population of clouds over a tropical ocean. Thin arrows represent convective scale updrafts and downdrafts. Wide arrows denote mesoscale updrafts and downdrafts. Other details and symbols for model parameters are described in Houze et al. (1980).

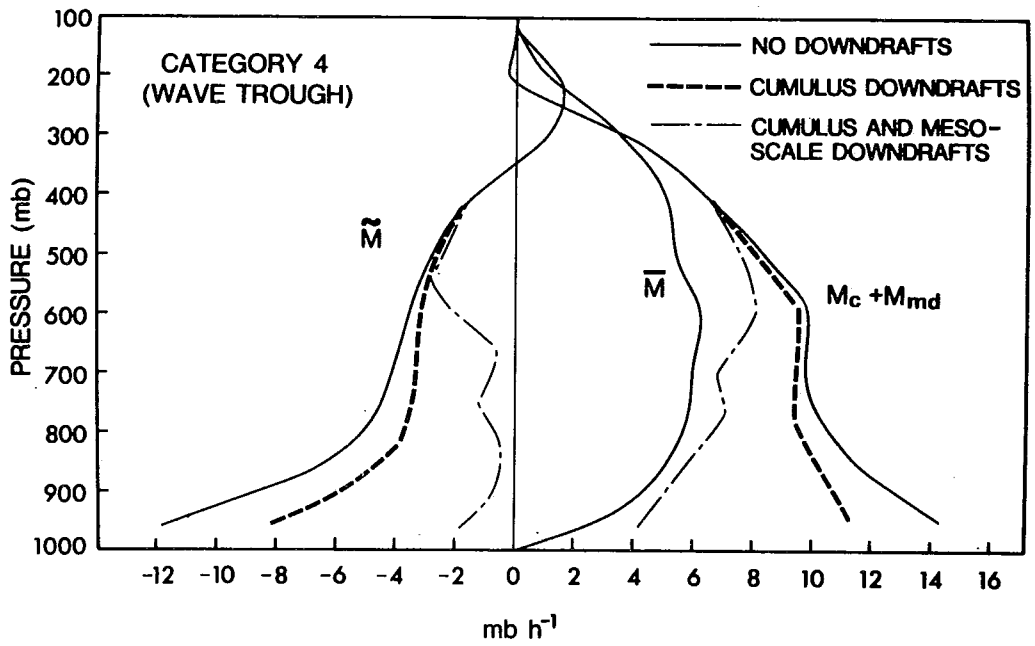

Fig. 9.35 Environmental mass flux $\tilde{M}$, mean mass flux $\bar{M}$ and net convective mass flux, $M_c + M_{md}$, for wave trough for cases with and without downdrafts. From Johnson (1980).

also show a mid-tropospheric positive vorticity source during undisturbed conditions, which could be associated with shallow to mid-level convection. However, both disturbed and suppressed budgets show a similar vorticity source at 200 mb, whose origin is unclear.

Cho et al. (1979b) and Cho and Cheng (1980) develop a theoretical basis for modeling vorticity transports by clouds using a continuous transient model for a cumulus cloud based on Cho (1977). They show the importance of horizontal transports of vorticity on the cloud scale, associated with the large vorticity couplets typically found in cumulonimbus. They also show, however, that average in-cloud vorticities are comparable to large-scale average vorticity (though somewhat larger). They find good agreement between A/B-scale budget residuals and parameterized values (Fig. 9.40). Their parameterization needs cloud boundary values of vorticity and these they estimate from a potential vorticity budget analysis (Cheng et al., 1980).

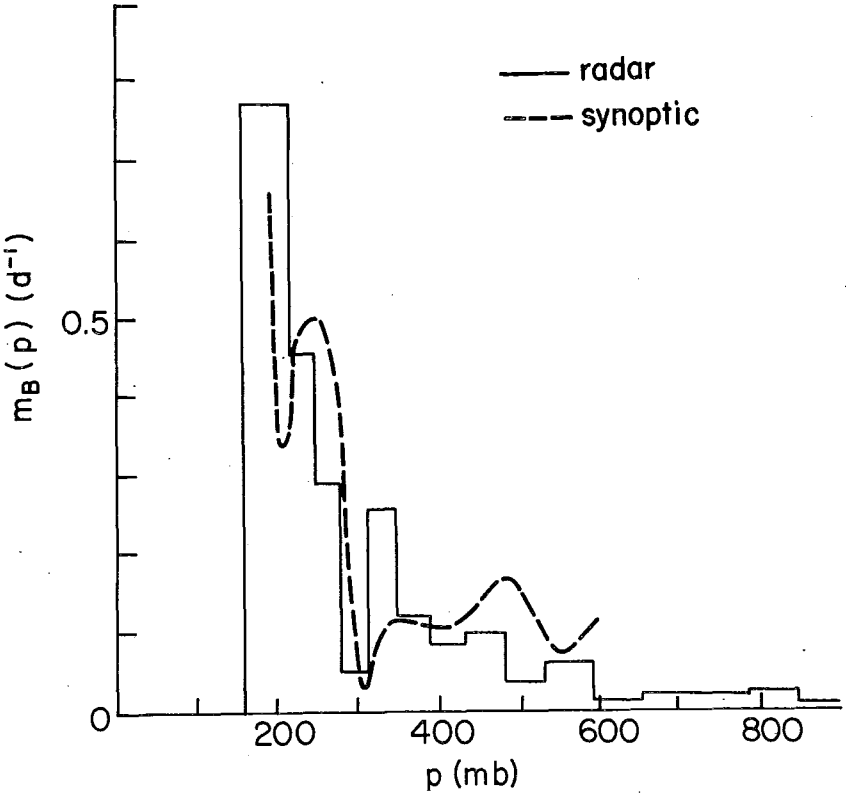

Fig. 9.36 Cell base mass transport spectrum diagnosed by the radar and synoptic approaches. From Houze et al. (1980).

The papers by Shapiro (1978), Stevens (1979), and Shapiro and Stevens (1980) explore the vorticity budget of the composite easterly wave. Their parameterization of the residual, using a single bulk cloud model, gives reasonably good agreement between observed and parameterized sources, but shows that spectral models are much worse because the vorticity budget for each cloud spectral type is unrealistic. They also found problems with the diagnosis of cloud mass flux. They concluded that their model was theoretically equivalent to the transient cloud model of Cho and Cheng (1980).

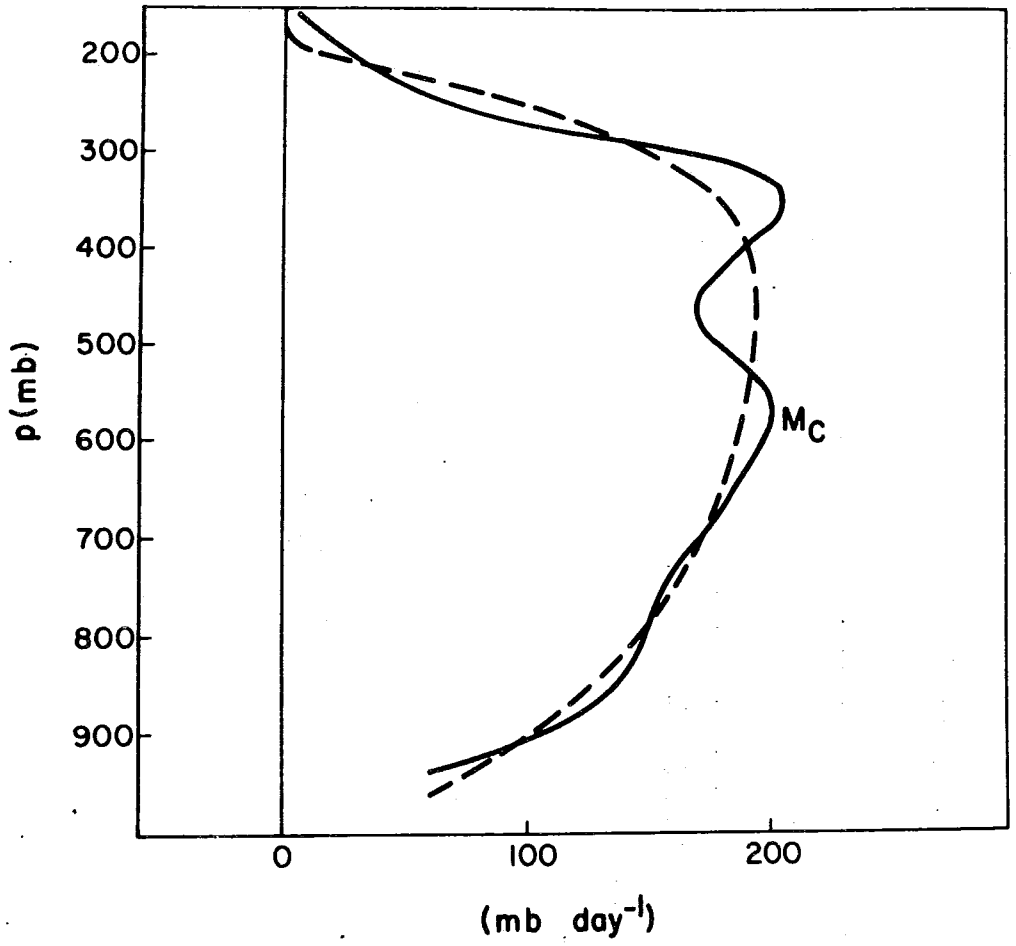

Fig. 9.37 GATE A/B-scale total cloud mass flux M_c (a) and recycling rate by cumulus clouds (b) for the period 0000-2400 2 September 1974. Dashed M_c curve is smoothed profile. From Cheng et al. (1980).

Stevens (1979) and Shapiro and Stevens (1980) attempt an analysis of the momentum budget for the wave, using the data of Thompson et al. (1979) and computing the wave pressure field by integrating the hydrostatic equation using wave perturbation virtual temperatures. The budgets tend to show, depending on wave phase, either sources of sinks or momentum at all heights. They concluded that simple interpretations or parameterizations, which only transport momentum, were not apparent.

9.7 PARAMETERIZATION TESTS AND CONVECTIVE MODELING

The testing of convective parameterization theories for use in numerical models was an important GATE objective. Some of this work has been done, but much remains to be accomplished. With the realization of the importance of convective transports of vorticity and momentum (Stevens et al., 1977; Shapiro and Stevens, 1980; Cho and Cheng, 1980), the large effects of clouds on the radiative divergence profile (Cox and Griffith, 1979) and the importance of mesoscale anvil circulations (Johnson, 1980b; Leary and Houze, 1980) the problem has become a much larger one.

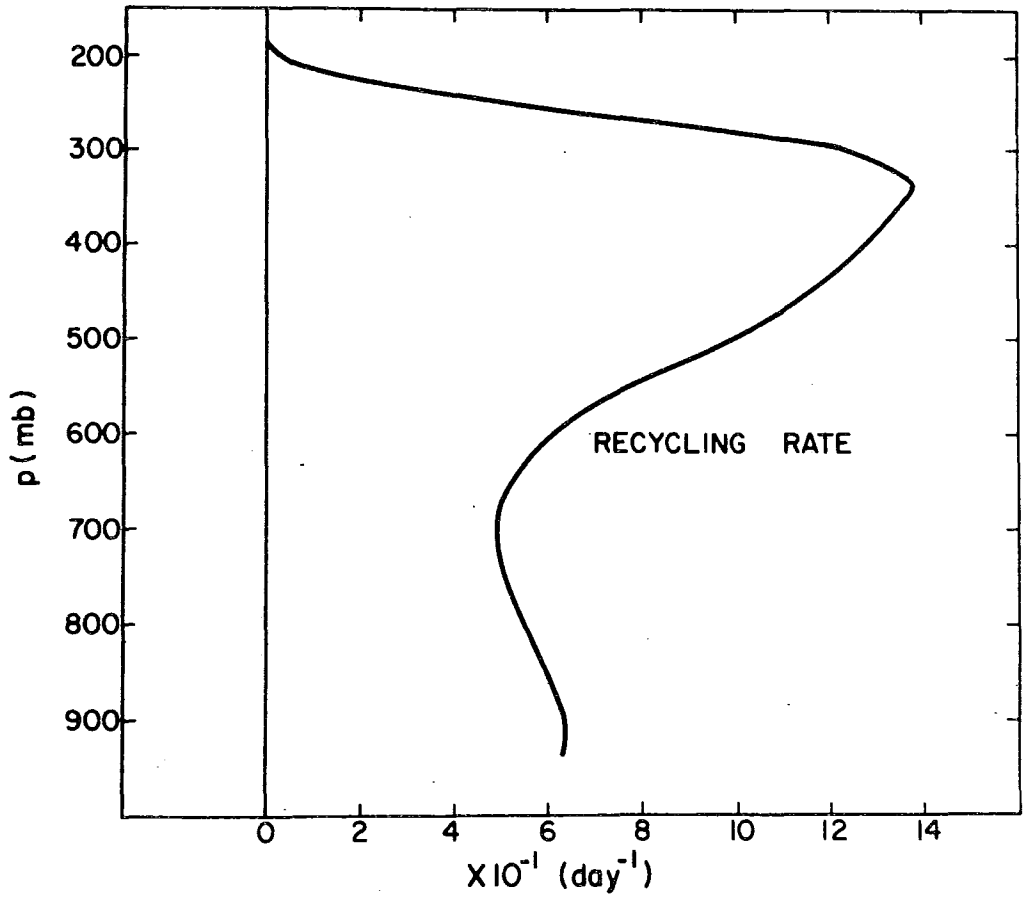

(b)

Fig. 9.37 (cont.)

The debate continues over whether all convective systems (including, for example, the squall line) are parameterizable, and whether in hurricane modeling it is necessary or desirable to parameterize convection. Rosenthal (1979) shows the extreme sensitivity of an axisymmetric hurricane model to different convective parameterizations. He further finds using horizontal grids of 10-20 km, which are sufficient to resolve mesoscale cloud structures but not individual convective towers, latent heat release on the resolvable scale is in some cases responsible for storm amplification. Rosenthal (1978, 1980) shows a hurricane simulation in which only latent heat release on the resolvable scales is included. The initial stages of the simulation show a squall-type mesoscale cloud structure that propagates in apparent independence of the vortex-scale flow, which shows no significant amplification. It is only later in the simulation with non-squall cloud structure that cooperative development of the CISK-type takes place.

9.7.1 Large-scale Numerical Modeling

The testing of parameterization schemes is inherent in large-scale numerical model simulations. Recently, Slingo (1980) has reported on a coupled cloud-radiation parameterization used in the British 11-layer tropical model and

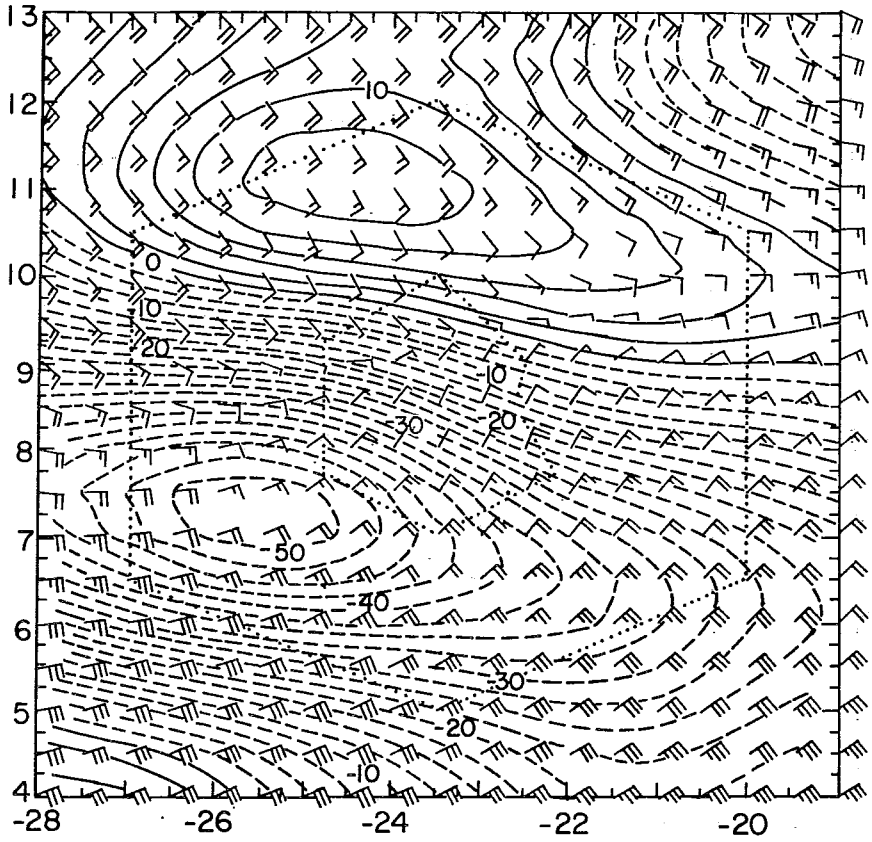

Fig. 9.38 Relative vorticity field at 227 mb at 1800 GMT 5 September 1974 showing cyclonic (solid lines) and anticyclonic (dashed lines) vorticity couplet (unit: 10^{-6} s^{-1}) across strongly divergent outflow over cloud cluster complex. The domain is centered on the A/B ship array (dotted). The ordinate and abscissa are latitude in degrees. The wind barbs are conventional (single long barb equals ten knots). From Ooyama, unpublished.

tested on GATE data. Layer clouds at low, middle and high levels are determined statistically from large-scale relative humidity and, for the low-level clouds (mainly stratocumulus under inversions), lapse rate. Deep convection is predicted using the parameterization of Lyne and Rowntree (1976). Tests show realistic distributions of stratocumulus off Africa and South America and upper and middle-level layer clouds developing in the vicinity of deep convection in a manner somewhat reminiscent of the anvil cloud development seen in case studies (Secs. 9.5 and 9.6). Other work has been done by Krishnamurti et al. (1979, 1980) **and Miyakoda and Sirutis (1977).**

9.7.2 Semiprognostic Tests

Semiprognostic tests involve computing the fluxes by an ensemble of convection in a region of space and period of time representative of a grid volume and time step of a large-scale numerical model and comparing the results with observations. Lord (1978) and Krishnamurti et al. (1980) have carried out such tests on GATE Phase III data with the ensemble fluxes computed by several parametric schemes, including hard and soft convective adjustment, Arakawa and Schubert's (1974) scheme, and Kuo's (1965) and (1974) schemes. Krishnamurti et al. show that hard convective adjustment gives massive rainfall at the first time-step, with a consequent radical change in the atmospheric thermal and moisture structure.

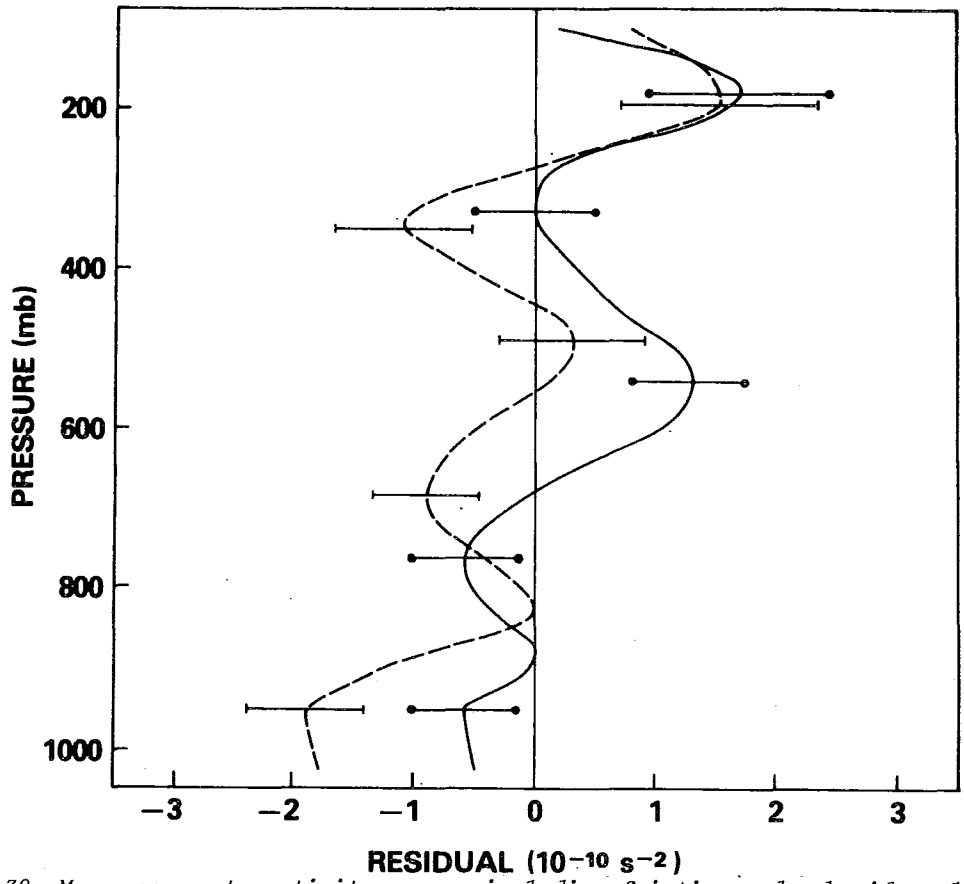

Fig. 9.39 Mean apparent vorticity source including friction and subgrid scale processes only for disturbed (dashed) and undisturbed (solid) conditions with confidence intervals indicated by bars. From Reeves et al. (1979).

Soft convective adjustment, which only adjusts over a fraction of the grid, can give reasonable mean rainfall rates for the entire period, but poor day-by-day agreement. Kuo's (1965) scheme, which partitions the moisture convergence, under-predicts rainfall, but has good phase agreement. Kuo's (1974) scheme and the Arakawa-Schubert scheme (tested by both Lord and Krishnamurti et al.) both give excellent agreement between observed and predicted precipitation (Fig. 9.41). Krishnamurti et al. found that the rainfall agreed very closely with the vertical advection of water vapor. Lord's work, however, shows that a successful precipitation comparison is not a sufficient test of the parameterization scheme's ability to reproduce realistic profiles of warming and drying of the environment by the convective fluxes.

Soong and Tao (1980) carried out semiprognostic tests on GATE data with a two-dimensional cloud ensemble model developed by Soong and Ogura (1980). Domain averaged vertical and horizontal wind and initial thermodynamic structure were prescribed for an observed deep convective situation. A randomly generated population of model clouds was allowed to develop for 6 h within a domain 64 km in horizontal dimension. Fluxes by the model clouds produced profiles of warming and drying over the model domain that compared favorably with observed profiles. Kuo's (1965) parameterization scheme gave a less favorable comparison.

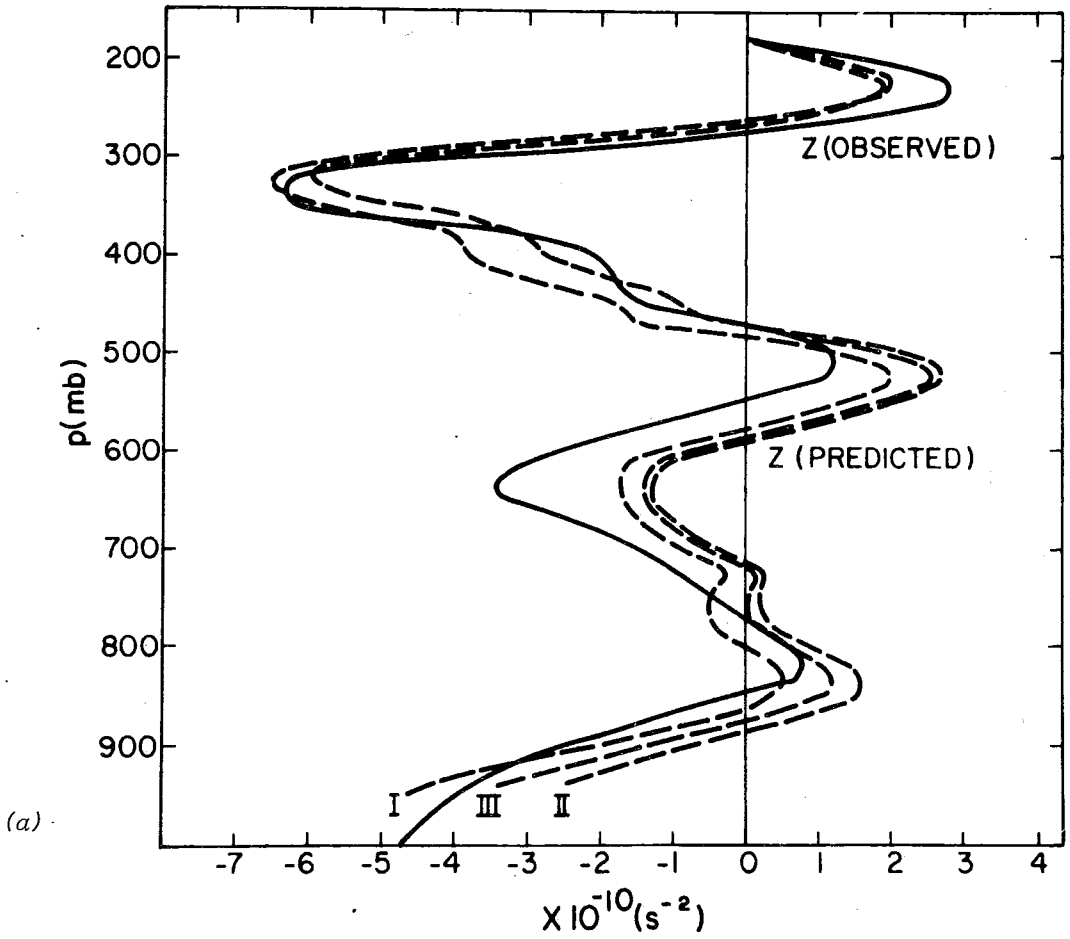

(a)

Fig. 9.40 Comparison between the observed (solid) and predicted (dashed) apparent vorticity sources for 2 September (a) and 9 September 1974 (b). Three different predicted sources are shown for different cloud-scale vorticity parameterizations. From Cho and Cheng (1980).

9.7.3 Shallow Cumulus and Stratocumulus Modeling

Although the modeling and parametric work described in this section has not been done using GATE data, much of it is relevant to GATE objectives and will be used for further analyses.

Work has been done on the construction of parametric models for shallow cumulus layers (Albrecht et al., 1979; Albrecht, 1979). These papers discuss the evolution of a mixed layer type model (Betts, 1973a) for the tradewind boundary layer, and show good agreement for atmospheric structure and convective fluxes with values observed during the Atlantic Tradewind Experiment (1969). This model was also used to simulate diurnal variations, and showed in the limiting case of a stratocumulus layer, good agreement with Schubert (1976). Schubert (1976) and Schubert et al. (1979a, b) extend Lilly's (1968) stratocumulus model and apply it to regions of horizontally inhomogenous sea-surface temperature and large-scale divergence. There has been considerable discussion of the appropriate parameterization of radiation for stratocumulus: specifically the degree to which

(b)

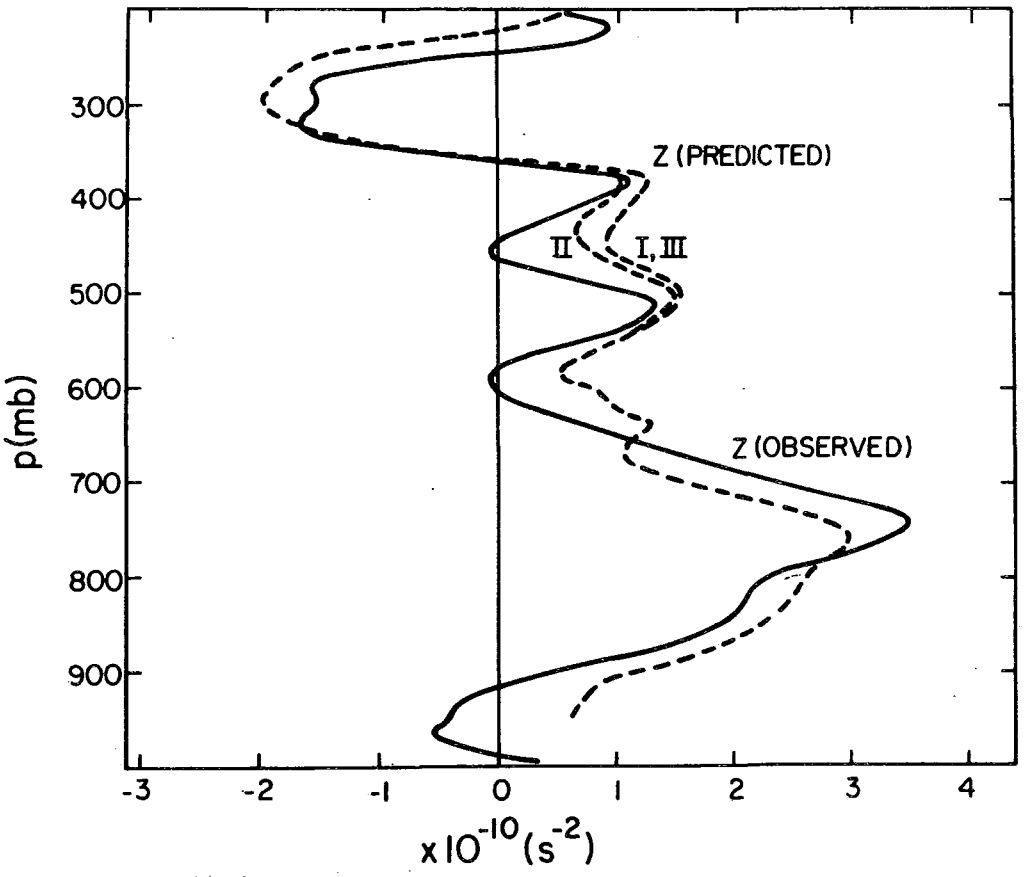

Fig. 9.40 (cont.)

radiative cooling can be regarded as part of a cloud-top boundary condition, or a mechanism for the generation of turbulence in the cloud layer (Deardorff, 1976; Kahn and Businger, 1979; Lilly and Schubert, 1980; Deardorff and Businger, 1980; Randall, 1980a). Slingo's (1980) cloud parameterization (Sec. 9.7.1) includes stratocumulus with radiative feedback. The breakup of a stratocumulus layer through cloud-top entrainment instability has been modeled by Randall (1980b) and Deardorff (1980). The three-dimensional modeling of shallow cumulus populations has advanced considerably (Sommeria, 1976; Sommeria and LeMone, 1978). In the latter paper the authors compare model parameters with experimental data and find good agreement for some parameters. Subsequently, Beniston and Sommeria (1981) use the three-dimensional model to test hypotheses of the parametric models of Yanai et al. (1973), Betts (1975, 1976b) and Fraedrich (1976). They show that the coupling of the convective thermodynamic fluxes through a bulk convective mass flux is a very accurate parameterization. They also confirm the usefulness of the coupling of the cloud and subcloud layers using two closure parameters, as proposed in Betts (1976b). The comparison with Fraedrich's (1976) cloud population parameterization scheme is less satisfactory. The model cloud population (whose realism is admittedly questionable) differs appreciably from the simple exponential distribution proposed by Fraedrich, with corresponding differences in the mass flux distributions.

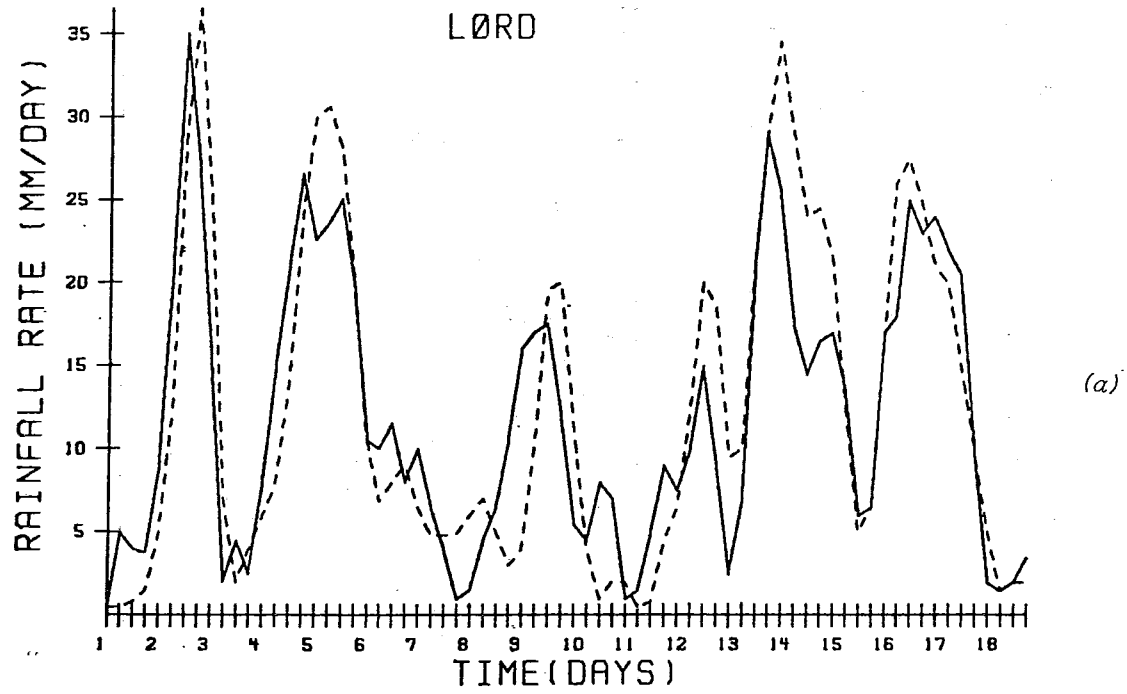

(a)

Fig. 9.41 Comparison between observed (dashed line) and predicted (solid line) rainfall rates (mm day $^{-1}$) for 1-18 September 1974, using Lord's (1978) scheme (a) and Kuo's (1974) scheme (b). From Krishnamurti et al. (1980).

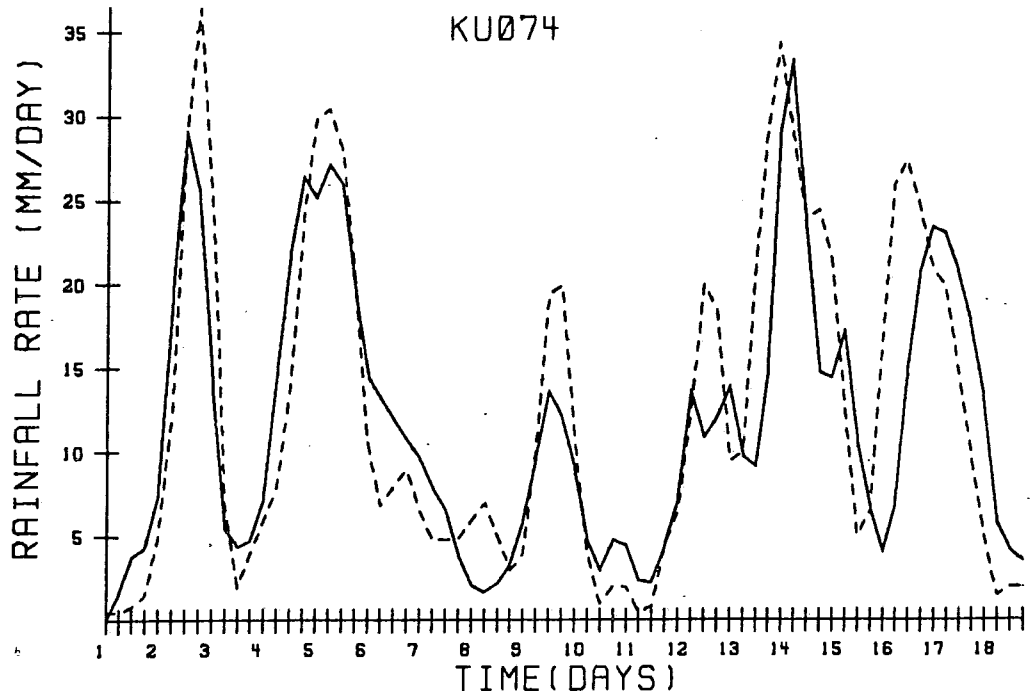

(b)

9.8 CONCLUSIONS

Convection that occurs in the region of planetary-scale lifting associated with the tropical Hadley cells was documented extensively in GATE by upper-air soundings, satellite, meteorological radar and instrumented aircraft. Though much of the data have yet to be analyzed, many aspects of the structure of the convection and its relation to larger-scale flow have been revealed by detailed studies of a few examples of GATE convective systems, by limited or preliminary studies of a somewhat larger number of systems, and by statistical overviews of the satellite, radar and aircraft data.

As had been hoped for in the planning of GATE, the convection sampled in the experiment resided in the center of the zone of ITCZ cloudiness extending across the eastern equatorial Atlantic Ocean and, as had been anticipated, the convection was dominated by cloud clusters. The frequency of clusters in time and space was modulated by synoptic-scale easterly waves and diurnal cycles of radiative heating and cooling.

The cloud clusters were of two types: squall clusters, which propagated rapidly and were associated with pronounced vertical wind shear, and non-squall clusters, which propagated slowly and were associated with weaker wind shear.

Cloud clusters were characterized by large upper-level cloud shields that emanated from penetrative cumulonimbus. Accompanying the deep cumulonimbus was a spectrum of smaller convective features ranging from moderate cumulonimbus down to tiny non-precipitating cumulus. The spectrum of sizes of these convective features, whether measured in terms of height, area, duration or rainfall rate, was lognormal. That is, there existed a great many smaller convective clouds and rain areas for each large cumulonimbus rain area in a cloud cluster.

However, the relatively few large cumulonimbus rain areas, referred to as "mesoscale precipitation features," accounted for about 90% of the rain in GATE. These mesoscale precipitation features were the preferred regions where the deepest convective cells, or "hot towers", hypothesized to exist by Riehl and Malkus (1958), actually formed and penetrated to the tropopause.

As a mesoscale precipitation feature matured, it developed a region of stratiform precipitation adjacent to its active cells. The stratiform portion of the feature consisted partly of older decayed cells and, in important cases, occupied the majority of the area covered by the mesoscale precipitation feature. A large fraction of the total rainfall in GATE fell as stratiform precipitation of this type. The stratiform precipitation fell from the middle-level base of the "anvil" cloud shield that interconnected the various mesoscale precipitation features of a cloud cluster. Associated with the stratiform precipitation below the base of the anvil was a mesoscale (as opposed to cumulus-scale) downdraft similar to that described by Zipser (1969). This downdraft originated at about the 0° C level and the air in it was generally unsaturated and cooled by melting and evaporation of the falling precipitation. A mesoscale region of ascent appeared to exist within the anvil cloud itself, above the mesoscale downdraft. The existence of the mesoscale updraft needs to be confirmed. However, both it and the mesoscale downdraft are consistent with the observation of large-scale convergence in the middle troposphere and divergence at the surface and at high levels in regions containing clusters that are in mid-to-late stages of development.

In the dissipating stage of a mesoscale precipitation feature, the convective cells become less numerous and weaker, and the stratiform precipitation dominates the feature.

The downdrafts, both cumulus-scale and mesoscale, from a mesoscale precipitation feature invade the planetary boundary layer and fill it with low moist static energy air. Moderate cumulonimbus, existing as part of the spectrum of smaller convective features associated with clusters also produce significant downdraft modification of the subcloud layer. As downdraft air spreads out in the boundary layer, it influences the patterns of new cloud formation. New clouds are suppressed everywhere within the downdraft-covered region, however, both small cumuli and incipient major clusters tend to form at the edges of the downdraft air, where low-level convergence becomes enhanced. Thus, cloud patterns are controlled not only by large-scale phenomena such as the Hadley cells, synoptic-scale waves and diurnal radiative cycles, but also by the existence of past clouds, the medium of communication between the past and present clouds being the downdrafts.

Representing tropical clouds in a mathematically suitable way for including their effects in numerical models of large-scale flow remains an objective of GATE research. The descriptive and statistical studies of GATE convective systems have led to the realization that a variety of physical processes must be accounted for in such models. Besides cumulus-scale updrafts, it now appears that cumulus-scale downdrafts, mesoscale downdrafts, mesoscale updrafts, downdraft-induced boundary-layer transformations and radiative feedbacks are all important in modifying the thermodynamic and dynamic structure of the large-scale environment. That controls over new convective cloud formation are not purely large-scale, but involve the history of past clouds, and that feedbacks to the environment may not be directly from convective to synoptic scale but involve the generation of intermediate-scale disturbances are now eminently apparent and must be considered in trying to understand and model scale interactions in the tropics.

Further diagnostic and parametric studies are needed. It is clear that on large enough scale (700 km and 24 h), precipitation and mean vertical motion are closely coupled. This gives encouragement for the parameterization of convection. However, it has not been shown that we can predict the detailed vertical structure of the convective fluxes with sufficient accuracy. GATE, moreover, has shown that the vorticity transports by convection cannot be neglected in favor of a purely thermodynamic convective parameterization. On space and time scales more comparable to the mesoscale precipitation areas (100 km and 4 h), we are far from understanding the parametric problem.

Much remains to be done to understand the mechanisms of scale interactions in the tropics and much GATE data remains unexamined. We anticipate that in future years these data will be used to study more examples of GATE convective systems and their interactions with their environments will be intensively studied and, as a result, the mechanisms involved will be closer to being unraveled.

ACKNOWLEDGMENTS

Dr. Edward Zipser has contributed many helpful comments. Both authors have been scientific visitors with Dr. Zipser's GATE group at the National Center for Atmospheric Research. Other colleagues who have critiqued the manuscript include A. Arakawa, R. H. Johnson, C. A. Leary, R. S. Pastushkov, R. J. Reed and C. Warner. Technical assistance with the manuscript, figures and references were provided by L. Link, S. Stippich and K. Moore. The authors are supported by the Global Atmospheric Research Program, Division of Atmospheric Sciences, National Science Foundation and the GATE Project Office, National Oceanic and Atmospheric Administration under Grants ATM78-16859 and ATM79-15788.

REFERENCES

Albrecht, B. A., A. K. Betts, W. H. Schubert and S. K. Cox, 1979: A model for the thermodynamic structure of the trade-wind boundary layer: Part I., Theoretical formulation and sensitivity tests. J. Atmos. Sci., 36, 73-89.

_____, 1979: A model for the thermodynamic structure of the trade-wind boundary layer: Part II., Applications. J. Atmos. Sci., 36, 90-98.

Arakawa, A. and W. Schubert, 1974: Interaction of a cumulus cloud ensemble with the large-scale environment. Part I. J. Atmos. Sci., 31, 674-701.

Arkell, R., M. Hudlow, 1977: GATE international meteorological radar atlas. US NOAA, EDS, Wash., D.C., 222p.

Aspliden, C. I., Y. Tourre and J. C. Sabine, 1976: Some climatological aspects of West African disturbance lines during GATE. Mon. Wea. Rev., 104, 1029-1035.

Augstein, E., 1978: The atmospheric boundary layer over the tropical oceans. Meteorology over the Tropical Oceans, 73-103, Roy Meteor. Soc., Bracknell, England.

Austin, P. M. and S. G. Geotis, 1979: Raindrop sizes and related parameters for GATE. J. Appl. Meteor., 18, 569-575.

_____ and R. A. Houze, Jr., 1973: A technique for computing vertical transports by precipitating cumuli. J. Atmos. Sci., 30, 1100-1111.

Ball, J. T., et al., 1980: Cloud-coverage characteristics during Phase 3 of GATE, as derived from satellite ans ship data. Mon. Wea. Rev., 108(9), 1419-1429.

Barnes, G. M., 1980: Subcloud layer energetics of precipitating convection. Ph.D. Dissertation. University of Virginia, Charlottesville, VA, 212 pp.

Beniston, M. G. and G. Sommeria, 1981: Use of a detailed planetary boundary layer model for parameterization purposes. J. Atmos. Sci., (in press).

Betts, A. K., 1973a: Non-precipitating cumulus convection and its parameterization. Quart. J. Roy. Meteor. Soc., 99, 178-196.

_____,1973b: A composite cumulonimbus budget. J. Atmos. Sci., 30, 597-610.

_____,1975: Parametric interpretation of trade-wind cumulus budget studies. J. Atmos. Sci., 32, 1934-1945.

_____, 1976a: The thermodynamic transformation of the tropical subcloud layer by precipitation and downdrafts. J. Atmos. Sci., 33, 1008-1020.

_____, 1976b: Modelling subcloud layer structure and interaction with a shallow cumulus layer. J. Atmos. Sci., 33, 2363-2382.

_____, R. W. Grover and M. W. Moncrieff, 1976: Structure and motion of tropical squall lines over Venezuela. Quart. J. R. Met. Soc., 102, pp. 395-404.

_____, 1978: Convection in the tropics. Meteorology over the Tropical Oceans. Roy. Meteor. Soc., Bracknell, England, 105-132.

Betts, A. K. and M. F. Silva Dias, 1979: Unsaturated downdraft thermodynamics in cumulonimbus. J. Atmos. Sci., 36, 1061-1071.

Bibikova, T. N., V. N. Kozhevnikov, E. V. Zhurba, Y. A. Romanov and A. K. Khrgian, 1977: Some results from cloud observations in the tropics. Soviet Meteor. Hydro., No. 8, 67-74.

Borovikov, A. M., I. P. Mazin, V. Melnichuk and P. Willis, 1975: Case study of analysis of individual Cb physical structure. GATE Report No. 14, Vol. II, ICSU/WMO, Geneva, 212-216.

_____, _____ and A. N. Nevzorov, 1978: Cloud structure peculiarities in the eastern zone of tropical Atlantic. Proc. Int. Scientific Conf. on the Energetics of the Tropical Atmosphere, Tashkent, published by ICSU/WMO, Geneva, 43-47.

Brown, J. M., 1979: Mesoscale unsaturated downdrafts driven by rainfall evaporation: A numerical study. J. Atmos. Sci., 36, 313-338.

Burpee, R. W., 1975: Weather forecasting for GATE. GATE Report No. 14, 98-100.

_____, 1979: Some features of synoptic-scale waves based on compositing analysis of GATE data. Mon. Wea. Rev., 103, 921-925.

Byers, H. R. and R. R. Braham, Jr., 1949: The Thunderstorm. Washington D.C., U.S. Govt. Printing Office, 287 pp.

Cheng, C.-P. and R. A. Houze, Jr., 1979: The distribution of convective and mesoscale precipitation in GATE radar echo patterns. Mon. Wea. Rev., 107, 1370-1381.

_____ and _____, 1980: Sensitivity of diagnosed convective fluxes to model assumptions. J. Atmos. Sci., 37, 774-783.

Cheng, L., T.-C. Yip and H.-R. Cho, 1980: Determination of mean cumulus cloud vorticity from GATE A/B-scale potential vorticity budget. J. Atmos. Sci., 37, 797-811.

Cho. H.-R., 1977: Contribution of cumulus cloud life-cycle effects to the large-scale heat and moisture budget equations. J. Atmos. Sci., 34, 87-97.

_____ and L. Cheng, 1980: Parameterization of horizontal transport of vorticity by cumulus convection. J. Atmos. Sci., 37, 812-826.

_____, _____ and R. M. Bloxam, 1979a: The representation of cumulus cloud effects in the large-scale vorticity equation. J. Atmos. Sci., 36, 127-139.

_____, R. M. Bloxam and L. Cheng, 1979b: GATE A/B-scale budget analysis. Atmos. Ocean, 17, 60-76.

Cox, S. K. and K. T. Griffith, 1979: Estimates of radiative divergence during Phase III of the GARP Atlantic Tropical Experiment: Part II. Analysis of Phase III results. J. Atmos. Sci., 36, 586-601.

Cunning, J. B. and R. I. Sax, 1977: A Z-R relationship for the GATE B-scale array. Mon. Wea. Rev., 105, 1330-1336.

_____ and _____, 1977: Raindrop size distribution and Z + R relationships measured on the NOAA DC-6 and the ship Researcher within the GATE B-scale array. NOAA TM ERL WMPO-37, 136p.

Deardorff, J. W., 1976: On the entrainment rate of a stratocumulus topped mixed layer in a strong inversion. Quart. J. Roy. Meteor. Soc., 101, 563-582.

_____, 1980: Cloud top entrainment instability. J. Atmos. Sci., 37, 131-147.

_____ and J. A. Businger, 1980: Comments on "Marine stratocumulus convection. Part I: Governing equations and horizontally homogeneous solutions". J. Atmos. Sci., 37, 481-482.

Degtyarev, A. I. and I. G. Sitnikov, 1976: Evaluation of methods for parameterization of penetrating convection based on GATE material. Soviet Meteor. Hydr., 1, 96-102 (Russian); 75-74 (English).

Eldridge, R. H., 1957: A synoptic study of West African disturbance lines. Quart. J. Roy. Meteor. Soc., 83, 303-314.

Echternacht, K. L. and M. Garstang, 1976: Changes in the structure of the tropical subcloud layer from the undisturbed to disturbed states. Mon. Wea. Rev., 104, 407-417.

Falkovich, A. I., 1978: On the problem of energy balance in the ITCZ. Proc. Int. Scientific Conf. on the Energetics of the Tropical Atmosphere, Tashkent, Published by ICSU/WMO, Geneva, 219-227.

_____, 1979: Dynamics and energetics of the ITCZ. Hydrometeorology, Leningrad, 247 pp.

Fitzjarrald, D. E., 1979: On using a simplified turbulence model to calculate eddy diffusivities. J. Atmos. Sci., 36, pp. 1817-1820.

Foltz, G. S. and W. M. Gray, 1979: Diurnal variation in the troposphere's energy balance. J. Atmos. Sci., 36, 1450-1466.

Fortune, M., 1980: Properties of African disturbance lines inferred from time-lapse satellite imagery. Mon. Wea. Rev., 108, 153-168.

Fraedich, K., 1973: On the parameterization of cumulus convection by lateral mixing and compensating subsidence. J. Atmos. Sci., 30, 408-413.

_____, 1976: A mass budget of an ensemble of transient cumulus clouds determined from direct cloud observations. J. Atmos. Sci., 33, 262-268.

Frank, N. L., 1970: Atlantic tropical systems of 1969. Mon. Wea. Rev., 98, 307-314.

Frank, W. M., 1978: The life cycles of GATE convective systems. J. Atmos. Sci., 35, 1256-1264.

_____, 1979: Individual time period analyses over the GATE ship array. Mon. Wea. Rev., 107, 1600-1616.

Fraser, A. B., 1968: The white box: The mean mechanics of the cumulus cycle. Quart. J. Roy. Meteor. Soc., 94, 71-87.

Fritsch, J. M., 1975: Cumulus dynamics: local compensating subsidence and its implications for cumulus parameterization. Pure and Appl. Geoph., V.113 (5/6) 851-867.

_____ and C. F. Chappell, 1980: Numerical prediction of convectively driven mesoscale pressure systems, Pt. 1, Convective parameterization. J. Atmos. Sci., 37 (8), 1722-1733.

GARP Publications Series No. 4, 1970: The Planning of GARP Tropical Experiments. ICSU/WMO, Geneva, 78 pp.

Garstang, M. A. and A. K. Betts, 1974: A review of the tropical boundary layer and cumulus convection: structure, parameterization and modeling. Bull. Amer. Meteor. Soc., 55, 1195-1205.

GATE Report No. 1, 1972: Experimental Design Proposal for the GARP Atlantic Tropical Experiment. Global Atmospheric Research Programme's Atlantic Tropical Experiment. ICSU/WMO, Geneva, 188 pp.

GATE Report No. 18, 1975: Report on the Field Phase of the GARP Atlantic Tropical Experiment, Aircraft Mission Summary. ICSU/WMO, Geneva, 143 pp.

Gaynor, J. E. and P. A. Mandics, 1978: Analysis of the tropical marine boundary layer during GATE using acoustic sounder data. Mon. Wea. Rev., 106, 223-232.

_____ and C. F. Ropelewski, 1979: Analysis of the convectively modified GATE boundary layer using in situ and acoustic sounder data. Mon. Wea. Rev., 107 (8), 985-993.

Gray, W. M., 1973: Cumulus convection and larger-scale circulations, I. Broadscale and mesoscale considerations. Mon. Wea. Rev., 101, 839-855.

_____ and R. W. Jacobson, Jr., 1977: Diurnal variation of oceanic deep cumulus convection. Mon. Wea. Rev., 105, 1171-1188.

Gruber, A., 1976: An estimate of the daily variation of cloudiness over the GATE A/B area. Mon. Wea. Rev., 104, 1036-1039.

Haman, K., 1969: On the influence of convective clouds on the large-scale stratification. Tellus, 21, 40-53.

Hamilton, R. A. and J. W. Archbold, 1945: Meteorology of Nigeria and adjacent territory. Quart. J. Roy. Meteor. Soc., 71, 231-262.

Holle, R. L., J. Simpson, and S. W. Leavitt, 1979: GATE B-scale cloudiness from whole-sky cameras on four U.S. ships. Mon. Wea. Rev., 107, 874-895.

Houze, R. A., Jr., 1975: Squall lines observed in the vicinity of the "Researcher" during Phase III of GATE. Prep. 16th Radar Meteor. Conf., Houston. Published by Amer. Meteor. Soc., Boston, 206-209.

_____, 1976: GATE radar observations in a tropical squall line. Prep. 17th. Conf. Radar Meteor., Seattle. Published by Amer. Meteor. Soc., Boston, 384-389.

_____, 1977: Structure and dynamics of a tropical squall-line system observed during GATE. Mon. Wea. Rev., 105, 1540-1567.

_____ and C.-P. Cheng, 1977: Radar characteristics of tropical convection observed during GATE: Mean properties and trends over the summer season. Mon. Wea. Rev., 105, 964-980.

_____ and C. A. Leary, 1976: Comparison of convective mass and heat transports in tropical easterly waves computed by two methods. J. Atmos. Sci., 33, 424-429.

_____, C.-P. Cheng, C. A. Leary and J. F. Gamache, 1980: Diagnosis of cloud mass and heat fluxes from radar and synoptic data. J. Atmos. Sci., 37, 754-773.

Houze, R. A., Jr. et al., 1981: Comparison of airborne and land-based radar measurements of precipitation during Winter MONEX. J. Appl. Meteor., 20, 772-783.

Hoxit, L. R. et al., 1976: Formation of mesolows or pressure troughs in advance of cumulonimbus clouds. Mon. Wea. Rev., 104, 1419-1428.

Hudlow, M. D., 1979: Mean rainfall patterns for the three phases of GATE. J. Appl. Meteor., 18, 1656-1669.

_____, V. Patterson, P. Pytlowany, F. Richards and S. Geotis, 1980: Calibration and intercomparison of the GATE C-band weather radars. NOAA Tech. Rept. EDIS 31, Center for Environmental Assessment Services, NOAA, 98 pp.

Iwanchuk, R. M., 1973: Characteristics and distribution of precipitation areas over the tropical Atlantic. S.M. thesis, Dept. of Meteorology, MIT, Cambridge, Mass. 106 pp.

Johnson, R. H., 1976: The role of synoptic-scale precipitation downdrafts in cumulus and synoptic-scale interactions. J. Atmos. Sci., 33, 1890-1910.

_____, 1978: Cumulus transports in tropical wave composite for Phase III of GATE. J. Atmos. Sci., 35, 484-494.

_____, 1980: Diagnosis of convective and mesoscale motions during Phase III of GATE. J. Atmos. Sci., 37, 733-753.

Kahn, P. H. and J. A. Businger, 1979: The effect of radiative flux divergence on entrainment of a saturated convective boundary layer. Quart. J. Roy. Meteor. Soc., 105, 303-306.

Kelley, J., 1974: Summary of aircraft missions in the GATE. NCAR GATE Report, published by the National Center for Atmospheric Research, Boulder, CO.

Kornfeld, J., A. F. Hasler, K. J. Hanson and V. E. Suomi, 1967: Photographic cloud climatology from ESSA III and V computer produced mosaics. Bull. Amer. Meteor. Soc., 48, 878-894.

Kreitzberg, C. W. and D. J. Perkey, 1977: Release of potential instability: Part II. The mechanism of convective / mesoscale interaction. J. Atmos. Sci., 34, 1569-1595.

Krishnamurti, T. N., H. L. Pan, C. B. Chang, J. Ploshay, D. Walker and A. W. Oodally, 1979: Numerical weather prediction for GATE. Quart. J. Roy. Meteor. Soc., 105, 979-1010.

_____, Y. Ramanathan, H. L. Pan, R. J. Pasch and J. Molinari, 1980: Cumulus parameterization and rainfall rates, I. Mon. Wea. Rev., 108, 465-477.

Kuo, H. L., 1965: On formation and intensification of tropical cyclones through latent heat release by cumulus convection. J. Atmos. Sci., 22, 40-63.

_____, 1974: Further studies on the parameterization of the influence of cumulus convection on large-scale flow. J. Atmos. Sci., 31, 1232-1240.

Kuusk, A., Yu.-A. Mullamaa, H. Niilisk, T. Nilson, M. Sulev, 1978: The structure of cloud cover in the trade-wind region on the basis of ship measurements. Proc. Int. Scientific Conf. on the Energetics of the Tropical Atmosphere, Tashkent, published by ICSU/WMO, Geneva, 155-160.

Leary, C. A., 1979: Behavior of the wind field in the vicinity of a cloud cluster in the Intertropical Convergence Zone. J. Atmos. Sci., 36, 631-639.

_____, 1980: Temperature and humidity profiles in mesoscale unsaturated downdrafts. J. Atmos. Sci., 37, 784-796.

_____ and R. A. Houze, Jr., 1976: Analysis of GATE radar data for a tropical cloud cluster in an easterly wave. Prep. 17th Conf. on Radar Meteor., Seattle, published by Amer. Meteor. Soc., Boston, 376-383.

_____ and _____, 1979a: The structure and evolution of convection in a tropical cloud cluster. J. Atmos. Sci., 36, 437-457.

_____ and _____, 1979b: Melting and evaporation of hydrometeors in precipitation from the anvil clouds of deep tropical convection. J. Atmos. Sci., 36, 669-679.

_____ and _____, 1980: The contribution of mesoscale motions to the mass and heat fluxes of an intense tropical convective system. J. Atmos. Sci., 37, 784-796.

Lebedeva, N. V. and N. A. Zavelskaya, 1980: Convection conditions over the tropical ocean on the basis of GATE data. Contributed paper. International Conference on the Scientific Results of GATE, Kiev, U.S.S.R., 17-23 September 1980.

LeMone, M.A., 1973: The structure and dynamics of horizontal roll vortices in the planetary boundary layer. J. Atmos. Sci., 30, 1077-1091.

_____, 1980: The marine boundary layer. Meteor. Monogr., (in press).

_____ and W. T. Pennell, 1976: The relationship of trade wind cumulus distribution to subcloud layer fluxes and structure. Mon. Wea. Rev., 104, 525-539.

_____ and E. J. Zipser, 1980: Cumulonimbus vertical velocity events in GATE, Part I: Diameter, intensity, and mass flux. J. Atmos. Sci. (in press).

Lilly, D. K., 1968: Models of cloud topped mixed layers under a strong inversion. Quart. J. Roy. Meteor. Soc., 94, 292-309.

_____, 1979: The dynamical structure and evolution of thunderstorms and squall lines. Ann. Rev. Earth Planet. Sci., 7, 117-161.

_____ and W. Schubert, 1980: The effects of radiative cooling on a cloud-topped mixed layer. J. Atmos. Sci., 37, 482-487.

López, R. E., 1973: Cumulus convection and larger scale circulations, II. Cumulus and mesoscale interactions. Mon. Wea. Rev., 101, 856-870.

_____, 1976: Radar characteristics of the cloud populations of tropical disturbances in the northwest Atlantic. Mon. Wea. Rev., 104, 268-283.

_____, 1977: The lognormal distribution and cumulus cloud population. Mon. Wea. Rev., 105, 865-872.

_____, 1978: Internal structure and development processes of C-scale aggregates of cumulus clouds. Mon. Wea. Rev., 106, 1488-1494.

Lord, S. J., 1978: Development and observational verification of a cumulus cloud parameterization. Ph.D. dissertation, Dept. of Atmospheric Sciences, University of California at Los Angeles, 359 pp.

Lyne, W. H., P. R. Rowntree et al., 1976: Numerical modeling using GATE data. Meteor. Magazine, 105, 261-271.

Mandics, P. A. and F. F. Hall, 1976: Preliminary results from the GATE acoustic echo sounder. Bull. Amer. Meteor. Soc., 57, 1142-1147.

Mansfield, D. A., 1977: Squall-lines observed during GATE. Quart. J. Roy. Meteor. Soc., 103, 569-574.

Martin, D. W., 1975: Characteristics of west African and Atlantic cloud clusters. GATE Report No. 14, ICSU/WMO, Geneva, 182-192.

_____ and O. Karst, 1969: A census of cloud systems over the tropical Pacific. Studies in Atmospheric Energetics based on Aerospace Probings. Ann. Rept., 1968, Space Science and Engineering Center, Univ. of Wisconsin.

_____ and V. E. Suomi, 1972: A satellite study of cloud clusters over the tropical North Atlantic Ocean. Bull. Amer. Meteor. Soc., 53, 135-156.

McBride, J. L. and W. M. Gray, 1978: Mass divergence in tropical weather systems, Paper I, Diurnal variation. Paper No. 289, Dept. of Atmospheric Science, Colorado State University, Fort Collins, Colo., 1-44.

McGarry, M. M. and R. J. Reed, 1978: Diurnal variations in convective activity and precipitation during Phases II and III of GATE. Mon. Wea. Rev., 106, 101-113.

Miyakoda, K. and J. Sirutis, 1977: Comparative integrations of global models with various parameterized processes of subgrid scale vertical transport: Description of the parameterization and preliminary results. Beitr. Phys. Atmos., 50, 445-487.

_____, J. Shelda and J. Sirutis, 1980: Four dimensional analysis experiment with the GATE data: Part II. (Submitted to J. Atmos. Sci.).

Moncrieff, M. W. and M. J. Miller, 1976: The dynamics and simulation of tropical squall lines. Quart. J. Roy. Meteor. Soc., 102, 373-394.

Mower, R. N., G. L. Austin, A. K. Betts, C. Gautier, R. Grossman, J. Kelley, F. Marks and D. W. Martin, 1979: A case study of GATE convective activity. Atmos. Ocean, 17, 46-59

Murakami, M., 1979: Large-scale aspects of deep-convective activity over GATE area. Mon. Wea. Rev., 107 (8), 994-10113.

Nitta, T., 1975: Observational determination of cloud mass flux distribution. J. Atmos. Sci., 32, 73-91.

_____, 1977: Response of cumulus updraft and downdraft to GATE A/B-scale motion systems. J. Atmos. Sci., 34, 1163-1186.

_____, 1978: A Diagnostic Study of Interaction of Cumulus Updrafts and Downdrafts with Large-scale Motions in GATE. J. Meteor. Soc., Japan, 56, pp. 232-241.

Nicholls, J. M., 1979: Aircraft measurements in the GARP Atlantic Tropical Experiment. Meteor. Mag., 108, 349-366.

Nicholls, S. and M. A. Le Mone, 1980: The fair weather boundary layer in GATE: the relationship of subcloud fluxes and structure to distribution and enhancement of cumulus clouds. J. Atmos. Sci., 37, pp. 2051-2067.

Obasi, G. O. P., 1974: Some statistics concerning the disturbance lines of West Africa. Prep., Symp. Tropical Meteorology, Part II. Nairobi, published by American Meteor. Soc., Boston, 62-66.

Ogura, Y. and Y. L. Chen, 1977: A life history of an intense mesoscale convective storm in Oklahoma. J. Atmos. Sci., 33, 1458-1476.

Ogura, Y. and H.-R. Cho, 1973: Diagnostic determination of cumulus cloud populations from observed large-scale variables. J. Atmos. Sci., 30, 1276-1286.

Ogura, Y. and M.-T. Liou, 1980: The structure of a mid-latitude squall line: A case study. J. Atmos. Sci., 37, 553-567.

_____, _____, J. Russell and S. T. Soong, 1979: On the formation of organized convective systems observed over the eastern Atlantic. Mon. Wea. Rev., 107, 426-441.

Ooyama, K., 1971: A theory of parameterization of cumulus convection. J. Meteor. Soc., Japan, 49, 744-756.

_____, 1980: Objective analysis of winds over the GATE ship array. (To be submitted to Mon. Wea. Rev.)

Payne, S. W. and M. M. McGarry, 1977: The relationship of satellite inferred convective activity to easterly waves over west Africa and the adjacent ocean during Phase III of GATE. Mon. Wea. Rev., 105, 413-420.

Peskov, B. E., 1980: Clouds and Convection. USSR National Report for the ICSU/WMO Monograph on GATE Scientific Results.

Petrossiants, M. A. and A. I. Falkovich, 1977: Diurnal variation of the meteorological elements in the region of the Atlantic tropical experiment. Soviet Meteor. and Hydr., 7, 67-72 (in English).

_____ et al., 1976: Tropex-74. Hydrometeorology, Leningrad, 736 pp.

_____, A. I. Snitkovsky and A. I. Falkovich, 1977: The air circulation in the intertropical convergence zone. Soviet Meteor. and Hydr., 5, 87-94 (Russian) 70-75 (English).

Ramage, C. S., 1971: Monsoon Meteorology. Academic Press, 294 pp.

Randall, D. A., 1980a: Conditional instability of the first kind upside down. J. Atmos. Sci., 37, 125-130.

_____, 1980b: Entrainment into a stratocumulus layer with distributed radiative cooling. J. Atmos. Sci., 37, 148-159.

Raymond, D. J., 1975: A model for predicting the involvement of continuously propagating convective storms. J. Atmos. Sci., 32, 1308-1317.

_____, 1976: Wave-CISK and convective mesosystems. J. Atmos. Sci., 33, 2392-2398.

Reed, R. J., 1975: An example of a squall line in the B-scale network. GATE Rep. No. 14, Vol. 1, ICSU/WMO, Geneva, 217-222.

_____ and E. E. Recker, 1971: Structure and properties of synoptic-scale wave disturbances in the equatorial western Pacific. J. Atmos. Sci., 28, 1117-1133.

Reed, R. J., D. C, Norquist and E. E. Recker, 1977: The structure and properties of African wave disturbances as observed during Phase III of GATE. Mon. Wea. Rev., 105, 317-333.

Reeves, R. W., C. F. Ropelewski and M. D. Hudlow, 1979: On the relationship of the precipitation to variations in the kinematic variables during GATE. Mon. Wea. Rev., 107, 1154-1168.

Riehl, H., 1969: Sound aspects of cumulonimbus convection in relation to tropical weather systems. Bull. Amer. Meteor. Soc., 50, 587-595.

_____ and J. S. Malkus, 1958: On the heat balance in the equatorial trough zone. Geophysica, 6, 503-538.

Rodenhuis, D. R. and A. K. Betts, 1974: The convection subprogramme for GATE. GATE Rep. No. 7, ICSU/WMO, Geneva, 83 pp.

Rosenthal, S. L., 1978: Numerical simulation of tropical cyclone development with latent heat release by the resolvable scales. I: Model description and preliminary results. J. Atmos. Sci., 35, 258-271.

_____, 1980: Numerical simulation of tropical cyclone development with latent heat release by the resolvable scales. II: Propagating small-scale features observed in the pre-hurricane phase. (Submitted to Mon. Wea. Rev.)

_____, 1979: The sensitivity of simulated hurricane development to cumulus parameterization details. Mon. Wea. Rev., 107, 193-197.

Sanders, F. and R. J. Paine, 1975: The structure and thermodynamics of an intense mesoscale convective storm in Oklahoma. J. Atmos. Sci., 32, 1563-1579.

_____ and K. A. Emanuel, 1977: The momentum budget and temporal evolution of a mesoscale budget and temporal evolution of a mesoscale convective system. J. Atmos. Sci., 34, 322-330.

Schubert, W. H., 1976: Experiments with Lilly's cloud-topped mixed layer model. J. Atmos. Sci., 33, 436-446.

_____, J. S. Wakefield, E. J. Steiner and S. K. Cox, 1979a: Marine stratocumulus convection, Part I: Governing equations and horizontally homogeneous solutions. J. Atmos. Sci., 36, 1286-1307.

_____, _____, _____ and _____, 1979b: Marine stratocumulus convection, Part II: Horizontally inhomogeneous solutions. J. Atmos. Sci., 36, 1308-1324.

Semyonov, Ye. K., 1975: Some features of the intertropical convergence zone (ITCZ) from meteorological satellite observations. Soviet Meteor. Hydr., No. 2., 22-29.

Shapiro, L. J., 1978: The vorticity budget of a composite African tropical wave disturbance. Mon. Wea. Rev., 106, 806-817.

_____ and D. E. Stevens, 1980: Parameterization by convective effects on the momentum and vorticity budgets of synoptic-scale Atlantic tropical waves. (Submitted to Mon. Wea. Rev.)

Shupiatsky, A. B., A. I. Korotov, V. D. Menshenin, R. S. Pastushkov, M. Jovashevic, 1975: GATE Rep. No. 14, V. II, ICSU/WMO, Geneva, 177-187.

Shupiatsky, A. B., A. I. Korotov and R. S. Pastushkov, 1976: Radar investigations of the evolution of clouds in the East Atlantic. Hydrometeorology, Leningrad, 508-514 (in Russian).

_____, G. N. Evseonok and A. I. Korotov, 1976: Complex investigations of clouds in the ITCZ with the help of satellite and ship radar equipment. Hydrometeorology, Leningrad, 515-520 (in Russian).

Sikdar, D. N. and S. J. Hentz, 1980: Kinematic structure of an Atlantic cloud cluster during GATE and its time variation. Tellus, 32, 439-455.

Silva Dias, M. F., 1979: Linear spectral model of tropical mesoscale systems. Atmos. Sci. Paper No. 311, Dept. Atmos. Sci., Colorado State University, Fort Collins, 213 pp.

Simpson, J. H., 1976: Boundary front in the summer regime of the Celtic Sea. Estuarine and Coastal Marine Science. N.Y., 4(1), 71-81.

_____ and G. van Helvoirt, 1980: GATE cloud-subcloud layer interactions examined, using a three-dimensional cumulus model. Contributions to Atmospheric Physics, Wiesbaden, W. Germany, 106-133.

Slingo, J. M., 1980: A cloud parameterization scheme derived from GATE data for use with a numerical model. Quart J. Roy. Meteor. Soc., 106(450), 747-770.

Sommeria, G., 1976: Three-dimensional simulation of turbulent process in an undisturbed tradewind boundary layer. J. Atmos. Sci., 33, 216-241.

_____ and M. A. LeMone, 1978: Direct testing of the three-dimensional model of the planetary boundary layer against experimental data. J. Atmos. Sci., 35, 25-39.

Soong, S.-T. and W.-K. Jao, 1980: Response of deep tropical cumulus clouds to mesoscale processes. J. Atmos. Sci., 37, 2016-2034.

_____ and Y. Ogura, 1980: Response of tradewind cumuli to large-scale processes. J. Atmos. Sci., 37, 2035-2050.

Stevens, D. E., 1979: Vorticity, momentum and divergence budgets of synoptic-scale wave disturbances in the tropical eastern Atlantic. Mon. Wea. Rev., 107, 535-550.

Suchman, D. and D. W. Martin, 1976: Wind sets from SMS images: As assessment of quality for GATE. J. Appl. Meteor., 15, 1265-1278.

_____, _____ and J. Simpson, 1977: The evolving circulation of an east Atlantic cloud cluster. Postprints 11th Tech. Conf. Hurricanes and Tropical Meteorology, Miami Beach, published by Amer. Meteor. Soc., Boston, 333-338.

Thompson, R. M., Jr., S. W. Payne, E. E. Recker and R. J. Reed, 1979: Structure and properties of synoptic-scale wave disturbances in the intertropical convergence zone of the eastern Atlantic. J. Atmos. Sci., 36, 53-72.

Tschirhart, G., 1958: Les conditions aérologiques à l'avant des lignes de graines en Afrique Equatoriale. Metéor. Nationale, Mono. No. 11, 28 pp.

Wallace, J. M., 1975: Diurnal variations in precipitation and thunderstorm frequency over the conterminous United States. Mon. Wea. Rev., 103, 406-419.

Warner, C., 1980: Cloud measurements on day 245 of GATE. Atmos. Ocean., 18, (in press).

_____ and G. L. Austin, 1978: Statistics of radar echoes on day 261 of GATE. Mon. Wea. Rev., 106, 983-994.

_____, J. Simpson, D. W. Martin, D. Suchman, F. R. Mosler and R. F. Reinking, 1979: Shallow convection on day 261 of GATE: Mesoscale arcs. Mon. Wea. Rev., 107, 1617-1635.

_____, _____, G. van Helvoirt, D. W. Martin, D. Suchman and G. L. Austin, 1980: Deep convection on day 261 of GATE. Mon. Wea. Rev., 108, 169-194.

Woodley, W., C. G. Griffith, J. S. Griffin, S. C. Stromatt, 1980: The inference of GATE convective rainfall from SMS-1 imagery. J. Appl. Meteor. 19, 388-408.

Yanai, M., S. Esbensen and J. H. Chu, 1973: Determination of bulk properties of tropical cloud clusters from large-scale heat and moisture budgets. J. Atmos. Sci., 30, 611-627.

_____, J. H. Chu, T. E. Stook and T. Nitta, 1976: Response of deep and shallow tropical maritime cumuli to large-scale processes. J. Atmos. Sci., 33, 976-991.

Zavelskaja, N. A., 1978: On the estimation of the convective cloud formation and the energy exchange with the entrainment and phase transforms. Proc. 1st. Scientific Conf. on the Energetics of Tropical Atmosphere, Tashkent, published by ICSU/WMO, Geneva, pp. 59-64.

Zipser, E. J., 1969: The role of organized unsaturated convective downdrafts in the structure and rapid decay of an equatorial disturbance. J. Appl. Meteor., 8, 799-814.

_____, 1977: Mesoscale and convective-scale downdrafts as distinct components of squall-line circulation. Mon. Wea. Rev., 105, 1568-1589.

_____, 1980: Kinematic and thermodynamic structure of mesoscale systems in GATE. Proc. of the Seminar on the Impact of GATE on Large-Scale Numerical Modelling of the Atmosphere and Ocean, Woods Hole, Mass., Aug. 26-29, 1979, published by National Academy of Sciences, Washington, D.C., 91-99.

_____ and C. Gautier, 1978: Mesoscale events within a GATE tropical depression. Mon. Wea. Rev., 106, 789-805.

_____ and M. A. LeMone, 1980: Cumulonimbus vertical velocity events in GATE, Part II: Synthesis and model core structure. J. Atmos. Sci., Vol. 37, No. 11, pp. 2458-2469.

CHAPTER 10

BOUNDARY LAYER PHENOMENA

THE SURFACE LAYER (AIR-SEA INTERACTION AND ITS PARAMETERIZATION)

by

Yu. A. Volkov*

THE STRUCTURE OF THE ATMOSPHERIC BOUNDARY LAYER UNDER DIFFERENT CONVECTIVE CONDITIONS

by

Ernst Augstein** and Hans Hinzpeter**

10.1 INTRODUCTION

The atmospheric phenomena of the tropical Hadley cell regime have been extensively investigated during the last two decades in the framework of several field experiments. Particular interest has been directed towards the air-sea exchange processes and the thermodynamics and dynamics of the maritime atmospheric boundary layer (ABL). Observations and model calculations consistently indicate that besides the large-scale flow characteristics, the lower boundary conditions and the radiative fluxes, the presence of clouds and the state of cloud convection plays an important role in controlling the boundary layer development and the energy transfer across the sea surface.

Surface fluxes are predominantly determined by the simplified bulk aerodynamic method from observed or model derived mean quantities in the surface layer and at the sea surface. Therefore, several attempts have been made during all GATE periods to study the applicability of the above-mentioned method and to estimate the empirical transfer coefficients with the aid of different experimental techniques. Unfortunately, the various measurements did not lead to a uniform result so that the validity of the bulk formulae for all large-scale conditions still remains unclear.

The complexity of the mean vertical structure of the ABL and consequently, of the mathematical concepts for its modelling increase from no cloud conditions via low-level stratiform and shallow non-precipitating cumulus convection to deep precipitating cumulo-nimbus clouds.

Low-level stratus and shallow cumulus clouds are generally observed in the upper part of the ABL when the near surface horizontal large-scale flow diverges and the air is heated and moistened from below. In this case, the transition from the perturbed boundary layer to the free atmosphere is clearly marked by a statical, strongly stable region in which the temperature increases and the water vapour decreases with height. In the past, most research activities have been concentrated on the investigation of this kind of ABL and of the inversion capped mixed layer. Observational facts and model treatments are well-documented in the literature, so that a brief compilation of the results may suffice in this connection.

We will focus our attention on situations with a horizontal convergent air flow in the lower troposphere, in which deep precipitating clouds gain predominant importance. The principal task of the GARP Atlantic Tropical Experiment (GATE) was based on

---

(* Institute of Atmospheric Physics, USSR Academy of Sciences, USSR
** Max-Planck-Institut für Meteorologie, Federal Republic of Germany)

the investigation of the inter-relationship between enhanced convection and other scales of motion in the atmospheric circulation. In particular, the boundary layer work was concerned with the effect of different stages of cloud activity on: (a) the vertical thermodynamic and kinematic structure of the lower troposphere; (b) the exchange processes across the air-sea interface; and (c) the vertical heat, water mass and momentum transport by various scales of motion in the lowest 2000 meters of the atmosphere. In order to satisfactorily cover a broad spectrum of motions in time and space, different technical means have been applied during the GATE field phases. Most of the results published so far are, by and large, based on single instrument systems, so that a synthesis of the findings of various authors might be useful.

We shall aim to make reference to most of the GATE experimental and modelling investigations we are aware of, but increased attention will be paid to studies concerned with the inter-relationship of boundary layer features and cloud convection.

10.2 THE SURFACE LAYER (AIR-SEA INTERACTION AND ITS PARAMETERIZATION)

10.2.1 Experimental methods

The turbulent fluxes of momentum, moisture and heat near the sea surface can be determined by different methods. For the investigations during GATE the following techniques have been applied: the eddy correlation and dissipation methods both of which are based on fluctuation measurements, the gradient approach which depends on vertical profile observations of wind velocity, specific humidity and air temperature, and the aerodynamic bulk method which requires standard meteorological measurements at the sea surface and at a certain reference height in the atmosphere. We can express the vertical turbulent fluxes of momentum (τ), sensible heat (H) and latent heat (E) in the form:

$$\tau = -\bar{\varrho}\,\overline{u'w'} = \bar{\varrho}\,K_D\frac{\partial \bar{u}}{\partial z} = \bar{\varrho}\,c_D\,\bar{u}_{10}^2 \qquad 10.1$$

$$H = c_p\,\bar{\varrho}\,\overline{\theta'w'} = -c_p\,\bar{\varrho}\,K_H\frac{\partial \bar{\theta}}{\partial z} = c_p\,\bar{\varrho}\,c_H\,(\bar{\theta}_0 - \bar{\theta}_{10})\,\bar{u}_{10} \qquad 10.2$$

$$E = L\bar{\varrho}\,\overline{q'w'} = -L\bar{\varrho}\,K_E\frac{\partial \bar{q}}{\partial z} = L\,\bar{\varrho}\,c_E\,(\bar{q}_0 - \bar{q}_{10})\,\bar{u}_{10} \qquad 10.3$$

(I) (II) (III)

In these equations u', w', θ', q' represent the fluctuations of the horizontal and vertical components of the wind velocity, of potential temperature and of specific humidity, respectively. ϱ denotes the air density, the specific heat at constant pressure and the latent heat of evaporation are indicated by c_p and L, respectively. K_D, K_H, K_E form the turbulent diffusion coefficients and c_D, c_H, c_E are the respective transfer coefficients of the turbulent momentum, sensible and latent heat fluxes. The subscripts 0 and 10 correspond to the values at the sea surface (q_0 = saturation value of specific humidity at the sea-surface temperature) and at a height of 10m. Terms (I) denote eddy correlation fluxes, expressions (II) refer to gradient values and notations (III) indicate the highly simplified bulk aerodynamic formulae.

During the entire GATE period vertical profiles of wind velocity, dry bulb and wet bulb temperature have been measured at an 8m high mast of a special buoy which was tethered to the R/V METEOR. The mast was equipped with cup anemometers and psychrometers. The signals of these sensors were recorded on board the ship. Vertical profiles of wind velocity, air temperature and specific humidity could be derived from

10 min. time averages of these data nearly continuously. Interruptions occurred during heavy rain and in cases when the wind speed exceeded 15 m/s. From the above-mentioned gradients, vertical turbulent fluxes in the surface layer have been calculated by Hasse et al. (1978).

The major contribution to the turbulent flux determination during GATE results from the aerodynamic bulk method using mean values of the wind speed, the temperature and the moisture measured at the ship boom or mast together with the sea-surface temperature. Although the simple version (III) of equations (10.1) to (10.3) is rather convenient for the estimation of the turbulent fluxes, one must bear in mind that the dimensionless exchange coefficients may depend in a still not fully known way on various properties of the surface layer. Variations of the spectrum of surface waves may for example lead to substantial modifications in the aerodynamic roughness of the sea surface, and, consequently, also in the drag coefficient c_D. The changes of the skin temperature of the ocean surface as observed by Gorodetsky et al. (1974) and Grassl and Hinzpeter (1975) may increase the uncertainty of the respective transfer coefficients for heat and water vapour c_H and c_E. Therefore, the scatter of these coefficients derived from measurements is quite large and the GATE observations are also not able to improve the situation considerably. Nevertheless, some attempts have been made to relate the vertical differences of the mean quantities to fluxes derived by the profile and eddy correlation method (Hasse et al., 1978; Volkov et al., 1976; Müller-Glewe and Hinzpeter, 1975 and Khalsa and Businger, 1977).

Fluctuation measurements in the surface layer have been conducted during the GATE period from the R/V PLANET, the R/V PROFESSOR ZUBOV, the R/V ACADEMIC KURCHATOV, the R/V DALLAS and the R/V FAY by boom-mounted instruments. The eddy correlation technique has been applied to the measurements of the PLANET, the PROFESSOR ZUBOV and the ACADEMIC KURCHATOV while the dissipation technique, which is based on considerations of the turbulence kinetic energy balance, has been used for evaluation of the DALLAS and FAY observations.

The influences of ship motion and obstacle effects have been corrected for by various methods. In spite of these procedures some uncertainty remains in the interpretation of such observations as we shall see subsequently.

10.2.2 The structure of the atmospheric surface layer

Characteristics of the atmospheric surface layer are primarily determined by several basic meteorological parameters such as the mean wind velocity, the mean air- and sea-surface temperatures and the mean water vapour content. All of these quantities experience modifications caused by large-scale or mesoscale processes in the tropical atmosphere.

For the undisturbed trade-wind zone the observed mean values of vertical differences $\theta_{w-a} = \theta_o - \theta_{10}$ and $q_{w-a} = \overline{q}_o - \overline{q}_{10}$ range around 0.5 K and 4 g kg^{-1}, respectively for average wind velocities of 6 to 8 $m \cdot s^{-1}$. The variability of the above values was rather small during the GATE observational period. This conclusion was violated only during the passage of a few atmospheric wave disturbances which are also reflected in the water temperature and salinity of the ocean as well as in the meandering of equatorial counter current near the Equator. Under such conditions Volkov et al. (1976) report temperature differences θ_{w-a} of 2-3 K and specific humidity differences q_{w-a} of 6-9 g/kg^{-1}. In the Inter Tropical Convergence Zone (ITCZ), however, much larger changes of the mean field parameters have been observed e.g. by Hasse et al. (1978). These authors report variations of the wind velocity, the precipitation rate and the air temperature of about 10 m s^{-1}, 20 mm $hour^{-1}$ and 3 K, respectively, as typical during the passage of convective or mesoscale disturbances. As a consequence of these modifications the sea-air temperature difference θ_{w-a} also varied between 1 and 4 K in the ITCZ while the specific humidity difference q_{w-a} fluctuated similarly as in the undisturbed trades.

The effect of an approaching precipitating gust front on the vertical temperature profiles is delineated in Figure 10.1. Hasse et al. (1978) have not only observed a tremendous drop in the air-temperature but also demonstrate that it takes nearly 10 minutes after the onset of rainfall until the temperature profile has readjusted to its state of equilibrium. These authors have estimated from heat balance considerations that the typical time scale t* for the readjustment of the vertical temperature profile up to a height z* may be expressed by $t^* = 69\ z^*\ \bar{u}_{10}^{-1}$.

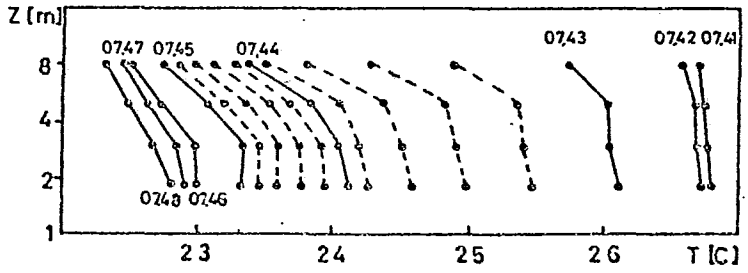

Figure 10.1 - Vertical temperature profiles measured on the "METEOR" buoy. Numbers indicate GMT time (hours and minutes) after Hasse et al. (1978).

Episodic measurements in different heights on-board the R/V ACADEMIC KURCHATOV at the Equator in the SE trades by Volkov et al. (1976) revealed a nearly adiabatic vertical temperature gradient in the layer between 4 and 10m above the water surface. Similarly, the mean vertical gradients of specific humidity turned out to be small with an average value of 0.03 $g(kg\ m)^{-1}$. In contrast to these findings, the turbulent fluxes of heat and moisture determined by the eddy correlation method resulted in substantial upward-directed fluxes of sensible and latent heat. Although there may be systematic errors in both the profiles and in the fluctuation measurements, one cannot exclude the possibility that heat and moisture fluxes by all turbulence scales are not always proportional to the local gradients of the mean quantities. Particularly under unstable static surface conditions ($\theta_{w-a} > 0$), convective elements may not greatly influence the low-level stratification but may considerably contribute to the vertical heat and water vapour fluxes. This conjecture is backed up by a typical example of fluctuations of T' and q' in Figure 10.2 observed by Volkov et al. (1974). It becomes obvious from these records that some warm and moist signals with time scales of 8 to 15 seconds are superimposed on the random turbulent fluctuations of other scales. Measurements of the water surface film made with the aid of radiometers by Grassl and Hinzpeter (1975) and Gorodetsky et al. (1975) showed temperature variations of 0.2 to 0.3 K with horizontal spatial scales between some 10 and several hundred meters. Such phenomena may for example be responsible for the generation of the above-quoted convective elements.

Furthermore the data of acoustic soundings by Mandics et al. (1975) also confirm the presence of a convective plume structure in the lowest levels of the atmospheric boundary layer with a typical horizontal scale of about 100 to 200m.

10.2.3 Spectral characteristics

The spectral characteristics of the meteorological quantities in the surface layer which have been derived from various series of measurements by the R/V PROFESSOR ZUBOV by Galushko et al. (1975) are categorized on the basis of the stratification parameter $\zeta = z/L$ (z = height and L = Monin-Obukhov length). The spectrum $S_{\alpha\beta}$ of the quantities α and β is delineated in the dimensionless form

$$S_{\alpha\beta}(\omega) = f\, S_{\alpha\beta}(f) / \overline{\alpha\beta} \qquad \ldots (10.4)$$

as a function of the dimensionless frequency $\omega = f\, z/\bar{u}_o$. Here $\bar{u}_o$ denotes the apparent wind velocity during the measurements.

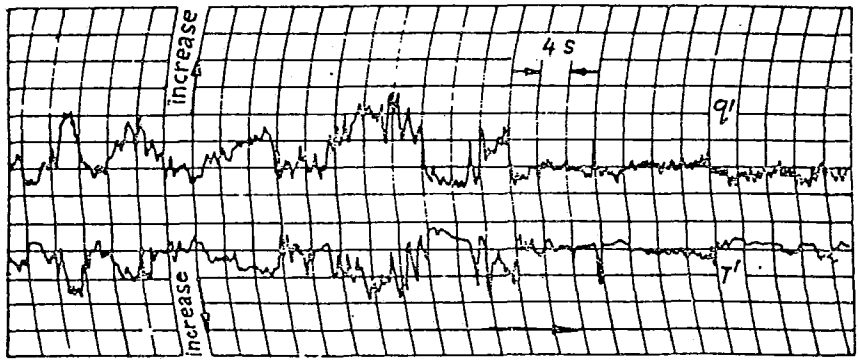

Figure 10.2 - Time series of temperature (T') and specific humidity (q') fluctuations observed on the R/V ACADEMIC KURCHATOV by Volkov et al. (1974).

The variance spectra of the horizontal (u) and vertical (w) wind components and of the temperature (T) as well as the co-spectra w'T' and w'u' for conditions of slightly unstable vertical density stratification are reproduced in Figure 10.3. For comparison, approximate curves of BOMEX and of the R/V KURCHATOV have been added. All of these measurements have similar characteristics, namely a high frequency peak for temperature and heat flux and a low frequency maximum for horizontal wind velocity, and momentum flux. The period of the strongest variations of the vertical wind component lies in between the maximal variations of temperature and horizontal wind velocity.

The variance spectra of the water vapour pressure in the SE trades in Figure 10.4 more or less correspond with those of the horizontal wind components. The dissimilarity between the temperature and both the moisture and the horizontal velocity spectra leads also to differences between the co-spectra of w'T', w'e' and w'u' in Figure 10.5 for a nearly neutral density distribution. We find the vertical heat flux to be concentrated in higher frequencies than the moisture and momentum transports.

One might speculate that momentum and water vapour are predominantly transported by larger convective elements in the surface layer, while the heat flux based on temperature fluctuations depends much more on mechanically generated small-scale turbulence. This picture could be considerably altered if the heat transport by water vapour fluctuations is considered as well. Brook (1978) has demonstrated that the latter may contribute as much as the dry effect to the total sensible heat flux particularly in the tropics where the Bowen ratio is generally small. This aspect has not been taken into account in the data which we are discussing here but for a proper understanding of certain processes in the surface layer it should not be omitted.

The fact that temperature and moisture fluctuations are closely correlated for frequencies around $\lg\omega < 0$, in spite of the dissimilarity of the variance spectra of these two quantities in this spectral part, is underlined by the co-spectra of e' and T' in Figure 10.5. The correlation $\sigma_{qT} = S_{qT} / (S_{TT}/S_{qq})^{1/2}$ is about 0.8 for $\lg\omega = 0$ and does not drop below 0.6 for $\lg\omega < 0$.

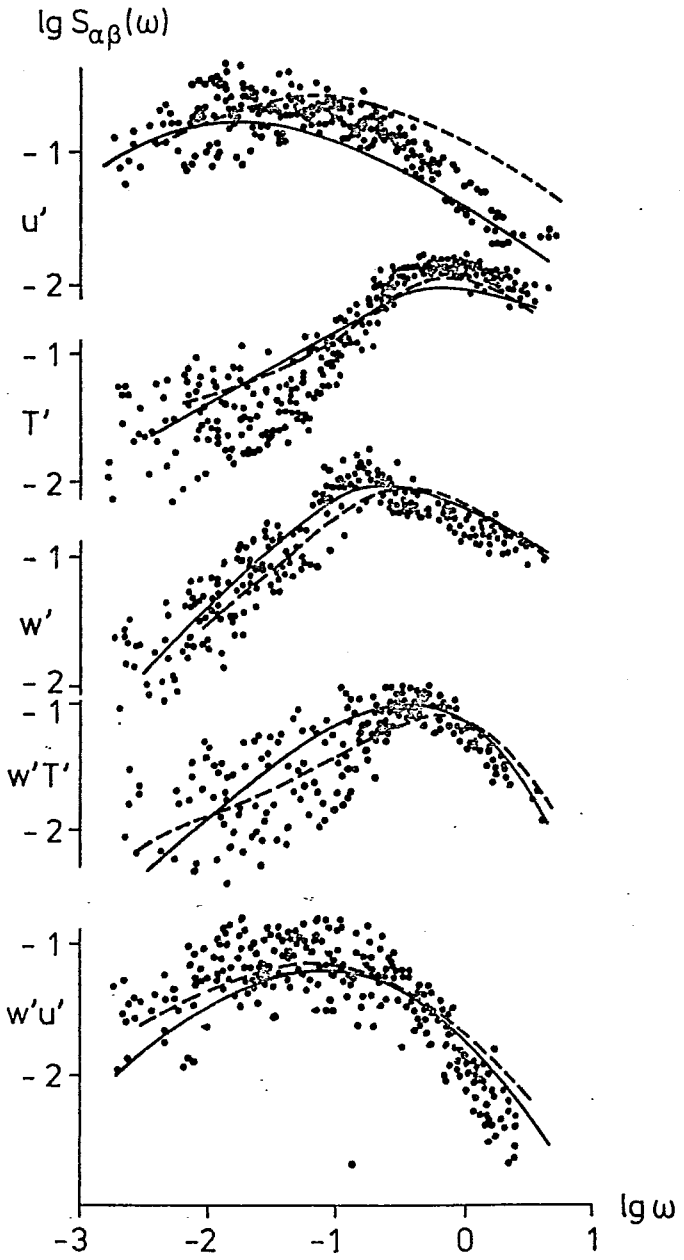

Figure 10.3 - Dimensionless variance spectra of the horizontal (u') and vertical (w') wind component and temperature (T) and co-spectra (w'T') and (w'u') measured on the R/V PROFESSOR ZUBOV: Dots: Results of BOMEX by Phelps and Pond (1971): full lines and of GATE by Elagina et al. (1974): dashed lines.

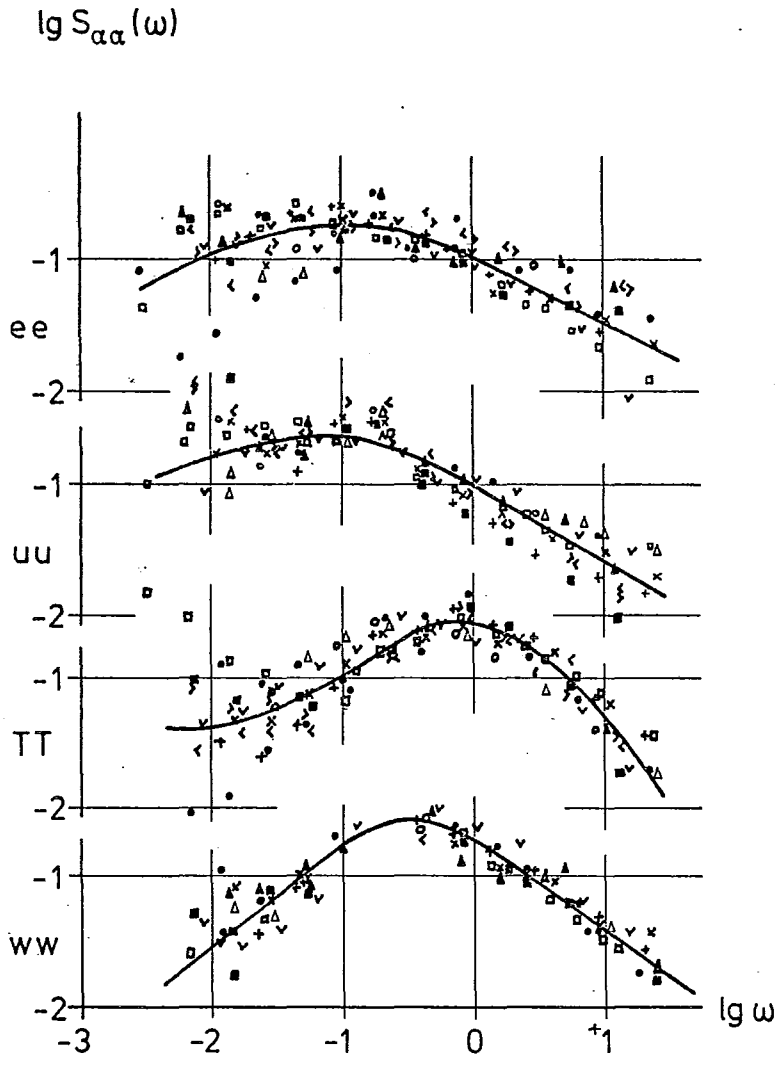

Figure 10.4 - Dimensionless variance spectra of water vapour (ee) horizontal wind speed (uu), temperature (TT) and the vertical wind component (ww) from the R/V ACADEMIC KURCHATOV. Different symbols indicate different runs.

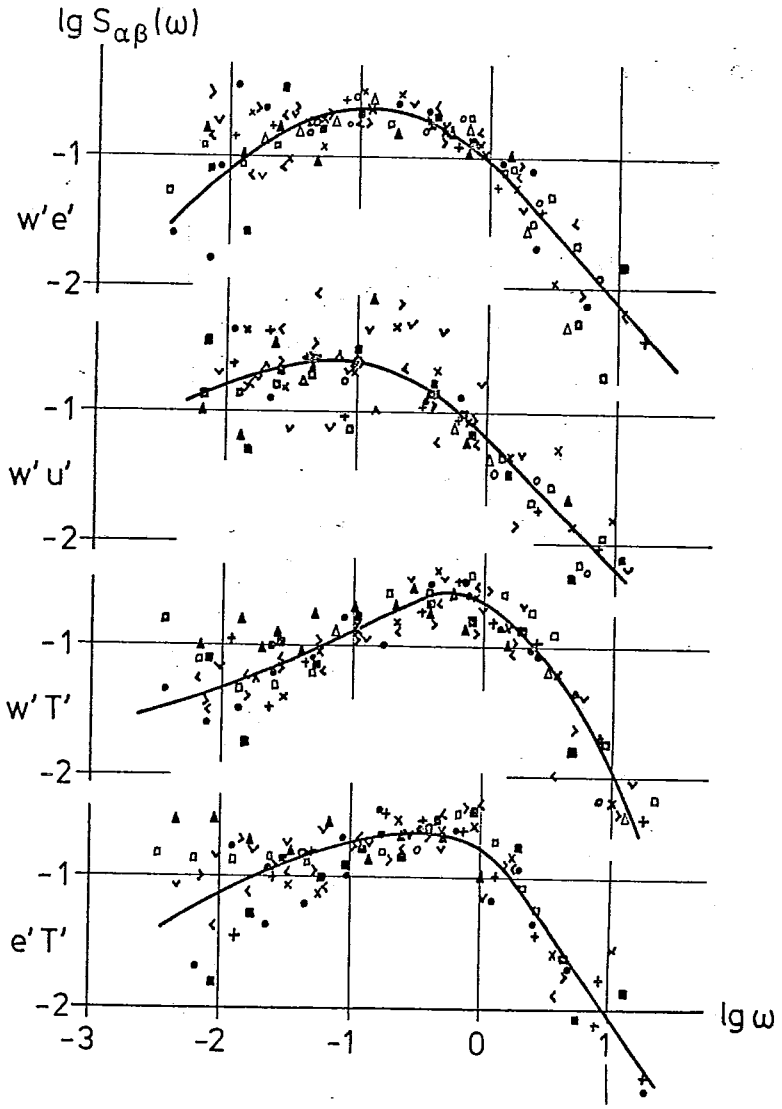

Figure 10.5 - Dimensionless co-spectra w'u', w'T', w'e' and e'T' from the R/V ACADEMIC KURCHATOV. Different symbols indicate different runs.

In cases of a more unstable density distribution, the temperature fluctuations tend to have a second maximum in the spectral region of the moisture peak as can be seen from Figure 10.6. Elagina et al. (1978) found from observations over land that the low frequency maximum of the temperature variance under unstable conditions moved to lower frequencies with an increasing Bowen ratio

$$B = \frac{c_p \bar{\varrho}\, \overline{T'w'}}{L\, \bar{\varrho}\, \overline{q'w'}}.$$

It might be useful to test during future experiments whether the same relationship holds over the ocean in order to better understand the relevant turbulence mechanism.

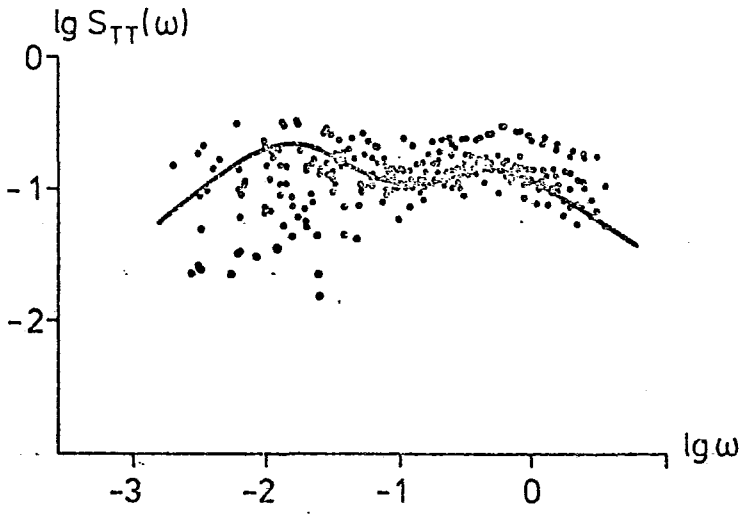

Figure 10.6 - Dimensionless temperature variance spectra under strongly unstable vertical density distribution. Dots: R/V PROFESSOR ZUBOV during GATE. Full line: San Diego after Phelps and Pond (1971).

10.2.4 The turbulent surface fluxes and their parameterization

In models of the general circulation as well as of the atmospheric boundary layer, the turbulent fluxes must normally be expressed with the aid of mean quantities such as those given by expressions (III) in equations (10.1) to (10.3). Therefore, it is an important task to test experimentally (a) if this formulation can be applied for the different atmospheric states in the tropics and (b) which transfer coefficients must be chosen. Principally such tests should be based on intercomparisons of the aerodynamic bulk formulae with eddy correlation measurements. But since the latter are rare over the ocean profile studies are occasionally used for this purpose as well.

A rather complete series of profile measurements has been obtained by Hasse et al. (1978) from a special buoy in the lowest 8m above the sea surface during all three phases of GATE. Their results based on 10-minute averages are portrayed in Figure 10.7. It is interesting to notice that enhanced cloud convection with rainfall leads to a significant increase in the upward sensible heat flux. The downward momentum transport is also higher in disturbed than in undisturbed periods but it is not as closely correlated with rainfall as the heat flux. The cloud processes obviously have only a small effect on the evaporation at the sea surface. For the entire GATE period Hasse et al. (1978) derived an increase on the average of about 15% for the latent heat and of about 400% for the sensible heat flux during disturbed periods compared to undisturbed situations. The Bowen ratio varied between 0.05 (undisturbed) and 0.19 (disturbed).

On the basis of the profile measurements Hasse et al. (1978) find the following mean values for the transfer coefficients $c_D = 1.44 \cdot 10^{-3}$, $c_H = 1.57 \cdot 10^{-3}$ and $c_E = 1.35 \cdot 10^{-3}$. As can be seen from Figure 10.8, the individual values scatter considerably for all three coefficients but no systematic differences appear between the disturbed and undisturbed conditions.

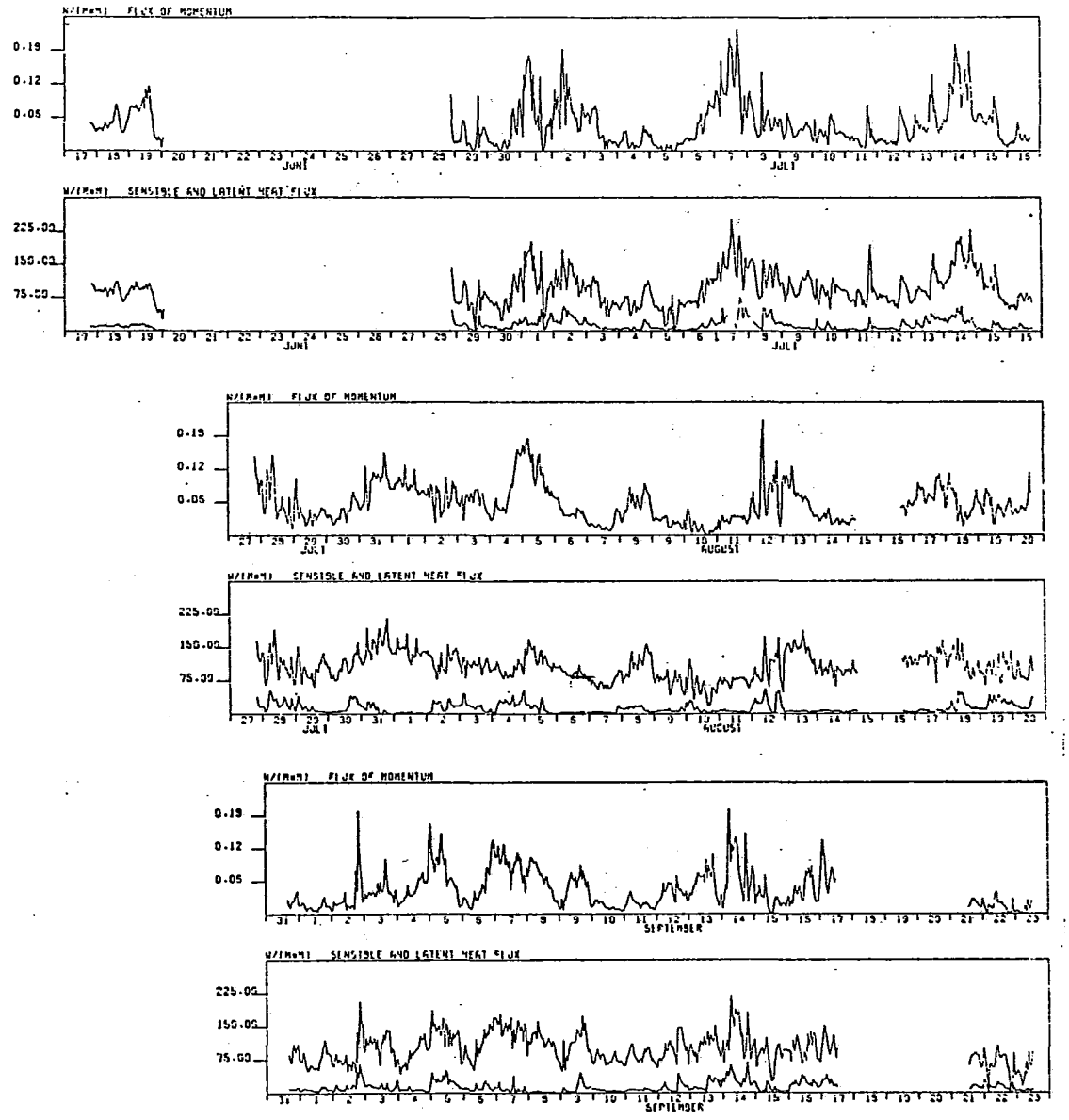

Figure 10.7 - Turbulent surface fluxes of momentum, sensible and latent heat during all three phases of GATE, derived from profile measurements on the METEOR buoy by Hasse et al. (1978).

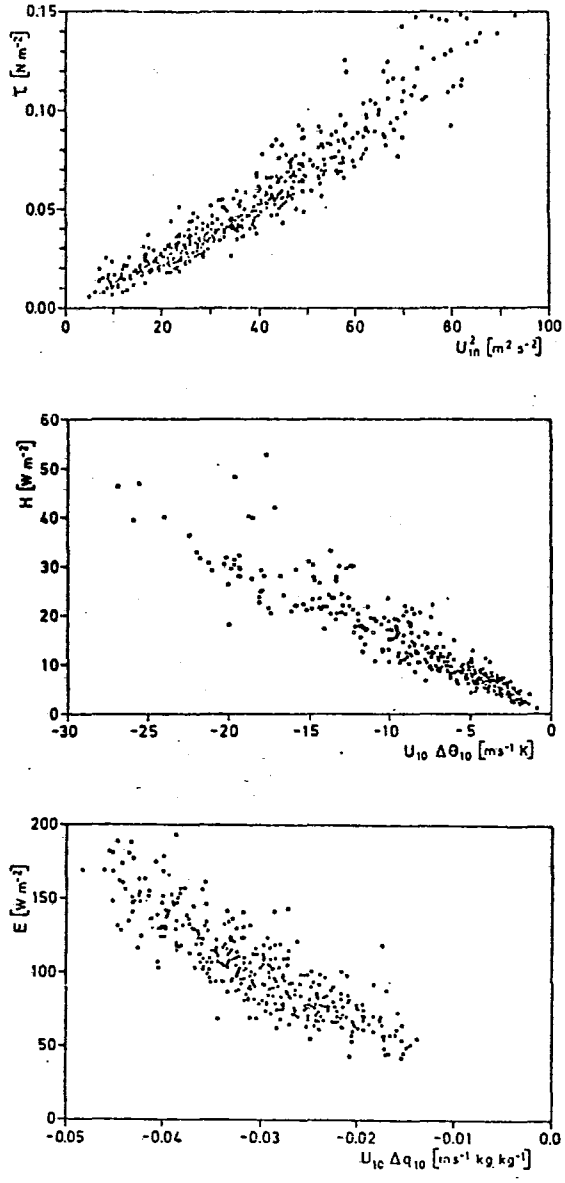

Figure 10.8 - Profile fluxes of latent heat (E), sensible heat (H) and momentum (τ) versus equivalent bulk parameters after Hasse et al. (1978).

For convectively undisturbed conditions in the SE trade winds Elagina et al. (1978) derived from eddy correlation measurements at the ship's boom of the ACADEMIC KURCHATOV the following results:

$$c_H = 1.58 \cdot 10^{-3}$$

and

$$c_E = 0.45 \cdot 10^{-3}.$$

The time series of their sensible and latent heat fluxes are displayed in Figure 10.9 with mean values of H = 7 Wm^{-2} and of E = 38 Wm^{-2} and of the Bowen ratio B = 0.18. The peak values of fluxes are primarily attributed to an increase of the sea-surface temperature caused by advection and not to variations of wind speed.

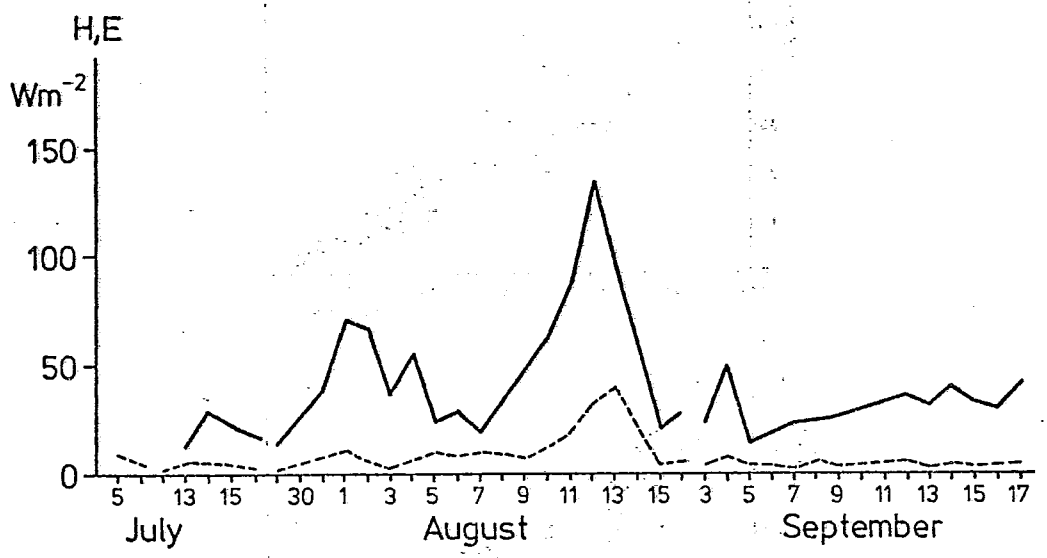

Figure 10.9 - Time series of daily averages of the eddy correlation fluxes of sensible (H) and latent (E) heat on the R/V KURCHATOV during GATE after Elagina et al. (1978).

The transfer coefficient obtained for sensible heat agrees closely with the value of Hasse et al. (1978) but a considerable difference appears for c_E. The diagrams in Figure 10.10, where sensible and latent heat fluxes are derived by the eddy correlation technique by different authors, are related to the bulk aerodynamic transfer rates with $c_H = c_E = 1 \cdot 10^{-3}$. It can be seen that the eddy latent heat fluxes of the ACADEMIC KURCHATOV are extremely low. At present we cannot offer a satisfactory explanation for this observational fact. Careful examination of the data leads us to believe that it is not caused by erroneous measurements or through perturbations of the ship. A similar tendency of the differences between c_H and c_E was found by Galushko et al. (1978) also from boom data during GATE with $c_H = 1.85 \cdot 10^{-3}$ and $c_E = 0.72 \cdot 10^{-3}$ and by Nicholls and Readings (1979) from aircraft gust probe measurements over the North Sea with $c_H = 1.6 \cdot 10^{-3}$ and $c_E = 1.0 \cdot 10^{-3}$. In contrast to the above values

Müller-Glewe and Hinzpeter (1975) obtain from flux measurements on a ship's boom during Phase III of GATE for c_E the considerably higher value of $1.3 \cdot 10^{-3}$.

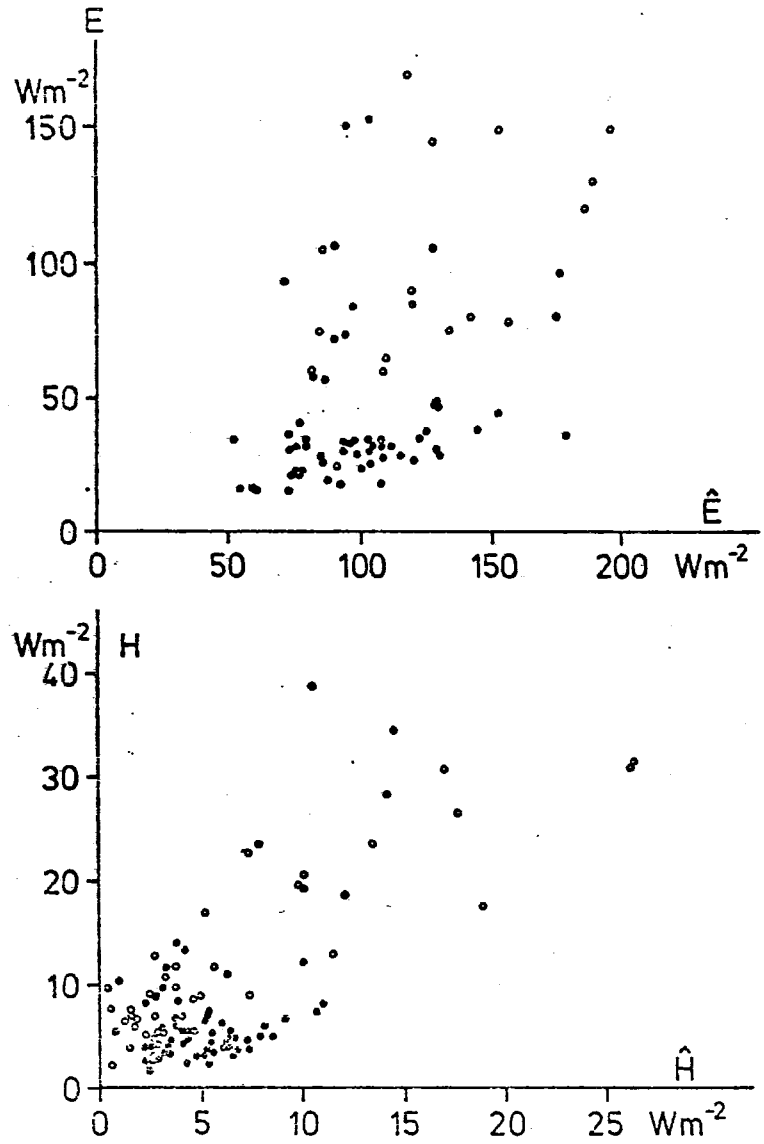

Figure 10.10 - Turbulent fluxes of latent (E) and sensible (H) heat obtained from eddy correlation measurements versus the respective aerodynamic values $\hat{E}$ and $\hat{H}$. Full dots: Volkov et al. (1976). Open circles: Müller-Glewe and Hinzpeter (1975).

The results firstly indicate that particularly the transfer coefficient for water vapour shows remarkable variations and secondly that c_E is generally distinctly lower than c_H. This latter tendency is also documented by the profile measurements of Hasse et al. (1978). Therefore, the GATE observations indicate that the sometimes

chosen simplified assumption $c_D = c_H = c_E = \text{const}$, with the constant ranging between $1.2 \cdot 10^{-3}$ and $1.5 \cdot 10^{-3}$ cannot be recommended for the low latitudes. According to the above results it seems more realistic to apply the following average values which result from the GATE measurements:

$$c_H = 1.7 \cdot 10^{-3}$$

$$c_E = 1.0 \cdot 10^{-3}$$

$$c_D = 1.3 \cdot 10^{-3}$$

The coefficient for momentum transfer c_D has been derived from profile, eddy correlation and dissipation measurements. The latter technique was employed by Khalsa and Businger (1977) for fluctuation measurements taken on board R/V DALLAS. The various results are marked by a considerable scatter so that an uncertainty of at least ± 25% must be taken into account when fluxes are calculated with the aid of the above constant, but in contrast to the latent heat transfer the various methods do not show a systematic difference for c_D and for c_H.

Considerable work has been devoted in the past to the derivation of more accurate transfer coefficients which, e.g. take into account changes of wind speed and of the vertical density distribution. On the basis of the GATE results we conclude that in the tropics such approaches would not lead to a significant improvement of the surface fluxes compared to constant values. Presumably the above-mentioned degree of uncertainty must be accepted in using the highly simplified bulk formulae.

10.2.5 Turbulent surface fluxes under disturbed and undisturbed conditions

The eddy correlation method, which can best be used to control the validity of the bulk aerodynamic method, suffers from technical shortcomings in rainy conditions. Therefore, our information about the surface fluxes in convectively strongly disturbed situations is extremely vague.

With respect to the averaging time Khalsa and Businger (1977) suggest that averaging periods of about 30 minutes are required for conditions of increased plume convection but with no rainfall in order to achieve reliable fluxes by the bulk aerodynamic formulae. In contrast Hasse et al. (1978) conclude from profile measurements that 10 minute averages may suffice for flux determinations in undisturbed as well as in disturbed situations. Only very unstable periods have to be excluded from this rule.

As indicated earlier already, the latter authors furthermore find no significant differences for the transfer coefficients in convectively disturbed and undisturbed conditions. This result should be interpreted with some reserve since the large scatter of the experimentally derived c_D, c_H and in particular c_E hardly enable us to clarify this matter with enough confidence.

Under the implication that the same transfer coefficients can be used at all large-scale conditions Hasse et al. (1978) and Barnes (1977) report considerably higher sensible heat fluxes at the sea surface within and in the rear of precipitating convective systems than before the storms. The latter author also finds a significant increase of the water vapour flux in the rain area where cold and relatively dry downdrafts penetrate down to the sea surface.

Statistical information on the surface fluxes under various large-scale situations in the trade wind regions and in the ITCZ has been reported by Augstein (1979). On the basis of several experiments in the low latitudes he finds that the latent heat flux is largest in the undisturbed trades ($\sim$160 W m^{-2}) and smallest in the ITCZ ($\sim$112 W m^{-2}). In contrast, the sensible heat flux is smallest in the trades ($\sim$8 W m^{-2}) and largest in the ITCZ ($\sim$16 W m^{-2}). Consequently the Bowen ratio varies from 0.05 in the trades to 0.13 in the ITCZ. But together with these values we wish to point out again that the transfer coefficients which have been used in the past for water vapour are 30% to 50% larger than the mean GATE value of $1.0 \cdot 10^{-3}$. Furthermore, the sensible heat flux by the water vapour fluctuations has not been taken into account so that the above-mentioned relative variations may be more or less realistic but the flux values may need a critical revision.

The GATE data analysis reveals independently of the afore-mentioned uncertainties of the flux calculations that the mean quantities in the surface layer and at the air-sea interface suffer from remarkable changes during the passage of intensive convective systems. According to Thompson et al. (1979), Petrossiants et al. (1975) and Günther (1980) convective perturbations are predominantly related to two synoptic wave disturbances. One of these, which was mainly discussed by Thompson et al. (1979) has a period of 3 to 4 days and the latter delineated by Petrossiants et al. (1975) and Günther (1980) ranges around a period of 32 hours.

Diurnal effects of the surface fluxes for all GATE ships within the A/B hexagon have also been investigated by Jacobs (1979). A semi-diurnal variation prevails in the sensible heat flux with maxima near 6 and 18 GMT. A similar behaviour is resolved in the latent heat transfer but here a diurnal mode with its maximum around 12 GMT becomes additionally obvious. Both modes are mainly due to changes in the air-sea differences of temperature T_{w-a} and of specific humidity q_{w-a}. In the ITCZ region these regular changes are frequently masked by the more irregular variations connected with convective perturbations.

10.3 THE STRUCTURE OF THE ATMOSPHERIC BOUNDARY LAYER UNDER DIFFERENT CONVECTIVE CONDITIONS

10.3.1 The atmospheric boundary layer in the undisturbed trade wind region

Measurements of several expeditions during the last 15 years, such as the international Atlantic Tradewind Experiment (ATEX) 1969, the U.S. Barbados Oceanographic and Meteorological Experiment (BOMEX) 1969, and the U.S.S.R. Tropical Experiment (TROPEX) 1972, have confirmed the earlier conclusion of Riehl et al. (1951) that the large-scale low-level horizontal flow is divergent on its way from the subtropical high pressure belts to the fringes of the Inter Tropical Convergence Zone (ITCZ). In this part of the Hadley cell the turbulence generated by shear and buoyancy in the lower atmosphere is considerably damped through the large-scale subsidence of relatively low density air across the top of the atmospheric boundary layer. In certain regions, especially over the areas of coastal upwelling of cold water, the turbulent vertical mixing is restricted to a shallow layer so that either no clouds or just a thin stratus deck may form below a strong capping temperature inversion. Such well-mixed boundary layers typically prevail in the trade wind areas off the western coasts of the continent (Reger, 1927; Neiburger et al., 1961; Wakefield and Schubert, 1976), off the coast of Somalia (Schott and Fernandes-Partagas, 1980) during the African Indian SW Monsoon, and for certain seasonal periods, also at other coastal regions.

If large-scale subsidence and horizontal advection are prescribed as external quantities, one-dimensional models, such as proposed by Lilly (1968) with the improvements of, e.g. Deardorff (1976 and 1981), Schubert (1976), Kahn and Businger (1979), and Kraus and Schaller (1978), permit a prognostic treatment of the mixed atmospheric boundary layer in close agreement with observations.

In the central part of the oceanic trade wind belts, the lower troposphere has a multi-layered structure with a well-mixed regime below the cloud base, and a conditionally unstable cloud layer above it. The latter is occupied by an ensemble of non-precipitating cumulus clouds (cumulus fractus, cumulus humilis) with members which extend into the topping trade wind inversion. The transition from the sub-cloud to the cloud layer is marked by a relatively thin stable region with a nearly isothermal vertical temperature distribution, and a distinct decrease of water vapour with height. The multi-layered ABL was first described by Bunker et al. (1949) on the basis of measurements over the Caribbean Sea. Succeeding experiments over various oceanic sites in low latitudes have confirmed their results as typical for the major area of the trade wind circulation (Augstein, 1979). Examples of the mean vertical temperature and specific humidity distribution of a mixed and a multi-layered ABL are reproduced in Figure 10.11.

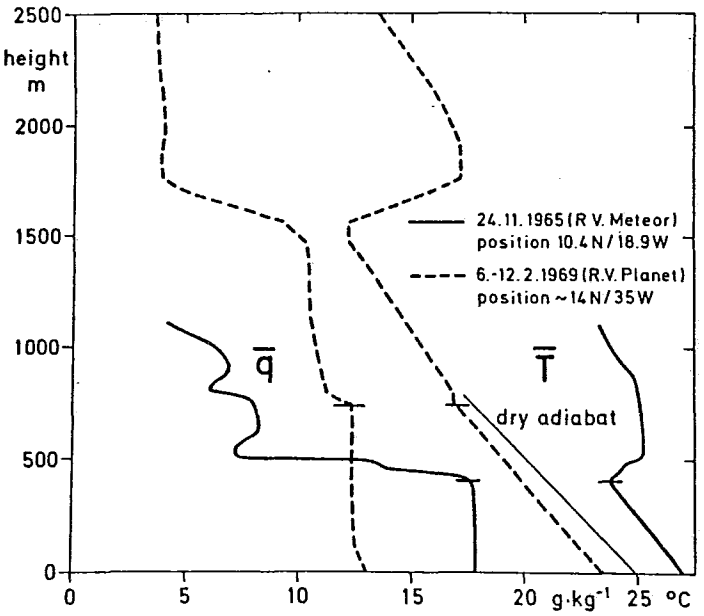

Figure 10.11 - Mean vertical profiles of temperature ($\overline{T}$) and specific humidity ($\overline{q}$) near the West African coast (solid lines) and in the central tropical Atlantic (broken lines), measured by radiosondes.

The physical principle of the formation and maintenance of a multi-layered structure in a subsiding large-scale air flow has already been formulated by Riehl et al. (1951) and by Malkus (1958). These authors clearly emphasized the importance of condensation and droplet evaporation, as well as the vertical thermal energy transports by cumulus clouds. The first prognostic numerical model for this kind of ABL was presented by Betts (1973), who treated the cloud process with the aid of an entraining, initially buoyant air parcel. The atmospheric boundary layer with cumulus clouds was further studied by Ogura and Cho (1973), Betts (1976a) and Ogura et al. (1977) with one-dimensional diagnostic models.

A direct simulation of clouds in the calculations is achieved by Sommeria (1976), and Sommeria and Deardorff (1977) in their three-dimensional prognostic numerical approach. But the application of this model is rather limited since it requires a large amount of computer time. Bougeault et al. (1979) furthermore show that many

features of the three-dimensional computations are as well reproduced by a one-dimensional treatment. More advanced one-dimensional time dependent models for boundary layers with non-precipitating clouds have been recently published by Johnson (1978), Albrecht et al. (1979), and Augstein and Wendel (1980). These authors principally apply mass flux schemes for the cloud parameterization, as proposed by Yanai et al. (1973), Arakawa and Schubert (1974) and Fraedrich (1973 and 1974). The so-called second-order closure principle has been used by Yamada and Mellor (1979) to study the multi-layered trade wind ABL also with a one-dimensional concept. Their simulation of a four-day BOMEX period reproduces some of the observed features of the ABL characteristics satisfactorily, but it fails to maintain the detailed structure of the mean vertical temperature and specific humidity profiles which are portrayed in Figure 10.11.

Several of the above-mentioned models reveal the strong influence that the large-scale subsidence and horizontal advection have on the ABL development. Furthermore, Sommeria (1976) and Augstein and Wendel (1980) emphasize the importance of the radiative flux divergence within the multi-layered ABL. The latter authors indicate that radiation not only generates the observed diurnal variation of convection, but also significantly affects the mean height of the cloud layer. Veyre et al. (1980) find from model considerations that cloud top infrared cooling has a strong impact on the cloud activity and the associated turbulence in the ABL.

The generation of inversion layers has been treated by Ivanov and Ingel (1976) with the aid of a refined "Austausch" concept. Their model, which has not yet been tested against observations, is able to create statical stable sublayers, but it cannot monitor such layered structures over longer time intervals.

The aforementioned one-dimensional models enable one, more or less, to simulate the time development of the first statistical moments of the ABL and of the various layer boundaries. However, with the exception of the last model, they are not designed e.g. to describe the transition from the pure mixed to the multi-layered structure and vice versa. In order to close this modelling gap, one needs criteria for the initiation and breakdown of cumulus clouds. A useful step in this direction was made by Mahrt (1979), who considered the penetration of convective elements into the stable regime atop a mixed boundary layer where they reach their level of water vapour condensation. Randall (1980) suggests that entrainment of potentially drier and warmer air across the cloud top could lead to a static instability of air parcels through evaporation of cloud droplets. This mechanism which was also addressed by Deardorff (1980) might under certain conditions break up a stratus deck below a temperature inversion into cumulus cells. The initial formation of regularly organized cloud patterns may also be described through linear theories such as the thermal Rayleigh criterion (see, e.g. Krishnamurti, 1975) or the inflection point instability (see, e.g. Lilly, 1966; Brown, 1970 and Etling, 1972). These concepts are basically valid for laminar flow but have been applied with some success also to turbulent conditions. Nevertheless, there exists still a considerable uncertainty about the detailed physics of the convection process. Further experimental efforts and theoretical studies are still necessary in order to sufficiently understand the development of the various kinds of clouds and their interaction with other scales of motion in the ABL.

10.3.2 The structure of the lower atmosphere in the ITCZ during GATE

10.3.2.1 The large-scale atmospheric field

Budget calculations with data of the GATE B- and A/B-array by Petrossiants et al. (1975), Antsipovich et al. (1975), and Reeves et al. (1979) show, for all experimental phases, a convergent horizontal flow in the lowest 1500m of the atmosphere (Figure 10.12). Maximum convergence occurs near the sea surface, indicating a concentration of the horizontal inflow of mass into the ITCZ on the subcloud layer.

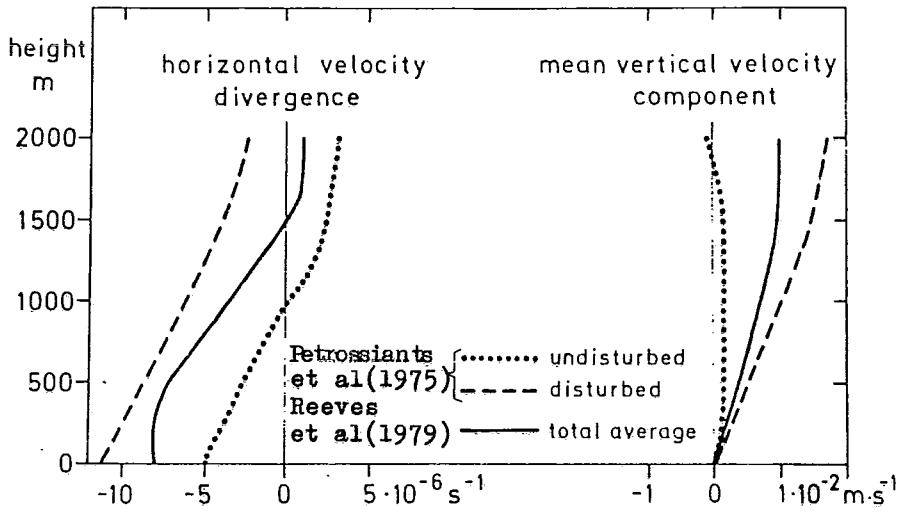

Figure 10.12 - Horizontal velocity divergence and mean vertical motion derived from wind measurements of the A/B-scale (Petrossiants et al., 1975) and of the A/B- and B-scale (Reeves et al., 1979).

Brümmer (1978) finds similar features for the C-array. The analyses of all GATE grid scales (A/B ~ 800 km, B ~ 300 km, C ~ 100 km) document a close correlation between the magnitude of low-level convergence of the horizontal mass transport and the cumulus cloud activity which is categorized here into undisturbed and disturbed conditions. The first one refers to situations with no or only shallow non-precipitating clouds and the latter to cases of deep precipitating convection. The time series of the surface divergence and the radar estimated precipitation rate of the C-array (Figure 10.13), derived by Jalickee and Ropelewski (1979), mark high precipitation rates when the horizontal air flow is strongly convergent.

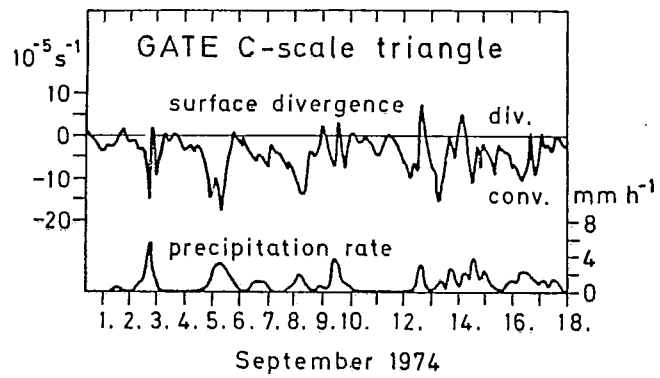

Figure 10.13 - Surface divergence and radar based precipitation rate for the C-array during Phase III. After Jalickee and Ropelewski (1979).

A more detailed investigation of the relationship between the large-scale flow characteristics and cloud convection is presented by Thompson et al. (1979). These authors - employing a compositing technique of Reed and Recker (1971) - use the surface and upper-air data of the GATE oceanic network in order to analyse the nearly periodic atmospheric variations with a sequence of about 3.5 days during Phase III. They determine the wave cycle by the meridional wind component at the 700 mb level. Several other quantities such as temperature, moisture, rainfall and vertical motion are then assigned to the different wave positions by subdividing each full oscillation into eight parts. In spite of such a relatively high resolution the compositing procedure applied obscures some details which are closely related to individual convective systems Therefore, one should try to diagnose the occurrence of the latter as good as possible and base averaging periods on the observed convection cycle.

Such an attempt was made by Günther (1977) and Brümmer (1979), who found from spectrum analysis of low-level divergence and precipitation that the largest peaks in the variance spectra lie at a period of about 32 hours (Figure 10.14).

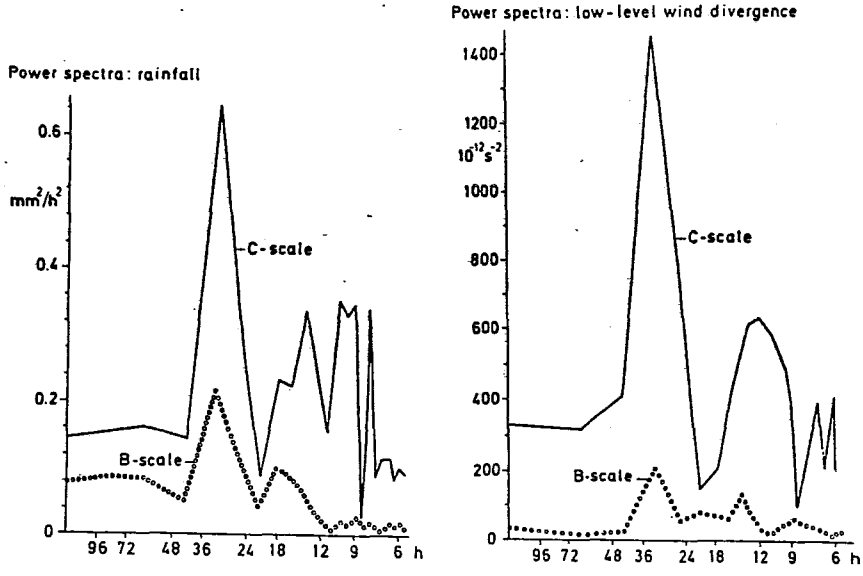

Figure 10.14 - Variance spectra of rainfall (left) and of velocity divergence at the sea surface (right) for the C-array (solid lines) and B-array (open circles). After Brümmer (1979).

These maxima are clearly expressed for the C-array and appear to be less pronounced in the B-array data. Obviously the phenomena consist of space scales which are not too well resolved by the B-grid, but distinctly show up in the C-array data. Therefore, one is lead to believe that the 3.5 day wave is superimposed by another one with a shorter period which is, in particular, strongly reflected in the cloud activity.

Tropical convective disturbances with periods around 32 hours have already been detected earlier by Ivanov et al. (1973) during TROPEX 1972. On the basis of GATE c-array measurements, Günther (1977) derived for these westward migrating waves a mean wavelength of about 800 km and a mean phase speed of nearly 10 ms^{-1}. Correlations between the horizontal velocity divergence, the thermodynamic properties at low levels,

and the precipitation rate of both the 3.5-day and the 32-hour wave show qualitatively similar features. Therefore, it seems in general to be favourable for the tropics to classify the observed ABL structures in relation to the large-scale tropospheric waves. Although we shall mainly refer to the 32-hour variation averaging, nevertheless, smears out several details. Therefore, studies of individual cloud systems must be carried out as well in order to delineate their effect on the structure of the lower troposphere more precisely.

10.3.2.2 The mean vertical structure of the low-level temperature, specific humidity and wind components in relation to the large-scale waves

High resolution vertical profile measurements of wind and thermodynamic quantities in the lower troposphere have been restricted mainly to the C-array ships during Phase III. Therefore, the consideration of the mean vertical structure of the lower atmosphere will be largely based on soundings of these platforms. In the subsequent discussion, we shall mainly rely on the data classification of Brümmer (1979), which is primarily related to the observed convective activity and much less to wave characteristics derived from the atmospheric field.

With reference to rainfall events of the GATE C-scale triangle he distinguishes between four different convective states as schematically shown in Figure 10.15. Conditions with no or shallow non-precipitating fair weather clouds are categorized as "undisturbed". The other three classes are related to the life cycle of deep cumulus convection. During the "growing" phase clouds are increasing in size and they start to precipitate. Then follows the "developed" period with mature cumulus clouds which produce the maximum of rainfall. Finally, when the convective activity is suppressed again and rainfall decreases the "decaying" phase is reached.

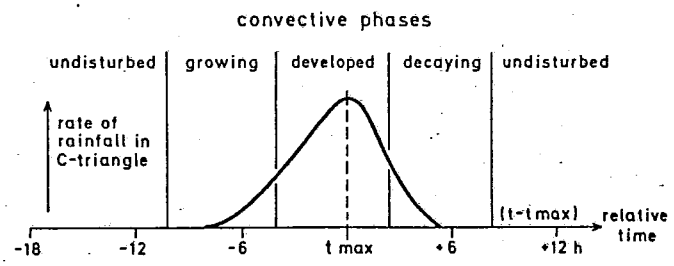

Figure 10.15 - Scheme of convective phases during GATE based on the rate of rainfall. Time axis is related to the time of maximum precipitation: t_{max}.

Günther (1977 and 1980) shows that these convective phases can be systematically related to different parts of the 32-hourly wave, which dominantly appears in the variance spectra of the horizontal divergence and precipitation as well as of temperature and specific humidity. In basic agreement with the findings of Thompson et al. (1979) for the 3.5 day easterly wave, the horizontal velocity divergence in Brümmer's (1979) analysis (Figure 10.16) has its largest negative values (strongest convergence) in the stage of growing clouds distinctly prior to the developed convection. Low-level divergence becomes even slightly positive in the wave part with decaying clouds. The variation of horizontal divergence during the wave passage is strongest in the sub-cloud layer and it decreases upwards. In the lowest 1000m of the atmosphere, the differences in the mean vertical motion, among the four phases, increase continuously with height (Figure 10.17).

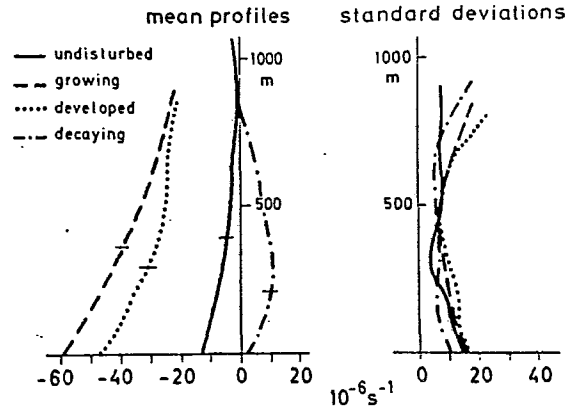

Figure 10.16 - Vertical profiles of horizontal velocity divergence for different convection modes (left side) based on C-array data and standard deviations for each category (right side). Horizontal bars mark the top of the mixed layer. After Brümmer (1979).

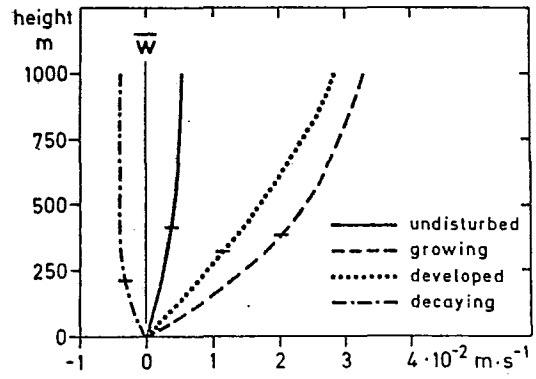

Figure 10.17 - Mean vertical motion for different convection modes based on divergence values of Figure 10.16.

The shape of the vertical profiles of the horizontal wind components is rather independent of the wave position with respect to the 32-hourly mode in the C-array (left side of Figure 10.18). For all four cases, the standard deviation is quite large (right side of Figure 10.18) so that not even the increase of the southerly wind component during developed convection is statistically significant. In contrast to this behaviour of the wind profiles in relation to the 32-hour wave the C-scale data as well as the analysis of Thompson et al. (1979) show distinct oscillations of the horizontal streamlines for the 3.5-day mode which increase from the sea surface up to about 700 mb. Furthermore, spectrum analysis of the C-array horizontal wind components indicates a pronounced signal in the 3 to 5 day range but not at or near the 32-hour period. Therefore, one might speculate that each of these two disturbances belongs to a different class of waves. The first one which is clearly documented in the horizontal and vertical field of motion has characteristics of Rossby-gravity-waves while the latter is mainly established in the vertical velocity component and thus appears more like a pure gravity wave.

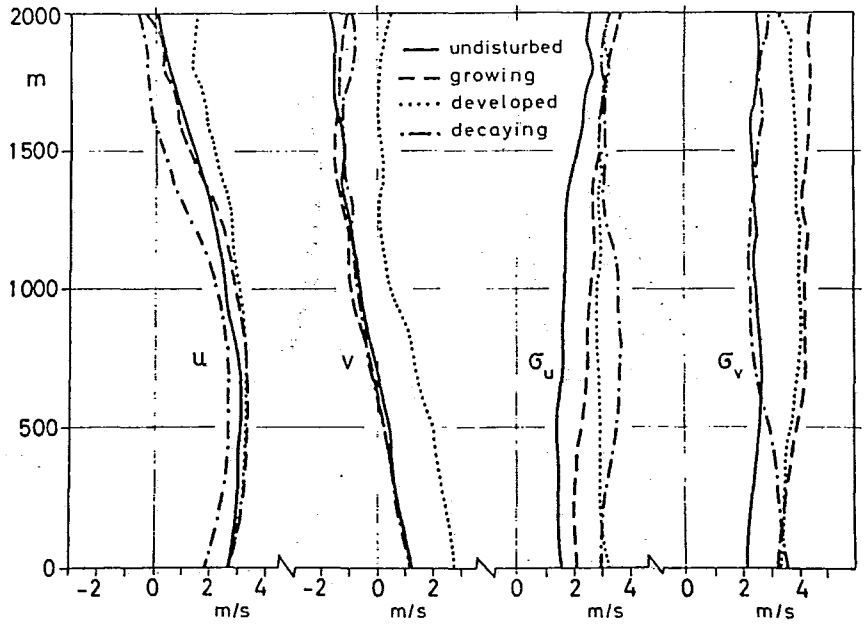

Figure 10.18 - Vertical profiles of the zonal (u) and meridional (v) wind components for different convection stages and the respective standard deviations σ_u and σ_v. (Courtesy of B. Brümmer).

The vertical distribution of the mean temperature and specific humidity, derived by Brümmer (1979) for different perturbation classes in the C-array as well as for ATEX-conditions, is reproduced in Figure 10.19. The typical layered structure was preserved during the averaging procedure by an adequate scaling of the vertical co-ordinate of the individual soundings (for details of the averaging method see Brümmer, 1979). Since the radiosonde sensors need some ten seconds to adjust from the start conditions on the ships to the unperturbed atmospheric values the profiles in the lowest 100 meters on Figure 10.19 are obtained by extrapolation to the sea surface. Therefore the near-surface regime, which generally has a superadiabatic temperature gradient and a distinct water vapour decrease with height, is not realistically documented by these graphs. A better representation of such details is obtained by Fitzjarrald and Garstang (1980), who analysed tethered balloon data. Before drawing conclusions from the temperature and moisture profiles, we may indicate that the rainfall maximum occurs during the developed section, but the growing and decaying phases also experience some precipitation. The graphs in Figure 10.19 portray the following facts, which agree with the radiosonde observations of Galushko et al. (1978) and with the tethered sond measurements of Gaynor and Ropelewski (1979) and Fitzjarrald and Gartstang (1980):

(a) The height of the mixed layer decreases from the undisturbed through the decaying convective stage and then recovers to its undisturbed value again.

(b) Above 100m height the vertical temperature gradient is nearly dry adiabatic within the sub-cloud mixed layer, and close to moist adiabatic in the lower cloud layer during the entire wave cycle. Precipitating convection causes cooling from the sea surface up to 2500m height. In the sub-cloud layer lowest temperatures occur during the decaying, and in the cloud layer during the developed cloud phase.

(c) In the mixed layer the specific humidity assumes maximum values during the undisturbed and further up during the developed convective period. Minimum water vapour content appears throughout the entire regime during the decaying phase. Certain differences in the temperature/water vapour correlation above and below cloud base during the wave passage, will be considered below.

(d) Comparison of the GATE ITCZ profiles with undisturbed trade wind conditions of ATEX - although not simultaneously measured - suggest that the boundary layer air gains considerable amounts of sensible heat and water vapour on its march from the subtropical high pressure belt to the Equatorial Trough. The mixed layer is nearly twice as deep in the central trades as in the ITCZ. The trade wind inversion clearly marks the transition between the ABL and the free atmosphere in the divergent flow regime, but such an upper lid of the ABL can hardly be detected in the mean temperature and specific humidity profiles of the lowest 2000m of the convergence zone.

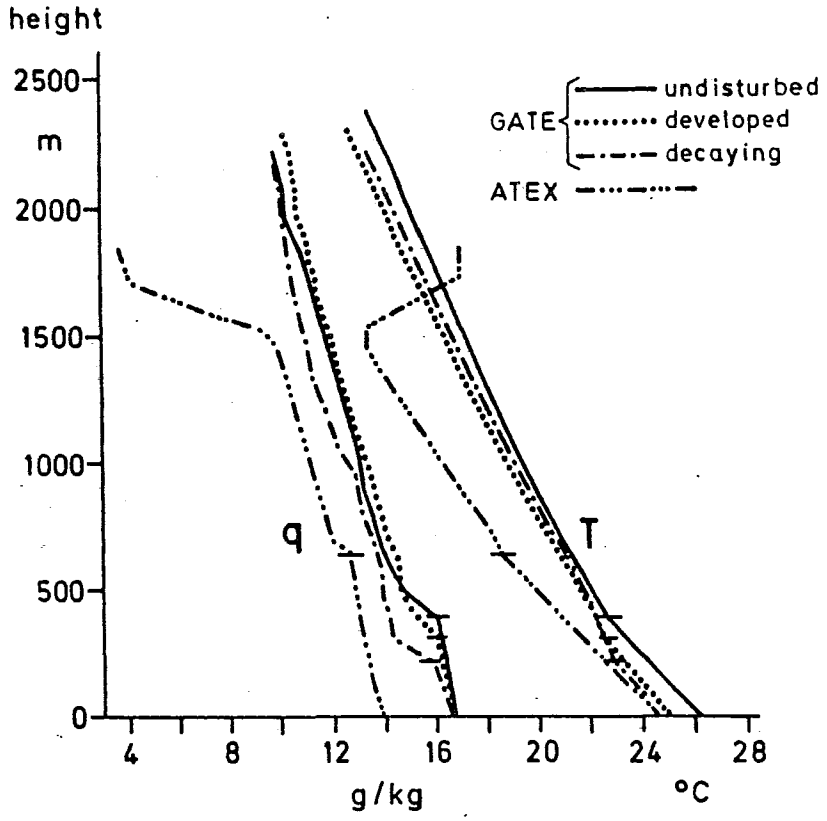

Figure 10.19 - Vertical profiles of air temperature (T) and specific humidity (q) for different convection stages during GATE and for the undisturbed trade wind area during ATEX. After Brümmer (1979).

The GATE measurements as well as earlier findings much more indicate that generally no distinct top of a boundary layer can be identified below the tropopause in the Inter Tropical Convergence Zone. Modelling of the ABL is quite useful under suppressed convection, when the dynamic and thermal lower boundary conditions predominantly act on the air flow. However, in the presence of precipitating cumulus clouds an atmospheric boundary layer cannot be clearly defined. Then the local influence of the lower boundary on the flow field is of minor importance, but the cloud processes dominate. Consequently, modelling in this case is primarily dependent on a satisfactory representation of the cloud effects, so that a separate treatment of just the lowest, say 2000 meters of the troposphere does not seem to be of great value.

The temperature (T) and specific humidity (q) variations in the sub-cloud and lower cloud layers may be deduced from the height dependence of the covariance and coherence spectra in Figure 10.20. The isolines of these illustrations, which have been analysed by Günther (1980) from spectra at 100m height intervals, are based on the structure sonde measurements of the C-array ships FAY, METEOR and PLANET during Phase III.

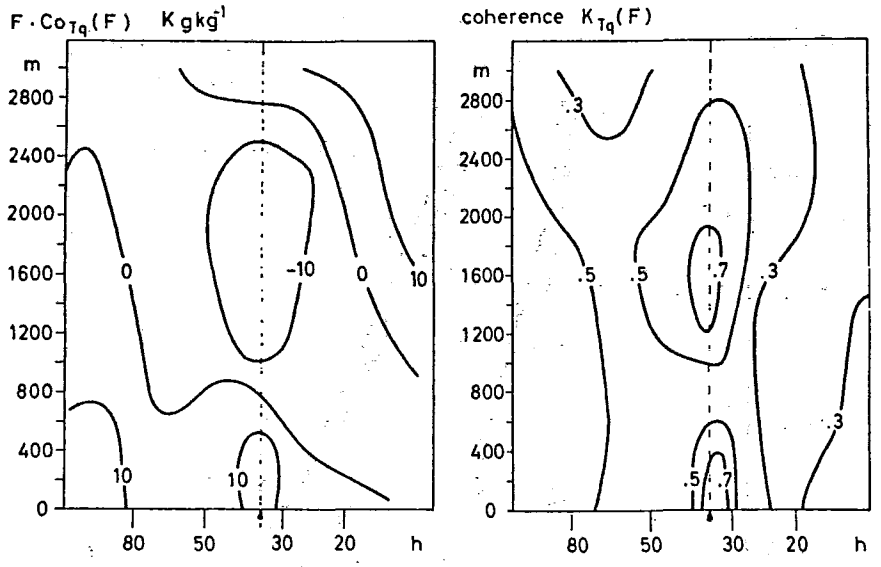

Figure 10.20 - Isolines of covariances (left side) and coherences (right side) of temperature and specific humidity for the C-array. The vertical broken line indicates the period of 32 hours. Abscissa: period in hours, ordinate: height in meters. After Günther (1980).

Both the covariance and coherence of T and q show maxima in the sub-cloud layer and at around 1600m height during the period of 32 hours (dashed vertical lines). The moisture and temperature variations are in phase below, and out of phase above the cloud base according to the respective positive and negative covariances on the left-hand side of Figure 10.20. This result clearly delineates that drying and cooling, or moistening and warming are correlated in the mixed layer while the combinations of drying and warming, or moistening and cooling dominate in the lower cloud layer during the passage of the wave. Similar correlations have been found by Zipser (1969) for a tropical squall line, by Miller and Betts (1977) for travelling convective systems over

Venezuela, by Seguin and Garstang (1976) for precipitating clouds over the Caribbean Sea, and by Gaynor and Ropelewski (1979) for disturbances during GATE at the ship OCEANOGRAPHER. All of these observations provide evidence that precipitating convection in the tropics systematically modifies the ABL as described above under item (a) to (d).

The spectra reproduced in Figures 10.14 and 10.20 suggest that the cloud activity in the Atlantic ITCZ is closely related to the large-scale tropospheric oscillation with a period of about 32 hours. This wave is distinctly coupled to the atmospheric boundary layer through the horizontal velocity divergence and the effects of precipitating cumuli. The latter act upon the lower troposphere through condensation, evaporation and vertical mixing.

A nearly conservative quantity during dry and moist adiabatic displacement of air parcels is the so-called moist static energy $h = c_p T + gz + Lq$. Therefore, its vertical fluxes reasonably reflect the cloud transports. The profiles in Figure 10.21 have been derived by Brümmer (1979) as residuals of C-array budget computations. This kind of procedure suffers generally from a considerable uncertainty but we may nevertheless draw some qualitative conclusions from the results. In situations of low cloud activity (undisturbed and decaying periods), the upward flux of moist static energy in Figure 10.21 decreases with height in a similar way as in the undisturbed trade wind belt.

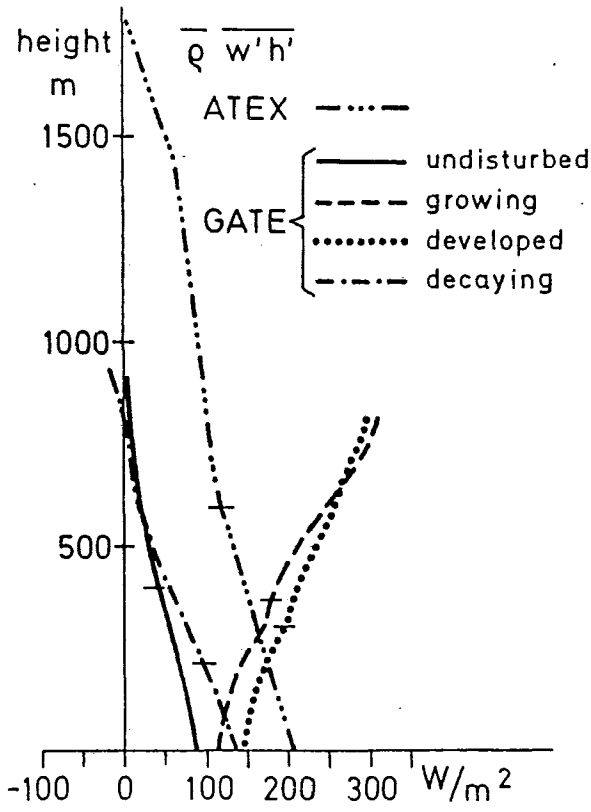

Figure 10.21 - Vertical profiles of subgrid scale fluxes of moist static energy for different convection stages in the GATE C-array and for ATEX. Horizontal bars mark the top of the mixed layer. After Brümmer (1979).

During the growing and developed wave sequences, the moist static energy transports increase with height and become already twice as large as the sea-surface values at about 600m height, slightly above cloud base. Consequently, in this situation subgrid scale transports would diminish the moist static energy in the lower troposphere. But Brümmer (1979) found, from budget calculations, that only minor local time changes of h are caused since the convergence of the subgrid scale vertical transports in the undisturbed and decaying phases, and their divergence under growing and developed conditions are mainly compensated for by large-scale advection. These facts support the hypothesis that the large-scale low-level flow and cloud convection are closely inter-related.

Reed and Recker (1971) derived from measurements that the synoptic scale waves over the tropical Pacific Ocean obtain their kinetic energy from the cloud induced condensational heating and evaporative cooling. But Thompson et al. (1979) found that instead of this thermodynamic mechanism the 3.5-day mode over the Atlantic Ocean is driven by barotropic energy conversion. Nevertheless, preliminary linear model computations by Günther (personal communication) seem to suggest that a 32-hour gravity wave and cloud convection may be positively backcoupled and thus support each other. If this CISK-like concept proves to be valid, the low-level atmospheric flow and cumulus convection play an important role in the generation and maintenance of the 32-hour tropospheric oscillation over the tropical Atlantic Ocean.

10.3.2.3 Processes in the near surface atmospheric region under various convective conditions

Atmospheric soundings at different positions of the observed large-scale tropospheric waves enable one to detect the effects of various processes on the kinematic and thermodynamic state of the lower troposphere. Studies of individual convective systems with reference to their stage of development - as portrayed in Figure 10.22 - support the view that precipitating clouds in the tropics systematically modify the lower atmosphere. The latter recovers to its undisturbed state within a time interval of 5 to 10 hours. Some insight into the processes which contribute to the observed modifications of the atmospheric mean properties can be gained from the high resolution data of tethered balloon sondes and aircraft gust probe measurements.

Emmitt (1978) treated nineteen individual clouds, which passed by the tethered balloon device of the R/V DALLAS. Up to five special radiosondes could be mounted at the tether line of the balloons in the height range between about 100m and 1200m. One example of the measured time series, including the ship's boom data at 10m height, is reproduced in Figure 10.23. The in-cloud time sequence is hatched on the graphs. The cloud base in this particular case was observed at 310m altitude. The following facts are of special interest: (a) the cloud induced signals can be traced down to the boom level at 10m height; (b) various quantities, primarily the horizontal wind component, exhibit remarkable fluctuations in connection with up and downdrafts within the range of the visible cloud; (c) in a detailed inventory of the nineteen cases, Emmitt resolves warm and moist updrafts and cold and dry downdrafts as dominant features at all levels. Nevertheless, other combinations also occur. Among these, the kinetic energy consuming cold and moist updrafts and warm and dry downdrafts gain importance near the cloud base and in the sub-cloud layer. Similar results have been reported by Riehl et al. (1978) from aircraft measurements. The negatively buoyant cloud mass fluxes are finally responsible for the small downward sensible heat flux at about 350m height in Figure 10.24.

The mean cloud fluxes can be converted into horizontal area averages, which are consistent with Brümmer's (1978) budget residuals, under the assumption that about 6% of the area is covered by actively transporting clouds of the observed kind. Since this value more or less agrees with other estimates it leads us to believe that the cloud transports in fact account for the majority of the subgrid scale fluxes in the upper mixed and lower cloud layers which have been obtained from C-array budget considerations.

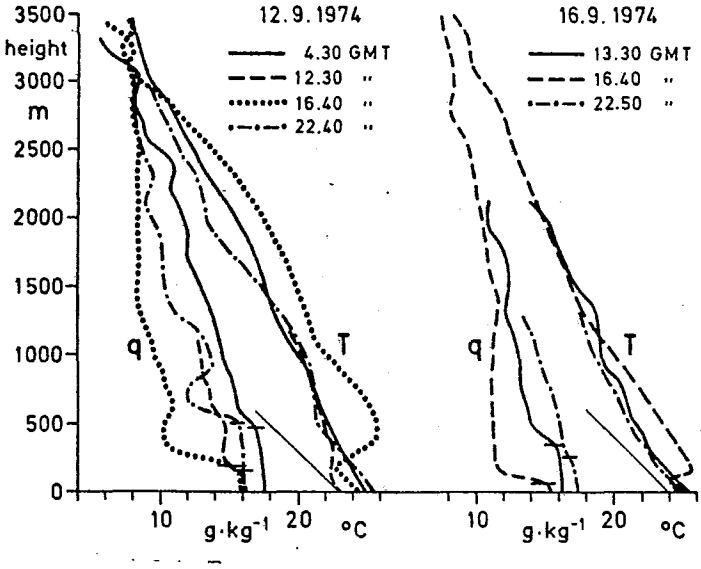

Figure 10.22 - Vertical profiles of temperature (T) and specific humidity (q) during two passages of convective systems at the "Meteor" position in the C-array. Solid lines: before, and dashed lines: immediately after the precipitation period. Dash-dotted: recovered ABL. Thin straight lines: dry adiabats. Horizontal bars indicate the top of the mixed layer. After Augstein (1979).

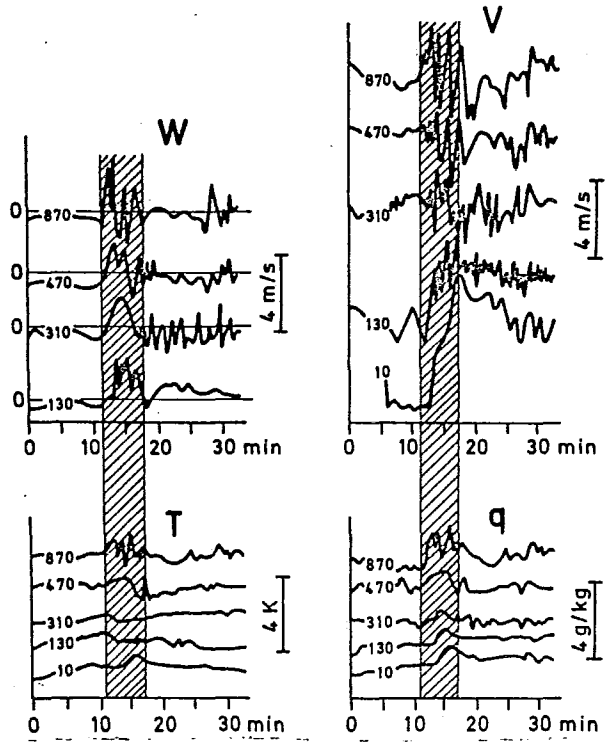

Figure 10.23 - Time series of tethered balloon measurements at 870m, 470m, 310m and 130m height, as well as of boom data at 10m height. w = vertical velocity, v = horizontal velocity, T = temperature, q = specific humidity. Hatched time period = in-cloud measurements. After Emmitt (1978).

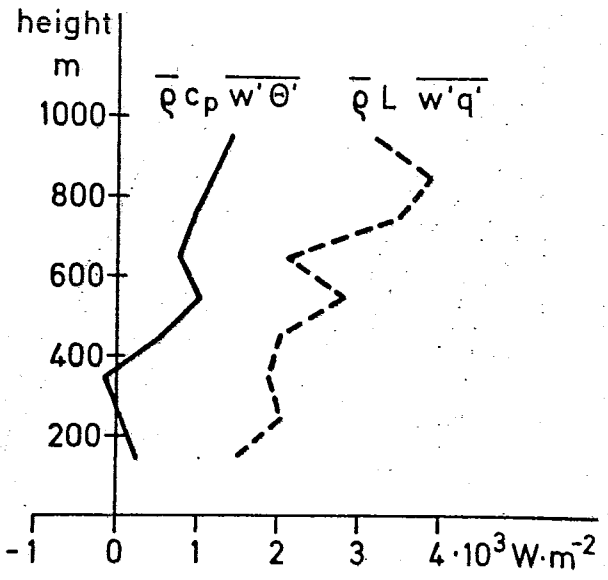

Figure 10.24 - Vertical profiles of sensible (solid line) and latent (dashed line) heat flux within the area covered by active cumulus clouds. After Emmitt (1978).

The processes within the sub-cloud layer, under suppressed and moderate cloud convection, have been investigated with tethered balloon turbulence sondes by Andreev et al. (1975) and Thompson et al. (1980); with the acoustic echo sounding technique by Gaynor and Mandics (1978); and with gust probe equipped aircraft by Riehl et al. (1978), Nicholls and Le Mone (1980), Greenhut (1980) and Reinking (1979). Unfortunately, all of these methods cannot be satisfactorily applied in rain conditions so that the results are either restricted to non-precipitating convection, or to the before and after situations of deep clouds.

Tethered balloon turbulence measurements averaged for the sub-cloud layer and under depressed cloud activity by Andreev et al. (1975) in Figure 10.25 are characterized by a peak at frequencies slightly higher than 10^{-3} Hz. The dominance of rather low frequencies in the mixed layer turbulence, which is obvious in the variance spectra of Figure 10.25, has also been reported by Thompson et al. (1980) from tethered balloon sonde measurements, and by Nicholls and Le Mone (1980) and Reinking (1979) from aircraft gusts probe analysis.

The covariance spectra of w'T', w'q' and w'u' are not as uniform throughout the mixed layer as the corresponding variance spectra. In general agreement with the aircraft data of Nicholls and Le Mone (1980) and Reinking (1979) the tethered balloon spectra of T'w' and q'w' reported by Thompson et al. (1980) clearly document that the peak wavenumber (or frequency) shifts from higher to lower values with height (Figure 10.26). The only exception to this finding is observed for suppressed convection near the top of the mixed layer at 400m altitude. The investigators point out that their data set is quite heterogeneous, but nevertheless speculate that smaller scales of turbulence may be generated near the top of the mixed layer under the given conditions.

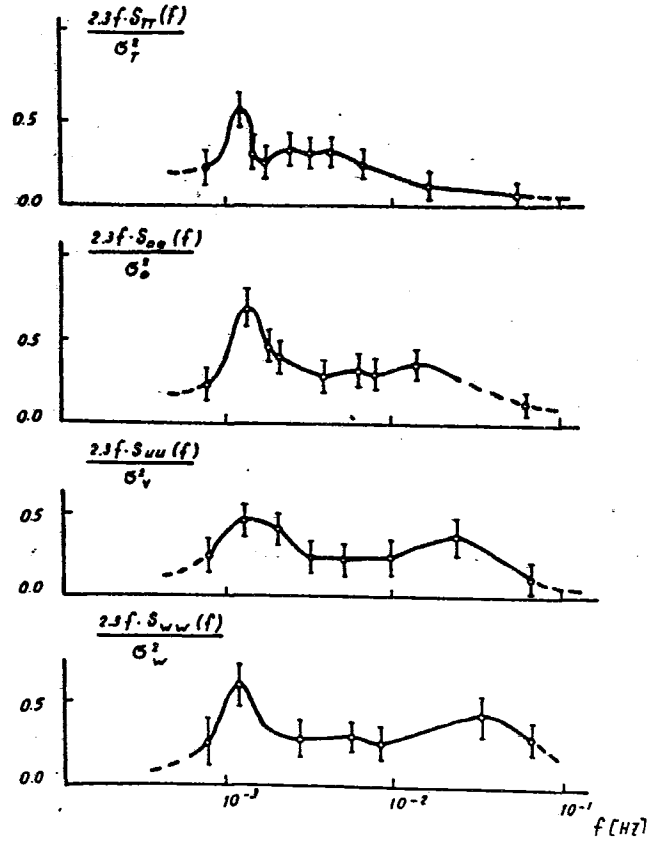

Figure 10.25 - Variance spectra of temperature (TT), absolute humidity (aa), horizontal wind speed (uu), and vertical wind velocity (ww), scaled by the total variance σ^2 for the mixed layer derived from tethered balloon measurements. After Andreev et al. (1975).

This may occur when buoyant elements are destroyed, during their strong damping in the stable regime between the mixed and cloud layers. Besides this detail, it is interesting to note from Figure 10.26 that the moisture flux by all scales of motion is upwards in the entire mixed layer during both convection categories. The sensible heat can, in contrast, flow upwards in certain spectral bands and downwards in others.

The momentum transport (upper curves of Figure 10.26) is downwards on all scales of motion in the lowest 200m of the atmosphere. The flux reverses its sign for wavenumbers centred at $5 \cdot 10^{-2}$ m^{-1} in the suppressed mode. In the moderate convective mode at 400m height it practically points upwards throughout the entire spectrum. Although these findings cannot be satisfactorily explained, due to incomplete information on the vertical distribution of the horizontal wind velocity, the results demonstrate at least certain differences between the processes in the lower and in the upper mixed layer.

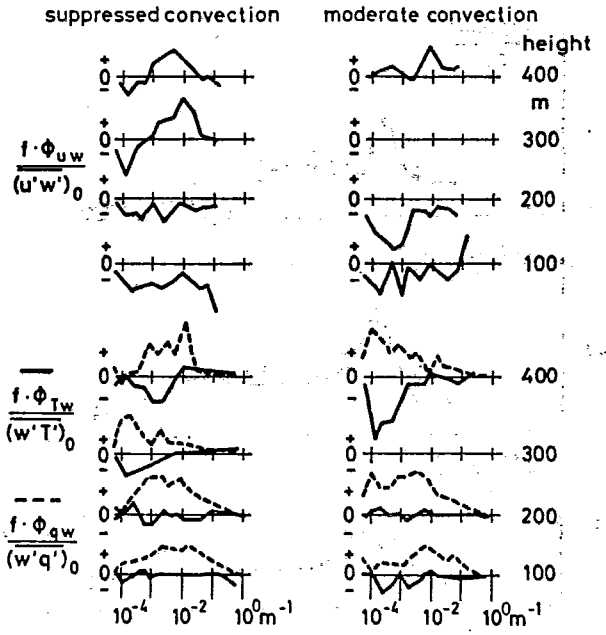

Figure 10.26 - Cospectra u'w' (upper solid curves), T'w' (lower solid curves) and q'w' (lower dashed curves) at 4 height levels in the mixed layer under suppressed and moderate convection during Phase III of GATE. The spectra are scaled by the surface fluxes. Abscissa: wavenumber in m^{-1}. After Thompson et al. (1980).

The latter impression gains further support from the acoustic echo sounder measurements of Gaynor and Mandics (1978) on the R/V OCEANOGRAPHER during all three GATE phases. The facsimile records in Figure 10.27 show, for convectively undisturbed conditions (on the lowest display), that the plume-like black signals, which start at the sea surface, weaken with height and more or less terminate at an altitude of about 300m. The change in turbulence characteristics above and below this level is also represented in Figure 10.28 in the variance of air temperature, specific humidity, and the wind velocity components derived from the aircraft measurements as well as from three-dimensional model computations by Nicholls et al. (1981).

The measured fluctuations of the horizontal wind components in the upper and lower mixed layer show a similar height dependence, as do the temperature and water vapour variances. The behaviour of the wind variances is not reproduced by the model simulation. The authors assume this difference to result from the fact that the long periods are not resolved in the computations. However, experimental field data and model products agree fairly well in the profiles of $\overline{T'^2}$, $\overline{q'^2}$ and $\overline{w'^2}$. The latter quantity has - in contrast to the other variances portrayed in Figure 10.28 - its maximum roughly in the centre of the mixed layer, and decreases to small values at the sea surface and at cloud base. Instrumental reasons for the obvious differences between the vertical profiles of the variance of the horizontal and vertical velocity variations are not very likely. Considering the variance spectra of w', Nicholls and Le Mone (1980), as well as Greenhut (1980), found that the most energetic wavelength increases from about λ_m = 200m at the 50m level to λ_m = 800m at an altitude of 250m.

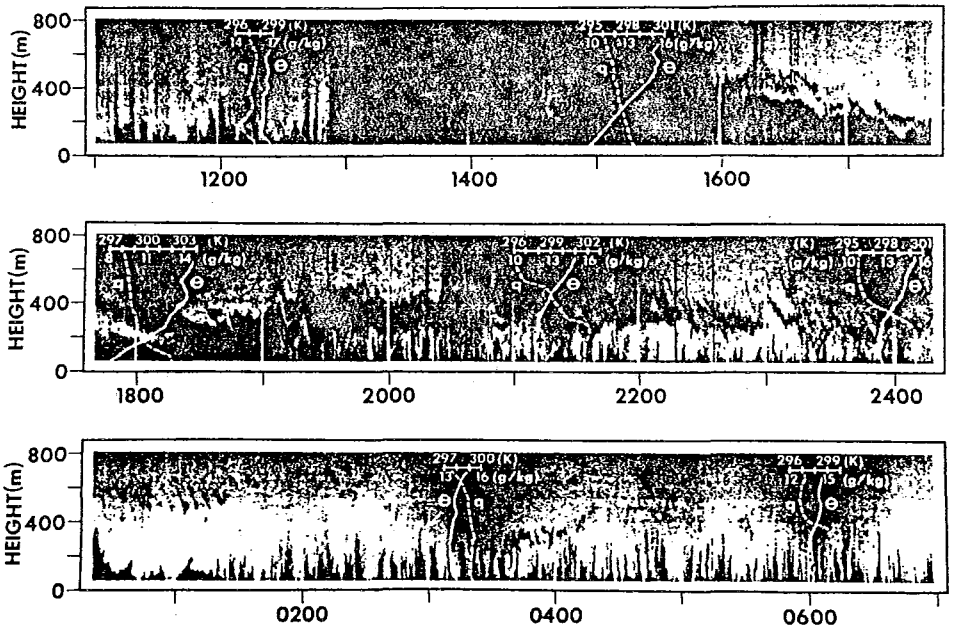

Figure 10.27 - Echo sounder facsimiles and radiosonde temperature and specific humidity profiles at the R/V OCEANOGRAPHER from the 12th to the 13th September 1971. After Gaynor and Mandics (1978).

Further upward λ_m is nearly constant with height. On the basis of this finding we conclude that the dominant scale of vertical motion grows with height in the lower positively buoyant regime of the mixed layer, and reaches its maximum near the level where the ascending air parcels become neutrally buoyant. In the upper negatively buoyant part of the mixed layer the large fast upward moving elements are superior to smaller and normally slower ones, due to lateral mixing and internal friction.

The large values of $\overline{T'}^2$, $\overline{q'}^2$, $\overline{u'}^2$ and $\overline{v'}^2$ in the upper mixed layer may result from cloud induced downdrafts, which start to mix shortly below the cloud base and do not contribute much to $\overline{w'}^2$. Although most of the quoted details are quite speculative at present, the above results qualitatively support the idea that under suppressed convection the turbulence in the lower mixed layer is dominated by effects of the lower boundary conditions on the atmosphere, while in the upper part convective mixing across the cloud base level gains increasing importance.

The situation is remarkably different in convergent regions with precipitating clouds. The acoustic sounder records, together with the radiosonde temperature and specific humidity profiles in Figure 10.27, show that the mixed layer may be totally stripped off by a squall-line-disturbance. This convective system appears in the observations at 12.50 and lasts for about three hours. Drying and cooling, especially near the sea surface and warming in the upper layer, become distinctly obvious in the profiles at 19.00 when a shallow mixed layer has formed again. It takes about eight hours until the lower atmosphere recovers to its undisturbed state. This is generally achieved by turbulent mixing from below, which has to work against a substantial subsidence in the rear of the disturbance.

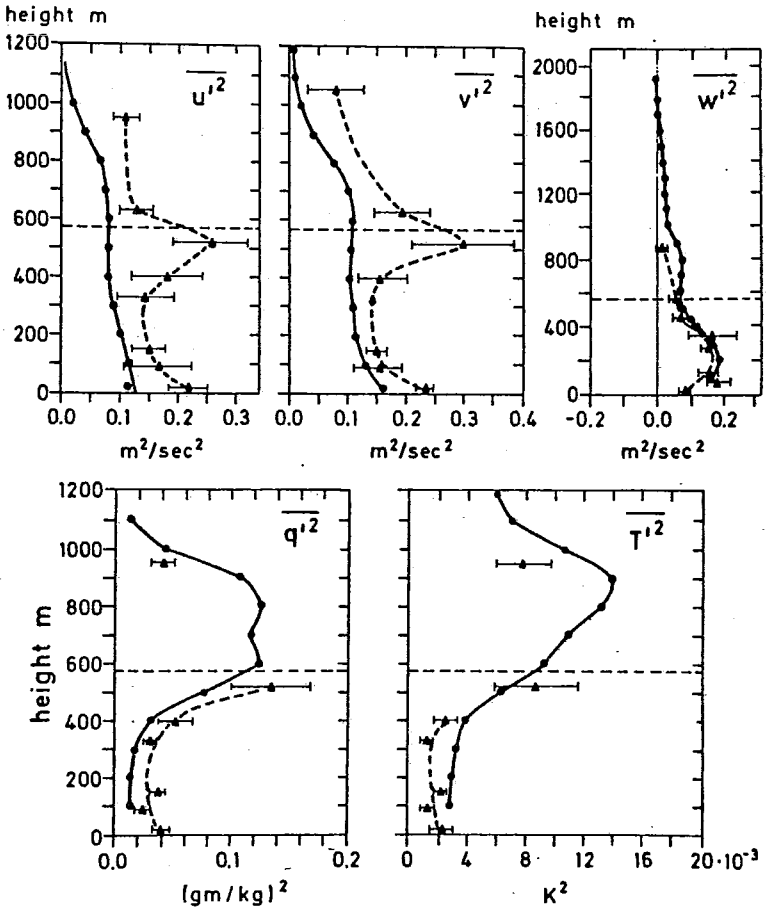

Figure 10.28 - Vertical profiles of mean variances of horizontal ($\overline{u'^2}$), ($\overline{v'^2}$) and vertical ($\overline{w'^2}$) velocity components, specific humidity ($\overline{q'^2}$), and temperature ($\overline{T'^2}$), derived from aircraft measurements (triangles) and from three-dimensional model calculations (dots). Horizontal bars indicate the standard deviation. Dashed horizontal lines: cloud base. After Nicholls et al. (1981).

Obviously, a mesoscale downward motion generally exists in the cloud free areas, even when the large-scale flow is convergent. Otherwise, the frequently detected stable transition regime between the mixed and cloud layers could not be explained as a rather permanent feature. Consequently, continuity of air mass requires that the net upward cloud flux at the cloud base overcompensates the horizontal mass inflow within the sub-cloud layer. Model calculations of Yanai et al. (1973), Nitta (1977), Johnson (1980), and Leary and Houze (1980), in fact, suggest that cloud updrafts are to a large extent balanced by downdrafts on the cloud or sub-cloud scale, as well as by mesoscale subsidence in the cloud free areas. Thus, a satisfactory understanding of the convective process and its effect on the development of the ABL requires a quantitative determination of not only the cloud updrafts, but also of the above quoted two scale regimes of downdrafts.

Augstein et al. (1979) have attempted to estimate the vertical transport of moist static energy by cloud up and downdrafts, which are superimposed on the area mean cloud upward flow. Using Emmitt's (1978) tethered balloon data and Brümmer's (1978) budget results, they concluded that about 70% of the subgrid scale vertical flux of moist static energy at the cloud base is performed by cloud related up and downdrafts on the sub-cloud scale. According to these derivations, the contribution of compensating subsidence in the cloud free area to the subgrid scale transports of energy is negligibly small. But Johnson (1980) concludes from model investigations that mesoscale subsidence, which particularly occurs in the wake of squall-lines (Zipser, 1977), may be of equal importance to the vertical exchange of thermodynamic properties as the smaller scale up and downdrafts. Further studies of the convective transports seem to be necessary in order to clarify this point of disagreement.

In spite of such uncertainties GATE studies indicate that a realistic treatment of the time development of the atmospheric state in the lower troposphere must pay attention to physical processes, which can hardly be taken care of by one-dimensional parameterization schemes. The latter seem to be restricted to diagnose some bulk modifications of the atmosphere by deep precipitating clouds and to describe the recovery of the mixed sub-cloud layer in the rear of active convection.

10.3.3 Modelling of the lower atmosphere under ITCZ conditions

Observational facts suggest that model simulation of the lower atmosphere in the presence of deep precipitating convection is critically dependent on a sufficient representation of the cloud effects on the mean properties of the lower atmosphere. Therefore, the development of parameterization methods for precipitating cumulus convection has gained high importance since several years. Yanai et al. (1973), Ogura and Cho (1973), Arakawa and Schubert (1974) and Fraedrich (1973 and 1974) have developed mass flux schemes in order to describe mainly the thermodynamic modification of the large-scale field by clouds. These concepts have been improved by Johnson (1976), Nitta (1977), and Brown (1979), who also considered the contribution of evaporatively driven downdrafts. Finally, Johnson (1980) also included a mesoscale circulation into the calculations, assuming that the updrafts in clouds are partly compensated for by downdrafts which are spread over a large area in the cloud free environment. While the above concepts are basically designed to simulate the thermodynamic properties, Moncrieff and Miller (1976) and Moncrieff (1978 and 1981) proposed models which also treat the dynamic effect of clouds on the mean atmospheric motion.

All these approaches more or less describe only the bulk influences of the entire cloud ensemble on the atmospheric state. They are not able to resolve much of the details of the vertical atmospheric structure during the passage of individual cloud systems. Such gross modifications of the sub-cloud layer thermodynamics, due to precipitation and cloud transports, have also been treated by Betts (1976) with the aid of a rather simple mass exchange principle. Guided by the results of Moncrieff and Miller (1976), he implies that the sub-cloud layer air is totally replaced by the equivalent air mass from just above the cloud base. The latter is assumed to possess the moist static energy of the air preceeding the convective disturbance. The cooling of the downdrafts by evaporative rainfall is expressed through an empirical function.

The thermodynamics of different scales of downdrafts have been considered by Betts and Silva Dias (1979). Their approach provides a means of obtaining some insight into the physics of the cloud induced mass exchange between the sub-cloud and lower cloud layers. However, it sacrifices the appealing high simplicity of Bett's (1976) former "black box" treatment.

The observational findings on the dependence of cloud growth on the large-scale low-level flow, the modification of the thermodynamics and kinematics of the sub-cloud and lower cloud layers during enhanced convection, and the recovery of the mixed layer to its unperturbed state lead us to believe that the convective schemes actually available are not sufficient to accurately predict the development of the mean properties of the lower atmosphere in the presence of deep precipitating clouds.

A one-dimensional entrainment model as proposed by Lilly (1968), has been applied by Gaynor and Ropelewski (1979) to convectively undisturbed GATE conditions and to the wake regions of deep cloud systems. Their attempt indicates that the undisturbed conditions cannot be satisfactorily monitored by such a simple model. The required extremely large mean subsidence rates of 5 to 10 cm s^{-1} would quickly lead to an imbalance of the heat and water vapour budgets of the mixed layer. The observations during GATE in contrast indicate small convergences of the low-level horizontal flow in convectively undisturbed areas of the ITCZ rather than the high divergences required by Gaynor and Ropelewski (1979). We suspect that the pure entrainment method fails, in this case, even if realistic horizontal advection of heat and water vapour could be prescribed because a considerable number of convective elements penetrates the top of the mixed layer and forms clouds. Augstein and Wendel (1980) have shown that under such conditions a large amount of the kinetic energy, generated in the mixed layer, is converted into potential energy by forcing air parcels upwards through the stable transition layer into the cloud layer. The calculations of Gaynor and Ropelewski (1979) seem to be more realistic for the wake of convective systems where no low level clouds are present. Here their subsidence rates are still high but they fall at least into the range which Zipser (1977) reports for the rear side of the squall-lines.

Fitzjarrald and Garstang (1980a) have also simulated the recovery of the mixed layer in the wake of the convective system, passing the C-array on 12 September 1974 with a quite similar entrainment model. The vertical temperature and humidity profiles related to this disturbance are delineated in Figure 10.22. The surface observations of the R/V DALLAS, the radar echo coverage, and the mixed layer horizontal velocity divergence of the C-array as well as the measured mixed layer depths at the DALLAS position are displayed on the left-hand side of Figure 10.29. The model computations were started with observed initial conditions at about 1350 GMT. This time is marked by the heavy dashed line on the left graph of Figure 10.29. The main purpose of the numerical computation was to see if the height, temperature and water vapour variations of the mixed layer can be explained by the simultaneous influence of mean subsidence through the top of the layer and of turbulent mixing from below.

The model results are shown together with the observed quantities on the right-hand side of Figure 10.29. Computations have been carried out taking again Lilly's (1968) entrainment factor k = 0.25 and prescribing the horizontal divergence by $5 \cdot 10^{-5}$ s^{-1} as obtained from the C-array data (dashed lines) as well as by a value twice as large (solid curves). The divergence was kept constant in time for seven hours and was then linearly changed to a convergence of $-6 \cdot 10^{-5}$ s^{-1} within a period of two hours. Both of the model runs achieved a reasonable qualitative simulation of the observations. A better quantitative agreement was obtained for the higher divergence rate of 10^{-4} s^{-1}. This result suggests that the local subsidence, in this situation, may be distinctly larger than the mean values for the C-array.

Independent of this uncertainty, the model calculations reproduce the initially observed negative correlation between the local time changes of temperature and water vapour in the wake area. This behaviour is primarily caused by the rapid growth of the mixed layer, which causes a strong entrainment of warm and dry air from above. The importance of the influence of the large-scale vertical motion on the mixed layer depth is quite evident in Figure 10.29. When horizontal divergence changes into convergence after eight hours of simulation, the mixed layer height rapidly increases.

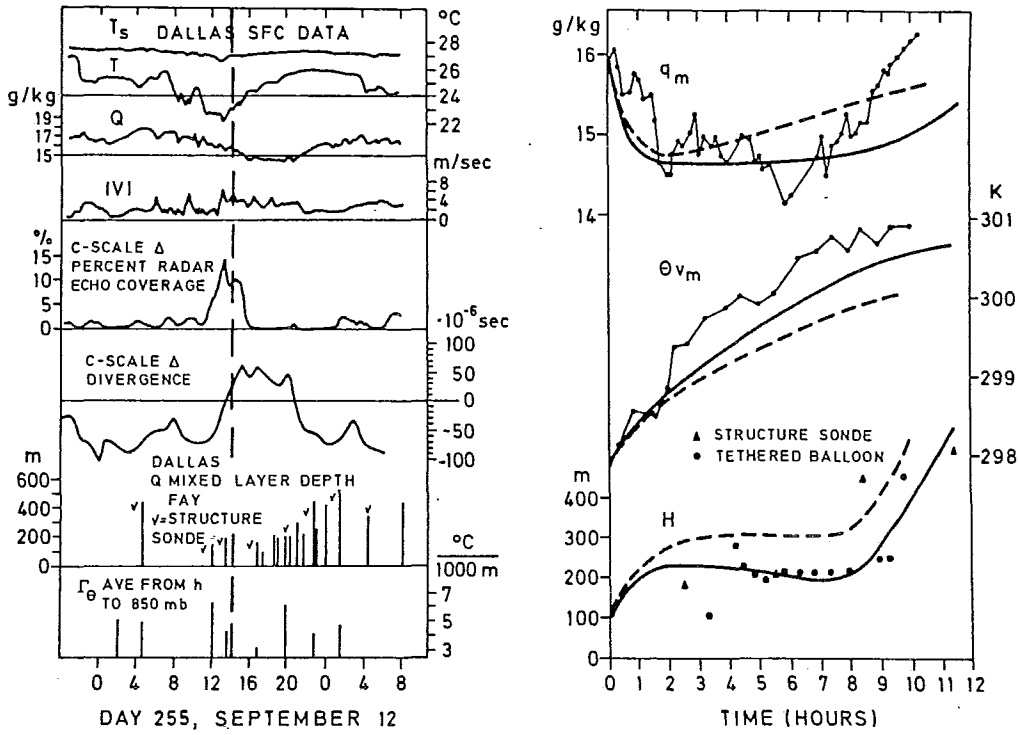

Figure 10.29 - Left side: Observed conditions during the passage of a convective disturbance at the R/V DALLAS. T_s = sea-surface temperature, T = air temperature, Q = specific humidity, V = wind speed, Γ_θ = gradient of potential temperature above the mixed layer. Dashed heavy line indicates start time of the model simulation.

Right side: Model simulation of mixed layer specific humidity q_m (upper curves), virtual potential temperature Θ_{vm} (middle) and the height of the mixed layer H (lower graph). Model values: Dashed lines for divergences = $5 \cdot 10^{-5}$ s^{-1}, heavy solid lines for divergence = 10^{-4} s^{-1}. Light full lines, circles and triangles indicate observations. After Fitzjarrald and Garstang (1980a).

During this development the top of the layer surmounts the water vapour condensation level so that low-level cumulus clouds form and the model becomes invalid. However, up to this point several observational facts are satisfactorily reproduced.

In principle, GATE measurements suggest that modifications of the large-scale low-level air flow cause changes of the vertical structure of the lower atmosphere and of the spectrum of motion in the convective and high wavenumber turbulence scale. Therefore, ideal modelling should take care of the interaction processes of the various scales of motion.

Such energy exchange mechanisms among processes of different scales have been investigated by Le Mone (1976) who studied the modulation of turbulence by longitudinal rolls. Ivanov et al. (1971) and Ivanov and Ordancvich (1973) have shown with the aid of model considerations that such variations of the turbulence characteristics in the atmospheric surface layer may be generated through roll induced mesoscale time changes of the mean flow. Since this concept is restricted to mechanical influences on the turbulence it is not sufficient for such as the GATE conditions. But it marks an interesting way of scale interaction considerations.

10.4 CONCLUSIONS

The GATE boundary layer measurements of various investigations compose a valuable data basis for the study of the influence of deep cumulus convection on the structure of the lower atmosphere. The results obtained during GATE support the following conclusions:

I. For the surface layer:

(a) The mean quantities at and near the sea surface experience considerable variations during the passage of convective disturbances.

(b) These effects lead to remarkable changes of the energy and momentum transfer across the sea surface.

(c) The shape of the co-spectra of w'O' differs considerably from those of w' q' and w' u'. Thus, it seems to be likely that near the sea surface the heat transfer is predominantly achieved by relatively small scales of motion while water vapour and momentum are much more transported by convective elements at a larger size.

(d) The parameterization of the momentum and sensible heat fluxes by the bulk aerodynamic equations with constant transfer coefficients seems to be possible if an uncertainty of $\pm$ 25% is admitted. The coefficient for water vapour has even a much larger scatter. This finding may on the one hand be attributed to deficiencies of the various instrumental procedures. But on the other hand the GATE measurements also suggest that the determination of the evaporation at the sea surface by the aerodynamic method may be rather insufficient in principle under conditions of strong cloud convection.

II. For the atmospheric boundary layer:

(a) The horizontal velocity divergence and the advection of water vapour in the lower troposphere dominantly control the development of deep cumulus convection. This relationship becomes obvious particularly during the passage of large-scale tropospheric easterly waves.

(b) The vertical mass transport by updrafts of convective clouds in the ITCZ generally overbalances the air mass supply through the large-scale horizontal flow convergence in the sub-cloud and lower cloud layers. This difference is compensated for by downdrafts on the sub-cloud and mesoscale. Each of these downward fluxes acts in a different manner on the thermodynamic state of the lower atmosphere.

Sub-cloud scale downdrafts of deep cumuli - which are mainly driven by evaporating rainfall - generally lead to a considerable cooling and a slight drying of the sub-cloud layer within short periods of time. Mesoscale subsidence seems to have its most important influence on the rear side of enhanced convective systems. Here the downward motion creates a relatively warm and dry regime in the lower atmosphere which effectively suppresses the growth of the mixed layer. Therefore, the recovery of the latter after the passage of a major cumulus cloud critically depends on the strength, duration and area coverage of the cloud induced mesoscale downdrafts.

(c) The actual processes occurring in areas covered by precipitating clouds are still vaguely known because of the breakdown of most observational tools under such environmental conditions. The measurements are mainly restricted to the description of bulk effects caused by clouds on the atmospheric state.

(d) Gross modifications of the sub-cloud layer by precipitating clouds can be reasonably reproduced by rather simple model schemes which ignore the details of the physical processes.

(e) In spite of this result it seems to be doubtful if a separate model treatment of the atmospheric boundary layer in conditions of enhanced convection is possible and useful since the clouds affect an intense coupling throughout the entire troposphere. The dominant influence of convective vertical mixing makes it practically impossible to detect a reasonable level up to which the lower boundary of the atmosphere significantly influences the air flow.

(f) Although special modelling of the lower atmosphere throughout the entire cloud cycle is not very promising periods of low convective activity and of decaying clouds can to some extent be treated even by one-dimensional boundary layer concepts. But the success of such studies is distinctly dependent on a proper prescription of the mesoscale flow characteristics.

The GATE investigations support the conclusion that a satisfactory model simulation of the lower atmosphere in cases of precipitating convection must include the three-dimensional field of motion and a rather detailed cloud parameterization.

Finally we may indicate that changes in the cloud activity can lead to distinct modifications of the sea-surface temperature which in principle might couple back on the atmospheric processes. Although this effect has not yet been adequately studied we conclude from bulk estimations that it is only of minor influence on time scales of convection. But it may gain importance on larger time periods.

ACKNOWLEDGEMENTS

This chapter has been reviewed partly by J. Businger and H. Charnock (The surface layer) and partly by C. Readings and G. Sommeria (The structure of the atmospheric boundary layer ...). We are grateful to all of these colleagues for valuable comments and suggestions which have lead to improvements and completion of our text. We are indebited to C. Johnson and E. Graber for their assistance during the preparation of the English text and to B. Zinecker for typing the manuscript.

REFERENCES

Albrecht, B.A., A. K. Betts, W. H. Schubert and S. K. Cox, 1979: A model of the thermodynamic structure of the trade-wind boundary layer: Part I. Theoretical formulation and sensitivity tests. J. Atm. Sci., 36, 73-89.

Andreev, V. D., V. N. Ivanov, V. C. Korolev, V. M. Linkin, T. F. Masagutov, A. V. Smirnov and Y. Holtz, 1975: The results of direct measurements of turbulent characteristics for the planetary boundary layer. GATE Rep., 14, I, 233-244, WMO, ICSU.

Antsipovich, V. A., A. I. Snitkovsky and A. I. Falkovich, 1975: On the order of values of the meteorological elements obtained in the A/B-array in the period of GATE. GATE Rep., 14, II, 99-116, WMO, ICSU.

Arakawa, A. and W. H. Schubert, 1974: Interaction of cumulus cloud ensemble with the large-scale environment, Part I, J. Atm. Sci., 31, 674-701.

Augstein, E., 1979: The atmospheric boundary layer over the tropical oceans. Meteorology over the tropical oceans. R. Met. Soc. Bracknell, edited by D. B. Shaw, 73-104.

_____ and M. Wendel, 1980: Modelling of the time dependent atmospheric boundary layer with non-precipitating cumulus clouds. Beitr. Phys. Atm., 53, 509-538.

_____, M. Garstang and G. D. Emmitt, 1979: Vertical mass and energy transports by cumulus clouds in the tropics. Deep Sea Research, 26, Supplement, Vol. 1, 9-21.

Barnes, G., 1977: In: Report of the U.S. Central Program Workshop, Boulder, Colorado, p. 453.

Betts, A. K., 1973: Non-precipitating cumulus convection and its parameterization. Quart. J. R. Met. Soc., 99, 178-196.

_____, 1976: The thermodynamic transformation of the tropical subcloud layer by precipitation and downdrafts. J. Atm. Sci., 33, 1008-1020.

_____, 1976a: Modelling the subcloud layer structure and interaction shallow cumulus layer. J. Atm. Sci., 33, 2363-2382.

_____ and M. F. Silva Dias, 1979: Unsaturated downdraft thermodynamics in cumulonimbus. J. Atm. Sci., 36, 1061-1071.

Bougeault, P., G. Sommeria and J. C. André, 1979: Méthode de modélisation unidimensionnelle de la couche limité planetaire nuageuse. Comparison avec un modéle tridimensionnel. J. Rech. Atm., 13, 243-259.

Brook, R. B., 1978: The influence of water vapour fluctuations on turbulent fluxes. Bound. Layer Met., 15, 481-487.

Brown, R. A., 1970: A secondary flow model for the planetary boundary layer. J. Atm. Sci., 27, 742-757.

Brown, J. M., 1979: Mesoscale unsaturated downdrafts driven by rainfall evaporation: a numerical study. J. Atm. Sci., 36, 313-338.

Brümmer, B., 1978: Mass and energy budgets of a 1 km high atmospheric box over the GATE C-scale triangle during undisturbed and disturbed weather conditions. J. Atm. Sci., 35, 997-1011.

_____, 1979: Boundary layer processes during the life cycle of GATE convective disturbances. Beitr. Phys. Atm., 52, 306-330.

Bunker, A. F., B. Haurwitz, J. S. Malkus and H. Stommel, 1949: Vertical distribution of temperature and humidity over the Caribbean Sea. Pap. Phys. Ocean. Met., Mass. Inst. Rech. and Woods Hole Ocea. Inst., 1-82.

Charney, J. and A. Eliassen, 1964: On the growth of the hurricane depression. J. Atm. Sci., 21, 68-75.

Deardorff, J. W., 1976: On the entrainment rate of a strato-cumulus topped mixed layer. Quart. J. R. Met. Sci., 102, 563-582.

_____, 1980: Cloud top entrainment instability. J. Atm. Sci., 37, 131-147.

_____, 1981: On the distribution of mean radiative cooling at the top of a strato-cumulus capped mixed layer. Quart. Roy. Met. Soc., 107, 191-202.

Elagina, L. G., B. M. Koprov and Yu. A. Volkov, 1974: Spectra and cospectra of the turbulent fluctuations of the velocity, temperature and humidity in the boundary layer over the ocean. GATE Rep., 2, WMO/ICSU.

_____, _____ and _____, 1978: Investigation of turbulent heat exchange between atmosphere and ocean in the Equatorial Atlantic. Proc. Int. Sci. Conf. on the Energ. of the Trop. Atm. Tashkent, WMO Publication, 113-118.

Emmitt, G. D., 1978: Tropical cumulus interaction with and modification of the sub-cloud region. J. Atm. Sci., 35, 1485-1502.

Etling, D., 1972: Einfluss der thermischen Schichtung auf die Stabilität der Ekman'schen Grenzschichtströmung. Beitr. Phys. Atm., 44, 560-576.

Fitzjarrald, D. R. and M. Garstang, 1980: Vertical structure of the tropical boundary layer. Submitted to Month. Weath. Rev.

_____ and _____, 1980a: Boundary-layer growth over the tropical ocean. Submitted to Month. Weath. Rev.

Fraedrich, K., 1973: On the parameterization of cumulus convection by lateral mixing and compensating subsidence: Part I, J. Atm. Sci., 30, 408-413.

_____, 1974: Dynamic and thermodynamic aspects of the parameterization of cumulus convection: Part II, J. Atm. Sci., 31, 1838-1849.

Galushko, V. V., V. N. Ivanov, I. V. Nekrasov, V. D. Pudov, A. V. Rostkov, A. S. Shushkov, 1975: Turbulent characteristic measurements in the marine boundary layer during GATE. ICSU/WMO. GATE Rep. No. 14, V. II, pp. 237-261.

_____, _____, T. F. Masagutov, V. V. Nekrasov and A. V. Rostkov, 1978: Experimental investigations of the atmospheric boundary layer structure in the tropical latitudes. Proceedings of Int. Sc. Conf. on the Energetics of the Trop. Atm., Tashkent 1977, WMO/ICSU, Geneva, 89-106.

Gaynor, J. E. and Ch. F. Ropelewski, 1979: Analysis of the convectively modified GATE boundary layer using in situ and acoustic sounder data. Month. Weath. Rev., 107, 985-993.

_____ and P. A. Mandics, 1978: Analysis of the tropical marine boundary layer during GATE using acoustic sounder data. Month. Weath. Rev., 106, 223-232.

Gorodetzky, A. K., A. P. Orlov, A. I. Pashkov, V. N. Stoliarov, 1974: The relation between radiation and kinetic temperature of the surface layer water. TROPEX 1872, Gidrometeoizdat, 511-519, Leningrad.

Grassl, H. and H. Hinzpeter, 1975: The cool skin of the ocean. GATE Rep. 14, 2, 229-236, WMO, ICSU.

Greenhut, G. K., 1980: Analysis of aircraft measurements of momentum flux in the sub-cloud layer over the tropical Atlantic Ocean during GATE. Boundary Layer Dynamics Group, NOAA/ERL, Boulder, Colorado 80303.

Günther, H., 1977: Spectral studies of disturbed and undisturbed situations with surface data in the GATE B- and C-scale. "Meteor" Forsch.-Ergb., B.12, 16-22.

_____, 1980: A convective mesoscale wave disturbance during GATE investigated by spectral methods. Beitr. Phys. Atm., 53, 74-89.

Hasse, L., M. Grünewald, J. Wucknitz, M. Dunckel and D. Schriever, 1978: Profile derived turbulent fluxes in the surface layer under disturbed and undisturbed conditions during GATE. "Meteor" Forsch.-Ergeb. B.13, 24-40.

Ivanov, V. N., A. E. Ordanovich and L. I. Petrova, 1971: Large-scale structure and its interaction with small-scale turbulence in the atmospheric surface layer. Izv. Atmospheric and Oceanic Physics Vol. 7, No. 3, 263-269.

_____ and _____, 1973: Mesoscale structure of the atmospheric boundary layer and its interaction with small-scale turbulence. Izv., Atmospheric and Ocean Physics, Vol. 9, No. 7, 685-698.

_____, M. A. Petrossiants, L. T. Myach and A. V. Nesterova, 1973: Certain characteristic time scales of the variation of meteorological elements in the Intertropical Convergence and Trade Zones. Izv. Atm. Ocean. Phys., 10, 1138-1147 (Engl. edit.).

_____ and L. Kh. Ingel, 1976: A simplified model of the trade-wind belt inversion. TROPEX-74, Vol. I, Gidrometeoizdat, 261-267, Leningrad.

Jacobs, C. A., 1979: Mean diurnal and shorter period variations in the air-sea fluxes and related parameters during GATE. Deep Sea Res., Supplement to Vol. 26, 65-98.

Jalickee, J. B. and Ch. F. Ropelewski, 1979: An objective analysis of the boundary-layer thermodynamic structure during GATE. Part I, Method. Month. Weath. Rev., 107, 68-76.

Johnson, R. H., 1976: The role of convective scale precipitation downdrafts in cumulus and synoptic-scale interactions. J. Atm. Sci., 33, 1890-1910.

_____, 1978: Characteristic structure and growth of the non-precipitating cumulus layer over South Florida. Month. Weath. Rev., 106, 1495-1504.

_____, 1980: Diagnosis of convective and mesoscale motions during Phase III of GATE. J. Atm. Sci., 37, 733-753.

Kahn, P. H. and J. A. Businger, 1979: The effect of radiative flux divergence on entrainment of a saturated convective boundary layer. Quart J. R. Met. Soc., 105, 303-306.

Khalsa, S. J. S. and J. A. Businger, 1977: The drag coefficient determined by the dissipation method and its relation to intermittent convection in the surface layer. Bound. layer Met., 12, 273-297.

Krauss, H. and E. Schaller, 1978: A note on the closure of Lilly-type inversion models. Tellus, 30, 284-288.

Krishnamurti, R., 1975: On cellular cloud patterns, Part I to Part II, J. Atm. Sci., 32, 1354-1383.

Leary, C. A. and R. A. Houze, 1980: The contribution of mesoscale motions to the mass and heat fluxes of an intense tropical convective system. J. Atm. Sci., 37, 784-796.

Le Mone, M. A., 1976: Modulation of turbulence energy by longitudinal rolls in an unstable planetary boundary layer. J. Atm. Sci., 33, 1308-1320.

Lilly, D. K., 1966: On the stability of Ekman boundary flow. J. Atm. Sci., 23, 481-494.

_____, 1968: Model of cloud-topped mixed layers under a strong inversion. Quart J. R. Met. Soc., 94, 292-309.

Mahrt, L., 1979: Penetrative convection at the top of a growing boundary layer. Quart. J. R. Met. Soc., 105, 469-485.

Malkus, J. S., 1958: On the structure of the trade wind moist layer. Pap. Ocean. Met., Mass. Inst. Tech. and Woods Hole Inst., 13, No. 2, 1-48.

Mandics, P. A., F. F. Hall and E. J Owens, 1975: Preliminary results of acoustic echo sounding of the marine boundary layer during GATE. GATE Rep., 14, 2, 225-228, WMO, ICSU.

Miller, M. J. and A. K. Betts, 1977: Travelling convective storms over Venezuela. Month. Weath. Rev., 105, 833-848.

Moncrieff, M. W., 1978: The dynamical structure of two-dimensional steady convection in constant vertical shear. Quart. J. R. Met. Soc., 104, 543-567.

_____, 1981: A theory of organized steady convection and its transport properties. Quart. J. Roy. Met. Soc., 37, 148-159.

_____ and M. J. Miller, 1976: The dynamics and simulation of tropical cumulo-nimbus and squall-lines. Quart. J. Roy. Met. Soc., 102, 373-394.

Müller-Glewe, J. and H. Hinzpeter, 1975: Turbulent fluxes in the ITCZ during GATE Phase III at station 27. GATE Rep., 14, 1, 224-232, WMO, ICSU.

Neiburger, M., D. S. Johnson and C. W. Chien, 1961: Studies of the structure of the atmosphere over the eastern Pacific Ocean in Summer. I. The inversion over the eastern North Pacific Ocean. Univ. of California Press, Berkeley.

Nicholls, S. and C. Readings, 1979: Aircraft observations of the structure of the lower boundary layer over the sea. Quart. J. Roy. Met. Soc., 105, 785-802.

Nicholls, S. and M. A. Le Mone, 1980: The fair weather boundary layer in GATE: The relationship of subcloud fluxes and structure to the distribution and enhancement of cumulus clouds. J. Atm. Sci., 37, 2051-2067.

_____, _____ and G. Sommeria, 1981: The simulation of a fair weather marine boundary layer in GATE using a three-dimensional model. Quart. J. R. Met. Soc. (in print).

Nitta, T. N., 1977: Response of cumulus updraft and downdraft to GATE A/B-scale motion system. J. Atm. Sci., 34, 1163-1186.

Ogura, Y., J. Russel and H. R. Cho, 1977: A semi-empirical model of the trade wind inversion. J. Met. Soc. Japan, 55, No. 5, 209-222.

_____ and H. R. Cho, 1973: Diagnostic determination of cumulus populations from large-scale variables. J. Atm. Sci., 30, 1276-1286.

Petrossiants, M. A., A. I. Snitkovsky and A. I. Falkovich, 1975: On the evolution of the Inter Tropical Convergence Zone. GATE Rep., 14, I, 12-28, WMO/ICSU.

Phelps, G. T. and S. Pond, 1971: Spectra of temperature and humidity fluctuations and of the fluxes of moisture and sensible heat in the marine boundary layer. J. Atm. Sci., 28, 918-928.

Randall, D. A., 1980: Conditional Instability of the First Kind Upside Down. J. Atm. Sci., 37, 125-130.

Reed, R. J. and E. E. Recker, 1971: Structure and properties of synoptic-scale wave disturbances in the equatorial western Pacific. J. Atm. Sci., 28, 1117-1133.

Reeves, R. W., Ch. F. Ropelewski and M. Hudlow, 1979: Relationships between large-scale motion and convective precipitation during GATE. Month. Weath. Rev., 107, 1154-1168.

Reger, J., 1927: Der Südostpassat. Beitr. Phys. Freien Atm., 13, 59-63.

Reinking, R. F., 1979: Vertical eddy motion and energy transfer at very low altitudes over the tropical Atlantic ocean. Deep Sea Research, 26, Supplement, Vol. 1, 23-50.

Riehl, H., C. Yeh, J. S. Malkus and N. E. La Seur, 1951: The north-east trade of the Pacific Ocean. Quart. J. R. Met. Soc., 77, 598-626.

_____, G. Greenhut and B. R. Bean, 1978: Energy transfer in the tropical subcloud layer measured with DC-6 aircraft during GATE. Tellus, 30, 524-536.

Schott, F. and J. Fernandez-Partagas, 1980: On the onset of the summer monsoon during the FGGE 1979 Experiment off the East African Coast: A comparison of wind data collected by different means. Submitted to J. Phys. Oc.

Schubert, W. H., 1976: Experiments with Lilly's cloud-topped mixed layer model. J. Atm. Sci., 33, 436-446.

Seguin, W. R. and M. Garstang, 1976: Some evidence of the effects of convection on the structure of the tropical subcloud layer. J. Atm. Sci., 33, 660-666.

Sommeria, G., 1976: Three-dimensional simulation of turbulent processes in an undisturbed trade wind boundary layer. J. Atm. Sci., 33, 216-241.

Sommeria, G. and J. W. Deardorff, 1977: Subgrid-scale condensation in models of non-precipitating clouds, J. Atm. Sci., 34, 344-355.

Thompson, R. M., S. W. Payne, E. E. Recker and R. J. Reed, 1979: Structure and properties of synoptic-scale wave disturbances in the Inter Tropical Convergence Zone of the Eastern Atlantic. J. Atm. Sci., 36, 53-72.

Thompson, N., K. L. Webber and B. P. Norris, 1980: Eddy-fluxes and spectra in the GATE sub-cloud layer. Quart. J. R. Met. Soc., 106, 277-292.

Veyre, P., G. Sommeria and Y. Fouquart, 1980: Modélisation de l'effet des hétérogénéités du champ radiatif infra-rouge sur la dynamique des nuages. J. Rech. Atm., 14, 89-108.

Volkov, Yu. A., L. G. Elagina, B. M. Koprov and T. K. Kravchenko, 1974: Turbulent fluxes of heat and moisture and some statistical characteristics of turbulence in the surface layer of atmosphere in the tropical zone of the Atlantic. TROPEX-1972, Gidrometeoizdat, Leningrad, pp. 305-312.

_____, _____, _____, B. A. Semenchenko, E. M. Feigelson, 1976: Heat and moisture exchange on the Equator. TROPEX-1974, Vol. 1, Gidrometeoizdat, Leningrad.

_____, A. S. Ginzburg, L. G. Elagina, E. T. Irshov, D. T. Matveev, B. M. Koprov, V. N. Kapustin, E. M. Kozlov, A. P. Orlov, S. M. Piragov, E. M. Feigelson, A. Kh. Shukurov, 1978: Investigation of heat fluxes in dependence on the determining factors in the Equatorial Zone of the Atlantic. Proc. Int. Sci. Conf. on the Energ. of the Trop. Atm. Tashkent, ICSU/WMO Publication, 149-154.

Wakefield, J. S. and W. H. Schubert, 1976: Design and execution of the marine stratocumulus experiment. Atm. Sc. Paper No. 256, Dept. Atm. Sci., Colorado State Univ., Fort Collins.

Yamada, T. and G. L. Mellor, 1979: A numerical simulation of BOMEX data using a turbulence closure model coupled with ensemble cloud relations. Quart J. R. Met. Soc., 105, 915-944.

Yanai, M., S. Esbensen and J.-H. Chu, 1973: Determination of bulk properties of tropical cloud clusters from large-scale heat and moisture budgets. J. Atm. Sci., 30, 611-627.

Zipser, E. J., 1969: The role of organized unsaturated convective downdrafts and the structure and rapid decay of an equatorial disturbance. J. Appl. Met., 8, 799-814.

_____, 1977: Mesoscale and convective-scale downdrafts as distinct components of squall-line structure. Month. Weath. Rev., 105, 1568-1589.

CHAPTER 11

RADIATION PROCESSES AND THEIR PARAMETERIZATION

by
E. M. Feigelson
(Institute of Atmospheric Physics, Academy of Sciences of the USSR, Moscow, USSR) sections 11.2-11.7*
and
K. Ya. Kondratyev and M. A. Prokofyev
(Main Geophysical Observatory, Leningrad, USSR) sections 11.8-11.10

11.1 INTRODUCTION

Objectives of the GATE Radiation Sub-Programme

GATE radiation studies constituted a separate Radiation Sub-Programme (RSP), since radiation is the primary source of energy generating and sustaining the atmospheric motions and evolution of weather systems. On the other hand, the minute details of this mechanism are still not quite understood, notwithstanding a number of successful attempts to incorporate the radiative processes into models of atmospheric dynamics. Therefore, the main objective of GATE being "to determine the mechanism of tropical convection and its interaction with the large-scale circulation", the two principal objectives of the GATE RSP were formulated as follows:

a) to determine the vertical profiles of radiative fluxes and of radiative temperature changes at the time and space resolution of the B and C-scale in dependence on principal parameters such as distribution of clouds and aerosol particles, there by providing an essential factor required to study the formation of tropical cumulus convection and the larger cluster phenomena;

b) to determine the net radiation and its components at the ocean surface in the B-scale area, since these parameters are essential for air-sea interaction studies and for objectives of the Boundary Layer and Oceanographic Sub-Programmes.

Moreover, "the accompanying radiation experiments" were envisaged aimed at studying the radiative properties of cloudiness, aerosol, improving the remote sensing techniques, etc.

It was expected that radiative effects generated in the dust layers associated with Saharan air outbreaks into the ocean could be important in affecting the build-up (blocking) of convection. Similar ideas stimulated the studies of the cloud-induced radiative cooling.

The attainment of the first of the RSP objectives required the vertical profiles of radiative fluxes and flux divergences to be determined with the spatial-temporal resolution corresponding to the B and C-scales of the GATE area:

t = 6-12 hours

p = 200 mb

$y = x$ = 100-500 km

in dependence of such principal factors as cloudiness distribution, aerosol number density, etc.

The second RSP objective called for determining the components of the surface radiation balance with the same spatial-temporal resolution. The state of art in radiation measurement techniques was decisive in choosing the vertical resolution p = 200 mb, which corresponded to approximately 10% relative error in characteristic

* Section 11.1 prepared jointly by all three authors

radiative warming of the atmospheric layer of 2°C/day and to an absolute error in the total radiative heat flux divergence of about 5 W/m^2.

The final result of implementing the GATE RSP should have been the construction of 4-D radiative heat flux divergence distributions over the GATE area in the chosen spatial-temporal scales under different characteristic conditions. The elementary calculation showed that even the most effective management of all the observational platforms available for GATE could not give more than 16% of the data needed for this task. Therefore, starting from the experiment planning stage, the question was risen of designing techniques for parameterizing the "sub-grid" (in the sense of the above scales) processes.

Three principal ways for such parameterization have been suggested: i) pure interpolation; ii) calculation of radiative characteristics followed by testing of the results against direct observational data; iii) working out of a parameterization scheme based on all the available primary and auxiliary data with further computation of radiative characteristics. The latter two more flexible techniques are more promising in accounting actual physical conditions.

Thus, in accordance with the structure of the main GATE RSP objectives, the analyses of the RSP results can be divided into:

a) studies aimed at solving the main RSP problem, including the dynamics of the tropical atmosphere, the radiation-cloudiness interaction, and modelling the properties of tropical cloudiness;

b) radiative measurements at the ocean surface and in the free atmosphere during GATE;

c) studies aimed at constructing the spatial-temporal distribution of radiative fluxes and flux divergences;

d) special radiative studies.

The GATE RSP results are reflected in this Chapter as much as possible in all listed problems.

11.2 RADIATION BALANCE AT THE SEA SURFACE

During expeditions TROPEX-72 and GATE-74 the standard actinometry was carried out on board of all the USSR ships (6 ships in 1972 and 13 ships in 1974). The integral fluxes of the direct and total solar radiation were measured in the day-time; the net or the downward atmospheric heat radiation fluxes was measured in the night-time. These fluxes for day-time were calculated (see below). On several ships the long-wave radiation was measured during day-time, with non-standard instruments. Aerosol-optical and cloud observational programmes were implemented which allowed study of the relation of near sea surface radiation components to atmospheric conditions. The averaged values of the radiation fluxes are shown on Figs.11.1-2, Tables 11.1-2 taken from Voitova (1980). The data were collected during the expeditions

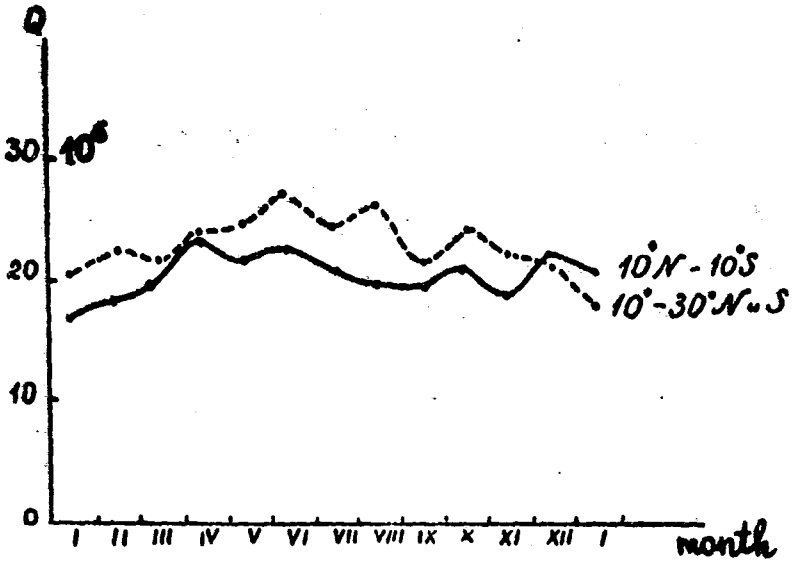

Fig.11.1a. Average daily sums of global solar radiation in J /m^2day

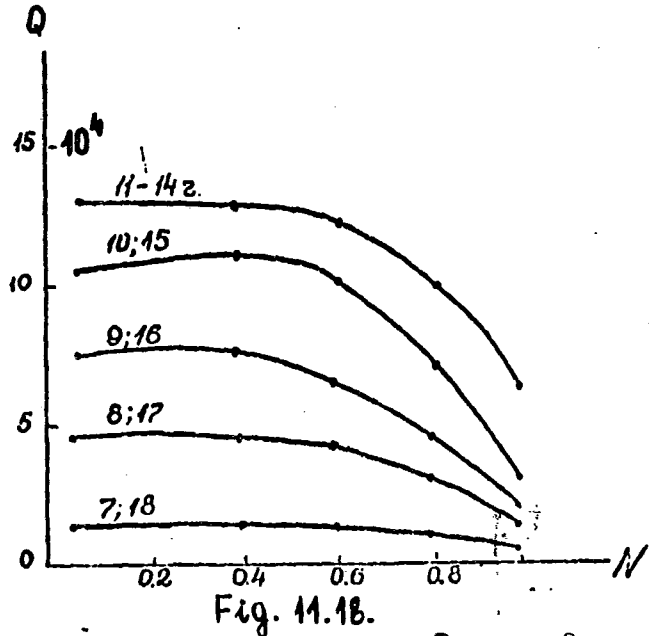

Fig. 11.1b.

Fig.11.2.

Fig.11.1b - Hourly sums of Q in J/m^2h versus cloud amount; numbers at the curves denote the observation local time. (Voitova,1980)

Fig.11.2 - Time variation (local time) of the integral albedo of the ocean; Curve 1 - N=0.0; 2 - N=0.1-0.3; 3 - N=0.4-0.6; 4 - N=0.7-0.9; 5 - N=1.0 (Voitova,1980).

"Polygon-70"*, TROPEX-72, GATE-74 and supplemented by additional observations from the USSR research ships.

Table 11.1. Frequency distribution of daily sums of the net thermal radiation. Column (1) ITCZ, (2) - outside ITCZ.

F(0) J/m^{2}day	% (1)	% (2)
(0-98) 10^4	1	0
98-196	9	0
196-294	40	16
294-392	31	16
392-490	16	9
490-588	3	34
588-686	0	20
686-784	0	5

Table 11.2. Frequency distribution of hourly sums of the net radiation. Columns (1), (2) and (3) refer to 0°; 5.0-7.5°N and 3-16,5°N, respectively

F(0) J/m^{2}day	% (1)	% (2)	% (3)
(0.0-2.5) 10^4	0	1	4
2.5-7.4	1	14	14
7.4-12.3	19	16	44
12.3-17.2	24	34	33
17.2-22.1	18	30	4
22.1-27.1	23	4	1
27.1-31.9	9	1	0
31.9-36.8	6	0	0

*This 6 month expedition in the oceanic area 14-17°N, 31-35°W started in February 1970 on board "Acad. Kurchatov" and "Dmitry Mendeleev".

The averaged field of Q flux within the GATE area is presented on Fig. 11.3 from Semenchenko and Kislov (1978).

The USSR ship "Semen Dezhnev" made 6 meridional cross-sections within the area: 13°N-9°S, 30°W-23°W. From the actinometric and meteorological data obtained the heat budget on the ocean's surface was computed (Belevich, 1976):

$$T = Q - R - F(0) - F_T - F_e \qquad (11.1)$$

The first two terms have been measured, the third calculated (see below). The two last fluxes have been approximated with the "bulk" formulae. The budget T is presented on Fig. 11.4. The extrema of T on Fig.11.4 are in agreement with direct measurements (see Table 11.16). Estimates of the budget T were given also by Grassl (1977).

Recently, Galindo (paper at the Int. Conf. on Scientific Results of GATE, Kiev, USSR 17-23 Sept. 1980) has performed the spectral analysis of net radiation, temperature, rainfall based on hourly values from some GATE ships. Nearly the same harmonics have been revealed in all the three cases. The range of oscillations covers those of mesoscale (squall lines, cloud clusters, synoptic (easterly waves) and planetary scale up to periods of 10-15 days (Fig. 11.5).

11.2.1 Empirical formulae

Empirical formulae for fluxes of the total solar radiation Q and the heat radiation $F_\downarrow(0)$ and $F(0)$ are widely used in practice. The relation of $F_\downarrow(0)$ to the total cloud amount N for prevailing air temperature at the sea surface 25-27°C and vapour pressure 25-30 mbar was presented in the form (Egorov, 1976):

$$F_\downarrow(0) = 400\,(1 + 0.16\,N^2)\ \frac{W}{m^2} \qquad (11.2)$$

and the relation to the temperature and to the amount of lower clouds N_L in the form (Bartenjeva et al., 1974).

$$F_\downarrow(0) = 0.936\,\sigma T(0)^4\,(1 + 0.05\,N_L) \qquad (11.3)$$

Both formulae show a weak dependence of $F_\downarrow(0)$ on the cloud amount and an approximate equality to $\sigma T^4(0)$ due to the high humidity of the tropical atmosphere. This result is supported by the emissivity values of the equatorial atmosphere given in Table 11.3 (Semenchenko and Nekrasov, 1974).

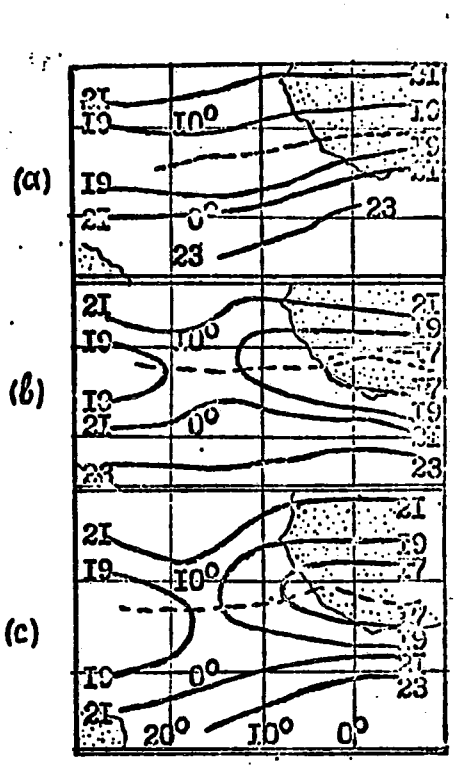

Fig. 11.3

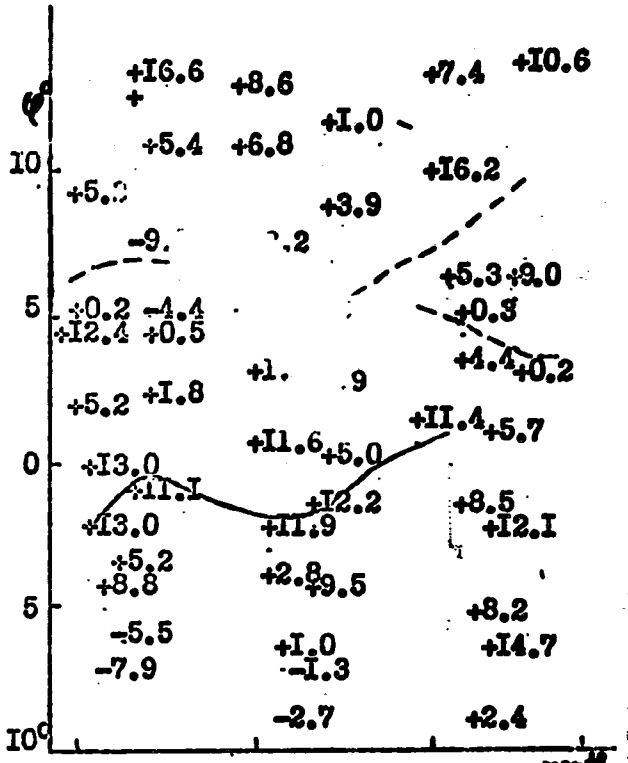

Fig. 11.4

Fig.11.3 - Daily mean values of Q in $J/m^2 day 10^6$. The dashed lines indicate the center position of the ITCZ averaged for the respective phase: a),b) and c) correspond to Phase I,II, and III. (Semenchenko and Kislov 1978)

Fig.11.4 - Surface heat balance $\bar{T}$ J/m^2 day 10^6: curves are T_{max} and T_{min} (Belovich,1978).

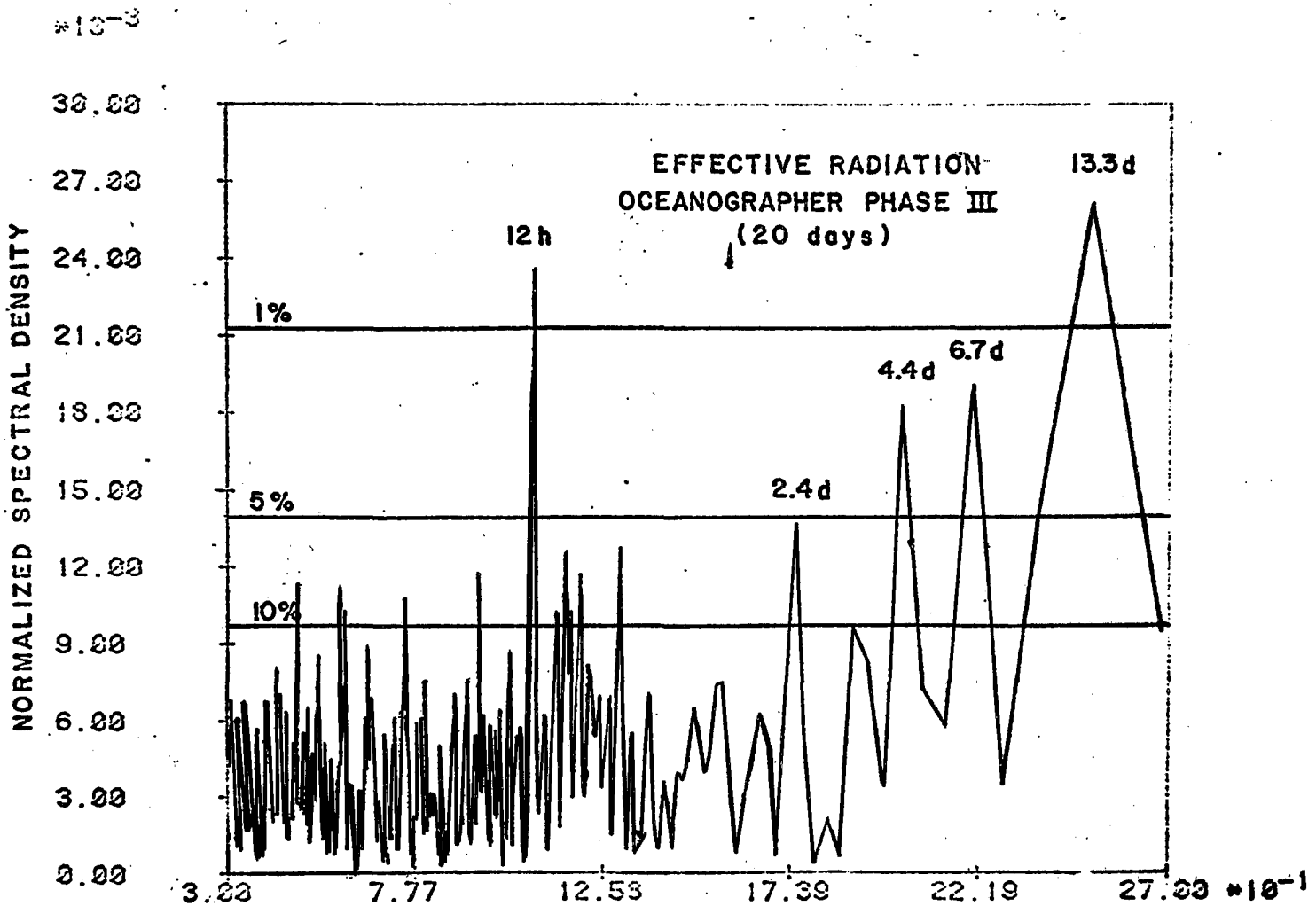

Fig.11.5 - Spectral density of the flux F(0).
(according to Galindo, paper at Kiev Conference, 1980)

Table 11.3. Emissivity $E = \frac{F_{\uparrow}(0)}{\sigma T^4(0)}$

Phase \ N	0.0-0.2	0.3-0.4	0.5-0.6	0.7-0.9	1.0
I	0.91-92	0.93	0.94	0.95	0.96
II	0.86-87	0.88-89	0.90-91	0.92-93	0.94

The higher humidities found in the tropical latitudes ($\varphi > 5°N$) increase E even more.

The connection of net radiation with the water vapour content was described as follows (Ginzburg et al., 1976):

$$F(0) = 174 - 21\, m_V \frac{W}{M^2} \qquad (11.4)$$

with $m_V = 3\text{-}5\ g/cm^2$

A semi-empirical equation was derived (Ginzburg, 1977):

$$F(0) = \Delta B + B(0)\left[\frac{a}{e(0)} - bN\right] \qquad (11.5)$$

where

$$\Delta B = B_s - B(0);\ B_s = \sigma T^4;\ B(0) = \sigma T(0)^4;\ a \approx 3;\ b \approx 0.5$$

The solar energy input per hour Q in relation to cloud amount and to the Sun elevation is described by Kirillova and Egorov (1977); Egorov and Kirillova (1979) as follows:

$$Q = Q_0 (\sin h)^{1.2} - a (\sin h)^b N^3 \qquad \text{with } Q_0 = 1 \frac{kV}{M^2} \qquad (11.6)$$

The coefficients a and b are given in Table 11.4 together with the relative error of the approximation σ.

Table 11.4. Coefficients a, b and σ

Clouds	a	b	σ	Clouds	a	b	σ
C_i	0.05	0.70	15	Sc	0.48	1.10	26
Ac	0.24	0.70	19	Cb	0.66	1.15	58
Cu	0.85	1.15	17				

Polavarapu (1979) derived regression equations between the radiative budget and its components:

$$B = a_1 Q + b_1 = a_2 (Q-R) + b_2 = a_3 [Q + F_\downarrow(o)] + b_3 \qquad (11.7)$$

The coefficients of these equations given in Table 11.5 are derived from measurements on board "Quadra"; a_i and b_i are the same for all phases of GATE for morning and evening hours. The standard error in all cases is less than 2%.

Table 11.5. The mean values of a_i and b_i (in $10^4 J/m^2 h$) in (11.7)

a_1	b_1	a_2	b_2	a_3	b_3
0.95	-17	0.98	-146	0.99	-168

This technique turns out to be successful due to the predominance of the flux Q in the budget. Equations (11.7) are useful for the reconstruction of the unmeasured components if the budget is measured.

11.2.2 Radiation in cumulus cloud conditions

On board ships "Acad. Kurchatov", "Acad. Korolev", "Ernst Krenkel" the special cloud tracing programmes were carried out for the statistical analysis of the cloud field and its relation to the radiation field (Djubkin et al., 1978; Kuusk et al., 1978; Abramov et al., 1976). It was found that the statistical characteristics of these fields can be described by the same formulae as in the middle latitudes (see Ross , 1972). The model parameters are different in ITCZ in trade-wind zones and in the middle latitudes.

In the North-East trade-wind region (φ = 13°N, ship "Acad. Korolev") as compared with the middle latitudes:

a. The sizes of Cu clouds are smaller by 30% on average with well pronounced trade-winds with the trade inversion and $N \leq 0.6$. These sizes are larger by 50% (as compared with middle latitudes) if the inversion weakens and the convection is a penetrative one ($N \geq 0.6$).

b. Cu clouds are less opaque and attenuate the solar radiation-less.

c. The input of high harmonics in the variability spectrum of Q is larger due to the smaller scattered radiation.

Some results of the investigations carried out on board the ships "Acad. Korolev" and "Ernst Krenkel" are presented on Figs. 11.6-8. The frequency distribution function of Q -flux in the cumulus cloud conditions is bi-modal as is found in the middle latitudes. The first mode corresponds to dense clouds and the second one to clear sky. The correlation radii on Fig. 11.7 are small due to the small sizes of Cu clouds.

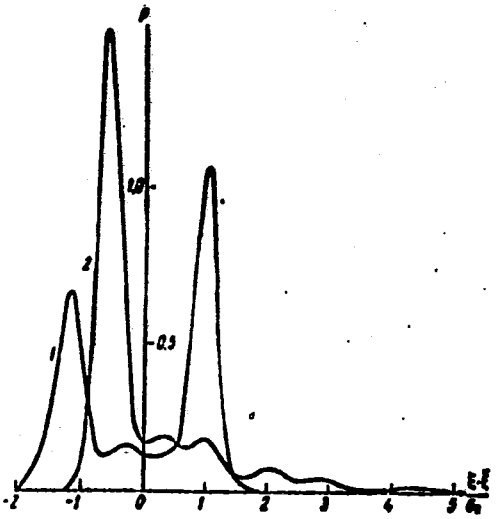

Fig.11.6.
Distribution functions of the global radiation (1) and the zenith brightness (2) in cumulus cloud conditions: ξ - the measured quantity; $\bar{\xi}$ - its mean value; σ_ξ - its standard deviation. (Kuusk et al.,1976).

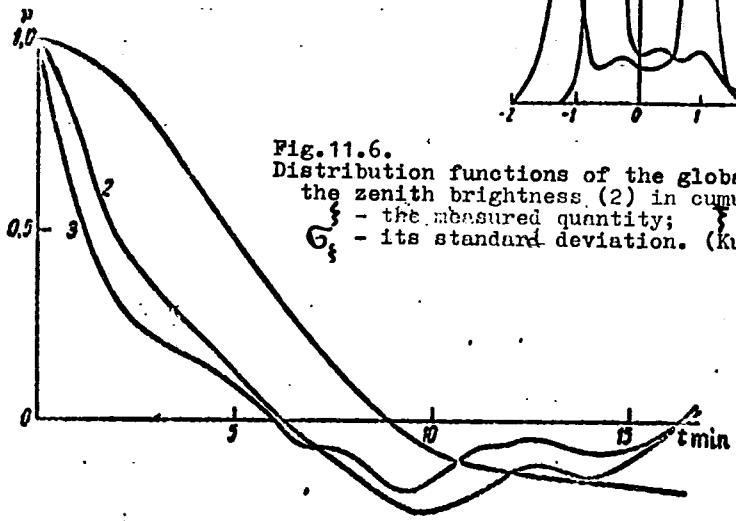

Fig.11.7. - Autocorrelation functions of F(0) (1), the zenith radiation temperature in "the window" of 8-12 μkm (2) and cloud amount at the zenith (3). (Kuusk et al.,1976).

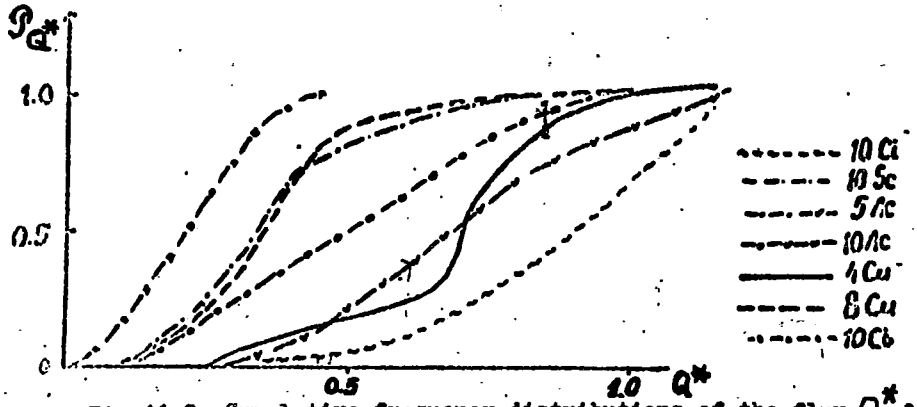

Fig.11.8. Cumulative frequency distributions of the flux Q^* for different cloud forms and amounts (Dubkin et al.,1978).

The values of the relative flux Q^* and its standard deviation are presented on Fig. 11.9 versus cloud amount. The flux Q is normalized to the average flux in the clear sky $Q_0 = I_0 \cos\zeta [1 + g \sec\zeta]^{-1}$ with $g = 0.1$ (empirical constant).
The dependence of Q^* upon N is approximated by the expression $Q^* = a - bN$ with an error of 20-25%; the parameter a varies from 0.75 to 1 depending on atmospheric turbidity, parameter b = 0.5.
Table 11.6 contains some parameters of the relative fluxes of I* and Q* (here $I^* = I[I_0 \exp(-\tau_0 \sec\zeta)]^{-1}$) with $\tau_0 = 0.3$.

Table 11.6. Statistical parameters of relative fluxes of the direct (I*) and total (Q*) solar radiation

N	I*, Q*	Mean value	Variance	Main parameters of differential distributions						
				Min.	Max.	Mode		Probability of mode		Median
						1	2	1	2	
0.2-0.3	I*	0.80-0.86	0.042-0.074	0	1.0	0-0.6	0.80-0.90	0.02-0.15	0.44-0.83	0.80-0.90
0.4	I*	0.65	0.10	0	0.95	0	0.85	0.20	0.50	0.80
0.4-0.5	Q*	0.43-0.70	0.020-0.040	0.05-0.35	1.0-1.20	0.30-0.50	0.70-0.85	0.03-0.50	0.10-0.37	0.45-0.75
0.6-0.7	Q*	0.44-0.55	0.024-0.036	0.10-0.25	1.00-1.20	0.30-0.50	0.80-0.90	0.08-0.15	0.04-0.08	0.40-0.55
0.8-0.9	Q*	0.32-0.46	0.016-0.044	0.15	1.00	0.20-0.30	0.70-0.90	0.17-0.33	0.02-0.06	0.20-0.40

11.3 HEAT RADIATION FIELD ACCORDING TO RADIOMETER-SOUNDING DATA

The radiometersounding (RS) of the atmosphere was carried out on ten Soviet ships. Radiometersondes were released once every day at 00 GMT during all three observation periods of the GATE. The integral hemispherical fluxes of upward and downward heat radiation, temperature, humidity, pressure were measured.

The heights of ascents were in 83% of all the cases higher than 15 km, in 56% exceeded 20 km and in 15% of the cases reached 30 km. In all, 565 successful soundings were performed during the GATE.

The data obtained have been described in Zaitseva et al. (1976). Some methodical aspects of interpretation were considered in Zaitseva and Feigelson (1979). Systematic analysis of the sounding results is given in Feigelson et al. (1980).

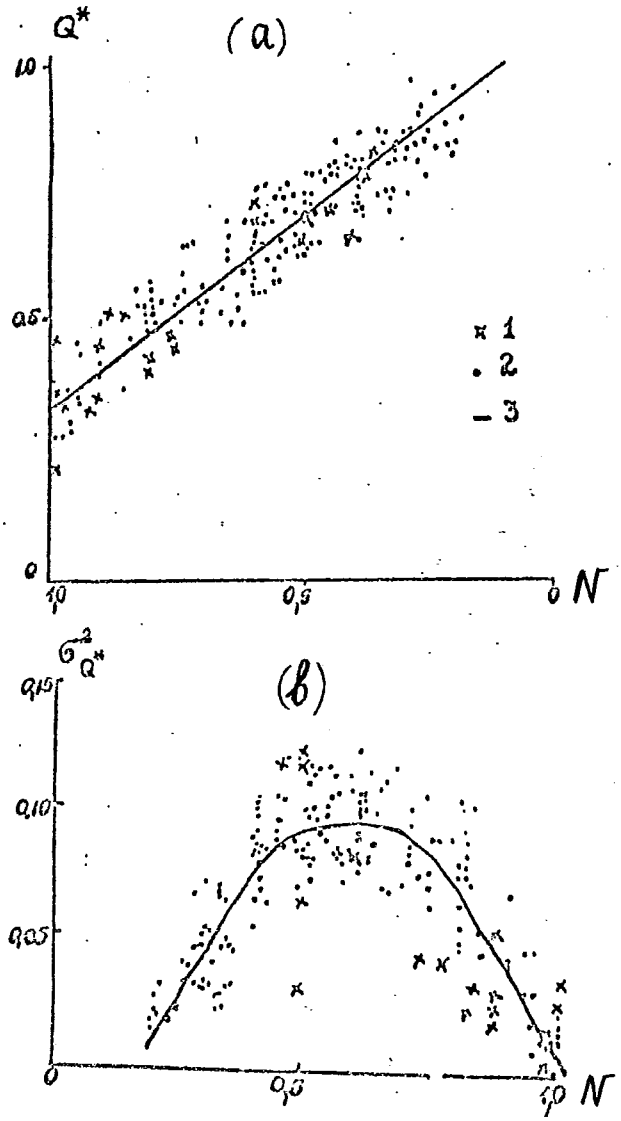

Fig. 11.9 - Dependence of the relative flux Q^* (a) and its variance (b) upon cloud amount. (Kirillova et al., 1977)

An equatorial model has been proposed based on data from the ships "Akademik Kurchatov" and "Passat". Cloudy and cloudless situations are not separated because the dominant thin trade-wind clouds in the equatorial zone influenced the radiative fluxes insignificantly.

The main GATE polygon of scales A/B and B was located at the tropical latitudes ($5°N \leq \varphi \leq 15°N$). There were 7 Soviet ships equipped with RS. For this polygon the cloudy and cloudless situations were examined both separately and jointly.

Thus, the bulk of the data was represented by four basic models given in Table 11.7: equatorial, tropical cloudless, tropical cloudy and general tropical; some additional models were also constructed. In each model the mean profile of all corresponding soundings and the relative variability is given.

The separation of the cloudy and cloudless situations was based on the peculiarities of the flux $F(p)$ in presence of clouds and on the stability of $F(p)$ in the clear sky tropical atmosphere (Zaitseva and Feigelson, 1979). The cloudless model includes also the cases of thin clouds to which the radiometersonde responded weakly. The "cloudy" model units all the situations when clouds actually influenced the radiation field.

The equatorial belt is clearly distinguished by the largest values of the average flux with small variability. In the inner tropics (A/B scale), the radiative regime of the cloudless atmosphere is rather close to the equatorial one with lower values of $F(p)$ due to larger humidity. In the absence of clouds, the radiation field here is isotropic: the means for the three ships of the main meridian ($\lambda = 23{,}5°W$) and for the four northern ships ($\varphi \geq 10°N$) almost coincide. The variability coefficients are also close to each other. Column 6 in Table 10.7 presents ships located in the southern part of the zone with the dust outbursts from the Sahara desert (Carlson and Prosper, 1977). From the means the dust effect is not ascertained, but perhaps it accounts for the enhanced variability (compare columns 6 and 4).

Clouds decrease the flux $F(p)$ and increase its variability. There is a latitudinal dependence: minimal fluxes at maximum variability correspond to ITCZ ($\varphi = 5\text{-}8°N$). Northwards from this zone the fluxes increase and the parameter v_F decreases.

The polygon A/B, as a whole, is represented by column 3. When comparing columns 3 and 5 one can see a small effect of cloudless cases on the mean radiative regime.

Similar data for one-direction fluxes $F_{\uparrow\downarrow}(p)$ show that $F_{\uparrow}(p)$ is stable at $p \geq 500$ mb owing to the temperature stability and remains insensitive to the appearance of clouds because of the high humidity of the lower troposphere. At levels of $p < 500$ mb, $F_{\uparrow}(p)$ decreases, while the variance $\sigma^2_{F_{\uparrow}}(p)$ increases. This increase in the vicinity of the tropopause is associated with the increase of σ^2_T. The variance $\sigma^2_{F_{\downarrow}}$ distinctly increases with height at p = 200 to 300 mbar. Evidently, the tops of clouds are often located in this layer and also σ^2_u increases here. The magnitude and variability of the outgoing radiation depends on the humidity of the upper atmosphere, on cloud top heights and on cloud amount. The temperature of the ocean does not influence this flux.

Table 11.7. Mean values of net long-wave radiation - F(p) in w/m^2 and variability $V_F\% = 100\frac{\sqrt{\sigma_F^2}}{F}$; σ_F^2 - variance

Model	Equatorial		Tropical general		Tropical cloudless		Tropical cloudy		Cloudless on 4 ships $\varphi \geq 10°N$	
1	2		3		4		5		6	
Pmb	F	V_f	F	V_f	F	V_f	V_f	V_f	F	V_f
970	50	21	34	11	45	22	26	45	43	23
900	63	22	39	90	57	16	29	50	54	22
850	71	20	43	100	64	15	32	50	61	21
800	81	17	40	61	70	17	36	51	68	21
750	89	16	55	54	75	16	41	47	74	20
700	97	17	61	49	82	14	47	44	82	17
650	103	18	67	47	89	14	52	45	89	17
600	112	20	72	46	97	12	56	47	97	16
550	121	20	77	49	105	12	59	53	105	16
500	132	19	84	47	114	12	66	51	112	17
450	142	16	94	47	124	13	75	45	121	15
400	151	13	103	41	134	12	84	42	131	14
350	157	12	112	39	140	11	94	39	138	13
300	164	12	118	36	147	11	101	37	148	13
250	173	10	126	34	153	11	109	38	155	12
200	177	09	130	31	154	13	114	31	156	13
150	177	09	132	29	152	16	117	27	154	17
100	183	09	141	26	155	13	127	23	156	17
70	191	10	152	22	165	13	138	20	165	17
50	194	10	158	17	170	12	144	20	168	17
30	198	09	162	16	183	07	151	17	171	16
20	201	10	167	16	191	07	155	16	171	20
10	203	10	163	17	170	13	157	20	197	09

The spatial structure of radiative fluxes, temperature and humidity show extrema in the ITCZ. In the lower troposphere all the fields may be considered approximately zonal. In upper layers ($p > 500$ mb) the zonality is significantly disturbed. An example is given on Fig.11.10.

Some special features of heat radiation in the tropics were revealed (Zaitseva and Feigelson, 1979). Heavy convective clouds strongly influence longwave radiation. The same holds for Ci clouds which are denser and occur more often in the tropics than in middle latitudes.

The radiative cooling (R) of the layer 970-100 mb in "pure" situations in average was: without clouds $R_{clear} = -1.3$ K/d (50 cases), in the presence of Ci clouds - $R = -1.0 \frac{K}{d}$ (10 cases), in case of heavy Cu clouds - $R_{ITCZ} = -0.7 \frac{K}{d}$ (20 cases); if there were Cu and Ci clouds together R diminishes to $-0.5 \frac{K}{d}$. The intensive diminishing of the radiative cooling of the entire troposphere by Cu and Ci clouds is one of the tropical peculiarities.

The second is the enhanced variability of the cooling of the upper troposphere (400-100 mb). The upper parts of the Cu clouds penetrating in this layer intensify its cooling to $-1.4 \frac{K}{d}$ instead of $-0.9 \frac{K}{d}$ without clouds. In case of Ci clouds the cooling of the same layer is down to $-0.4 \frac{K}{d}$ in average.

The net radiation near the ocean surface $F(o)$ in the tropics is about half the value in middle latitudes and it is less sensitive to clouds. That is due to the high humidity of the tropical atmosphere and to the small difference $T_s - T(o)$ (see equation 11.3 , Table 11.3)).

11.3.1 Radiative cooling

Table 11.8 presents the average cooling rates in various layers, calculated from using Table 11.7.

Examining this Table, one should remember that with an error in the flux measurement of the order of 1 or 2% (Kostyanoy , 1975) the error in determining the net radiation turns out to be about 10% and in the flux divergence about 20% at $\Delta p = 200$ mb in the middle troposphere. This may partly cause the nonuniformity of the radiative cooling profiles. But to a greater extent the latter is determined by the location of cloud and aerosol layers boundaries, inversions of temperature and humidity.

The evident physical features inferred from Table 11.8 are as follows:

(1) the biggest cooling of the middle troposphere;

(2) the smaller cooling of the whole cloudless tropical troposphere as compared with the equatorial one;

(3) the smaller cooling of the lower layers (970-600 mb) in the presence of clouds than without them; within the layer of 600-400 mb the cooling is also smaller and in the layer of 400-200 mb it is bigger than in the first case;

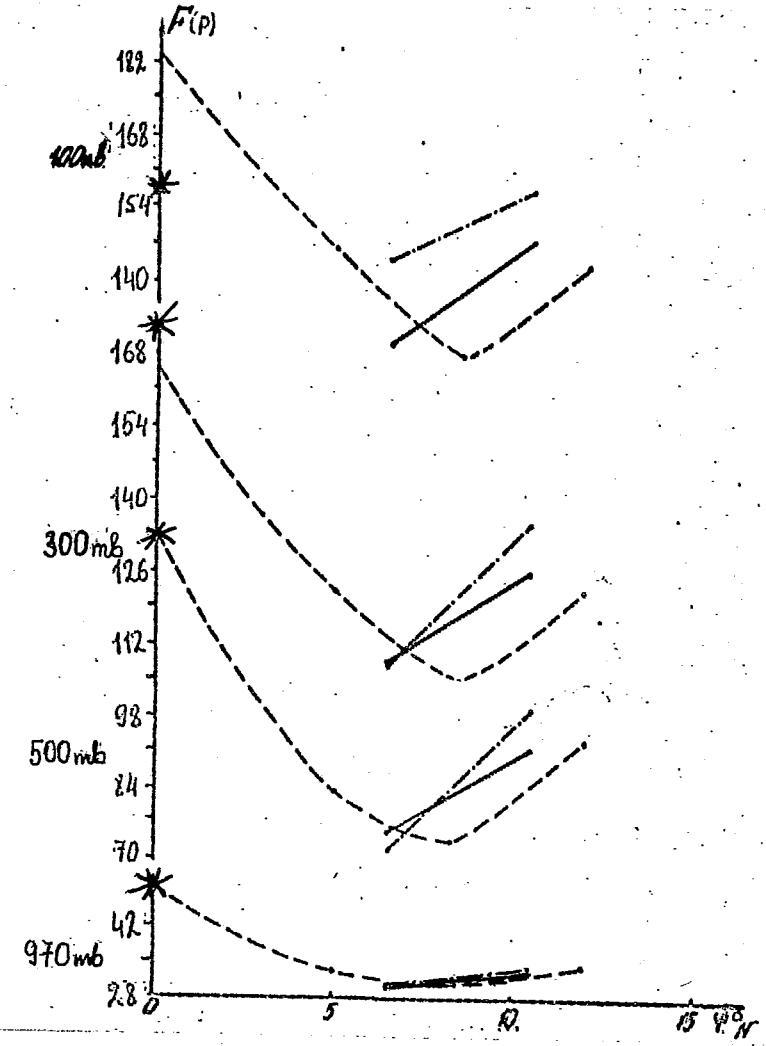

Fig.11.10 - The latitudinal distribution of net radiation in w/m^2 at different meridians and isobaric levels; the lines represent the data of the following ships: —— λ =20°00'W ("Krenkel", "Poryv") – – λ =23°30'W ("Kurchatov", "Zubov", "Vieze", "Korolev") —·— λ =27°00'W("Ocean", "Priboy"), • λ =30 ÷ 33°W ("Volna"), * λ =10°00'W("Passat") (Feigelson et al.,1980).

(4) the cooling of the troposphere is smaller in the presence of clouds.

Table 11.8. Radiative cooling rates in K/day for various atmospheric layers and different models

Model P_{mb}	Equatorial	Cloudless tropical	General tropical	Cloudy tropical	Cloudless for the 4 northern ships
970-800	1.56	1.24	0.76	0.49	1.21
800-600	1.33	1.15	0.97	0.86	1.24
600-400	1.65	1.56	1.30	1.21	1.45
400-200	1.06	0.83	1.15	1.22	1.06
970-150	1.30	1.10	1.01	0.94	1.14
900-500	1.46	1.21	0.96	1.17	1.22

The first of these features is explained by high cloud tops. The second - by the higher humidity of the innertropical latitudes. The third and fourth have been explained in detail in Feigelson (1973). Zaitseva and Feigelson (1979): under the clouds, near their bases and within them the cooling is small. On the whole, the cloudy atmosphere with high cloud tops is radiatively warmer than the cloudless one.

The 900 – 500 mb layer and column 5 in Table 11.8 are given in order to reveal the aerosol effect. According to Carlson, 1977; Carlson and Prospero, 1977 outbreaks of the Saharan dust are observed to the north of $\varphi = 10°N$ and in the layer at $500 \leq p \leq 900$ mb. However, as indicated above, the averaged data don't show any additional aerosol effect in radiative cooling.

Some individual cases of RS on board "Akademik Korolev" under cloudless conditions were considered. Table 11.9 presents the ratios (r) of the heating rates in these cases to the average data from Table 11.8, column 5.

In the sounding on 30.06 this ratio is $r < 1$ at $p > 800$ mbar and $r > 1$ within the layer $400 \leq p \leq 800$ mb. Possibly, this is just the aerosol effect. Apparently, the upper boundary of the aerosol layer is located where the value of r sharply increases. In other cases (01.07; 11.07; 16.07; 30.07) too when r sharply increases above a certain layer of small values of r, an aerosol effect may be expected.

Table 11.9. Ratio-r of radiative cooling rates in some individual soundings on RV "Akademik Korolev" to the means for cloudless atmosphere

Date / P_{mb}	29.06	30.06	01.07	11.07	16.07	30.07	31.07	04.08	31.08
970-800	0.88	0.75	0.91	0.84	0.62	0.99	1.22	1.23	1.15
800-600	0.80	1.23	0.85	1.39	1.21	0.84	1.03	1.47	0.88
600-400	1.05	1.44	0.67	0.88	1.27	1.26	1.09	0.50	1.13
400-200	0.86	0.77	1.20	1.20	1.19	1.16	1.07	1.09	0.92
970-150	0.98	1.12	0.92	1.08	1.14	1.08	1.07	1.03	0.99
900-500	0.79	1.03	0.81	1.07	1.05	1.06	1.13	1.23	0.94

11.3.2 Correlation analysis

The RS data allow calculations of correlations between the flux fluctuations on different levels. The normalized auto-correlation matrices $r(p_k, p_l)$ and cross-correlations with temperature and humidity were calculated by Feigelson et al., 1980.

Table 11.10 presents the matrices $r(p_k, p_l)$ for the fluxes $F_{\uparrow\downarrow}(p)$ and $F(p)$. A more rapid decrease of $r(p_k, p_l)$ with the increased $|p_k - p_l|$ was discovered, as compared with the middle latitude case (see Feigelson, 1973). For temperature and humidity auto-correlation and for their cross-correlations with radiative fluxes, this effect is the most pronounced. An example is given on Fig. 11.11. The GATE RS data as well as the estimates made earlier (Koprova et al. 1977), Kaznacheeva and Rudenkova (1976) show that the tropical latitudes are characterised by small-scale fluctuations in the temperature and humidity and by associated small-scale fluctuations in the radiation field. Radiation correlations are also weakened by the high optical density (high humidity and thick clouds) of the atmosphere and, consequently, by the short-range acting of the radiation.

The eigenvectors of the correlation matrices were calculated too (See Feigelson et al., 1980). An example is given in Table 11.11. Expansions of meteorological quantities in series by corresponding eigenvectors have found wide applications in atmospheric physics and meteorology.

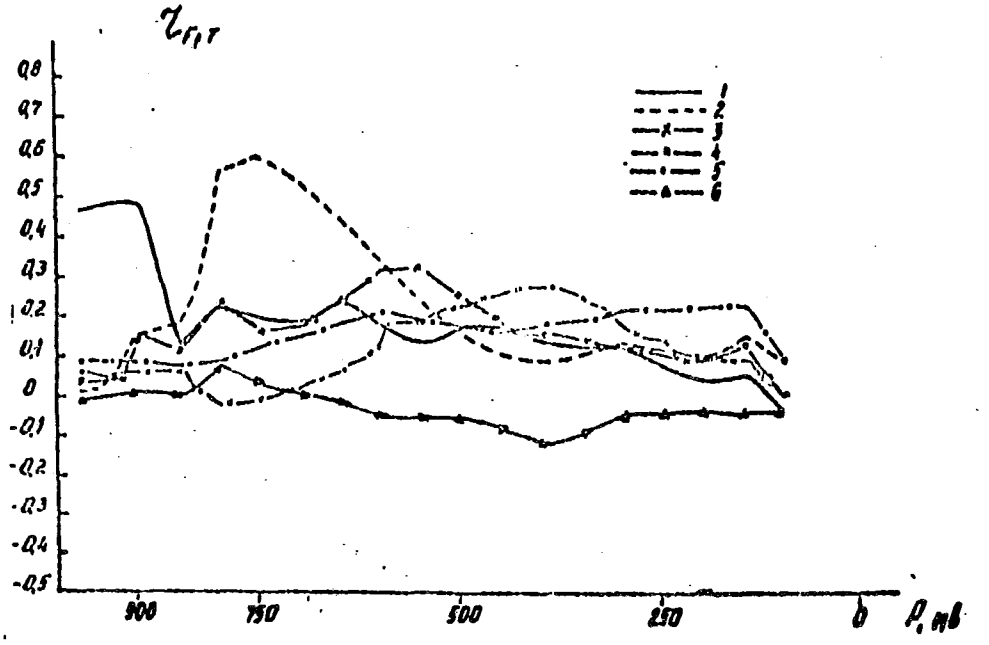

Fig. 11.11. The normalized cross-correlation matrix of upwapd flux and temperature. The flux at one selected level is correlated with the temperature at all the other levels: 1 - $F_{\uparrow}$ (970); 2 - $F_{\uparrow}$ (800); 3 - $F_{\uparrow}$ (600); 4 - $F_{\uparrow}$ (400); 5 - $F_{\uparrow}$ (200); 6 - $F_{\uparrow}$ (100) ;

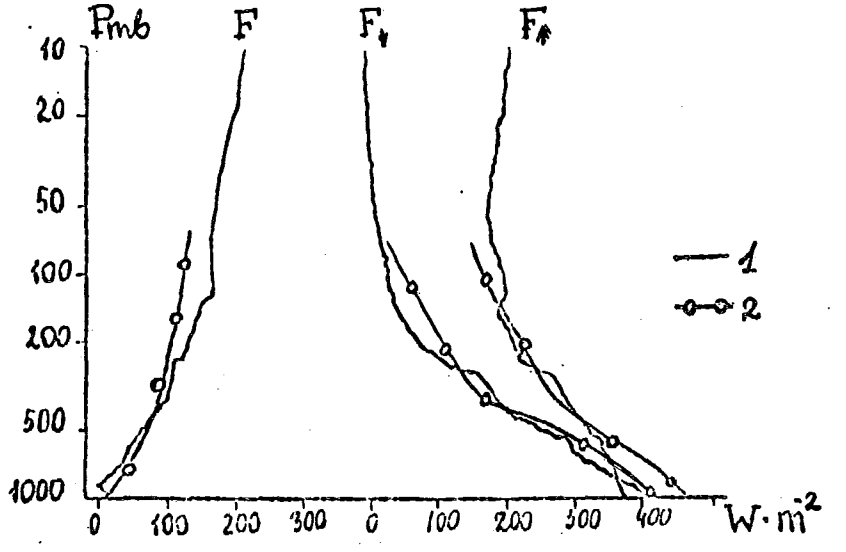

Fig. 11.12. - Fluxes of $F_{\uparrow\downarrow}$ and F from the RS data; curves 1-measurements on 16 August 1974 with 5/8 Cb, 8/8 Ac (Fimpel et al., 1977) ; curves 2-the data from Table 11.7, column 5.

Table 11.10 Autocorrelation coefficients

A. Fluxes $F_{\uparrow\downarrow}(p)$

P_{mb} \ P_{mb}	970	900	800	700	600	500	400	300	200	100
				$F_{\uparrow}(p)$						
970	1.00	0.67	0.34	0.30	0.30	0.20	0.20	0.26	0.18	0.11
900	0.92	1.00	0.62	0.50	0.46	0.36	0.30	0.28	0.20	0.16
800	0.76	0.87	1.00	0.77	0.60	0.37	0.28	0.31	0.30	0.29
700	0.62	0.70	0.86	1.00	0.82	0.59	0.49	0.49	0.44	0.41
600	0.54	0.63	0.76	0.94	1.00	0.78	0.66	0.61	0.52	0.45
500 $F_{\downarrow}(p)$	0.46	0.54	0.67	0.83	0.91	1.00	0.86	0.76	0.61	0.51
400	0.44	0.51	0.61	0.71	0.75	0.85	1.00	0.87	0.69	0.55
300	0.38	0.43	0.52	0.60	0.63	0.71	0.89	1.00	0.86	0.71
200	0.36	0.39	0.46	0.53	0.55	0.59	0.73	0.82	1.00	0.88
100	0.13	0.13	0.23	0.30	0.36	0.38	0.40	0.42	0.56	1.00

B. Fluxes of net radiation F(p)

P_{mb} \ P_{mb}	970	900	800	700	600	500	400	300	200	100
970	1.00	0.90	0.79	0.66	0.60	0.53	0.51	0.47	0.40	0.32
900		1.00	0.87	0.73	0.66	0.57	0.54	0.49	0.42	0.34
800			1.00	0.87	0.78	0.67	0.63	0.57	0.48	0.42
700				1.00	0.94	0.84	0.76	0.69	0.60	0.53
600					1.00	0.92	0.81	0.73	0.64	0.58
500						1.00	0.83	0.79	0.69	0.63
400							1.00	0.91	0.80	0.70
300								1.00	0.90	0.78
200									1.00	0.87
100										1.00

Table 11.11. Eigenvalues μ_i and eigenvectors $\varphi_i(p)$ for the flux $F(p)$

μ_i = 0,0280		0.00388	0.00232	0.00139	0.00121	0.000950	0.000384
P_{mb} \ i =1		2	3	4	5	6	7
970	0.073	0.125	0.122	0.169	-0.050	-0.216	0.145
900	0.008	0.188	0.147	0.261	-0.046	-0.242	0.194
800	0.140	0.255	0.117	0.824	-0.126	-0.118	-0.008
700	0.172	0.250	0.012	0.150	-0.003	0.145	-0.225
600	0.215	0.254	-0.032	-0.002	0.006	0.287	0.036
500	0.270	0.191	-0.069	-0.304	0.054	0.215	0.232
400	0.280	0.016	-0.161	-0.242	-0.008	-0.182	-0.093
300	0.281	-0.137	-0.251	0.047	-0.037	-0.271	-0.309
200	0.250	-0.275	-0.169	0.249	0.188	-0.046	0.264
100	0.204	-0.313	0.313	0.108	0.181	- 0.016	-0.035

Table 11.12. Auto- $R_Q(S)$, $R_N(S)$ and cross-correlation $R_{Q,N}(S)$ coefficients.
Values at S=0 were obtained by extrapolation.

S_m	$R_Q(S)$	$R_N(S)$	$R_{QN}(S)$
0	0.98	0.82	-0.65
50	0.96	0.63	-0.69
300	0.27	0.35	-0.26
500	0.08	0.22	-0.14
700	0.02	0.07	-0.02
900	-0.03	0.03	-0.08
1300	0.00	0.06	-0.04
1700	-0.20	-0.03	-0.11
2400	0.12	0.08	-0.10

The small scale of the radiation field fluctuations in tropics is manifested in the horizontal structure too, due to the small sizes of cumulus clouds. The spatial auto-correlations of diurnal sums of Q and daily mean cloud amount N and the cross-correlations are computed by Dvorkina et al. (1977). The computational data are presented in Table 11.12. Values of correlation coefficients at S=0 were obtained by extrapolation of R(S).

The US-FRG experiment of the radiometersounding was carried out on board the ship "Meteor". Thirty seven successful soundings were made of which two examples of fluxes corresponding to well-developed convective clouds and to clear sky, as well as averaged heating rates for several cases are reproduced in Fimpel et al., 1977. These data compared with the mean data of the USSR radiometersounding are represented in Figs. 11.12-14. Of course, it is not too good to compare individual measurements with the mean data; nevertheless the two sources of data appear to be consistent (see also Zaitseva and Fimpel, 1977).

11.4 COMPUTATION OF THE RADIATION BUDGET OF THE TROPICAL ATMOSPHERE

11.4.1 Methodology

Computations of the long-wave flux divergence - R_h, the short-wave flux convergence - R_s and the total budget $R_t=R_h+R_s$ of the tropical atmosphere in 100 mbar layers and in the layer (1000 - 1012 mb) are presented in Cox and Griffith (1979 a and b).

Calculations were made for the time intervals t = 6 hrs for meshes ΔS = 0.5°N x 0.5°W for the A/B-scale polygon GATE phase III. Temperature and humidity were obtained from the upper-air sounding on board of 5 US ships located within the B-scale area. The satellite data of cloud top pressures - P_t, cloud amounts at these levels - $N(P_t)$ and radar data of the relative amounts of thick clouds were used.

The procedure for computing the heat radiation fluxes was rather conventional with respect to gas components of the atmosphere (H_2O; CO_2; O_3) the additional "e-absorption" in "the window" of 8-12 μm was accounted for (see Cox , 1973).

Clouds were suggested to be "grey"; their emissivity was determined from the formula:

$$E(\tilde{z}) = 1 - e^{-K w \tilde{z}} \qquad (11.8)$$

at K = 0.045 m^2/g. Here, w is the liquid water content of the cloud; the vertical coordinate $\tilde{z}$ is read from cloud tops (when calculating $F_\downarrow$) or bases (when calculating $F_\uparrow$).

For the cloudy atmosphere with given P_t and $N(P_t)$ calculations were made twice:

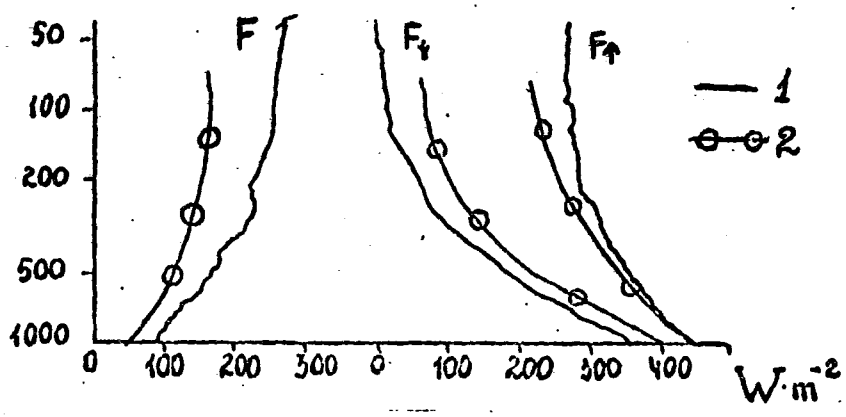

Fig. 11.13. - A_s in fig.11.12; curves 1 are measurements on 13 August in the clear sky conditions; 2 the data from Table 11.7, column 4.

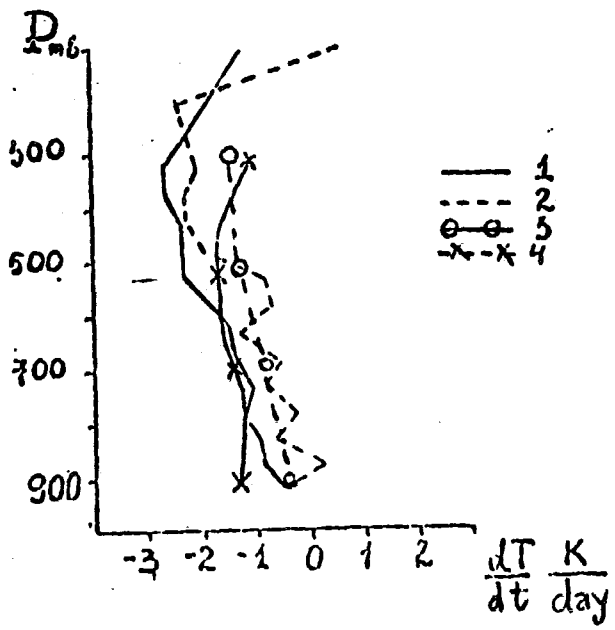

Fig.11.14. - Mean cooling profiles: curves 1 - clear sky (9cases); 2-low - and middle-level clouds overcast sky (8cases); 3 - Ci clouds (5cases); Fimpel et al., 1977): curve 4 - Table 11.7, column 3.

(a) In assumption of a thick cloud with the base at p = 950 mb;

(b) A cloud was assumed to be a thin one contained in the same layer $\Delta p = 100$ mb as its top.

A portion of thick clouds in their total amount $N(P_t)$ at each level P_t was derived from measurements of the area of radar echo sent only by dense cloud parts.

Clouds always were taken as horizontal uniform layers.

The atmospheric heating by the solar radiation is equal to $R_s = \frac{\partial A(p_o, p)}{\partial p}$ where $A(p_o, p)$ was calculated as follows:

$$A(p_o, p) = I_o \int_{\pi/2}^{\zeta_o} \cos\zeta \sum_{i=1}^{4} f_i\left[\sec\zeta\, M_i(p_o, p)\right] d\zeta \qquad (11.9)$$

where $p_o = 0$; ζ_o refers to the midday; $Mi(p_o, p)$ is the optical density of the i-th absorbing substance (CO_2, H_2O - vapour and droplets; O_3) f_i is the corresponding integral absorption function. It was assumed that the thickness of clouds is H = 1 km and at $z < z_t - 1$km the absorption is negligible.

Despite a number of simplifications and sources of errors referred to by Cox and Griffith (1979 a and b) one may agree with the following statement of these authors: "In summary, it should be emphasized that this is the first regional radiation budget study of this time and space resolution in which the computational algorithms have been verified by comparison with observations and in which the cloud-sampling problem has been minimized by using detailed cloud-height and areal coverage data from satellite".

11.4.2 Results of calculation*

In Table 11.13 are given the values of $R_h(\Delta p)$ versus total water vapour content m_v for clear sky. The quantity R_s is also presented with unknown m_v.

Fig. 11.15 presents the A/B-scale mean profiles $R_h(p)$ and $R_s(p)$ from all the data for Phase III. These profiles are compared with calculations of Dopplick (1972) and with heat radiation divergencies calculated from the radiometersounding data for the general tropical model (see column 3 of Table 11.7).

The significant differences of the first and last profiles will be discussed below.

---

* All results in this section (excluding Fig. 11.18-20) belong to Cox and Griffith (1979 a and b).

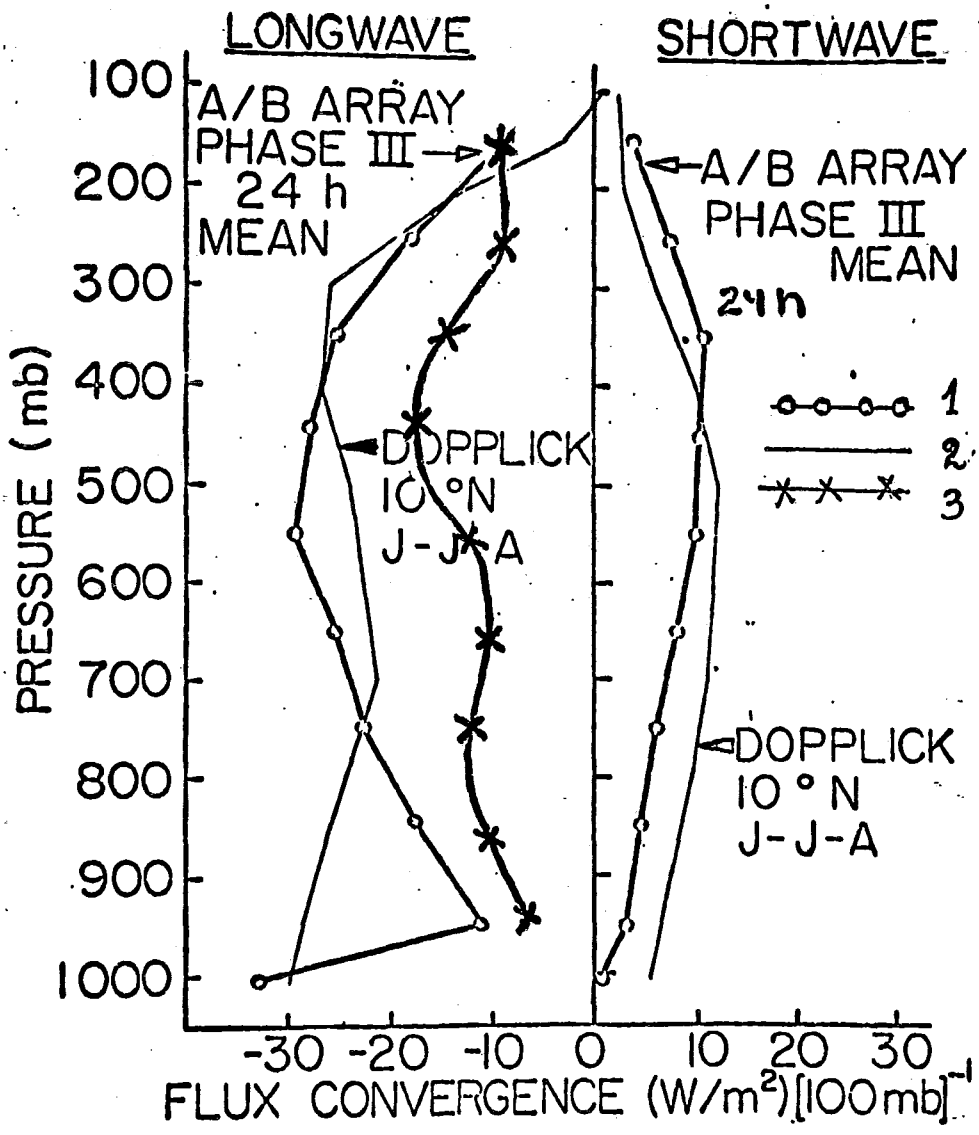

Fig.11.15. - Mean profiles of longwave cooling and shortwave heating (1) by Cox and Griffith (1979 a and b); Dopplick (1972) (See Cox and Griffith (1979 a and b); 3-mean RS data Table 11.7, column 3

Table 11.13. Negative R_h and R_s in $\frac{W}{m^2 100\ mb}$; clear sky conditions

ΔPmb \ m_{5day}	5.8	5.4-5.2	5.0-4.8	4.8	R_s^*
100-200	5.81	5.81	5.81	5.81	5.41
200-300	15.98	15.21	14.69	14.44	10.58
300-400	22.90	22.72	22.60	22.54	21.07
400-500	24.56	23.97	23.61	23.37	22.59
500-600	29.07	26.81	25.39	24.80	21.64
600-700	31.32	28.48	26.58	25.75	18.32
700-800	36.07	34.64	33.22	32.39	16.23
800-900	30.97	33.10	33.81	34.05	15.23
900-1000	12.70	20.59	25.85	28.48	14.59
1000-1012	4.00	4.20	4.74	5.10	1.68

The differences between the curves 1 and 2 are attributed (by Cox and Griffith, 1979 a and b) to the negelect of "e-absorption" and to the use of the mean climatic cloudiness by Dopplick.

To distinguish more clearly the effect of convective cloud in Fig. 11.16 and in Tables 11.14-15 the 5-day means with the most and the least pronounced convection ("disturbed" and "suppressed" days) are given in conjunction with the mean data for Phase III - clearly sky days. The relationship between day and nighttime values R_h, R_s and R_t is different because of the diurnal variation of cloudiness.

Appreciable horizontal gradients of the radiative fluxes occur due to rather small dimensions of the convective clouds. This gradients can be evaluated as the differences between the "disturbed" and "suppressed" data of Tables 11.14-and 11.15. This allows to isolate the height ranges where disturbed areas release heat to undisturbed ones and vice versa.

*Here and below if the time is not indicated, R_s refers to the integral for the day-time which is always considered to be equal to 12 hrs from 6.00 to 18.00 local time.

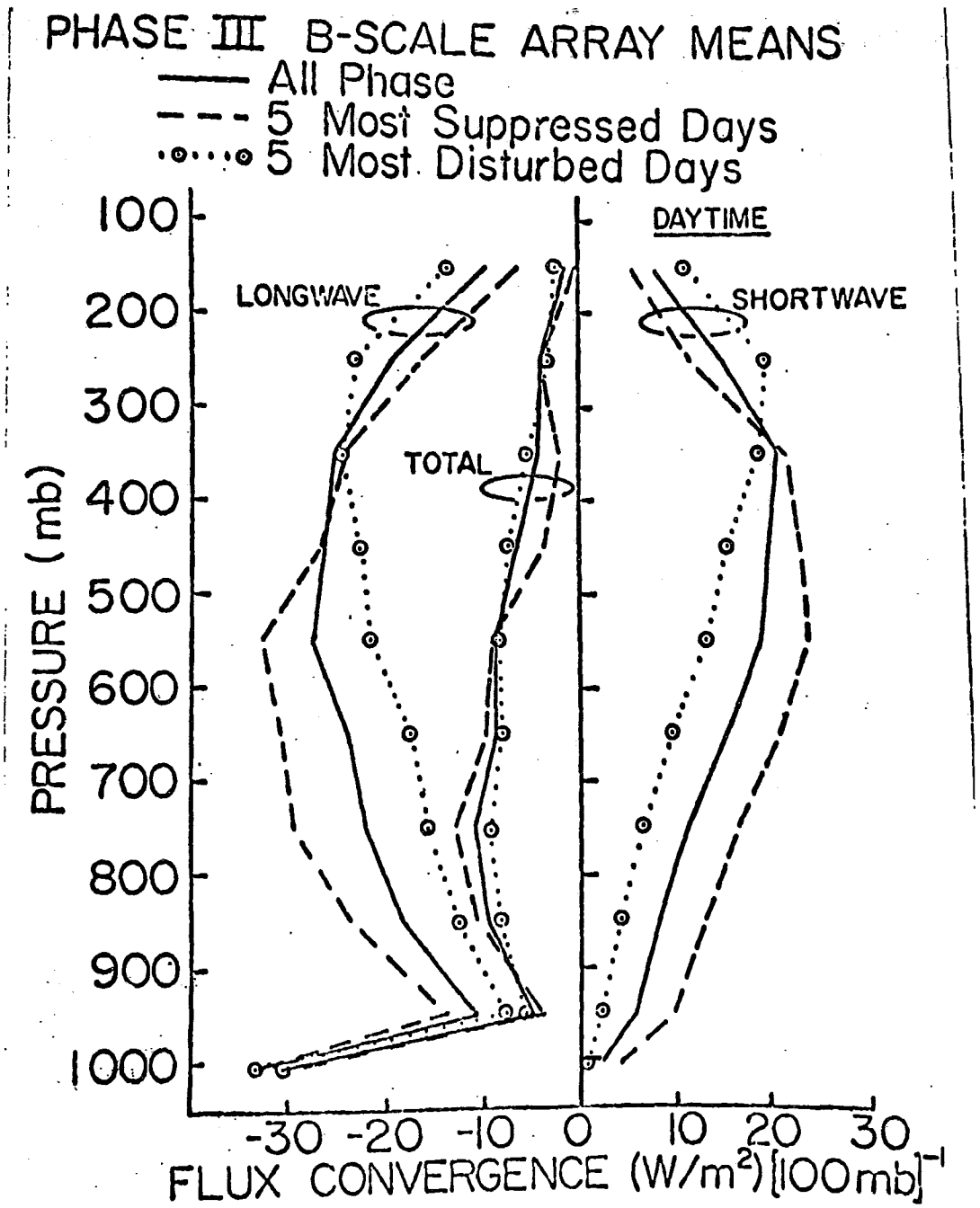

Fig.11.16. - Comparison of GATE Phase III mean data with means for the 5 "disturbed" days and the 5 "suppressed" days (Cox and Griffith, 1979 a and b).

Table 11.14. $R_t(\Delta P)$ w/m$^2\Delta$p for increasing day time and at night (18.00-06.00). The last line $\bar{R}_t$ w/m^{2}912 mb. The numerator - 5 "Suppressed" days; denominator - 5"disturbed" ones; numbers in brackets relate to cloudless conditions.

Pmb	t - local time in hrs				
	11-13	09-15	07-17	06-18	18-06
1	2	3	4	5	6
100-200	$\frac{2.7}{4.0}$ (2.5)	$\frac{1.9}{2.4}$ (1.8)	$\frac{0.5}{-0.4}$ (0.4)	$\frac{-0.3}{-2.2}$ (-0.4)	$\frac{-6.2}{-11.0}$(-5.8)
200-300	$\frac{2.5}{7.5}$ (1.4)	$\frac{0.9}{4.8}$ (-0.1)	$\frac{-2.1}{-0.1}$ (-2.7)	$\frac{-4.0}{-3.1}$ (-4.4)	$\frac{-16.8}{-21.3}$(-10.0)
300-400	$\frac{9.9}{5.1}$ (9.8)	$\frac{6.9}{2.5}$ (7.0)	$\frac{1.3}{-2.3}$ (1.7)	$\frac{-2.0}{-5.3}$ (-1.6)	$\frac{-25.6}{-26.5}$ (-2.27)
400-500	$\frac{9.2}{1.0}$ (11.0)	$\frac{6.1}{-1.0}$ (7.9)	$\frac{0.2}{-4.9}$ (2.3)	$\frac{-3.4}{-7.3}$ (-1.3)	$\frac{-28.8}{-26,8}$ (23.9)
500-600	$\frac{4.2}{-1.1}$ (7.3)	$\frac{0.9}{-2.9}$ (4.3)	$\frac{-5.1}{-6.2}$ (-1.1)	$\frac{-8.7}{-8.3}$ (-4.5)	$\frac{-33.9}{-24.9}$ (-26.1)
600-700	$\frac{2.1}{-2.5}$ (0.6)	$\frac{-0.8}{-3.9}$ (-1.9)	$\frac{-6.1}{-6.3}$ (-6.5)	$\frac{-9.4}{-7.9}$ (-9.3)	$\frac{-28.0}{-19.2}$ (-27.6)
700-800	$\frac{-3.6}{-5.8}$ (-9.0)	$\frac{-5.9}{-6.7}$ (-11.2)	$\frac{-10.1}{-8.3}$ (-15.3)	$\frac{-12.7}{-9.2}$ (-17.8)	$\frac{-24.5}{-16.3}$ (-34.1)
800-900	$\frac{-3.6}{-5.9}$ (-10.1)	$\frac{-5.4}{-6.5}$ (-12.2)	$\frac{-8.7}{-7.5}$ (-16.0)	$\frac{-10.6}{-8.2}$ (-18.4)	$\frac{-20.1}{-12.9}$ (-33.6)
900-1000	$\frac{-1.9}{-4.3}$ (-0.7)	$\frac{0.5}{-4.6}$ (-2.7)	$\frac{-2.0}{-5.1}$ (-6.4)	$\frac{-3.6}{-5.5}$ (-8.6)	$\frac{-12.9}{-8.6}$ (-23.2)
1000-1012	$\frac{-3.2}{-3.8}$ (-1.8)	$\frac{-3.3}{-3.9}$ (-2.0)	$\frac{-3.4}{-3.9}$ (-2.4)	$\frac{-3.5}{-3.9}$ (-2.7)	$\frac{-4.1}{-4.0}$ (-4.4)
$\bar{R}_t$ (100÷1012)	$\frac{22.1}{-5.8}$ (11.0)	$\frac{1.8}{-19.8}$ (-9.1)	$\frac{-35.5}{-45.0}$(-46.0)	$\frac{-58.2}{-60.9}$ (-69.0)	$\frac{-200.9}{-171.6}$ (-216.2)

Table 11.15. Hourly means of $R_t(\Delta p)$ w/m^2 Δ p and $\bar{R}_t$ w/m^2 912 mb.

The numerator-"suppressed" days, denominator - "disturbed" ones.

P_{mb} \ loc. time	11-12	10-11	09-10	08-09	07-18	06-07	
	12-13	13-14	14-15	15-16	16-17	17-18	18-06
100-200	2.7 / 4.0	2.1 / 2.8	1.0 / 0.5	-0.7 / -2.7	-2.6 / -6.7	-4.8 / -11.1	-6.2 / -11.2
200-300	2.5 / 7.5	1.3 / 5.5	-1.1 / 1.5	-4.5 / -4.1	-8.7 / -11.0	-13.4 / -18.6	-16.8 / -21.3
300-400	9.9 / 5.1	7.6 / 3.1	-3.2 / -0.8	-3.1 / -6.2	-10.8 / -12.8	-19.3 / -20.2	-25.6 / -26.5
400-500	9.2 / 1.0	6.8 / -0.6	2.1 / -3.6	-4.5 / -8.0	-12.6 / -13.3	-21.6 / -19.3	-28.8 / -26.8
500-600	4.2 / -1.1	1.7 / -2.5	-3.1 / -5.1	-9.9 / -8.9	-18.2 / -13.5	-27.4 / -18.7	-23.9 / -24.9
600-700	2.1 / -2.5	-0.1 / -3.5	-4.4 / -5.5	-10.4 / -8.2	-17.7 / -11.6	-25.9 / -15.4	-28.0 / -19.2
700-800	-3.6 / -5.8	-5.4 / -6.5	-8.7 / -7.8	-13.5 / -9.6	-19.3 / -11.8	-25.7 / -14.3	-24.5 / -16.3
800-900	-3.6 / -5.9	-5.0 / -8.4	-7.6 / -7.2	-11.3 / -8.4	-15.8 / -9.8	-20.9 / -11.5	-20.1 / -12.9
900-1000	1.9 / -4.3	0.8 / -4.5	-1.2 / -5.0	-4.1 / -5.6	-7.6 / -6.4	-11.5 / -7.3	-12.9 / -8,6
1000-1012	-3.2 / -3.8	-3.3 / -3.9	-3.4 / -3.9	-3.5 / -3.9	-3.7 / -3.9	-3.9 / -4.0	-4.1 / -4.0
$\bar{R}_t$ (100÷1012)	22.1 / -5.8	6.5 / -16.5	-23.2 / -36.9	-65.5 / -65.6	-117 / -100.8	-174.4 / -140.4	-200.9 / -171.6

The temporal variability of the radiation flux divergence for the troposphere (100 −1012 mb) $\overline{R}_{s,h,t}$ is illustrated on Fig. 11.17. The observed periodicity is related by Cox and Griffith (1979a,b) to propagation of the eastern dynamical waves and appropriate cloud structure. The time and space average behaviour of the quantities $\overline{R}_{s,h,t}$ was investigated in the same paper by increasing the scales of averaging.

The temporal variability diminishes almost to zero during the 6 day period of two easterly-wave passages. The spatial variability is reduced to 1.5÷2 by an increase of the areal averaging within the possible limits. The latitudinal and longitudinal variability of $\overline{R}_{h,s,t}$ along cross sections made through the centre of area (8.5°N, 23.5°W) clearly illustrate the extremes for R_h and R_t in the centre of the ITCZ (see also Fig. 11.10).

The radiative cooling of the boundary layer $z \leq 1$ km has been discussed in Augstein and Garstang (1977) and Ellingson (1977). On the basis of the spectral measurements made on the aircraft "Electra" regression ratios were constructed which allowed one obtain the radiative cooling rate profiles with clear sky and under a "Black" cloud cover presented in Fig. 11.18-20.

In conclusion of this Section let us consider the causes of the significant discrepancies between the calculated and measured values of R_h shown in Fig. 11.15.

1. The hemispheric actinometric sensor of the radiometersonde averages over a large area. The instrument response time and the ascending speed lead to smoothing. Clouds are seldom continuous and uniform in the space of averaging. This leads to smaller values $R_{h,t}$ compared with the computational results for a "black" model cloud with a flat homogeneous horizontal surface.

2. In statistical processing of RS data the flux values are interpolated to the standard levels. In this procedure intensive cooling at cloud tops may be omitted or smoothed.

3. It is reasonable to intercompare the one-direction fluxes instead of R_h values being extremely sensitive to measurement or calculation errors, to details of the model in computations or of the atmospheric structure in measurements.

11.5 RADIATION IN THE EQUATORIAL BELT

The equatorial belt (5°N - 5°S) differs from the proper tropical latitudes ($\varphi > 5°$) with respect to the nature of dynamic processes, the transfer of heat and humidity.

During all three phases of GATE the ship "Academik Kurchatov" was located at $\varphi = 0.0$, $\lambda = 23.5$W, i.e. in the center of the equatorial Atlantic at the maximum off-shore distance, in particular, from dust sources - the African deserts. This location caused some special features in the data collected. Direct measurements of the turbulent fluxes

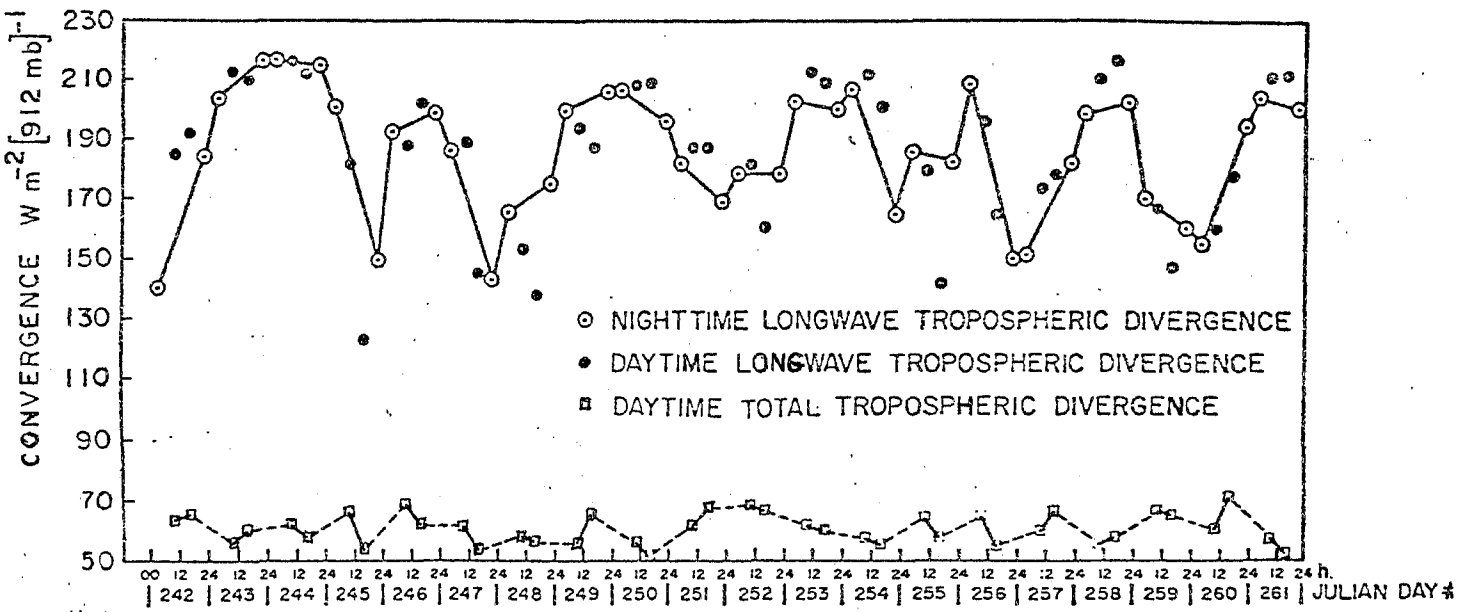

Fig.11.17.- Temporal variability of flux convergence of the troposhere.

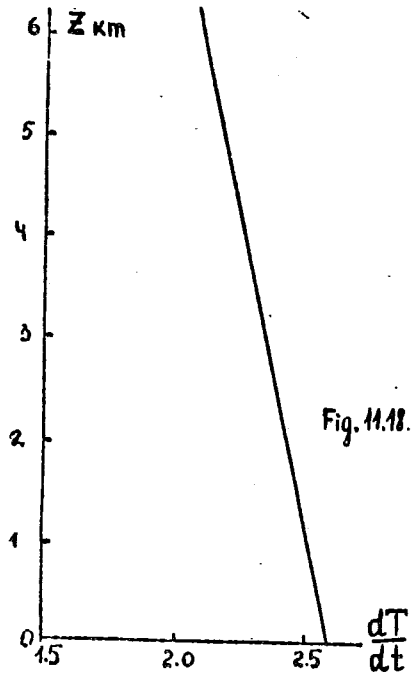

Fig.11.18.

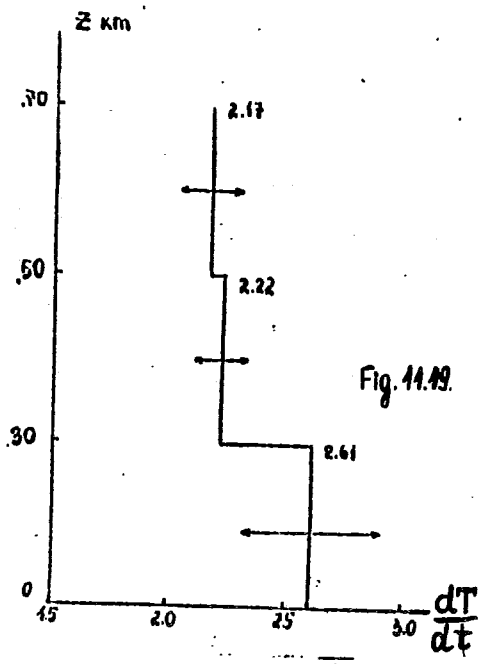

Fig.11.19.

Fig.11.18. Variation of the cooling rate of a layer (0;Z) in K/d with increasing Z for clear sky (Augstein and Garstang, 1977)

Fig.11.19. - Cooling rates (mean for 7 days in clear sky conditions in K/d) for the layers 0.0-0.3 Km, 0.3-0.5 km, 0.5-0.7km (Augstein and Garstang, 1977).

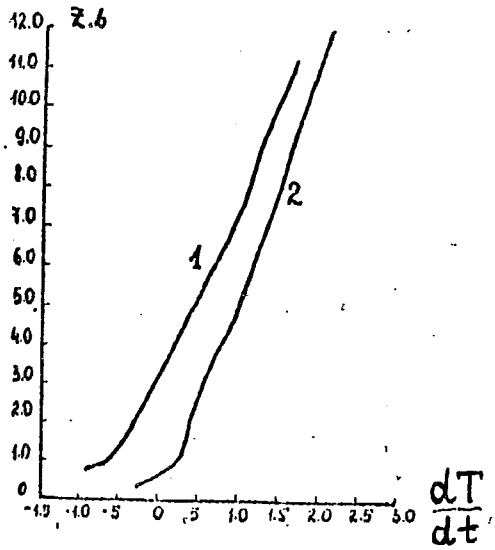

Fig.11.20. Variation of the cooling rate (in K/d) of the suboloud layer with cloud base height (Z_b) : (1) - the layer of (0; 0.3 km); (2) - that of (0.5-0.7 km). Positive values mean cooling, negative ones heating rates (Augstein and Garstang, 1977).

of heat and moisture, in conjunction with actinometry, allowed one to make reliable estimations of the heat budget at the Equator and the solar heating of the ocean.

The average characteristics of the equatorial atmosphere are briefly presented in Volkov et al. (1978). The SE trade-wind with mean velocities of 5.8 m/s prevailed in the lower 1.5-3 km layer. The temperature at the 14 m-level was equal to 24.4-24.9° and differed from the sea surface temperature by 0.4-1.0°C. The mean relative humidity at the sea surface and the total atmospheric moisture content were equal to 77-80% and 3.7-3.9 g/cm^2, respectively. The total cloud amount was on the average 0.35-0.50. The prevailing clouds were Cu hum., Cu med., their mean amount was 0.2, and the prevailing horizontal size D = 500 m.

The features of aerosol composition of the atmosphere are presented in Kapustin et al. (1976). The scattering coefficient in visual range near the ocean surface is closely correlated to the number of small particles with radius $r \leq 0.2$ μkm and weakly correlated to larger ones ($r > 1$ μkm). There has been no correlation to the humidity and wind velocity revealed but there is a clear correlation to wind direction: one day after a change in wind direction from SE to E the total number of particles increased (from 3 particles/sm^3 to 15-17 particles/cm^3 approximately). Thus, in the center of the equatorial Atlantic the variability of aerosol particles is caused by dust invasions from Africa.

The mean optical thickness of aerosols τ_a in visible light was 0.1 -0.2; the background* scattering coefficient near sea surface $\sigma_a = 0.4 \cdot 10^{-4}$ m^{-1}. The good correlation between parameters τ_a and σ_a indicates a mixing of aerosols in height (Kapustin and Pirogov, 1976).

The variability of the direct solar radiation coming to ocean surface in cloudless conditions was almost fully due to the variability of the aerosol composition and was not related to the humidity variation. The latter affected significantly the net radiation.

The distribution function of individual components of the radiation budget for each phase of GATE is shown on Figs. 11.21-22. The smaller values of $F(o)$ for the phase I in Fig. 11.21 are explained by the smaller temperature differences $T_s - T(o)$ compared to phases II and III.

Fig. 11.22 presents the frequency distribution of hourly sums of relative fluxes of the global solar radiation. The values $Q^* > 1$ in this figure may be explained, to some extent, through the reflection of the light by the side walls of cumulus clouds. But at least partialy values $Q^* > 1$ might be attributed to an inadequate choice of mean Q values in clear sky conditions used for normalizing the total radiation flux. The F(p) profile for equatorial belt is given in Table 11.7.

---

* i.e. without dust outbreaks.

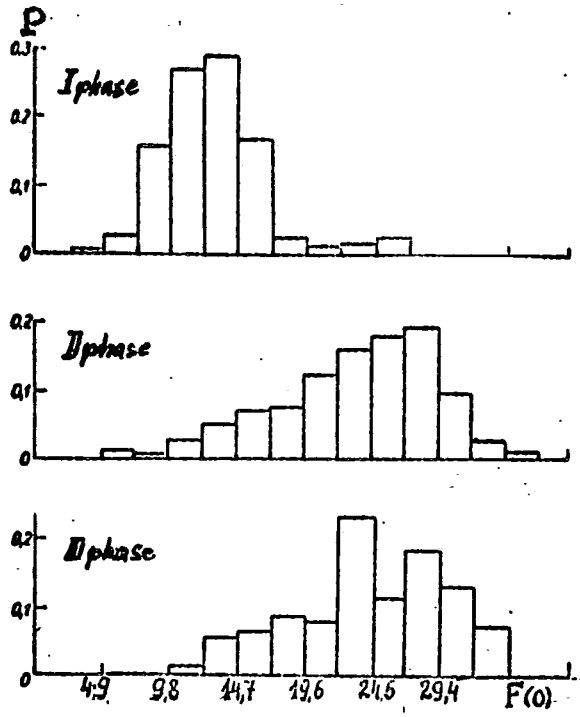

Fig.11.21. Frequency distribution of hourly sums of net longwave flux F(0) in $\frac{4}{m^2 h}\ 10^4$ (Samoilenko and Semenchenko, 1976)

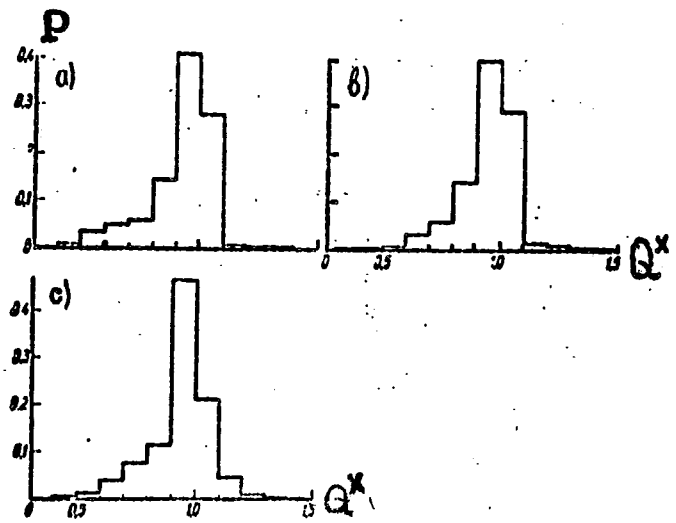

Fig. 11.22. Frequency distribution of the relative fluxes of the total solar radiation (Semenchenko and Semenchenko, 1976) a,b,c - the I,II,III, GATE phases.

Table 11.16 contains the mean values of the heat budget at the sea surface and its individual components for Phase II and III, in conjuction with similar data obtained by the same team by means of the same instrumentation for turbulence measurements on board the same "Acad. Kurchatov" during TROPEX-72 and FGGE-79 (Volkov et al., 1976; Koprov, 1980; see also Chapter 10).

The estimates of T and its components by Grassl (1977) are given in Table 11.16 too. These data were obtained at the point 9°45'N, 23°W - on board of the ship "Planet "(FRG)during the 3-d Phase of GATE. All the radiative fluxes were measured: turbulent fluxes were calculated from "bulk" formulae. The variations of data got by using somewhat different "bulk" parameterization are given in the corresponding columnes of the Table 11.16.

Table 11.16. Mean daily values of the heat budget and its components in w/m^2

	Experiment	Q	R	F(o)	F_T	Fe	T
1.	Phase II 0°N; 23.5°W	262	12	53	11	62	124
2.	Phase III 0°N, 23,5°W	238	13	55	5	38	127
3.	TROPEX-72, June 1972 7.5°N; 20.8°W ITCZ axis by 7°N	153	8	28	7	83	27
4.	TROPEX-72 August 1972 7.5°N; 21.8°W ITCZ axis by 10°N	219	9	23	4	78	103
5.	FGGE August 1979 0°N; 23.5°W	276	12	48	11	64	147
6.	"Planet" Phase III GATE 9°45'N, 23°W	124	7	43	10-15	95-102	

This table shows that the main loss to the atmosphere is the turbulent flux of latent heat which is comparable to the net heat radiation flux in the equatorial belt. The latter flux increases at the Equator due to lower humidity. The sum of the fluxes T is always positive; it represents the part of solar energy which actually heats the ocean. At the Equator this quantity is by 20% larger than that in the inner tropical latitudes outside the ITCZ. Inside ITCZ almost no solar heating of the ocean occurs. The data of FGGE-79 fully confirm the results of GATE. Some differences with Grassl's data in radiative fluxes are evidently due to the different cloud conditions at the observation points.

The more significant differences in the flux F_e values are reasonable due to the "bulk" formulae.

11.6 THE "WINDOW" 8-12 μkm

Attenuation of radiation in the range 8-12 mkm is rather significant in the tropics but its nature is still debatable. It is attributed to the continuous absorption by water vapour ("e-absorption") or to the absorption by aerosol particles.

The spectra of the direct solar radiation in the range of 2-14 μkm with resolution of 1-2 cm^{-1} and of the downward atmospheric radiation in the ranges of about 0.4 μkm and space angles of about 2°x4° were measured on board the ship "Acad. Kurchatov" (Shukurov and Chavro, 1978; Malkevich et al., 1976).

$K_\lambda = \frac{\tau_\lambda}{\tilde{m}_v}$ Fig. 11.23 presents the effective absorption coefficients where τ_λ is the optical thickness derived from direct solar radiation measurements. The results of similar measurements on land in the middle latitudes are presented too. This allows one to consider a wide range of the temperature values from -25° to +25° and humidity from 0.3-3.5 cm, respectively (the humidity $\tilde{m}_v$ is reduced to the normal pressure). The water vapour pressure at ocean surface $e(o)$ varied from 2 to 25 mb.

$\tilde{m}_v = 3$ cm; Fig. 11.23 shows a significant variability of K_λ at values that is impossible to explain by the dependence on $T(o)$ and $e(o)$ (i.e. by the "e-absorption") which are practically constant in the equatorial Atlantic.

The close correlations of K_λ within the range (8-14 μkm) and $\lambda = 2.2$ mkm as well as of K_λ and the actinometry data indicate that the variations of K_λ are basically due to aerosols. To distinguish effects of the water vapour and aerosols the minimum values of K_λ are considered. The dependence of $\min(K_\lambda)$ on $\tilde{m}_v$ is shown in Fig. 11.23 by solid lines. The minima are accepted as the water vapour absorption coefficients. The values of $K_{\lambda a} = K_\lambda - \min K_\lambda$ are taken as the attenuation coefficients of aerosol particles.

The spectral distribution of $\min K_\lambda = K_{\lambda, H_2O}$, of the aerosol optical thickness $\tau_{\lambda a} = K_{\lambda a} \cdot \tilde{m}_v$ and of its maximum values $\max \tau_{\lambda a}$ are presented in Table 11.17.

Table 11.17. Spectral values of parameters

parameters	λ (μm)				
	8.11	8.90	10.20	12.20	13.10
$\tau_{\lambda a}$	0.10	0.05	0.10	0.20	0.20
$\max \tau_{\lambda a}$	0.25	0.16	0.25	0.40	0.50
K_{λ, H_2O} $\frac{cm^2}{g}$	0.10	0.08	0.08	0.15	0.25

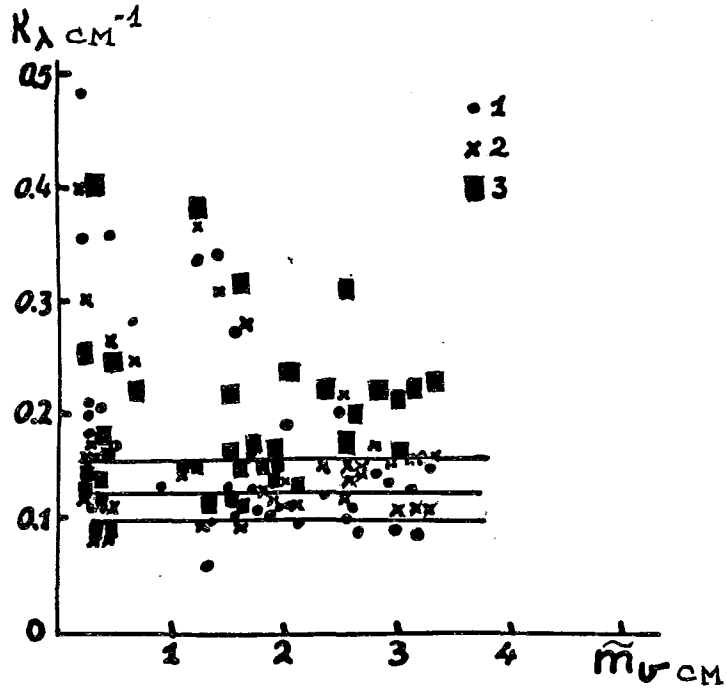

Fig.11.23. - Relations of the effective coefficients of the attenuation K_λ cm^{-1} to the reduced water vapour mass $\tilde{m}_v$ cm; 1 is λ =10.2 μkm, 2 - λ =11.2 μkm, 3 - λ =12.0 μkm (Shukurov and Chavro, 1978)

Measurements of the sky radiation at λ = 8.38; 9.00; 10.74; 11.50; 12.30 μkm were made on board the FRG ship "Planet" during Phase III of GATE. Half-widths of the spectral ranges were within 0.2-0.6 mkm (Grassl, 1975). These data, together with upper air soundings were used toisolate the effects of various absorbing substances by the technique given in Grassl (1973). The aerosol effect has been neglected as a small one. The water vapour content and the optical thicknesses are given in Table 11.18 for two days of measurements:

Table 11.18. Total moisture content and spectral optical thicknesses

	λ μkm / ms g/cm²	8.38	9.00	10.7	11.5	12.3
31 August	4.84	0.757	0.391	0.569	0.930	1.164
	4.84	0.823	0.475	0.677	1.035	1.271
	4.83	0.831	0.462	0.688	1.053	1.328
	4.83	0.852	0.508	0.712	1.060	1. 410
	4.87	0.785	0.439	0.651	0.984	1.250
3 Sept.	5.28	0.720	0.362	0.658	1.007	1.225
	5.28	0.775	0.463	0.686	1.061	1.265

Table 11.19 gives optical thicknesses of the net "e-absorption" ($\tilde{\tau}_e$) which are free from the influence of CO_2, O_3, CH_4. The parameter $\tilde{\tau}_e$ is compared with computed data of Grassl (1973) (column 4), Burch (1970) (column 3).

Table 11.19. Measured values of $\tilde{\tau}_e$ and their difference from computed ones

(1)	Measured (2)	Measurements minus calculation (3)	(4)
0.38	0.451	0.006	0.043
9.00	0.307	-0.137	-0.023
10.74	0.580	-0.079	0.018
11.50	0.855	-0.030	0.101
12.30	1.010	-0.038	0.080

The spectral optical thicknesses in the „window" of 8-12 mkm have been interpreted above from the opposite points of view.

May be the reality is that this spectral range (and other atmospheric "windows") is influenced by the aerosol and "e-absorption" as well as by gas traces.

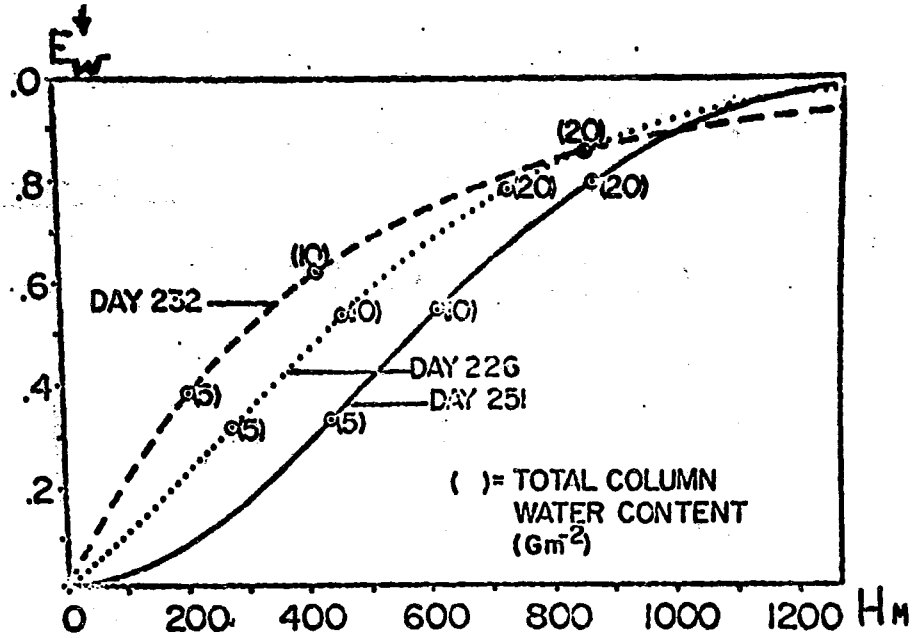

Fig.11.24. - Emissivity of cirrus clouds versus distances to cloud layers tops H for 3 days. The crystal water content in the Layer (Z_t ; Z) in g/m^2 is given in brackets (Griffith and Cox, 1977).

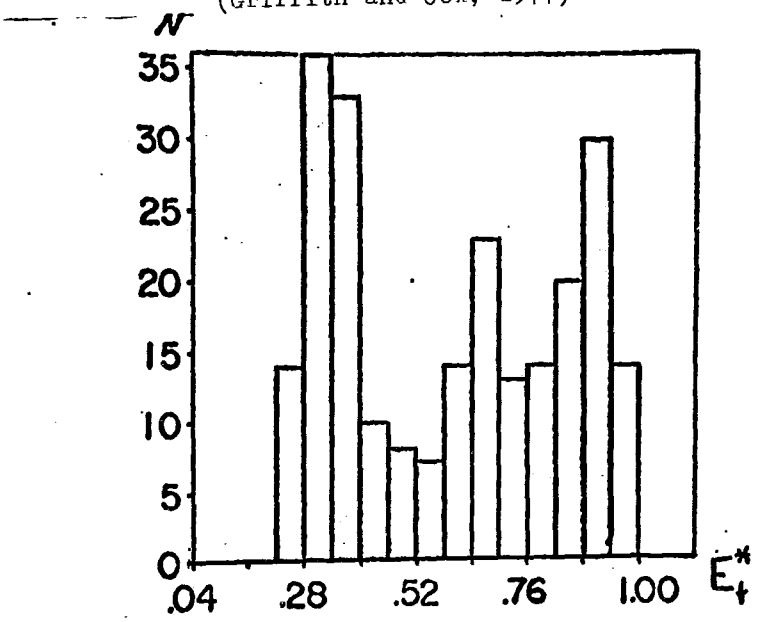

Fig.11.25. Frequency distribution of the effective emissivity; the 232-th day; the horizontal flight at the level of 1.3 km below Z_t; N is the number of cases (Griffith and Cox, 1977).

Table 11.20

Effective $E^*_{\downarrow}$ and proper - $E_{\downarrow}$ emissivity of Ci clouds

	date	Z_b, km	Z_t, km	$E^*_{\downarrow}$	$E_{\downarrow}$
"Priboy"	I2.IX	7,9	I2,I	0,64	0,44
" - "	" "	7,9	I0,0	0,80	0,44
"Prof.Vieze"	6,IX	I2,I	I6,5	0,53	0,I3
"Volna"	I5.УШ	I0,8	I3,7	0,I9	0
"Volna"	I3.IX	II,3	I4,5	0,48	0
"Acad.Korolev"	I9.IX	8,0	9,7	0.27	0.23
" - "	" "	8,0	I0,7	0.46	0,23
"Acad.Kurchatov"	4.IX	8,7	I2,8	0.42	0
" - "	" "	8,7	I4,0	0,49	0
" - "	I4.УП	I2,2	I4,6	0,25	0,I3
" - "	" "	I2,2	I6,0	0,43	0,I3
"Priboy"	6.IX	I0,3	I2,8	0,42	0,I2
"Volna"	II.IX	6,8	I2,7	0,6I	0
"Acad.Kurchatov"	8.IX	I3,2	I5,4	0,I7	0
" - "	" "	I3,2	I6,5	0,33	0

11.7 EMISSIVITY OF Ci CLOUDS

Ci clouds are frequent in the tropics and they are optically denser than in the middle latitudes. The radiative effect of these clouds is significant and for its evaluation the emissivity E needs to be known.

Measurements of the integral fluxes of thermal radiation F and the temperature at the cloud boundaries make it possible to derive useful parameters: the effective emissivity - $E^*_{\uparrow\downarrow}$ (see Feigelson, 1973; Cox, 1976).

Approximate evaluations of the emissivity $E_{\uparrow\downarrow}$ of Ci clouds proper were made on the GATE data by Griffith and Cox (1977) , Zaitseva and Feigelson (1979). The emissivity of the gaseous components of the cloud layer was excluded in both cases.

The data of several days from USA aircraft "Sabreliner" was used in the first paper. The results are given on Fig. 11.24-25. The second paper was based on RS data; the results are presented in Table 11.20. In some cases two positions of the cloud bottom were considered as the exact position was unknown.

The emissivity $E^{\downarrow}_{w}$ on Fig. 11.24 is calculated by the equation (11.8). It turned out to be much bigger than in Table 11.20. The reason of this discrepancy partially may be attributed to the approximate approach of Zaitseva and Feigelson (1979). Partially it may be due to the exponential form of the emissivity in Griffith and Cox (1977). Such form is not typical for integral absorptivity.

11.8 RADIATIVE EFFECTS OF SAHARAN AEROSOL

The mighty phenomenon of the Saharan dust outbreaks into the Atlantic drew particular attention of radiation experts during GATE.

The spatial expansion of the Saharan aerosol layer (SAL) was studied in the course of GATE by means of surface optical observations and satellite images.

A comprehensive study of the Saharan aerosol outbreaks was undertaken by Kondratyev et al. (1976) based upon ship, aircraft and satellite data from GATE together with geographical and climatological data from other sources. The authors discussed the sources of dust in the Western Sahara and dry savanna of the North-Western Africa within the "amphitheatre" of the mountain systems of Atlas, Ahagsar and the Guinea upland. Prevailing forms of the aeolian relief, the baren bedrock, destructed to gravel and sand provide an inexhaustible source for dust flows (Fig. 11.26).

The sands of the Saharan ergs are composed mainly of quartz particles in the 0.25-1.1 μm range, coated with the "desert crust" - ferric oxides.

The dust outflows from the Sahara into the Atlantic were traced in the visible and IR images from the "SMS-1" satellite. The dust clouds are easily identified over the water surface because of the brightness contrast. Formation of cloudiness at the outer edge of the flow is quite characteristic (Fig. 11.27).

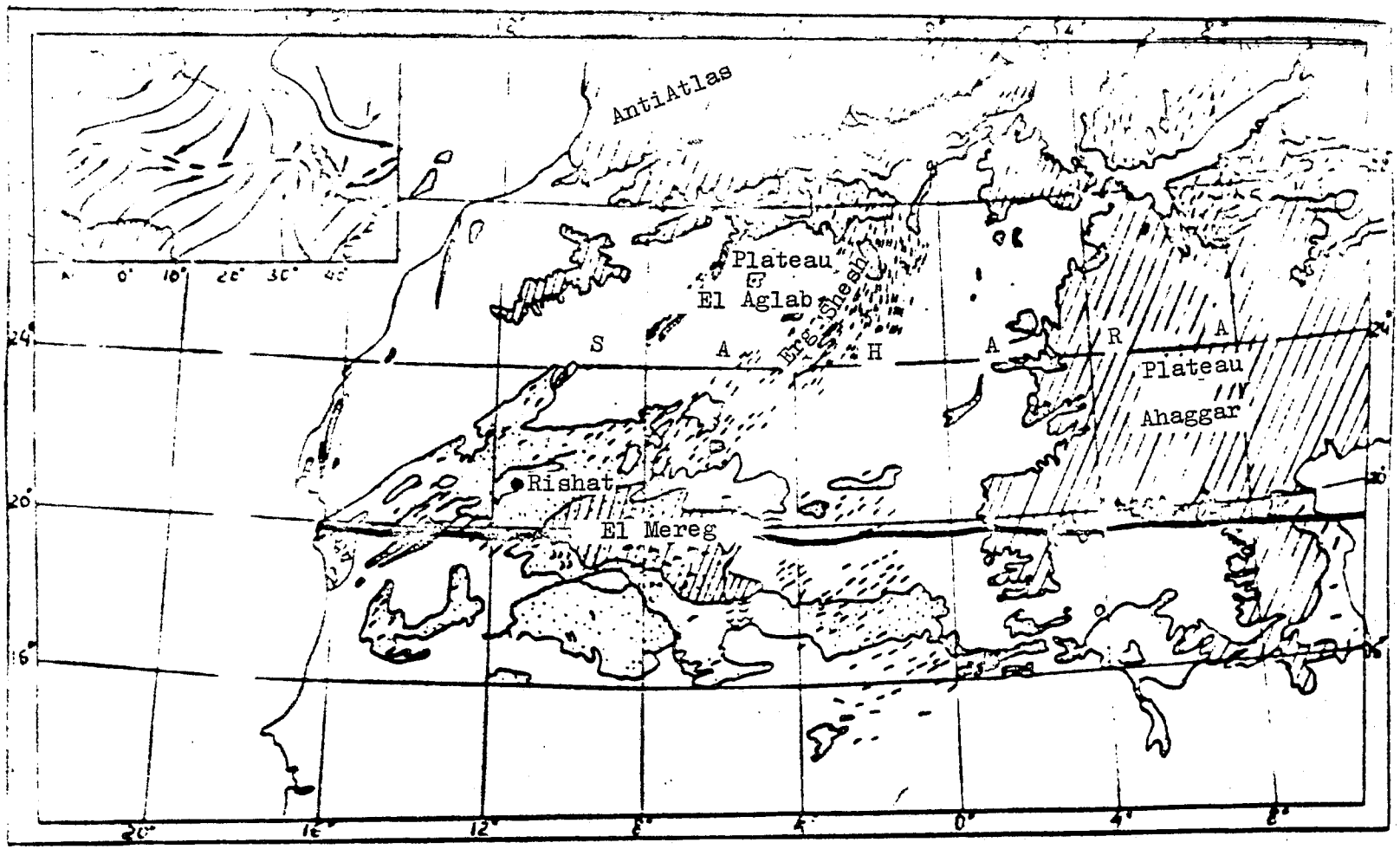

Figure 11.26 Dominant types of the Saharan relief.
1. Ergs
2. Bedrock
3. Relief boundaries
4. ITCZ axis

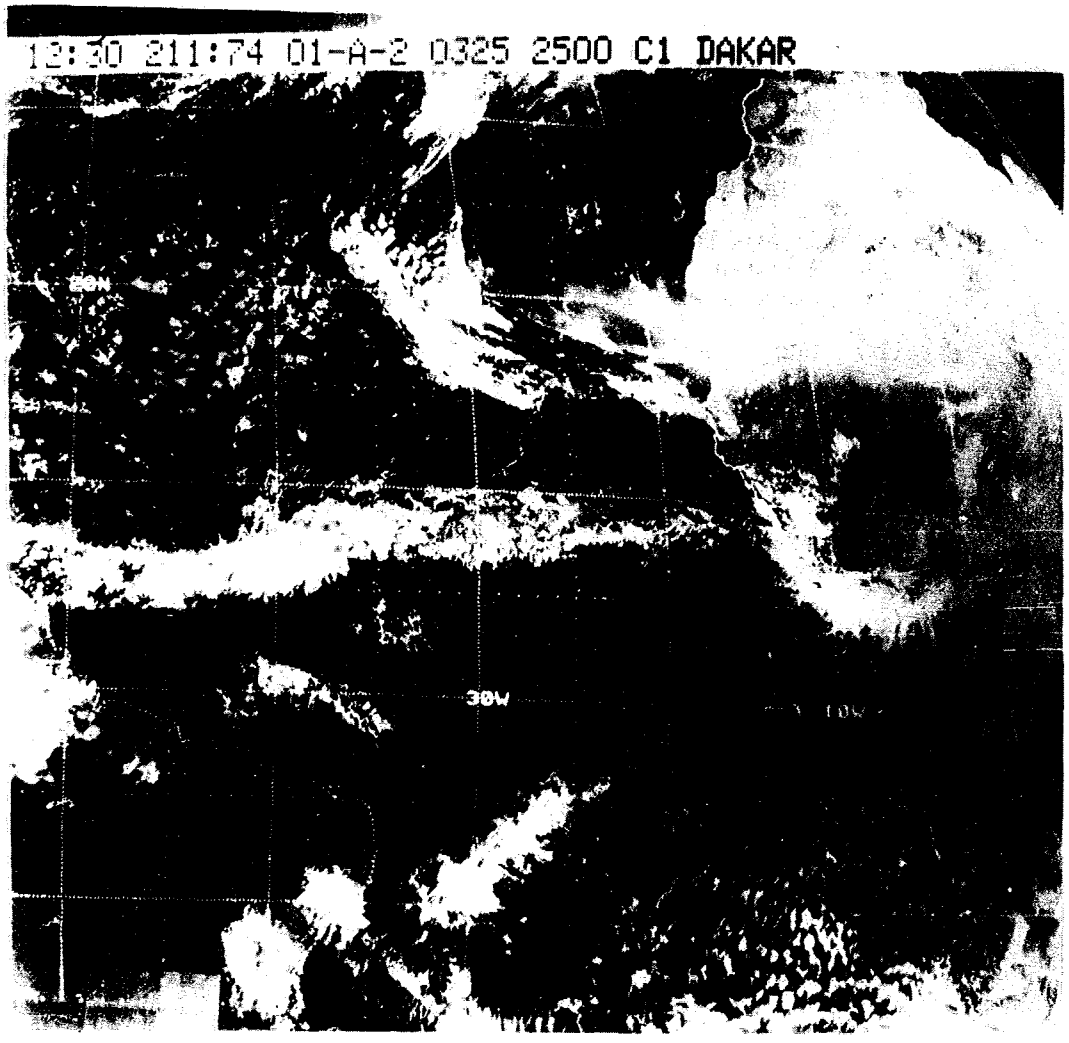

Figure 11.27 SMS-1 image of the Saharan dust outbreak on July 4,1974.

The most extensive outbreaks were registered on July 4, 30, and September 4, 1974. The area of dust clouds during these outbreaks reached $5-5.5 \times 10^6 km^2$. The existence of a secondary source of continental aerosol was noted to the South-West of the Ahaggar foothills at the Tassilin-Ahaggar plateau.

The dynamics of the outbreak on July 29-30, 1974 was studied in connection with atmospheric synoptic processes over North-Western Africa and the GATE A/B-scale array.

The principal dynamical characteristics and some radiative properties of SAL were described by Carlson and Prospero (1972) and Diaz et al. (1976) on the basis of observations made during BOMEX. The qualitative model of the dynamics of SAL, as suggested by Carlson and Prospero (1972) included the folowing features (Figs. 11.28-29):

(a) Lower level troughs, identified with the axes of the African wave disturbances, often traced in satellite images as "inverted V-structures" of cloudiness;

(b) Dust front behind the trough, relatively free of clouds;

(c) Large-scale anticyclonic eddies behind the dust front at the level of 600-700 mb;

(d) Inflow of the dust-free air from the northern latitudes along the coast at lower levels. (Part of the flow passing over the continent can capture small but significant amounts of dust);

(e) Inflow of the dust-free air from the northern latitudes at lower levels, also invading the continent and the trough;

(f) The predominance of winds from the Sahara at the upper levels over the coastal winds at low levels.

The pulsative character of the air flow from the Sahara is connected with its periodic interruption by the disturbances coming from the African continent.

The maximum potential temperatures in SAL decrease at a rate of about 1 K/day as it moves across the Atlantic westward, which corresponds to a cooling of about 0.7 K/day in units of regular temperature. As a rule the Saharan air leaves the African continent having mean potential temperatures of 43-44K, mixing ratio of 2-4 g/kg, and the upper border at the level of 540-560 mb.

This air reaches the Caribbean Basin with the same mixing ratio , but its potential temperature lowered to about 40K, and the upper border is already at 600 mb. At the same time calculations neglecting aerosol effects give an IR cooling rate of about 2 K/day for average conditions and approximately 1.6K/day for cloudless skies.

Entering the Atlantic as a relatively narrow "tongue" from the Mauritanian and Senegalese coast the dust outbreak is gradually captured by the anticyclonic motion which broadens the front of the dust flow as it moves forward. The possible explanation of such

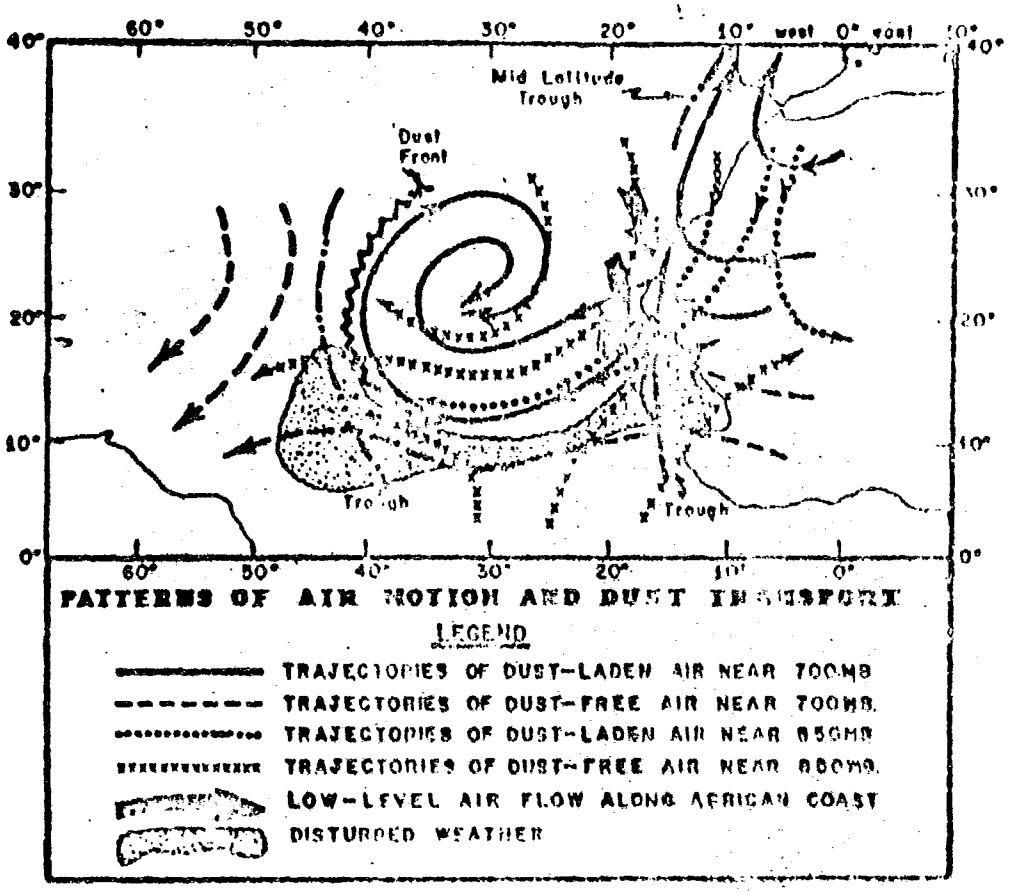

FIG. 11.28 Schematic model of air motions accompanying the movement of African disturbances and the associated dust pulses from Africa.

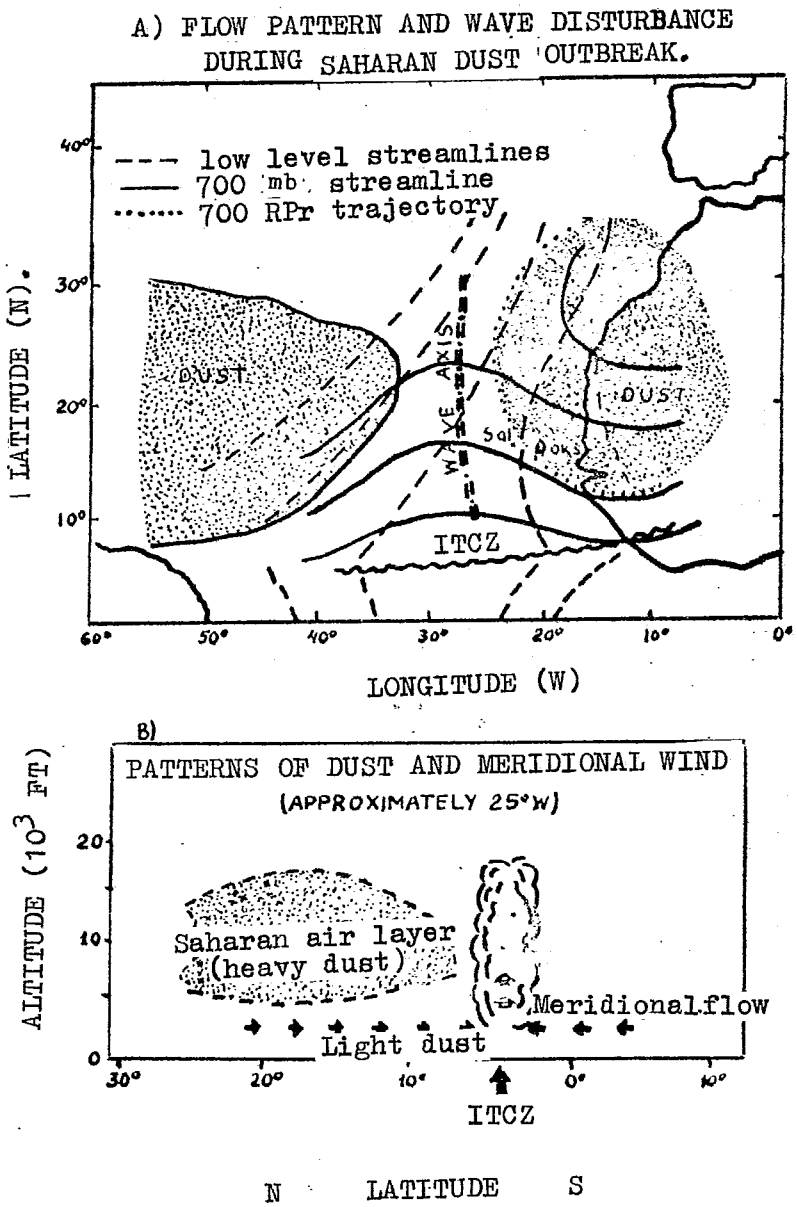

Figure 11.29A Schematic representation of the flow patterns associated with an easterly wave and a Saharan air outbreak.

Figure 11.29B Schematic cross-section of a Saharan air outbreak along 25°W looking toward Africa. Small arrows indicate the meridional component of the wind which will tend to transport material into the ITCZ.

a circulation is conservation of potential vorticity so that the decrease of SAL thickness when it is undercut by the trade winds during its outbreak into the ocean, leads to the development of the vortex (Diaz, et al., 1976).

The most characteristic feature of the wind field in SAL is the jet stream close to 700 mb with a maximum near the southern border of the layer. Most probably this jet is associated with the horizontal temperature gradient between the SAL and the surrounding dust-free air. The maximum horizontal temperature gradient is observed close to 750 mb level, the warmest air being between the jet maximum and the top of the layer (cf. Fig. 11.29).

Suppression of cloud development in the presence of SAL can be explained by two reasons: first, the presence of a temperature inversion at the base of the layer; second, large-scale downward motions near the top of the layer; especially close to the southern front of the outbreak where intensification of the downward motions (< -0.5 cm/sec) compensates for the weaker effect of the temperature inversion.

The features of the vertical profile of aerosol number density in SAL are explained by a combination of two factors: the small-scale convective mixing constantly introduces clear air into the lower layers of SAL, thus decreasing the concentration of aerosol particles; gravitational setting decreases the particle concentration near the top of the SAL, while the inner turbulence in the isentropic layer equalizes it in the layer itself. In the result the highest aerosol concentrations must be (and actually are) observed in the middle part of SAL.

Carlson (1979) has demonstrated that high resolution satellite radiometric data can be used for estimating the large-scale spatial distribution of aerosol optical thickness. The applicability of this technique is, however, limited to water as underlying surface and lifted aerosol (as is the case for SAL) for which the microphysical characteristics and the complex index of refraction can be estimated from surface or aircraft data. In the study discussed the model calculations of the aerosol optical thickness were made according to data by Carlson and Caverly (1977) for the value of $m = 1.54 - 0.0025i$ ($\lambda = 0.66 \mu m$) and 30° zenith angle of the sun.

The aerosol optical thickness τ_d is retrieved from the data of a super-high resolution radiometer on board the NOAA-3 satellite in a polar-synchronous orbit during GATE. The technique of retrieving τ_d consisted in choosing the element of minimum brightness in the histogram of brightness of the elements of one scan. These elements (50-100 for every case) are assumed to correspond to a cloud-free atmosphere and the respective values of brightness are transformed into radiation fluxes according to the technique by Carlson and Wendling (1977). The values thus obtained are used as references to plot the isopleths of τ_d .

The outlined technique was used for analyzing 7 cases of SAL outbreaks into the GATE area. The spatial distributions of τ_d ($\lambda = 0.66 \mu m$) were obtained over the area 10-25°N, 24-44°W. The values of τ_d in the centre of the outbreak (14-20°N) exceeded 2.0 and even reached 3.0. The area of such high values of τ_d was to the north of the GATE array, which explained why such values were not observed from

the surface. The analyses of radiometric data showed that SAL reached far wider than it could be traced from images in the visible.

Characteristic forms of cloudiness and sharp changes of atmospheric turbidity were observed in the region of the propagating front of the outbreak.

The estimate of the total mass from the formula relating the optical thickness to the total aerosol load in the vertical atmospheric column yielded the average value 8 Megatons (Mt). The Saharan dust mass monthly carried out into the Atlantic reaches 30-40 Mt.

In the study by Prospero et al. (1977) the results of the atmospheric turbidity network were summarized for 5 surface stations and 10 ships in GATE. Measurements were made at wavelenghts 0.5 and 0.88 μm. The average Volz turbidity values for SAL, Barbados, and Miami were 0.297, 0.130, and 0.100 respectively at $\lambda = 0.5$ μm. Atmospheric turbidity in the central and eastern parts of the northern tropical Atlantic was similar to that obtained in large industrial centres.

The values of the α exponent in Angstrom's formula for the mentioned sites were 0.348, 0.285 and 0.899 respectively. Low values of α testify the neutral character of extinction, which is supported by visual observations of sky color. Values of $\alpha \sim 1$ were observed only in Miami in the absence of SAL. From these observations the following conclusion was drawn: the optically active component of Saharan aerosol does not suffer noticeable transformations upon the crossing of the Atlantic.

No simple relationship was found between the daily averaged atmospheric turbidity in observational sites and the daily averaged concentrations of mineral aerosol measured at the surface.

The movement of SAL across the Atlantic was also traced in studies by Galindo et al. (1978) and Kondratyev et al. (1977a). In the work by Galindo et al. (1978) two cases of September 5 and 8 1974 were concerned when one of the most clear and most turbid days, respectively, were registered for the whole GATE field phase at the position of the Mexican R/V "Mariano Matamoros" (8.5N, 45.5°W). A comparison to the B-scale array data yielded an average speed of the outbreak of 18 km/h. The front of the outbreak is marked by an intense development of cumulus clouds while clouds are practically absent within the outbreak.

Kondratyev et al. (1977a) and Adnashkin et al. (1979) tracked the progress of SAL using data of 6 Soviet GATE ships: "Poryv", "Akademik Korolev", "Professor Vise", "Priboy", "Musson", "Okean".

Meteorological features of SAL have been studied by a number of authors and can be summarized (Kondratyev et al. (1976), Carlson and Benjamin (1980) as follows (cf. Fig. 11.30):

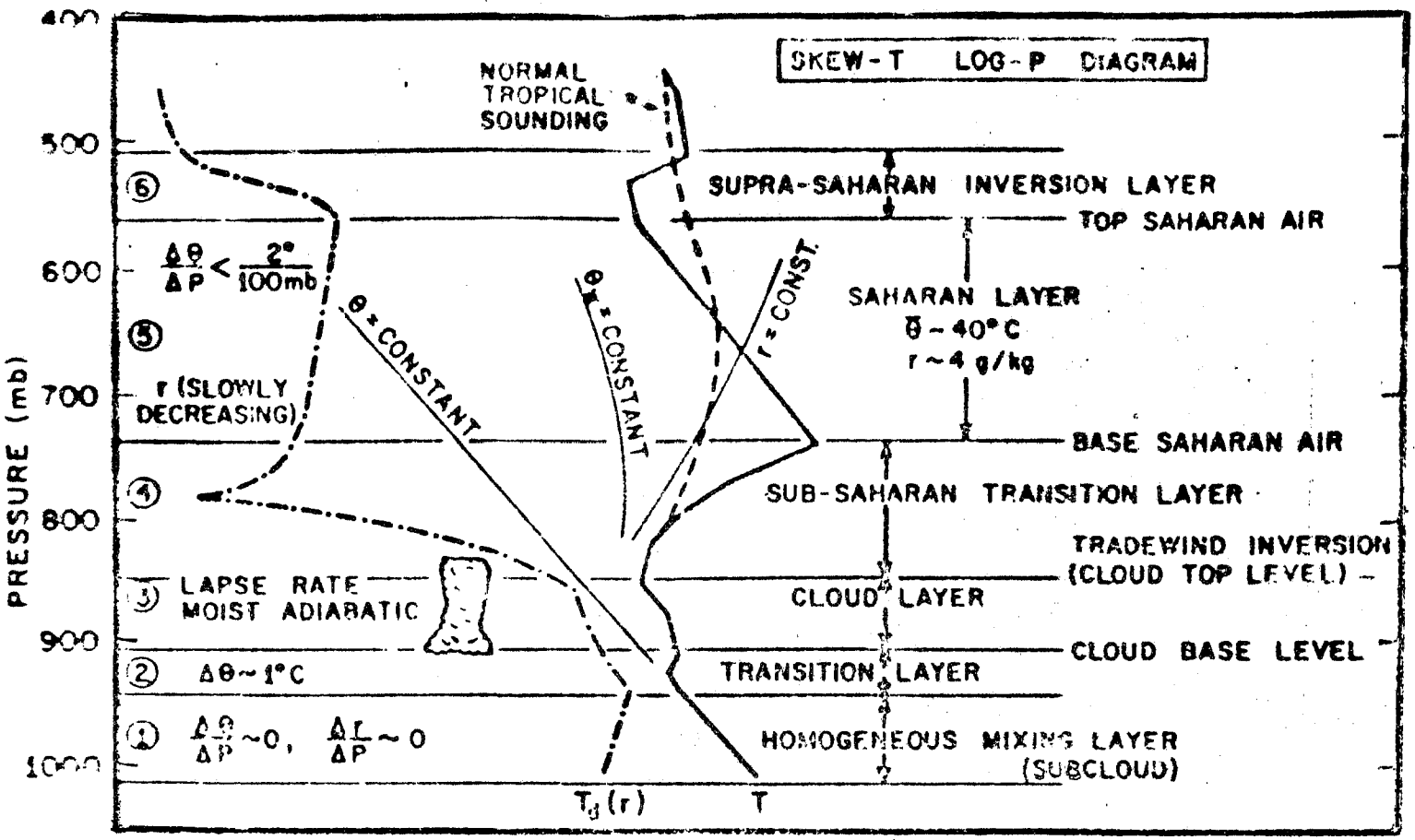

Figure 11.30 Idealized concept of meteorological conditions in the Saharan air outbreak.

(1) The SAL reaches from 0.5-1 to 4-6 km altitude moving with the mean air flow at speeds of 15-20 km /hr;

(2) The SAL base usually coincides with the trade wind temperature inversion;

(3) The temperature of SAL base is 4-7 K higher than that of the regular tropical airmass;

(4) The potential temperature is conversely 10 K higher;

(5) The water vapour mixing ratio is considerably below "normal";

(6) A step-like reduction of absolute humidity at the base of SAL is characteristic.

The microphysical and optical characteristics of the Saharan aerosol were studied by Kondratyev et al. (1976, 1977a), Carlson and Caverly (1977), Galindo et al. (1978), Patterson et al. (1977), Laktionov et al. (1976), Adnashkin et al. (1979) and many others. In studies by Kondratyev et al. (1976) and Adnashkin et al. (1979) the meridional profiles of the following aerosol characteristics obtained during the TROPEX-72 expedition are given: large and giant particles and condensation nuclei number density, aerosol extinction of direct solar radiation and particle size spectra (Fig. 11.31). The atmospheric integral transparency coefficient P_2, aerosol optical thickness τ_a and wavelength exponent is Angstrom's formula:

$$\tau_a = \beta \lambda^{-\alpha} \tag{11.10}$$

were computed. Characteristic values of P_2 in the area of the outbreak are 0.5-0.6, τ_a reaching 0.7-0.5. The exponent α varies from 0.2 (almost neutral extinction) to 0.9. The increase of solar radiation extinction is noted at $\lambda = 0.38\,\mu m$, which fact is interpreted as proof of the absorption of radiation by hematite.

The scattering phase functions in the surface layer are given in Fig. 11.32. The presence of aerosol leads to the increase of the asymmetry factor K (K = 1.8 for meteorological visibility S_m = 100 km, and K = 12 for S_m = 7.7 km). Phase function minimum shifts to 110-120°.

The aircraft measurements of aerosol particle number density ($r \geq 0.2\,\mu m$) and the chemical (elemental) composition ($r \geq 0.03\,\mu m$) showed that SAL has particular vertical structure. The maximum number densities fall to the layer boundaries while the minimum number density in the middle of the layer corresponds to the largest mass lead. The authors explain this feature by a number of factors: short life history of the layer, turbulence and updrafts in the layer which promote intensive particle coagulation.

The above particularity together with the fact that the maximum of shortwave heating in SAL falls exactly to the levels of minimum number density forces one to stipulate that radiation absorption due to large conglomerate particles takes place, the actively absorbing small particles of high imaginary part of the complex index of refraction being embedded in these.

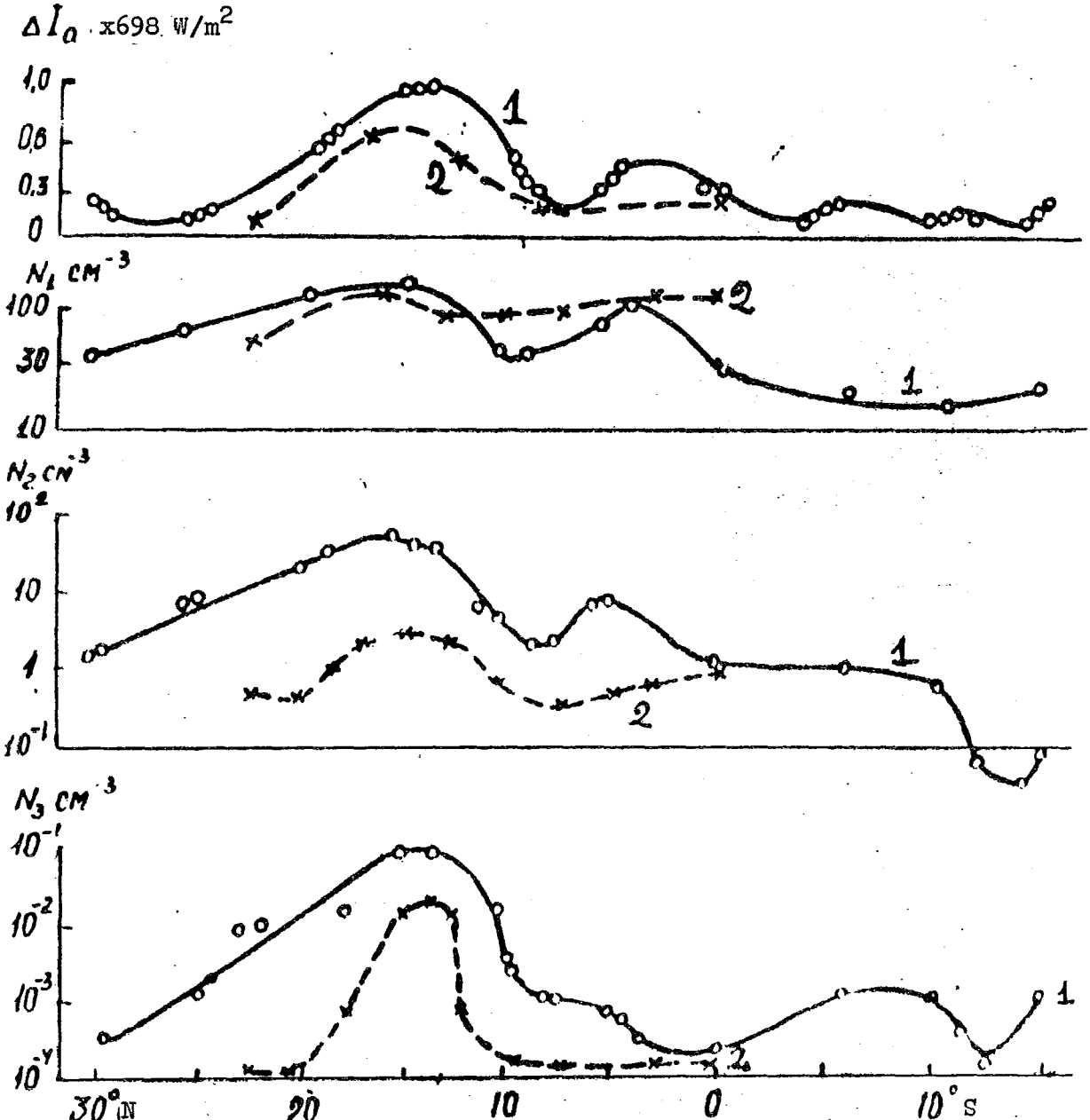

Figure 11.31 Meridional profiles of direct solar radiation aerosol extinction (1) and large and giant particles number density (2) from the TROPEX-72 expedition.

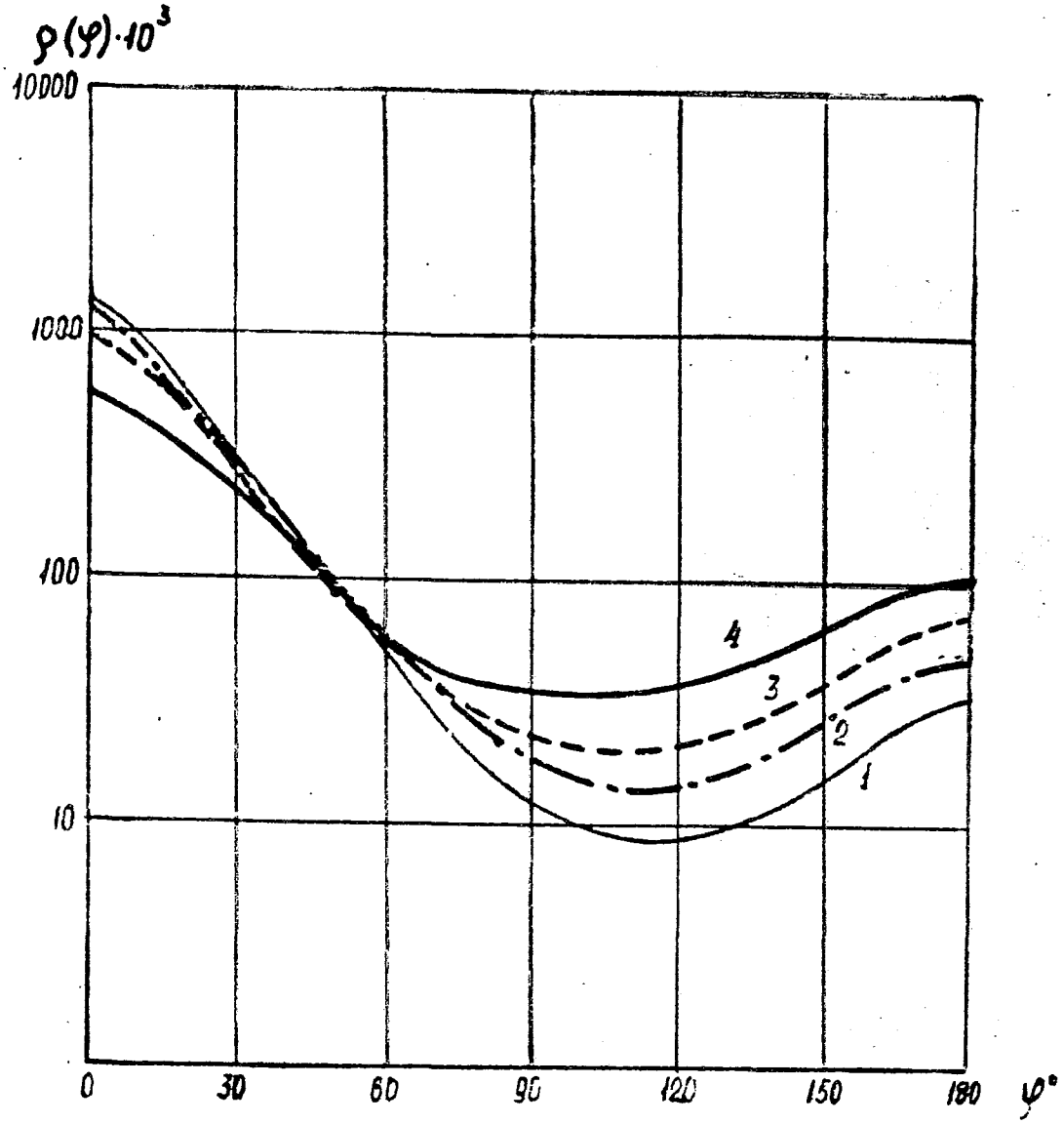

Figure 11.32 Scattering phase functions in the surface layer from the TROPEX-72 expedition.
1 - 4 - heavy to negligible dust load.

The chemical analysis revealed the presence of elements characteristic for continental aerosols. Contents of Fe ($\geqslant 10\ \mu g/m^3$) and Al (5-10 $\mu g/m^3$) were particularly high. The samples did not yield elements or morphological structures characteristic for marine aerosols. In the laboratory Patterson et al. (1977) determined the complex index of refraction of Saharan aerosol in the wavelength range 300-700 nm sampled at Barbados, Sal and Tenerife during GATE and also on board the FRG R/V "Meteor" in November 1973 at point 17°N, 26°W.

The samples were taken on polystyrene Delbag Microsorban filters at a flux of 2.8 m^3/min and with a sampling time of 24 hrs. The aerosol particles were removed from the filters by solving the latter in toluene with further multiple washing of the sedimented aerosol matter.

Elemental composition of the samples was determined by means of neutron activation technique. Concentration of marine salts was 14 $\mu g/m^3$ on the average, that of Saharan mineral aerosol 76 $\mu g/m^3$, so that marine salts made up 16% of the total aerosol mass. These results agree with the data by Kondratyev et al. (1976) and Pueschel (1975).

The prevailing constituent are the brownish aggregated particles of radii $\geqslant 0.3\ \mu m$, coated with clay dust. All the samples are quite similar. The real part of the complex index of refraction determined through Beck's technique (illumination of the particles suspended in oil of known optical properties by visible light) constituted:
$n' = 1.558 + 0.004$ ($\lambda = 550\ \mu m$) and $n'' = 1.552 \pm 0.004$ ($\lambda = 630\ \mu m$).

The imaginary part of the complex index of refraction (n'') was determined from the measurements of absolute reflectivity using the technique of sample dilution that enables one to apply the Kubelka-Munck theory to data thus obtained. Calibrated barium sulphate powder was used for diluting.

Estimation of the technique errors, accounting for the noise of a spectrophotometer in an integrating sphere, the uncertainties in scattering, variations in the aerosol sample density, and also the uncertainties in the Kubelka-Munck theory itself yields a measurement error of 40% for n''.

The measurements showed the n'' value for Saharan aerosol to be at least an order of magnitude higher than for marine salt, so that salt may be considered a non-absorbing additive, decreasing n'' by some constant value. Considering the mass ratio for salt and mineral aerosols in the samples, n'' for Saharan aerosol varies from 0.025 ($\lambda = 300$ nm) to 0.0038 ($\lambda = 600$-700 nm), and slightly starts to increase again within the near-IR.

During GATE aerosol filter sampling in order to determine its optical properties was performed by Pueschel (1975). The data on particle shape and size distribution were obtained with a scanning electron microscope. Elemental composition was determined from dispersion x-ray analysis, which confirmed the already available data on mineral origin of the aerosol and its complex index of refraction.

The particle size distribution is of Junge type with mode diameter $D = 0.5\ \mu m$ and exponent factor $\gamma = -3$.

On the basis of these data the Mie calculations of total scattering, absorption and back-scattering were performed. The following climatologically significant results were obtained at $\lambda = 0.5\,\mu m$: (1) with a real part of the refractive index $n' = 1.6$ the total scattering exceeds absorption if the imaginary part of the refraction index is within the limits $0 \leq n'' \leq 0.05$; (2) the critical value of the absorption to backscattering ratio above which the surface warming exceeds cooling is reached at $n'' = 0.015$. Thus the effect of the Saharan dust should be cooling at the surface if one assumes the value $n'' = 0.0045$, which is commonly referred to; (3) the total or "effective" system albedo approximately doubles in comparison to ocean surface albedo in the presence of aerosol with the complex index of refraction $n = 1.0 - 0.005i$.

The IR computations ($\lambda = 10\,\mu m$) show that: (1) total scattering exceeds absorption for $n'' = 0.25$; (2) for $n'' = 1.0$ (the value usually given in literature for Saharan aerosol) only 17% of the total radiation extinction falls to absorption.

The author concludes that the optical density of SAL is generally lower than for industrial aerosols, but its climatological effects must be considerable because of its wider spatial extent.

The light-scattering properties of Saharan aerosol were studied by Grams et al. (1977) with the help of a laser polar nephelometer mounted on board the US NCAR aircraft L-188 "Electra". The nephelometer measures the scattered radiation intensity ($\lambda = 0.633\,\mu m$) within 15°-165° at 5° step.

On the basis of simultaneous measurements of aerosol size distribution and number density by means of an optical counter and impactor the intensity of scattered light was calculated according to Mie formulas with different complex refractive indices. The value yielding the best agreement with nephelometer results was chosen as the one corresponding to reality. The analyses of 14 samples taken on July 9, 1974 give the value $m = 1.525 - 0.0067i$, its real part remaining constant, and imaginary part being determined to the uncertainty factor of 4. Within these limits the result agrees with the data of preceding measurements in Texas (Big Sprongs), at Barbados and Canary Islands.

Carlson and Caverly (1977) made the analysed radiation observations from Cape Verde Islands during GATE. The aerosol optical thickness according to Volz sun photometer observations was about 0.7-1.0 during SAL outbreaks and ~ 0.5 in other cases. The aerosol turbidity factor (wavelength exponent) in Angstrom's formula was close to zero, which testifies to neutral character of the aerosol extinction.

The SAL particle size distribution was studied from the US NOAA DC-6 aircraft by means of a Royco-220 electro-optical aerosol spectrometer that covers the range $D = 0.4\text{-}11\,\mu m$. The curves of the dependence $\Delta S_v / (\Delta \ln D)$ are presented (Figure 11.33) where D is the particle diameter, $\Delta S_v = \Delta N_v \pi D^2$, ΔN_v - unit volume number density for particles of diameter D. The area under such a curve presents the total particle surface within the given size range, i.e. a measure of their optical activity. The diameter D_m, corresponding to the maximum shows the particles with the main input influence on radiation. In most cases $D_m = 2\text{-}4\,\mu m$. The corresponding logarithmic distributions $dN_v/d\ln D$ have a bend in the region $D \sim 5\,\mu m$. In the most dense part

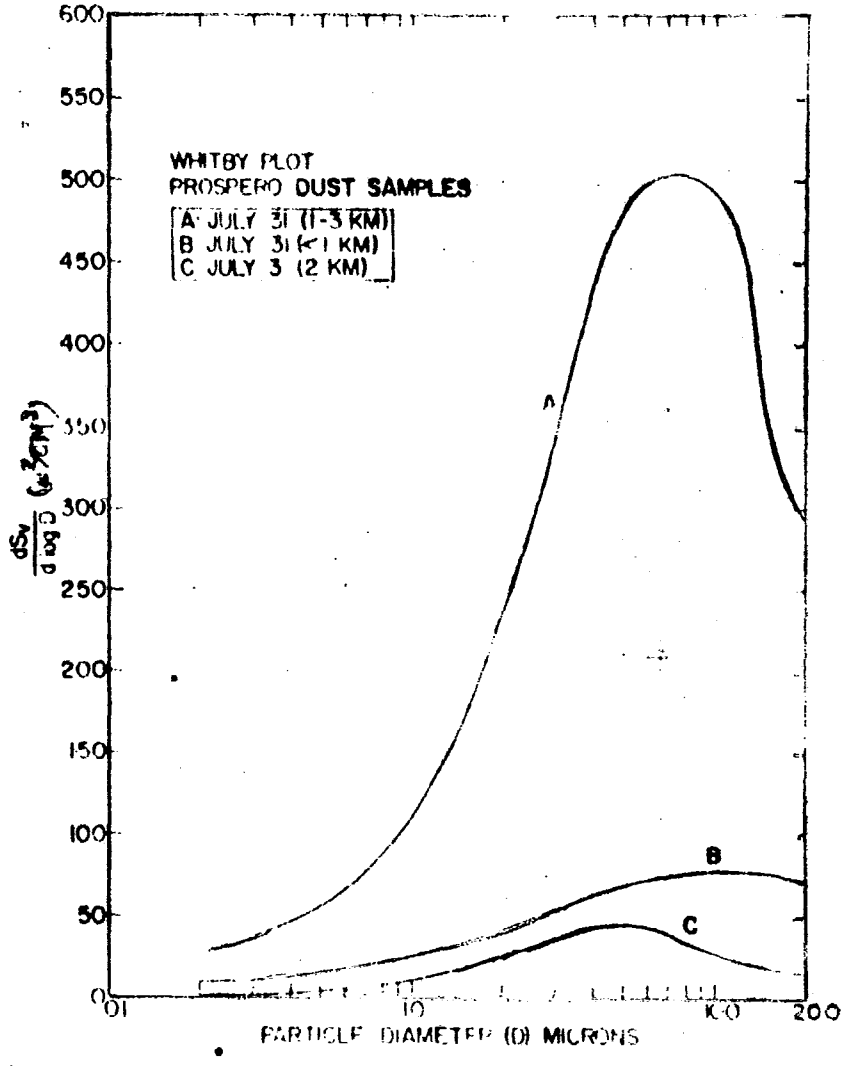

Fig11.33 Whitby plot for composite dust spectra measured with a Royco 220 aerosol spectrometer aboard the NOAA DC-6 aircraft near Sal on July 31 (spectra A and B) and south of Dakar on July 3 (spectrum C). Flight altitudes are listed in the inset

of the layer (measurements of July 31 , 1974) D_m = 8-10 μm and over 50% of the mass of Saharan aerosol is in the range D > 20 μm.

Optical characteristics of the Saharan dust are calculated from Mie formulae, using the above microphysical characteristics with the complex index of refraction m = 1.54 - 0.005i. The comparison of monochromatic aerosol attenuation coefficient thus obtained with values calculated through Koschmieder's formula from the surface observations of horizontal visibility at Sal disclosed the discrepancy of more than half an order of magnitude. The authors explain such a discrepancy by the errors associated with the use of Koschmieder's formula and the particular vertical profile of number density of SAL (the "empty" layer in the lower kilometer of the atmosphere).

Kondratyev et al. (1977a) paid particular attention to the problem of the influence of Saharan aerosol upon radiation transfer and atmospheric circulation using vertical and horizontal visibility observations on board the "Passat" at position 0°, 10°W. The most powerful dust outbreak on August 11, 1974 was characterized by values P_2 = 0.50, τ_2 = 0.694, S_m = 8.0 km, α = 0.372 km^{-1} with particle number density in the surface layer

$$N_D > 0.63\ \mu m = 30\ cm^{-3}$$

The spectral radiative effects of SAL were studied by Kondratyev et al. (1976) (Fig. 11.34). The spectral and integral radiation measurements showed in many cases the presence of an "optically empty" layer below SAL, where practically no changes of atmospheric radiative characteristics with height were observed.

The spectral albedo of the layer increased with height, this increase being more expressed in the near IR part of the solar spectrum (0.8-1.0 μm). The spectral course of the aerosol radiative heat flux divergence in SAL in the 0.4-1.0 μm range qualitatively coincided with the spectral dependence of the imaginary part of the complex index of refraction for hematite (Fe_2O_3), which was considered the primary absorbing agent. The maximum relative absorption of radiation by aerosol registered on September 4, 1974 reached 20%.

The relative input of the aerosol absorption in the 1-2 μm range was calculated as difference between the total (measured) and molecular (calculated) absorption. It varied from 8 to 25% for SAL as a whole. Aerosol input was most stable in the 1.65-2.10 μm range. Considerable variability of the spectral course of aerosol absorption in the IR was registered. The analyses of the vertical profiles of spectral albedo at fixed wavelengths in the 0.5-1.4 μm range, of the brightness phase functions, and of coefficient of anisotropy for reflected radiation showed that the albedo maximum and anisotropy minimum for the upward flux corresponded to a level of maximum concentration of metal-containing absorbing aerosol particles. On the whole the Saharan aerosol appeared to be spectrally neutral in this range.

The integral radiation measurements performed by Kondratyev et al. (1977b, 1978, 1979) revealed considerable total extinction of the shortwave radiation in SAL, reaching 25-30W/(m^2km). The increase of albedo with height is uniform inside the layer becoming somewhat sharper in its upper part (due to increased scattering). The long-wave upward radiation sharply decreases with height in the presence of

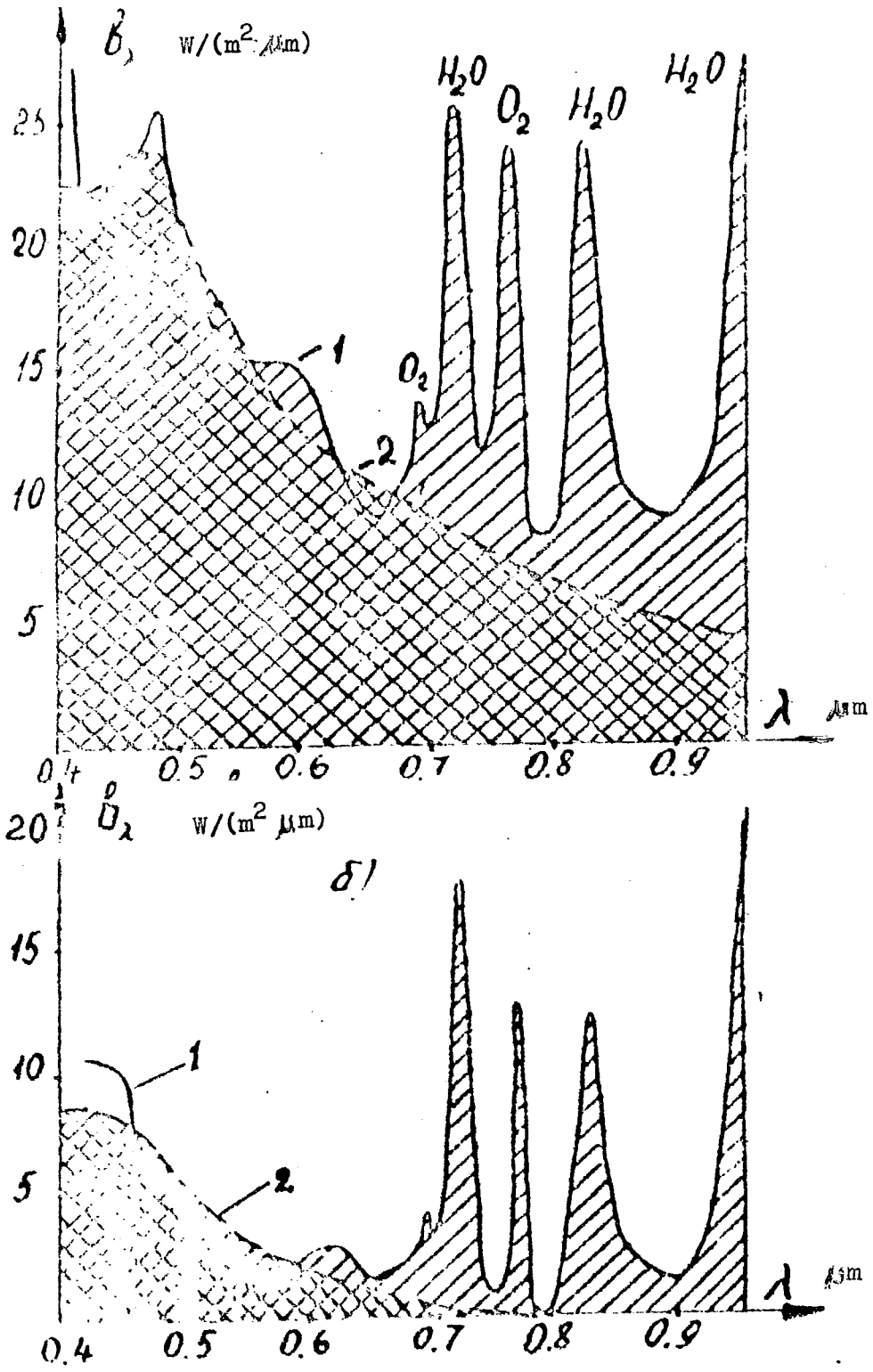

Figure 11.34 Plots of shortwave radiation spectral absorption in the presence (a, July 4, 1974) and absence (b, August 13, 1974) of SAL. Data from IL-18 MGO K-2 spectrometers. 1 - total absorption in the 6100-450 m layer; 2 - aerosol absorption.

aerosol (by up to 40 W/(m^2km) in the lower part of the layer up to 3 km height), which leads to a decrease of the radiative cooling within the layer to negligibly low values. Radiative heating of the lower 5-km atmospheric layer in the presence of SAL increases by 80-100 W/m^2, this additional heat being released in the middle troposphere inside the layer.

The results of measurements of the spectral flux divergence in the absence of clouds showed that it was determined solely by aerosol absorption in the 0.4-1.0 μm range. The spectral signature of aerosol absorption was qualitatively interpreted as hematite (Fe_2O_3) absorption. In the case of a heavily turbid atmosphere it reached about 31 W/m^2 in the layer 6.1-0.5 km over the range 0.4-1.0 μm (approximately 3.3% of the solar constant), while the gaseous component was approximately 10 W/m^2. The aerosol and gaseous absorption over the whole shortwave range (0.3-3.0 μm) were comparable in highly turbid atmosphere.

According to the data by Grams et al. (1977), the diffuse radiation flux increases by 40-90% when passing through SAL, the turbidity coefficients by 60%; the wavelength exponent for total radiation extinction (α) drops from $\sim$1 to $\sim$0.

The largest radiative heating rates due to shortwave radiation absorption are registered in the 1-2 km layer (up to 0.43°C/hr) in contrast to aircraft observations in the region of the "sea of darkness". In the absence of SAL the radiative heating rate is at maximum in the 0-1 km layer (about 0.12 K/hr).

Carlson and Caverly (1977) found that solar radiation extinction at the surface determined by diffuse to global flux ratio technique constituted on the average 20-25% daily for July 1974 with the optical aerosol thickness $\tau_d = 0.74$ ($\lambda = 0.5$ μm).

During GATE measurements of direct solar radiation in the 0.3-3.0 μm range were performed from aboard the US NASA "Convair-990" aircraft in the Schott filter bands with the shortwave cut-offs at 0.395, 0.495, 0.530, 0.630, 0.695, and 0.805 μm.

Hickey and Griffin (1975) presented the results of measurements on June 30 and July 31, 1974 at the levels 150, 1500, 3050, 6100, 9150, and 12200 m. At 20.2° solar zenith angle the solar flux attenuation at the upper level reached 10.8% (1309 W/m^2).

On June 30, 1974 the SAL reached from 1650 to 5700 m and on July 31, 1974 in the Cape Verde Islands area - from the ocean surface to 5800 m. In an attempt to reach the base of the layer on July 31 "Convair-990" performed the touch-and-go at the air field runway on Sal.

The uniform character of extinction in all the spectral bands points to "neutral" character of the extinction by Saharan aerosol. The total extinction of the direct solar radiation in SAL amounted to 891 W/m^2 on July 31, 1974 (64.8% of the extraterrestrial value).

Cox and Minnis (1978) examined the radiative properties of Saharan aerosol on the basis of aircraft actinometric data (four integral hemispheric fluxes were measured) obtained in 6 GATE missions by the NCAR "Sabreliner".

The observational results were compared to those calculated from shortwave and longwave radiation transfer models (0.285-2.8 and 4-50 μm, respectively). The shortwave model considered the absorption by H_2O, CO_2, O_3 for specified concentrations of the given components and included 7% Rayleigh scattering. The longwave (IR) model included the same gases and also H_2O-CO_2 band overlap, similar to that used by Carlson and Wendling (1977).

Applying both models the sensitivity of the results to input parameter errors was estimated. It was shown that relative shortwave radiative characteristics were negligibly sensitive to variations in water vapour amount. On the whole, the errors to be expected were in the range ± 0.005 for absorptivity and ±0.002 for reflectivity of the layer, corresponding to ±0.012K/hr/140 mb.

With the accuracy of data on absolute humidity of ±10% and on temperature ±1K, the emissivity errors amount to ±8% for downward radiation, and ±7% for upward. The combined effect of these uncertainties led to 10% error (±0.01K/hr/100 mb) in radiation temperature changes.

The comparison of calculation results to measurement data demonstrate good agreement (within the above accuracies) in the absence of dust outbreaks. Therefore the radiative effects of aerosol are estimated as difference between the measurement data in presence of aerosol and the model calculation results.

The increase of absorption of shortwave radiation in a sounded layer (up to 550 mb) during aerosol outbreaks was 9% on the average. The increase of reflectivity was twice as large. Extinction of the layer increased by 20% (61 W/m^2). In the result 6% less radiative energy reaches the surface. It is noted that the lower part of the aerosol layer mainly contributes to scattering, while the upper contributes to absorption (this result agrees with the conclusions by Kondratyev et al. (1976), and Carlson and Caverly (1977)). The radiative heating in the upper part of the layer (in comparison to "clear" atmosphere) increases by 0.025K/hr, 0.01 K/hr in the middle layer and the maximum of heating is shifted to the 700 mb level.

The comparison of calculated and measured emissivities leads the authors to the conclusion that the Saharan dust does not significantly contribute to the balance of IR radiation. The possible effect of aerosol consists in weakening the cooling at lower levels, but scanty data do not permit any final conclusion.

Carlson and Caverly (1977) made calculations of the imaginary part of the refractive index with the use of delta-Eddington approximation by inverting the model calculations at three wavelenghts : 0.365, 0.468 and 0.610 μm. The respective values found are 0.018, 0.008 and 0.0029.

The total dust load in the atmospheric column was estimated through its relation to aerosol extinction coefficient calculated from Mie formulae. From the results of 7 days of observations from aboard NOAA DC-6 a practically linear dependence was obtained which made it possible to express the mean mass concentration (c) of aerosol and its total load (M) through aerosol optical thickness (τ_d) and

geometrical thickness of SAL (h). The respective values for July, 1974 are: $c = 550\ \mu g/m^3$, $M = 2.8\ g/m^2$ for $\tau_d = 0.74$ ($\lambda = 0.5\ \mu m$) and $h = 5$ km.

On the basis of these results, the conclusion was made that the decrease of solar radiation by Saharan aerosol is to a large extent due to absorption at shorter wavelengths though backscattering plays an important role too. The general effect of aerosol in the total system reflectivity over the spectrum should, however, not be larger since the increase of absorption may be almost compensated by backscattering.

Carlson and Benjamin (1980) calculated the fluxes and flux divergences in SAL, based on the idealized presentation of Saharan dust properties. The size distribution and spectral dependence of the complex index of refraction and also the vertical distribution of meteorological parameters were synthesized from a number of papers dedicated to SAL and its properties. The electromagnetic spectrum was divided into 4 bands within the shortwave range (up to 4 μm), and into 12 within the longwave range (up to 250 μm).

The calculations were made by means of the delta-Eddington approximation and were also compared to the more accurate doubling technique. Radiation transfer in the IR absorption bands was calculated with application of the random band model.

Calculations were made for cloudless and cloudy conditions over the ocean (surface albedo A = 0.05) and desert (A = 0.30) surfaces. Cloudiness was represented by a Sc layer between 950 and 900 mb with an emissivity of 1.0 and optical thickness of 10.

It appeared that the results in IR are hardly sensitive to variations in aerosol optical thickness and the particle size spectrum: the change of the complex refractive index by the factor of 2 leads to 8% change in the IR fluxes.

The outgoing fluxes over ocean in the absence of cloudiness are no indicator for cooling or warming of the Earth-atmosphere system, since it appeared that they are almost insensitive to changes in the aerosol optical thickness. The cooling at the surface due to a decrease of the downward flux is practically compensated by the increase of warming in the middle troposphere. The increase of aerosol load over the desert or cloud layer leads to total heating of the system because of the decrease of reflectivity.

The radiation interaction of aerosol and cloud must be critically important since the increase or decrease of stratiform cloudiness underlying the aerosol layer will change the system reflectivity.

Additional radiative heating rates in SAL for the optical thickness $\tau_d \sim 1.0$ reach 1-2 K/day in the 600-800 mb layer. This is important for the radiative forcing generated by horizontal gradients of the heat flux divergence between the dusted belt from 10-20°N and the "clear" ITCZ around 5°N.

The role of SAL in altering the atmospheric radiative regime was also discussed by Prospero et al. (1977). The presence of Saharan aerosol may increase the absorption of solar radiation by 100% and strongly inhibit an IR cooling. The resulting decrease of cooling may be an important factor in explaining the stability of the temperature inversion at SAL base. This inversion, in turn, strongly inhibits the development of penetrative convection over large areas of the Atlantic. Particularly this lack of cloudiness makes detection of SAL so easy in satellite images.

The role of dust in cloud formation may be qualitatively assessed on the basis of data by Weickman (1975) who has shown that the concentration of ice nuclei active at -20°C in the GATE area often reaches 10 to 100 dm^{-3} while the typical value over continents is less than 1 dm^{-3}. Therefore the penetration of dust-loaded air into powerful convective cloudiness may lead to quick and intensive formation of ice particles. This, in particular, can explain the existence of extensive fields of opaque cirrus decks so often observed in the GATE area.

11.9 RADIATION ROLE IN TROPICAL CONVECTION

Theoretical and experimental studies prior to GATE have provided a certain level of understanding of the dynamical processes in the tropical atmosphere. Thus in a fundamental study by Riehl and Malkus (1958) it was shown that the vertical mass and energy transport in the equatorial trough zone was determined by 1500-5000 gigantic convective clouds, assumed to be grouped in approximately 30 clusters. This result has put forward the problem of the relationship between the penetrative convection and the large-scale atmospheric motions as the central subject of tropical meteorology.

The earlier studies have shown the depth of penetration of the warm air parcel into the stable atmospheric layer above the mixing layer and the entrainment of the stable air into that layer to be the crucially important factors for the build up of the convective layer. The lapse rate γ of the stable layer, the depth of the convective layer and the turbulent heat exchange between the underlying surface and the atmosphere are among the most essential features of the process considered. Noonkester and Jansen (1977) discussed the temporal variations of the convective layer depth and its dependence on the stability near the top of the mixing layer and on surface temperature changes. The observations during September-October 1973 in cloudless conditions have shown the convective layer height "h" to have an asymmetric daily course. The maximum of "h" is reached before the maximum temperature of the underlying surface. The rate of increase of "h" does not change with time during the erosion of the "constant layer", but sharply changes upon reaching the layer with a different lapse rate. The convective layer depth decreases during the late afternoon hours after a period of high variability of "h" in the vicinity of its maximum value. The increase of the rate $\Delta h/\Delta t$ does not depend on the convective layer depth during the period from the early morning hours until approximately one hour prior to the maximum of "h".

The GATE ship, aircraft and satellite data provided for the first time the possibility for analyzing the tropical meso- and synoptic scale weather systems with high time resolution. For example, Foltz (1976) undertook a diagnostic study of moisture (specific humidity "q") and dry static energy balances ($S = T + gz/C_p$), (where T is the air temperature, g is acceleration of gravity, C_p is specific heat at constant pressure) on the basis of aerological soundings (from B-scale and A/B-scale ships) and satellite data. From rawinsonde soundings from eight ships the divergence was computed at 32 levels from the surface to the 100 mb layer with 3-6 hours time resolution. The q and S balances integrated over the whole atmospheric layer were calculated for all three phases of GATE. The averaged moisture budget of one phase presents a balance between the large-scale moisture convergence, surface evaporation and condensation. The balance of S shows that the mean dry static energy convergence over the A/B scale together with radiative cooling is almost totally compensated by condensation. The heat storage and heat exchange between the ocean surface and the atmosphere are smaller by one to two orders of magnitude on the average, but during certain short time periods the heat and moisture storage can become significant due to short-term fluctuations of S and q.

The advection of dry air to the A/B scale area with a maximum close to the jet stream layer at about 650 mb was important for all the phases, leading to an imbalance of the moisture budget. Radar derived precipitation was observed to lag by 4-6 hours the computed values for intensive precipitation periods. Accumulation of liquid water in clouds during formation of precipitation should be considered the most probable cause of such a lag. The total condensation rate is quite closely connected with the instant vertical motions at the 700 mb level, no largescale lifting being observed prior to intensification of convection. The total condensation is the most reliable parameter for calculating the latent heat released in the tropical convective systems, as determined by the instant mass convergence below 700 mb. The condensation maximum as obtained from the q and S balances is reached at approximately 07:30 hr LT.

The analysis of a large set of various observations (precipitation, rawinsonde, satellite images, radar, etc.) has shown (Jackobson (1976)) that a pronounced diurnal course of the convection responsible for the build-up of cumulus cloudiness is characteristic for most of the tropical and subtropical regions. The rawinsonde combined data and the satellite images over the Western Pacific have revealed a considerably more pronounced convergence in the morning hours (around 10:00 LT), as compared to evening (around 22:00 LT).

From 13 years of hourly precipitation observations at eight atolls and minor islands in the Pacific a considerably higher frequency of heavy showers in the morningthan in the afternoon or early evening hours was derived. The intensification of convection during the 22:00-10:00 period, LT, in comparison to that during 10:00 - 22:00 was also confirmed by the analysis of the cloud cover images from the US Defence Department meteorological satellite. The retrieval of the daily course of penetrative convection from satellite data alone is hampered by the difficulty to discern separate convective cells, while the surface data analysis of cloud amount is complicated by the masking due to other clouds.

It should be particularly noted that Jackobson (1976) while explaining the afternoon-to-early-evening maximum of convective cloudiness over land by the daily course of solar heating (especially so with strong diurnal temperature changes in the zone of weak evapotranspiration: deserts, semi-arid zones), points out that the morning maximum and afternoon-to-evening minimum are characteristic for the convective regime over the ocean.

Thus, the studies even prior to GATE have shown the necessity to review certain theoretical notions about the development of convection, the role of dynamical, radiative and other diabatic factors in the formation of powerful convective clouds in the tropical zone.

The GATE-based studies started with analyzing separate episodes of cloud formation and development during some chosen experiment days.

The new prospects of studying the relationship between the penetrative convection and large-scale motions were opened by the successive cloud cover images from geostationary satellites used for retrieving the wind field at the trade wind cumulus and the cirrus level.

Suchman et al. (1977) outlined a technique for determining the spatially averaged vertical mass transport (M) inside and around the cloud clusters on the basis of the assumption that M was caused by the divergence in the lower tropospheric inflow and upper tropospheric outflow layers, which could be retrieved from the cloud motions. A three-layer model of the atmosphere, consisting of two passive and one active layer was introduced. The outflow layer embraced the anvils of Cb clouds. The vertical velocity in the upper part of the inflow and the lower part of the outflow layers was estimated from the data on the divergence field. The vertical mass transport M was determined for two mature tropical disturbances from the "SMS-1" images of September 5, 1974.

The cloud clusters formed along the boundary between the strong NE trade wind flow and the SW monsoon. A strong cyclonic vorticity in the lower troposphere and a convergence maximum at the same level were typical for all clusters in the disturbance. In both cases the strongest upward motions in the lower layer occurred some hours earlier than in the upper one. The velocity of the upward flows decreased with the increasing cluster dimensions, remaining, nevertheless, considerable causing appreciable upward transport even outside the clusters. The mass transport on the cluster scale varied from 15 to almost 35 mb/hr. The slight negative transport in the inflow layer of the more mature clusters was an exception, which testified the presence of powerful mass transport into the cluster zone in the middle troposphere.

Loranger (1975) studied the spatial and temporal variability of the tropical Sc and convective cloudiness for 29 days of the first and second phase of GATE from the "SMS-1" data. The data refer to the 0-15°N, 17.5-27.5°W area. The maximum probability of occurence of cloud rings was around a 4-6 day period during the first phase while a shorter one is typical for the second. This period correlated with the passage of the easterly waves and with convective intensity as determined from ship observations (there was also negative correlation between the cloud-ring frequency and convective intensity). The analysis of the spatial distribution of cloud occurence frequency revealed 5 maxima of 10-30%. These maxima correlated with the areas of dissipating, extending or weak convection.

During the third phase of GATE, on September 14, 1974 a well-organized line of S-N oriented Cb clouds formed together with an associated cloud mesosystem. It formed within the B- and C-scale ship arrays and slowly drifted to the West. This mesosystem was thoroughly studied through ship rawinsonde soundings and observations from 5 aircraft in the 990-190 mb layer by Emmanuel (1977). Each aircraft passed 4 to 12 times through the mesosystem approximately along the cloud line.

The aircraft data processing revealed considerable difficulties in determining the aircraft position with an accuracy sufficient for obtaining the spatial structures of convective cloudiness. A resolution of about 1.8 km and 30 min was reached in measuring the separate elements of the convective system.

The preliminary wind field, temperature, and humidity data analysis showed unexpected features of the mesosystem structure including the region of strong vorticity, the generation of negative absolute vorticity over large areas and the discretness of the cloud line movements. Two strong maxima of the upward motions were observed: one before the surface gust front, and the second, elevated, caused by either the buoyant force or the mesoscale warming. In the updraft region the vorticity is generated, reaching its maximum in the middle troposphere. The mesosystem moved eastward for a few hours against the general direction of momentum transport. However, separate cloud cells having a life time from 0.6 to 1 hr moved to the NW with the mean flow.

Warner et al. (1979) have traced a cloud cluster on September 18, 1974 (day 261) including data from the SMS-1 geostationary satellite, the B and A/B scale ship arrays and five aircraft. The clouds generated within and above the moist surface flow drifted towards the cluster and banded into lines or arcs of small ($\sim$500 m) cumulus clouds at the 500-700 m level with a mean spacing of 1-2 km. With 15 min satellite images the cloud could be tracked for more than 2 hours, and the aircraft photographs showed them to consist of a lot of small clouds. The ship radar data demonstrated that the clouds appeared after precipitation fallout. Apparently these small convective clouds are indicators of the downdraft structure which accompanies precipitation and stimulates their generation. Finally, the small clouds developed into isolated precipitating Cb clouds. The synchronous aircraft data showed that the cloud areas existed as a consequence of the mesoscale circulation (the constantly renewed convection), caused by the release of latent heat in clouds, but not by the primary air flow at the ocean surface.

The influence of the surface processes reaches up to only 500 m. The vertical transport of heat above this layer is mainly caused by cloud arcs and larger clouds. Circulation was most intense close to and just above the lower cloud boundary, but weakened with height in the lower 1 km layer. The horizontal scale of the whole mesoscale circulation system was about 40 km, the characteristic life cycle $\sim$2 hrs. Apparently the mesoscale cloud structures in the moist surface layer are a dominant factor in the interaction between convection in the moist surface layer and the lower troposphere up to 6 km.

The results of atmospheric studies in the GATE area were to a certain extent summarized by the US GATE Central Program Workshop in 1977. The following conclusions of this workshop are important with regard to the GATE RSP problems:

(1) In the ship array, the continental aerosols are more plentiful than sea salt particles below cloud base on most days. At levels above 900 mb, very few salt particles are observed, but the dust particles which can act as ice nuclei are quite numerous during major dust outbreaks.

(2) A significant diurnal change of atmospheric parameters is present in the GATE area and over other tropical oceans. Within the GATE A/B-scale area this is best observed in troposphere divergence profiles and heavy rainfall from well-organized weather systems. Maximum convergence and rainfall occurs in the late morning and afternoon. This rainfull maximum is 6 hrs later than that observed in the West Pacific.

(3) Emissivity of cirrus clouds and high middle clouds was observed to be significantly higher than expected. Cloud and cloud-free radiation divergence differences are as large as the cloud free IR cooling itself. These cloud and cloud-free differences may significantly feedback to the mesoscale circulation.

The above results appeared to be somewhat unexpected in the sense that the powerful convective clouds were generally supposed not to have any predictable diurnal course, because the lower tropospheric stability over oceans does not suffer considerable diurnal variations.

The composite analyses of observational results, referring to the Western Pacific, the GATE area and other tropical areas, that revealed the existence of a pronounced daily variation of convective cloudiness and precipitation were performed by Gray (1977). Observations in tropics over land demonstrated the presence of an early to late morning maximum of powerful convective cloudiness in contrast to only one maximum during the afternoon. The analysis of the data from Pacific island stations showed a pronounced maximum of powerful convection either in the morning or afternoon hours throughout the year (in the afternoon maximum the island influence is probably manifested). The more powerful the convection is, the stronger its diurnal course with a morning maximum is expressed. The heavy rainfall occurence from cloud clusters (>1.0 cm/hr) is three times higher during the morning hours.

According to the GATE data the daily maximum occurs in the early afternoon hours. Apparently the 6 to 7 hours lag of the penetrative convection maximum is caused in this case by the influence of the continent of Africa and is associated with close connection of the heavy rainfall in the GATE area with lines of deep convective clouds. A considerably weaker diurnal course is characteristic for low clouds and total cloudiness.

Gray (1977) suggested that the diurnal course of powerful convective cloudiness, peaking in the early morning, is driven by spatial variations of the vertical profiles of longwave cooling. A considerably more powerful radiative cooling of the cloud-free atmosphere surrounding convective cloudiness enhances the downward motions there, thus stimulating the convergence in the lower layers into the convection zones. The subsidence-induced heating of the atmosphere and the low level convergence considerably weaken during the day. During the night due to increased radiative cooling in the upper tropospheric

convection zone, the discussed processes intensify as compared to the cloud-free atmosphere, the situation being reversed during the day. Only mesoscale weather-forming systems have the life-span and dimensions large enough for the radiative processes to become important. Naturally, there must be a lag between the radiative processes and reaction of convective cloudiness and precipitation.

Foltz (1976) treated the hypothesis of the radiatively modulated diurnal course of convection from the point of view of the atmospheric energy balance formation. It is known that the tropospheric radiative cooling is compensated, globally, by condensation or latent heat release (70-80%), and the transport of sensible heat (20-30%). The ratio between latent and sensible heat flux over oceans usually is 10-20, i.e. the latent heat totally dominates the sensible heat exchange.

The calculations based on three-years of meteorological observations from the Northern Hemisphere (time step of 12 hrs), the GATE area (time step of 3 hrs) and from a number of specialized tropical field programs (time step from 3 to 6 hrs) have shown the need for a pronounced diurnal course of tropospheric heating in order to compensate for the radiative cooling. The calculations support the earlier suggestion that there is a strong diurnal course of heating (2:1) with a maximum in the morning and a minimum in the late afternoon to evening hours. Since subsidence was observed to intensify during the early morning period, it must be responsible for the temperature increase. Apparently the principal mechanism generating the downward motions is the relatively stronger radiative cooling of the nocturnal atmosphere in comparison with the daytime. The above speculations are illustrated by Figures 11.35 A and B. The comparison of all the components of the heat balance for the 850-350 mb layer under cloud-free and average cloudy conditions in the 0-10°N band calculated from routine meteorological observations shows the layer minimum temperature around 5:00, LT, the maximum - around 14:00 - 15:00. Accounting for the diurnal course of radiative cooling for the average cloudy conditions does not introduce any noteworthy changes into the diurnal course of the needed heating, but decreases systematically its values.

The large contrasts in the radiative heat flux divergence between the cloudy and cloud-free zones are obviously a significant source or available potential energy for the tropical weather-forming systems.

During the daytime the radiative cooling of the cloudfree air weakens as well as the contrast between cloudfree and cloudy areas. The upper tropospheric radiative cooling in the cloud zone is stronger during the night but weaker in the daytime as compared to surrounding cloud-free area. In addition to the input by processes at the lower levels this intensifies the divergence in the upper part of cloudy zones during the night. Gray (1976) has reasoned that generation of the deep convective clouds forestalls the changes in the lower and midlevel cloudiness.

It may appear strange that radiation is suggested as the main factor determining the diurnal course of penetrative convection instead of condensation, the amount and diurnal amplitude of latent heat in cloud clusters exceeding 3 to 5 times those induced by radiation contrasts between the cloudy and cloud-free areas. Radiation is a

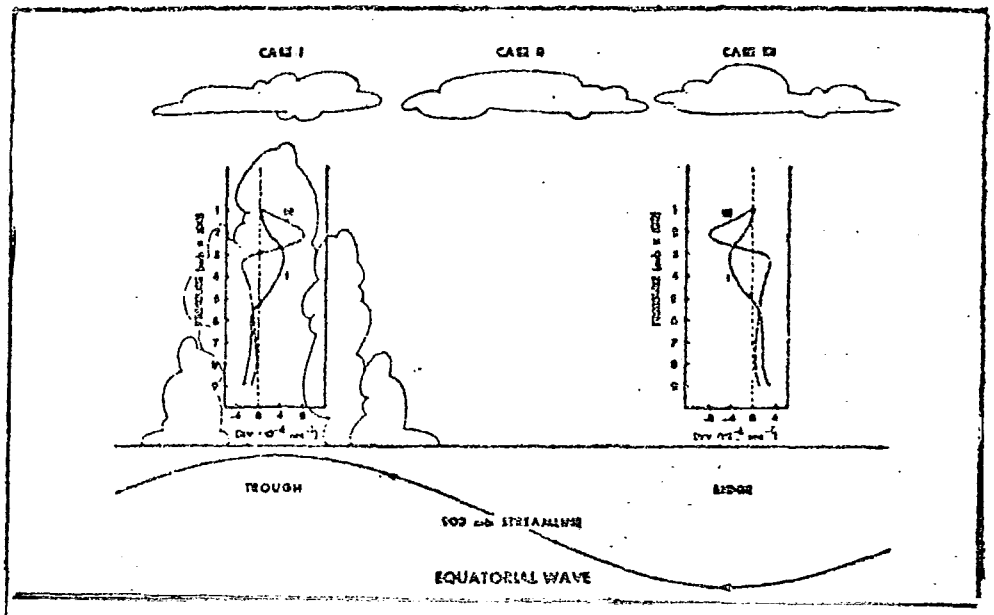

Figure 11.35A .Cloud-induced radiative forcing of tropospheric synoptic-scale mass divergence.

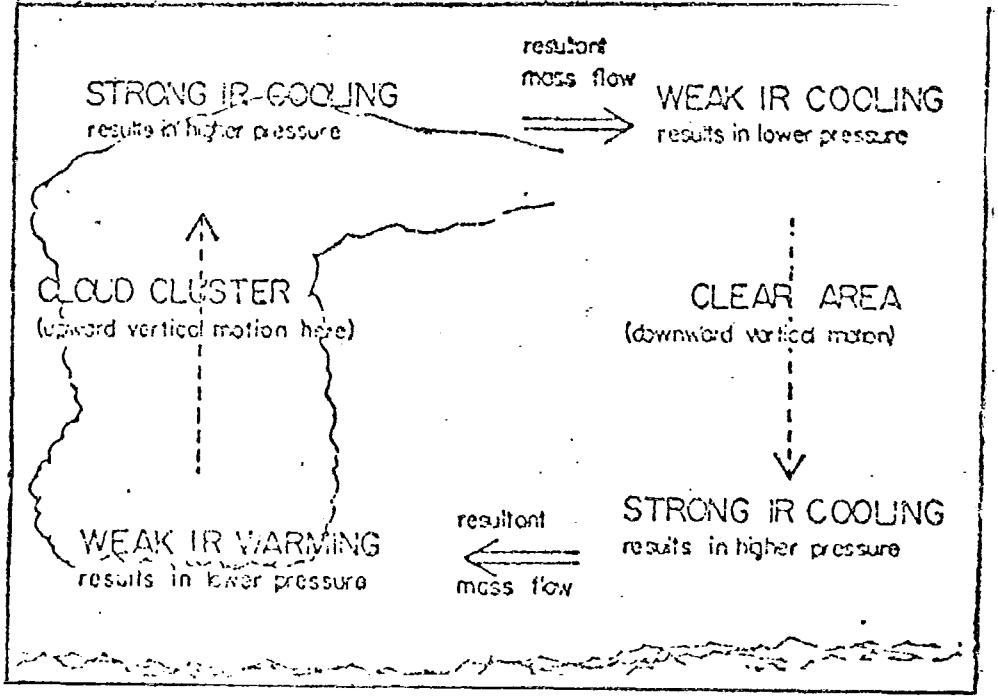

Figure 11.35B. Cloud-induced radiative forcing of tropospheric cluster-scale circulation.

continuous direct heat source or sink, which does not, in contrast to condensation heat, depend on vertical motion. The heating due to condensation is mainly transferred into the adjacent cloud-free subsidence areas. This is exactly why the cloud to cloud-free radiative contrasts appear so important.

In such conditions condensation in the cloud clusters occurs as a response to radiative forcing. If radiation is the primary mechanism for energy pumping in the tropical weather-forming systems, then one must anticipate a strong diurnal course of convergence and penetrative convection, which induces the formation of cumulus clouds. Since such a diurnal course is actually observed, a thorough analysis of the GATE data is needed, aimed at unveiling the physical factors responsible for it. The necessity to study the diurnal course of powerful (penetrative) convection in cumulus clouds in preference to the lower tropospheric convection must be particularly stressed. The weak diurnal course of total cloudiness is no indicator of absence of a strong one for penetrative convection.

In order to test such qualitative notions a number of studies in cloud-radiation interaction was undertaken. Fingerhut (1978) developed a theoretical model of a tropical cloud cluster (CC) that takes the diurnal course of radiation into account. The model is based on the complete system of equations and starts from the following facts: axial symmetry; separate treatment of the boundary leayer, the 5-layer troposphere and the stratosphere; three zones: the inner disturbance zone with unbroken multilayer cloudiness (it occupies about 20% of the CC area), the outer cloudiness zone, and the intermediate zone of partial cloudiness; radius of the disturbance zone is 3° latitude, the radius of the total area is 6.7° latitude.

Numerical modelling was carried out for a 17-point radial grid with 46 km spacing. The time step was 120 s. Heat divergence was diagnostically retrieved from the condition of the best fit of calculations to observations. The computational results demonstrated that almost all the latent heat was transformed to potential energy, only a minor portion was spent for direct air heating. The potential energy was transported to the atmosphere surrounding the disturbance zone, where the downward motions finally led to potential energy conversion into heat, thus causing an indirect heating of the cloudfree atmosphere by clouds.

Radiative factors play the main role in sustaining the CC. Accounting for the diurnal course of radiative flux divergence in the disturbance zone and the cloud-free atmosphere leads to diurnal variations of mass divergence and rainfall in the CC.

The maximum heat storage and associated horizontal pressure gradient lag by 2 hours the maximum heating rate. The radial wind velocity lags by additional 4 hours the pressure gradient. Therefore the mass divergence lags the maximum of heating by 6 hours. Thus, the low level convergence maximum (minimum) occurs at 06:00 (18:00) hr LT. The high (low) moisture conversion values at the lower levels together with the corresponding vertical motions at 06:00 (18:00) hr LT cause the observed rainfall maximum (minimum).

In order to study the heat and moisture balances in CC's, Rodenhuis (1977) suggested a model of the cellular structure of clouds allowing the description of the convective cloud ensemble. Calculations of the influence of radiative flux divergence profiles on the size spectrum and the depth of convective clouds for GATE data from September 6, 1974 were made. The cloud geometry was set as circular cylinder with "cavity" inside, occupied by the updraft zone. The calculations showed that climatological values of radiative flux divergence from Dopplick (1972) are important for describing the bimodal structure of the mass flow in the boundary layer and the distribution of cloud amount. This is particularly true for the lower levels of cloud and sub-cloud layers, but is also important for the upper layers where the negative radiative flux divergence is an important component of the total heat divergence. Updating is needed of the cloud model to account for realistic radiative flux divergence.

The diurnal course of meteorological parameters and convective activity over the A/B GATE array was also demonstrated by Petrossiants and Falkovich (1977) from ship observational data. The work discusses two possible diurnal courses: (1) the arrival of a disturbance from the continent, strongest during daytime; (2) generation by local conditions.

The "continental" hypothesis makes it possible to explain the difference in diurnal courses between the Pacific and Atlantic oceans by the different "running" times for disturbances, generated over continents to the given ocean area. The study suggests the strongdiurnal variation of the radiative cooling of the atmosphere up to 200 mb as another possible cause for the diurnal variations of convection intensity.

Ellingson and Serafino (1978) obtained the estimates of the dependence of various cloud ensemble characteristics on heat flux divergence. The ensemble was featured as a set of cylinders with fixed base height and varying vertical dimension (1 to 14 km) and 3 vertical profiles of heat flux divergence were applied to the GATE data from September 5 and 6, 1974. The analysed characteristics were: the area coverage for clouds of the given height; heat and moisture fluxes for separate clouds; rainfall and mass flow. A considerable sensitivity of these characteristics to radiative flux divergence (RFD) was found, especially in the lower and upper troposphere, where RFD is comparable to total heat flux.

11.10 RADIATIVE EFFECTS IN GATE-BASED ATMOSPHERIC CIRCULATION MODELS

In this section the studies are discussed that attempt to put together the GATE experimental results on radiative properties of tropical cloudiness and include them in the local circulation models.

Krishnamurti et al. (1978) used a local primitive equations model, integrated for 96 hours with high spatial-temporal resolution (100x100 km^2, 3 minutes) to reproduce 10 realistic situations from GATE. The model embraces the region 5°S-25°N, 40°W-20°E and describes in detail the radiation transfer processes including the cloud feedback and diurnal course.

Comparing three runs of the model: (a) with fixed solar zenith angle without cloud feedback; (b) allowing the solar zenith angle to vary but without cloud feedback; (c) allowing the solar zenith angle to vary and including the cloud feedback with the actually observed distribution of meteoparameters, showed that the account of the feedback is decisive for successive reproduction of the actual meteorological fields.

Slingo (1978) attempted to estimate the impact of a cloud-modulated radiative flux divergence on the intensity of convection. Actually, it was a direct test of the hypothesis by Gray and Jackobson on the decisive role of radiative heating contrasts in forming the tropical convective cloudiness over ocean. Radiation and cloud fields on a 2° grid within 35°N-15°S, 77°W-49°E were calculated with an 11-layer model of the tropical atmosphere specifically designed for GATE studies and described by Lyne and Rowntree (1976), Lyne et al. (1976) and Walker (1978). The interaction of radiation with cloudiness of 4 types: low, middle, high, and convective differing in height, thickness, and radiative properties was included. The heat sources and sinks were given directly in the form of "dry" and "moist" static energy and vertical heat transport, which was a measure of convective activity at the same time.

The cloud amount was parameterized for each cloud type through relative humidity and lapse rate. It took into account the difference in mass flows for convection over ocean and land and particularly distinguished the cases of the development of low cloudiness in tropical disturbances and below the trade-wind inversion.

It was assumed that clouds of different form and type overlap randomly. If the model predicted the development of deep convection, only in 10% of the area convective clouds were allowed to reach the level $\sigma = 0.195$ (the model was realized in σ-coordinates) and the rest 90% were treated as shallow low-level convection. In accordance with the results by Griffith and Cox (1977), the emissivity of tropical cirrus clouds associated with penetrative convection is assumed to be equal to 1.0. The outlined assumptions directly took into account the results of GATE field phase. The integration of the model for 3 days with a 2-hr step was performed starting with the initial conditions also taken from the GATE data set, namely - the situation on 12Z, September 4, 1974. In order to assess the sensitivity of the results to the presence of time-dependent cloudiness, two numerical experiments were made, one of which utilized the fully interactive cloudiness and radiation, the second with no clouds, so that fluxes and flux divergence values corresponding to the cloud-free atmosphere were used.

The results demonstrated high sensitivity of the model both to the radiation-cloudiness interaction and to the type of underlying surface above which the convection occurs. The model quite successfully predicted the principal features of the cloudiness distribution by the end of the experiment (12Z, September 7, 1974).

The radiation-cloudiness interaction over land led to reduction of the rainfall amount and to weakening of the disturbances.

The decrease of the incoming radiation over sea cannot directly affect the dynamics of the atmosphere, since the ocean temperature surface is fixed in the model. It corresponds physically to high heat capacity of the ocean which must not react to variations of the irradiance over characteristic life-spans of the synoptic systems. At the same time

the radiation-cloudiness interaction over the ocean leads to the increase of convective activity and heavier rainfall. This fact is explained by the influence of the extended cirrus cloudiness outflowing from the convective Cb clouds which is a usual feature of the tropical disturbances. Since only a small part of the grid could be occupied by powerful convective clouds, high cirrus cloudiness became decisive for an additional radiative warming, in contrast to the cloudless case. The total radiative effect of such clouds is a warming, since its radiative temperature is considerably lower than the equivalent blackbody temperature of radiation upwelling from the lower layers.

Such an additional warming, first, intensifies the upward motions at the upper and middle levels and, second, also intensifies the convergence into the disturbance at lower levels. Both these effects contribute to deepening of penetrative convection and, consequently, to the increase of rainfall over oceans.

LIST OF SYMBOLS

I_o - solar constant

I - integral flux of the direct solar radiation flux at sea surface

Q - global solar radiation flux

R - reflected solar radiation flux

ζ - zenith angle of the sun

$\tau_o, \tau_{o\lambda}$ - integral and spectral optical thicknesses of the atmosphere

$F_{\uparrow\downarrow}(\zeta)$ - upward and downward fluxes of heat or longwave radiation

$F = F_{\downarrow} - F_{\uparrow}$ - net radiation

$B = Q - R - F_o$ - radiative balance at sea surface

$T = B - F_T - F_e$ - energy balance at sea surface

F_T, F_e - turbulent fluxes of sensible and latent heat

$T(z), t°(z)C$ - the temperature in Kelvin and Celsius

T_s - sea surface temperature

N - cloud amount in parts of unit

u - relative humidity in %

m_s - the water vapour content of the atmosphere in $g \cdot cm^{-2}$

W - liquid water content of clouds in gm^{-3}

$e(z)$ - water vapour pressure in mb

z - altitude in m or km

p - pressure in mb

λ - wavelength

τ_d - aerosol optical thickness

m - complex index of refraction

n' - real part of the complex index of refraction

n'' - imaginary part of the complex index of refraction

α - Angström's formula exponent

P_2 - atmospheric integral transparency coefficient for atmospheric optical mass 2

S_m - meteorological visibility

r - aerosol particle radius

D - aerosol particle diameter

γ - Yunge exponent factor

REFERENCES

Abramov, R.V. et al., 1976. Convective clouds in the equatorial Atlantic from the instrumental and visual observations - In: "TROPEX-74", vol. 1, Leningrad, Gidrometeoizdat, p.475-482 (in Russian).

Adnashkin, V.N. et al., 1979. Optical characteristics of the atmosphere over the Tropical Atlantic - Meteorology and Hydrology, No. 11, p. 62-69 (in Russian).

Augstein E., M. Garstang, 1977. The structure of and transports through the lower atmosphere. US GATE Central Program Workshop NCAR, Boulder, Colorado. 25 July - 12 August 1977, p.455-544.

Bartenyeva, O.D., et al., 1974. On a technique for measuring the radiative balance of the ocean surface - In: "TROPEX-72", Leningrad, Gidrometeoizdat, p. 675-681 (in Russian).

Belevich, V.V., 1976. Some information on the thermal balance along the meridional cuts of the tropical Atlantic from the data of the research ship "Semyon Dezhnev" - In: "TROPEX-74", vol. 1, Leningrad, Gidrometeoizdat, p. 675-678 (in Russian).

Burch, D.E., 1970. Investigation of infrared radiation absorption by atmospheric gases. AFCRL F 19628-69-c-0263.

Carlson, T.N., 1979. Atmospheric turbidity in Saharan dust outbreaks as determined by analyses of satellite brightness data. Month. Wea.Rev., vol. 107, No. 3, p. 322-335.

Carlson, T.N., R.J. Benjamin, 1980. Radiative heating rates for Saharan dust. J.Atm.Sci., vol. 37, No. 1, p. 193-213.

Carlson, T.N., R.S.Caverly, 1977. Radiative characteristics of Saharan dust at solar wavelenghts. J.Geophys.Res., vol. 82, No. 21, p. 3141-3152.

Carlson, T.N., J.M.Prospero, 1972. The large-scale movements of Saharan air outbreaks over the Northern Equatorial Atlantic. J.Appl.Meteorol., vol. 11, No. 2, p. 283-297.

Carlson, T.N., P. Wendling, 1977. Reflected radiance measured by the NOAA-3 VHRR as a function of optical depth for Saharan duts. J.Appl.Meteorol., No. 16, p. 1368-1371.

Carlson, T.N., 1977. Large scale distribution of turbibity over the Northern Equatorial Atlantic. Proceedings of the symposium on radiation in the atmosphere. Garmisch-Partenkirchen, FRG, 19-28 August 1976. Published by Science Press, USA. p. 555.

Carlson, T.N., J. Prospero, 1977. Saharan air outbreaks: meteorology, aerosols and radiations. Report of the U.S. GATE Central Program Workshop held by NCAR, 25 July - 12 August 1977. p. 57-58.

Cox, S.K., K.T.Griffith, 1979 a. Estimates of radiative, divergence during Phase III of the GARP Atlantic Tropical Experiment: Part I. Methodology. J.Atm.Sci., vol. 36, No. 4, p. 576-585.

Cox, S.K., K.T.Griffith, 1979 b. Estimates of radiative divergence during Phase III of the GARP Atlantic Tropical Experiment: Part II. Analysis of Phase III results. J.Atm. Sci., vol. 36, No. 4, p. 586-601.

Cox, S.K., 1973. Infrared heating calculation with a water vapour pressure broadened continuum. Quart. J.Roy.Met.Soc., vol. 99, No. 422, p. 669-679.

Cox, S.K., 1976. Observations of cloud infrared effective emissivity. J.Atm.Sci., vol. 33, No. 2, p. 287-289.

Cox, S.K., 1975. Relating broadband shortwave irradiance measurements to radiative properties of the atmosphere. AMS Second Conf. on Atmosph. Rad., Collection of Abstracts. October 29-31, Arlington, Va., p. 237-240.

Cox, S.K., P.Minnis, 1978. Magnitude of rhe radiative effects of the Saharan dust layer. Atm.Sci. Paper No 283, Dept. Atm. Sci., CSU, Fort Collins, Co., 111 pp.

Diaz, H.E., T.N.Carlson, J.M.Prospero, 1976. A study of the structure and dynamics of the Saharan air layer over the Northern Equatorial Atlantic during BOMEX - NAA Techn. Memo ERL WMPO-32. 61 pp.

Dopplich, T.C., 1972. Radiative heating of the global atmosphere. J.Atm.Sci., vol. 29, No. 7, p. 1278-1294.

Dvorkina, M.D., B.N.Egorov, T.V.Kirillova, 1977. Some information about the statistical structure of the fields of the total radiation and cloudiness over ocean. Trudy GGO, issure 382, p. 29-35 (in Russian).

Dyubkin, I.A., et al., 1977. The statistical structure of direct radiation in cloudy atmosphere in the tropical Atlantic. Symposium on Radiation, Garmisch-Partenkirchen, FRG. 19-28 August 1976. Publisched by Science Press, USA.

Dyubkin, I.A., et al., 1978. The statistical structure of shortwave radiation fluxes depending on the clouds of different forms for the tropical Atlantic. Proceedings of the Int. Sci.Conf. on the Energetics of the Tropical Atmosphere, Tashkent, September 1977. p. 197- 208

Egorov, V.N., T.V.Kirillova, 1979. Attenuation of the total radiation by clouds of different forms from the GATE-74 data. Izvestiya, Academy of Sciences of the USSR, Atmospheric and Oceanic Physics (Izvestiya AN USSR. Fizika Atmosfery i Okeana), No. 9, p. 987-990 (in Russian).

Egorov, V.N., 1976. Cloud effect on atmospheric emission in the tropical Atlantic. In book "TROPEX-74", vol. 1, p. 594-599 (in Russian).

Egorov, V.N., T.V.Kirillova, 1977. On consideration of the cloud effect on the total radiation in the tropical Atlantic. Trudy GGO, issue 388, p. 102-105 (in Russian).

Ellingson, R.C., 1977. Results from a GATE longwave radiation experiment. Proc. of the Symp. on Radiation in the Atmosph. Garmisch-Partenkirchen, FRG. 19-28 August 1976. Science Press, p. 536-538.

Ellingson, R.C., G.Serafino, 1978. The sensitivity of ensemble cumulus characteristics to changes in the bulk radiative heating rate. Third Conf. Atmosph. Rad., p. 276-278.

Emmanuel, K., 1977. Preliminary investigation of a tropical squall mesosystem as observed during GATE. NCAR Techn. Note No.119 - PROC., p. 39-70.

Feigelson, E.M., 1973. Radiant heat transfer in a cloudy atmosphere. Translated from Russian. Published for NOAA by the Israel programme scientific translations.

Feigelson, E.M., et al., 1980. Heat radiation fluxes in tropical atmosphere. Preprint. Academy of Sciences USSR. Space Research Institute. 59 p.

Fimpel, H.P., et al., 1977. Results of IR-Radiometersonde flight during GATE from R.V. "Meteor". Proceedings of the Symposium on Radiation. 19-28 August, Garmisch-Partenkirchen, FRG, p. 533-535.

Fingerhut, W.A., 1978. A numerical model of a diurnally varying tropical cloud cluster disturbance. Month.Wea.Rev., vol. 106, No. 2, p. 255-264.

Foltz, C.S., 1976. Diurnal variation of the tropospheric energy budget. Atm.Sci.Pap. No.262, Dept. Atm.Sci., CSU, Fort Collins, Co., 141 pp.

Galindo, I., A.Muhlia and A.Leyva, 1975. Atmospheric turbidity and sky radiation at maritime environments: Gulf of Mexico and Tropical Atlantic. Beitrage zur Physik der Atmosphare (Contribution to Atmospheric Physics), 48, Band. p. 168-184.

Galindo, I., A.Muhlia and J.L.Bravo, 1978. Radiation experimental data on the energetics of the Saharan aerosol layer in the GATE synoptic scale. ICSU/WMO. Proc.Internat. Conf.Energ.Trop.Atm. (Tashkent, 14-21 September 1977). Geneva, pp. 175-188.

Ginzburg, A.S., 1977. Calculation of the thermal emission fluxes from the GATE data. In coll. of papers "Meteorological studies under the program of the International Tropical Experiment", Moscow, "Nauka" Publ. House, p. 15-24 (in Russian).

Ginzburg, A.S., et al., 1976. The emission of fluxes in the center of the equatorial Atlantic calculated and measured on the "Akademik Kurchatov" research ship. In: "TROPEX-74", vol. 1, Leningrad, Gidrometeoizdat, p. 577-586 (in Russian).

Grams, G.W., et al., 1977. Measurements of the light-scattering of the Saharan dust layer. Proc. of the Symp. on Rad. in the Atmosph. Garmisch-Partenkirchen, FRG, 19-28 August 1976. Science Press, p. 78-81.

Grassl, H., 1973. Separation of the atmospheric absorbers in the 8-13 μm region. Contr. Atm. Phys., vol. 46, p. 75-88

Grassl, H., 1975. "E-Type" absorption in the tropics. GATE Report No. 14, vol. 1, p. 298-302.

Grassl, H., 1977. Gemessene Strahlungs - und Wärmeflüsse über dem tropischen Ozean. "Meteor" Forschunggergebnisse, Reihe B, No. 12, "Meteorologie und Aeronomie" (in German, abstract in English), pp. 42-50.

Gray, W.M., 1976. Diurnal variation of oceanic deep cumulus convection. Paper II. Physical Hypothesis. Atm.Sci.Paper No. 243. Dept.Atm.Sci., CSU, Fort Collins, CO., p. 49-106.

Gray, W.M., 1977. Diurnal variation of deep cumulus convection over the tropical oceans. Preprint. WMO Techn.Conf. on the Energetics of the Trop.Atm., Tashkent, 14-21 September. 15 pp.

Griffith, K.T., S.K.Cos., 1977. Infrared radiative properties of tropical cirrus clouds as inferred from broadband measurements. Atm.Sci.Paper No.269. Dept.Atm.Sci., CSU, Fort Collins, Co., 102 pp.

Hickey, J.P., P.J. Griffin, 1975. Normal incidence solar radiation measurements from NASA Convair - 990 during GATE. Abstract, AMS Second Conf. on Atmosph.Rad., 29-31 October, Arlington, Va., p. 230-233.

Ivanov, V.N., et al., 1976. Meteorological fields spectra in the equatorial Atlantic. In: "TROPEX-74", vol. 1, Leningrad, Gidrometeoizdat, p. 207-217 (in Russian).

Jackobson, R.W., Jr., 1976. Diurnal variation of oceanic deep cumulus convection. Paper I. Observational evidence. Atm.Sci. Paper No. 243. Dept.Atm.Sci., CSU, Fort Collins, Co., p. 1-78.

Kapustin, V.N., et al., 1976. The effect of the aerosol and water vapour on director solar radiation fluxes in the centre of the equatorial Atlantic. In: "TROPEX-74", vol. 1, Leningrad, Gidrometeozdat, p. 630-637. (in Russian).

Kapustin, V.N., S.M.Pirogov, 1976. The sea surface layer aerosol in the equatorial atmosphere. In: "TROPEX-74", vol. 1, Leningrad, Gidrometeoizdat, p. 644-651 (in Russian).

Kaznacheeva, V.P., T.V.Rudenkova, 1976. The statistical structure of the vertical profiles of the meteorological elements in the tropical Atlantic. Trudy VNIIGMI-MCD, issue 13 "Statistical methods for analysis and in meteorology". p. 143-165 (in Russian).

Kirillova, T.V., R.C. Timanovskaya, A.V. Gudimenko, 1977. The statistical sturcture of the total radiation incident on the ocean surface in cumulus clouds conditions. Trudy GGO, issue 388, p. 93-101 (in Russian).

Kirillova, T.V., B.N. Egorov, 1977. Estimation of the cloud effect on the total radiation from the GATE-74 observational data. Trudy GGO, issue 398, p. 112-117 (in Russian).

Kirillova, T.V., Yu.K. Fedorov, 1967. On the vertical structure of the longwave radiative fields. Trudy GMC SSSR, issue II "Problems in Satellite Meteorology", p. 148-158 (in Russian).

Kondratyev, K.Ya., et al., 1976. Aerosol in the GATE area and its radiative properties. Atm.Sci. Paper No. 247. Dept.Atm.Sci., CSU, Fort Collins, Co., 109 pp. (Also available as Trudy GGO, 1977, issue 381, in Russian).

Kondratyev, K.Ya., et al., 1977a. Preliminary results of the GATE aircraft Radiation Subprogramme studies. Meteorology and Hydrology, No.3, p. 97-104 (in Russian).

Kondratyev, K.Ya., et al., 1977b. Impact of aerosols on radiative energetics of the tropical atmosphere. Proc.Int.Sci.Conf. Energetics of the Trop.Atmosph., 14-21 September, Tashkent. ICSU/WMO, Geneva 1978. p. 143-149.

Kondratyev, K.Ya., et al., 1979. The impact of aerosol on the radiative energetics of the tropical atmosphere. Trudy GGO, issue 415, Leningrad, Gidrometeoizdat, p.3-7.

Kondratyev, K.Ya., M.A.Prokofyev, 1978. Attempt of determining the total diurnal radiative heat flux divergence from the GATE data. Doklady Akademii Nauk SSSR, vol. 242, No.4, p. 804-807 (in Russian).

Koprov, B.M., 1980. The energy balance in the near-equatorial atmosphere and the meridional heat transfer. Izvestia AN SSSR. Fizika Atmosfery i Okeana, No. 1, p. 11-19 (in Russian).

Koprova, L.I., et al., 1977. Characteristic features of the statistical structure and possibilities for objective analysis of the airtemperature field over the equatorial Atlantic. Izvestia AN SSSR. Fizika Atmosfery i Okeana, vol. 13, No. 6, p. 629-637. (in Russian).

Koprova, L.I., V.G.Boldyrev, 1970. On the statistical characteristics of the vertical structure of the temperature and humidity fields up to high altitudes. Izvestia AN SSSR. Fizika Atmosfery i Okeana, vol. VI, No. 2, p. 154-167 (in Russian).

Kostyanoy, G.N., 1975. On accuracy of the longwave radiation measurements with an actinometric radiosonde. Meteorology and Hydrology. No. 4 (in Russian).

Krishnamurti, T.N., et al., 1978. Limited area numerical weather prediction with the GATE data. Proc. of the Int.Conf. on the Energetics of the Trop.Atmosph., Tashkent, 14-21 September, ICSU/WMO, Geneva 1978, p. 329-344.

Kuusk, A.E., Yu.A.R. Mullamaa, 1976. On the diurnal course of the total radiative flux in the cloudless sky in the tropical Atlantic and Pacific oceans. In: "TROPEX-74", vol.1, Leningrad, Gidrometeoizdat, p. 659-663 (in Russian).

Kuusk, A.E., et al., 1976. On the studies of the cloud and radiation fields' variability during the 13'th voyage of the "Akademik Korolov" research ship. In: "TROPEX-74", vol. 1, Leningrad, Gidrometeoizdat, p. 600-608 (in Russian).

Kuusk, A.E., et al., 1978. The structure of the cloud cover in the tradewind region on the basis of ship measurements. Proceedings of the Int.Sci.Conf. on the Energetics of the Tropical Atmosphere, Tashkent, Sept., p. 155-160.

Laktionov, A.G., et al., 1976. On connection between the optical and aerosol characteristics of the atmosphere over the eastern equatorial Atlantic. In: "TROPEX-74", vol. 1, Leningrad, Gidrometeoizdat, p. 630-637 (in Russian).

Loranger, D., 1975. Spatial and temporal frequency distribution of cloud ring occurence during GATE. Preprint, Dept.Atm.Sci., CSU, Fort Collins, Co., 8 pp.

Lyne, W.H., P.R.Rowntree, 1976. Development of a convective parameterization using GATE data. Met.O.20 Techn.Note.No. 11/70, UK Meteorological Office, Bracknell.

Lyne, W.H., et al., 1976. Numerical modelling using GATE data. Met.Mag., vol. 105, p. 261.

Malkevich, M.S., et al., 1976. A complex method for studying the water vapour contribution into atmospheric transparency in the 8-12 μm transparency window. Trudy GGO, issue 369, Leningrad, Gidrometeoizdat, p.143-156 (in Russian).

McClatchkey, R., et al., 1972. Optical properties of the atmosphere (3d ed.). Env.Res.Paper, AFCRL No. 411, 108 p.

Noonkester, V.N., D.R.Jansen, 1977. The growth and decay of the convective field revealed by surface-based remote sensors. 16th Radar Meteorol. Conf., Houston, Texas, 1975, Boston, MA., p. 304-311.

Patterson, B.M., et al., 1977. Complex index of refraction between 300 and 700 nm for Saharan aerosols. J.Geophys.Res., vol. 82, p. 3153-3160.

Petrossiants, M.A., A.I. Falkovich, 1977. On the diurnal course of meteorological elements in the Atlantic Tropical Experiment area. Meteorology and Hydrology, No.7, p. 83-90 (in Russian).

Pinkov, A.M., 1960. On statistically orthogonal expansions of the empirical functions. Izvestia AN SSSP. Sr.Geofizica, No.3. p. 432-439 (in Russian).

Polovarapu, R.J., 1979. Estimation of net radiation at sea. Atmosphere-Ocean v.17 No.1, p. 24-35.

Prospero, J.M., R.T.Nees, 1977. Dust concentration in the atmosphere of the equatorial North Atlantic: Possible relationship to the Sahelian drought. Science, vol. 196, p. 1196-1198.

Prospero, J.M., et al., 1977. Monitoring Saharan aerosol transport by menas of atmospheric turbidity measurements. Preprint. Saharan Dust Workshop. Göteborg, Sweden, 20 p.

Pueschel, R.F., 1975. Optical properties of the aerosol over the Eastern Atlantic Ocean. Second AMS Conf. on Atmosph. Radiation. Collection of Abstracts. October 29-31, Arlington, Va., p. 227.

Proceedings of the Seminar on the Impact of GATE on Large-Scale Numerical Modelling of the Atmosphere and Ocean, 1979. August 20-29, Woods Hole, MA., 1980. NAS, 276 pp.

Report of the US GATE Central Program Workshop, 1977. NCAR, Boulder, CO., 25 July - 12 August, 732 pp.

Riehl, H., J.Malkus, 1958. On the heat balance of the equatorial trough zone. Geophysica, No.6, p. 503-538.

Rodenhuis, D.R., 1977. The influence of the bulk radiational cooling rate on the apparent bimodal cloud distribution in GATE. Preprint. The IV Int.Meet.Exp. on GATE Radiation Sub-programme, Leningrad, 21-26 November, 27 pp.

Ross, Yu.K., 1972. Stochastic structure of cloud and radiation fields. Tartu, Institute of Physics and Astrophysics, 281 pp. (in Russian).

Samoilenko, V.S., B.A.Semenchenko, 1976. On the radiative heat exchange between the ocean surface and atmosphere at the equator. In: "TROPEX-74", vol. 1., Leningrad, Gidrometeoizdat, p. 564-567 (in Russian).

Semenchenko, B.A., V.P.Nekrasov, 1974. The role of the effective emission in the thermal balance of the ITCZ. In: "TROPEX-74", Leningrad, Gidrometeoizdat, p. 506-510 (in Russian).

Semenchenko, B.A., et al., 1977. On the constituents of the radiative balance at the equator. Trudy GGO, issue 398, p. 568-576 (in Russian).

Semenchenko, B.A., A.V,Kislov, 1978. The factors of variability of radiative fluxes on the oceanic surface in the tropics. Proceedings of the Intern.Sc.Conf.Tashkent, 14-21 Sept., 1977, p. 189-196.

Shukurov, A.Rh., A.I.Charov, 1978. On the variations of the atmospheric spectral transmittance in the "windows" of the infrared region over the tropical ocean area. Proc.Int.Conf. on the Energetics of the Trop.Atmosph., Tashkent, 14-21 September 1977. ICSU/WMO, Geneva, p. 167-172.

Slingo, J.M., 1978. The effect of the interactive clouds and radiation on convective activity in a numerical model of the tropics. Met.O.20 Techn.Note No.11/130. 29 pp. Unpubl.

Smith, W.L., et al., 1977. A radiative heating model derived from the GATE MSR experiment. J.Appl.Meteorol., vol. 16, No. 4, pp. 384-392.

Stochastic Structure of Cloud and Radiation Fields, 1972. Tartu, Institute of Physics and Astrophysics. 281 pp. (in Russian).

Suchman, D., et al., 1977. Deep convective mass transports: an estimate from a geostationary satellite. Month.Wea.Rev. vol. 105, No.8, p. 943-955.

Voitova, K.V., 1980. Clouds as a regulator of the radiative and thermal balances in the tropical latitudes of ocean. In: "Atmospheric Circulation and its Interaction with Ocean in the Tropical Latitudes of the Atlantic". Coll. of Papers. "Nauka", Publ. House, Moscow (in Russian).

Volkov, Yu.A., et al., 1976. On the heat - and water exchange at the equator. In: "TROPEX-74", vol. 1, Leningrad, Gidrometeoizdat, p. 379-393 (in Russian).

Volkov, Yu.A., et al., 1978. "Investigation of heat fluxes as dependent on determining factors in the equatorial zone of the Atlantic", p. 149-154. Proceedings of the Int.Sci.Conf., Tashkent, 14-21 September 1977.

Vonder Haar, T.H., D. Loranger, E.A.Smith, 1977. Earth-atmosphere system radiation budgets for selected days during the AMTEX and GATE. Proc.Int.Symp. on Radiation in the Atmosph. Garmisch-Partenkirchen, FRG, 19-28 August 1976. Science Press, p. 539-543.

Walker, J., 1978. Interactive cloud and radiation in the 11-Layer model. Part II: Cloud Scheme. Met.O.20 Techn.Note. No.II/122, UK Meteorological Office, Bracknell.

Warner, C., et al., 1979. Shallow convection on Day 261 of GATE: Mesoscale area. Month. Rev., vol. 107, No. 12, p. 1617-1695.

Weickman, H., 1975. Observations on convective clouds over the tropical Atlantic. GATE Report No. 14, Part II, p. 145-155.

Zaitseva, N.A., E.M.Feigelson, 1979. Characteristic features of the radiative heat exchange in the tropics from the data of the TROPEX-74 actionmetric sounding. Izvestia AN SSSP. Fizika Atmosfery i Oceana, vol. XV, No. 2, p. 154-168 (in Russian).

Zaitseva, N.A., H.P.Fimpel, 1977. On comparisons of actinometric radiosondes of the USSR and FRG made during the GATE-74. Meteorology and Hydrology, No. 8, p. 91-95 (in Russian).

Zaitseva, N.A., T.M.Krasnova, 1976. Variability of the longwave radiation at the GATE grounds. In: "TROPEX-74", vol. 1, Leningrad, Gidrometeoizdat, p. 712-721 (in Russian).

CHAPTER 12

MAIN ACHIEVEMENTS OF GATE AND ITS IMPACT ON FGGE

by

M. A. Petrossiants*

(Hydrometeorological Research Centre of the U.S.S.R., Moscow, U.S.S.R.) with co-operation of all other authors of this Monograph, participants of the International Conference on Scientific Results of GATE (Kiev, September 1980), and I. Sitnikov** (WMO/ICSU Joint Planning Staff).

12.1 INTRODUCTION

12.1.1 The concept of carrying out international tropical experiments for studying atmospheric processes in the tropics prior to the First GARP Global Experiment was brought up for the first time in 1966 in the report of the CAeM Working Group on Tropical Meteorology (Report of the First Meeting of CAeM Working Group on Tropical Meteorology, 14-18 November 1966, Geneva, WMO, 1966). This concept was supported and further developed at the Conference on Global Atmospheric Research Programme held in Skepparholmen (Stockholm) from 28 June to 11 July 1967. The GARP programme itself was originated at this Conference.

In the report of the Conference on GARP there is section 3.2 which deals with problems of tropical meteorology and contains the first draft plan of the tropical experiment. It took seven years for planning and design since that very time up to the beginning of the field phase of GATE. The following experiments carried out by different countries had significantly contributed to the success of GATE: Line Islands Experiment in the mid-Pacific (1967), Atlantic Trade Wind Experiment (ATEX, 1969), Barbados Oceanographic and Meteorological Experiment (BOMEX, 1969), the USSR National Atlantic Tropical Experiment (1972). Along with the experiments in the oceans some special observations were also arranged on land: the Venezuela International Hydrological and Meteorological Experiment (VIMHEX) during rainy seasons of 1969 and 1972, and ASECNA pre-GATE experiments in Africa in 1972 and 1973.

12.1.2 GATE was implemented during the period of 17 June to 23 September 1974. The observations conducted in the course of GATE were divided into three phases:

Phase I - from 26 June to 16 July

Phase II - from 28 July to 16 August

Phase III - from 30 August to 19 September.

During the periods of 17-19 June and 21-23 September the first and the final intercomparisons were made. Seventy nations participated in the implementation of GATE. Ten countries at different times provided thirty-nine research ships, four countries sent twelve aircraft. The SMS-1 geostationary satellite and polar-orbiting satellites were used for taking cloud pictures over the area of the experiment. Four countries provided shipborne weather radars for measuring precipitation and depicting the internal structure of cloud systems.

---

*Present affiliation: The Moscow State University, U.S.S.R.

**Present affiliation: The Hydrometeorological Research Centre of the U.S.S.R., Moscow, U.S.S.R.

12.1.3 The scientific processing and analysis of data obtained during GATE started already in the course of the experiment and then were intensively continued for subsequent years. Several conferences and scientific meetings were arranged, the most important of which are as follows: the Third and the Fourth International Meetings of Experts on the GATE Radiation Sub-programme (Leningrad, 1975 and 1977); the GATE B/C-Scale Oceanography Workshop (Southampton, June 1975), the GATE Equatorial and A-Scale Oceanography Workshop (Geneva, July 1975); the JOC Study Conference on the Development of Numerical Models for the Tropics (Exeter, England, April, 1976), the GATE Oceanography Workshop (Brest, France, September 1976), the Advisory Group Meeting of the Boundary-Layer Sub-programme (Hamburg, 1976), the GATE Equatorial Experiment Workshop (Miami, March 1977), US GATE Central Program Workshop (Boulder, July-August 1977), the International Scientific Conference on the Energetics of the Tropical Atmosphere (Tashkent, September 1977), the GATE Symposium on Oceanography and Surface Layer Meteorology (Kiel, Federal Republic of Germany, May 1978), the International Conference on Meteorology over the Tropical Oceans (London, August 1978), the Seminar on the Impact of GATE on Large-Scale Numerical Modelling of the Atmosphere and Ocean (Woods Hole, U.S.A., August 1979), and others.

Internationally co-ordinated GATE research culminated in the International Conference on Scientific Results of GATE held in Kiev, U.S.S.R. in September 1980. The Kiev Conference actually served as a basis for the preparation of this publication.

12.1.4 The experiment was designed by the International Scientific and Management Group (ISMG) operating under the direction of Dr. J. P. Kuettner (GATE Report No. 1). It is due to the activities of ISMG that the preliminary scientific results of GATE were published as soon as the experiment was over (GATE Reports No. 14, Volumes I, II) as well as the Report on the Field Phase (GATE Reports Nos. 15-19) which made available to the scientific community the data obtained at the GATE Operations Control Centre in Dakar.

12.1.5 Within the period of seven years after the completion of the field phase of GATE, the preparation of the final GATE data set has been carried out at the World Data Centres A and B and the Subprogramme Data Centres (GATE Report No. 20) and a great variety of papers (about 1000) have been published. A list of these publications partly appeared in "The GATE Bibliography" (ICSU/WMO, Geneva. First issue, January 1978; second issue, January 1979) and several periodically updated national bibliographies. It is impossible to review all the papers contained in the GATE Bibliography. However, some of the summarized publications are worthy of mentioning:

(a) "TROPEX-74", Proceedings of the Soviet National Expedition on GATE Programme. Vol. I, Atmosphere, 736 pp; Vol. II, Ocean, 217 pp. Gidrometeoizdat, Leningrad, 1976.

(b) "GATE International Meteorological Radar Atlas" by R. Arkell and M. Hudlow, Center for Experimental Design and Data Analysis, EDS, NOAA, U.S.A., April 1977, 222 pp.

(c) Report of the U.S. GATE Central Program Workshop. Sponsored by National Science Foundation, NOAA, U.S.A. Boulder, Colorado, 25 July - 12 August 1977, 723 pp.

(d) "Weather maps of the Atlantic Tropical Experiment (GATE)", Vols. I, II and III, edited by B. S. Chuchkalov, The Hydrometeorological Research Centre of the U.S.S.R. Obninsk, U.S.S.R., 1977.

(e) "Sea Surface Temperatures for GATE"; "An Atlas of the Motion Field over the GATE Area", Part I (200 mbs), Part II (250 mbs), Part III (300 mbs), by T. N. Krishnamurti and co-authors. Report Nos. 76-3, 78-2, 78-3 and 78-4, Department of Meteorology, Florida State University, Tallahassee, U.S.A., 1976-1978.

(f) "Numerical modelling of the tropical atmosphere". ICSU/WMO, GARP Publications Series No. 20, Geneva, July 1978, 79 pp.

(g) Proceedings of the International Scientific Conference on the Energetics of the Tropical Atmosphere, Tashkent, 14-21 September 1977. ICSU/WMO, Geneva, October 1978, 442 pp.

(h) "GATE Radar Rainfall Atlas" by M. D. Hudlow and V. L. Patterson, Center for Environmental Assessment Services, EDIS, NOAA, U.S.A. NOAA Special Report, March 1979, 155 pp.

(i) "Meteorology over the Tropical Oceans", published by the Royal Meteorological Society. Bracknell, Berkshire, U.K., 1979.

(j) "Dynamics and Energetics of the Intertropical Convergence Zone" by A. I. Falkovich. Gidrometeoizdat, Leningrad, 1979, 247 pp.

(k) "Graphical presentation of the U.S.S.R. oceanographic observations in the tropical Atlantic during GATE (June to September 1974)" by V. A. Bubnov, V. D. Egorkhin, Z. N. Matveeva, S. E. Navrotskaya and D. I. Philippov. Technical Report TR-79-1, 1979, University of Miami, 163 pp.

(l) "Satellite-derived Precipitation Atlas for GATE" by C. G. Griffith, W. L. Woodley, J. S. Griffin and S. C. Stromatt. Environmental Research Laboratories, NOAA, U.S.A., February 1980, 280 pp.

(m) "The Synoptic (A) Scale Circulations during the third (20 August - 23 September), the second (17 July - 19 August 1974) and the first (26 June - 16 July 1974) Phase of GATE, and Means for Phases I, II and III by J. C. Sadler and L. K. Oda, Department of Meteorology, University of Hawaii, U.S.A., UHMET 78-02, 79-14 and 80-01, 1978-1980.

(n) Proceedings of the Seminar on the Impact of GATE on Large-Scale Numerical Modeling of the Atmosphere and Ocean, Woods Hole, Massachusetts, U.S.A., 20-29 August 1979. National Academy of Sciences, Washington, D.C., 1980, 276 pp.

(o) "Dynamics of the Equatorial Atmosphere" by E. M. Dobryshman. Gidrometeoizdat, Leningrad, 1980, 288 pp.

(p) "Oceanography and Surface Layer Meteorology in the B/C-Scale", edited by G. Siedler and J. D. Woods. Deep-Sea Research, GATE Suppl. 1 to Vol. 26, 1980, 294 pp.

(q) "Equatorial and A-Scale Oceanography" edited by W. Düing. Deep-Sea Research, GATE Suppl. 2 to Vol. 26, 1980, 356 pp.

(r) "Physical Oceanography of the Tropical Atlantic during GATE", edited by W. Düing, F. Ostapoff and J. Merle. University of Miami, U.S.A., 1980, 117 pp.

GATE data have been used in all the above-mentioned studies which testifies to the fact that the experiment has had great impact on tropical meteorology and oceanography.

12.2 MAIN RESEARCH RESULTS

The scientific programme of the Experiment was based on the knowledge and experience of operational work gained by tropical meteorologists prior to the beginning of GATE. Thus it is obvious that the scientific data obtained through analysing the GATE observational data collected during the experiment are closely connected with the pre-GATE investigations. In some cases GATE data have refined the pre-GATE results, in others they have confirmed hypotheses, revealed new facts, increased our understanding of the physical processes in the tropics. Owing to such an uninterrupted process of investigations it is not always easy to determine the contribution of GATE itself. Here we shall try to mention only the most important results.

12.2.1 Large-scale mean state

A detailed description of the mean state of the atmosphere and ocean has been obtained in the A-scale area. An objective analysis of the motion field at the sea surface and also at 850, 300, 250 and 200 mb, and sea-surface temperature field for the period of 100 days and individual phases has been developed with the GATE data. Objective analyses of some derived characteristics such as the wind stress, the curl of the wind stress, and also of the surface heat balance of the GATE oceans have been carried out as well.

A manual analysis of the wind field at the sea surface (850 mb over land) and at 250 mb for all the three phases of GATE has been performed.

The analysis of the surface pressure and geopotential heights at 850, 700, 500, 300, 200 and 100 mb for the most part of the A-scale area and for all three phases of GATE beginning from 1 July has been carried out.

The mean cloudiness distribution derived by means of satellite measurements of brightness in the infrared part of the spectrum over the entire GATE period in the A-scale area has been determined.

Rain estimates for significant part of the A-scale area and for time scales ranging from 85 days to 6 hours, from infrared geosynchronous satellite data have been made and compared with the shipboard rain gauge, radar and Nimbus 5 electrically scanning microwave radiometer estimates. On the basis of these data analyses of the diurnal variation in rainfall and maps showing satellite-inferred locations of new cloud formations, cloud mergers and cloud evaporation have been produced. These studies of the large-scale mean state of the atmosphere have provided a valuable climatology for various meteorological parameters over the tropical Atlantic and West Africa during the Northern summer season. They will serve for a long time as a basis for studying atmospheric processes in the tropics and for testing the results of the numerical experiments including those for the FGGE period for the tropical regions.

12.2.2 Easterly waves

GATE data have made it possible to refine our pre-GATE understanding of easterly or African waves, it has been possible to determine more precisely their structure, the position of the areas of convective activity and precipitation in relation to the trough and ridge axes of a wave. Composite analyses of easterly waves, which determine their average structure normalized relative to the average wavelength, have proved to be very useful in these studies but other techniques and approaches should not be discarded.

It was shown that waves with a nearly 2,500 km length and with a period of about 3.5 days were the most essential feature of the synoptic-scale processes. A detailed structure of these waves was determined by means of budget calculations, involving complicated mechanisms of energy transformations, and produced for Phase III over the A/B-scale area.

As to the origin of easterly waves there is no yet definite conclusion on the comparative role of barotropic and baroclinic instability in these processes. A very common view is, however, that the waves are generated as a result of barotropic instability of the midtropospheric easterly jet in eastern and central Africa (caused by horizontal shift in the wind field), but continue to develop in western Africa largely as a result of latent heat release in deep convective clouds (baroclinic instability). They may maintain again in the eastern Atlantic, because of greater homogeneity in heat distribution over the underlying surface, through barotropic processes.

The growth mechanisms and structure of easterly waves suggested by the observational studies have been tested in simple linear models which proved to be useful for this purpose. Dry models reproduce the low-level structure well. Moist models yield qualitatively correct upper-level structure as well but the features are too weak. Non-linear models are needed to handle better the effects of latent heat release.

Synoptic-scale disturbances affecting the ITCZ region, upper tropospheric disturbances and hurricanes originated from disturbances over the tropical Atlantic have also been productively studied with the GATE data.

12.2.3 Theoretical aspects

The GATE presented an exceptionally favourable opportunity for testing various theoretical concepts in what regards tropical and equatorial waves, the development and location of the ITCZ, formation of tropical cyclones. Since GATE the theory of Rossby, Kelvin and mixed Rossby-gravity waves in the tropical and equatorial atmosphere has been further developed. Small-scale waves in the narrow equatorial belt have been analysed. The role of non-linear effects in the interaction of different types of those waves has been accentuated. Studies of the barotropic and baroclinic instability and of the wave-CISK mechanism in the context of the generation and maintaining of tropical waves, have been stimulated.

Although, more often than not, the above studies did not involve the GATE data directly, there is a wide spectrum of theoretical problems where these data would be of great help. The problem of instability of tropical motions, in its general formulation or individual applications, may serve as one of the most important examples.

12.2.4 Large-scale numerical modelling

12.2.4.1 Impact of GATE on objective analysis techniques

Analyses utilizing four-dimensional data assimilation for the GATE period are progressing very well. An objective analysis of the wind field in the tropical zone turns out to be of similar quality compared to the subjective ones, that is manual analyses. The use of dynamic assimilation and an optimum interpolation method as well as the successive correction method or a variational adjustment (or a combination of these methods) is equally typical. The full (final) GATE data set makes it possible to get a better resolution of easterly waves than that using quick-look data. The significance of the results of objective GATE analysis for further studies of the tropical circulation and its interaction with systems outside the tropical zone should be emphasized. An example is the development of the four-dimensional analysis scheme at GFDL based on the GATE data sets.

12.2.4.2 Modelling of tropical atmospheric circulation

The present atmospheric general circulation models describe a great number of large-scale phenomena and processes typical of the tropical zone. They include the ITCZ, easterly waves, Kelvin and Rossby-gravity waves as well as tropical cyclones although the latter are oversimplified. More often use of high resolution spectral models is characteristic. The models show a high sensitivity, especially, to the initial moisture conditions, to parameterizations of and interaction between cloudiness and radiation fields in the tropical zone. This is confirmed by latest numerical experiments on monsoon circulation modelling.

12.2.4.3 Forecasting for the GATE area

Experimental forecasts for the GATE area made with the help of limited area models showed that many features of the tropical flow and rainfall for periods of a few days (given adequate data) are predicted well enough. Advances in the application of relatively simple models to the prediction of wave troughs and squall lines should especially be noted. Energetics of modelled waves somewhat differ, though, from diagnostic studies made using composited data. To overcome this and other deficiences, the GATE should continue to be used.

12.2.5 GATE oceanography

Oceanographic and sea-surface layer studies gave a detailed picture of sea-surface temperature fluctuations T_s for different periods. The amplitude of these fluctuations increases with the length of periods. A passage of squall lines and cloud clusters over the B/C array as well as diurnal and 3-4 days fluctuations do not cause a change of more than 0.5°C. They may, however, reach several degrees C for 14- and 30-day periods (within a few hundred kilometers from the equator). Of considerable magnitude are the large-scale seasonal (a period of a month and more) fluctuations of T_s in the tropical zone. The heat budget of the upper ocean is primarily balanced by surface flux and advection. Therefore local ocean heat content changes can not be related to local surface flux variations. Mean horizontal and vertical fluxes as well as the frequency dependent variance of the upper ocean heat content can, however, be obtained.

Major advances were made in the understanding of processes that contribute to the re-distribution of heat in the ocean. These included results on internal waves and on the turbulent structure of the upper ocean in the ITCZ region as well as results on large-scale equatorial waves and on turbulent transfer processes in the Equatorial Undercurrent (Lomonosov Current) region.

12.2.6 ITCZ processes and balances

Significant progress has been made in studying the ITCZ, its structure on the average as well as cases of a developed ITCZ (active convection) and a weak or suppressed ITCZ (suppressed convection).

12.2.6.1 The convection in the ITCZ area has appeared to depend on the sign and magnitude of the large-scale controlled vertical motions in the 500-300 mb layer. Thus, in case of a developed ITCZ the area of the controlled upward motions extends from the sea level up to 100 mb and the area of maximum precipitation and cloudiness is located $1\text{-}2^{\circ}$ latitude southwards of the surface convergence line. The temperature field reveals a very weak warm core in the upper troposphere and a similarly weak cold core in the lower troposphere. In case of a suppressed ITCZ, on the contrary, the entire troposphere above 700 mb experiences large-scale downward motions.

12.2.6.2 When active convection takes place in the ITCZ, practically all the water vapour, which was brought into a unit atmospheric column by the large-scale motions and turbulent fluxes from ocean, condenses and falls out as precipitation. It means that almost all the latent heat of condensation is converted into the sensible heat which is then transferred into subtropical regions.

Precipitation estimates from the water vapour influx into a unit atmospheric column of ITCZ between surface and the 100 mb level calculated by different authors, have provided reasonable results when compared with radar measurements.

12.2.6.3 The total energy exchange between ITCZ and subtropical regions depends on the type of the ITCZ convection. For a developed ITCZ an energy influx is observed in the lower troposphere up to 700 mb and above it there occurs energy outflow with maximum in the 300-100 mb layer. For a suppressed ITCZ total energy influx takes place in the low layer up to 850 mb, and in the 300-100 mb layer energy outflow occurs in the 700-500 mb layer.

12.2.6.4 Processing of satellite data for cloud brightness showed that in the ITCZ cloud belt over land near the African coast at about 10°N, 17°W there exists the centre of maximum convective activity. Convection intensity in this centre oscillates with a period of 1 and 4 days.

The diurnal variation over the A/B ship array is in the co-phase with the diurnal variation over the centre of maximum convective activity.

However, unlike the western Pacific where the maximum of vertical motions, deep convection and precipitation occurs in the morning, in the A/B area it is observed in the afternoon. The phases of the diurnal variation north and south of the A/B ship array (and of this centre) are, however, quite different.

12.2.7 Convection in GATE

12.2.7.1 Mesoscale systems

Radar, aircraft and satellite data have been used to obtain a unique description of the mesoscale squall and non-squall systems that occurred during GATE. These mesoscale systems have been shown to account for a dominant fraction of the precipitation (about 90%) and vertical mass transfer that was associated with larger-scale convergence during certain phases of passing easterly waves.

These mesoscale systems showed a typical time evolution, starting with a band of convective cells, followed by the development of a mesoscale precipitation area under an extensive anvil, and the subsequent decay of active deep convection. Approximately 40% of the precipitation from these systems fell as stratiform rain from the mesoscale precipitation areas. Studies have revealed that in addition to convective scale updrafts and downdrafts in the convective cells, the mesoscale rain areas are characterized by upper tropospheric mesoscale ascent, and a lower tropospheric mesoscale downdraft. This two cell circulation may be in part driven by condensation and freezing aloft and evaporation and cooling below, but other dynamical processes appear to be involved.

Quantifying the effect that these systems have on the large-scale is of utmost importance. B-scale data may be useful in increasing our understanding of the scale interaction problem. A more complete theoretical understanding of the dynamics and thermodynamics of these systems is needed.

12.2.7.2 Studies of cloud and convective elements

Extensive cloud updraft and downdraft data were obtained from aircraft penetrations of convective systems. Convective-scale downdrafts in these systems transport approximately one half to three fourths as much mass as updrafts.

New data on structure, evolution and movement of the cumulonimbus cloud bands in the ITCZ have been obtained by means of weather radars installed on board research vessels. A shift of the cumulonimbus cloud band to the south of the ITCZ axis has been discovered.

Radar data of convective elements have been processed which showed a log-normal distribution of clouds. A similar distribution has been earlier obtained through processed cloud pictures covering the entire sky. The physical explanation for this distribution and its possible implications to parameterization should be further studied.

12.2.7.3 Diagnostic studies of cumulus convection

Diagnostic budget studies of cumulus convection carried out mainly on the basis of GATE radiosonde data have been an important tool for increasing our understanding of how convection alters the thermodynamic structure of the large-scale environment. Physically reasonable mass fluxes have been obtained from these diagnostic studies by using more sophisticated cloud models (which account not only for updrafts but also for convective and mesoscale downdrafts).

Considerable progress has been made using GATE data in the study and interpretation of vorticity budgets, though more work remains to be done. It appears that the convection acts to oppose the concentration of low-level cyclonic vorticity by the large-scale convergence.

12.2.7.4 Convective modelling and parameterization

Models that simulate the detailed life cycles of whole populations of clouds including cloud clusters have begun to appear. Since these models allow for large-scale forcing mechanisms to be externally specified, such models are powerful tools in the effort to understand how large-scale processes control a cloud ensemble. Analysis of GATE data has shown that the ITCZ cloud clusters and precipitation are triggered by large-scale processes, with the convergence preceeding the convective activity by about six hours.

The above models, however, being of diagnostic nature, do not yet represent parameterization schemes applicable to operational prognostic models. Initial work has begun on the testing of different cumulus parameterization schemes in numerical models using GATE data.

12.2.8 Boundary-layer phenomena

12.2.8.1 The surface layer

Main characteristics of the turbulent exchange near the ocean surface were obtained during GATE by direct measurements in the surface layer along 23.5°W with the aid of different experimental techniques.

The turbulent fluxes of momentum, sensible and latent heat under different weather conditions allowed to describe the exchange regime for the ITCZ and the trade-wind zone during the whole experiment time and should serve as the basis for the development of parameterization schemes of the interaction between the ocean and the tropical atmosphere.

The mean quantities of the turbulent fluxes experience considerable variations during the passage of convective disturbances. These effects lead to remarkable changes of energy and momentum transfer across the ocean surface.

The dissimilarity between the temperature and the moisture spectra and consequently the differences between the spectra of sensible and latent fluxes indicate that most likely the heat transfer near the sea surface is predominantly achieved by relatively small scales of motion while water vapour is transported by convective elements of a larger size. The transfer coefficient for latent heat fluxes was in general distinctly lower than that for sensible heat.

Finally the GATE measurements also suggest that the determination of the evaporation at the sea surface by the aerodynamic method may be rather insufficient in principle under conditions of strong cloud convection.

12.2.8.2 Atmospheric boundary layer under different convective conditions

Aircraft and tethered balloon measurements together with budget studies have greatly increased our understanding of the convectively undisturbed and disturbed boundary layers in the tropics. In a horizontally divergent flow with suppressed cumulus cloud activity the top of the atmospheric boundary layer is generally well marked by a temperature inversion. When deep precipitating convection dominates during low-level convergence the vertical extension of the boundary layer is ill-defined. Under these conditions cloud generated up- and down-drafts lead to a distinct modification of the thermodynamic properties of the subcloud and lower cloud layer. After the passage of a convective system several hours are required until the boundary layer has recovered to its undisturbed state.

Simple one-dimensional models enable us to satisfactorily simulate the time development of the undisturbed boundary layer even in the presence of non-precipitating cumulus clouds. These models can also be applied to describe the recovery of the subcloud mixed layer in the rear of convective systems. In the case of deep convection modelling of the boundary layer separate from the other parts of the troposphere seems not to be reasonable since the structure of the low-level atmosphere is critically determined by the convection process. Current model schemes have been applied to such conditions with some success but further improvements seem to be necessary.

Variable knowledge gained from the GATE boundary layer investigations has been advantageously used in between in studying the air flow over the Arabian Sea during different stages of the Indian monsoon circulation.

12.2.9 Radiation in GATE

For the first time the three-dimensional radiation field in the tropics has been described and the role of clouds and aerosols in its formation has been specified. Differences between the equatorial radiation band (equatorward of 5° of latitude) and the radiation regime of the proper tropical zone (poleward of 5° latitude) have been established. Spatial fluctuations of radiative fluxes, caused by characteristic dimensions of convection clouds, have been shown to the small-scale phenomena.

The radiative profiles in the tropics have been shown to considerably alter the radiative budget of the atmosphere. Basic modulations of the radiative budget are determined by horizontal variations in cloudiness: the latter produce horizontal gradients in the daily averaged divergence of the radiative fluxes. The above gradients have been considered as one of possible factors determining the diurnal variability of the penetrative convection.

Furthermore, substantial day-night differences between clear and cloudy regions are also observed, horizontal differences being much greater in the meridional than in the latitudinal direction. The considerable role of the dust transport from the African continent in the radiative characteristics of the atmosphere has also been shown.

Response of the dynamical processes in the tropical atmosphere to the radiation changes has been spectacularly shown in some numerical experiments, in particular in tropical forecasts of synoptic-scale features and associated rainfall over land and ocean with interactive clouds alternating solar and long-wave radiation.

12.2.10 Unanswered questions

We must agree that many of the basic questions of tropical meteorology are still unanswered. Examples are: the question of the mechanism by which easterly waves are maintained during their crossing the Atlantic, in particular, the role of cumulus convection in that maintaining; the question in what (rather rare) cases hurricanes might form from easterly waves or other weak disturbances; the question of an interaction of Hadley-type circulation with synoptic formations; the question of mesoscale circulations development and their interaction with synoptic-scale phenomena; a wide scope of questions of the equatorial atmospheric dynamics. FGGE data may serve as an additional basis for all these questions to be answered.

12.3 TECHNOLOGICAL DEVELOPMENT AND ITS IMPACT ON FGGE

A wide use of new observational means during GATE made it possible to develop new techniques which later were of great help for FGGE. That refers, in particular, to satellite observations.

12.3.1 New techniques were very useful in processing cloud pictures taken by geostationary satellites to obtain a wind speed and direction data derived from the movement of high- and low-level clouds. These techniques have found an extensive use during FGGE.

12.3.2 Various techniques have been developed for determining precipitation using satellite products over the GATE area. The above-mentioned techniques provided the extremely needed precipitation values over oceans where there is a lack of surface-based precipitation observations.

12.3.3 The experience in the application of "Omega" and "VLF" signals in "Navaid" systems to wind measurements in free atmosphere with the GATE ships data, showed their potential value and revealed the deficiencies. To overcome these deficiences a more sophisticated "CORA" system was developed. It was then used for carrying out wind measurements on a large scale in the tropics during FGGE.

12.3.4 The quantitative weather radar network in GATE was an important advance in radar meteorology. The highly successful radar network established for the measurement of precipitation in GATE was one of the first to make full use of digital processing of multiple inter-calibrated radars co-ordinated in their operation to give simultaneous horizontal and vertical precipitation structure over a large area continuously in time for a long period. Such radar networks are now being implemented in operational forecasting networks by several countries. The radars in GATE demonstrated dramatically the potential of such networks to measure rainfall and depict the internal structure of cloud systems.

12.3.5 The techniques for calculating the balances in the ITCZ area were proposed. The physical conclusions derived from them should be compared with the techniques and results performed by ships during FGGE, in particular, during the Monsoon Experiment in which the configuration of ship arrays was in great part determined by the experience gained during GATE.

12.4 USE OF GATE EXPERIENCE FOR IMPLEMENTATION AND MANAGEMENT OF FGGE

GATE was the first experiment of the Global Atmospheric Research Programme to co-ordinate the work of such a great number of countries and various observing systems in field conditions. Its implementation required the development of certain

organizational procedures and joint efforts on an international scale. The experience thus gained was further used for FGGE implementation in the following way.

12.4.1 The planning of the GATE was carried out by a special International Scientific and Management Group (ISMG). The Central Programme, five subprogrammes, operation plans of ship movement, aircraft missions, satellite flights, telecommunication requirements, data management plan and other activities have been worked out by the ISMG. The practice was then used by the GARP Activities Office when working at the FGGE Implementation/Operations Plan.

12.4.2 GATE implementation was ensured by national contributions in the establishment of the observing system and the observational data processing system. Contributions and their co-ordination were made by a Tropical Experiment Board. Its members were the designated representatives of the Meteorological Services which have stated their intention to contribute to GATE implementation on a voluntary basis. The experience gained from these arrangements was further used by establishing the WMO Executive Committee Inter-governmental Panel on the FGGE.

12.4.3 The operational control of the implementation of the GATE field phase was performed by the GATE Operations Control Centre (GOCC) which was planning and implementing the aircraft missions, confirmed periods for intensive observations, carried out data collection and real time analysis and kept under review the general course of the Experiment. The experience proved to be very useful for the operational control of FGGE and MONEX.